Edited by
Evangelos Tsotsas and
Arun S. Mujumdar

Modern Drying Technology

Modern Drying Technology

Edited by E. Tsotsas and A. Mujumdar

Other Volumes

Volume 1: Computational Tools at Different Scales

ISBN: 978-3-527-31556-7

Volume 2: Experimental Techniques

ISBN: 978-3-527-31557-4

Volume 3: Product Quality and Formulation

ISBN: 978-3-527-31558-1

Forthcoming Volumes

Volume 5: Process Intensification

ISBN: 978-3-527-31560-4

Modern Drying Technology Set (Volumes 1 – 5)

ISBN: 978-3-527-31554-3

Edited by
Evangelos Tsotsas and Arun S. Mujumdar

Modern Drying Technology

Volume 4: Energy Savings

WILEY-VCH Verlag GmbH & Co. KGaA

The Editors:

Prof. Evangelos Tsotsas
Otto von Guericke University
Thermal Process Engineering
Universitätsplatz 2
39106 Magdeburg
Germany

Prof. Arun S. Mujumdar
National University of Singapore
Mechanical Engineering/Block EA 07-0
9 Engineering Drive 1
Singapore 117576
Singapore

Library of Congress Card No.: applied for

British Library Cataloguing-in-Publication Data
A catalogue record for this book is available from the British Library.

Bibliographic information published by the Deutsche Nationalbibliothek
The Deutsche Nationalbibliothek lists this publication in the Deutsche Nationalbibliografie; detailed bibliographic data are available on the Internet at http://dnb.d-nb.de.

Composition Thomson Digital, Noida, India

Printing and Binding

Cover Design Adam Design, Weinheim

Printed in the Federal Republic of Germany
Printed on acid-free paper

Print ISBN: 978-3-527-31559-8
ePDF ISBN: 978-3-527-63169-8
oBook ISBN: 978-3-527-63168-1

Contents

Series Preface

The present series is dedicated to drying, that is, to the process of removing moisture from solids. Drying has been conducted empirically since the dawn of the human race. In traditional scientific terms it is a unit operation in chemical engineering. The reason for the continuing interest in drying and, hence, the motivation for the series concerns the challenges and opportunities. A permanent challenge is connected to the sheer amount and value of products that must be dried – either to attain their functionalities, or because moisture would damage the material during subsequent processing and storage, or simply because customers are not willing to pay for water. This comprises almost every material used in solid form, from foods to pharmaceuticals, from minerals to detergents, from polymers to paper. Raw materials and commodities with a low price per kilogram, but with extremely high production rates, and also highly formulated, rather rare but very expensive specialties have to be dried.

This permanent demand is accompanied by the challenge of sustainable development providing welfare, or at least a decent living standard, to a still-growing humanity. On the other hand, opportunities emerge for drying, as well as for any other aspect of science or living, from either the incremental or disruptive development of available tools. This duality is reflected in the structure of the book series, which is planned for five volumes in total, namely:

Volume 1: Computational tools at different scales
Volume 2: Experimental techniques
Volume 3: Product quality and formulation
Volume 4: Energy savings
Volume 5: Process intensification

As the titles indicate, we start with the opportunities in terms of modern computational and experimental tools in Volumes 1 and 2, respectively. How these opportunities can be used in fulfilling the challenges, in creating better and new products, in reducing the consumption of energy, in significantly improving existing or introducing new processes will be discussed in Volumes 3, 4 and 5. In this sense, the first

two volumes of the series will be driven by science; the last three will try to show how engineering science and technology can be translated into progress.

In total, the series is designed to have both common aspects with and essential differences from an extended textbook or a handbook. Textbooks and handbooks usually refer to well-established knowledge, prepared and organized either for learning or for application in practice, respectively. On the contrary, the ambition of the present series is to move at the frontier of "modern drying technology", describing things that have recently emerged, mapping things that are about to emerge, and also anticipating some things that may or should emerge in the near future. Consequently, the series is much closer to research than textbooks or handbooks can be. On the other hand, it was never intended as an anthology of research papers or keynotes – this segment being well covered by periodicals and conference proceedings. Therefore, our continuing effort will be to stay as close as possible to a textbook in terms of understandable presentation, and as close as possible to a handbook in terms of applicability.

Another feature in common with an extended textbook or a handbook is the rather complete coverage of the topic by the entire series. Certainly, not every volume or chapter will be equally interesting for every reader, but we do hope that several chapters and volumes will be of value for graduate students, for researchers who are young in age or thinking, and for practitioners from industries that are manufacturing or using drying equipment. We also hope that the readers and owners of the entire series will have a comprehensive access not to all, but to many significant recent advances in drying science and technology. Such readers will quickly realize that modern drying technology is quite interdisciplinary, profiting greatly from other branches of engineering and science. In the opposite direction, not only chemical engineers, but also people from food, mechanical, environmental or medical engineering, material science, applied chemistry or physics, computing and mathematics may find one or the other interesting and useful results or ideas in the series.

The mentioned interdisciplinary approach implies that drying experts are keen to abandon the traditional chemical engineering concept of unit operations for the sake of a less rigid and more creative canon. However, they have difficulties of identification with just one of the two new major trends in chemical engineering, namely process-systems engineering or product engineering. Efficient drying can be completely valueless in a process system that is not efficiently tuned as a whole, while efficient processing is certainly valueless if it does not fulfill the demands of the market (the customer) regarding the properties of the product. There are few topics more appropriate in order to demonstrate the necessity of simultaneous treatment of product and process quality than drying. The series will try to work out chances that emerge from this crossroads position.

One further objective is to motivate readers in putting together modules (chapters from different volumes) relevant to their interests, creating in this manner individual, task-oriented threads through the series. An example of one such thematic thread set by the editors refers to simultaneous particle formation and drying,

with a focus on spray fluidized beds. From the point of view of process-systems engineering, this is process integration – several "unit operations" take place in the same equipment. On the other hand, it is product engineering, creating structures – in many cases nanostructures – that correlate with the desired application properties. Such properties are distributed over the ensemble (population) of particles, so that it is necessary to discuss mathematical methods (population balances) and numerical tools able to resolve the respective distributions in one chapter of Volume 1. Measuring techniques providing access to properties and states of the particle system will be treated in one chapter of Volume 2. In Volume 3, we will attempt to combine the previously introduced theoretical and experimental tools with the goal of product design. Finally, important issues of energy consumption and process intensification will appear in chapters of Volumes 4 and 5. Our hope is that some thematic combinations we have not even thought about in our choice of contents will arise in a similar way.

As the present series is a series of edited books, it cannot be as uniform in either writing style or notation as good textbooks are. In the case of notation, a list of symbols has been developed and will be printed at the beginning of every volume. This list is not rigid but foresees options, at least partially accounting for the habits in different parts of the world. It has been recently adopted as a recommendation by the Working Party on Drying of the European Federation of Chemical Engineering (EFCE). However, the opportunity of placing short lists of additional or deviant symbols at the end of every chapter has been given to all authors. The symbols used are also explained in the text of every chapter, so that we do not expect any serious difficulties in reading and understanding.

The above indicates that the clear priority in the edited series was not in uniformity of style, but in the quality of the contents that are very close to current international research from academia and, where possible, also from industry. Not every potentially interesting topic is included in the series, and not every excellent researcher working on drying contributes to it. However, we are very confident about the excellence of all research groups that we were able to gather together, and we are very grateful for the good cooperation with all chapter authors. The quality of the series as a whole is set mainly by them; the success of the series will primarily be theirs. We would also like to express our acknowledgements to the team of Wiley-VCH who have done a great job in supporting the series from the first idea to realization. Furthermore, our thanks go to Mrs Nicolle Degen for her additional work, and to our families for their tolerance and continuing support.

Last but not least, we are grateful to the members of the Working Party on Drying of the EFCE for various reasons. First, the idea for the series came up during the annual technical and business meeting of the working party 2005 in Paris. Secondly, many chapter authors could be recruited among its members. Finally, the Working Party continues to serve as a panel for discussion, checking and readjustment of our conceptions about the series. The list of the members of the working party with their affiliations is included in every volume of the series in the sense of acknowledgment, but also in order to promote networking and to provide access to national working

parties, groups and individuals. The present edited books are complementary to the regular activities of the EFCE Working Party on Drying, as they are also complementary to various other regular activities of the international drying community, including well-known periodicals, handbooks, and the International Drying Symposia.

December 2006

Evangelos Tsotsas
Arun S. Mujumdar

Preface of Volume 4

As already stressed in the general preface, the contents of modern drying technology are subjected to the dual requirement of producing high-quality products with highly efficient processes. Moreover, drying is energetically expensive – a major consumer of energy in modern societies – which makes energy use a crucial aspect of process efficiency. In times of abundant and inexpensive energy, one might ignore – and many people did – the respective consumption, concluding that any drying process is a good process as long as the desired product properties can be preserved or established. However, cheap energy seems to belong to history, and serious environmental concerns have appeared, related to climate change. Consequently, modern drying technology must address the complete challenge, regarding product quality and process efficiency as the two faces of the same coin, and treat them concurrently. Having discussed "Product quality and formulation" in Volume 3 of this series, we turn our attention to "Energy savings" in Volume 4. The optimistic title should by no means conceal difficulties arising from thermodynamic and economic restraints, but it does express our confidence that modern drying technology can fulfill the task. This confidence stems from a number of available methods, emerging approaches and innovative ideas, which can seriously serve and significantly contribute to the ultimate goal of energetically efficient drying processes, as presented in the following eight chapters:

Chapter 1: Fundamentals of energy analysis of dryers
Chapter 2: Mechanical solid-liquid separation processes and techniques
Chapter 3: Energy considerations in osmotic dehydration
Chapter 4: Heat pump assisted drying technology – Overview with focus on energy, environment and product quality
Chapter 5: Zeolites for reducing drying energy usage
Chapter 6: Solar drying
Chapter 7: Energy issues of drying and heat treatment for solid wood and other biomass sources
Chapter 8: Efficient sludge thermal processing: From drying to thermal valorization

Chapter 1 sets the fundamentals of energy analysis, breaking down the total energy consumption of a dryer in its constituent parts, defining efficiency, and

identifying sources and reasons for inefficiency and losses. Pinch analysis is discussed in detail as a powerful tool for assessing the potential of and designing heat transfer from hot to cold material streams. Various other methods that can lead to energy savings are classified and presented – from altering operating conditions to the combination of heat and power. Specific examples that range from learning exercises to industrial case studies are used to put figures and numbers behind the principles. Most important, Chapter 1 points out very clearly that dryer energy savings should always be considered in the context of the overall process or even production cite, in a systemic approach.

An evident systemic aspect is that the energy consumption of any dryer decreases with decreasing moisture content in the feed. Unfortunately, the respective potential for energy savings is not always fully utilized, because thermal drying and the preceding solid-liquid separation are designed separately, often by different people. Therefore, solid-liquid separation processes are highlighted in Chapter 2, including an exhaustive taxonomy, the detailed presentation of equipment, and criteria for selection and design. Modern techniques for the enhancement of such separations by electric or magnetic forces are presented. Furthermore, improvements that can be attained by the consecutive, parallel or combined use of equipment are discussed, referring to both purely mechanical steps and to the combination of mechanical separation with thermal drying in the batch or continuous mode of operation.

Another possibility to remove water out of soft materials previously to drying, namely osmosis, is treated in Chapter 3. Osmotic dehydration is relevant to food processing and can lead to significant energy savings in the drying step, but it has also an impact on food quality, which must be simultaneously considered. Experiences with and benefits from the combination of osmotic dehydration with different kinds of thermal drying are comprehensively reviewed.

One major source of energy loss from conventional one-pass hot-air dryers is "over the chimney". Therefore, heat recovery from the warm and moist exhaust air is a key to the enhancement of the energetic efficiency of dryers. Since such recovery can be achieved by heat pumps, heat pump drying is discussed in detail in Chapter 4. A distinctive advantage of this technology lies in its add-on character – it can be applied to virtually any kind of dryer, though it is most reasonable in combination with low to moderate temperature dryers for the processing of sensible goods. Chapter 4 explains the principles of different types of heat pumps, presents various methods for their combination with dryers, and quantifies the merits that can be obtained in terms of improved energetic efficiency. Extensive records of successful application to various products – food and agricultural, wood and timber, pharmaceutical and biological – are presented, design methods are discussed, and opportunities for future development are outlined.

Similarly to heat pumps, particulate adsorbents – especially zeolites – can also be used for heat recovery from dryer exhaust gases. Zeolite drying is highlighted as a powerful and promising technology in Chapter 5. It is pointed out that zeolites can be used for heat recovery from the exhaust, but they can also serve the purpose of inlet air dehumidification, or even be mixed to and subsequently separated from the drying material. The resulting energy savings are evaluated in a systematic way,

starting with simple configurations and moving step-by-step to more complex multi-stage or steam-operated systems. Examples of already realized facilities for the drying of dairy products, sludge and seeds are presented. Finally, economic aspects are analyzed in terms of pay-back times for the necessary additional investment.

In Chapter 6, solar drying is treated as a further energetically promising alternative. Solar energy is for free, but reaches the Earth with a relatively low flux and a strongly fluctuating rate. To use it for drying, solar energy must be harvested in an efficient way that does not require too much additional investment. This leads to special constructions of solar collectors and dryers, which are classified and discussed in detail. Applications of such equipment are presented for various agricultural products, and the necessity for relaxing the influence of variable energy input by appropriate control strategies is stressed. Case studies on timber and tobacco are used to show that solar drying can be economically viable and beneficial in comparison to both, primitive sun drying but also conventional hot-air drying.

It is well known that the harvesting of solar energy is very efficiently carried out by plants, creating biomass. Some kinds of biomass, namely wood, can be used to, for example, make furniture, some others as renewable fuels. Since both applications are closely related to drying and of a very large scale, they are discussed thoroughly in Chapter 7. First, benchmarks are provided for the energy demand of wood drying kilns, and methods for saving energy by improved kiln design and operation are presented. It is, then, shown, that preconditioning by drying can enhance the efficiency of processes aiming at the energetic valorization of biomass, such as combustion or gasification. Various drying technologies for fuel biomass are discussed. Dual-scale models applicable to the drying of both, timber pieces and fuel biomass particles are presented. Apart from the assessment of energetic efficiency, such models can also track product quality in terms of, for example, timber distortion or uniformity of residual moisture in a fuel biomass particle system.

Finally, Chapter 8 addresses the energetic issues of one more large-scale application of drying, namely the drying of sludge from wastewater treatment facilities. The case is similar to woody biomass, because the main component of sludge is bacterial biomass that may just need to be dried before, for example, landfill, or may require drying in combination with subsequent processes of thermal valorization, such as – again – combustion or gasification. After a presentation of sludge composition and properties, the various types of drying equipment and processes that can be used for sludge are discussed thoroughly, along with their energetic efficiency. Specific case studies illustrate that the proper integration of drying in municipal wastewater treatment plants can significantly reduce the energy demand, and that sludge can have a significant value as a fuel, if efficiently pre-dried.

Due to nature of the topic, the present volume of Modern Drying Technology has interdisciplinary links to thermodynamics, energy and environmental engineering, process systems engineering, food engineering, meteorology, forestry, biology and biotechnology, but also to economics. Concerning the scale, single particles and processing equipment (particle systems) are considered, but also entire production sites and global environmental and economic systems.

Thematic threads within the Modern Drying Technology series exist from the present:

- Chapter 1 to Chapter 7 of Vol. 1 (systems engineering)
- Chapters 2 and 5 to Chapter 6 of Vol. 2 (particle characterization)
- Chapters 3 and 4 to Chapters 1 and 2 of Vol. 3 (food processing)
- Chapter 7 to Chapter 1 of Vol. 1 (wood drying)
- Chapter 8 to Chapters 4 of Vol. 2 and Chapter 5 of Vol. 3 (gel materials)

Additionally, the entire present volume is closely related to Vol. 3, as the already mentioned two faces of the same coin. The overall message is that of drying science and technology in good shape for doing exactly what the title of the volume describes, namely saving energy.

Acknowledgements for Volume 4 are the same as in the series preface, we would like to stress them by reference, but not repeat them here.

August 2011

Evangelos Tsotsas
Arun S. Mujumdar

List of Contributors

Editors

Prof. Evangelos Tsotsas
Otto von Guericke University
Magdeburg
Thermal Process Engineering
PSF 4120
39106 Magdeburg
Germany
Email: Evangelos.Tsotsas@ovgu.de

Prof. Arun S. Mujumdar
National University of Singapore
Mechanical Engineering
Block EA 07-0
9 Engineering Drive 1
Singapore 117576
Singapore
Email: mpeasm@nus.edu.sg

Authors

Dr. Giana Almeida
AgroParisTech
1 avenue des Olympiades
91744 Massy cedex
France
Email: giana.almeida@agroparistech.fr

Dr. Harald Anlauf
Karlsruhe Institute of Technology (KIT)
Institute of Mechanical Process
Engineering and Mechanics (MVM)
Straße am Forum 8
76131 Karlsruhe
Germany
Email: harald.anlauf@kit.edu

Dr. Patricia Arlabosse
Université de Toulouse
Mines Albi, CNRS
Campus Jarlard
81013 Albi
France
Email: Patricia.Arlabosse@mines-albi.fr

Dr. Moniek A. Boon
TNO
Postbus 360
3700 AJ Zeist
The Netherlands
Email: floor.boon@tno.nl

Dr. Paul J. Th. Bussmann
TNO
Postbus 360
3700 AJ Zeist
The Netherlands
Email: paul.bussmann@tno.nl

Dr. Julien Colin
AgroParisTech
ENGREF
14 rue Girardet
54 042 Nancy
France
Email: julien.colin@nancy-engref.inra.fr

Prof. Michel Crine
University of Liège
Department of Applied Chemistry
Laboratory of Chemical Engineering
Bâtiment B6c – Sart-Tilman
4000 Liège
Belgium
Email: M.Crine@ulg.ac.be

Dr. Yohann Dumont
Aix-Marseille Université
M2P2, UMR CNRS 6181
Europôle de l'Arbois, BP 80
13545 Aix en Provence Cedex 4
France
Email: yohann.dumont@
univ-cezanne.fr

Dr. Jean-Henry Ferrasse
Aix-Marseille Université
M2P2, UMR CNRS 6181
Europôle de l'Arbois, BP 80
13545 Aix en Provence Cedex 4
France
Email: jean-henry.ferrasse@etu.
univ-cezanne.fr

Dr. Sachin V. Jangam
National University of Singapore
Mechanical Engineering Department
Blk EA, #06-15
9 Engineering Drive 1
Singapore 117576
Singapore
Email: mpejsv@nus.edu.sg

Ir. Ian C. Kemp
Glaxo Smithkline, R&D
Gunnels Wood Road
Stevenage SG1 2NY
United Kingdom
Email: ian.c.kemp@gsk.com

Prof. Didier Lecomte
Université de Toulouse
Mines Albi, CNRS
Centre RAPSODEE
Campus Jarlard
81013 Albi
France
Email: didier.lecomte@2ie-edu.org

Prof. Angélique Léonard
University of Liège
Department of Applied Chemistry
Laboratory of Chemical Engineering
Bâtiment B6a – Sart-Tilman
4000 Liège
Belgium
Email: a.leonard@ulg.ac.be

Prof. Werner Mühlbauer
Universität Hohenheim
Institute of Agricultural Engineering
Garbenstrasse 9
70593 Stuttgart
Germany
Email: wernermuehlbauer@yahoo.de

Prof. Arun S. Mujumdar
National University of Singapore
Mechanical Engineering Department
Blk EA, #06-15
9 Engineering Drive 1
Singapore 117576
Singapore
Email: mpeasm@nus.edu.sg

Prof. Joachim Müller
Universität Hohenheim
Institute of Agricultural Engineering
Garbenstrasse 9
70593 Stuttgart
Germany
Email: joachim.mueller@uni-hohenheim.de

Prof. Patrick Perré
Ecole Centrale Paris
Grande Voie des Vignes
92295 Châtenay-Malabry
France
Email: patrick.perre@ecp.fr

Prof. Hosahalli S. Ramaswamy
McGill University
Department of Food Science
Macdonald Campus
21111 Lakeshore Road
Ste-Anne-de-Bellevue
PQ H9X 3V9
Canada
Email: hosahalli.Ramaswamy@Mcgill.ca

Dr. Yetenayet Bekele Tola
McGill University
Department of Food Science
Macdonald Campus
21111 Lakeshore Road
Ste-Anne-de-Bellevue
PQ H9X 3V9
Canada
Email: yetenayet.tola@mail.mcgill.ca

Dr. Antonius J.B. van Boxtel
Wageningen UR
Department of Agrotechnology and Food Sciences
Systems and Control Group
Postbus 17
6700 AA Wageningen
The Netherlands
Email: ton.vanboxtel@wur.nl

Ir. Henk C. van Deventer
TNO
Postbus 360
3700 AJ Zeist
The Netherlands
Email: henk.vandeventer@tno.nl

Recommended Notation

- Alternative symbols are given in brackets
- Vectors are denoted by bold symbols, a single bar, an arrow or an index (e.g., index: i)
- Tensors are denoted by bold symbols, a double bar or a double index (e.g., index: i, j)
- Multiple subscripts should be separated by colon (e.g., $\rho_{p,dry}$: density of dry particle)

A	surface area	m^2
a_w	water activity	–
B	nucleation rate	$kg^{-1}\ m^{-1}\ s^{-1}$
b	breakage function	m^{-3}
$C(K)$	constant or coefficient	various
c	specific heat capacity	$J\ kg^{-1}\ K^{-1}$
D	equipment diameter	m
$D(\delta)$	diffusion coefficient	$m^2\ s^{-1}$
d	diameter or size of solids	m
E	energy	J
F	mass flux function	–
$F(\dot{V})$	volumetric flow rate	$m^3\ s^{-1}$
f	relative (normalized) drying rate	–
f	multidimensional number density	–
G	shear function or modulus	Pa
G	growth rate	$kg\ s^{-1}$
g	acceleration due to gravity	$m\ s^{-2}$
H	height	m
H	enthalpy	J
H	Heaviside step function	–
h	specific enthalpy (dry basis)	$J\ kg^{-1}$
$h(\alpha)$	heat-transfer coefficient	$W\ m^{-2}\ K^{-1}$
$\tilde{h}(h_N)$	molar enthalpy	$J\ mol^{-1}$
Δh_v	specific enthalpy of evaporation	$J\ kg^{-1}$
I	total number of intervals	–

J	numerical flux function	–
J	Jacobian matrix	various
$j(\dot{m}, J)$	mass flux, drying rate	kg m^{-2} s^{-1}
K	dilatation function or bulk modulus	Pa
$k(\beta)$	mass transfer coefficient	m s^{-1}
L	length	m
M (m)	mass	kg
$\tilde{M}(M, M_N)$	molecular mass	kg kmol^{-1}
$\dot{M}(W)$	mass flow rate	kg s^{-1}
$\dot{m}(J, j)$	mass flux, drying rate	kg m^{-2} s^{-1}
$\dot{m}$	volumetric rate of evaporation	kg m^{-3} s^{-1}
N	number	–
N	molar amount	mol
$\dot{N}(W_N)$	molar flow rate	mol s^{-1}
n	molar density, molar concentration	mol m^{-3}
n	number density	m^{-3}
n	outward normal unit vector	
$\dot{n}(J_N)$	molar flux	mol m^{-2} s^{-1}
P	power	W
P	total pressure	kg m s^{-2}
p	partial pressure/vapor pressure of component	kg m s^{-2}
$\dot{Q}(Q)$	heat flow rate	W
$\dot{q}(q)$	heat flux	W m^{-2}
R	equipment radius	m
R	individual gas constant	J kg^{-1} K^{-1}
$\tilde{R}(R_N)$	universal gas constant	J kmol^{-1} K^{-1}
r	radial coordinate	m
r	pore (throat) radius	m
S	saturation	–
S	selection function	s^{-1}
s	boundary-layer thickness	m
T	temperature	K, °C
t	time	s
u	velocity, usually in z-direction	m s^{-1}
u	displacement	m
V	volume, averaging volume	m^3
$\dot{V}(F)$	volumetric flow rate	m^3 s^{-1}
v	specific volume	m^3 kg^{-1}
v	general velocity, velocity in x-direction	m s^{-1}
W	weight force	N
$W(\dot{M})$	mass flow rate	kg s^{-1}
w	velocity, usually in y-direction	m s^{-1}
X	solids moisture content (dry basis)	–
x	mass fraction in liquid phase	–
x	particle volume in population balances	m^3

x	general Eulerian coordinate, coordinate (usually lateral)	m
x_0	general Lagrangian coordinate	m
$\tilde{x}(x_N)$	molar fraction in liquid phase	–
Y	gas moisture content (dry basis)	–
y	spatial coordinate (usually lateral)	m
$y(\omega)$	mass fraction in gas phase	–
$\tilde{y}(y_N)$	molar fraction in gas phase	–
z	spatial coordinate (usually axial)	m

Operators

∇	gradient operator
∇	divergence operator
Δ	difference operator

Greek Letters

$\alpha(h)$	heat-transfer coefficient	W m^{-2} K^{-1}
$\beta(k)$	mass-transfer coefficient	m s^{-1}
β	aggregation kernel	s^{-1}
δ	Dirac-delta distribution	
$\delta(D)$	diffusion coefficient	m^2 s^{-1}
ε	voidage	–
ε	emissivity	–
ε	small-scale parameter for periodic media	–
ε	strain	–
η	efficiency	–
θ	angle, angular coordinate	rad
κ	thermal diffusivity	m^2 s^{-1}
λ	thermal conductivity	W m^{-1} K^{-1}
μ	dynamic viscosity	kg m^{-1} s^{-1}
μ	moment of the particle-size distribution	various
ν	kinematic viscosity	m^2 s^{-1}
π	circular constant	–
ρ	density, mass concentration	kg m^{-3}
Σ	summation operator	
σ	surface tension	N m^{-1}
σ	Stefan–Boltzmann constant for radiative heat transfer	W m^{-2} K^{-4}
σ	standard deviation (of pore-size distribution)	m
σ	stress	Pa
τ	dimensionless time	–
Φ	characteristic moisture content	–
φ	relative humidity	–
φ	phase potential	Pa
ω	angular velocity	rad
$\omega(y)$	mass fraction in gas phase	–

Subscripts

a	at ambient conditions
as	at adiabatic saturation conditions
b	bound water
bed	bed
c	cross-section
c	capillary
cr	at critical moisture content
D	drag
dry	dry
dp	at dewpoint
eff	effective
eq	equilibrium (moisture content)
f	friction
g	gas (dry)
H	wet (humid) gas
i	inner
i, 1, 2, ...	component index, particle index
i, j, k	coordinate index, $i, j, k = 1$ to 3
in	inlet value
l	liquid (alternative: as a superscript)
m	mean value
max	maximum
mf	at minimum fluidization
min	minimum
N	molar quantity
o	outer
out	outlet value
P	at constant pressure
p	particle
pbe	population balance equation
ph	at the interface
r	radiation
rel	relative velocity
s	solid (compact solid phase), alternative: as a superscript
S	at saturation conditions
surf	surface
V	based on volume
v	vapor, evaporation
w	water
w	wall
wb	at wet-bulb conditions
wet	wet
∞	at large distance from interface

Superscripts, Special Symbols

v	volumetric strain
*	rheological strain
*	at saturation conditions
$\overline{\ }$ or $\langle\rangle$	average, phase average
$\overline{\ }^{\alpha}$ or $\langle\rangle^{\alpha}$	intrinsic phase average
$\sim$	spatial deviation variable

EFCE Working Party on Drying: Address List

Prof. Odilio Alves-Filho
Norwegian University of Science and Technology
Department of Energy and Process Engineering
Kolbjørn Hejes vei 1B
7491 Trondheim
Norway
odilo.fihlo@gmail.com

Prof. Julien Andrieu *(delegate)*
UCB Lyon I/ESCPE
LAGEP UMR CNRS 5007
batiment 308 G
43 boulevard du 11 novembre 1918
69622 Villeurbanne cedex
France
andrieu@lagep.univ-lyon1.fr

Dr. Paul Avontuur
Glaxo Smith Kline
New Frontiers Science Park H89
Harlow CM19 5AW
United Kingdom
Paul.Avontuur@gsk.com

Prof. Christopher G. J. Baker
Drying Associates
Harwell International Business Centre
404/13 Harwell Didcot
Oxfordshire OX11 ORA
United Kingdom
ChristopherGJ.Baker@gmail.com

Prof. Antonello Barresi *(delegate)*
Politecnico di Torino
Dip. Scienza dei Materiali e Ingegneria Chimica
Corso Duca degli Abruzzi 24
10129 Torino
Italy
antonello.barresi@polito.it

Dr. Rainer Bellinghausen *(delegate)*
Bayer Technology Services GmbH
BTS-PT-PT-PDSP
Building E 41
51368 Leverkusen
Germany
rainer.bellinghausen@bayertechnology.com

Dr. Carl-Gustav Berg
Abo Akademi
Process Design Laboratory
Biskopsgatan 8
20500 Abo
Finland
cberg@abo.fi

Dr. Catherine Bonazzi *(delegate)*
AgroParisTech – INRA
JRU for Food Process Engineering
1 Avenue des Olympiades
91744 Massy cedex
France
Catherine.Bonazzi@agropartistech.fr

Paul Deckers M.Sc. *(delegate)*
Bodec
Process Optimization and Development
Industrial Area 't Zand
Bedrijfsweg 1
5683 CM Best
The Netherlands
deckers@bodec.nl

Prof. Stephan Ditchev
University of Food Technology
26 Maritza Blvd.
4002 Plovdiv
Bulgaria
sditchev@gmail.bg

Dr. German I. Efremov
Pavla Korchagina 22
129278 Moscow
Russia
efremov_german@mail.ru

Prof. Trygve Eikevik
Norwegian University of Science and Technology
Dep. of Energy and Process Engineering
Kolbjørn Hejes vei 1B
7491 Trondheim
Norway
Trygve.M.Eikevik@ntnu.no

Dr. Ioannis Evripidis
Dow Deutschland GmbH & Co. OHG
P.O. Box 1120
21677 Stade
Germany
evripidis@dow.com

Prof. Istvan Farkas *(delegate)*
Szent Istvan University
Department of Physics and Process Control Pater K. U. 1.
2103 Godollo
Hungary
Farkas.Istvan@gek.szie.hu

Dr. Dietrich Gehrmann
Wilhelm-Hastrich-Str. 12
51381 Leverkusen
Germany
Dietrich.Gehrmann@t-online.de

Prof. Adrian-Gabriel Ghiaus *(delegate)*
Thermal Engineering Department
Technical University of Civil Engineering
Bd. P. Protopopescu 66
021414 Bucharest
Romania
ghiaus@instalatii.utcb.ro

Prof. Gheorghita Jinescu
University "Politehnica" din Bucuresti
Faculty of Industrial Chemistry,
Department of Chemical Engineering
1, Polizu street
Building F, Room F210
78126 Bucharest
Romania
g_jinescu@chim.upb.ro

Prof. Gligor Kanevce
St. Kliment Ohridski University
Faculty of Technical Sciences
ul. Ivo Ribar Lola b.b.
Bitola
Macedonia
kanevce@osi.net.mk

Prof. Markku Karlsson *(delegate)*
UPM-Kymmene Corporation
P.O. Box 380
00101 Helsinki
Finland
markku.karlsson@upm-kymmene.com

Ir. Ian C. Kemp *(delegate)*
Glaxo SmithKline, R&D
Gunnels Wood Road
Stevenage SG1 2NY
United Kingdom
ianckemp@btinternet.com

Prof. P. J. A. M. Kerkhof
Eindhoven University of Technology
Dept. of Chemical Engineering
P.O. Box 513
5600 MB Eindhoven
The Netherlands
p.j.a.m.kerkhof@tue.nl

Prof. Matthias Kind
Universität Karlsruhe (TH)
Institute für Thermische
Verfahrenstechnik
Kaiserstr. 12
76128 Karlsruhe
Germany
matthias.kind@ciw.uni-karlsruhe.de

Prof. Eli Korin
Ben-Gurion University of the Negev
Chemical Engineering Department
Beer-Sheva 84105
Israel
ekorin@bgumail.bgu.ac.il

Prof. Ram Lavie
Department of Chemical Engineering
Technion – Israel Institute of Technolgy
Technion City
Haifa 32000
Israel
lavie@tx.technion.ac.il

Prof. Angélique Léonard *(delegate)*
Laboratoire de Génie Chimique
Département de Chimie Appliquée
Université de Liège
Bâtiment B6c – Sart-Tilman
4000 Liège
Belgium
A.Leonard@ulg.ac.be

Prof. Avi Levy *(delegate)*
Ben-Gurion University of the Negev
Department of Mechanical Engineering
Beer-Sheva 84105
Israel
avi@bgu.ac.il

Prof. Natalia Menshutina
Mendeleyev University of Chemical
Technology of Russia (MUCTR)
High Technology Department
125047 Muisskaya sq.9
Moscow
Russia
chemcom@muctr.edu.ru

Jun.-Prof. Thomas Metzger
Otto-von-Guericke University
Thermal Process Engineering
P.O. Box 4120
39016 Magdeburg
Germany
thomas.metzger@vst.uni-magdeburg
.de

Prof. Antonio Mulet Pons *(delegate)*
Universitat Politecnica de Valencia
Departament de Tecnologia d'Aliments
Cami de Vera s/n
46071 Valencia
Spain
amulet@tal.upv.es

Prof. Zdzislaw Pakowski *(delegate)*
Technical University of Lodz
Faculty of Process and Environmental Engineering
ul. Wolczanska 213
93-005 Lodz
Poland
pakowski@wipos.p.lodz.pl

Prof. Patrick Perré *(delegate, chairman of WP)*
Ecole Centrale Paris
Laboratoire de Génie des Procédés et Matériaux
Grande Voie des Vignes
92295 Châtenay-Malabry
France
patrick.perre@ecp.fr

Dr. Romain Rémond *(WP secretary)*
Research Engineer
AgroParisTech - Engref
14, Rue Girardet
54000 Nancy
Remond@nancy-engref.inra.fr

Dr. Roger Rentröm
Karlstad University
Department of Environmental and Energy Systems
Universitetsgatan 2
65188 Karlstad
Sweden
roger.renstrom@kau.se

Prof. Michel Roques
Universite de Pau et des Pays de l'Adour
5 Rue Jules-Ferry
ENSGTI
64000 Pau
France
michel.roques@univ-pau.fr

Dr. Carmen Rosselló *(delegate)*
University of Illes Baleares
Dep. Quimica
Ctra. Valldemossa km 7.5
07122 Palme Mallorca
Spain
Carmen.rossello@uib.es

Prof. G. D. Saravacos *(delegate)*
Nea Tiryntha
21100 Nauplion
Greece
gsaravac@otenet.gr

Dr. Scarlatos Panayiotis *(Panos)*
SusTchem Engineering LTD
144 3rd September Street
11251 Athens
Greece
pscarlatos@suschem.gr

Dr. Michael Schönherr
Research Manager Drying
Process Engineering
BASF Aktiengesellschaft
GCT/T – L 540
67056 Ludwigshafen
Germany
michael.schoenherr@basf.com

Dr. Milan Stakic
Vinča Institute for Nuclear Sciences
Center NTI
P.O. Box 522
11001 Belgrade
Serbia
stakicm@yahoo.com

Prof. Stig Stenstrom *(delegate)*
Lund University
Institute of Technology
Department of Chemical Engineering
P.O. Box 124
22100 Lund
Sweden
stig.stenstrom@chemeng.lth.se

Prof. Ingvald Strommen *(delegate)*
Norwegian University of Science and Technology
Department of Energy and Process Engineering
Kolbjørn Hejes vei 1b
7491 Trondheim
Norway
ingvald.strommen@ntnu.no

Prof. Czeslaw Strumillo *(delegate)*
Technical University of Lodz
Faculty of Process and Environmental Engineering
Lodz Technical University
ul. Wolczanska 213
93-005 Lodz
Poland
cstrumil@wipos.p.lodz.pl

Prof. Radivoje Topic *(delegate)*
University of Belgrade
Faculty of Mechanical Engineering
27 Marta 80
11000 Beograd
Serbia
r.topic@eunet.yu

Prof. Dr.-Ing. Evangelos Tsotsas *(delegate, immediate past chairman of WP)*
Otto-von-Guericke University
Thermal Process Engineering
P.O. Box 4120
39016 Magdeburg
Germany
evangelos.tsotsas@vst.uni-magdeburg.de

Dr. Henk C. van Deventer *(delegate)*
TNO Quality of Life
P.O. Box 342
7300 AH Apeldoorn
The Netherlands
henk.vandeventer@tno.nl

Michael Wahlberg M.Sc.
Niro
Gladsaxevej 305
2860 Soeborg
Denmark
mw@niro.dk

Dr. Bertrand Woinet *(delegate)*
SANOFI-CHIMIE, CDP
Bâtiment 8600
31-33 quai armand Barbès
69683 Neuville sur Saône cedex
France
bertrand.woinet@sanofi-aventis.com

Prof. Ireneusz Zbicinski
Lodz Technical University
Faculty of Process and Environmental Engineering
ul. Wolczanska 213
93-005 Lodz
Poland
zbicinsk@mail.p.lodz.pl

1
Fundamentals of Energy Analysis of Dryers

Ian C. Kemp

1.1
Introduction

Drying is a highly energy-intensive process, accounting for 10–20% of total industrial energy use in most developed countries. The main reason for this is the need to supply the latent heat of evaporation to remove the water or other solvent. There are thus clear incentives to reduce energy use in drying: to conserve finite resources of fossil fuels, to reduce carbon footprint and combat climate change, and to improve process economics, but it is a challenging task facing real thermodynamic barriers.

Effective analysis of current energy use is a vital first step in identifying opportunities for savings. An initial lower bound of dryer energy needs is provided by calculating the evaporation load for the amount of water to be removed (Section 1.3). This shows how much energy is inherently required and, by comparing with current measured energy usage, what opportunities exist to reduce energy consumption. These fall into three main categories;

1) Reduce the evaporation load – for example, by upstream dewatering to reduce initial moisture content, or avoiding overdrying.
2) Increase the dryer efficiency – for example, by improving insulation and reducing heat losses, installing heat recovery or changing operating parameters.
3) Improve the energy supply (utility) system – for example, by increasing boiler efficiency, or using combined heat and power (CHP), heat pumps, waste incineration, or other alternative low-cost fuels.

Frequently, the evaporation load will be less than 50% of the actual process energy consumption in terms of fuel supplied. The numerous causes for this difference include:

- Additional energy required to break bonds and release bound moisture
- Heat losses in the exhaust (particularly for convective dryers) or through the dryer body
- Heating solids and vapor to their discharge temperature
- Steam generation and distribution losses and condensate losses

Modern Drying Technology Volume 4: Energy Savings, First Edition.
Edited by Evangelos Tsotsas and Arun S. Mujumdar.

- Losses in non-routine operation, for example, startup, shutdown or low load periods
- Ancillary steam use, for example, trace heating, steam ejectors and turbine drives

In addition, there will be power consumption for fans, vacuum pumps, chillers, mechanical drives and other general uses. The dryer's energy use must also be seen in the context of the complete process and, indeed, of the site as a whole.

One key tool is pinch analysis (Section 1.4.2), which shows the temperatures at which the dryer heat load is required and where heat can be recovered from the exhaust vapor, and places this in the context of the overall production process. This shows the feasibility of heat recovery, CHP, heat pumps and process changes, and helps to generate realistic targets for how much energy the process should be using. Practical methods to help achieve these targets are reviewed in Section 1.5, and the whole analysis methodology is shown in action in the case study in Section 1.6.

An engineer – maybe a reformed gambler – once restated the three laws of thermodynamics (conservation of energy, increasing entropy and increasing difficulty of approaching absolute zero) as follows:

1) You can't win – you can only break even.
2) You can't break even – you can only lose.
3) You can't get out of the game.

Energy consumption, like taxes, is an unavoidable fact of life. Nevertheless, it is sensible, and feasible, to use our ingenuity to reduce it as far as possible.

1.2 Energy in Industrial Drying

Industrial dryers are major energy users. A survey by Wilmshurst (1988) (reported by Bahu, 1991) estimated that drying processes accounted for at least 10% of industrial energy demand in the UK and Europe – not just 10% of process engineering, but of all industrial consumption. Since then, if anything, the figure has increased; a similar survey by Kemp (1996) for the UK Government's Department of Energy evaluated the figure at 12–15% of total industry energy use. Similar figures are thought to apply for most developed countries.

Why should this be, in an era of increasing focus on energy efficiency and work by manufacturers to improve their equipment? The answer is that drying processes have an unavoidable constraint – they must supply enough heat or energy to provide the latent heat of evaporation for all the vapor which is removed – over 2000 kJ kg^{-1} for the most common solvent, water. All industries have been working to reduce their energy consumption, but many have been able to make energy savings more easily than drying, which is limited by its thermodynamic barrier. Furthermore, dryers tend to have inherently low thermal efficiency (often below 50% for convective dryers) and many new products requiring drying have appeared on the market (e.g., special foods, pharmaceuticals, videotapes).

In the 1970s and 1980s, energy prices were high, and this provided the major cost incentive for installing energy-saving projects – an incentive that was markedly reduced when oil prices fell to much lower levels in the following years. Now, in the twenty-first century, energy is recognized to be only part of the bigger picture of sustainability. Major associated benefits of energy reduction include reducing CO_2 and other greenhouse gases, and pollutants and acid gases including SO_x and NO_x. With oil prices volatile again, and the principles of dryer energy reduction better understood than in the past, it is an excellent time to revisit the challenge of making drying systems more energy efficient. This should involve the entire process, including the energy supply systems, rather than treating the dryer in isolation.

An economic point which is often overlooked is that energy is a direct cost, so that a saving of £1000 (GBP) goes directly onto the bottom line and appears as £1000 extra profit. In contrast, a £1000 increase in sales is diluted by a corresponding increase in production costs, including raw materials, transport and, of course, energy itself. Nevertheless, the tight constraints on budgeting and economic return on energy-saving schemes make it essential that a clear analysis of the principles is made before embarking on a project.

1.3
Fundamentals of Dryer Energy Usage

1.3.1
Evaporation Load

We will use the common definition of a drying process as being one where liquid is removed from a solid specifically by evaporation. This excludes mechanical dewatering processes such as filtration and centrifugation. Hence, to achieve drying, the latent heat of evaporation must be supplied to turn each kilogram of moisture into vapor. Thus the absolute minimum amount of heat or other energy, $E_{v,min}$, (J), which must be supplied for a drying process is:

$$E_{v,min} = M_v \Delta H_v \tag{1.1}$$

It is often more convenient to use the corresponding heat supply rate, $Q_{v,min,}$ (J s^{-1} or W), which is given by:

$$Q_{v,min} = W_v \Delta H_v \tag{1.2}$$

For a continuous process it is

$$Q_{v,min} = W_s (X_{in} - X_{out}) \Delta H_v \tag{1.3}$$

and for a batch process (at any instant)

$$Q_{v,min} = M_s \left(\frac{-dX}{dt} \right) \Delta H_v \tag{1.4}$$

Latent heat varies with temperature. For the most common solvent, water, the latent heat of evaporation is 2501 kJ kg^{-1} at 0 °C and 2256 kJ kg^{-1} at 100 °C. At ambient temperatures, around 20 °C, a figure of 2400 kJ kg^{-1} is a good working approximation. So, for a drying process which requires the evaporation of 1 kg s^{-1} of water from the solid, an absolute minimum of 2400 kJ s^{-1} (2400 kW) must be supplied to the process in some way. Note, however, that if the liquid enters with the solid at one temperature, and emerges as a vapor at a higher temperature, additional sensible heat will be needed to achieve this, in addition to the latent heat at a fixed temperature.

1.3.2
Dryer Energy Supply

The evaporation load is the minimum energy demand for drying, but this energy has to be transferred to the solids in a practical way; for example, from hot air (convective drying), a hot wall or surface (contact or conduction drying), or by absorbing electromagnetic radiation (infrared, radiofrequency or microwave drying). The process of supplying heat typically consumes significantly more energy than the latent heat of evaporation.

For a continuous convective (hot air) dryer, the heater duty for the inlet air heat exchanger (excluding heater losses) is given by:

$$Q_{\text{heater}} = W_{\text{g}} c_{P\text{g}} (T_{\text{g,in}} - T_{\text{g,a}}) \tag{1.5}$$

Here $T_{\text{g,in}}$ is the inlet temperature to the dryer and $T_{\text{g,a}}$ is the temperature at which the air is supplied. Conversely, when the hot air is supplied to the dryer, the exhaust emerges at a mean temperature of $T_{\text{g,out}}$. A simple heat balance on a continuous dryer (as developed for debottlenecking by Kemp and Gardiner, 2001) gives:

$$W_{\text{g}} c_{P\text{g}} (T_{\text{g,in}} - T_{\text{g,out}}) \approx W_{\text{s}} (X_{\text{in}} - X_{\text{out}}) \Delta H_{\text{v}} + W_{\text{s}} c_{P\text{s}} (T_{\text{g,out}} - T_{\text{g,in}}) + Q_{\text{loss}} \tag{1.6}$$

that is, heat given up by hot air $\sim$ evaporation load + sensible heating of solids + heat losses.

Combining Eqs. 1.5 and 1.6 we find that, to a first approximation:

$$Q_{\text{heater}} = \frac{(T_{\text{g,in}} - T_{\text{g,a}})}{(T_{\text{g,in}} - T_{\text{g,out}})} \left[W_{\text{s}} (X_{\text{in}} - X_{\text{out}}) \Delta H_{\text{v}} + Q_{\text{s,sens}} + Q_{\text{loss}} \right] \tag{1.7}$$

This would be the heat energy required to run a perfect adiabatic dryer, and also the amount of fuel needed if the heat was supplied by a perfect energy conversion system with zero losses. We see that, compared to the basic evaporative load, there are additional terms for heat losses in the exhaust gas, sensible heating of the solids and heat losses from the dryer body.

In some cases, filter cakes can be dewatered by blowing ambient air through them, so that evaporative cooling occurs and the damp exhaust air emerges below ambient. No heat is then required, but there is a significant pressure drop across the cake, so

power is needed to run the fans. Moreover, the process is very slow – typically taking many hours or days – because the driving forces are so low.

Likewise, if heat is supplied by conduction, there is no need for a large air flow to transmit heat, and the heat requirement with no carrier gas would fall to:

$$Q_{\text{heater}} = \left[W_s(X_{\text{in}} - X_{\text{out}})\Delta H_v + Q_{s,\text{sens}} + Q_{\text{loss}}\right] \tag{1.8}$$

However, a partial pressure or humidity driving force is needed to carry the vapor away from the solids, otherwise the local air becomes saturated with vapor and drying rates fall towards zero. A flow of carrier gas is required, or a vacuum must be pulled. This requires additional electrical power for fans or pumps, or steam for ejectors.

Finally, if a system incorporates water adsorption by zeolites, as described in Chapter 5, this reduces the evaporation load. However, energy will then be needed to regenerate the zeolite to its dry state for reuse (or to manufacture new zeolite if it cannot be recycled).

Hence, in practice, the actual energy which must be supplied is normally considerably greater than the evaporation load calculated in Section 1.3.1. The various additional energy penalties can be broken down into the following categories:

1) Thermal inefficiencies in the dryer: exhaust heat content in convective dryers, sensible heating of solids, heat losses from dryer body.
2) Thermal inefficiencies in the utility (heat supply) system: steam generation efficiency, steam leaks and mains losses.
3) Additional energy demands: power for solids transport, vacuum pumps and air fans.

These will now be illustrated by a detailed practical example.

1.3.3
Evaluation of Energy Inefficiencies and Losses: Example

Assume a continuous process with a flowrate $1\,\text{kg s}^{-1}$ of dry solid, being dried from 12 to 2% moisture (dry basis) so that $\Delta X = 0.1\,\text{kg kg}^{-1}$ and the evaporation rate $W_v = 0.1\,\text{kg s}^{-1}$. Hence, from Eq. 1.2, $Q_{v,\text{min}} = 240\,\text{kW}$.

A psychrometric chart provides a convenient and rapid way to estimate enthalpies and outlet conditions. Either a Grosvenor (temperature–humidity) or Mollier (enthalpy–humidity) chart can be used. It allows for additional factors, such as the extra heat required to heat water vapor from 20 °C to exhaust temperature. By reading off the exhaust humidity, the required airflow can be calculated using a mass balance on the solvent; alternatively, if dryer airflow is known, the maximum evaporation rate can be found. Assuming negligible leaks, the mass balance is:

$$W_g(Y_{\text{out}} - Y_{\text{in}}) = W_v = W_s(X_{\text{in}} - X_{\text{out}}) \tag{1.9}$$

For convective dryers, the heat is supplied by hot air. Assume the inlet air is at 150 °C, which is heated by steam from ambient (20 °C), and the ambient humidity is $7.5\,\text{g kg}^{-1}$ ($0.0075\,\text{kg kg}^{-1}$, corresponding to a dewpoint of 10 °C). Either by

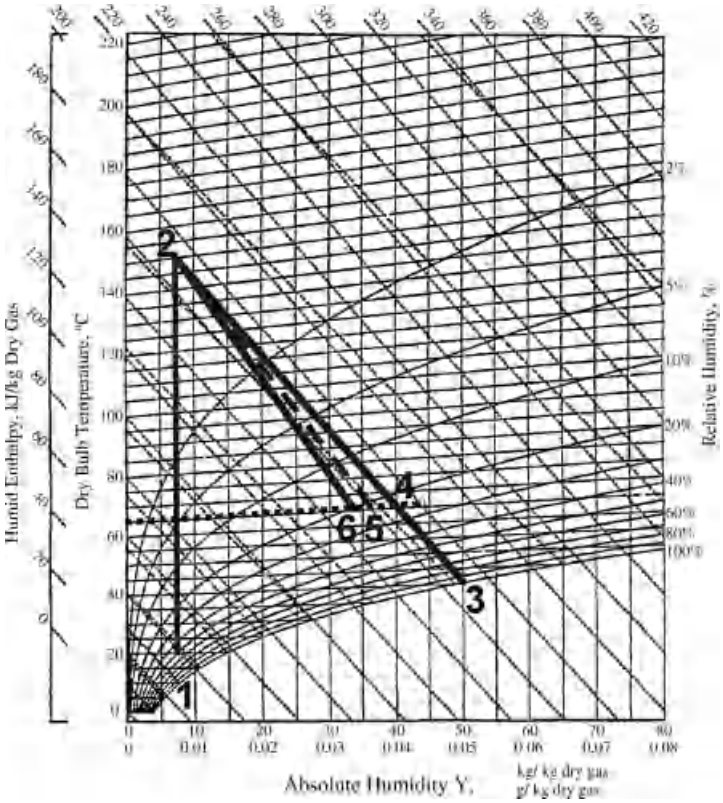

Fig. 1.1 Mollier psychrometric chart with operating lines for an indirect-heated convective dryer.

calculation or by reading from a psychrometric chart (see Fig. 1.1), the enthalpy is approximately 40 kJ kg^{-1} for the ambient air (point 1 on the chart) and 170 kJ kg^{-1} for the inlet air (point 2), so that 130 kJ kg^{-1} must be supplied in the air heater. For illustrative purposes, these and other enthalpy figures will be rounded throughout the following calculations. Also, by substituting the appropriate numbers into Eq. 1.9, we obtain the useful relationship $W_g = 0.1/(Y_{out} - 0.0075)$.

1.3.3.1 Dryer Thermal Inefficiencies

Exhaust Heat Losses The absolute minimum exhaust temperature is the adiabatic saturation temperature T_{as}. For inlet air at 150 °C and humidity 7.5 g kg^{-1}, T_{as} is approximately 40 °C (point 3), reading along the adiabatic saturation line on the psychrometric chart (or, as a good approximation at low to moderate humidity, using lines of constant enthalpy which are roughly parallel to adiabatic saturation lines). Hence there is about 40 kJ kg^{-1} of sensible heat in the exhaust compared to 20 kJ kg^{-1} in the ambient air, and of the 130 kJ kg^{-1} supplied to heat the air, at most 110 kJ kg^{-1} could be used for evaporation. This can be roughly confirmed from the adiabatic

saturation humidity which is about 50.5 g kg^{-1}; hence, 43 g kg^{-1} has been evaporated and, with a latent heat of about 2400 kJ kg^{-1}, requires 103 kJ kg^{-1}; the additional heat above this is needed to raise the water vapor to exhaust temperature.

Thus if dryer efficiency η is expressed as latent heat of evaporation divided by actual heat supplied to the air, this is (103/130) or approximately 80%, so that 20% is inherently lost in the exhaust. This efficiency will vary with inlet air temperature, falling further for lower inlet temperature.

Likewise, from Eq. 1.9, $W_g = (0.1/0.0043) = 2.33\,\text{kg s}^{-1}$, and from Eq. 1.5, $Q_{\text{heater}} = 2.33 \times 1.0 \times (150 - 20) = 302.3\,\text{kW}$, so that $\eta = 240/302.3 = 79.4\%$, as above.

Exhaust Air Temperature Above Dewpoint The ideal efficiency above can only be achieved for a dryer where the exhaust gas reaches equilibrium with the solids. This implies extremely good heat transfer because the driving forces for heat and mass transfer will be very low. It can be closely approached in a batch fluidized bed during constant rate drying, as heat and mass transfer in the bed is excellent and the number of transfer units is high (typically 5–10). For most dryers, however, to reduce dryer size and avoid condensation, exhaust temperature will be significantly above its dewpoint. Taking a typical value of 25 °C, the exhaust temperature is now 65 °C (point 4), the sensible heat component is about 65 kJ kg^{-1}, the exhaust humidity is 40.5 g kg^{-1}, and this corresponds to a latent heat component of (33/1000 × 2400) or 79 kJ kg^{-1}. Dryer efficiency has now fallen to just over 60%.

To achieve the dryer duty with the lower exhaust humidity, airflow W_g must rise to 3.03 kg s^{-1}, from Eq. 1.9, and heater duty to 394 kW, from Eq. 1.5, hence the lower efficiency.

Heating of Solids If the solids enter at ambient (20 °C) but are heated to 50 °C during the falling-rate section of the drying process to remove bound moisture, and the specific heat capacity of the solids is 1 kJ kg^{-1} K^{-1}, the sensible heat supplied is $W_s c_{Ps} \Delta T = 1 \times 1 \times 30 = 30\,\text{kW}$. The total Q_v has risen to 270 kW, just over 10% above the base value. Conversely, of the 79 kJ kg^{-1} calculated above, about 10% is used to heat solids rather than for evaporation, so the evaporation load falls to 70 kJ kg^{-1} and the efficiency to 54%. The result of this is that the outlet humidity falls to approximately 37 g kg^{-1} for the same exhaust temperature (point 5), and the dryer operating line is no longer parallel to an adiabatic saturation line or a line of constant enthalpy.

Using Eq. 1.9 again, $W_g = 3.39\,\text{kg s}^{-1}$, and from Eq. 1.5, $Q_{\text{heater}} = 441\,\text{kW}$.

Heat of Wetting of the Solids When removing bound moisture, extra heat will be required to break the bonds between the water and the substrate. This appears as an increase above the normal latent heat of evaporation, becoming greater as the moisture content falls. This is material-specific and is not included in these calculations, but should be borne in mind. It can sometimes be rolled in with heat losses (below).

Heat Losses from the Dryer Body These are typically 5–10%, but can be greater if the dryer is poorly insulated or of small capacity (higher surface-to-volume ratio). As well as convection and radiation from the outer surfaces, heat conduction along the

Tab. 1.1 Outlet conditions, airflow and heater duty for different scenarios.

Condition	$T_{g,out}$ (°C)	Y_{out} (kg kg^{-1})	ΔH_{latent} (kJ kg^{-1})	W_g (kg s^{-1})	Q_{heater} (kW)	η (%)
Adiabatic saturation	40	0.0505	103.2	2.33	302	79.4%
Exhaust approach 25 °C	65	0.0405	79.2	3.03	394	60.9%
Including solids heating	65	0.037	70.8	3.39	441	54.5%
Including heat losses	65	0.034	63.6	3.77	491	48.9%

supporting framework must also be taken into account. Losses may be expressed in various ways – an absolute value, a percentage of inlet air enthalpy or a percentage of evaporation load. Assuming for this case a loss of 10% of evaporation, the evaporation load has now fallen to 63 kJ kg^{-1} and efficiency to 49%. A further reduction in outlet humidity also takes place, to 34 g kg^{-1} assuming the same exhaust temperature of 65 °C is maintained (point 6 on the psychrometric chart). Hence $W_g = 3.77$ kg s^{-1} and $Q_{heater} = 491$ kW.

Overall, we see that a typical convective dryer, even if well-designed and well-operated, can be less than 50% efficient. Table 1.1 summarizes the outlet conditions, air flow requirement and heater duty for the different situations. The various operating lines are shown on the Mollier psychrometric chart in Fig. 1.1.

1.3.3.2 Inefficiencies in the Utility (Heat Supply) System

Boiler Efficiency Assuming the dryer is heated by steam, this must be raised in a boiler where fuel is burned in an air stream. Significant heat is lost in the exiting flue gases. Modern boilers will recover as much heat as possible from the flue gas, for example, by economizers which heat boiler feedwater and the incoming air. However, even then, the flue gases will leave at 120–150 °C and the maximum boiler efficiency will be about 80–85%. Boiler efficiency is usually stated on the air side, as the ratio between heat passed to the process fluid and the heat released from combustion of the fuel. Lower flue gas temperatures would give condensation in the exhaust gas, which can lead to stack corrosion due to acid gases, even with relatively clean fuels such as natural gas.

Boiler Feedwater Heating The steam will be condensed in the process to provide heat to the dryer and will release its latent heat. For example, 10 bara steam (10 bar absolute pressure, 9 bar gage) condenses at 180 °C with a latent heat of 2015 kJ kg^{-1}. Hot condensate emerges. If this is returned at the same temperature and pressure to the boilers to act as feedwater, with no leaks or temperature losses, the same amount of heat (2015 kJ kg^{-1}) can be supplied in the boiler to produce steam. However, in practice, this never happens. Some water is blown down to avoid build-up of salts, and must be made up with cold water which requires additional heating. Some plants do not have a pressurized condensate return system, which limits the boiler feedwater return temperature to about 85–90 °C before cavitation (boiling) occurs. Others

Tab. 1.2 Heat required to raise steam from boiler feedwater at different temperatures.

Fluid	Temperature (°C)	Enthalpy (heat content) (kJ kg^{-1})	Heat required to raise 10 bar steam (kJ kg^{-1})	Fuel for boiler at 80% efficiency (kJ kg^{-1})
10 bara steam	180	2778	0	0
10 bara water	180	763	2015	2519
Water at 90 °C	90	377	2401	3001
Water at ambient	20	84	2694	3368

return only part of their condensate, or none at all. If all boiler feedwater is raised from ambient (20 °C) to 180 °C, this gives an additional 679 kW heat requirement, and a loss of 25% (because 2694 kJ kg^{-1} heat must be supplied but only 2015 kJ kg^{-1} is recovered on condensation). If condensate is heated from 90 °C, the additional heat requirement is 386 kW and the loss is 16%. See Tab. 1.2, which also includes the loss due to boiler efficiency. Thus, for a boiler which is 80% efficient in raising 10 bara steam, but is supplied with feedwater at ambient temperature which is not heated by flue gas in an economizer, the actual heat delivered to the process is only 60% of the fuel used (2015/3368).

Steam Distribution Losses Steam is passed from the boiler to the dryer along steam mains. Ideally, these will be short, well-insulated and well-maintained, and heat losses and steam leakage will be below 5%. However, many large and old sites have extensive networks of steam mains which suffer significant losses from long pipe runs, missing or damaged insulation, redundant sections which have not been blanked off, steam leaks and poorly maintained steam traps. In an extreme case (Kemp, 2007), half the steam generated at the boilers was unaccounted for.

Assuming a modest steam distribution loss of 10% and a condensate return temperature of 90 °C, Tab. 1.3 (left-hand side) and Fig. 1.2 show how the different losses add up for a typical steam-heated convective dryer, combining the dryer losses from Section 1.3.3.1 and the utility system losses from Section 1.3.3.2. The evaporative load is less than 30% of the gross calorific value of the fuel, illustrating starkly how a large number of apparently unimportant losses can add up to a major overall penalty. Even if the mains distribution losses were only 5% and the condensate return system heat loss was 10%, so that most condensate is returned above 100 °C in a pressurized system, the overall system efficiency is still only 33.5%, as shown in the right-hand side of Tab. 1.3; or, putting it another way, the amount of fuel required in the boiler in heating terms is three times the minimum heat required for the required evaporation duty.

In Fig. 1.2, the top right-hand segment represents losses in the dryer, the top left-hand segment is losses in the utility system, while the bottom solid region is the actual evaporation load.

Overall, it can be seen that for an indirect-heated convective dryer it will be extremely rare to get an overall thermal efficiency greater than 50% (expressed as

Tab. 1.3 Breakdown of fuel use for a typical convective steam-heated dryer.

Situation	Steam Distribution Loss 10%, 90 °C Condensate Return			Steam Distribution Loss 5%, Condensate Return Loss 10%		
Component	Heat Required	Marginal Heat, kW	Marginal %	Heat Required	Marginal Heat, kW	Marginal %
Minimum evaporation load	2400	2400	29.6	2400	2400	33.5
Adiabatic saturation	3023	623	7.7	3023	623	8.7
Exhaust approach 25 °C	3939	916	11.3	3939	916	12.8
Including solids heating	4407	467	5.8	4407	467	6.5
Including heat losses	4906	499	6.1	4906	499	7.0
Steam distribution loss	5451	545	6.7	5164	258	3.6
Condensate losses	6495	1044	12.9	5740	576	8.0
Boiler efficiency (80%)	8118	1623	20.0	7174	1434	20.0

latent heat of evaporation compared to gross calorific value of fuel), and this will require a highly efficient steam system as well as an efficient dryer. For a contact dryer, exhaust airflow and exhaust heat losses are much lower, but the maximum practicable figure is likely to be 70%. Neither of these figures include power for vacuum pumps, fans, and so on, which are covered in Section 1.3.3.3.

Water and Thermal Oil Systems Some dryers are heated by circulating loops containing hot water (at lower temperatures) or thermal fluid (at high temperatures). These still have to be heated by furnaces, and heat losses in these are similar to those in boilers. Flue gas heat losses will depend on the circulating fluid temperature,

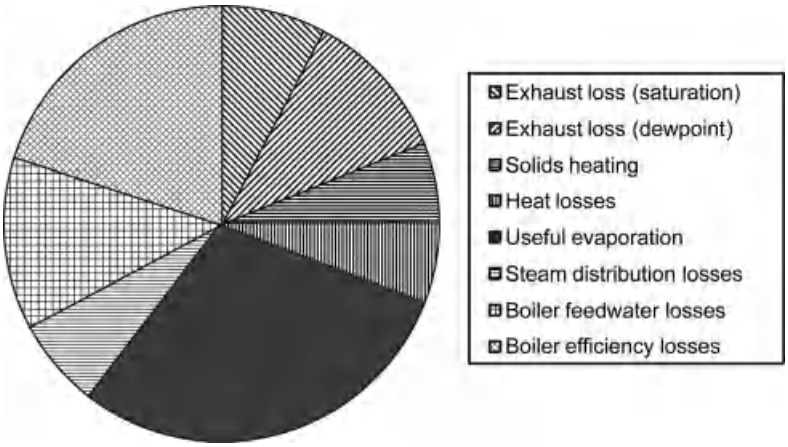

Fig. 1.2 Breakdown of overall usage of heat supplied as fuel for a typical steam-heated convective dryer.

although the flue gas can still be used to heat the incoming air to the boiler. Condensate losses should be lower, as all the heat transfer fluid is recirculated, but heat losses from the pipework must still be allowed for.

Direct-Fired Dryers In some dryers, fuel can be burned and the combustion gases can be used directly as the hot inlet gas for a convective dryer. This eliminates the losses involved in the steam-raising boilers. The system can only be used where it is acceptable for the product to come into direct contact with the combustion gases, and the inlet air has a higher humidity due to the additional water produced in combustion. Normally, natural gas is used and the additional water added to the air is given by:

$$\begin{aligned} CH_4 + 2O_2 &= CO_2 + 2H_2O \\ 16\,\text{kg} + 64\,\text{kg} &= 44\,\text{kg} + 36\,\text{kg} \end{aligned}$$

Typically, the gross calorific value of natural gas is $54\,000\,\text{kJ kg}^{-1}$ and the net calorific value $47\,000\,\text{kJ kg}^{-1}$. The latter is more convenient for calculations here, as the water generated by combustion ends up as water vapor. Hence 1 GJ heat is released from 21.3 kg fuel and generates 47.9 kg water vapor. In this case, where 130 kJ per kg air needs to be added, an additional 0.0062 kg water vapor is added and the inlet humidity rises from 7.5 to $13.7\,\text{g kg}^{-1}$. The new enthalpy is $190\,\text{kJ kg}^{-1}$ instead of $170\,\text{kJ kg}^{-1}$, because of the extra energy contained in the latent heat of the water vapor – this in effect has been supplied by the difference between the gross and net calorific values.

The psychrometric chart in Fig. 1.3 shows a direct-fired system working with the same air inlet temperature and exhaust ΔT as an indirect system. The dryer now works between point 7 (inlet) and 8 (exhaust), as against points 2 and 6 for the dryer heated by an indirect heat exchanger. Both cases allow for heat losses and solids heating, as before. The useful heat released as a percentage of heat in the fuel can be expressed as (47 000/54 000) in terms of calorific value or $(170 - 40)/(190 - 40) = 130/150$ in terms of inlet enthalpy, both equating to an efficiency of 87%; the remaining 13% is used to heat the additional water vapor. This is better than the boiler efficiency of an indirect steam heated system, even if a small additional allowance is made for heat losses from the burner (usually well under 5%). In addition, all steam distribution and condensate return losses are eliminated entirely.

Table 1.4 shows the outlet conditions and burner duty, and can be compared with Table 1.1. To a first approximation, the required airflow will be the same as for the indirect heater, but the outlet humidity is higher by $0.0062\,\text{kg kg}^{-1}$ throughout and the burner duty is greater than the heater duty.

Likewise, we can generate Tab. 1.5 showing a breakdown of the energy losses, equivalent to Tab. 1.3, and the corresponding pie chart, Fig. 1.4. In this case, we have broken out the heat required for the water vapor from combustion as a separate entity, and added a notional 5% heat loss from the burner itself. Despite these, the overall efficiency is more than 40%, which is considerably better than an equivalent steam-heated system. Comparing Fig 1.4 with Fig 1.2, the top left segment corresponding to utility system losses is much smaller.

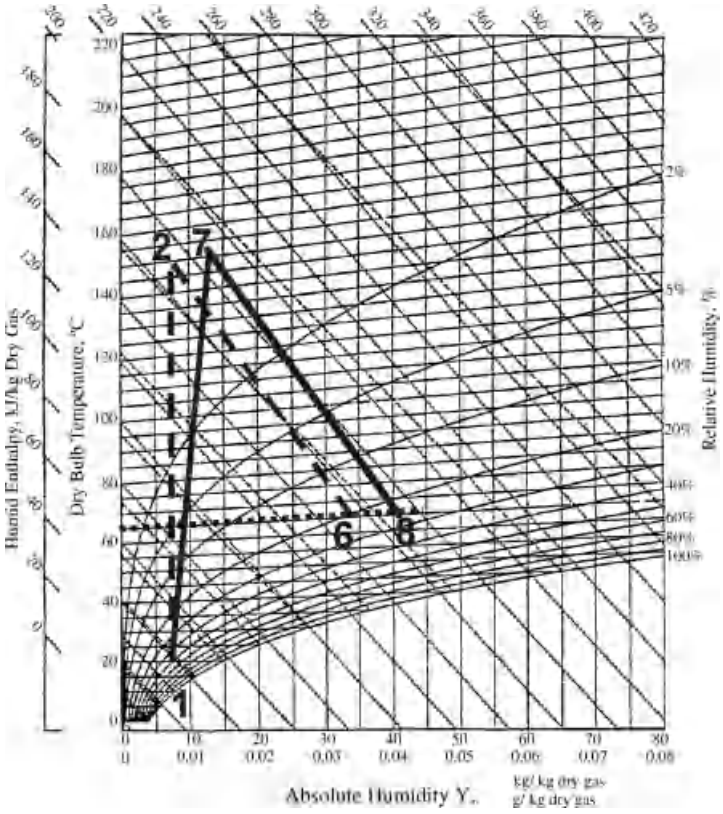

Fig. 1.3 Psychrometric chart for direct-fired and indirect-heated convective dryers.

Electrical Heating Electrical heating can be used, for example, by infrared heater or RF and microwave systems. However, the electricity must be generated somewhere. For typical thermal power stations, efficiencies are typically around 30–40% (though over 50% for modern combined cycle systems). Hence, allowing for capital costs and distribution losses, it is a reasonable rule of thumb that electrical power typically costs three times more per kWh than fuels in most countries. The exceptions are where

Tab. 1.4 Outlet conditions, airflow and heater duty for direct-fired dryer.

Condition	$T_{g,out}$ (°C)	Y_{out} (kg kg^{-1})	ΔH_{latent} (kJ kg^{-1})	W_g (kg s^{-1})	Q_{burner} (kW)	η (%)
Adiabatic saturation	40	0.0567	103.2	2.33	349	68.8
Exhaust approach 25 °C	65	0.0467	79.2	3.03	454	52.8
Including solids heating	65	0.0432	70.8	3.39	508	47.2
Including heat losses	65	0.0402	63.6	3.77	566	42.4

Tab. 1.5 Breakdown of fuel use for a typical convective dryer with direct-fired burner.

	Heat Required	Marginal Heat, kW	Marginal %
Minimum evaporation load	2400	2400	40.3
Adiabatic saturation	3023	623	10.5
Exhaust approach 25 °C	3939	916	15.4
Including solids heating	4407	467	7.8
Including dryer heat losses	4906	499	8.4
Burner vapor heating	5660	755	12.7
Burner efficiency (95%)	5958	298	5.0

cheap hydro-electric power is available (see also Section 1.3.4.2). Moreover, losses also occur in electrical heating; the magnetrons used for microwave heating typically only have an efficiency of 50% (delivered microwave energy compared to input power).

1.3.3.3 **Other Energy Demands**

These are as electrical power, and it must again be remembered that this typically costs three times as much as heat per unit energy (kW or kWh).

1) Solids transport costs, for example, screw feeders, bucket or belt conveyors, or fans for pneumatic conveying systems; also rotary discharge valves, and so on.
2) Vacuum pump power. For conductive (contact) dryers, where vacuum is almost invariably used to give better driving forces and achieve acceptable drying times.
3) Steam ejectors. These are used as an alternative method of pulling vacuum. Obviously they eliminate the power required for vacuum pumps, but extra steam is required (which cannot be recovered as condensate). As ejectors often work

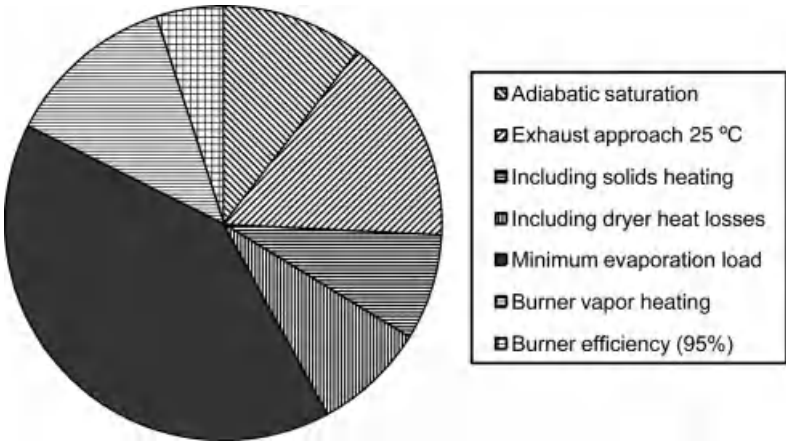

Fig. 1.4 Breakdown of fuel usage for a typical convective dryer with direct-fired burner.

best with ratios of around 1:1 for driver steam to vacuum flow, the steam consumption of the ejectors can be similar to that used in the dryer itself, thus almost doubling steam use.

4) Fan power. Depending on the system pressure drop, the exhaust fan power for the calculated airflow of 3.8 kg s^{-1} (13 700 kg h^{-1}) will typically be in the range 50–100 kW. This is a significant demand compared with steam usage (bearing in mind the price differential).
5) Boiler feedwater pumps and other liquid pumping duties. Usually small.

1.3.4 Energy Cost and Environmental Impact

1.3.4.1 Primary Energy Use

Dryers typically use both heat and electrical power. Sometimes these have been lumped together and quoted as a total energy consumption for the unit operation or site. This is often inappropriate. It is often more helpful to state energy use in terms of primary energy, total energy cost or, in these days of climate change, carbon footprint (total carbon dioxide released into the atmosphere).

Primary energy is the usage of the original source of fuel. Hence, for a dryer heated by steam, the primary energy use is the fuel burned in the boilers, which will typically be at least 20% higher than the heat delivered from the steam. However, the difference between point-of-use and primary energy consumption becomes far more significant for electrical power. If, as in most countries, this is generated from fossil fuels, the typical primary energy consumption can be about three times higher than the power use. So supplying 1 kW of evaporation by steam heating may require 1.2 kW of primary energy, but doing so by electrical heaters requires no less than 3 kW of primary energy.

1.3.4.2 Energy Costs

Relative costs of energy sources tend to reflect the primary energy use, so the cost of electric power is typically three times that of fuel. The exception comes where power is mainly generated as hydro-electricity, in which case the fossil fuel use is zero and the generating cost is also very low. The charge made for hydro-electric power is usually based on amortization of the high capital costs, with a small amount for operating costs (principally labor and maintenance). Likewise, nuclear power tends to have relatively low fuel cost but high capital charges, which should also allow for final decommissioning costs.

For energy cost estimation, normally one should use fuel and power prices applicable at the specific site studied. If for any reason there are no data available, the following values can be used (2010 figures) for a ballpark costing only – remembering that energy prices can fluctuate widely:

Fuel £6 per GJ = £21.6 per MWh
Power £18 per GJ = £64.8 per MWh

1.3.4.3 Carbon Dioxide Emissions and Carbon Footprint

Carbon footprint varies between different fossil fuels because of their different ratios of carbon to hydrogen and calorific value. Typical figures for CO_2 produced per kWh of energy for different fuel sources are:

Natural gas: 0.184 kg kWh^{-1}
Diesel oil and fuel oil: 0.25 kg kWh^{-1}
Coal: 0.324 kg kWh^{-1}

The values for oil and coal vary with grade, and for natural gas the figure depends on the proportion of other hydrocarbons and gases mixed with the main constituent, methane (CH_4).

The value for electric power will depend on how it is generated, which will be a mix of technologies varying with the country. Using the general rule of thumb that electricity requires three times as much primary energy per kW as heat, for a country which generates all its power from fossil fuels, the expected figure would be roughly 0.55 kg kWh^{-1} if natural gas is the main source, 0.75 kg kWh^{-1} for oil and 0.95 kg kWh^{-1} for coal. This will be reduced if a significant proportion of a country's power is hydroelectric or nuclear power, which have virtually zero CO_2 emissions.

In practice, typical values are 0.4–0.6 kg kWh^{-1} for Europe, 0.6 kg kWh^{-1} for North America, 0.8–1.0 kg kWh^{-1} for developing countries, but with significant exceptions. The highest values are for countries using a high proportion of coal, such as Australia (0.953 kg kWh^{-1}). As expected, values are substantially lower for countries which generate much of their power from renewable sources (hydroelectricity, wind, etc.) or nuclear, both of which give an effectively zero carbon footprint. For example, for France (where over 70% of electricity is nuclear) the 2010 figure is only 0.088 kg kWh^{-1}. Table 1.6 and Fig 1.5 show comparative figures for a range of major energy-using countries.

Tab. 1.6 Carbon footprint for fuels and electric power for selected countries; Data from National Energy Foundation, UK, 2010, all figures in kgCO_2 kW h^{-1}.

Fossil Fuels	Natural Gas	0.184
	Fuel oil	0.25
	Diesel oil	0.25
	Coal	0.324
Electricity	France	0.088
	Germany	0.458
	UK	0.541
	USA	0.613
	China	0.836
	India	0.924
	Australia	0.953
CHP	Gas engine	0.27

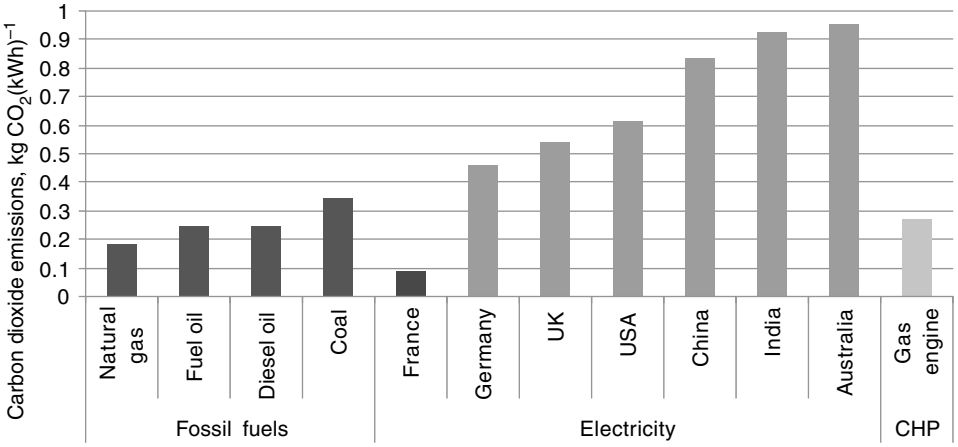

Fig. 1.5 Carbon footprint for fuels and electric power for selected countries.

1.4 Setting Targets for Energy Reduction

1.4.1 Energy Targets

Logically, we should aim to achieve a significant energy reduction by setting a target to aim at. How do we evaluate these energy targets? There are three levels:

1) "Management" or "arbitrary" targets – aiming for a specified percentage reduction year-on-year, say 5 or 10%. Kemp (2007) points out that this takes no account of the reality of the process, and unfairly penalizes efficient ones! However, these targets can be appropriate for "good housekeeping" type measures, especially if there are very little process data available.
2) Rigorous targets for the existing process – based on a calculation of what it should be using, given a specified evaporation load and expected dryer efficiency. To calculate this, reliable values of key process heat loads are needed, preferably obtained from a consistent heat and mass balance.
3) Further reduced targets for an improved process – specifically redesigned to inherently use less energy, by reducing the evaporation requirement or substituting a more efficient dryer.

In the case study at the end (Section 1.6) we can see how these are applied in a specific case.

Key tools for analysis include:

1) Heat and mass balance on the dryer; need not be precise, but must be consistent.

2) Overall energy consumption data for the process plant, including heat and power supplied (fuel, steam, imports from grid) and local usage (broken down by process).
3) Pinch analysis; see Section 1.4.2.

1.4.2 Pinch Analysis

1.4.2.1 Basic Principles

In the last 30 years, pinch analysis (also known as pinch technology or process integration) has been shown to be a vital tool for assessing minimum required energy consumption and setting rigorous targets, and hence identifying energy saving opportunities. It allows a systematic analysis of the overall plant, and has developed into the broader subject of process synthesis.

This section summarizes the basic principles. The overall methodology is described in detail by Kemp (2007), Smith (2005), Linnhoff *et al.* (1982) and in ESDU Data Items (1987, 1989, 1990). Kemp (1991, 2005, 2007) and Smith (2005) have applied the method specifically to dryers.

Pinch analysis examines the flows and unit operations in processes which require or release heat. These are categorized into "hot streams" (which give up heat, e.g., a hot dryer exhaust stream as it cools and condenses) and "cold streams" (which require heat, e.g., the wet solids entering the dryer which need to be heated to evaporate off the moisture). All the heating requirements could be fulfilled by hot utilities (e.g. steam, hot water, furnace gases) and likewise the cooling needs could be fulfilled by cold utilities (e.g., cooling water, chilled water or refrigeration). However, heat can be recovered between hot streams at a higher temperature and cold streams at a lower temperature. All heat exchange reduces both hot and cold utility use, and hence reduces fuel and power use and emissions. Pinch analysis allows rigorous *energy targets* to be calculated for how much heat exchange is possible, and hence the minimum possible levels of hot and cold utility use.

Most processes have a *pinch temperature*. Above this temperature they have a net heat requirement; below the pinch, there is net waste heat rejection. Heating below the pinch, cooling above the pinch, or heat exchange across the pinch all incur an energy penalty. Conversely, heat pumps only achieve a real energy saving if they work backwards across the pinch, upgrading useless below-pinch waste heat to useful above-pinch heat. Hence, a pinch analysis of a system is an important prerequisite of any energy saving project, to ensure that it will achieve its aims.

Streams are characterized by their temperature and heat load (kW), the latter being calculated as:

$$Q_{\text{stream}} = Wc_P(T_{\text{in}} - T_{\text{out}}) \tag{1.10}$$

In terms of potential heat recovery, the main hot and cold streams in a typical dryer are:

Hot streams

H1. The exhaust gas from the dryer. This includes both sensible and latent heat.

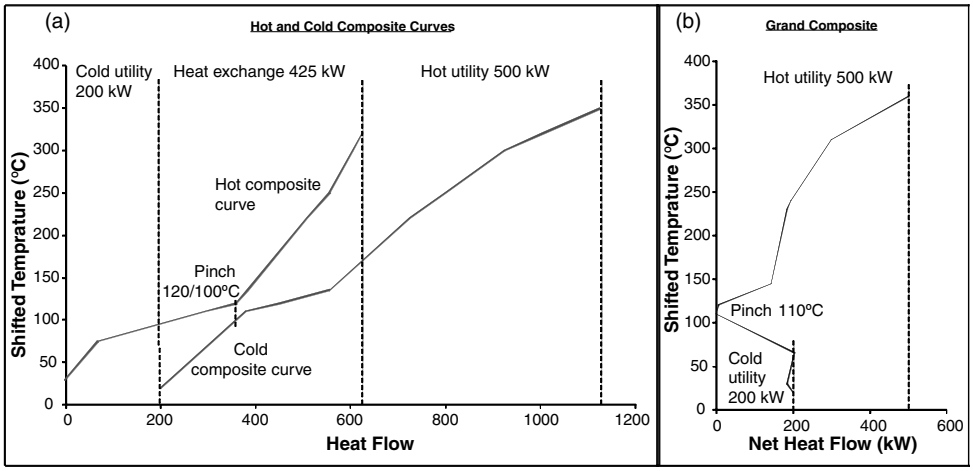

Fig. 1.6 (a) Composite and (b) grand composite curves for a typical liquid-phase process.

H2. The hot solids emerging from the dryer. A sensible cooling load, normally much less than H1.

Cold streams

C1. (For convective dryers) Heating the drying air, usually from ambient to dryer inlet temperature.
C2. (For contact dryers) Heat supply to the dryer via the jacket.
C3. Preheating the solids before they enter the dryer.

C1 or C2 are normally the dominant heat loads, as these will supply the heat used for evaporation.

The hot and cold streams can be effectively represented on a temperature–heat load diagram, as shown in Fig. 1.6 for a typical liquid-phase process. Where there are multiple hot and cold streams, their heat loads can be summed together to produce composite curves. The hot composite curve is the sum of the heat loads of all the hot streams over the temperature ranges where each one exists. Likewise, the cold composite curve is the sum of the heat loads of all the cold streams. A minimum temperature difference for heat exchange, $\Delta T_{\min}$, must be selected, and has been chosen as 20 K. This gives the vertical distance between the curves. The point of closest vertical approach is the pinch, which here corresponds to a temperature of 100 °C for the cold streams and 120 °C for the hot streams. The region of overlap between the hot and cold composite curves shows the opportunity for heat exchange, recovering heat from hot to cold streams. The remaining heating and cooling in the non-overlapping region must be supplied by heating or cooling utilities.

A further useful calculation is to subtract the total heat required for the cold streams from that available from the hot streams at any temperature, to give the net requirements for hot or cold utility (external supply of heating or cooling) at any temperature. This gives the grand composite curve (GCC), shown in Fig 1.6b. Above

the pinch, hot utility is required; below the pinch, cold utility is needed. To allow for the minimum temperature difference for heat exchange ΔT_{min}, hot stream temperatures must be reduced by half this amount (10 °C) and the cold stream temperatures increased, to give "shifted temperatures". The grand composite curve shows the exact location of the pinch more clearly than the composite curves.

A heat exchange system can then be designed to try to achieve the energy targets. It must be remembered that pinch analysis targets give the maximum feasible heat recovery and that some aspects of this, particularly heat exchangers with small loads, may be uneconomic. Very often, there is a capital-energy tradeoff where some potential heat recovery is sacrificed to give a cheaper, simpler project with a better economic rate of return.

1.4.2.2 **Application of Pinch Analysis to Dryers**

Virtually all dryers use air as the carrier gas and water as the solvent to be evaporated. The high heat requirement of dryers is almost entirely due to the latent heat of evaporation of the water. Much of the heat supplied to the dryer emerges as the latent heat of the vapor in the exhaust gas, which can only be recovered by condensing the water vapor from the exhaust. However, as saturation humidity increases almost exponentially with temperature, the dewpoint of exhaust air is generally 50 °C or lower. It is very rare for this to be above the process pinch and the heat must thus be wasted. Hence, it is usual to simply vent the dryer exhaust from a stack, possibly recovering a small proportion of the heat as sensible heat.

Heat supply to convective dryers is in the form of hot air. Ambient air is drawn in and heated in either a direct-fired or indirect-fired furnace. The heat load of the dryer therefore plots as a sloping line. Composite curves for a typical dryer are shown in Fig. 1.7. It is clear that the scope for heat recovery in the basic system is limited. Some heat can be recovered from the dryer exhaust to the cold feed air. Usually this is only a

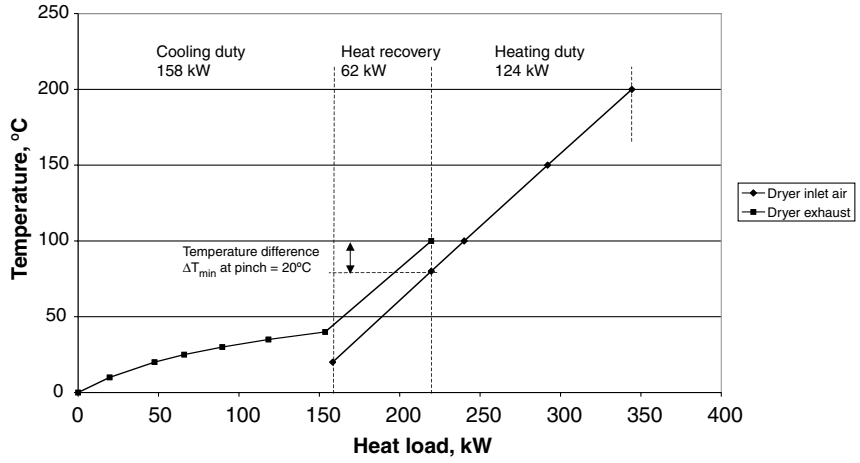

Fig. 1.7 Hot and cold composite curves for a simple convective dryer.

Tab. 1.7 Stream data for simple convective dryer example.

Hot Stream H1 (Dryer Exhaust)			Cold Stream C1 (Inlet Air Heating)		
Temperature (°C)	**Heat Load (kW)**	**Adjusted (kW)**	**Temperature (°C)**	**Heat Load (kW)**	**Adjusted (kW)**
100	229	220	20	45	158
40	163	154	80	107	220
30	99	90	100	127	240
20	56	47	150	179	292
0	9	0	200	231	344

small proportion of that available, but nevertheless, the actual cost savings can be significant because dryers are so energy-intensive.

Let us take a simple practical example. A convective dryer operates with 1 $kg\,s^{-1}$ of dry airflow at an inlet humidity of 0.01 $kg\,kg^{-1}$. This hot air is heated from 20 to 200 °C and used to evaporate moisture from solids. The exhaust gas temperature is 100 °C. From calculation, or a psychrometric chart, we can see that the enthalpy of the inlet air rises from 45 $kJ\,kg^{-1}$ to 230 $kJ\,kg^{-1}$. Ignoring both heat losses and the sensible heating of the solids, the exhaust air emerges with a humidity of 0.048 $kJ\,kg^{-1}$ and a dewpoint of 40 °C. Hence 0.038 $kg\,s^{-1}$ of water is evaporated, and (taking latent heat as 2450 $kJ\,kg^{-1}$) the inherent requirement is approximately 93 $kJ\,s^{-1}$ (93 kW). In fact, approximately 185 kW has been used to heat the incoming air, so the dryer is barely 50% efficient – or significantly less when heat losses and the heating of the inlet solids are included. Table 1.7 tabulates the resulting temperature–heat load data for the key streams.

The "adjusted" data shifts the heat load figures so that the hot stream begins at zero heat load and the cold stream lies below it. ΔT_{min} has again been chosen as 20 K. The pinch is calculated as 80 °C for the cold streams and 100 °C for the hot streams, at an adjusted heat load of 220 kW. The resulting plot is shown in Fig. 1.7. The range over which the hot and cold streams overlap, where heat can be recovered from the hot exhaust stream to the cold inlet air, can be seen at a glance.

Likewise the grand composite curve (Fig. 1.8) shows the net heating and cooling requirements for the dryer. The heat loads of the dryer exhaust and inlet air do not quite match over the range 30–90 °C (shifted temperature) because the exhaust has a higher humidity, and hence a higher specific heat capacity. The cooling requirement is calculated to condense all the water in the exhaust and reduce its temperature to 0 °C, but in practice this will not normally be necessary; indeed, in many cases the dryer exhaust can be discharged directly at its final temperature after all useful heat has been recovered by heat exchange, and no cooling is required at all.

Compare with the composite and grand composite curves of the typical liquid-phase process shown in Fig 1.6. The overlap region for the liquid process composite curves is much greater than for a typical dryer, showing that there are proportionately more opportunities for heat recovery within the process.

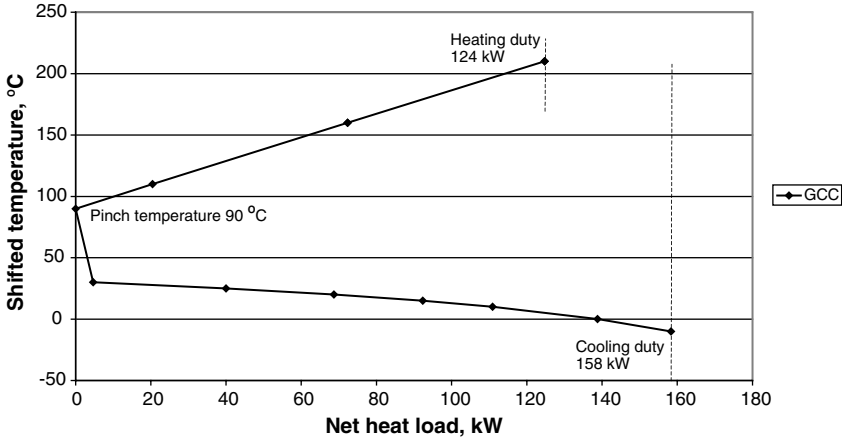

Fig. 1.8 Grand composite curve for a convective dryer.

1.4.2.3 **The Appropriate Placement Principle Applied to Dryers**

Pinch analysis enables us to see not only how much energy the dryer is using, but whether it is able to exchange with other parts of the process, and whether these opportunities can be increased.

Let us consider the general process whose composite and grand composite curves are shown in Fig. 1.6, and the dryer shown in Figs. 1.7 and 1.8. If these are on the same site, are there possibilities for heat exchange between them? And are the operating conditions of the dryer and background process (particularly temperatures) such that this heat recovery is maximized? Or can we change the operating conditions to increase the potential for heat exchange between them?

The Appropriate Placement principle for a unit operation or a utility states that, to minimize energy use, it should ideally be placed so that it releases all its heat above the pinch temperature and above the GCC of the process, or receives all its heat below the pinch and below the GCC. Visually, if the heat demands of a unit operation, such as a dryer, are plotted on the same graph as the remaining "background process", the dryer should fit either entirely above or entirely below the GCC. This means that it can exchange all its heat with the rest of the process, rather than requiring a separate supply.

To see whether this is the case, we can "split the grand composite curve", plotting two separate lines for the dryer and the background process, as shown in Fig. 1.9a. The dryer GCC is reversed to allow this. The total target for the separate processes is 624 kW (124 kW for the dryer and 500 kW for the liquid process), while that for the combined processes is 604 kW, so that only 20 kW extra can be recovered by heat exchange.

It is clear that the dryer is working across the pinch; it is not so clear what can be done about it. The only possibilities are:

1) Reduce the temperature at which the dryer requires heat.

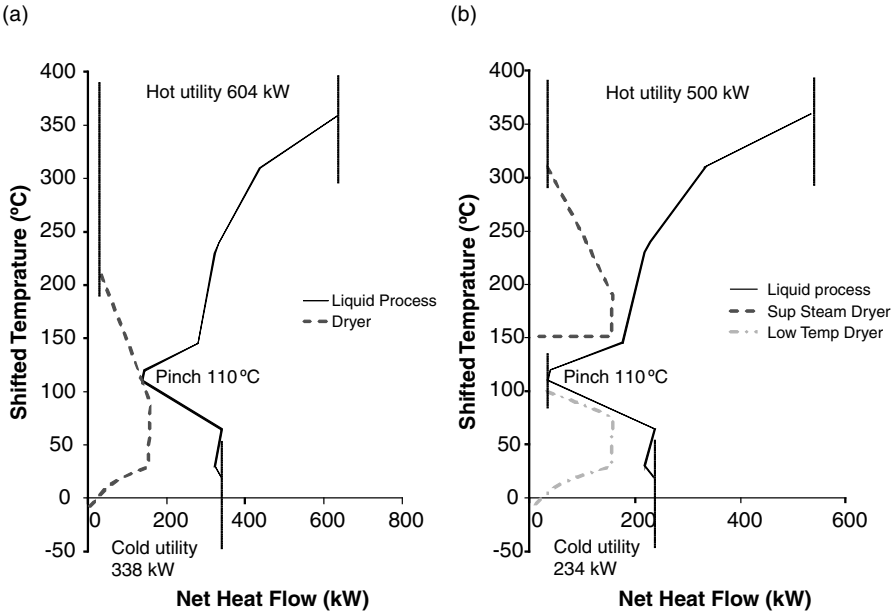

Fig. 1.9 Split grand composite curves for (a) standard convective dryer, (b) pressurized superheated steam or low-temperature convective dryers.

2) Raise the temperature at which the dryer exhaust stream releases heat.
3) Alter the background process so that more of it fits above or below the dryer heat profile.

The first can be achieved by using a low-temperature dryer extracting heat below the pinch as warm air or warm water. The reduced temperature driving forces would normally cause a huge increase in the size and capital cost of the dryer. However, if a dispersion dryer (e.g., a fluidized bed or cascading rotary dryer) can be substituted for a layer dryer (e.g., an oven or tray unit), the much enhanced heat transfer coefficients may allow low-temperature drying with a small unit. Warm air can be fed directly to the dryer; warm water can heat it indirectly via internal coils. Alternatively, some preheating of the wet feed solids may be carried out in a pre-dryer working on below-pinch waste heat. This has particular advantages for sticky or temperature-sensitive materials.

The second option is virtually impossible with conventional air dryers as the dewpoint cannot be altered significantly. Recycling exhaust gases and raising the humidity will raise the dewpoint; however, it may adversely affect drying. In any case no heat can be recovered above the boiling point, 100 °C, unless the entire system is placed under high pressure – an extremely expensive option. However, in some cases a heat transformer has been used to absorb moisture from the exhaust gas and recover some of its heat.

If, instead, the superheated form of the solvent being evaporated is used as the carrier gas instead of air, a very different picture emerges. The recovered vapor can

then be condensed at high temperature, above the pinch. The commonest case is superheated steam drying, which also has the advantage of a better heat transfer coefficient between vapor and solids than for air. The steam is recirculated and reheated; a bleed equal to the evaporation rate is required, and this steam can be condensed to yield useful heat – at 100 °C when working at atmospheric pressure, or significantly above 100 °C if operating at elevated pressures. Superheated steam drying has previously been advocated for heat transfer or safety reasons, but it clearly has energy advantages too. The main drawback is that a large fan or compressor is required to recirculate the steam, and the power consumption of this can cancel out the savings from heat recovery. An interesting solution to this problem is the airless dryer (Stubbing, 1993, 1999), where no gas recirculation is used; the water driven off from the solids in the early stages of drying forces the air out of the system to create the superheated steam atmosphere. This system works at atmospheric pressure. In contrast, large-scale continuous superheated steam dryers used, for example, for pulp and paper processing, typically operate at high pressures and temperatures.

Figure 1.9b illustrates the placement of a pressurized superheated steam dryer above the process GCC, or a low-temperature dryer below the GCC.

Conversely, if the operating conditions of the dryer cannot be changed, it may be possible to alter those of the rest of the process instead. An example (Kemp, 2007; Linnhoff *et al.*, 1982) is for a gelatin plant where a three-stage dryer (working at 60–80 °C) followed a three-stage evaporation system. The composite and grand composite curves are shown in Fig. 1.10, highlighting the heat loads due to the evaporator (E1-E3) and dryer (D1-D3). The pinch was initially at 40 °C and it was impossible to bring the dryer below that. Instead, the operating pressure of the evaporator train was raised so that it discharged vapor at a higher temperature; in effect, shifting the pinch upwards to 97 °C and bringing it above the temperature of the dryer heat loads. The net result was that the vapor from evaporator effect 2 was then hot enough to heat the dryer directly, giving an overall energy reduction of nearly a third, from 1517 to 1027 kW, as shown in Fig. 1.11. Although increased pressure

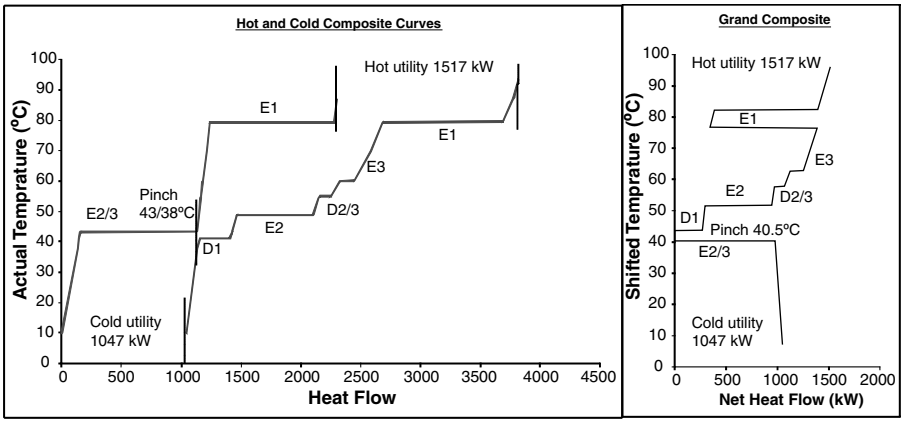

Fig. 1.10 Composite and grand composite curves for gelatin process, original form.

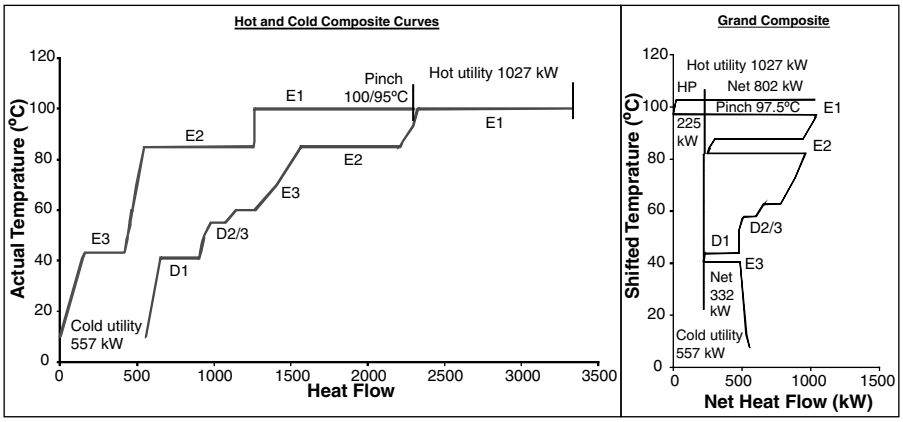

Fig. 1.11 Composite and grand composite curves for gelatin process, modified form.

normally entails increased equipment cost, in this case the evaporator train was working under vacuum, so all that was needed was to reduce the vacuum pulled (also reducing vacuum pump power and cost). The evaporator had been designed as a unit operation, with a multiple effect configuration over a range of temperatures; this was correct design taken in isolation, but not when a holistic analysis was made over the complete plant! There was also a thermocompressor across the first evaporator effect. Being a heat pump, this should be working across the pinch, but in the original configuration it was above the pinch; in the revised layout it was correct. This saves another 225 kW and brings the heat required from external utilities down to 802 kW, a total saving of no less than 46%. Another example of linking evaporators and dryers appears in the case study in Section 1.6.

1.4.2.4 **Pinch Analysis and Utility Systems**

The grand composite curve is also helpful for optimizing configuration of the utility systems that supply the heating and cooling requirements. The operating line of the hot utility system needs to lie entirely above the process GCC, and the cold utility system below it. If heat is provided by condensing steam, this plots as a horizontal line at the condensation temperature; multiple steam levels may be used. Alternatively, heat may be supplied from a hot gas stream (air or flue gas); this releases sensible heat over a range of temperatures and plots as a sloping line. Both methods are illustrated in Fig. 1.12.

In many cases, the dryer inherently lies across the process pinch, and it is very difficult to reduce its energy consumption significantly using pinch technology. However, the net cost of supplying the heat can be substantially reduced by using a co-generation (CHP) system; the exhaust from either a gas turbine or a reciprocating engine is hot enough to supply almost any hot gas dryer. The exact inlet temperature is easily controlled by adding a varying amount of cool dilution air. CHP is described further in Section 1.5.4.3. The main limitations on such a system are the capital cost and the cleanness of the exhaust; gas turbines and gas engines are more acceptable in the latter respect than diesels. The heat profile of the exhaust should again lie above

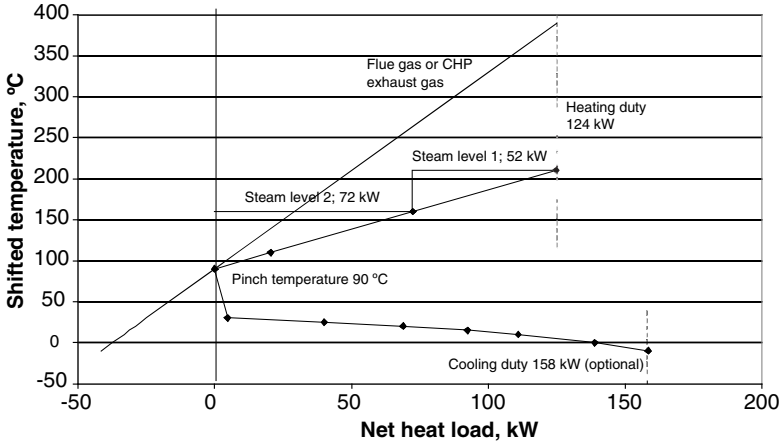

Fig. 1.12 Fitting utility heating to the process grand composite curve.

the process GCC as much as possible, under the Appropriate Placement principle, to minimize the overall heat requirement of the process plus utility system. See Figs. 1.12 and 1.14.

Heat pumps can be an option. Again, the Appropriate Placement principle applies, but in this case, as the heat is released at a higher temperature than the cooling, the heat pump should be placed so that the heat is released above the GCC, and any heat absorbed from the process should come below the GCC. In other words, the heat pump should work backwards across the pinch. For many dryers, the temperature lift is too high to achieve this. However, for dryers using a large air recycle with a low temperature lift, including many food and agricultural dryers, heat pumping may be economic. Further details are given in Section 1.5.4.4.

1.4.3
Drying in the Context of the Overall Process

Dryers are normally part of a larger solids processing operation, and two major types can be distinguished.

1) Insoluble solids. Typically formed by crystallization from solution, mechanically separated by filtration or centrifugation, and then dried. As much water as possible is removed in the mechanical separation step, but even if a high vacuum or pressure is used in the filter, or a high speed in a centrifuge, there will be a significant amount of both unbound and bound moisture which cannot be removed mechanically. The thermal energy required to dry this off is far greater than that used for mechanical separation.
2) Soluble solids. Here a chemical or biological entity may be formed in solution, concentrated by evaporation until handling or pumping becomes too difficult, and then dried. Even where the majority of water is removed in the evaporation, the energy consumption of that step can be greatly reduced by using multiple

effects and reusing the latent heat of evaporation. For drying, by contrast, the temperature drop is such that only a single-stage unit can normally be used. Moreover, evaporators can give efficiencies close to 100%, whereas dryers can frequently be at 50% or below, due to driving force losses, heat lost in exhaust air and additional energy required to remove bound moisture.

One of the best ways to reduce the energy load on a dryer is to reduce the initial moisture content (or increase the % solids) of the incoming feed.

The methods for doing this will obviously depend on the upstream process. Typical situations are:

1) Filtration or centrifugation. Probably the most common upstream unit operations, occurring in processes such as bulk and fine chemicals, primary pharmaceuticals and other situations where solids have been formed (e.g., by crystallization or precipitation) and are being concentrated as a slurry. Obviously, the inlet moisture to the dryer and the dryer heat load will be minimized by maximizing mechanical dewatering of the slurry in the filter or centrifuge.
2) Granulation, as in secondary pharmaceutical processes. Minimize the water required to achieve granulation by careful design, effective mixing and good choice of operating conditions such as agitation speed. In some cases, alternative granulation methods such as roller compaction can be considered which inherently use little or no added water.
3) Evaporation to a solid, slurry or paste, as in many food and mineral processes. Use multiple effects and temperature stacking in evaporators wherever possible, so that energy (particularly latent heat) can be reused. Mechanical and thermal vapor recompression (basically heat pumping using vapor) may also be applicable. As the solution becomes more concentrated and viscous, and boiling point rise becomes greater, all these techniques become harder to apply and a basic 1:1 condensation/evaporation system becomes the norm. Nevertheless, this is often still more thermally efficient than a dryer, so it is desirable to get the solids as dry as possible before transferring to the dryer.
4) Liquid processing or evaporation to a liquid feed form (slurry or solution), for feeding to a spray dryer, film-drum or thin-film (scraped-surface) dryer. Again, one would normally try to increase the concentration as far as possible by evaporation or (for a slurry) mechanical dewatering, as long as the feed remains sufficiently pumpable.

See also Section 1.5.2.1.

1.5
Classification of Energy Reduction Methods

An initial overview analysis of the energy requirements of the process, based on the evaporation load, shows how much energy is inherently required and, by comparing with current measured energy usage, what opportunities there are for savings.

Opportunities to reduce energy consumption can be classified into three main categories;

a) Reduce the evaporation load – for example, by upstream dewatering to reduce initial moisture content, or avoiding overdrying.
b) Increase the dryer efficiency – for example, by improving insulation and reducing heat losses, installing heat recovery or changing operating parameters.
c) Improve the energy supply (utility) systems – for example, increase boiler efficiency, reduce distribution losses, install combined heat and power (CHP), heat pumps, waste incineration or other alternative low-cost fuels.

It is also useful to subdivide further:

a) Reduce the evaporation load by:
   1) Reducing the inherent energy requirement for drying, for example, by dewatering the feed, or avoiding the need for drying altogether.
   2) Increasing the efficiency of the dryer, by reducing heat losses, total air flow or batch times.
b) Increase the dryer efficiency by:
   3) Heat recovery within the dryer system, between hot and cold streams.
   4) Heat exchange between the dryer and surrounding processes.
c) Improve the utility systems by:
   5) Using lower-cost heat sources to supply the heat requirement, for example, low-grade heat or renewable energy (including alternative fuels, biofuels and waste).
   6) Improving the efficiency of the energy supply system, for example, by reducing losses in the boiler or steam distribution system.
   7) Using CHP; co-generate power while supplying the heat requirement to the dryer.
   8) Using heat pumps to recover waste heat to provide dryer heating.

Hence, methods 1 and 2 can be categorized as ways of directly reducing the dryer heat duty, methods 3 and 4 use heat recovery to reduce the amount required from external utilities (heating and cooling systems), and methods 5–8 reduce the cost of the utilities or the primary energy requirement. The order of classification represents the logical order in which the steps should be investigated practically; there is little point in sizing a heat recovery scheme if it is possible to alter the dryer heat flows significantly. In all cases, the ultimate aim and benefit is the same; to reduce the net usage of fossil fuels and other non-renewable energy sources, and to minimize emissions of CO_2, greenhouse gases, pollutants such as NO_x and SO_x, and other waste materials.

Likewise, from a pinch analysis viewpoint, heat duty reduction (methods 1 and 2) is a process change which reduces energy targets, methods 3 and 4 are heat recovery or heat exchange which help to achieve calculated targets, and methods 5–8 improve the efficiency or reduce the cost of the utility systems meeting the residual energy demands.

These eight methods will be considered in more detail in Sections 1.5.2–1.5.4.

1.5.1 Reducing the Heater Duty of a Convective Dryer

Referring back to Section 1.3.2, we derived two alternative expressions for the heater duty of a convective dryer:

$$Q_{\text{heater}} = W_{\text{g}} c_{P\text{g}} (T_{\text{g,in}} - T_{\text{g,a}}) \tag{1.5}$$

$$Q_{\text{heater}} = \frac{(T_{\text{g,in}} - T_{\text{g,a}})}{(T_{\text{g,in}} - T_{\text{g,out}})} \left[W_{\text{s}} (X_{\text{in}} - X_{\text{out}}) \Delta H_{\text{v}} + Q_{s,\text{sens}} + Q_{\text{loss}} \right] \tag{1.7}$$

Here $T_{\text{g,in}}$ is the inlet temperature to the dryer and $T_{\text{g,a}}$ is the temperature at which the air is supplied. From Eq. 1.5, we see that to reduce the heat duty Q_{heater}, we will need to reduce the airflow W_{g}, decrease $T_{\text{g,in}}$ or increase $T_{\text{g,a}}$. If we know the dryer heat load and the air inlet and outlet temperatures, we can calculate the required air flow by combining Eqs. 1.5 and 1.7, or rearranging Eq. 1.6:

$$W_{\text{g}} = \frac{W_{\text{s}} (X_{\text{in}} - X_{\text{out}}) \Delta H_{\text{v}} + Q_{s,\text{sens}} + Q_{\text{loss}}}{c_{P\text{g}} (T_{\text{g,in}} - T_{\text{g,out}})} \tag{1.11}$$

Likewise, from Eq. 1.7, we have the following alternative ways to reduce Q_{heater} for a fixed production rate W_{s}:

- Reduce the inherent evaporative duty by reducing inlet moisture content X_{in}, increasing final moisture content X_{out} or reducing the latent heat of evaporation ΔH_{v} (Section 1.5.2.1).
- Reduce heat loss Q_{loss} or change operating conditions by increasing inlet gas temperature $T_{\text{g,in}}$ or decreasing outlet gas temperature $T_{\text{g,out}}$ (Section 1.5.2.2).
- Preheat the air entering the heater (increase $T_{\text{g,a}}$) by heat recovery or exhaust air recycle (Section 1.5.3).

We will continue to use our worked example from Section 1.3 as a base case: W_{s} (dry basis) $= 1\,\text{kg s}^{-1}$, $X_{\text{in}} = 0.12\,\text{kg kg}^{-1}$, $X_{\text{out}} = 0.02\,\text{kg kg}^{-1}$, $T_{\text{g,in}} = 150\,^{\circ}\text{C}$, $T_{\text{g,a}} = 20\,^{\circ}\text{C}$, $T_{\text{g,out}} = 65\,^{\circ}\text{C}$, $Q_{s,\text{sens}} = 30\,\text{kW}$, $Q_{\text{loss}} = 30\,\text{kW}$, $c_{P\text{g}} = 1\,\text{kJ kg}^{-1}\,\text{K}^{-1}$.

There is a complication with the latent heat of evaporation. We have generally taken $\Delta H_{\text{v}} = 2400\,\text{kJ kg}^{-1}$. However, the evaporated water enters with the solid at 20 °C, with $h_{\text{l}} = 84\,\text{kJ kg}^{-1}$ (from steam tables), and emerges with the exhaust air at 65 °C, with $h_{\text{v}} = 2618\,\text{kJ kg}^{-1}$. So for use in Eq. 1.7, we need to use $\Delta H_{\text{v}} = 2534\,\text{kJ kg}^{-1}$. The difference is due to the additional sensible heat taken up by the vapor. Hence $Q_{\text{heater}} = (313 \times 130/85) = 479\,\text{kW}$. The slight difference from the value of 491 kW in Table 1.1 is due to the difference between the calculation and reading from a psychrometric chart. Heat of wetting, which would further increase ΔH_{v} at low moisture content, is assumed zero (or rolled into Q_{loss}).

From Eq. 1.11, W_{g} (dry basis) $= (313/85) = 3.69\,\text{kg s}^{-1}$. Using Eq. 1.5 as a cross-check, $Q_{\text{heater}} = (3.69 \times 1.0 \times 130) = 479\,\text{kW}$. This will be used as the base case for all the following calculations.

1.5.2 Direct Reduction of Dryer Heat Duty

1.5.2.1 Reducing the Inherent Heat Requirement for Drying

The dominant component is the evaporative heat load, and reducing this requires a reduction in the moisture removed in the dryer (or, in special cases, in the latent heat of evaporation).

1) Reduce the inlet moisture X_{in}; this can only be achieved by altering the upstream process, and a holistic approach to overall solids process design as described by Kemp (2004) will be helpful. Typical methods include improved mechanical dewatering by centrifuging, vacuum or pressure filtration, or gas blowing of the filter cake supplied to the dryer. A promising development in recent years has been the use of superheated steam for filter cake dewatering, for example, by the Hi-Bar pressure filter manufactured by Bokela (Karlsruhe, Germany). This provides some heat for evaporation, but the more significant mechanism appears to be that the surface tension forces binding the water to the cake are reduced and substantially more liquid is removed in the mechanical dewatering step. A similar phenomenon has been observed in paper dryers, where heating the felt rollers allowed more water to be detached mechanically from the sheet surface. If X_{in} can be reduced from 12 to 10%, $W_g = (2534 \times 0.08 + 30 + 30)/85 = (263/85) = 3.09\,kg\,s^{-1}$ from Eq. 1.11. From Eq. 1.5, $Q_{heater} = (3.09 \times 130) = 402\,kW$, a substantial reduction of 77 kW, or 16% of the base case heater duty.

   Another method of reducing initial moisture content is by absorption or adsorption of some of the liquid in the material. However, the absorbent material needs to be regenerated and, as this will normally be done thermally, the latent heat of evaporation must still be removed. There can only be a net gain in energy usage if either (i) the absorbent can be regenerated at a low temperature using low-grade waste heat which would otherwise be thrown away, or (ii) the absorbent can be regenerated at a high temperature giving a more thermally efficient system than normal drying. (i) will never normally occur, but (ii) can occur for drying of foodstuffs where there are severe temperature limitations on the product; see Chapter 5 and also van Deventer (2002).

   The absorbent solid must also be easily separable from the main product.

2) Increase the outlet moisture X_{out} by relaxing the product specification. This rarely makes a large difference to the heat balance; however, avoiding a stringent requirement for low final moisture content can substantially reduce drying time, and bring major benefits because drying efficiency is low in the tail end of the falling-rate drying period. A common consequence is a reduction in outlet gas temperature $T_{g,out}$. Hence $(T_{g,in} - T_{g,out})$ is greater, the heat obtained from 1 kg of air increases proportionally, and from Eq. 1.11, the airflow can be reduced. For example, if X_{out} is relaxed to 2.5% ($0.025\,kg\,kg^{-1}$), the evaporative heat duty only falls from 253.4 to 240.7 kW, a 5% saving. However, if $T_{g,out}$ also falls from 65 to 55 °C, $W_g = (302/95) = 3.17\,kg\,s^{-1}$. From Eq. 1.5, $Q_{heater} = (3.17 \times 130) = 412$ kW, a total saving of 67 kW or nearly 15%.

3) Reduce the latent heat of evaporation ΔH_v, by substituting a solvent with lower latent heat. Bahu (1991) suggested displacing water by toluene in a pre-drying step. However, this approach has not been adopted in practice, because there are now very severe emissions limits on VOCs (volatile organic compounds) such as toluene. Hence, the solution is worse than the problem, as the potential environmental damage and gas cleaning costs from using toluene far outweigh the benefits from the energy savings.

1.5.2.2 Altering Operating Conditions to Improve Dryer Efficiency

1) Increase inlet gas temperature $T_{g,in}$; usually $T_{g,out} > T_{g,a}$, so the first term in Eq. 1.7 will decrease. The limitation is the risk of thermal damage. From Eq. 1.5, to achieve a lower drying duty, W_g must fall. For example, suppose $T_{g,in}$ is increased to 170 °C and $T_{g,out}$ can be maintained at 65 °C. From Eq. 1.11, $W_g = (313/105) = 2.98\,kg\,s^{-1}$, and from Eq. 1.5, $Q_{heater} = (2.98 \times 150) = 448\,kW$, a saving of 31 kW. In practice, however, it is difficult to avoid an increase in $T_{g,out}$, which increases exhaust heat losses and reduces the gain in efficiency. If $T_{g,out}$ rises to 70 °C, $W_g = (313/100) = 3.13\,kg\,s^{-1}$, and $Q_{heater} = (3.13 \times 150) = 470\,kW$.
2) Decrease outlet gas temperature $T_{g,out}$. From Eq. 1.11, W_g falls and exhaust heat losses are reduced. However, outlet humidity and relative humidity increase, along with dust concentrations and condensation problems, while temperature and humidity driving forces fall. Hence, drying times will tend to increase, and it may become difficult to achieve the final moisture specification.
3) Reduce heat losses Q_{loss} by adding insulation, removing leaks and so on. For example, if Q_{loss} is halved from 30 kW (~10%) to 15 kW (~5%), Eq. 1.11 shows that the required airflow also falls: $W_g = (298/85) = 3.51\,kg\,s^{-1}$, and $Q_{heater} = (3.51 \times 130) = 456\,kW$, saving 23 kW (5%).

Important benefits can also arise from improved control to ensure that a dryer is always working at its preferred design conditions, or to ensure that batch drying is stopped as soon as the product has reached its target moisture content.

Table 1.8 summarizes the various options for reducing heater duty, including heat recovery possibilities described in Section 1.5.3.

Tab. 1.8 Effect of energy-saving changes on airflow and heater duty for indirect dryer.

Parameter	$T_{g,in}$ (°C)	$T_{g,out}$ (°C)	Q_{loss} (kW)	W_g (kg s^{-1})	Q_{heater} (kW)	Saving (%)
Operating Conditions						
Base case	150	65	30	3.69	479	0
Inlet moisture 10%	150	65	30	3.09	402	16
Outlet moisture 2.5%	150	65	30	3.54	460	4
Outlet 2.5%, lower $T_{g,out}$	150	55	30	3.17	412	14
Increased $T_{g,in}$	170	65	30	2.98	448	7
Increased $T_{g,in}$ and $T_{g,out}$	170	70	30	3.13	470	2
Reduced heat loss	150	65	15	3.51	456	5
Air preheat to 45 °C	150	65	30	3.69	387	19

1.5.3 Heat Recovery and Heat Exchange

1.5.3.1 Heat Exchange Within the Dryer

The heating and cooling profiles in Fig. 1.7 show that, for a typical dryer, only a small proportion of the exhaust heat can be recovered to heat incoming cold air, and none of the latent heat of evaporation as it is released below 40 °C. Hence dryers, especially convective dryers, tend to have low efficiencies, measured in terms of the external heat requirement, compared to that theoretically necessary to evaporate the moisture from the solids. In Fig. 1.7, heat recovery has reduced the dryer heat requirement by one-third, from 186 to 124 kW. However, this is still substantially greater than the evaporative heat load of 93 kW, and this is before taking into account the numerous other barriers to efficiency, such as heat losses, solids heating and utility system losses.

Moreover, the assumed minimum temperature difference $\Delta T_{\min}$ of 20 K between the hot and cold streams is very optimistic for gas-to-gas heat exchange. For higher $\Delta T_{\min}$, the curves are pushed laterally apart, the overlap is reduced and the heat recovery falls, becoming zero for $\Delta T_{\min} > 80$ K. Krokida and Bisharat (2004) presented a detailed analysis of heat recovery from dryer exhaust air in a form suitable for computation, including the effect of heat pumping.

For our worked example, let us assume that we do not wish to bring the exhaust gas below its dewpoint, to avoid condensation. For the base case, where $T_{g,out} = 65$ °C and $Y_{out} = 0.034\ \text{kg kg}^{-1}$, the psychrometric chart shows that the dewpoint is about 34 °C. However, this would give a $\Delta T_{\min}$ of only 14 K. Hence, taking $\Delta T_{\min} = 20$ K instead, the inlet air can be warmed from 20 to about 45 °C, and the heater duty becomes $Q_{heater} = 3.69 \times (150 - 45) = 387$ kW, a saving of 92 kW or 19%. Again, if higher $\Delta T_{\min}$ is used, heat recovery falls and becomes zero at $\Delta T_{\min} = 45$ K.

A number of schemes for heat recovery from dryer exhaust gases have been installed and some were supported by the UK Government as demonstration projects in the 1980s and 1990s. However, the results were disappointing. The wet, dusty nature of dryer exhaust streams led to severe fouling problems on heat exchanger tubes (Kaiser *et al.*, 2002), and sometimes corrosion. Special units such as glass tube heat exchangers were tried, but the capital cost was high, while the relatively small proportion of heat being recovered meant that savings were only modest. When the price of energy fell from its early 1980s peak, plans for further schemes were discreetly abandoned.

An alternative heat recovery method is exhaust air recycle. However, to prevent build-up of humidity in the circuit, most of the water vapor must first be condensed out. Typically this reduces the air temperature to below 40 °C, which gives very little gain compared to once-through heating with ambient air, as can be seen from the temperature–heat load profile in Table 1.7 and Fig. 1.7. If, however, it is feasible to expel the air from the dryer and create an atmosphere of water vapor, as in "airless drying" systems, the vapor can be condensed at atmospheric pressure at 100 °C and the losses due to the heated air in the dryer exhaust also disappear.

1.5.3.2 Heat Exchange with Other Processes

There are two possibilities; either heat from below the dryer pinch can be used to heat other processes, or heat rejected from other processes can be used to heat the dryer. The GCC (Fig. 1.8) shows what heat can be recovered to or from an external process at any given temperature or range. Unfortunately, net heat sources well above 100 °C or sinks below 30 °C would be needed, and few industrial sites meet these criteria. For atmospheric pressure (and vacuum) dryers, the latent heat in the dryer exhaust is released at too low a temperature to be useful, as the dewpoint will be well below 100 °C.

Superheated steam dryers are significantly different. The exhaust will condense at or above 100 °C, at the saturation temperature corresponding to the applied pressure, and this may be hot enough to supply other moderate temperature processes on site. The economics of a superheated steam drying system may stand or fall on the ability to use this heat effectively. In a closed-loop system, the steam is recirculated and recompressed, and the vapor removed by drying is purged as steam, with a heat load corresponding to the latent heat of evaporation. If this steam can be condensed for process heating duties, replacing steam from standalone boilers, a major operating cost saving is achieved.

Conversely, waste heat from other site processes is rarely hot enough to supply conventional dryers. A special low-temperature dryer could be used, but the low driving forces will push up the required size, and hence the capital cost. Opportunities might arise where the dryer inherently has to work at low temperatures, for example, agricultural crop dryers, vacuum dryers heated by hot water, or even low-pressure superheated steam dryers (Devahastin *et al.*, 2004). However, it is rare to find agricultural dryers on the same site as high-temperature industrial processes, while low-temperature vacuum dryers tend to be batch dryers in intermittent use and with low energy consumption.

The remaining possibility is that, on a site with other furnaces or boilers present, it may be possible to use heat from the flue gases to heat the dryer. Often this is more effectively done as part of a CHP scheme, as described below. Energy recovery from incinerators is also possible.

A point to beware of when integrating between different processes (or between two sub-sections of the same process) is that heat recovery is only possible when both processes are operational. There can be some loss of flexibility. If one process has to be shut down, the other must also be shut down, or alternative utility heating or cooling must be supplied. The same can apply at process start-up, even with internal heat recovery within the process; until the exhaust streams have reached operating temperature, heat cannot be recovered from them to the inlet streams.

1.5.4
Alternative Utility Supply Systems

The objective here is not to reduce dryer energy consumption directly, but to supply the heat load using low-cost utilities or by thermodynamically efficient methods that reduce primary energy consumption.

1.5.4.1 Low Cost utilities

Providing heat at a high temperature may be significantly more expensive than at a lower temperature. For example, in a steam system, higher temperature levels require much higher pressures, and hence much more expensive boilers and pipelines. A hot water recirculating system may obviate the need for steam altogether for low-temperature heat duties: or it may be possible to utilize solar heating. The grand composite curve evaluates these opportunities. The utility heat must be supplied at or above the temperature of the cold stream it is heating (allowing for necessary temperature differences in heaters etc.). In Fig. 1.12, we see that it is possible to supply more than half the total heat duty (72 kW) at a temperature of 160 °C (6 bar steam) instead of 210 °C (20 bar).

To utilize lower temperature utilities, lower driving forces must be tolerated, requiring larger heat exchangers. Also, a low-temperature drying process such as solar heating, may need different processing methods from a higher-temperature one; for example, drying times will normally need to be lengthened, often substantially.

Renewable sources and waste products should be considered as fuel options. Where security of supply is insufficient, or the calorific value is too low, dual fuel boilers can be used, supplementing fossil fuels by alternative fuels. Emission levels need to be investigated, particularly odors from waste-derived fuel. When considering alternative fuels such as biofuels, sustainability and land use should be carefully checked. It would be inappropriate to cause irreversible deforestation by excessive timber burning, or to use a biofuel which is grown on land desperately needed for local food production. On the other hand, an unwanted by-product or waste product of that food production process, such as rice husk, makes a highly appropriate and sustainable fuel.

1.5.4.2 Improving Energy Supply System Efficiency

Section 1.3.3.2 demonstrates many of the changes to heat supply systems which can make them more efficient. For steam boilers, efficiency is maximized by use of flue gas heat recovery and economizers, boiler feedwater heating and condensate return. Steam distribution systems should be well maintained, steam leaks promptly repaired, steam traps monitored for leakage, "dead legs" closed off promptly, and local meters installed and recalibrated regularly. Direct fired burners eliminate all costs associated with steam raising and distribution, and should be considered where the product quality is not impaired by coming into direct contact with exhaust gases. Modern burners, giving low emissions of nitrogen oxides (NO_x) and sulfur oxides (SO_x), should be used; retrofitting of older burners can be considered. Localized boilers are another way to eliminate steam mains, as are localized CHP generators, covered in the next section.

Cold utilities are usually cheaper than hot utilities, but note that low-temperature refrigeration loops are very expensive and the circulating temperature should therefore be maximized, and cooling water used where temperatures allow, in preference to chilled water or refrigeration.

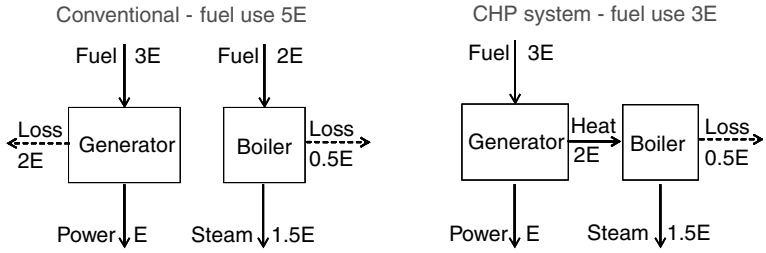

Fig. 1.13 Schematic representation of a typical CHP (combined heat and power) system.

1.5.4.3 **Combined Heat and Power**

The dryer heat requirement is supplied in conjunction with power generation in a heat engine. This power can be used on the site or exported to the electricity supply grid. In effect, the power is generated at a marginal efficiency of nearly 100%, compared with 40% in a typical stand-alone power station. The principle is shown schematically in Fig. 1.13. The heat that would otherwise be rejected through the stack is usefully used in the process. In effect, instead of using $3E$kW of fuel to generate power E, we have only used E, so the power has been generated at 100% marginal efficiency!

In practice, this is an oversimplification. Usually, the heat must be supplied from a CHP system at a higher temperature than it is rejected at in a stand-alone power station, so that power typically falls from 40 to 33% of fuel energy and heat rises from 60 to 67%. Nevertheless, the reduced power generation (or increased fuel to generate the same power) is far outweighed by the value of energy recovered from the exhaust heat (plus the substantial reduction in environmental emissions compared with separate systems). A very clear example of this is shown in the case study, in Section 1.6.3.

CHP is increasingly used to heat buildings via district heating schemes, but industrial applications require the heat to be generated at much higher temperatures. Table 1.9 lists the three main forms of industrial CHP.

Steam turbines are the earliest form of CHP system, and have been extensively used for decades in pulp and paper mills. However, they give a relatively low power output for a given heat production. Hence, they have been used infrequently in recent installations. They are usually large-scale systems, providing several megawatts of heat from the low-pressure steam and more than 1 MW of electricity. The

Tab. 1.9 Types of combined heat and power system.

CHP System	Scale	Power/Heat Ratio	Heat/Power Ratio	Main Heating Range (°C)
Steam turbines	Large	<0.2	>5	100–200
Gas turbines (natural gas or fuel oil)	Large	0.67–0.2	1.5–5	100–400
Diesel or gas reciprocating engines	Small	1.25–0.5	0.8–2	100–300, <80

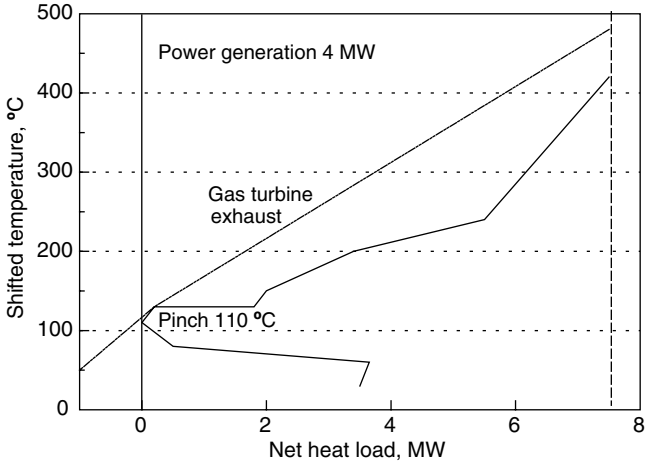

Fig. 1.14 Gas turbine CHP system fitted to a grand composite curve.

temperature and pressure of the steam levels can be optimized by using the GCC, as in Fig. 1.12.

Gas turbines are often the most effective form of CHP; they produce a good proportion of power, plus high-grade heat in the form of hot exhaust gas, which can be used to heat a dryer directly, or to raise steam for indirect heating. Again, the required heat load can be found from the GCC; the hot exhaust gases plot as a sloping line, as in Fig. 1.12. An excellent example is the 1982 installation by Scottish Grain Distillers at Port Dundas, Glasgow. Here a gas turbine generates 3.5 MW of power, sufficient for all the site needs, and the hot exhaust gases at approximately 450 °C are fed directly to a pneumatic conveying dryer, which dries the spent grain residues from the fermentation to produce animal feed. The grand composite curve for a similar system is shown in Fig. 1.14. Here, 4 MW of power and 7.5 MW of useful above-pinch heat is being generated, while about 2 MW of above-ambient exhaust heat is rejected as it is low-grade heat below the pinch and, therefore, useless.

Gas and diesel engines also produce a high power output, but less high-grade heat than gas turbines, with a large amount of waste heat at around 80 °C from the jacket cooling water. This is often useless for process duties, especially if the pinch is around 100 °C as the heat is released below the pinch. However, if there are nearby offices or warehouses, the jacket heat can provide central heating and domestic hot water to them. Conversely, if the pinch is at ambient, there must be some low-grade process heating duties, which can thus be fulfilled by the jacket water.

Scale is another factor; gas turbines are mainly used for large installations (2 MW power production and above, generating at least 3 MW heat) whereas gas engines are usually substantially smaller than 1 MW power output, giving heat loads well under 500 kW. An interesting small-scale example is a sewage sludge dryer developed around 2000 by NMA (Netherlands) with an integral gas engine; the power generated is used for the agitator drive, overcoming the high resistance of the sticky sludge in the early stages, and the exhaust heat is fed into the dryer for final thermal drying.

So, the big question; which CHP system is most appropriate for a dryer? As usual, the answer is, "It depends". Key factors are the required temperature range, the shape of the GCC, the site power-to-heat ratio and the total power and heat requirements. For most small- and medium-sized chemical and process plants, gas engines are more appropriately sized than steam turbines or gas turbines. More than one gas engine is often used in parallel, to match site heat demand and give operating flexibility (see the case study, Section 1.6.3).

The relative costs of heat and power are also very important; obviously CHP schemes are more worthwhile in countries where power is mainly provided from fossil fuels and is relatively expensive, and are unattractive where cheap power sources such as hydro-electricity are available.

1.5.4.4 **Heat Pumps**

A heat pump can recover heat from the exhaust gas to heat the dryer. In thermodynamic terms, this needs to work backwards across the pinch, recovering useless below-pinch waste heat for duties above the pinch. Again, the GCC shows how much heat can be upgraded at any temperature. The coefficient of performance (COP) is the heat upgraded per unit power supplied, and falls as the temperature lift increases. In most countries, electrical power is generated from fossil fuels in power stations, with an efficiency of 30–40%. Hence, a COP of 3 is required just to break even in primary energy terms, and to give some economic return for the cost of the heat pump, the COP needs to be at least 5 and preferably nearer 10. This will only be possible where the temperature lift is very low. Good opportunities are agricultural dryers and grain stores where exhaust air is recycled and reheated; drying is very slow, the heating duty is low and the temperature difference between exhaust and inlet air is only a few degrees. On the GCC, this would show up as a "sharp" pinch. In contrast, our example dryer in Fig. 1.8, where a temperature lift of over 100 °C is required to upgrade any significant amount of heat, is totally unsuitable for heat pumping. Inappropriate placement of a heat pump destroys any potential energy savings; Sosle *et al.* (2003) noted that a heat pump dryer for apple, although giving good product quality, had a higher energy consumption than an equivalent hot air dryer because the heat lost in the secondary condenser could not be usefully recovered. However, Krokida and Bisharat (2004) suggest that a heat pump can still be economic, even over a fairly wide pinch region.

In countries where electrical power is available cheaply, for example, from hydroelectric sources, the economics of heat pump systems are substantially better. Lower COPs can be tolerated and the use of heat pumps on industrial dryers becomes economically feasible in some more cases.

The analysis above is for conventional closed-cycle heat pumps taking in a given amount of exhaust heat and releasing a slightly greater amount at a higher temperature. There can be considerable differences for other systems, for example, open-cycle (mechanical or thermal vapor recompression), absorption heat pumps and heat transformers/splitters. In all cases, however, the temperature/heat load profiles of the heating and cooling stages should be compared with the process GCC to ensure that the most appropriate system is selected and that it is working over the optimum range of temperature and heat load.

1.6
Case Study

A case study on a food processing plant gives an example to compare different dryer types, both in terms of energy performance and other operational and economic parameters.

1.6.1
Process Description and Dryer Options

The plant is producing a dry final product with approximately 2% final moisture content from an initial solution with about 30% dissolved solids. The upstream process is of interest; in the early stages of evaporation, multiple-effect evaporators and either thermal or mechanical vapor recompression are used to reduce the energy consumption to a small fraction of the total evaporation latent heat load. As the concentration increases, viscosity rises and the solution also shows a substantial boiling-point rise (vapor temperature lower than solution temperature), reducing temperature driving forces so that multiple effects can no longer be used. Finally, a paste is formed and this must be dried from about 20% moisture wet basis, 25% dry basis. There are three technology options for this:

- Batch vacuum tray (oven) dryers
- Continuous vacuum band (belt) dryers
- Continuous spray dryer (working from a more dilute initial solution).

Vacuum tray dryers are the original historic process. They are simple to construct and operate, and operate at an absolute pressure of 70–100 mbar, which can be achieved by liquid ring vacuum pumps. However, they are of relatively small capacity (about 150 kg) and the manual loading and unloading is highly labor-intensive. Drying cycle time is 1 h and loading adds 20 min to the cycle. Hence up to 20 ovens in parallel are required to give a production rate of $2\,t\,h^{-1}$, as the effective throughput of each oven is little more than $100\,kg\,h^{-1}$.

Vacuum band dryers are the continuous equivalent of the batch tray dryers. They have a larger throughput, and feed and discharge are automatic, so that labor requirements are far lower. They can be operated under similar conditions of temperature and vacuum to the batch dryers, giving a drying time of about 50 min, as, unlike batch ovens, they do not need time for heating up or pulling and releasing vacuum at the start and end of each cycle. However, by pulling a higher vacuum, with absolute pressures down to about 30 mbar, falling-rate drying can be substantially accelerated and the drying time falls to about 30 min. The disadvantage is that to pull this level of vacuum, either a chilled water condenser (using power) or a steam ejector (using steam) is required, and the energy consumption of the latter is comparable to the latent heat load. Moreover, if the nozzles are worn, steam consumption becomes even higher with no gain in vacuum, so regular maintenance and replacement is necessary – yearly is recommended. Between 2 and 5 band dryers in parallel, depending on scale and vacuum conditions, could be used to meet a $2\,t\,h^{-1}$ production requirement.

The third option is a spray dryer. This is a convective dryer working at atmospheric pressure, giving a significantly different temperature history from the vacuum dryers, so that product physical properties may be different. A single unit can easily achieve $2\,t\,h^{-1}$, or indeed far higher throughput. The feed must be pumpable and is, therefore, considerably more dilute than for the tray and band dryers, at approximately 50% solids. This reduces the need for evaporation equipment, saving capital cost, but the energy efficiency of the convective spray dryer is inherently lower than that of a comparable evaporator, even of single-stage type. For this product, tolerable inlet temperature is about 180 °C and exhaust temperature 100 °C, while ambient air supply averages about 20 °C over the year. Some energy is lost in solids heating and post-drying rather than used for direct evaporation, so efficiency expressed in terms of evaporative heat load is around 40% rather than the 50% which might be expected from the temperatures. To produce $2\,t\,h^{-1}$ of product, an evaporation rate of $2\,t\,h^{-1}$ is required, giving an evaporative load of $4000\,MJ\,h^{-1}$. With a temperature drop of 80 °C and air specific heat capacity of $1\,kJ\,kg^{-1}\,K^{-1}$, this means that an airflow of no less than $50\,t\,h^{-1}$ will be needed.

1.6.2 Analysis of Dryer Energy Consumption

For drying, the heat demand is significantly higher than the evaporation load, for several reasons:

- The solids need to be heated from their initial temperature to their final temperature in the dryer before discharge
- For batch ovens, the trays and ovens need to be reheated during each cycle, and some steam is supplied during loading and unloading
- For spray dryers, the whole of the airflow needs to be heated from ambient temperature to the final exhaust temperature

Measurements of steam consumption and comparison with calculated evaporation load reveal that:

- Vacuum tray ovens have typical efficiencies of about 30–40% for this product.
- Vacuum band dryers at the same conditions have higher efficiencies of 50–60%.
- Band dryers working at a higher vacuum have a substantial additional energy demand for the vacuum system.
- Spray dryer efficiency depends strongly on the inlet and exhaust temperatures; for this product, as noted above, the calculated efficiency is about 40%.

A pinch analysis shows that there is very little overlap between the composite curves (Fig. 1.15) and hence there is little opportunity for heat recovery within the plant or on the dryer. The dryer is working across the pinch, as shown by the grand composite curve (Fig. 1.16) and split GCC (Fig. 1.17) but it is not possible to alter the operating temperatures of either the dryer or other process units (notably the evaporators) to allow heat exchange between them. However, there may be opportunities to exchange heat with the utility system. In particular, below-pinch waste heat

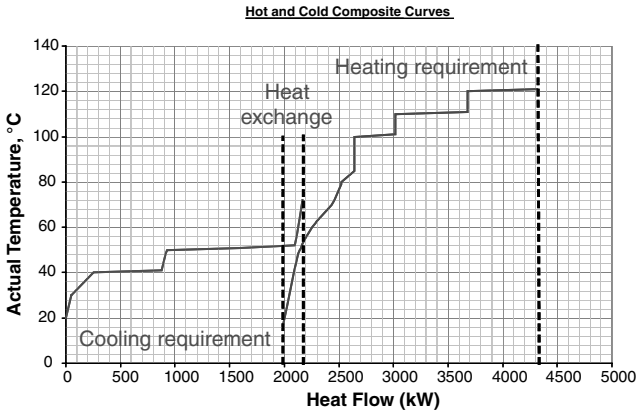

Fig. 1.15 Composite curves for a food process.

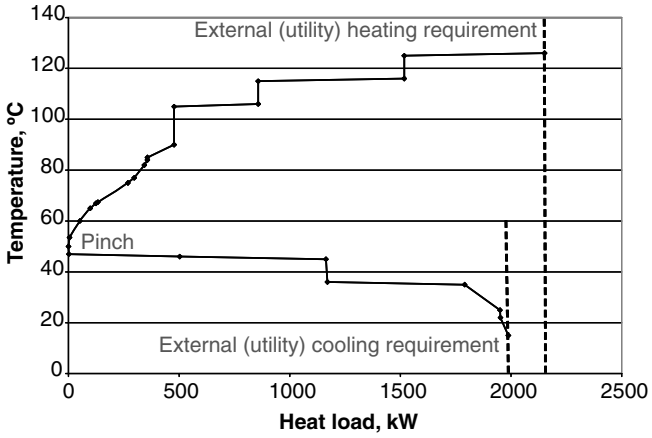

Fig. 1.16 Grand composite curve for a food process.

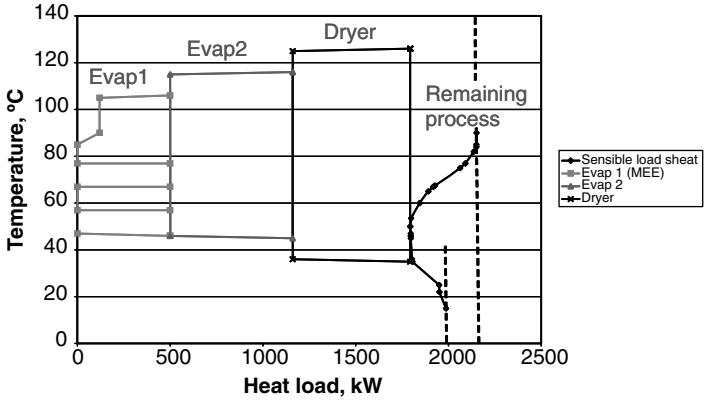

Fig. 1.17 Split grand composite curve for a food process.

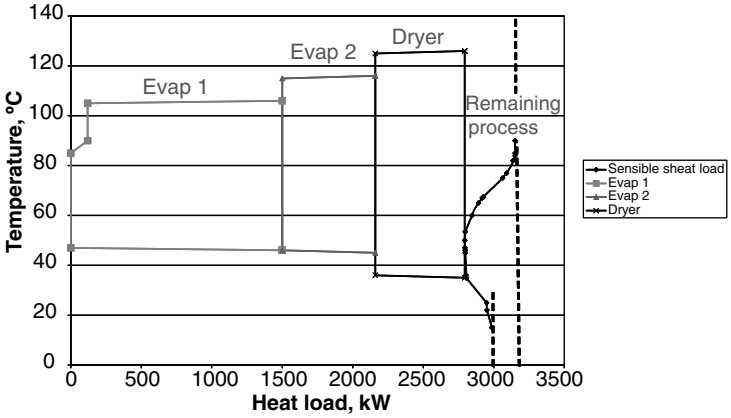

Fig. 1.18 Split GCC for a food process, with single-effect instead of multi-effect evaporator.

can potentially be used to preheat make-up water for the boiler feedwater system, as condensate return is well below 100%. The first-stage evaporators are multi-effect, which reduces their energy consumption substantially; compare Fig. 1.18 for the corresponding single-effect system, which shows that an extra 1000 kW of energy is required – a 45% penalty. As the solution is concentrated, the temperature driving forces are squeezed by the boiling point rise effect, where evaporated vapor is at a lower temperature than the solution. This, coupled with high viscosity, which reduces heat transfer coefficients, and the tight temperature limitations on the product, prevents the use of multiple effects in the second stage evaporators.

For the spray dryer, there is an opportunity to recover heat from the exhaust to preheat the inlet air. This can be done either with a direct air-to-air heat exchanger or by two separate exchangers with a circulating fluid to transfer heat, typically hot water. In both cases, it is desirable to use extended heat transfer surfaces to maximize the heat transfer coefficient. However, there is then a high risk of fouling for the dust-laden exhaust gas stream; either the heat transfer surfaces must be relatively plain for easy cleaning (giving a physically large exchanger) or the dust must be removed prior to the exchanger by a cyclone or bag filter, which incurs both extra capital cost and higher pressure drop. Exhaust heat recovery could bring exhaust temperature down from 100 to about 70 °C and improve efficiency from 40 to 55%.

Power use also needs to be considered. The power consumption of vacuum pumps is modest, and both primary energy use and costs are normally less than for steam ejectors. Spray dryers use substantial power for the fans, due to the high airflow (over 300 kW for the 2 t h^{-1} unit here). Moreover, in countries with high humidity, the inlet airflow may need to be dehumidified, requiring chilled water, which in turn incurs a power cost for the refrigeration system.

Table 1.10 compares the alternative dryer systems and their energy usage, and Fig. 1.19 shows the breakdown of steam consumption; note that for the tray and band dryers, the actual dryer evaporation load is a very small proportion of the overall process steam consumption.

Tab. 1.10 Comparison of alternative dryer options for food processing plant.

Dryer Type	Vacuum Tray (Oven) Dryers	Vacuum Band Dryers	Band Dryers – High Vacuum	Spray Dryer, no Heat Recovery	Spray Dryer With Heat Recovery
Mode of operation	Batch	Continuous	Continuous	Continuous	Continuous
Mode of heating	Conduction	Conduction	Conduction	Convective	Convective
Initial solids (%)	80	80	80	50	50
Residence time (min)	80	50	30	1	1
Holdup/Capacity (kg)	140–170	300–500	300–500	30–40	30–40
Production rate (per unit) ($kg\,h^{-1}$)	100–130	400–600	660–1000	2000	2000
Number required	16–20	4–5	2–3	1	1
Vacuum equipment	Vacuum pump	Vacuum pump	Steam ejector	None	None
Pre-evaporator	Yes	Yes	Yes	No	No
Evaporator:					
Evaporation rate ($kg\,h^{-1}$)	1600	1600	1600	0	0
Efficiency (%)	88	88	88		
Steam consumption ($kg\,h^{-1}$)	1800	1800	1800		
Dryer:					
Evaporation rate ($kg\,h^{-1}$)	400	400	400	2000	2000
Efficiency (%)	33	50	50	40	55
Steam consumption ($kg\,h^{-1}$)	1200	800	800	5000	3700
Ejector steam use ($kg\,h^{-1}$)	0	0	800	0	0
Total steam use ($kg\,h^{-1}$)	*3000*	*2600*	*3400*	*5000*	*3700*
Steam use (kW)	1700	1500	1900	2800	2100
Electrical power use	Medium	Medium	Low	High	Very High
Capital cost	Medium	High	Low	Medium	High
Labor cost	High	Low	Low	Low	Low
Maintenance cost	Low	Low	High	Low	Low

Clearly, each dryer type has its advantages and disadvantages, and, for selection, the preference will be based on the relative importance of capital, energy and labor cost. In practice, the batch drying option is only economic in developing countries with very low labor costs, and can be eliminated from consideration elsewhere. It is noteworthy, however, that the heat energy consumption of the spray drying system is substantially higher than the vacuum dryers, and the main reason is that the spray dryer is much less efficient than the pre-evaporators for concentrating the liquid from 50 to 80% solids.

Power consumption can be a substantial factor whose importance can be overlooked. The fan power requirement of 300 kW is a further penalty for the spray dryer, but if this is expressed in terms of primary energy, it rises to about 900 kW, giving a

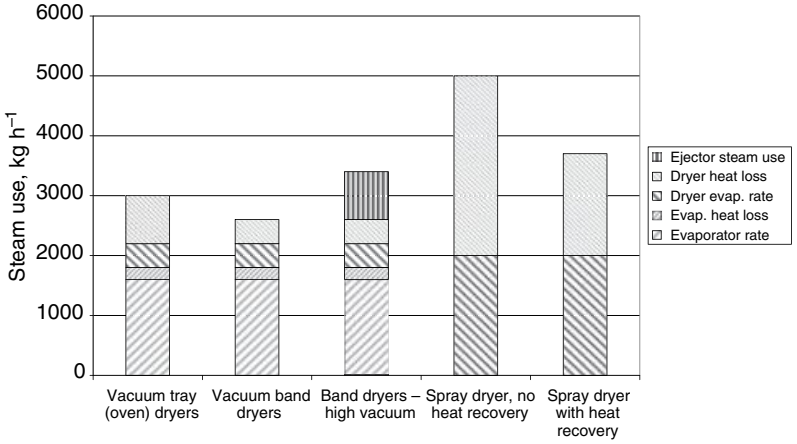

Fig. 1.19 Breakdown of steam consumption for alternative drying systems.

total energy use for the spray dryer of no less than 3700 kW. Although heat recovery from the exhaust lowers dryer steam consumption, there is an additional pressure drop through the heat exchanger and any additional dust collection equipment, giving an even higher fan power requirement. In addition, if inlet air dehumidification by chilled water is required during summer, particularly in tropical countries, the refrigeration power load can be several hundred kilowatts during those months.

Choice of the vacuum level for the band dryers also shows a clear capital-energy trade-off. In practice, careful temperature profiling in the dryer and combined pump/ejector systems can be used to optimize performance and reduce residence time while not incurring excessive steam costs. Hence, in practice, the preferred choice in normal circumstances will be one of the variants of vacuum band drying systems.

1.6.3
Utility Systems and CHP

Combined heat and power should always be considered as an option. The process is well suited for it; a gas engine is appropriately sized, the exhaust gas can be used to generate steam for the dryers and evaporators, and the jacket hot water can be used to heat parts of the upstream process (around 50–80 °C). The payback on a basic scheme is around 5–10 years, which is typical of CHP schemes in general.

However, for some sites in developing countries, the picture is very different. In some areas, rapidly increasing power demand has outstripped local generating capacity and power grid supply. For example, one site has random power outages for 25–30% of the day, and the site has five diesel generators which frequently need to be brought into action at a moment's notice. Because of the high cost of diesel fuel, this is an expensive method of power generation. Converting three of the diesel engines to gas or dual-fuel engines (cheaper than buying new gas-fueled generators), and installing heat recovery from the exhaust gases gives an excellent retrofit project

Tab. 1.11 Energy use and carbon dioxide emissions with and without CHP.

	Original		With CHP	
	kW	$t_{CO2}\,y^{-1}$	kW	$t_{CO2}\,y^{-1}$
Natural gas use	1667	2700	3333	5400
Steam/hot water raised	1333		1333	
Losses to exhaust	333		1000	
Power generated	0		1000	
Power imported (70%)	700	3297	0	0
Power from diesel	300		0	
Diesel oil used	1021	1276	0	0
Total primary energy	4788		3333	
Total carbon dioxide		7273		5400

with a payback of barely 2 years, because of the large savings from eliminating diesel fuel. The primary energy and carbon footprint benefits are similarly considerable, as shown in Tab. 1.11. The figures are based on a power consumption of 1000 kW and to calculate annual emissions, a working year of 5000 h has been assumed.

For imported electricity, primary energy is taken to be 3 times the power use. Overall, the CHP system gives 30% savings in primary energy and 26% in carbon footprint. These figures would be similar even if all power was imported and none generated locally from diesel.

One factor which needs to be checked is whether the local gas supply infrastructure is able to supply the large gas flows required for a major CHP scheme. This has in the past ruled out some promising CHP schemes, even in developed countries.

Additional steam use is generated from coal-fired boilers. In some locations, alternative fuels such as rice husk can be considered as supplementary fuel. Also, the steam is generated and distributed at high pressure. Where a heating duty requires only low pressure steam, the steam can be let down through a small local steam turbine, instead of a let-down valve. Rather than generate a small amount of electrical power, requiring expensive alternators, the most cost-effective use of the shaft work is as direct drive to pumps and other process machinery on that process stage. Hence, if the stage is shut down and the steam is not required, the power load is also not needed and does not have to be separately supplied.

1.7 Conclusions

Although dryers are intensive energy users, it is often difficult to find obvious major energy savings. Their energy use needs to be considered in the context of the overall process.

Pinch analysis of a typical dryer shows that heat recovery is severely limited by thermodynamic as well as economic considerations. Dryers usually have a high net heat demand above 100 °C; the main heat output is the latent heat of evaporation held in the vapor in the exhaust gas, which cannot usually be recovered except as low-grade waste heat. In a few specific situations, heat may be exchanged with a nearby process whose pinch is substantially above (or, more rarely, below) the dryer pinch temperature. Heat pumps are possible, but only in specific circumstances; there are often opportunities in agricultural drying, and solar heating is also an important possibility. In many industrial situations, the biggest opportunity comes from CHP (combined heat and power), particularly gas turbines on large sites and gas engines on small or medium ones. Reduction of the inlet moisture content to the dryer is the other major possibility, but the changes needed to achieve this must be made to the upstream process rather than the dryer itself.

Despite these difficulties, energy analysis of dryers is very worthwhile and can lead to major energy and cost savings. Key tools are the formation of a consistent heat and mass balance, and a systematic comparison between fuel use, steam generated and delivered to plants, and the energy actually required and consumed by the process itself.

Additional Notation Used in Chapter 1

ΔH_v	specific enthalpy of evaporation	$J\,kg^{-1}$
ΔT_{min}	minimum temperature difference (at pinch)	K

Subscripts

burner	for a direct-fired burner
heater	for an indirect heater (heat exchanger)
latent	latent heat
loss	heat loss
sens	sensible heat
stream	for a stream (in pinch analysis)

Abbreviations

CHP	combined heat and power
COP	coefficient of performance
GBP	Great Britain pound
GCC	grand composite curve
RF	radio frequency
VOC	volatile organic compound

References

Bahu, R. E., 1991. Energy considerations in dryer design. *Proceedings of 7th International Drying Symposium* (IDS'90), Prague, pp. 553–557.

Devahastin, S., Suvarnakutura, P., Soponronnarit, S., Mujumdar, A. S., 2004. A comparative study of low-pressure superheated steam and vacuum drying of a heat-sensitive material. *Drying Technol.* **22**(8): 1845–1868.

ESDU 1987–1990. ESDU Data Items 87030, 89001 and 90027; *Process integration and pinch technology.* Available by subscription from ESDU International plc, London, UK.

Kaiser, S., Antonijevic, D., Tsotsas, E., 2002. Formation of fouling layers on a heat exchanger element exposed to warm, humid and solids-loaded air streams. *Exper. Therm. Fluid Sci.* **26**: 291–297.

Kemp, I. C., 1991. Some aspects of the practical application of pinch technology methods. *Trans. Inst. Chem. Eng.* **69**(A6): 471–479.

Kemp, I. C., 1996. Unpublished survey on energy use in industrial drying for ETSU (Energy Technology Support Unit), UK Department of Energy.

Kemp, I. C., 2004. Drying in the context of the overall process. *Drying Technol.* **22**(1 & 2): 377–394.

Kemp, I. C., 2005. Reducing dryer energy use by process integration and pinch analysis. *Drying Technol.* **23**(9–11): 2089–2104.

Kemp, I. C., 2007. *Pinch analysis and process integration (User guide to process integration for the efficient use of energy)*, 2nd edn, Butterworth Heinemann, Elsevier, Oxford, UK and New York, USA.

Kemp, I. C., Gardiner, S. P., 2001. An outline method for troubleshooting and problem-solving in dryers. *Drying Technol.* **19**(8): 1875–1890.

Krokida, M. K., Bisharat, G. I., 2004. Heat recovery from dryer exhaust air. *Drying Technol.* **22**(7): 1661–1674.

Linnhoff, B., Townsend, D. W., Boland, D., Hewitt, G. F., Thomas, B. E. A., Guy, A. R., Marsland, R. H., 1982. *User guide to process integration for the efficient use of energy,* 1st edn, Institution of Chemical Engineers, Rugby, UK. For 2nd edition see Kemp 2007.

Smith, R., 2005. *Chemical process design and integration,* John Wiley & Sons.

Sosle, V., Raghavan, G. S. V., Kittler, R., 2003. Low-temperature drying using a versatile heat pump dehumidifier. *Drying Technol.* **21**(3): 539–554.

Stubbing, T. J., 1993. Airless drying: Its invention, method and application. *Trans. Inst. Chem. Eng.* **71**(A5): 488–495.

Stubbing, T. J., 1999. Airless drying: Developments since IDS'94. *Drying Technol.* **17**(7&8): 1639–1651.

van Deventer, H. C., 2002. Advanced drying concepts: Superheated steam and adsorption. Presentation at EFCE Drying Working Party meeting, University of Magdeburg.

Wilmshurst, A., 1988. *Industrial energy use in drying with special reference to infra-red.* Diss., University of Cambridge, UK. Reported by Bahu (1991).

2
Mechanical Solid–Liquid Separation Processes and Techniques

Harald Anlauf

2.1
Introduction and Overview

Thermal or mechanical means can be used to more or less efficiently separate a suspension into the continuous liquid and the disperse solid phase. One important aspect of modern drying technology consists in the integration of the process steps before and behind the thermal dryer to attain an optimal overall process design. Mechanical liquid separation is an important process step, located upstream of the thermal dryer, and should, therefore, be discussed here in more detail. As a rule, the thermal methods are usually quite energy-intensive compared with the mechanical liquid separation because they require a phase transition from the liquid to the gaseous aggregate state and the appropriate evaporation enthalpy must be supplied. For this reason, and also because of the often undesirable thermal exposure of sensible products, it is mostly advantageous to separate as much liquid as possible mechanically. For physical reasons a final amount of liquid always remains in the particle structure after the mechanical liquid separation. This portion of liquid can only be removed from the solid material by thermal means. If a completely dry powder is required as the final product, one of the tasks for the optimization of the whole separation process consists in determining the most favorable point of transition from the mechanical to the thermal separation step. This transition point is very variable and depends on the requirements of the selected thermal drying process. For spray drying a slurry that can still be pumped and sprayed is necessary, whereas the solids should be dehumidified down to mechanical flowability for fluidized bed drying.

At the interface of these two basic processes for solid–liquid separation, combined mechanical–thermal processes have also been developed and established, such as centrifuge dryers, nutsch dryers and, in recent times, steam pressure filters (see Section 2.5). The advantages of these systems consist in synergies, which result in energy savings, compact and simplified process design.

Figure 2.1 gives a schematic survey of the physical possibilities for mechanical solid–liquid separation. For each of the shown physical principles different separation techniques can be identified, and for each of these techniques a large

Modern Drying Technology Volume 4: Energy Savings, First Edition.
Edited by Evangelos Tsotsas and Arun S. Mujumdar

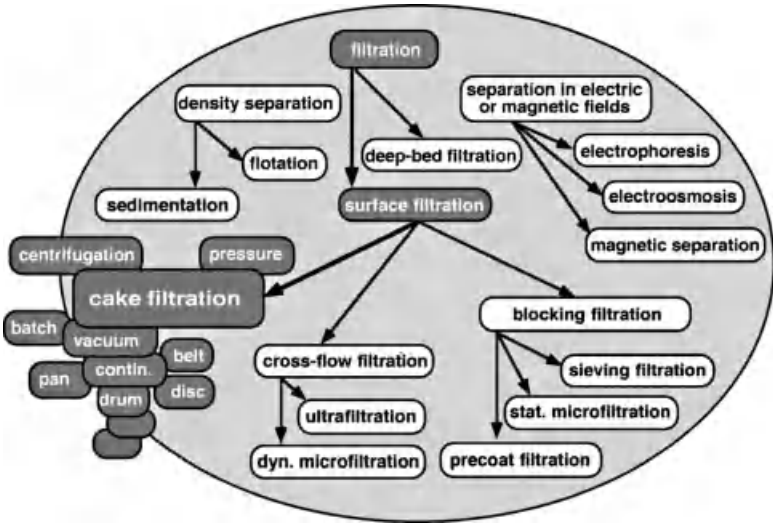

Fig. 2.1 Survey of the physical processes for mechanical solid–liquid separation.

number of different separation apparatuses exist. As an example we consider cake filtration, which can be carried out in a centrifugal field under the influence of a mechanically produced pressure, or by generation of vacuum behind a filter medium. The respective cake filter can be operated discontinuously or continuously. Considering, for example, the family of continuously operating rotary vacuum filters, one can find drum, disc, belt and pan filters as the basic types. Each of these apparatuses can be optimally adapted by special constructive means to the individual task of a specific separation problem. The reason for this variety is that mechanical separation processes must be effective over extreme ranges of particle size, size distribution and shape, specific weight of solids and liquid, suspension concentration, suspension and liquid rheology, flow rate, chemical composition of the suspension, process and technical boundary conditions and, last but not least, the demands on the separation results. For instance, the particle diameter can vary from a few nanometers to some centimeters. In addition, the general principle of mechanical separation of particles from liquid allows a further differentiation into different special settings of tasks. The primary goal of a mechanical solid–liquid separation process can be distinguished as follows:

- ***Dehumidification of the solids.*** As much liquid as mechanically possible should be displaced from sediments or filter cakes by squeezing or desaturation.
- ***Concentration of suspensions.*** Only a part of the clear liquid is to be withdrawn from a diluted suspension in order to relieve the following apparatus or to make it applicable at all.
- ***Clarification of a liquid.*** As far as possible, particle free liquid should be withdrawn from a suspension.

- ***Classification of solids according to particle size***. A particle system is to be separated at a defined cut size into a fine fraction and a coarse fraction, or a defined particle fraction has to be produced.
- ***Sorting of solids according to material properties (specific weight, shape, color, etc.)***. A particle system has to be separated according to properties other than particle size.
- ***Washing of solids to remove soluble substances***. To purify a particle system from soluble substances a liquid, which has to be molecularly miscible with the suspension liquid, is used. One can basically distinguish between permeation washing and dilution washing. During permeation washing the wash liquid is filtrated through a packed bed of already separated particles. In the case of dilution washing the previously separated particles are resuspended with wash liquid and separated again. In multistage processes the mode of wash liquid application can be co-current or counter-current. By counter-current flow operation wash liquid can be saved in comparison to the co-current flow operation. However, counter-current flow operation is not always applicable.
- ***Three-phase separation of solids and two molecularly immiscible liquids***. In general, for this task the necessary difference in specific weight of the materials involved is utilized.
- ***Extraction and following phase separation***. Here the same density separation processes are applied as for the three-phase separation. Additionally, intensive mixing of the extraction agent and the suspension to be extracted has to be realized.

Figure 2.1 shows that the equipment variety can, nevertheless, be systematically arranged into physically well defined and distinguishable separation mechanisms. The mechanical separation processes can be split basically into three main groups.

The density separation processes utilize a difference in the specific weight of solids and liquid for the separation of particles by sedimentation in the direction of, and by flotation against, the direction of the earth's gravity or a centrifugal field (see Section 2.2).

The filtration processes are characterized basically by the flow of the liquid phase through a porous filter medium due to a pressure difference, while the solid particles are held back. One differentiates thereby between depth filtration (see Section 2.3.4), in which the particles to be separated are deposited inside the structure of a filter layer, and surface filtration, in which the particles are retained at the surface of a filter medium. Surface filtration can be subdivided into cake, cross-flow and blocking filtration.

Cake filtration is characterized by the fact that the solids are deposited as a macroscopic porous layer on the filter medium, while the liquid must flow through the already formed filter cake and the filter medium. In subsequent post-treatment steps the filter cake can be first washed and then desaturated in the case of incompressible, or squeezed in the case of compressible cake structure. In comparison to other filtration procedures, cake filtration permits extensive dehumidification of the solids. In order to be realized economically, cake filtration requires, however,

the fulfillment of certain conditions, like sufficiently high suspension concentration and particle size (see Section 2.3.1).

In comparison to cake filtration, the procedures of cross-flow filtration are based on tangential suspension flow over the filter medium, which consists usually of a microporous membrane. In this manner filter cake formation is avoided nearly totally and the suspension can be concentrated up to its limit of flowability. This technique is applied to separate very small particles and highly dilute suspensions, which would lead to uneconomically high filter cake resistances and long filtration time with cake filtration (see Section 2.3.3).

As an alternative, highly diluted suspensions containing very small or even coarse particles can be treated by blocking filtration. Here, one permits the gradual blockage of the filter medium pores by single particles; after reaching a defined critical pressure loss the particles are detached, for example by a back-flushing procedure (see Section 2.3.2).

Finally, particle separation can be influenced by applying an additional electric or magnetic field, if the particles show an appropriate material behavior (see Section 2.4).

Modern mechanical solid–liquid separation technology has, beside the versatile apparatus spectrum, further important possibilities to optimize the separation process. One of these possibilities consists of a suspension pre-treatment to make the subsequent separation easier (see Section 2.6.3). Furthermore, one has to check whether a batchwise or a continuously operating separation process should be chosen (see Section 2.6.1). Both modes of operation feature special advantages and disadvantages. In the rarest cases a solid–liquid separation process is fulfilled by one single apparatus. Very often a combination of apparatuses is the best choice to gain the physically and economically best solution, despite comparatively large expenditure on equipment (see Section 2.6.2).

Last but not least, several alternative solutions exist for nearly every separation problem, so that only a careful and deep analysis of all relevant aspects can lead to optimal results. For the choice of a separation process, in a first step the separation problem has to be analyzed, and a specification of requirements regarding the separation results has to be formulated. This leads to first ideas for eventually suitable processes. The second step typically involves bench-scale separation experiments, to provide a proof of principle and to get the data necessary for scaling up the considered types of equipment. On the basis of the laboratory results and after comprehensive analysis of economic and other important aspects, pilot-scale tests must be carried out in most cases. Specific apparatus parameters, which cannot be determined by bench-scale tests, can now be investigated. From the successfully realized pilot test the final quantitative scale-up to the industrial process can be accomplished.

The procedures and apparatuses for mechanical solid–liquid separation are under permanent research and development in view of new challenges and requirements of the separation (Anlauf, 2006, 2007a, b, 2008; Höflinger, 2008; Kopf *et al.*, 2008; Lyko, 2008; Ripperger, 2008). Actual research results are permanently transferred to apparatus construction. New materials and methods of production engineering are used. Modern sensor and data transfer technology allow the remote monitoring of

separation processes and result-dependent control and regulation. The trend is toward the "intelligent" machine, which reacts to changes in the feed conditions automatically. However, on the way to this target a number of still unsolved questions of basic research have to be answered. One of these questions is the quantitative correlation between filter separation results and real particle system characteristics (Sorrentino, 2002).

General information about the theory, processes and apparatuses of mechanical solid–liquid separation can be found in several books (Jornitz and Meltzer, 2001; Dickenson, 1997; Leung, 1998, 2007; Rushton *et al.*, 1996; Sutherland, 2005; Svarovsky, 2000; Wakeman and Tarleton, 2005a, b, 2007).

2.2
Density Separation Processes

2.2.1
Froth Flotation

Flotation processes are generally based on the fact that suspended particles have a smaller specific weight than the surrounding liquid phase and thus rise up against the direction of the earth's gravity or a centrifugal field. Even if the particles have a larger specific weight than the surrounding liquid phase, they can still be made to rise up against gravity to the top of a so-called "flotation cell" as a froth, by adhering to gas bubbles. Figure 2.2 illustrates the general principle of froth flotation. Industrially, flotation in aqueous suspensions is most frequently used for sorting particles of different materials. Flotation is used, in particular, in ore, mineral and coal processing to separate fine-grained particle mixtures of liberated minerals and tailings. In the field of paper recycling, flotation is applied for de-inking of the pulp. However, flotation is also applied as an energetically favorable and low-cost process for the total

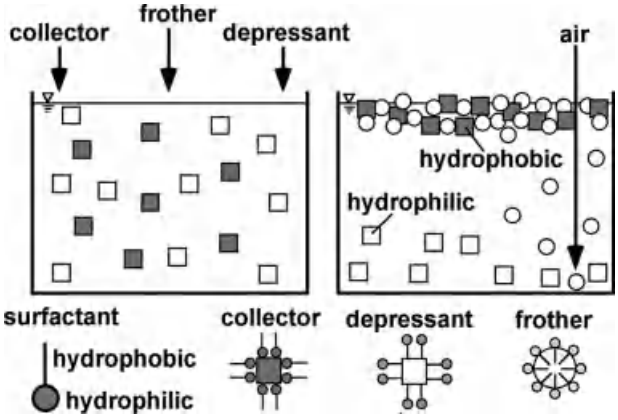

Fig. 2.2 Principle of the froth flotation process.

separation of organic particles that have only small differences in specific weight to the surrounding liquid. This is used increasingly in sewage water treatment as an alternative to sedimentation processes. The required clarification area can be reduced significantly in this way, under certain circumstances.

In order to enable the attachment of gas bubbles to the particle surfaces, these must be hydrophobic. If they are not hydrophobic by nature, they can be made hydrophobic by adding special surfactants, which are called "collectors". Surfactants or tensides are surface active molecules that consist of a hydrophobic nonpolar hydrocarbon chain and a hydrophilic polar group. According to the kind of polarity, one differentiates between anionic, cationic and nonionic surfactants. Anionic collectors are, among others, xanthanates, carboxylates, alkylsulfates or mercaptanes. Cationic collectors are alkylamines. The particles that are not to be discharged with the froth must show hydrophilic surface properties and settle in the direction of gravity to the bottom of the flotation cell. If they are not hydrophilic by nature, they can be made hydrophilic by special surfactants, which are called "depressants". Typical depressants are alkali cyanide, lime hydrate, zinc sulfate or water glass. The froth itself can be stabilized against coalescence by so called "frothers". Typical frothers are, among others, polypropylene glycol or aliphatic alcohols. The optimally flotable particle diameters are in the range 40–150 μm for solids with specific weights of more than $3000\,kg\,m^{-3}$. Upwards the flotation process is limited by the particle weight and downwards by the decrease in selectivity. Due to the ascending particle-loaded bubbles, three-phase froths are obtained in a flotation process. In the froth product are present not only particles adhering to the bubbles by heteroagglomeration but also a small amount of the finest hydrophilic particles. This phenomenon limits the selectivity of the process. Generally, several process steps such as basic flotation, secondary flotation, and purification flotation are necessary to produce the final solids concentrate. From the equipment point of view one can differentiate between mechanical and pneumatic apparatuses. Furthermore, special constructions such as pressure-release flotation and electro-flotation (see Section 2.4) are available. Flotation apparatuses are usually operated continuously.

In mechanical flotation apparatuses the energy necessary for mixing and dispersing is supplied to the aerated suspension by means of rotor/stator systems, as shown in Fig. 2.3. The air is sucked into the liquid through the hollow shaft of the stirrer, or it is supplied from outside by means of a nozzle. It is then dispersed in the rotor/stator system to small bubbles and mixed with the suspension under highly turbulent flow conditions. After turbulent dispersion and mixing, the froth must have the possibility to rise up under calm conditions.

In pneumatic flotation apparatuses no rotor/stator system exists. Here, the required air is supplied from the outside under pressure and dispersed to bubbles by means of a suitable aeration system. In Fig. 2.4 such a flotation column is shown. The height of flotation columns can vary from 5 to 15 m with a diameter of up to 4 m. Gas and suspension are fed in countercurrent configuration. This leads to an improved selectivity compared with the mechanical flotation systems, which show a cross-flow principle.

With the modern process of pressure-release flotation the pressure dependence of the gas solubility in water is utilized for bubble generation. The water is saturated

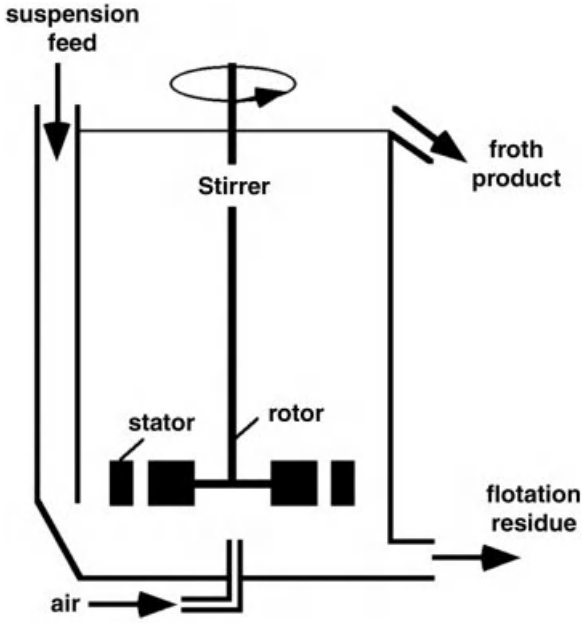

Fig. 2.3 Mechanical flotation apparatus.

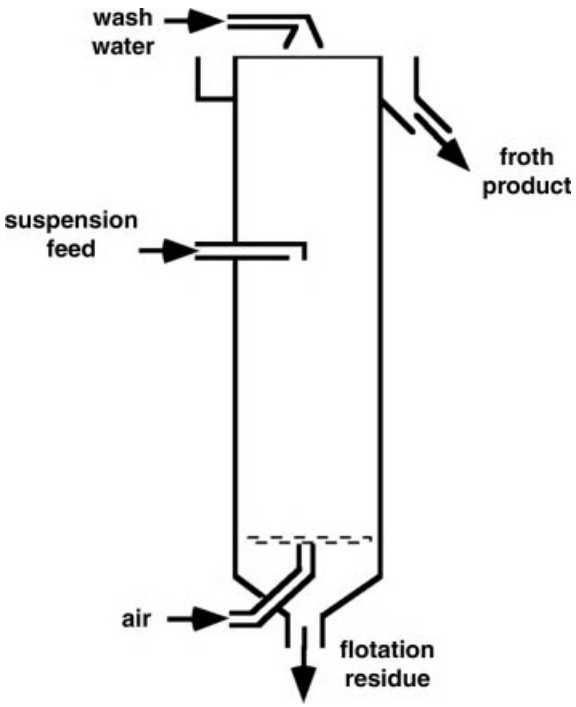

Fig. 2.4 Pneumatic flotation apparatus.

with air under increased pressure, and afterwards released to atmospheric pressure. In comparison to mechanical and pneumatic flotation with bubble diameters of more than 100 µm, here particularly small bubbles of 50 to 80 µm can be produced for relatively high pressures of approximately 450 to 700 kPa. Many bubbles emerge directly at the particle surfaces, where the nucleus formation work is lowest.

Further and more detailed information about froth flotation can be found in Rao (2004) and Fuerstenau and Yoon (2007).

2.2.2 Sedimentation

Sedimentation processes have the task of separating solids from liquid over a wide range of conditions that start with the concentration or clarification of dilute suspensions and end with the extensive dehumidification of the separated solids. Classification and sorting can also be realized. A specific feature of sedimentation processes is the ability to separate suspensions that contain, beside solid particles, two molecularly immiscible liquids of different specific weight (water/oil) among their components. In contrast to flotation, the solid particles are separated in sedimentation processes in the direction of gravity g or a centrifugal acceleration a toward a solid and impermeable wall (Fig. 2.5).

While the acceleration due to gravity is constant, the centrifugal acceleration depends on the rotor radius R and the angular velocity of the rotor ω:

$$a = R \cdot \omega^2 \tag{2.1}$$

Although the angular velocity of a centrifuge may remain constant, the acceleration of a settling particle increases due to the increasing radius. Sufficiently accurate calculations can often be conducted with a constant mean centrifugal acceleration, if the centrifuge radius is large in relation to the thickness of the liquid layer in the rotor ("long arm approximation"). A dimensionless centrifugal factor

$$C = \frac{a}{g} = Fr \tag{2.2}$$

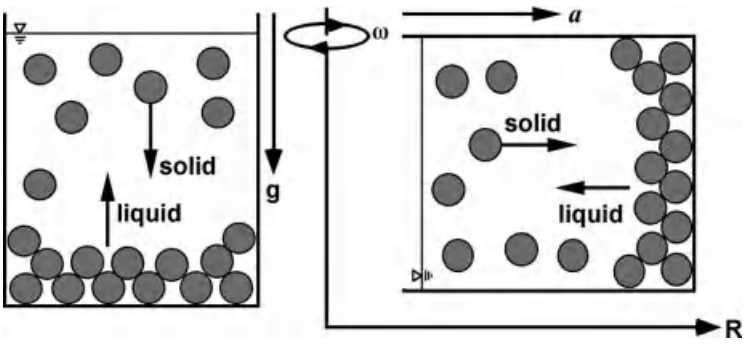

Fig. 2.5 Principle of sedimentation.

indicates the multiple of acceleration due to gravity that can be realized in the respective centrifuge, and serves to compare the efficiency of centrifuges. This characteristic number is also known as the Froude number and is used in mixing, agglomeration and comminution technology for rotating equipment.

In the case of sedimentation, the specific weight of the particles ϱ_s is always larger than the specific weight of the surrounding liquid phase ϱ_l. The liquid displaced by the downwards settling particles must move upwards. Apart from the density difference between the solids and liquid $\Delta\varrho$ and the acceleration g or a, the settling velocity v is influenced by the dynamic viscosity of the liquid μ_l, the particle diameter d and the solids volume concentration of the suspension. For the settling velocity v_{St} of single spherical particles (highly diluted suspension), laminar flow and Newtonian fluids, Stokes law is valid:

$$v_{St} = \frac{\Delta\varrho \cdot g \cdot C \cdot d^2}{18 \cdot \mu_L} \tag{2.3}$$

If one assumes constant acceleration in a centrifuge, the centrifugal settling velocity can be calculated easily by multiplication of the settling velocity in the earth's field and the C-value. As the solids concentration increases during sedimentation, the particles hinder each other more and more until, finally, they start to move with the same velocity, independently of their individual characteristics. A sharp and distinct sedimentation front is formed, with no particles in the clear liquid zone above it. This phenomenon is called "swarm sedimentation". The settling velocity of the swarm is sensitively dependent on the suspension concentration. After a sediment has formed by settling, a further displacement of liquid can take place only by compression (consolidation). This consolidation results from the dead weight of the particle layer, which is exposed either to gravity or to a centrifugal field. The pores of the sediment, however, remain completely filled with liquid. The first layers of the sediment are most strongly consolidated. At the surface of the sediment no further compression takes place. Consequently, a nonlinear concentration (porosity) gradient is built up over the sediment height.

A physical limit for sedimentation in the earth's field is set at a particle size of approximately 1 μm, because thermal convection and Brownian motion keep smaller particles permanently in suspension. Nevertheless, by means of agglomeration (see Section 2.6.3) one can make even the smallest particles accessible to gravity sedimentation. If a change in suspension properties is not permitted, the mass forces must be increased by changing from the earth's field to a centrifugal one.

Continuously operated circular and rectangular basins, as well as lamella clarifiers, are most frequently used for gravity sedimentation. Figure 2.6 shows a circular thickener/clarifier. The suspension is supplied centrally by means of a feed pipe and then spreads radially in the basin. Swarm sedimentation behavior of the suspension is desired, to separate the clear liquid from the sedimentation zone by a sharp sedimentation front. If this behavior is not given by the feed conditions, flocculation may help to enforce swarm sedimentation. In addition the smallest particles are bound in the floc structure and the overall sedimentation velocity increases.

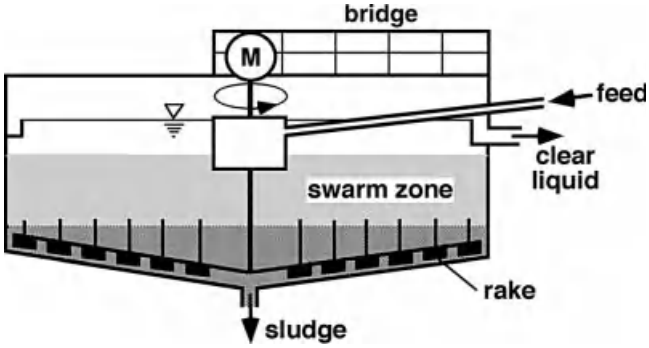

Fig. 2.6 Circular sedimentation basin.

In modern, high efficiency basins the suspension is led into the swarm zone, which then works like a dynamic filter for the ascending clear liquid. The sludge collected at the bottom of the basin is transported by means of a slowly rotating rake mechanism towards the central discharge opening. To increase the efficiency of the apparatus thin sticks can be installed on top of the rabble arms, which cut drainage channels into the sediment. In this way the sediment consolidates faster, and the sludge concentration can be increased. Large circular sedimentation basins are built in concrete with diameters up to 200 m.

Figure 2.7 shows a rectangular sedimentation basin. In this case the suspension flow and settling direction are perpendicular to each other. In Fig. 2.7 it can be recognized that density separation processes are well suited for multiphase separation. Floating substances can be separated here by a special discharge construction, which separates floating sludge and clarified liquid. For a given feed stream, the separation condition for the particles can be adjusted by the so-called "clarification area" of the basin. The feed volume flow rate divided by the clarification area determines the up-flow velocity of the liquid, which must be less than the sedimentation velocity of the particles. Continuously operated apparatuses for gravity sedimentation need relatively large clarification areas because of the usually low settling velocity of the particles.

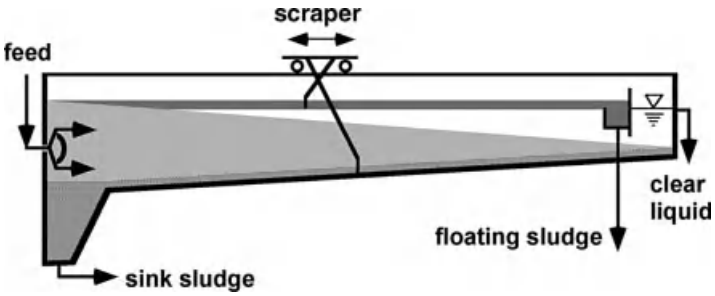

Fig. 2.7 Rectangular sedimentation basin.

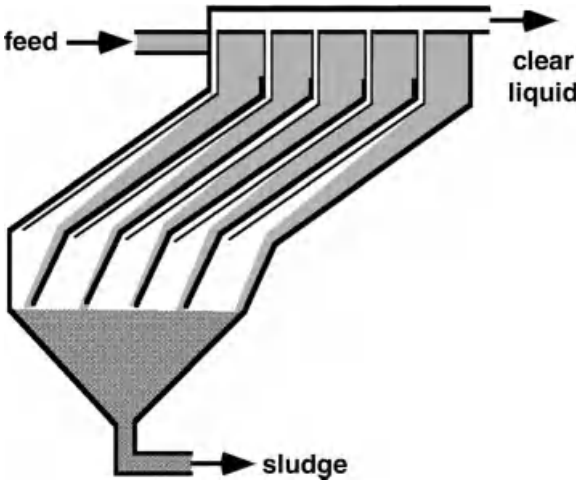

Fig. 2.8 Lamella clarifier.

Very large clarification areas on a small footprint area can be made available by a lamella clarifier, as demonstrated schematically in Fig. 2.8. Angularly arranged plates in the settling chamber lead to a drastic shortening of the distance necessary for settling until the particles are separated. A precondition for the operability of this apparatus is that the separated particles are able to slide down the plates without sticking on their surface. This can be ensured within certain limits by adjustment of the plate inclination.

As an alternative to the gravity sedimentation processes, sedimentation centrifuges can be chosen. For this purpose the following basic types of centrifuges are available:

- Beaker centrifuges
- Tube and overflow centrifuges
- Hydrocyclones
- Decanter centrifuges
- Disc stack separators

In the laboratory, discontinuously operating beaker centrifuges can be used for analytic purposes and preparation of small product samples.

For extremely difficult separation conditions tube centrifuges with centrifugal values C of up to 50 000 are applied. Figure 2.9 shows the principle of such a centrifuge. Tube centrifuges are quasi-continuous, but, in reality, operate rather discontinuously. During permanent feeding through a central feed pipe a sediment grows up in the rotor. On top of the sediment a stagnant zone of liquid is standing, which is overflowed by a thin and fast moving liquid layer. As soon as the particles enter the stagnant zone they can be considered as separated and settle down to the surface of the sediment. As soon as the sediment has achieved a certain critical height, the centrifuge must be shut down and, in most cases, dismantled and released

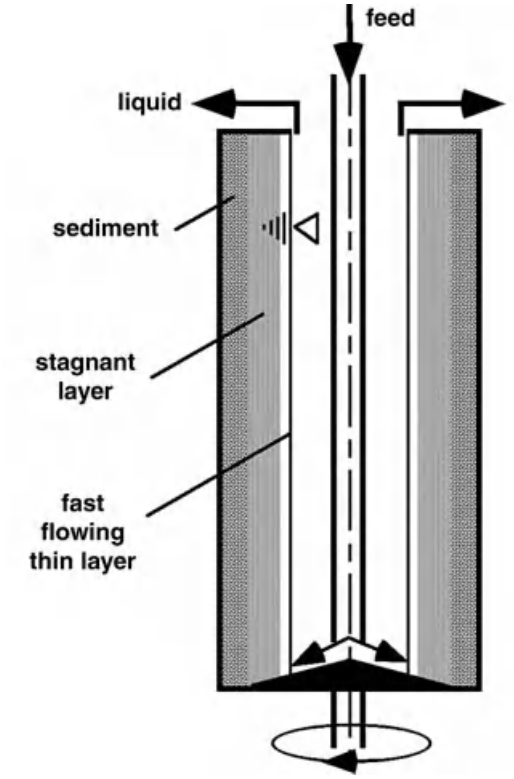

Fig. 2.9 Tube centrifuge.

manually from the solids. An extreme case for the pharmaceutical industry is a tube centrifuge for only one single use. On the other hand, some types of tube centrifuges are equipped with an automated mechanical sediment discharge. Similar types of centrifuges operating discontinuously at much lower *C*-values with automated or manual solids discharge are used for the cleaning of cooling lubricants and similar slurries.

A well-known representative of continuously operating centrifugal separators is the hydrocyclone. As shown in Fig. 2.10, hydrocyclones are very simply designed apparatuses. The suspension to be separated is accelerated here not by the rotation of a solid bowl, but by tangential injection under pressure. The liquid is forced by the tangential inlet into the cylindrical/conical process space on spiral circular paths. Particles up to a certain cut size settle outwards through a potential vortex; they are separated at the solid wall of the cylinder and discharged as a concentrate through the underflow apex orifice. The smaller particles follow the streamlines and are removed, together with the main part of the liquid, through a cylindrical tube fixed in the center of the top and projecting some distance into the cyclone. This overflow pipe is called the "vortex finder". In this way, both a separation and, in particular, a classification of the particles can be realized. The centrifugal acceleration is determined by the

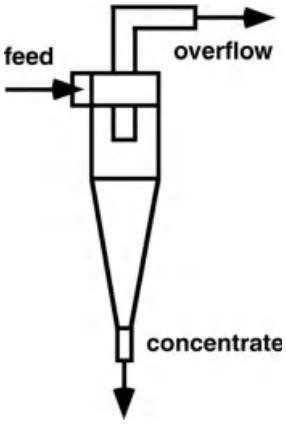

Fig. 2.10 Hydrocyclone.

injection pressure and the cyclone diameter. Maximum pressure losses of about 400 kPa and minimum cyclone diameters of about 10 mm limit the cut size to approximately 5 μm. Therefore, for large amounts of liquid and small cut size, several small cylones must be arranged in parallel. Agglomeration to improve the separation is not meaningful in hydrocyclones, since the strong shear stresses of the vortex flow would destroy the previously formed agglomerates. Because of the simple construction, hydrocyclones can be built of very different materials, such as metal, polymers or ceramic and, thus, can be optimally adapted to the conditions of a process.

Figure 2.11 shows the principle of a decanter centrifuge in a standard design. In contrast to the hydrocyclone, the suspension is fed into a rotating cylindrical/conical solid bowl by an axially arranged inlet pipe. A liquid layer ("pond") is formed, the height of which can be adjusted by a weir at the end of the cylindrical part of the drum. In modern centrifuges the weir height can be adjusted directly during operation by different technical systems. Over the weir, the clarified liquid is removed from the centrifuge. The settled solid particles must be transported along the solid wall of the bowl to the opposite side of the centrifuge by a screw. This requires a differential speed between the screw and the solid bowl. The differential speed can be adjusted by various types of special gearings. During the transport

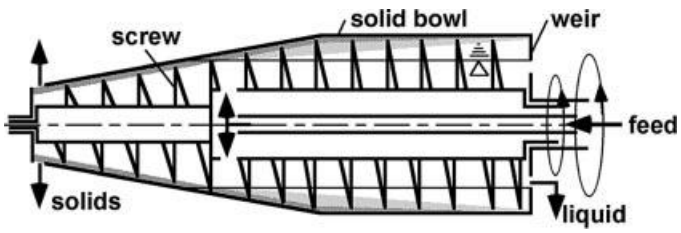

Fig. 2.11 Decanter centrifuge.

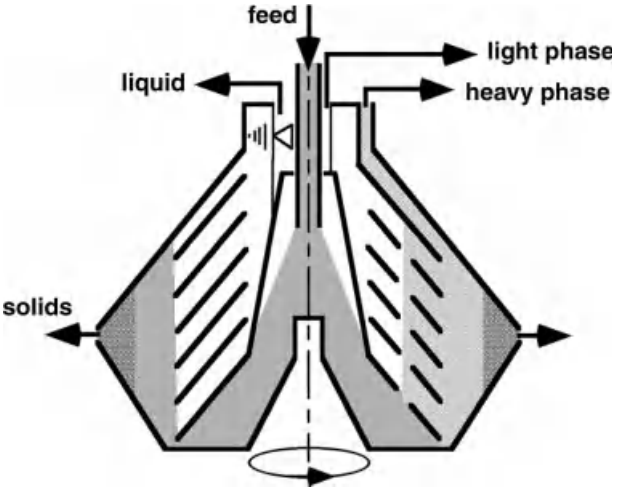

Fig. 2.12 Disc stack separator for solid–liquid separation (left side) and solid–liquid–liquid separation (right side).

from the cylindrical to the conical part of the bowl the solids leave the liquid level ("beach") and thus some liquid is able to drain back to the pond. In decanter centrifuges the separation can be greatly improved by agglomeration of the particles to be separated, because they can then settle with comparatively low stress. By adaptations to their structure, decanter centrifuges can be used very flexibly for three-phase separation, extraction, sorting and, partly, for classifying (Anlauf, 2007b). Decanter centrifuges can reach centrifugal values C up to about 5000 and are built with drum diameters of up to 1800 mm.

If the decanter centrifuge represents the translation of the gravity settling basin into the centrifugal field, then the principle of the disc stack separator represented in Fig. 2.12 corresponds to the gravity lamella clarifier. The clarification area is increased remarkably in this centrifuge by a plate package. The suspension, supplied centrally by a feed pipe, flows, in the case of solid–liquid separation (Fig. 2.12, left side) from the outer radius through the plate package to the inner radius of the centrifuge, where the clarified liquid is discharged. The solid particles settle to the outer radius of the double conical drum and are collected there. The consolidated, though still flowable, sludge is discharged from there, depending on its amount, either by permanently open or periodically opened nozzles. If, besides a solid material, a second liquid has to be separated (Fig. 2.12, right side), then the plate package has some rising channels which are distributed equally on the circumference. Their radial position corresponds to the volume ratio of the two liquids to be separated. The supplied suspension penetrates into the rising channels and the lighter liquid is led inwards. The heavier liquid and the solids move outwards. Light and heavy liquid are discharged from separate openings. Disc stack separators can realize centrifugal values C of up to 15 000. Due to the large clarification area in connection with high centrifugal values, a disc stack separator can replace gravity clarification surfaces of

up to 300 000 m^2 on a very small foot print area and separate even very small particles of less than 1 μm. Disc stack separators are often used in the biotechnological and pharmaceutical sector to separate not only very small but also very sensitive particles. Modern disc stack separators are equipped with special suspension feeding and solids discharge systems for gentle particle treatment. The suspension is not added to the surface of the fast rotating liquid in the centrifuge but directly into the liquid in order to realize a smooth acceleration. The solids are discharged through self-regulating nozzles near the axis of rotation to avoid the high pressures, up to 20 MPa, for nozzle discharge at the outer periphery. The self-regulation of the nozzles can, furthermore, compensate changing feed conditions and guarantee constant separation results (Anlauf, 2007b).

2.3 Filtration

2.3.1 Cake Filtration

During cake filtration the particles are separated on the surface of a porous filter medium, as shown in Fig. 2.13. The liquid flows as filtrate through the pores of the cake and the filter medium. Particles and liquid move due to a pressure difference ΔP between the absolute pressure at the suspension surface P_1 and the pressure underneath the filter medium P_2 ($P_1 > P_2$) in the same direction. This pressure difference can be generated pneumatically, hydraulically, mechanically or by a centrifugal field. In order to avoid blockage of the filter medium, its pores are usually chosen so large that for a very short time, at the very first moment of filtration, single particles are able to escape into the filtrate before particle bridges can form

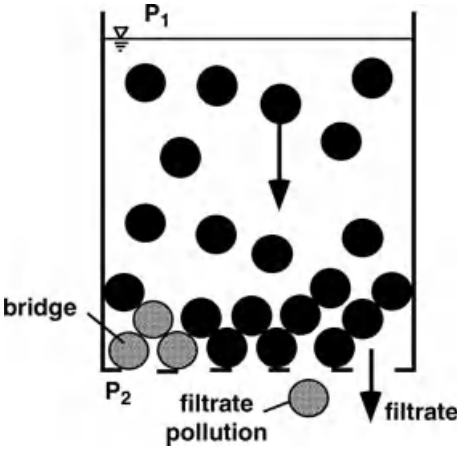

Fig. 2.13 Principle of cake filtration.

across the meshes and seal them. On top of these bridges, the filter cake then grows up without further filtrate pollution. Cake filtration processes are applied for moderately to highly concentrated suspensions within the particle size range 1 to 1000 µm. Smaller particles cannot be separated reasonably by cake filtration due to extremely high pressure losses. However, the range of application for cake filtration processes can be shifted, by particle agglomeration, to even smaller particles (see Section 2.6.3). Larger particles separate spontaneously by gravity on screens and are dehumidified on a dump.

The calculation of filtration processes is generally based on the law of Darcy, which describes laminar flow of liquids through porous layers:

$$v = \frac{\Delta P}{\alpha \cdot H \cdot \mu_l} \tag{2.4}$$

The superficial flow velocity v (empty pipe) depends on the effective pressure difference ΔP, the layer thickness dependent specific flow resistance α, the layer thickness H itself, and the dynamic viscosity of the liquid μ_l. This generally formulated law has to be adapted and modified for the special conditions of each filtration process. In this way the law of Darcy can also be adapted to the conditions of compressible gases, two-phase flow of liquid and gas during cake desaturation, and liquid permeation during cake washing. During the cake formation period the porous filter medium and the increasing filter cake are permeated by the liquid. From the law of Darcy the time t necessary to form a certain cake height H can be derived from:

$$t = \frac{H^2 \cdot \alpha \cdot \mu_l}{2 \cdot \kappa \cdot \Delta P} + \frac{H \cdot \beta \cdot \mu_l}{\kappa \cdot \Delta P} \tag{2.5}$$

Here, the flow resistance of the filter medium β is taken into consideration. The concentration parameter κ is calculated from the solids volume concentration of the suspension c_V and the cake porosity ε:

$$\kappa = \frac{c_V}{1-\varepsilon-c_V} \tag{2.6}$$

Cake and cloth resistance have to be determined experimentally. An appropriate measuring regulation is described in the VDI guideline No. 2762. After the step of filter cake formation, follows, if necessary, a cake washing procedure, in order to remove soluble components of the suspension liquid from the filter cake. For this purpose the filter cake is either resuspended in washing liquid and filtered again, or is permeated by the washing liquid (see Section 2.1). After the washing, or directly after the formation, follows a mechanical dehumidification of the filter cake. As can be seen in Fig. 2.14, two principally different possibilities of cake dehumidification can be distinguished. These are desaturation (Fig. 2.14a) and squeezing (Fig. 2.14b). For particles with diameters of more than about 10 µm, or if particle adhesion forces do not matter, nearly incompressible filter cake structures are formed. In this case the pore liquid can be displaced by gas (Fig. 2.14a). Capillary forces, which hold the liquid back in the pores of the cake, result from the interface between liquid and gas. If, in

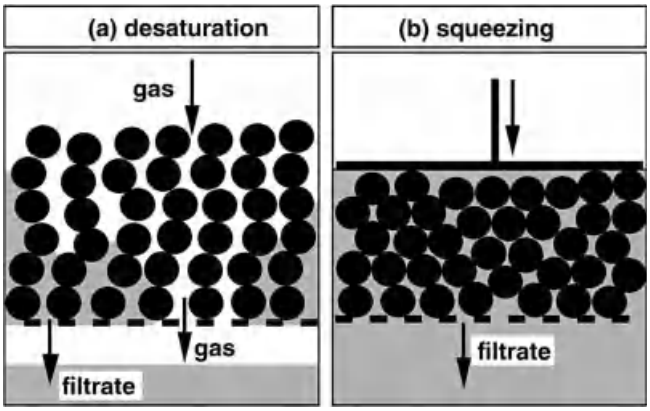

Fig. 2.14 Mechanisms of filter cake dehumidification: (a) desaturation, (b) squeezing.

the case of pneumatic dehumidification, the external pressure difference is larger than the capillary pressure, gas penetrates into the pores and displaces liquid until a pressure equilibrium is reached. The filter cake becomes desaturated and a two-phase flow of gas and liquid develops. At the contact points of the particles, on their surfaces, and in eventually existing inner pores, some liquid remains, which cannot be further removed mechanically. The capillary pressure P_c of a circular pore depends on the surface tension of the liquid σ_l and on the radius of interface curvature R_{surf}, which is correlated with the wetting angle δ and the capillary radius r, as can be seen in Fig. 2.15. The force balance at the interface can be formulated by the Laplace equation:

$$P_c = \frac{2 \cdot \sigma_l \cdot \cos \delta}{r} \tag{2.7}$$

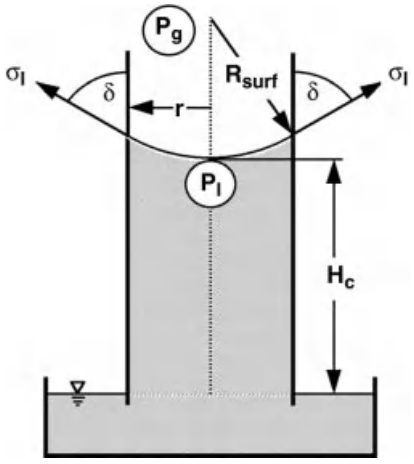

Fig. 2.15 Capillary pressure in a circular pore.

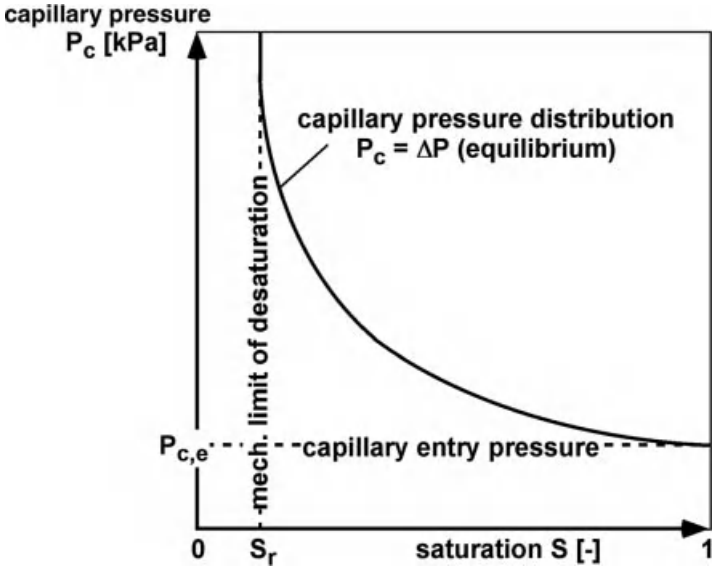

Fig. 2.16 Capillary pressure curve.

In the equilibrium state the liquid rises up to the capillary height H_c. The distribution of pore sizes in a filter cake entails a capillary pressure distribution. This is characterized by the capillary pressure curve shown in Fig. 2.16.

The capillary pressure curve has to be determined experimentally and provides information on what minimum saturation degree S appears in the filter cake for the applied pressure difference ΔP. The saturation degree S is defined as the ratio of liquid volume V_l and void volume V_v in the filter cake:

$$S = \frac{V_l}{V_v} \tag{2.8}$$

The capillary pressure curve is limited from below by the capillary entry pressure $P_{c,e}$, which must be at least overcome to initiate desaturation. The mechanical limit of desaturation S_r cannot be exceeded with any increase in the pressure difference. If, in particular with small particles with diameters of less than about 10 µm, adhesion forces act between the particles, a noticeably compressible filter cake structure is formed. In this case the cake can be squeezed (Fig. 2.14a). Thus liquid from the pores of the filter cake is displaced, although the cake remains completely saturated. The pressure for cake consolidation can be generated:

- hydraulically by pressing additional suspension into a filter chamber already filled with cake,
- mechanically by a diaphragm or a piston, or by
- mass forces in a centrifugal field.

The cake filtration processes can be distinguished systematically according to the kind of filtration pressure.

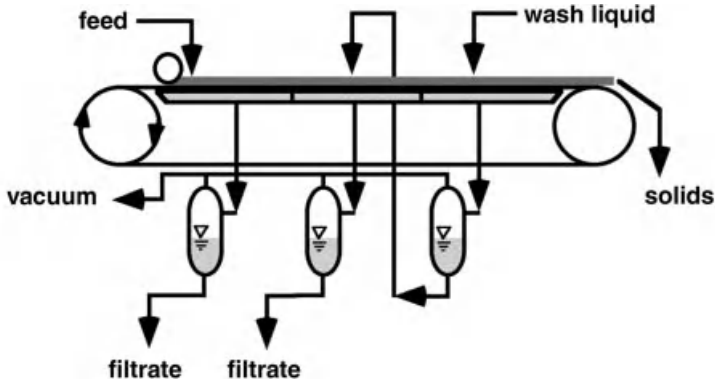

Fig. 2.17 Vacuum belt filter.

Gas differential pressure can be generated both by creation of a vacuum behind the filter medium, or by application of an overpressure above the suspension. While vacuum filters are limited by the vapor pressure of the liquid to pressure differences below 0.1 MPa, gas overpressure can be chosen freely within technically reasonable limits. The technical upper limit for encased gas overpressure filters is about 1 MPa. The pressure difference usually remains constant during filtration. Modern vacuum filters are built only for the continuous mode of operation. Discontinuous vacuum filters, like the Buchner-funnel, are used only in the laboratory. Drum filters, disc filters, belt filters and pan filters are the main types of continuous vacuum filters used in industry.

Figure 2.17 shows a vacuum belt filter. This type of filter is particularly well suited for filter cake washing, however, it needs comparatively large floor space for installation.

Drum and disc filters are not only used as vacuum filters but also as encased overpressure filters (hyperbar filters). Figure 2.18 shows a disc filter installed

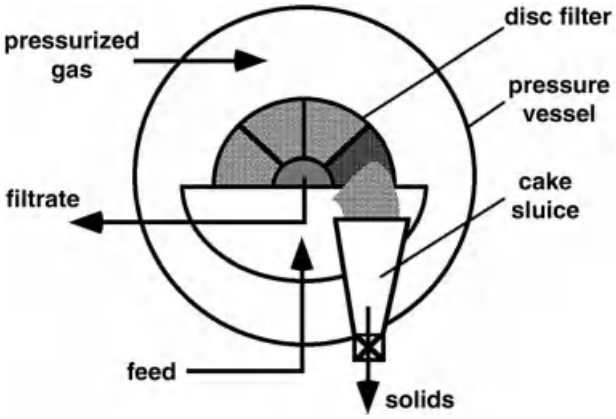

Fig. 2.18 Hyperbar disc filter.

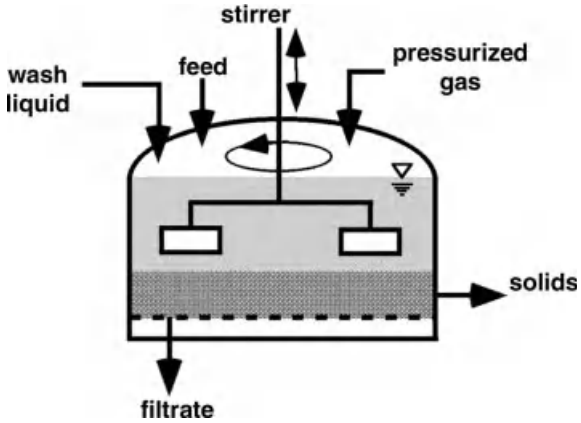

Fig. 2.19 Stirred pressure nutsch filter.

completely in a pressure vessel. The filter disc of modern filters consists of up to 40 segments, which filter on both sides. The slender segment shape leads to a very homogeneous filter cake. On the central filter shaft several filter discs can be mounted, one behind the other, to increase the capacity of the filter unit. In this way up to 200 m^2 of filter area can be installed in one pressure vessel. The special advantage of disc filters is their high capacity, whereby drum filters are exceptionally flexible in adjusting to different slurry and cake behavior.

In a drum filter, rectangular filter cells are arranged axially on the surface of the horizontally mounted filter drum. To react to different cake consistencies various possibilities for a safe cake discharge are available. This is unique for drum filters.

Pan filters are used for the fast settling of coarse particles and correspond in their construction to a 90-degree turned and horizontally arranged disc filter with one single disc.

In contrast to vacuum filtration, overpressure filters are operated continuously and batchwise. The stirred pressure nutsch filter, represented in Fig. 2.19, is an example of a batchwise operating, gas overpressure filter for the separation of relatively easy to filter suspensions. This apparatus, with filter areas up to 15 m^2, is very easily adaptable to changing product properties. Thus it is used frequently in pharmacy or fine chemistry for small product quantities of often varying compositions. The stirred pressure nutsch filter provides a relatively small filter area in relation to the process space. For relatively hard to filter suspensions several filter discs, cylindrical filter candles, flat rectangular filter leafs or filter bags are installed in the pressure vessel to increase the active filter area.

Alternatively to the gas differential pressure, mass forces can also be used for filtration. For coarse particles with diameters of more than 1 mm the force of gravity is used. Such particles are separated by bended or vibrating screens. With vibrating screens *C*-values of even 5 can be realized. Further dehumidifying then usually takes place via drainage in the earth's field. In order to obtain larger accelerations,

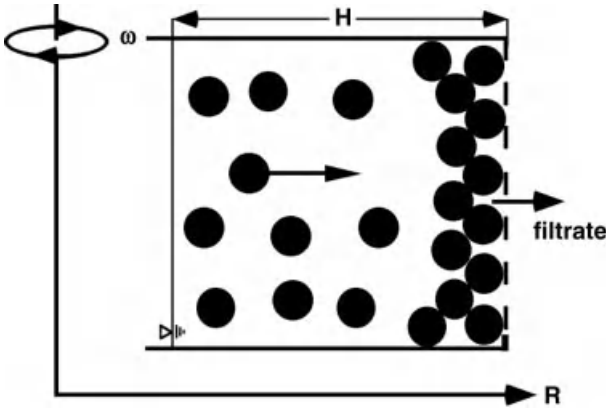

Fig. 2.20 Principle of centrifugal cake filtration.

centrifuges have to be used. Figure 2.20 clarifies the principle. The centrifugal pressure can be calculated as the hydrostatic pressure difference ΔP of a liquid column of height H in the centrifugal field:

$$\Delta P = \varrho_l \cdot g \cdot C \cdot H = \varrho_l \cdot R \cdot \omega^2 \cdot H \tag{2.9}$$

The centrifugal pressure changes with the height H of the liquid layer in the centrifuge bowl. This is a remarkable difference in comparison to the gas differential pressure, which can be held constant.

As in the case of gas overpressure filters, centrifugal pressures up to 1 MPa are realized technically. Due to the fast settling of particles in the centrifugal field, filter cakes in centrifuges are mostly formed by quick sedimentation, and subsequent drainage of the clear liquid layer above the sediment. During desaturation a moisture gradient appears along the cake height, because the centrifugal pressure becomes smaller and smaller in the emptying pores. The capillary pressure in a pore of constant diameter remains constant. If both pressures become equal in the equilibrium state, a capillary liquid height H_c remains in the cake, which cannot be further removed with a constant rotational speed of the centrifuge:

$$H_c = \frac{P_c}{\varrho_l \cdot g \cdot C} = \frac{2 \cdot \sigma_l \cdot \cos \delta}{r \cdot \varrho_l \cdot g \cdot C} \tag{2.10}$$

A large number of discontinuously and continuously operating machines are available for centrifugal filtration. To the family of discontinuous filter centrifuges belong, mainly, the horizontal and vertical peeler centrifuges, the inverting filter centrifuge and centrifuge dryers (see Section 2.5). Discontinuous filter centrifuges can realize centrifugal pressures of up to 1 MPa and are built with drum diameters of up to 1500 mm.

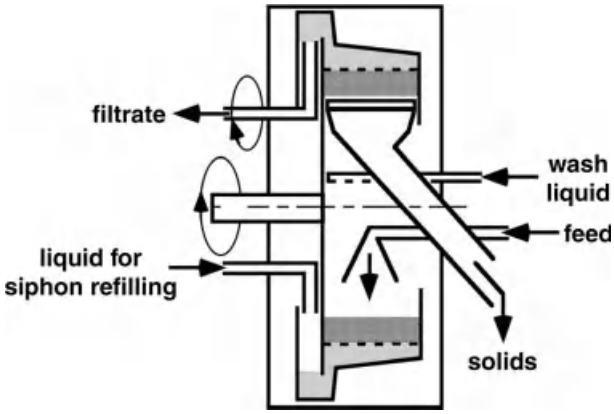

Fig. 2.21 Horizontal siphon peeler centrifuge.

As an example of these centrifuges a horizontal siphon peeler centrifuge is represented in Fig. 2.21. The suspension to be separated is supplied to the continuously rotating filter drum. After cake formation the filter cake can be washed and then desaturated. Finally, the filter cake is removed from the rotating drum by an advancing knife. Inevitably, a thin product layer remains on the filter cloth. This heel must be removed or regenerated periodically. While with conventional peeler centrifuges the filtrate goes directly into the housing and is removed from there by a fixed pipe, in the case of a siphon peeler centrifuge it is collected in a solid filtrate collecting room and then removed from a ring cup by a pivoting pipe. This has two advantages. If a part of the previously produced filtrate is returned again into the ring cup, the filter cloth can be cleaned by back-flushing and the clogged heel becomes resuspended. If, with the next load, the pivoting pipe is immersed below the level of the filter medium into the ring cup, the liquid column behind the filter medium generates a vacuum, which gives additional support to the filtration process.

In contrast to the peeler centrifuge, a heel can be avoided totally in the inverting filter centrifuge, where the filter medium for cake discharge is pushed axially out of the centrifuge drum by a special installation. The filter cloth is turned and the solids are detached completely.

In a centrifuge dryer thermal drying by hot gas follows the mechanical dehumidification, so that dry powder is finally produced (see Section 2.5).

In continuously operating filter centrifuges the separated solids are transported axially along the filter medium to the open end of the rotating perforated drum. To realize safe transport for a sufficient life-time, wear-resistant metallic wedge wire screens are necessary. In these centrifuges the residence time of the product in the process room amounts to less than 1 min for filtration pressures of about 0.1 MPa. Therefore, these centrifuges are used for large quantities of easy to filter and highly concentrated suspensions. The particle diameters are usually above 100 μm. Sliding discharge centrifuges and vibrating screen centrifuges possess a conical rotor and, as a result of the centrifugal force, the solids slide towards the greater drum diameter

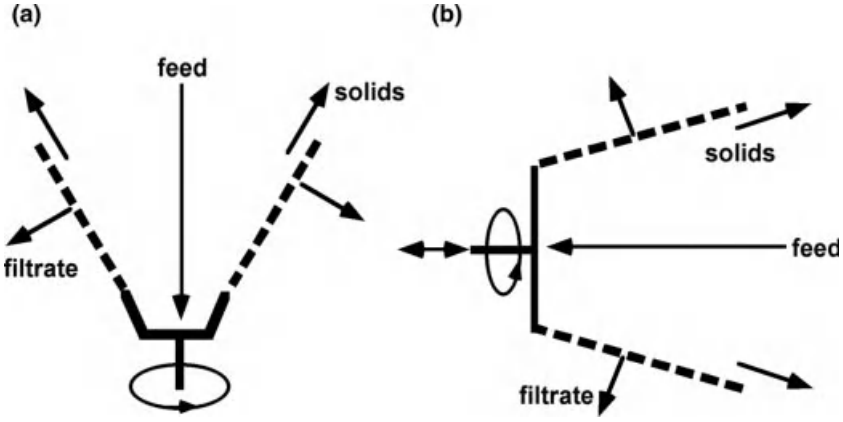

Fig. 2.22 Principle of (a) sliding discharge centrifuge and (b) vibrating screen centrifuge.

and its open end. For better traction control of the solids, the static friction between the product and the drum can be overcome in vibrating screen centrifuges by an overlay of drum rotation and axial oscillation. In Fig. 2.22 the principle of these centrifuges is outlined.

Worm screen centrifuges possess a screw similar to the decanter centrifuge. Pusher centrifuges are equipped with an axially oscillating pusher plate for discharging the filter cake. In Fig. 2.23 the principle of these centrifuges is sketched.

Continuously operating filter centrifuges are often combined with settling basins to guarantee enough concentrated feed for a safe function. The filtrate of these machines contains, in many cases, too many particles and is returned to the thickening device (see Section 2.6.2).

Continuous filter centrifuges can also be equipped with an internal machine part in which the slurry is pre-thickened by pure sedimentation. The screen bowl decanter centrifuge is an example of such machines.

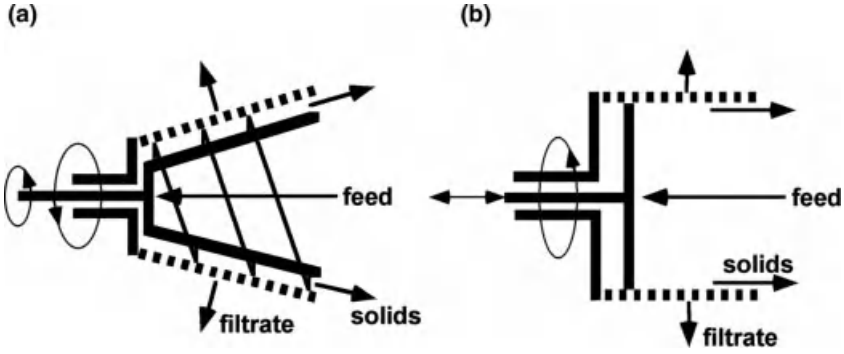

Fig. 2.23 Principle of (a) worm screen centrifuge and (b) pusher centrifuge.

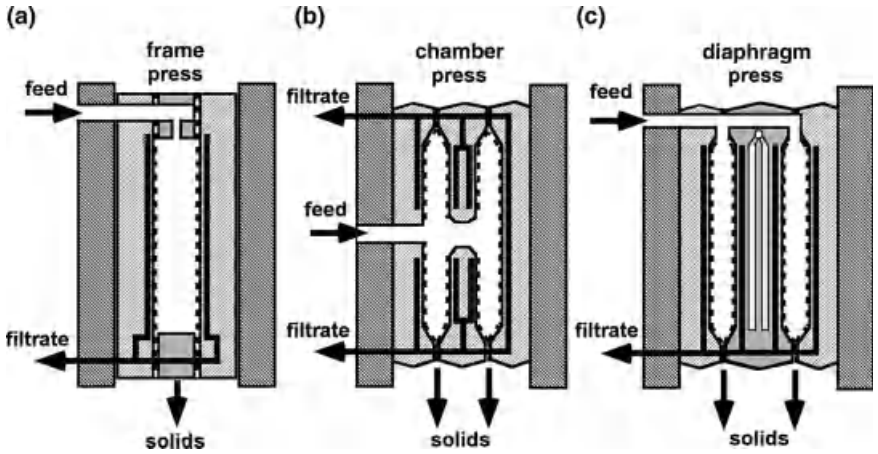

Fig. 2.24 (a) Frame, (b) chamber and (c) diaphragm filter press.

Last but not least, a hydraulic or mechanical pressure can be utilized for press filtration of suspensions that form a compressible filter cake. Depending on the flow resistance of the developing filter cakes, maximal filtration pressures of approximately 10 MPa are used in the relatively rare case of discontinuous piston and tube presses. Up to 2 MPa are used for discontinuous frame, chamber and diaphragm presses, and the relatively low pressure of about 0.1 MPa is applied to continuous screw and belt presses.

One of the most frequently used filter apparatuses for relatively difficult to separate suspensions is the discontinuous separate press. Figure 2.24 illustrates the three basic constructions of these apparatuses.

In the case of the historically oldest frame presses, the filter chamber is formed by a frame between two flat filter plates. The filter plates are covered on both sides with a filter cloth. This applies to all types of filter presses. The filter chambers of a chamber filter press are formed by the geometry of the filter plates themselves. While the filter cake in frame and chamber filter presses is consolidated hydraulically by additional pressing of suspension into the already cake-filled chambers, the filter cake in modern diaphragm filter presses can be squeezed mechanically by means of a flat diaphragm. This squeeze is very efficient and homogeneous. In all filter presses the filter plates must be pressed together by hydraulic or mechanical means in order to avoid leakages. For cake discharge, the plates are separated from each other and the cake is removed downwards from the chambers. The cake discharge turns out to be most difficult in the case of frame presses, because the cake sticks in the frame. In chamber and diaphragm presses gravity helps, but an additional mechanical support is often necessary to detach the cake from the filter cloth. The latest developments are fully automated diaphragm filter presses with horizontally arranged filter plates. The automated cake discharge is guaranteed here by an endless filter belt around all the plates, which can be moved. The moving filter belt transports the cake out of the filter chamber and detaches the solids by a sharp change of direction.

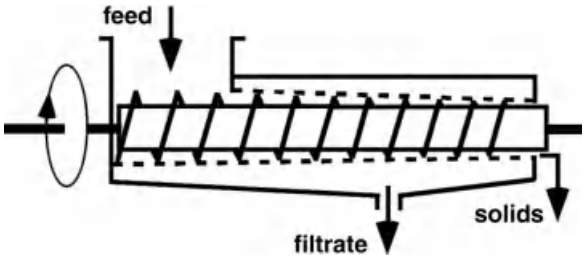

Fig. 2.25 Screw press.

Continuously operating press filters are built mainly as screw or belt presses and are used for relatively easily filtrable fiber suspensions or for strongly flocculated suspensions.

In Fig. 2.25 the principle of a screw press is depicted. The suspension to be separated is supplied to a transport and press screw, which is slowly rotating in a sieve basket. Metallic wedge wire screens are used as the filter medium. The diameter of the conical sieve basket and the distance between the screw blades decrease in the transport direction.Thus, the volume available for the solids is reduced continuously and they are squeezed. The filtrate penetrates the filter medium, gets into the housing of the screw press and is led away from there. The squeezed and dewatered solids are discharged from the sieve basket at the end of the press channel. The screen has to be cleaned periodically from outside by means of a strong water spray to avoid pore blockage.

In contrast to the screw press, Fig. 2.26 shows a double belt press filter. The suspension is fed continuously between two filter belts and is squeezed by press rollers. The smaller the roller diameter, the greater the squeezing pressure. Due to the enlacement of the rollers by the filter belts, the cake is not only pressed uniaxially but also sheared. This leads to a further cake consolidation and, therefore, to lower residual cake moisture.

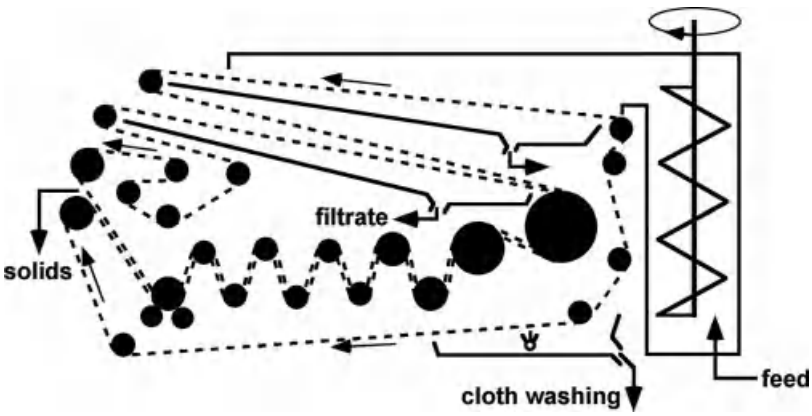

Fig. 2.26 Double belt press filter.

According to the described variety of apparatuses for cake filtration, very different demands are made on the filter media. From filter fabrics with various weave construction, fleeces and felts, porous sinter materials and metallic wedge wire screens to microporous membranes, very different filter media are used (Purchas, 1996). The filter medium represents the interface between the filter apparatus and the suspension. Only with the right adjustment between filter medium, filter apparatus, operating conditions, and suspension properties can a separation process be realized successfully (Anlauf, 2004). The application of recently developed new microporous membrane filter media can lead, in the case of vacuum filtration, to perfect particle retention and, in addition, to avoidance of the undesired gas flow during desaturation of the filter cake. If the capillary pressure in the pores of the filter medium is larger than in the pores of the filter cake, the cake can be desaturated by means of a gas differential pressure, however, the gas cannot penetrate into the fully saturated pores of the filter medium. A semipermeable behavior of the filter medium with respect to liquid and gas is generated. This could save energy for the operation of the vacuum pump (Anlauf, 2008).

2.3.2
Sieving and Blocking Filtration

If liquids do not contain particles with diameters of more than about 5 μm and these particles are present only in very low concentration, surface filters, such as sieve or blocking filters are applied. As "police filters" they protect, for example, hydrocyclones or disc stack separators (see Section 2.2.2) against oversized particles which could block the solids discharge nozzles. In water or oil cycles impurities, such as rust particles or particles from abrasion in a motor or gearing, are removed from the liquid by sieve filters. Each separated particle blocks one pore of the screen and the pressure loss of the filter rises with time. As soon as it exceeds a critical value, the filter must be regenerated. This takes place mechanically via rotating brushes or other devices or via back-flushing with its own or external liquid. The filter media can be sieve fabrics or wedge wire screens.

Figure 2.27 shows, as an example of this filter family, the principle of a quasi-continuously operating back-flushing sieve filter in the filtration and back-flushing period. The liquid to be purified enters the lower part of the filter housing with pressure P_1 and flows into several parallel and circularly arranged filter candles. The filtrate passes the filter medium, flows into the upper part of the filter housing and is discharged from there with pressure P_2. Due to the low pressure loss of the sieve filter P_2 is only slightly lower than P_1. The absolute pressure inside the filter is about 100 to 200 kPa higher than the atmospheric pressure P_3 outside the filter. If a filter candle is blocked on the inner surface by particles a back-flushing tube is moved under the candle. This tube connects the filtrate space with pressure P_2 and the atmospheric pressure P_3. Now the filtrate flows from outside inwards into the candle and washes away the separated particles from the filter surface. After the end of a very short cleaning period the back-flushing tube moves to the next blocked candle.

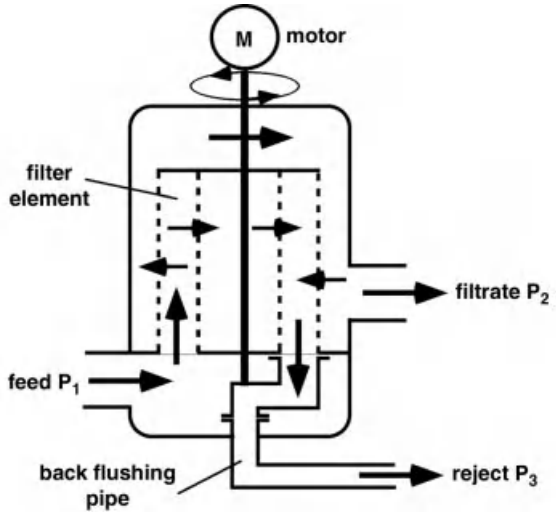

Fig. 2.27 Back-flushing filter.

2.3.3
Crossflow Micro- and Ultra-Filtration

The crossflow filtration depicted in Fig. 2.28 is a basic modification of surface filtration. Microporous membranes are normally used as filter media. Crossflow filtration is used, in particular, for the separation of very small particles of less than 1 μm diameter, colloids and dissolved macromolecules. Especially, the mechanical separation of large molecules in solution represents direct competition for thermal evaporation. In the case of solid particles, the crossflow filtration competes with high speed centrifuges like disc stack separators or tube centrifuges (see Section 2.2.2) and depth or precoat filtration processes (see Section 2.3.4). Compared with depth or precoat filtration and non-regenerable filter layers, crossflow filtration is characterized by the separation of the particles in a pure form. Crossflow filtration is also called shear stress, dynamic or delayed cake filtration. The solids (concentrate) as well as the liquid (permeate) can represent the required product. The suspension to be separated is pumped under pressure through the filter module. The liquid permeates the filter medium and is discharged as permeate. Particles try to follow the liquid and to build

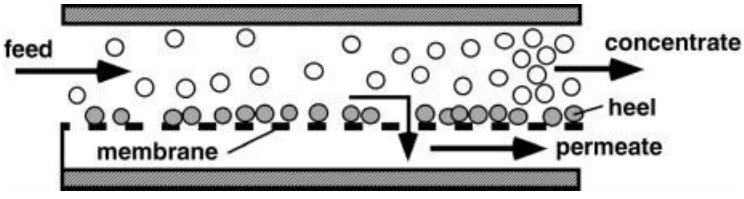

Fig. 2.28 Principle of crossflow filtration.

up a cake on the filter medium. However, during the flow of the suspension tangentially to the filter medium, particles are removed from the membrane surface, mainly by shear forces, and are consecutively concentrated. Only a very thin layer remains on the surface of the membrane. In this manner the transmembrane pressure loss can be kept low and the filter can be operated for a longer time. With declining filtrate flow, due to successive blockage or fouling of membrane pores and/or to increasing heel, the filter system must be periodically regenerated. This is done by back-flushing and/or various washing procedures. There are also attempts to prevent a heel by creation of an electrical field across the feed/concentrate channel to generate electrical repulsion of the charged particles from the filter medium (see Section 2.6.3). Concentration of the suspension or solution takes place along the direction of flow, and is maximal near to the outlet. Thus a crossflow filter is suitable for the concentration of suspensions or solutions over a broad spectrum of possible degrees of enrichment. With shear thinning or thixotropic flow behavior the concentrate can be kept flowable by the creation of high shear rates, despite high thickening at the discharge valve of the filter apparatus. In such cases the sludge may solidify, after discharge, to a semirigid mass. The principle of crossflow filtration is often limited by too high levels of moisture content in the concentrate. In some cases an irreversible blockage of the filter medium will appear after some time, despite regeneration measures.

In discontinuous operation liquid is withdrawn from the suspension by permanent filtration and the concentrate is recycled until the target concentration is reached. In the batch feed mode concentrate is also fed back, but fresh suspension is added to the filtrate until the total volume of the feed vessel has reached the final concentration. In fully continuous operation no concentrate recycling takes place, so that the target concentration can be achieved, usually, only by connecting several filter modules in series. Dia-filtration is a procedure of dilution washing in which substances dissolved in the suspension are rinsed through the filter medium. Similarly to the batch feed procedure, the concentrate is recycled, but it is topped up again with fresh wash liquid, not with suspension. Dia-filtration can be operated very effectively by counter-current flow of the wash liquid in continous mode and a series arrangement of modules (see Section 2.6.2).

The shear flow to prevent the particles from becoming deposited on the filter medium can be increased in dynamic filters by rotor/stator or rotor/rotor systems. Figure 2.29 depicts this for the example of overlapping counter-rotating filter discs.

Furthermore, the filter module can be mounted on a torsion rod and be oscillated at up to 50 Hz. Figure 2.30 summarizes all three possibilities of creating relative motion between the suspension and the filter medium.

Because of the extremely small particle diameters, microporous membranes are used as filter media for crossflow filtration processes. Such membranes can be manufactured in tubular shape for pipe or capillary modules, or in flat form for cushion, spiral or sheet modules. Various polymers, ceramics, glass and other materials can be employed for the membrane production. In crossflow processes one distinguishes, according to the particle sizes to be separated, between microfiltration with feed pressures of about 0.1 MPa and ultrafiltration with feed pressures of about 1.0 MPa. The pore diameters of membranes for microfiltration lie in the

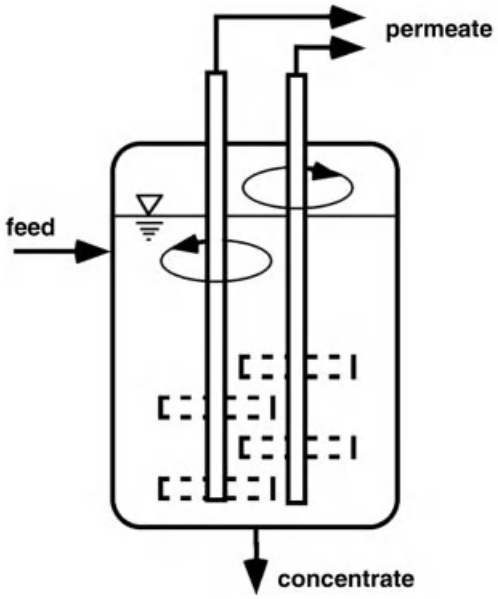

Fig. 2.29 Dynamic crossflow filter.

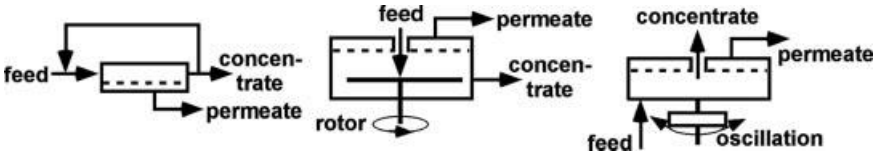

Fig. 2.30 Modifications for crossflow generation.

range 1.0–0.05 μm. Membranes for ultrafiltration are still porous membranes with convective mass flow, but with very small pore sizes, in the range 0.1–0.005 μm. They are, therefore, often denoted as molecular sieves. Purely diffusive mass transfer takes place when using poreless membrane structures for processes like reverse osmosis, which is used, for example, to desalinate seawater.

2.3.4
Depth and Precoat Filtration

Depth filtration is used when slightly turbid liquids have to be clarified. The liquid is usually the required product. The solids concentration here totals some g m^{-3} or less, and the particle diameters are below 1 μm. As shown in Fig. 2.31, the particles present in the suspension are separated inside a three-dimensional, highly permeable porous filter layer. Figure 2.31 shows the standard case of depth filtration, where a porous filter layer is permeated by the liquid to be purified. The filter cycle has to be shut down as soon as the capacity limit of the filter layer is reached. This capacity limit is

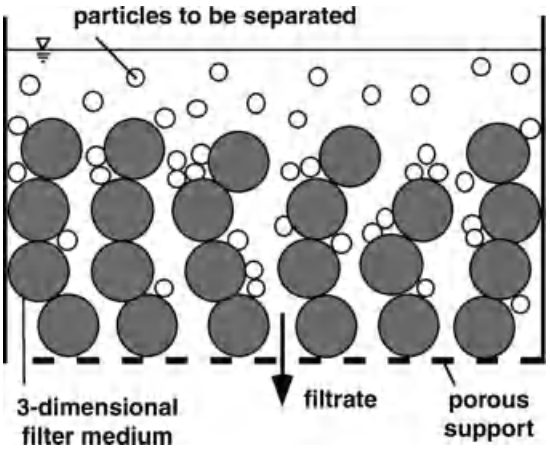

Fig. 2.31 Principle of depth filtration.

reached when either the pressure loss of the flow exceeds a critical value or the turbidity of the filtrate reaches an unacceptable level. The solids concentration in the filter feed may not exceed a critical maximum value, in order to avoid blockage of the filter surface. Such blocking appears when, in the case of high concentrations, several particles try to enter a filter pore at the same time and hinder each other, or when pores are gradually blocked by separated particles. In the case of cake filtration (see Section 2.3.1) this bridge formation by particles is necessary to initiate the cake formation. In depth filtration, however, such particle bridging would prevent following particles from penetrating into the filter layer and lead to failure of the process due to a drastic rise in flow resistance. Particle separation in depth filters requires a transport mechanism that brings the particles to the surface of the filter medium (collector) and an adhesion mechanism that holds the particles on the collector. The mechanisms of particle separation inside the filter layer are very complex, as can be seen in Fig. 2.32 for three essential examples of particle transport.

Case (a) is called "interception". The particle follows a streamline of the liquid and touches the collector compulsorily due to its physical dimension. Case (b) describes the "inertia effect", if a particle due to its mass cannot follow the streamline around the collector and settles on its surface. Finally, case (c) represents the "diffusion effect". This is relevant for very small particles, which are subject to diffusion and come into contact with the collector by stochastic movement. A further mechanical dehumidification of the separated solids is not possible in depth filtration processes. The separated solids are either removed, more or less efficiently, by back-flushing of the filter layer with a small part of the previously clarified liquid, or they are discharged together with the filter layer from the filter apparatus. One distinguishes between different depth filtration process variants in

- packed bed filters,
- cartridge and sheet filters or
- discontinuous and quasi-continuous precoat filters.

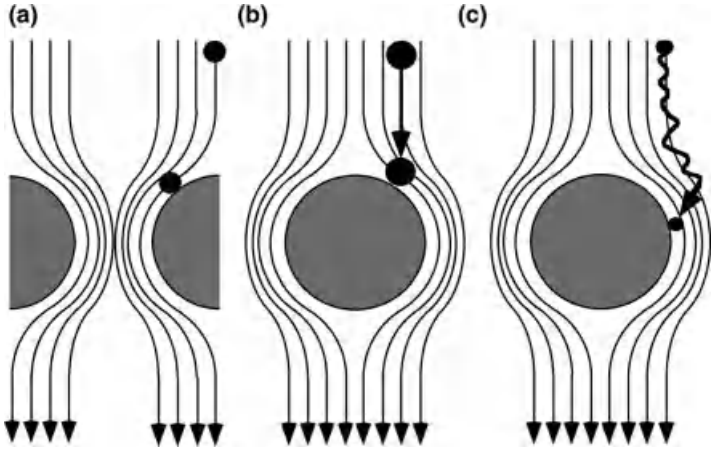

Fig. 2.32 Mechanisms of particle deposition in depth filters: (a) interception, (b) inertia and (c) diffusion.

The packed bed filters consist of discrete particle layers, which are regenerated after the filtration by back-flushing, or must be exchanged. This type of filter is used very frequently in water purification (Gimbel *et al.*, 2006). Gravel, sand, diatomaceous earth, perlite, filter coke, activated charcoal or others are used as the filter material. Materials like activated charcoal or ion-exchange resins are able, in addition to the purely mechanical separation of particles, to bind dissolved substances by adsorption. Figure 2.33 shows, as an example, a capsulated packed bed filter during filtration and back-flushing. Here an optimized two-layer filter is depicted. A coarse-grained coke layer is located on top of a fine-grained sand layer. Thus, the pores of the filter decrease in size from top to bottom, and the total capacity of the filter is increased in

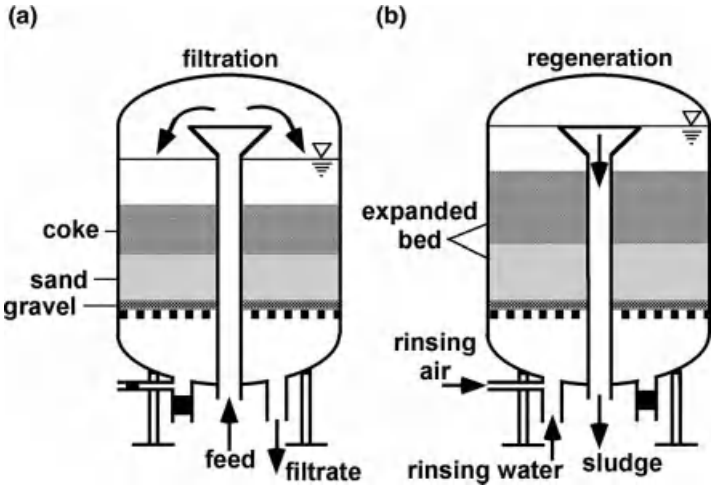

Fig. 2.33 Packed bed filter in (a) filtration mode and (b) back-flushing mode.

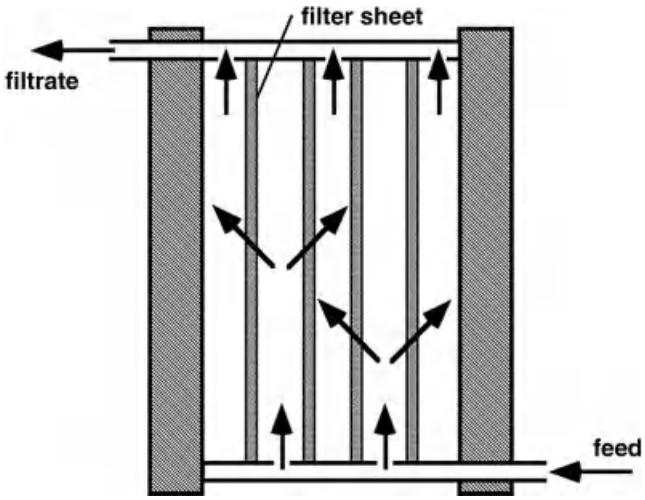

Fig. 2.34 Sheet filter.

comparison to a monolayer filter. To avoid a mixture of coarse and fine particles during back-flushing, the upper coarse particle fraction (coke) must have lower specific weight than the lower fine particle fraction (sand).

Cylindrical non-pleated or pleated cartridge filters or flat-shaped sheet filters use prefabricated filter media, which are, as a rule, not regenerable, and must be exchanged after reaching their limit of capacity. In the case of cartridge filters, yarn wound candles, sintered or resin-bound porous layers are normally used. Flat filter sheets are mostly composed of fibers (cellulose) to form a structure and particles (diatomaceous earth) for separation, which are mixed and bound together by resins. Recently, filter layers from pure cellulose have also been produced. The specific surface area of the cellulose fibers, and thus the separation capability, is increased by a special defibration process, which is called "fibrillation". Cartridge and sheet filters are applied for very different types of tasks and a very broad product spectrum.

A sheet filter with rectangular sheets is shown in Fig. 2.34. The apparatus is designed similarly to a frame filter press and consists of a package of filter plates and frames. The suspension is pumped into several filter chambers arranged in parallel. The liquid penetrates the filter media and is discharged as clarified filtrate through the filtrate channel. The particles are separated inside the porous filter sheet structure. As soon as the particle storage capacity of the sheets runs out, they must be replaced by new ones.

A further variant of depth filtration can be realized on many different apparatuses for cake filtration, such as discontinuous candle or leaf filters (see Section 2.3.1). Here, an auxiliary porous particle layer, which serves as a depth filter, is formed as a cake on a filter medium before the actual product filtration can take place. This kind of filtration is called precoat filtration. After reaching the limit of dirt-holding capacity the entire precoat layer is discharged and the cycle starts again forming a new precoat layer.

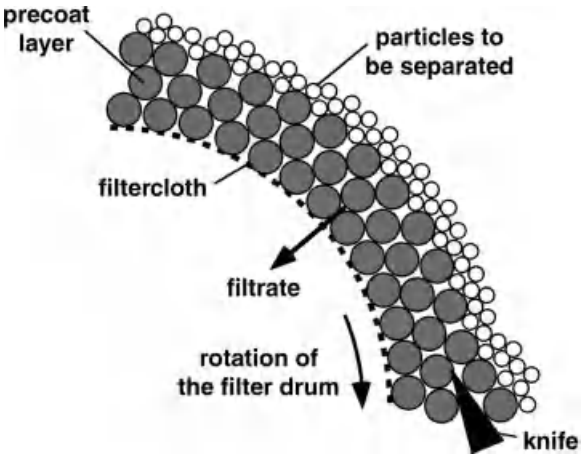

Fig. 2.35 Principle of particle discharge from precoat drum filters.

The precoat filtration on continuous vacuum drum filters offers the possibility of peeling off a very thin layer from the surface of the precoat, which is clogged by separated particles after one drum revolution. Thus a fresh and clean precoat surface is again immersed into the suspension in the filter trough. This allows the filtration of very small, highly concentrated particles, providing a transition from depth to cake filtration. Many applications for this technique can be found in the purification of beverages or the production of baker's yeast. Both the liquid and the solids can represent the required product.

Figure 2.35 demonstrates the principle of particle discharge from a continuous precoat drum filter. In a first working step a filter aid layer of several centimeters thickness ($H_c \approx 10$ cm) is built up on the drum covered with a well suited filter fabric. In the second working step the suspension to be clarified is filtered. The particles are separated in the uppermost layers of the precoat material and a very thin filter cake ($H_c < 1$ mm) is formed on top of the clogged precoat surface. Then the layer containing the separated particles is scraped off continuously by a sharp knife and fresh precoat surface is immersed again into the suspension. Most modern precoat drum filters have a knife feed motion of 50 to 100 μm per drum revolution. It is, thus, possible to filter continuously for several hours, without interruption to build up a new precoat layer.

In a special variant of precoat filtration, called "body feed filtration", the filter aid is mixed directly with the suspension to be clarified, as shown in Fig. 2.36. The particles of the filter aid form a framework into which the target particles are incorporated. Precoat filtration is often combined with body feed filtration in order to improve the filtration characteristics of the suspension, and thus to increase the service life of the precoat layer. Filter aids for precoat filtration are either of mineral or organic origin. Diatomaceous earth, perlite, coke, and starch, among others are used as particulate materials. Depending upon the requirements of the process, various fibrous materials, such as wood flour, extract-free cellulose, or ultrapure cellulose can be applied.

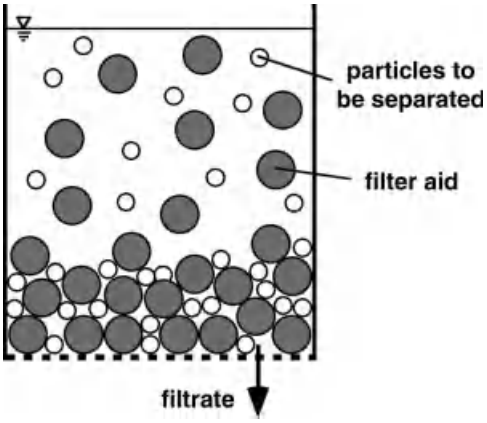

Fig. 2.36 Principle of body feed filtration.

In the selection of a suitable filter aid, acquisition and disposal costs play an important role, beside separation characteristics and purity requirements. In particular with regard to the waste disposal, organic filter aids possess advantages in comparison to mineral materials. Such advantages are low bulk density, biological degradability, and nearly ash-free combustion. A general trend can be observed towards the increased use of organic filter aids based on cellulose rather than mineral filter aids.

2.4 Enhancement of Separation Processes by Additional Electric or Magnetic Forces

If particles dispersed in liquid carry an electrical charge, or if they can be magnetized in a magnetic field, then two additional field forces are available to move particles and liquid relatively to each other. The use of electric and magnetic fields for technical solid–liquid separation is not normally a standard procedure and is thus limited to special applications or to basic research.

If one exposes a suspension to an electrical field, then charged particles move towards the electrode of opposite charge. This process is called electrophoresis. If hydrated ions are moving in an aqueous environment to the electrodes of opposite charge, they are transporting water molecules, and this is called electroosmosis. These effects can be used in technical solid–liquid separation processes. However, it should be noted that, apart from the transport processes, electrolysis at the electrodes also occurs and the temperature of the liquid rises. Due to the electrolytic effects, foreign ions from the electrodes get into the suspension, or decomposition of water into gaseous oxygen and hydrogen occurs (Delgado *et al.*, 2007).

A rather special application in the area of water purification is represented by electroflotation (Chen *et al.*, 2002), where the gas bubble formation takes place via electrolytic decomposition of the water. The oxygen bubbles used for flotation (see Section 2.2.1) simultaneously reduce organic impurities in the water by oxidation.

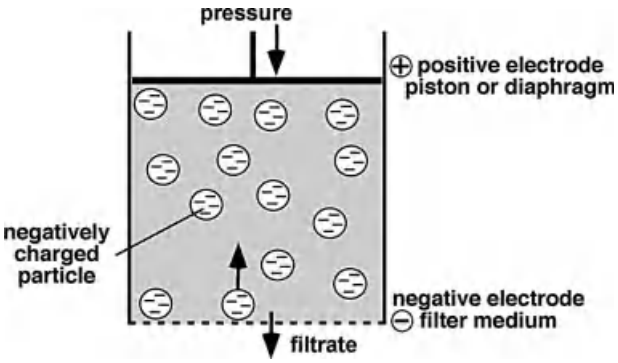

Fig. 2.37 Principle of electro/press-filtration.

Cationic materials are floated very well by the hydrogen bubbles. With the choice of a suitable electrode material, ions can become free, supporting the flocculation of the particles to be separated (see Section 2.6.3).

Electrochromatography is used only for analytic purposes and has yet no technical relevance.

One approach in current research work in the area of crossflow filtration is to position behind the microporous membrane an electrode which possesses the same charge as the particles to be separated. Thus particles are prevented from adhering to the membrane surface by electrostatic repulsion (Huotari *et al.*, 1999). The application of electrical fields to support cake filtration of very hard to filter suspensions has been realized already occasionally in filter presses (see Section 2.3.1). The principle of this process is explained in Fig. 2.37. Due to the arrangement and the polarity of the electrodes the particles are moved against the filtration direction. Thus a delayed formation of a filter cake with very high flow resistance on the filter medium results, and the liquid can be removed much more easily.

In this way the necessary filtration time in many cases can be shortened drastically. Disturbing effects that accompany the process, like electrolysis, have to be taken into account (Weber and Stahl, 2002).

If particles are magnetizable they can be separated from liquids with weak and strong magnetic field separators (Svoboda, 1987). Such procedures find application in classical mineral processing, where drum separators are preferred. A slowly rotating drum containing a magnet is immersed in a trough filled with suspension and the magnetizable particles adhere to the exterior surface of the drum. After the drum emerges from the suspension and the magnetic field is switched off, the separated particles are removed from the drum.

The latest proposals for mechanical separation in biotechnological production, which are still under academic research and technical development, are summarized under the name "Magnetic Fishing" (Eichholz *et al.*, 2008). Ferromagnetic microparticles are integrated into a polymeric matrix and then coated with specifically active ligands, which are able to bind selectively a target substance from a fermentation broth by the principle of lock and key. During the following separation process

a magnetic field is overlaid on a conventional filter or sedimentation apparatus. The target substance bound to the magnetic beads is held back and the undesired materials are led away. Subsequently, the isolated and concentrated target substance is purified and removed from the magnetic beads which are recycled to the process.

Magnetic separation can be realized in high gradient magnetic separation (HGMS) or open gradient magnetic separation (OGMS). With HGMS the slurry to be separated flows, as in a depth filtration (see Section 2.3.4), through a comparatively very open wire mesh, which is located in a magnetic field. The streamlines of the magnetic field are distorted remarkably by the wires and strong field gradients ∇H_{mag} originate, which directly influence the magnetic force F_{mag}. The magnetic force depends, apart from the permeability number μ_0, on the particle volume V_p, the susceptibility χ, the magnetic field strength H_{mag} and the field gradient ∇H_{mag}:

$$F_{mag} = \mu_0 \cdot V_p \cdot \chi \cdot H_{mag} \cdot \nabla H_{mag} \tag{2.11}$$

Figure 2.38 shows the distortion of the magnetic streamlines and the principle of separation in a HGMS filter for the example of one single wire. Using electromagnets the filter can be released after switching off the magnetic field from the separated particles by rinsing out the wire mesh.

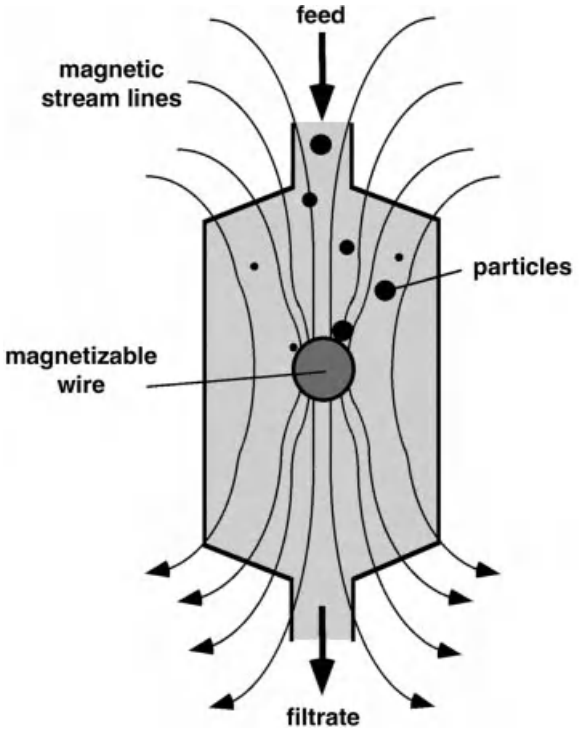

Fig. 2.38 Principle of high gradient magnetic separation (HGMS).

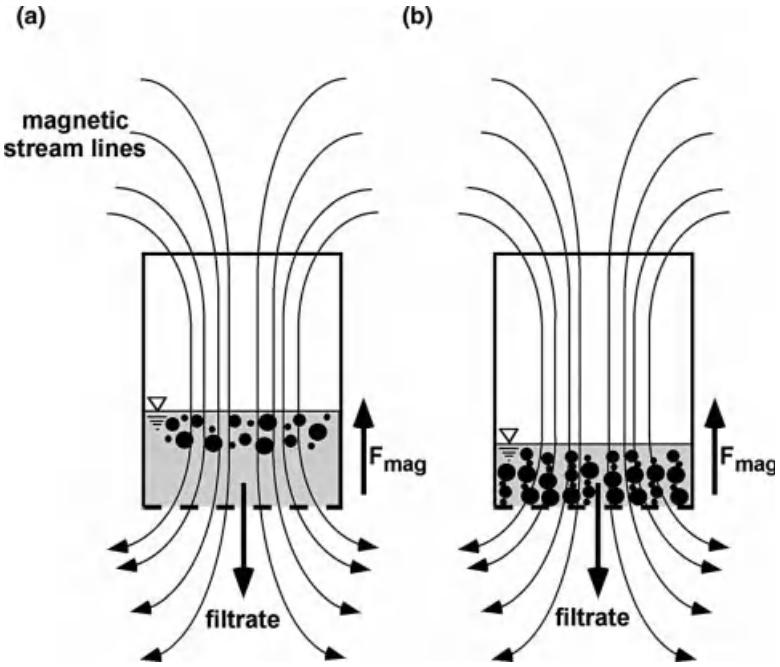

Fig. 2.39 Principle of open gradient magnetic separation (OGMS).

The OGMS procedures work in accordance with Fig. 2.39 without a field-strengthening matrix, and use the gradient of an external magnetic field to influence the magnetizable particles. By appropriate placement of the magnet the direction in which the particles should move can be determined. In a nutsch filter the particles can be kept away from the filter medium, analogously to the filtration in an electrical field (see Fig. 2.39a). The filtration time can be reduced greatly in this way. It is additionally favorable that the particles are deposited chain-like along the stream lines of the magnetic field in the cake, and thus form a very open and permeable cake structure (see Fig. 2.39b, and Fig. 2.37). By treatment in the feed pipe of the separation apparatus the particles can agglomerate, which improves the following separation. In these agglomerates even non-magnetizable particles can be included. This phenomenon is called heterocoagulation.

2.5
Mechanical/Thermal Hybrid Processes

Apart from the purely mechanical liquid separation, in various filter apparatuses the solids can also be thermally dried. This is realized in discontinuous stirred nutsch filters or filter centrifuge dryers by means of hot gas, which flows through the previously desaturated filter cake. In this way a separate thermal dryer can be saved. Real synergetic effects can be created with industrially established steam pressure

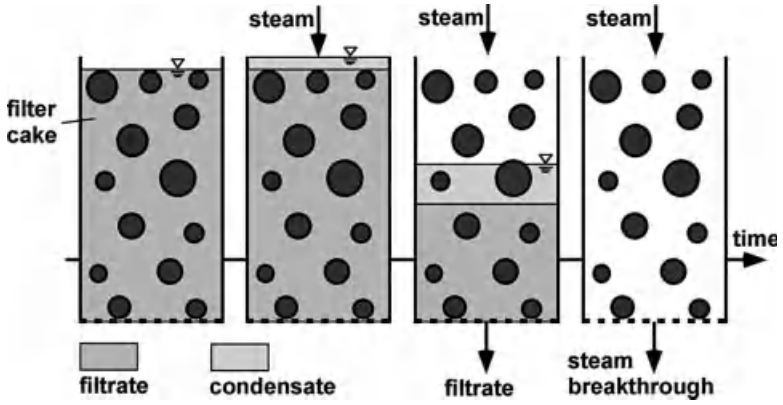

Fig. 2.40 Course of cake dehumidification in steam pressure filtration.

filtration processes (Peuker and Stahl, 2001). In this process pressurized steam serves as a gaseous displacement medium for the pore liquid contained in the filter cake. During the conventional desaturation of a filter cake with air or nitrogen the larger pores empty faster than the smaller ones, leading inevitably to an early and unwanted gas breakthrough at the filter medium. The gas flowing through these pores must be supplied by the compressor in order to maintain the filtration pressure. This "fingering" effect can be avoided completely with steam pressure filtration, where the liquid is displaced in an almost ideal piston-like way from the entire filter cake, as shown in Fig. 2.40. Pressurized steam possesses a high temperature according to its vapor pressure curve, and condenses first at the cold filter cake surface. This is heated, and the steam standing under pressure penetrates into the cake pores. When a coarse pore empties faster, the steam gets into the cold region of the cake. Thus the steam condenses, the pore is filled up with liquid again, and a planar, evenly advancing desaturation front develops. The produced condensate is an excellent washing medium, so that one can very efficiently purify the particles during the dehumidification of the cake. After the steam breakthrough, the hot filter cake is dehumidified to a low moisture content. Conventional contact or perfusion drying can be carried out additionally.

The steam pressure filtration is realized in industry by means of discontinuous diaphragm filter presses and continuous hyperbaric filtration on drum or disc filters. Figure 2.41 shows the principle of a diaphragm filter press with heatable filter plates. The filtrate outlet pipe is connected to a vacuum pump in order to lower the boiling temperature of the liquid. After the steam breakthrough the filter cake can be further dehumidified by means of thermal contact drying. A shrinkage of the filter cake during drying is compensated by the diaphragm.

In the case of steam pressure filtration using continuously operating hyperbar filters, the pressurized steam is, as shown in Fig. 2.42, fed into a special steam hood (Bott *et al.*, 2003).The filter cake emerges from the cold suspension and enters the hot steam hood. The pressure in the steam hood is equal to the gas pressure in the filter vessel. The process is designed in such a way that the cake leaves the steam hood at the

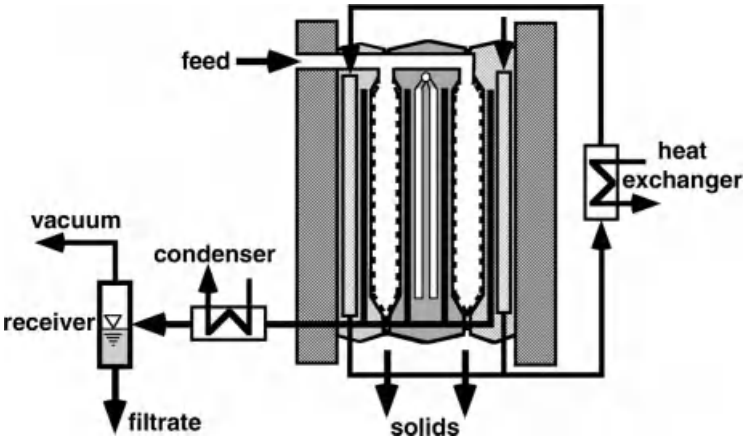

Fig. 2.41 Steam pressure filtration with diaphragm filter press.

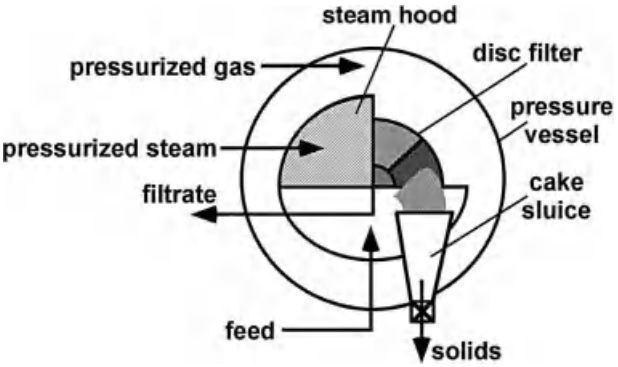

Fig. 2.42 Steam pressure filtration with hyperbar filters.

moment when the steam breakthrough occurs in the filter medium. After leaving the steam hood, pressurized air flows through the hot and still moist cake, so that a thermal postdrying by perfusion takes place.

2.6
Important Aspects of Efficient Solid–Liquid Separation Processes

2.6.1
Mode of Apparatus Operation

Discontinuously and continuously operating apparatus alternatives exist for almost any solid–liquid separation process. Due to the mode of operation they exhibit specific advantages and disadvantages.

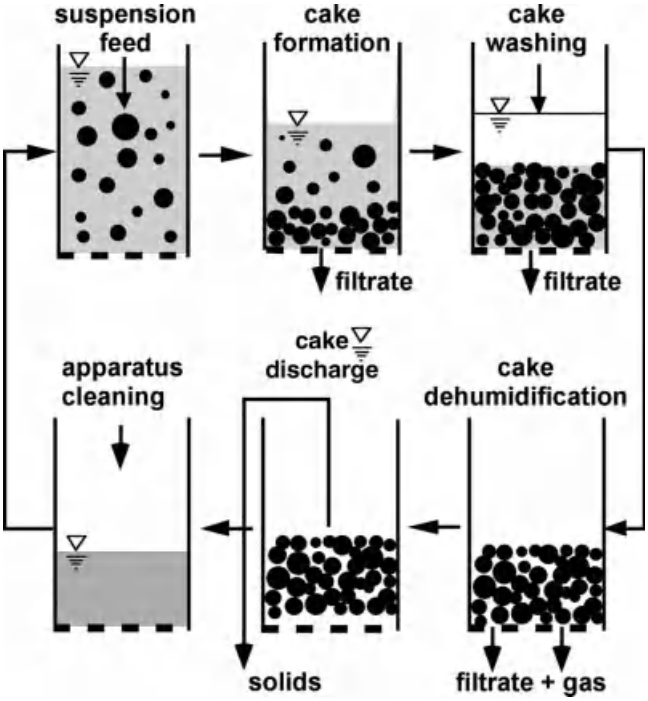

Fig. 2.43 Discontinuous solid–liquid separation process.

The principle of the discontinuous mode of operation can be explained with the example of a simple vacuum nutsch filter for cake filtration, as depicted in Fig. 2.43. The duration of each single process step, such as feeding, filter cake formation, cake washing, cake dehumidification, solids discharge, and apparatus cleaning can be adjusted independently from the other steps. Thus the separation apparatus can be adapted with maximum flexibility to the requirements of the respective product. On the other hand, cake is produced only during the filtration time. However, the solids throughput of the apparatus is specified by the cake mass formed during the entire time of the batch. The total batch time is subdivided into the active cake formation time and the so-called "dead time". The dead time includes all process steps without filter cake formation. One can show, for constant pressure filtration, that the maximum throughput of a discontinuously operating apparatus is reached when the cake formation time and the dead time are commensurate. If the flow rate is kept constant, the maximum throughput is achieved when the maximum pressure given by the pump is reached. A quasi-continuous mode of operation of batchwise operating apparatuses can be realized by parallel connection and time-shifted operation of several units. Another possibility for this exists in the installation of a suspension buffer tank. The continuous feed, which flows into the buffer tank, must correspond to the capacity of the discontinuous separation apparatus fed from that tank.

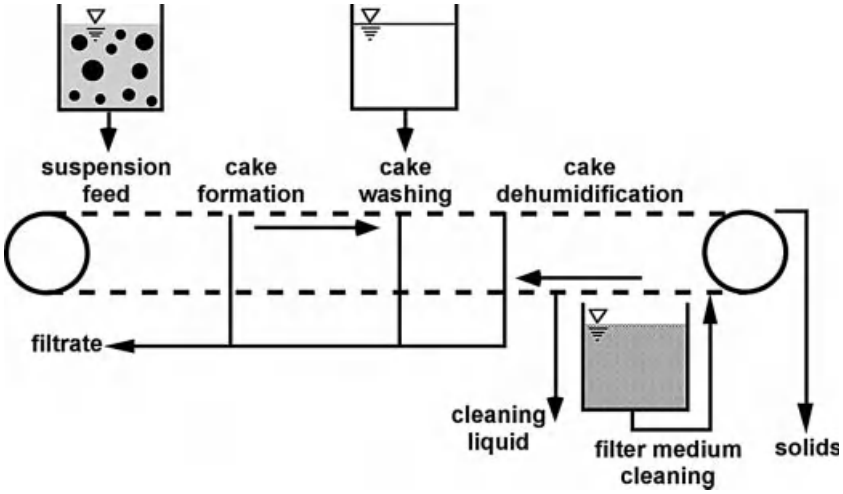

Fig. 2.44 Continuous solid–liquid separation process.

The fully continuous mode of operation of a solid–liquid separation apparatus can be described in contrast to the discontinuous principle, as shown in Fig. 2.44, by the example of a vacuum belt filter. In the continuous mode of operation, the residence time of the product in each process step is fixed by the common transport velocity and the geometrical length of the process zone. All process steps are coupled with each other by the common transport velocity. A change in the time relationship of individual process steps is only possible by adjusting the geometrical length of the respective zones. This can be realized only in relatively narrow limits by a change in the construction. On the other hand, the throughput of such a continuously operating apparatus is affected positively due to the omission of dead times. A continuously operating separation apparatus can be integrated in a batch production process, either by connection with a suspension storage tank, or by periodical shut-down of the separation apparatus.

2.6.2
Combination of Separation Apparatuses

A solid–liquid separation task is solved in most cases not via one single apparatus, but by means of a combination of several separation devices. During the separation process the mechanical properties of the solid–liquid mixture to be separated can change so much that the limits of application of one single apparatus are exceeded, or its operation is no longer economical. Sometimes it is advantageous to split a suspension at the beginning of the separation process, and to supply each part to a different separation apparatus. Depending upon the task, different principles of apparatus combinations can be classified into

- function separation,
- function integration,

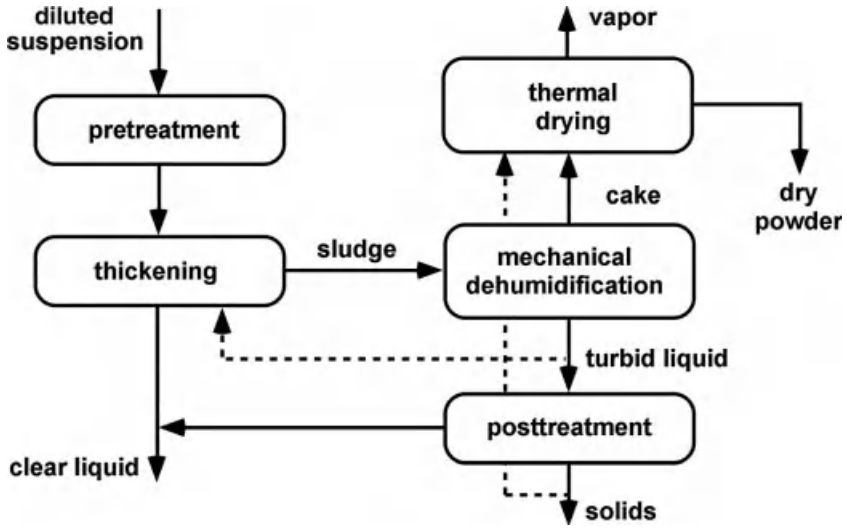

Fig. 2.45 Function separation.

- serial arrangement,
- parallel arrangement and
- cross arrangement.

If, for example, completely dry solids must be gained from an initially dilute dispersion, then this task can hardly be solved in a reasonable way in only one single separation apparatus. A combination of several interconnected apparatuses should usually be chosen, as represented schematically in Fig. 2.45.

The whole task of separation is divided into single steps, and an optimally suitable apparatus is assigned to each step. An initially low concentration suspension of small particles is often submitted first to a pretreatment by agglomeration to facilitate the following separation (see Section 2.2.2). In a subsequent concentration step, a significant part of clear liquid is withdrawn from the suspension in order to relieve the following dehumidification of the solids (see Section 2.2.3). The concentrate coming from this thickening step is then supplied to a separation apparatus whose role is to provide an extensive mechanical separation of the liquid. Since the separated liquid is often not yet perfectly particle-free, it can be led back into the thickening stage or it can be processed in a specialized post-clarification device. The mechanically dehumidified sediment or filter cake is finally passed to a thermal dryer to evaporate the last adhering liquid and appears at the end of the process as a completely dry powder.

Contrary to the principle of function separation, a combination of several process steps in only one apparatus can also represent the optimal solution of a solid–liquid separation problem. As follows from Fig. 2.46, steps for the generation of a particle system, as well as the mechanical dehumidification, and the final thermal drying can be integrated.

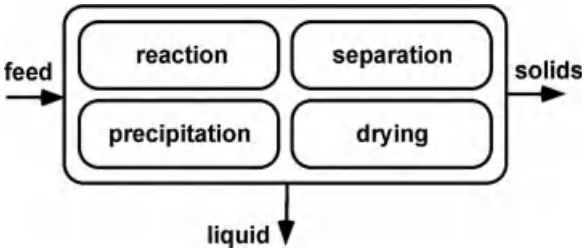

Fig. 2.46 Function integration.

Such configurations make sense if product losses have to be avoided as far as possible, and if the operation must be realized under extremely clean conditions. This is, for example, the case with very expensive pharmaceutically active substances. If such a process is realized in several individual apparatuses, then these apparatuses must be interconnected by pipings, flanges and armatures. This entails a large expenditure for cleaning. In addition, product is lost in every process step. The greater the number of single steps, the smaller becomes the product yield. Examples of such integrated apparatuses are modern filter reactors, filter dryers und centrifuge dryers.

The serial arrangement of identical apparatuses is used for the intensification and improvement of the process result. Figure 2.47 represents this principle schematically.

An example is continuous cross-flow filtration. If after one passage of the suspension through a membrane module the required concentration is not yet reached, then one can further increase the concentration by additional modules. A parallel arrangement of identical separation devices serves the capacity increase of a separation step by modular extension. Figure 2.48 shows the principle.

An alternative to a parallel arrangement would be the installation of one larger and more efficient apparatus. However, this is not always possible or meaningful. In the case of hydrocyclones, the throughput rises with the cyclone diameter, but the cut-size increases likewise. If a small cut-size is required, and a large amount of liquid has to be handled, then several hydrocyclones of small diameter must be arranged in parallel. As already mentioned in Section 2.6.1, a quasi-continuously operating process can be made possible by parallel arrangement of discontinuously operating separation apparatuses. A further aspect of the parallel arrangement of several apparatuses is the larger operational reliability, if one apparatus should fail. This is similar to the redundancy created by installation in parallel arrangement of a spare apparatus, which is normally not used.

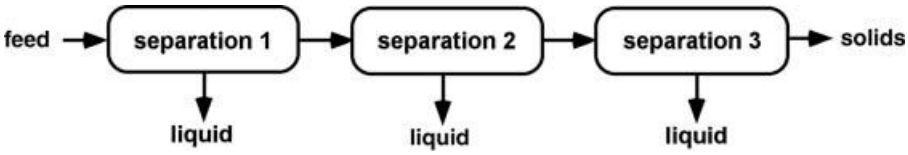

Fig. 2.47 Serial arrangement.

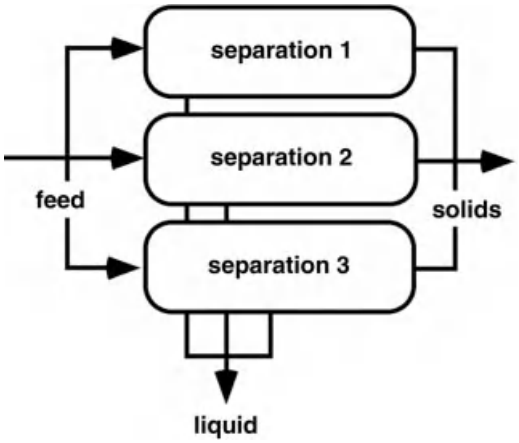

Fig. 2.48 Parallel arrangement.

No separation apparatus works perfectly. In a cross arrangement two apparatuses are combined in such a way that their respective strengths are of benefit for the solid and liquid product, whereas their weak points are mutually compensated. In Fig. 2.49 this is shown by the example of the combination of an apparatus for thickening and an apparatus for maximal dehumidification of the solids.

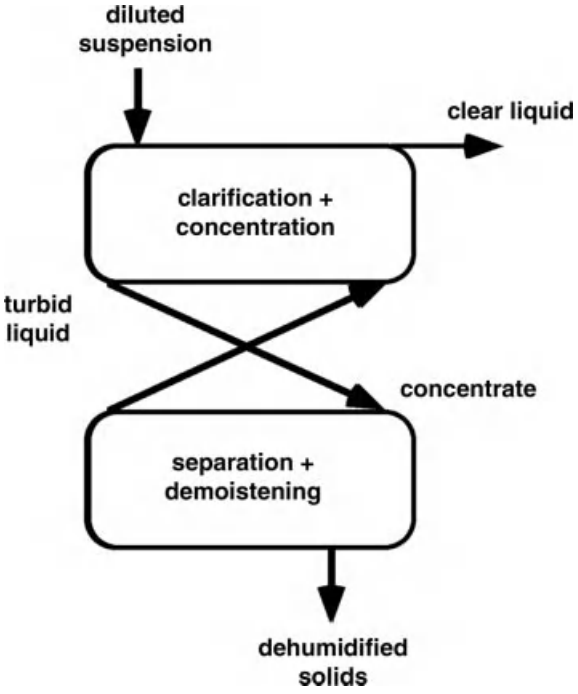

Fig. 2.49 Cross arrangement.

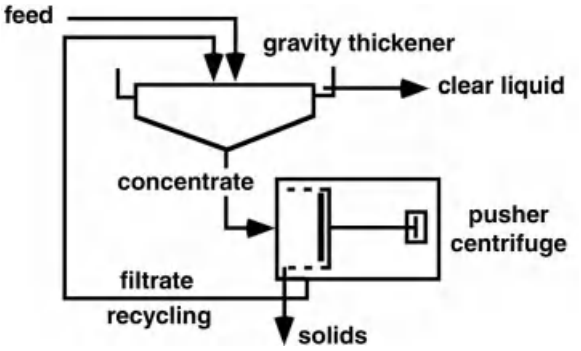

Fig. 2.50 Cross arrangement of sedimentation tank and filter centrifuge.

The apparatus for thickening a low concentration suspension can be optimized to produce particle-free liquid, which means it works as a clarifier. The concentrate, which then still contains much liquid, is supplied to an apparatus suitable for maximal solids dehumidification. As a consequence of these conditions, the separated liquid may contain an unacceptable amount of particles. This turbid liquid is returned to the thickener to be clarified again. A practical example is shown in Fig. 2.50 for the combination of a circular static sedimentation basin and a continuously operating filter centrifuge. The pusher centrifuge of Fig. 2.50 transports the separated solids, with the help of an axially oscillating pusher plate, continuously to the discharge at the open end of the rotating filter basket. The residence time of the product in the filter basket is approximately 10–20 s. To guarantee filter cake formation, and, eventually, washing and dehumidification within such a short time, the suspension must be highly concentrated and the filter medium must be as permeable as possible. The relatively open wedge wire screen produces a cloudy filtrate which is led back for post-clarification to the thickener/clarifier. This takes over the clarification and guarantees the physical function of the centrifuge by delivering a sufficiently concentrated suspension.

2.6.3
Suspension Pre-Treatment Methods to Improve Separation Conditions

The particle separation from liquids can be made easier, or possible at all, by different methods of suspension pre-treatment. The most important procedures for suspension pre-treatment are

- agglomeration of very small particles,
- preconcentration of the suspension,
- addition of filter aid material,
- suspension degritting or desliming, and
- defoaming of suspensions.

Classifying and the pre-concentration of highly diluted suspensions are independent steps of solid–liquid separation. However, they often serve in a combination

arrangement as necessary preliminary stages for a downstream apparatus that provides a more extensive mechanical liquid separation. The pre-concentration of a suspension serves, above all, the purpose of withdrawing a significant part of clear liquid at minimal possible expenditure in order to relieve the following, more effective and more costly separation equipment. Separation procedures that deliver the solids in a still flowable form are particularly well suited for this operation. Static and centrifugal sedimentation, cross-flow filtration and back-flushing filters are normally used for this purpose. Especially, the sedimentation processes are frequently combined with particle agglomeration.

The separation of particles with diameters less than approximately 10 μm is substantially facilitated by agglomeration. On the one hand, agglomerates settle faster than single particles. On the other hand, the individual sedimentation of single particles, which is usually undesired in separation processes, can be transformed into swarm sink behavior. The latter is characterized by the fact that all particles, independently of their size, shape or specific weight, settle with nearly the same velocity, and a sharp sedimentation front forms. The integration of the whole particle size distribution into the agglomerates prevents an undesirable demixing of the particles according to their size. Moreover, the necessary clarification surface of a sedimentation apparatus need no longer be laid out according to the smallest single particle to ensure particle-free overflow. In filtration processes, more permeable filter cakes are formed after particle agglomeration. This leads to faster cake formation. Furthermore, the filtrate pollution by particles able to get through the filter medium in the very first moment of cake formation can be reduced, or even totally prevented, by agglomeration. In order to avoid pore blockage of the filter medium, its pore size is often chosen so large that, for a good separation, particle bridges need to be formed across the meshes. Finally, particle demixing can also be avoided in filtration processes by agglomeration, because gravity cannot be switched off and sedimentation takes place in the suspension anyway. To build up agglomerates, van-der-Waals forces are mainly used in the case of coagulation, and polymer molecules of large molecular weight in the case of bridging flocculation (Russel *et al.*, 1989). Less important at present are processes presently in development, such as electrocoagulation and magnetic flocculation (see Section 2.4). Particles which are dispersed in ion-containing liquids carry, in general, surface charges and repel each other. In order to enable particle adhesion by van-der-Waals forces the electrostatic repulsion must be reduced to a level which allows the particles to come close enough together. The balance between attractive and repulsive forces is described in the DLVO theory.

Figure 2.51 shows this in a simplified representation. In the depicted case, a strong primary and a weaker secondary maximum of adhesion occur as a result of the balance between repulsive and adhesive forces. With accordingly large kinetic energy, particles can overcome the remaining barrier ("potential wall") and create very stable agglomerates in the primary maximum of adhesion. The physicochemical conditions favorable for coagulation can be adjusted by the pH value and/or the ion concentration of the suspension (Lyklema, 1991, 2001). The zeta potential, which can be determined by measurement, serves as a measure of the electrostatic charge and, derived from

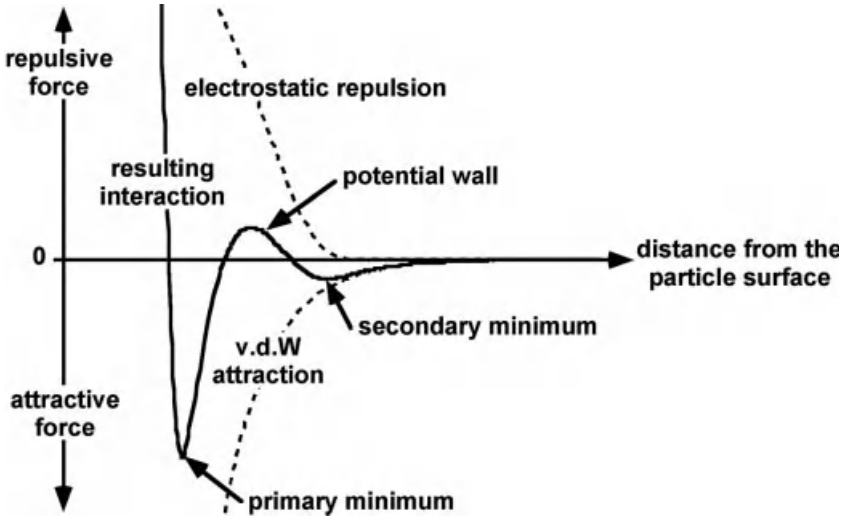

Fig. 2.51 Attraction and repulsion as a function of distance from the particle surface.

this, of the mutual repulsion of the particles. When the zeta potential becomes zero, at the isoelectric point, the particles have no external, outwardly oriented electrostatic charges. In this condition they are able to adhere maximally.

Furthermore, particles can be flocculated by addition of special soluble polymers. The adhesion between the particles is realized here by partial adsorption of the polymers, and thus by direct interlinking of the particles. According to the electric charge one can distinguish between anionic, cationic and nonionic polymers. Polyacrylamide is a frequently used polymeric chain. The molecular weight is of the order of magnitude of 10 million. The solids mass concentration of a ready to use solution is usually chosen between 0.03 and 0.1%. The preparation of the flocculant solution, the dosage, the mixing of flocculant and suspension, and the controlled floc formation are independent steps in the entire solid–liquid separation process. The necessary amount of flocculant is analyzed by charge detectors; the analysis of the result of agglomeration to find an optimal flocculant can be done by modern analytic centrifuges (Sobisch and Lerche, 2000). Depending on the real technical separation process, the agglomerates must withstand different kinds of mechanical load. Flocs which are separated in a centrifuge or in a pressure filter must be much more stable than those in a gravity settling tank. The strength of agglomerates can be adjusted in special flocculation reactors.

However, in many separation processes in the food or pharmaceutical industries the addition of foreign matter is forbidden. In such cases the driving forces must usually be increased to solve the separation problem.

The mixture of a hard to separate suspension with mineral or organic filter aid materials can lead to an increased permeability of filter cakes. This procedure is called "body feed filtration". It is mainly used when the liquid represents the required product. The range of the materials used here is very large. Today mineral filter aids, such as diatomaceous earth (kieselguhr) or perlite, are being displaced increasingly

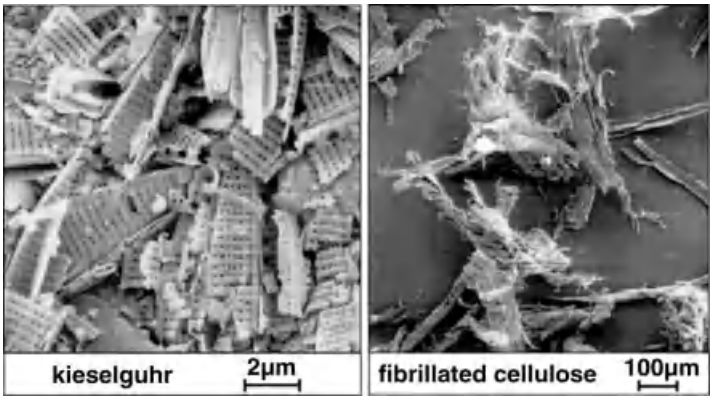

Fig. 2.52 Examples of filter aid materials.

by organic filter aids based on cellulose from renewable raw materials. Figure 2.52 shows microscopic pictures of diatomaceous earth and cellulose fibers.

In the case of very broad particle size distributions the largest as well as the smallest particles can turn out to be disturbing the separation process. Separation apparatuses, such as disc stack separators or hydrocyclones with nozzle discharge, and also cross-flow modules with very close flow channels must be protected against coarse particles, which can block the nozzle or flow channel. On the other hand, even a small quantity of the finest particles can clog the pores of a filter cake and generate a very high pressure loss. Depending on the particle size and flow rate, most apparatuses can be used to separate such disturbing particle fractions. Coarse particles can be removed for example by strainers or bended screens, fine particles by hydrocyclones, up-stream classifiers, or micro-membrane filters.

With foaming suspensions, it can be advantageous or necessary for safe and trouble-free operation of separation apparatuses to degrade the foam by chemical or mechanical means. Foams occur in flotation processes and in the presence of organic substances like proteins. Foam condensation by chemical means is usually not preferred due to the necessary addition of substances. More advantageous is mechanical foam suppression via water spray or special defoaming turbines.

2.7 Conclusions

Mechanical liquid separation is an important process step, located upstream of the thermal dryer. For each of several physical principles, different mechanical separation techniques can be identified, and for each of these techniques a large number of different separation apparatuses exist. The reason for this variety is that mechanical separation processes must be optimized for extreme ranges of particle size, size distribution and shape, specific weight of solids and liquid, suspension concentration, suspension and liquid rheology, flow rate, chemical

composition of the suspension, process and technical boundary conditions and, last but not least, demands on the separation results. Several alternative solutions exist for nearly every separation problem so that only a careful and deep analysis of all relevant aspects can lead to optimal results. The procedures and apparatuses for the mechanical solid–liquid separation are under permanent research and development in view of new challenges and requirements of the separation results. Actual research results are permanently transferred to innovative apparatus constructions.

Additional Notation Used in Chapter 2

a	centrifugal acceleration	$\mathrm{m\,s^{-2}}$
C	centrifugal number	
c_v	volume concentration	
F	force	N
Fr	Froude number	
H	field strength	$\mathrm{A\,m^{-1}}$

Greek Letters

α	specific filter cake resistance	$\mathrm{m^{-2}}$
β	filter medium resistance	$\mathrm{m^{-1}}$
δ	wetting angle, degrees	
κ	concentration parameter	
μ	permeability number	$\mathrm{Vs\,A^{-1}\,m^{-1}}$
χ	volume-based susceptibility	

Subscripts

e	entry
mag	magnetic
r	residual
St	Stokes
surf	surface
v	void
0	vacuum

References

Anlauf, H., 2004. The filter medium – Crucial interface between apparatus and suspension. *Proceedings of the 9th World Filtration Congress*, New Orleans, USA, session 336.2.

Anlauf, H., 2006. Recent research and machinery of solid liquid separation processes. *Drying Technol.* **24**: 1235–1241.

Anlauf, H., 2007a. Overview and recent developments in effective particle

decontamination by washing processes. *Filtration* **7**(1): 20–25.

Anlauf, H., 2007b. Recent development in centrifuge technology. *Sep. Purif. Technol.* **58**: 242–246.

Anlauf, H., 2008. Solid-liquid separation by cake filtration – State of the art and future expectations. *Proceedings of the 10th World Filtration Congress*, Leipzig, Germany, Volume I, 21–28 and Global guide of the filtration and separation industry, VDL, Rödermark, Germany, pp. 108–114.

Bott, R., Langeloh, T., Meck, F., 2003. Recent developments and results in continuous pressure and steam pressure filtration. *At Miner. Process.* **44**(5): 5–18.

Chen, X., Chen, G., Yue, P. L., 2002. Novel electrode system for electroflotation of wastewater. *Environ. Sci. Technol.* **36** (4): 778–783.

Delgado, A. V., González-Caballero, F., Hunter, R. J., Koopal, L. K., Lyklema, J., 2007. Measurement and interpretation of electrokinetic phenomena. *J. Colloid Interf. Sci.* **309**: 194–224.

Dickenson, T. C., 1997. *Filters and filtration handbook*. Elsevier, Oxford, UK.

Eichholz, C., Stolarski, M., Goertz, V., Nirschl, H., 2008. Magnetic field enhanced cake filtration of superparamagnetic PVAc-particles. *Chem. Eng. Sci.* **63**: 3293–3300.

Fuerstenau, M. C., Yoon, R.-H., 2007. *Froth flotation – A century of innovation*, SME, Sci-Tech Book News. Portland, USA.

Gimbel, R., Graham, N. J. D., Collins, M. R., 2006. *Recent progress in slow sand and alternative biofiltration processes*. IWA Publishing, London, UK.

Höflinger, W., 2008. Depth filtration with fibrous filter layers, in *Global guide of the filtration and separation industry*. VDL, Rödermark, Germany, pp. 136–138.

Huotari, H. M., Trägårdh, G., Huismanet, I. H., 1999. Crossflow membrane filtration enhanced by an external DC electric field: A Review. *Chem. Eng. Res. Des.* **77** (5): 461–468.

Jornitz, M., Meltzer, T., 2001. *Sterile filtration*. Marcel Decker, NewYork, USA.

Kopf, M. H. *et al.* 2008. The centrifuges of today and tomorrow: Larger, more efficient and more specific, in *Global guide of the filtration and separation industry*. VDL, Rödermark, Germany, pp. 125–130.

Leung, W. W.-F., 1998. *Industrial centrifugation technology*. McGraw-Hill, NewYork, USA.

Leung, W. W.-F., 2007. *Centrifugal separations in biotechnology*. Elsevier, Oxford, UK.

Lyklema, J., 1991. *Fundamentals of interface and colloid science: Fundamentals*. Academic Press, London, UK.

Lyklema, J., 2001. *Fundamentals of interface and colloid science: Solid-liquid interfaces*. Academic Press, London, UK.

Lyko, H., 2008. Membrane technology: Innovative separation techniques for many fields of application, in *Global guide of the filtration and separation industry*. VDL, Rödermark, Germany, pp. 144–148.

Peuker, U., Stahl, W., 2001. Steam pressure filtration: Mechanical-thermal dewatering process. *Drying Technol.* **19**(5): 807–848.

Purchas, D., 1996. *Handbook of filter media*. Elsevier, Oxford, UK.

Rao, S. A., 2004. *Surface chemistry of froth flotation*. Springer, Heidelberg, Germany.

Ripperger, S., 2008. Filter media for cake filtration, in *Global guide of the filtration and separation industry*. VDL, Rödermark, Germany, pp. 115–124.

Rushton, A., Ward, A. S., Holdich, R. G., 1996. *Solid-liquid filtration and separation technology*. VCH, Weinheim, Germany.

Russel, W. B., Saville, D. A., Schowalter, W. R., 1989. *Colloidal dispersions*. Cambridge University Press, Cambridge, UK.

Sobisch, T., Lerche, D., 2000. Application of a new separation analyzer for characterization of dispersions stabilized with clay derivates. *Colloid Polym. Sci.* **278**, 369–374.

Sorrentino, J. A., 2002. *Advances in correlating filter cake properties with particle collective characteristics*. Shaker, Aachen, Germany.

Sutherland, K. S., 2005. *Solid/liquid separation equipment*. Wiley-VCH, Weinheim, Germany.

Svarovsky, L., 2000. *Solid-liquid separation*. Butterworth Heinemann, Oxford, UK.

Svoboda, J., 1987. *Magnetic methods for the treatment of minerals*. Elsevier, Amsterdam, Netherlands.

Wakeman, R. J., Tarleton, E. S., 2005a. *Solid liquid separation – Principles of industrial filtration*. Elsevier, Oxford, UK.

Wakeman, R. J., Tarleton, E. S., 2005b. *Solid liquid separation – Scale-up of industrial equipment*. Elsevier, Oxford, UK.

Wakeman, R. J., Tarleton, E. S., 2007. *Solid liquid separation – Equipment selection and process design*. Elsevier, Oxford, UK.

Weber, K., Stahl, W., 2002. Improvement of filtration kinetics by pressure electrofiltration. *Sep. Purif. Technol.* **26**: 69–80.

3
Energy Considerations in Osmotic Dehydration

Hosahalli S. Ramaswamy and Yetenayet Bekele Tola

3.1
Scope

Osmotic drying, a partial dehydration process, is often considered as a pretreatment to improve the quality of the product over its conventionally dried counterpart. The osmotic treatment involves soaking of food in a hypertonic solution of sugar and/or salt for specific times under controlled conditions. The process involves two countercurrent mass flows, water from the food to the solution and solids from the solution to the food. The overall mass transfer phenomena are governed by pretreatment, osmotic solution, product and osmotic environment related factors. The treatment has generally been considered to give major advantages when combined or compared with other drying methods. The first advantage is quality enhancement, since the quality of osmotically pretreated products is better and the associated shrinkage is considerably lower than for products from conventional drying processes. The second advantage is that the technique helps to conserve the overall energy relative to other drying procedures. The quality aspects have been widely studied while energy issues have been addressed sporadically.

The purpose of this chapter is to briefly review the advantage of osmotic dehydration in terms of quality and then to focus on energy reduction and its potential contribution to maximize profit by reducing the associated costs. Studies related to the factors which influence mass transfer in the osmotic dehydration step are also important with respect to energy issues because the mass transfer rate and treatment time determine the residual moisture required to be removed by other methods. After the osmotic treatment, the moisture content of fruits and vegetables is usually reduced by 30–50% (wet basis). This reduction in moisture has significant impact on energy conservation because the latent heat normally required for moisture evaporation is reduced. Moisture removal in osmotic treatment is a physical separation governed by osmotic forces rather than the conventional vaporization involved in other drying methods. This is the principal reason for the energy savings in osmotic drying. Novel approaches in food drying are constantly explored to minimize the energy demand and maximize economic performance.

Modern Drying Technology Volume 4: Energy Savings, First Edition.
Edited by Evangelos Tsotsas and Arun S. Mujumdar.

3.2 Introduction

Osmotic dehydration is a process of partial removal of moisture from fruits, vegetables, meat or fish through the process of osmosis. The process involves immersion of the food particles in a hypertonic solution, which is either a sugar or a salt solution, or a mixture of both. During the process three simultaneous counter-current flows occur. The first is water flow out of the food into the solution, the second is a simultaneous transfer of solute from the solution into the food, and the third (usually small) is flow of natural solutes, such as sugars, organic acids, vitamins, reducing sugars, some flavor compounds, volatiles, minerals, and so on, leaking out from the food particles into the solution (Le Maruer and Biswall, 1988). Figure 3.1 is a simplistic representation of the osmotic dehydration process. The mass transport in osmotic dehydration is generally driven by the osmotic forces. Since the hypertonic solution has higher osmotic pressure with reduced water activity, it serves as the driving force for water withdrawal from the food particles into the osmotic solution. Rahman and Perera (2007) indicated that the removal of water during the osmotic process is primarily driven by diffusion and capillary flow, whereas solute uptake or leaching is by diffusion. These mass exchanges between the osmotic solution and food particles have been demonstrated to have an effect on the overall yield and quality of the dehydrated product.

In a perfectly semi-permeable membrane, the solution is unable to transfer through the membrane into the cells, but such membranes are rather rarely associated with food particles because of their complex internal structure and possible damage during processing (Shi, 2008). Hence, the osmotic dehydration processes generally allow counter flow of solute and water. The flux of water coming out of the food is, however, much larger than the counter flux of osmo-active substance. This is because semi-permeable plant tissues resist the free entry of

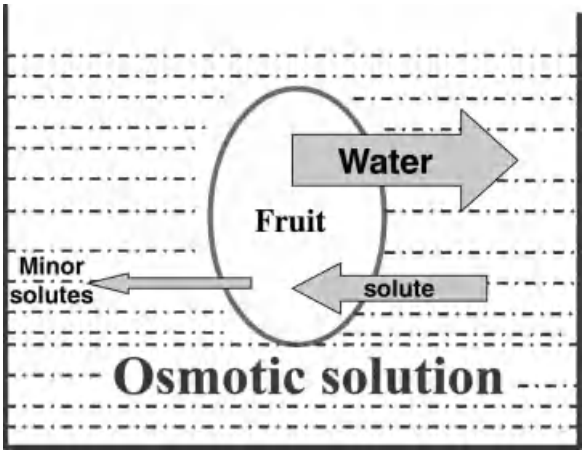

Fig. 3.1 Osmotic dehydration principle and relative mass flows of water and solutes.

larger osmo-active substances, while lower molecular weight water migrates out of the solution in a larger proportion. This results in a decrease in the water content of the product until an equilibrium condition is established. Depending on the concentration of solute in the osmotic solution, up to 50% reduction in the fresh weight of fruits or vegetables may be brought about by osmotic dehydration (Rastogi and Raghavarao, 1997).

3.3 Mass Transfer Kinetics

Osmotic dehydration is a mass transfer process. The kinetics of mass transfer is usually described using terms such as water loss (WL), solids or solutes gain (SG) and weight reduction (WR). There are several models available to predict the mass transfer between osmo-active substance and food. The overall mass transfer kinetics during osmotic dehydration is affected by several factors. By manipulating processing factors affecting mass transfer kinetics, and the nature of the product subjected to dehydration it is possible to reach different levels of dehydration or impregnation of the material under treatment.

3.3.1 Pretreatments

Pretreatment before osmotic dehydration can affect the inherent integrity of the product, which has an influence on mass transfer. The osmotic dehydration rate is largely affected by cell membrane permeability (Toupin and Le Maguer, 1989). Good membrane permeability will lead ultimately to more rapid osmotic dehydration. However, the cellular membrane of plant cells exerts high resistance to transfer of water and solutes and slows down the overall osmotic drying rate (Erle and Schubert, 2001). Therefore, the partial damage of cell membranes using different pretreatment methods can be advantageous for acceleration of the mass transfer process. Blanching, peeling, coating, freeze/thawing, high pressure, and high intensity electric field pulses are some of the pretreatment operations which are used before the osmotic dehydration process to enhance mass transfer.

Blanching is mainly done for fruits and vegetables, to inactivate endogenous enzymes that result in spoilage and, thus, to control their detrimental effects during and after the drying process. However, the mild heat treatment also disrupts and softens some of the tissue structures, creating damaged surfaces for easier solute–water movement. Meanwhile peeling, as a process of removing the external structural cover and damaging of the tissue, has an evident impact on mass transfer. Freeze/thawing is another pretreatment commonly used to improve the osmotic dehydration mass transfer kinetics. Frozen/thawed fish has fleshy characteristics that commonly increase the rate of salt absorption (Hilderbrand, 1992). Maestrelli *et al.* (2001) reported that moisture reduction by osmotic dehydration of muskmelon, prior to the freezing process, improved the quality by decreasing loss of exudates and giving

better texture after thawing. Furthermore, pre-dehydrated strawberry samples exhibited a better tissue organization after thawing treatment than the frozen slices without pretreatment (Sormani *et al.*, 1999).

One of the limitations of osmotic dehydration in the food industry is the infiltration of excess osmotic solute inside the material. Coating the food to be dehydrated with an artificial barrier on the surface may efficiently hinder the infiltration of solute inside the food, while not affecting much the rate of water removal (Lazarides, 2001). In such a way the desired dehydration will be achieved without accumulation of solutes in the foodstuff. For successful application in osmotic dehydration, the properties of coating materials should fit several requirements: good mechanical properties, satisfactory sensory properties, easy and rapid film formation, high water diffusivity, and prevention of excessive solute uptake by the tissue. Some of the coating materials suggested are: malto-dextrin, carboxymethylcellulose, gelatin, amylopectin, pectin, methylcellulose, wheat gluten, sodium alginate, cellulose ethylene, acetyl-monoglycerol, chitosan gel, aqueous solutions of potato and corn starches, and alcoholic solution of beeswax (Lewicki *et al.*, 1984; Camirand *et al.*, 1992; Wong *et al.*, 1994).

High pressure (100–800 MPa) treatment can increase the permeability of the cell structure (Rastogi *et al.*, 2000; Tedjo *et al.*, 2002). Micro-structural observation of high pressure treated samples has demonstrated the breaking down of cell walls and the softening of the tissue (Lazarides, 2001). Rastogi and Niranjan (1998) confirmed that high pressure pretreatment of pineapple (up to 400 Mpa) enhanced mass transfer rates, favoring higher water loss to solid gain (WL/SG) ratios. The application of high intensity electric field pulses is another pretreatment reported to enhance mass transfer during dehydration (Rastogi *et al.*, 1999); this is probably due to increased permeability of cells caused by large cell wall perforations occurring during the pulse.

3.3.2 Product

Product species, variety, and maturity level all have a significant effect on natural tissue structure, cell membrane structure, protopectin to soluble pectin ratio, amount of insoluble solids, intercellular spaces, tissue compactness, entrapped air and so on, and can lead to differences in the associated mass transfer rates (Lazarides, 2001). The chemical composition (protein, carbohydrate, fat, and salt), and physical structure (porosity, arrangement of the cells, fiber orientation, and skin), may also affect the kinetics of osmosis in food (Rahman and Perera, 2007). Particularly, porosity of the raw material has a significant effect on both shrinkage phenomena and mass transfer rates (Mavroudis *et al.*, 1998). Soft-textured fish tends to absorb salt faster than tough or firm-textured fish, and high-fat-content fish absorbs salt slower than low-fat fish. The shape/geometry and size of the product affect the surface area to volume ratio of the product with the solution. Since solute impregnation is a surface-controlled phenomenon, high specific surface values favor solute uptake (Torreggiani, 1993). In terms of thickness of the product, with decrease in thickness the rate of mass transfer of water and solute is enhanced.

3.3.3
Osmotic Solution

The osmotic process is affected by the physico-chemical properties of the solutes employed. Differences in osmotic dehydration arise mainly from differences in molecular weight, ionic state, and solubility of the solute in water (Rahman and Perera, 2007). The selection of the solute of the osmotic solution is very important. During this selection we have to consider the following three main factors: (i) the impact of the solute on the sensory characteristics of the product, (ii) the relative cost of the solute in relation to the value of the final product, and (iii) the molecular weight of the solute. Some of the solutes often used in osmotic dehydration processes are sodium chloride, saccharose, glucose, fructose and corn sirup.

The rate of solute penetration is directly related to the solution concentration and inversely related to the size of the sugar molecule (Giraldo *et al.*, 2003). According to the principle of osmosis, the rate of water loss from the product to a solution of large molecular weight solute is lower than that to a solution having small molecular weight solute, when both osmo-active solutions are at the same mass concentration (Lazarides, 1995). This is due to the low vapor pressure of the solution having low molecular weight solute. By using higher molecular weight sugars (i.e., lower dextrose equivalent corn sirup solids) it may be possible to reduce solute gain and allow better migration of moisture. Panagiotou *et al.* (1999) confirmed that solute molecular weight strongly affected both the rate and the equilibrium value of solid gain during osmotic dehydration of banana, kiwi and apple fruits in sucrose and glucose osmotic solutions. Furthermore, the rate of water loss from the food is directly proportional to the concentration of a solution. The higher the concentration, the higher the solute gain and water loss by the product. The pH of the solution can also affect the osmotic process. Acidification increases the rate of water removal by changes in tissue properties and consequential changes in the texture of fruits and vegetables (Moy *et al.*, 1978).

3.3.4
Treatment Conditions

Treatment conditions (temperature and treatment time, agitation, product to solution ratio, etc.) play an important role in the mass transfer during osmotic dehydration. Solution temperature and treatment time, in addition to solute concentration, are the most frequently evaluated factors in osmotic dehydration studies. Water loss increases with increase in temperature, whereas solid gain is less affected by temperature (Li and Ramaswamy, 2006a, b). In the case of high temperature, the solute cannot diffuse as easily as water through the cell membrane, and thus the approach to osmotic equilibrium is achieved primarily by flow of water from the cell (Rahman and Lamb, 1990). During osmotic dehydration high temperature limits are naturally set by the heat tolerance of the specific tissue to be processed and, especially, the heat stability of its cell membrane (Lazarides, 2001). With an increase in osmotic treatment time, the mass transfer process proceeds until both water and solute

concentrations attain their equilibrium conditions (Ramaswamy and Nsonzi, 1998; van Nieuwenhuijzen *et al.*, 2001).

Osmotic dehydration can be enhanced by agitation or circulation of the sirup around the sample (Lenart and Flink, 1984). The degree of mixing has a higher effect on WL than on SG. WL is higher in the turbulent flow region than in the laminar flow region. Therefore, turbulent solution flow due to agitation may result in higher WL/SG ratios (Lazarides, 2001). Ultrasound has also been used as a means to enhance mass transfer during osmotic dehydration of fruits. Rodrigues *et al.* (2009) elucidated the effect of ultrasonic waves with an analogy to the sponge effect. The wave can cause a rapid series of alternate compressions and expansions, in a similar way to a sponge when it is squeezed and released repeatedly. Continuous compression and relaxation of the wave may be the main cause for the creation of microscopic channels in porous materials such as fruits (Fuente-Blanco *et al.*, 2006). Osmotic dehydration under vacuum results in a change of behavior of mass transfer in fruit sugar or salt solution systems (Shi *et al.*, 1995). The reduction in pressure causes the expansion and escape of gas enclosed in the pores, and pores can be occupied by osmotic solution, thus increasing the mass transfer rate (Rahman and Perera, 2007).

3.4 Modeling of Osmotic Dehydration

Modeling of osmotic dehydration is generally employed in the optimization of the osmotic dehydration process and subsequent drying processes. Two basic approaches can be used to model osmotic dehydration (Salvatori *et al.*, 1998). The first, the macroscopic approach, assumes that the tissue is homogeneous, and the modeling is carried out on the cumulated properties of cell walls, cell membranes and cell vacuoles. The second, the microscopic approach, recognizes the heterogeneous properties of the tissue and is based on cell microstructure.

Existing models are mostly based on the assumption that the mass transfer can be described by a diffusion model in an unsteady state. This allows estimation of the diffusion coefficients for both water loss and solid gain, individually or simultaneously. The mass transfer is assumed to be unidirectional and the interactions of the other components on the diffusion of the solute are generally neglected. Analytical solutions of the equation are available for idealized geometries, that is, spheres, infinite cylinders, infinite slabs, and a semi-infinite medium. For these analytical solutions of the unsteady state diffusion model to exactly apply, it is necessary either to keep the external solution concentration constant or to have a fixed volume of solution. The resistance at the surface of the solid is assumed to be negligible compared to the internal diffusion resistance in the solid (Ramaswamy and van Nieuwenhuijzen, 2002). Azuara *et al.* (1992) developed a model based on mass balances of water and sugar to predict the kinetics of water loss and solids gain during osmotic dehydration. Correlative models have been proposed, either to compute the time required for a given weight reduction as a function of the processing temperature and of the solution concentration, or to estimate the dehydration parameters.

The use of Azuara's model to predict mass transfer in osmotic dehydration of fruits at atmospheric pressure has been favored relative to Page's, Magee's, and Crank's models, because Azuara's model fits the SG data better and it turns out to be good enough for fitting WL data. Also, the model has the advantage of allowing the calculation of the equilibrium values of moisture loss and solids gain (Ochoa-Martinez *et al.*, 2007). Azarpazhooh and Ramaswamy (2010b) evaluated diffusion and Azuara models for mass transfer kinetics during microwave-osmotic dehydration of apple cylinders under continuous flow medium-spray conditions. Their results showed that the Azuara model can be used to describe the transient mass transfer kinetics in this osmotic dehydration process. They indicated also that the model is useful in computing the equilibrium point for the moisture loss and solids gain based on short duration osmotic treatments, rather than waiting for the real equilibration to be achieved.

A major limitation of the models is that the obtained transport coefficients are global. They do not enable either to dissociate the respective contributions of each mass transfer, or to take into account the probable interactions between water and solute flows. Their usefulness is then limited as far as technological control of the process is expected. However, once the coefficients have been obtained in a well-defined range of temperature and concentration by experimental design, they can be used to predict and optimize parameters relevant to the process.

For transport in living tissues, the cell structure plays a major role in the transport mechanisms (Welti-Chanes *et al.*, 2005). Cellular structure modeling is extremely challenging since it attempts to take into account the internal changes that take place as the solute penetrates the material. Models involving cellular properties of the material (diffusivity, tortuosity and porosity), properties of the solution (viscosity, diffusivity and density), and process conditions (temperature and shape of the sample) have also been developed in order to integrate the contribution of each component, that is, osmotic solution and water, to the osmotic dehydration process, as well as to account for the natural tissue action, for example, shrinkage that occurs during osmotic dehydration (Le Maguer *et al.*, 2002).

3.5
Osmotic Dehydration – Two Major Issues

There are two major advantages of the osmotic dehydration process in the food industry (i) quality improvement and (ii) energy efficiency. The importance of osmotic dehydration in terms of quality aspects has been extensively discussed in several articles. However, only a few deal with energy issues.

3.5.1
Quality Issues

Osmotic pre-concentration is an effective way to reduce the water content with minimal damage to fresh product quality. This is largely due to the use of a

mild product treatment at relatively low process temperatures (30–50 °C); such temperatures do not affect the semi-permeable characteristic of cell membranes, which is an essential requirement for maintaining the osmotic phenomenon (Lazarides, 2001). Because of constant product immersion in the osmotic medium, the plant or animal tissue is not exposed to oxygen; therefore, there is no need to use antioxidants (i.e., sulphur dioxide in the case of fruits) for protection against oxidative and enzymatic discoloration. Hence, osmotic treatment before convective air-drying improves the quality of the final product by minimizing the oxidative browning. The partial dehydration and solute uptake are also helpful in preventing structural collapse during subsequent drying processes (Lazarides and Mavroudis, 1995). More importantly, osmotic treatment offers quality advantages to the final product, in most cases providing a more desired blend of sugars and acids, thereby reducing the tartness resulting from concentration of acids in many conventionally dried fruits. The finished product would also be more bulky and at the same time less fragile.

Osmotic treatments prior to freezing are used to produce several kinds of fruits that can be stored for long periods of time with good retention of texture, color and flavor after thawing, and prevention of extensive drip loss in freeze/thawing (Lazarides and Mavroudis, 1995). Water content reduction and sugar gain during osmotic dehydration have been observed to have some cryo-protectant effects on color and texture in several fruits (Chiralt *et al.*, 2001). The use of osmotically dried fruits to make high quality chips is another application area to get good quality vacuum fried product. Because of the high sugar content of the product after osmotic dehydration, vacuum frying is a method to produce high-quality (in both sensorial and textural quality parameters) deep-fat fried fruit chips. According to Nunes and Moreira (2009) the best mango chip in vacuum frying was produced with an osmotic solution concentration of 65% (w/v) and a temperature of 40 °C, which resulted in the highest water loss to sugar gain and provided a good texture characteristic.

3.5.2
Energy Issues

Drying is one of the most energy intensive unit operations in food and non-food products processing industries (e.g., ceramic, textile and wood industries). This is mainly because of the high latent heat of vaporization of water to be removed from a product. According to Kudra (2004), for batch drying, the energy efficiency is given as an average value over a drying time, and for continuous drying the energy efficiency is averaged over the range of moisture content, or the dryer length, or volume, depending on the dryer configuration. In both cases the drying efficiency and energy demand related to drying time is highly associated with the quantity of moisture in a material to be removed, or the rate of drying.

Osmotic dehydration of foods has significant advantages in the fruit and vegetable processing industry. This process generally does not produce a product of sufficiently low moisture content that can be stored for a long period of time. To get a stable product after osmotic dehydration, with a long shelf life, the technique requires a final stage (finish drying) of convection air-drying, freeze-drying, microwave-assisted

drying or vacuum drying. Complementing osmotic dehydration with these drying technologies is one of the selected methods for saving energy. Therefore, harmonization of osmotic dehydration with these energy demanding drying technologies has a merit in terms of maximizing energy use efficiency and reduction of production cost. This is because a significant amount of water is removed during the osmotic process in liquid (and not in vapor, i.e., no energy required to achieve the phase change) form, which demands little external energy supply. Thus, by reducing the moisture content of a product to any extent, using either a mechanical or osmotic dehydration method, ultimately facilitates reduction in the energy demand required in the subsequent finish drying process. Consequently, this moisture removal during osmotic dehydration has a twofold advantage from the energy point of view. First, the savings in the energy required for vaporization of the amount of moisture removed by the osmotic process. Second, such removal of moisture reduces the product load for the second stage drying, and reduces the drying time, and the associated secondary operational costs. In the following sections the different combinations of drying techniques with osmotic treatment are discussed individually with a focus on the energy issues.

3.5.2.1 **Osmo-Convective Drying**

The majority of artificial drying operations are based on air drying, where air is heated by the combustion of fossil fuels, or with an electric heater prior to being forced through the product. According to Mujumdar and Beke (2003), typical convective dryers account for about 85% of all industrial dryers. Heating of air before drying is the most energy-intensive process in the food drying industry. Thus, novelty in drying technology that focuses on minimizing the energy demand is very important. The food industry, in general, could save a lot of money by reducing the energy demand and wise use of energy, as well as by eliminating its waste. Beedie (1995) stated that improving the energy efficiency by only 1% could result in as much as 10% increase in profits. According to the author, energy can be saved by (i) reducing drying time or increasing throughput, (ii) avoiding heat losses from different sources (heat loss with exhaust air, with the product, radiation heat loss from the dryer, heat loss due to leakage of air from the dryer, and heat loss due to over-drying of products), and (iii) heat recovery from exhaust gas and dried product. By reducing the moisture content before the actual final drying step, the drying time and heating load can be significantly reduced. Therefore, osmotic dehydration as an upstream pretreatment of a convective air drying process enables us to reduce the energy demand for heating and evaporation of moisture from the product.

Removal of water in its liquid state rather than the vapor state allows the latent heat of vaporization to be captured, and only a small amount of sensible heat is lost with the condensate (Rahman and Perera, 2007). Mujumdar (2007) pointed out that almost 99% of the applications in drying involve removal of water in the vapor form. This means that the energy needed to raise the product temperature and to boil the water off must be supplied; this amounts to 2676 kJ kg^{-1} at 100 °C. The more water that needs to be removed during the convective drying process, the more latent heat of vaporization is demanded. By reducing the volume of moisture in the product by osmotic dehydration before the actual drying process the demand for energy can be

decreased. For instance, fresh fruits and vegetables contain 75 to 95% water, and one way to reduce this high water content, before the actual drying process, is the use of an osmotic dehydration step. As stated before, osmotic dehydration can remove up to 50% of the water in the original fruit or vegetable (Rastogi and Raghavarao, 1997). Hence, as compared to the original moisture content, the energy demand to remove the remaining moisture to attain the target moisture level is far less. Let us take the following simple hypothetical example.

Assume that a 100 kg batch of apples is being dried by both conventional air drying and osmo–conventional combination drying. Let us assume that the moisture content of fresh apples is 85% and we need to dry the product to a final moisture content of 15% (wet base) using the convective air drying method. Before the actual drying, let us say that another batch of the product is subjected to osmotic dehydration treatment and that the process results in a 50% weight reduction with a simultaneous solids infusion of 10% (all based on original weight), after which the treated product is dried in the same way to a final moisture content of 15% (wet basis).

In the direct convective air drying the amount of moisture removed can be calculated as follows:

Initial moisture in the 100 kg batch is 85 kg and the original solids content is 15 kg. Since the solids will remain the same during the conventional drying, in order to achieve the 15% (wet basis) final moisture content, the total product weight must be 17.65 kg. Check: moisture = (17.65–15) kg of the total 17.65 kg, and 2.65/17.65 is 15%. Hence, the amount of moisture removed during the process is (100 − 17.65) kg = 82.35 kg (same as (85–2.65) kg). The product is 17.65 kg.

In the osmotic process:

There is 50% weight reduction. So the product weight after osmotic treatment is 50 kg. In addition to moisture loss, there is solids gain associated with the osmotic drying, and, hence, the reduction in weight does not represent the real magnitude of the moisture loss. Since all are expressed on fresh weight basis and there is a reported 10% solids gain, the solids infused will be 10 kg. Which means the moisture lost during the process is actually (50 + 10) kg = 60 kg. So the residual moisture in the sample after the osmotic treatment is (85 − 60) kg = 25 kg. This quantity of moisture in the 50 kg osmotically treated product gives a wet basis moisture content of 25/50 or 50%. Hence the osmotic process results in reducing the product moisture from 85 to 50% on a wet weight basis, but has also contributed to significant infusion of solids from the sirup into the product. From the energy point of view the 60 kg moisture removed does not need to be vaporized, and, hence, the associated latent heat is saved.

Back to completing the remaining drying in the conventional dryer, we now have 50 kg product with 50% moisture which is reduced to 15%. The solids weight in the product is now 25 kg instead of 15 kg in the original case. Hence, the final product weight will be 29.4 kg with 4.4 kg water in it (check: 4.4/29.4 = 15%). Consequently, the amount of moisture removed by conventional drying will be only (25 − 4.4) kg = 21.6 kg which is a reduction of (82.35 − 21.6) kg = 60.75 kg. Relative to the 82.35 kg water removed in the case of only conventional drying, this combination results in 75% reduction in the vaporization energy. The latent heat of vaporization of water is

about 2250 kJ per kg of evaporated water. For a 1000 kg batch (one metric ton) of apples, this will mean an energy reduction of 2250 kJ kg^{-1} × 600 kg or 1350 MJ per ton. The product weight is now 29.4 kg which is an increase of 11.7 kg compared to the direct conventional drying product weight of 17.7 kg (66% higher product weight, mostly coming from the infused solutes – never the less from an economic point of view an increase in production yield).

According to various research studies, convective drying of osmotically dehydrated apples shows no constant rate period because the water content is below its critical value, and, hence, the application of osmotic dehydration preceding convective drying reduces the total energy consumption by 24 to 75%, depending on the process conditions and the method to reconstitute the hypertonic solution (Kudra, 2009). According to Kudra (2009), convective drying of apples consumes about 5000 kJ per kg evaporated water (double what is required for evaporation), and nearly 40% of the water is evaporated during the constant rate period, even though there may be 10 to 25% reduction in drying rate due to a surface layer of concentrated sirup. Lewicki and Lenart (1992) estimated that a reduction in the water content of apples by 76% decreases the specific energy consumption by 46–51%, depending on the temperature of the osmotic dehydration. The same authors also indicated that, in osmotic dehydration of apples from 7.6 to 4.0 kg kg^{-1} (dry basis) carried out at 20 to 40 °C, the dehydration process consumes only 100 to 500 kJ per kg water removed, whereas concentration of the diluted solution by evaporation may increase the energy consumption to 2500 kJ kg^{-1} unless multiple effect evaporators are used. However, it has also been recognized that osmotic dehydration with sirup re-concentration demands two to three times lower energy (per unit) than convection drying (Lenart and Lewicki, 1988). Strumillo and Adamiec (1996) also confirmed the significant benefit of osmotic treatment before the convective drying step to minimize the energy demand in the overall drying process.

Grabowski *et al*. (2002) evaluated the osmotic dehydration of cranberries and noticed that the conventional drying of raw cranberries starts at the high moisture content of 87.4% (wet basis) while the finish drying of osmotically dehydrated cranberries begins at a moisture content of about 50% (wet basis). This means, according to Kudra (2009), that osmotic treatment allows nearly 75% of the water to be removed non-thermally from the berries, which is equivalent to about 2250 kJ of energy per kilogram of fresh berries when convective vibrating fluid bed or pulsed fluid bed drying methods follow the osmotic dehydration process. Complementing osmotic dehydration with convective drying methods has, therefore, considerable merit, due to the less energy-intensive character of the process, and more profitability as compared to the solitary use of conventional air drying methods.

3.5.2.2 **Osmo-Freeze Drying**

The freeze drying process consists mainly of two stages: (i) the product is frozen, and then (ii) the product is dried by direct sublimation of ice under reduced pressure. Freeze-dried products that have been adequately packaged can be stored for unlimited time, maintaining most of the physical, chemical, biological, and sensorial properties of the fresh product.

In freeze drying, frozen material is subjected to a pressure below the triple point and heated by conduction or radiation to cause ice sublimation to vapor. This method is usually used for high-quality dried products which contain heat-sensitive components, such as vitamins, antibiotics, volatiles or microbial culture. The virtual absence of air and low temperature prevents deterioration due to oxidation or chemical modification of the product. It also gives very porous products, which results in high rehydration rates. In addition, since there is no movement of liquid water, the sublimation process leaves the structure pretty intact except for the porosity created by the escaping vapor. Hence, there is practically no shrinkage but, since the product weight is reduced due to moisture removal, the bulk density will be very low and the porous structure makes the product very fragile. However, freeze drying is a slow and expensive process and mainly used for high-value products (Cohen and Yang, 1995). Due to high capital and operating costs the industrial application of freeze drying to a wide range of fruits and vegetables has been limited (Hammami and Rene, 1997). A long processing time requires additional energy to run the refrigeration and compressor units, which makes the process very expensive for commercial use. The extended processing time during freezing and sublimation processes is mainly due to the high water content of fruit and vegetable crops. Hence, by reducing the moisture level there is a possibility to shorten the required processing time and associated energy demands, as well as costs.

In the freeze drying process high energy levels are also used for freezing, because of the large quantity of water present in fresh foods. Robbers *et al.* (1997) carried out an experiment to evaluate the effect of osmotic dehydration of kiwi fruit during the freezing process. They conducted the experiment first by immersing fresh kiwi fruits in 68% (w/w) aqueous sucrose solution to dehydrate for 3 h, then subjecting them to an air-blast freezer with an air velocity of $3\,m\,s^{-1}$ and temperature of $-3\,^{\circ}C$. The experiment showed that freezing began at a lower temperature in the dehydrated product and the temperature of the dehydrated samples was reduced to $-18\,^{\circ}C$ in 19–20 min, which was about 20–30% faster than with untreated kiwi, which required a freezing time of 23–24 min. Generally speaking, lower water content of dehydrated food always induces a lower freezing point and a shorter freezing time as there is less water to freeze and, consequently, less heat to remove (Spiazzi *et al.*, 1998). This confirms that a reduction in the moisture content of food can reduce the refrigeration load during freezing, which has a significant impact on energy reduction.

The energy distribution and consumption of individual operations of freeze drying were evaluated by Liu *et al.* (2008). They investigated the effect of various operating conditions on the exergy (available energy to be used) losses in the three stages of freeze drying operations. According to their result, the exergy consumption in the primary drying reaches 35.7%, in vapor condensing 31.8%, and in the vacuum pumping 23.3% of the total exergy input. According to these figures almost 67% of the total energy input is used in the primary drying step and condensation of the vapor. Therefore, by reducing the volume of moisture to be frozen through osmotic dehydration, the volume of water to be evaporated during primary drying and condensed can be minimized. Reduction in moisture content through osmotic dehydration contributes to reducing freezing, primary drying and condensation

loads, and, consequently, a reduced energy demand is obtained for the overall freeze drying process. Therefore, a significant proportion of energy will be saved if the plant materials are concentrated prior to freezing (Robbers *et al.*, 1997).

3.5.2.3 **Osmo-Microwave Drying**

The major draw-back of the convective hot-air drying method, from an energy point of view, is the longer drying period, higher drying temperature and, therefore, high energy consumption, which may be as high as 6000 kJ per kg of water evaporated (Mujumdar and Menon, 1995; Alibas, 2007). To cope with these limitations microwave-assisted drying is used as an alternative solution. The removal of moisture by microwave drying has the following benefits when compared with convective drying: no need for a heating medium, fast and volumetric heating, higher drying rate, shorter drying time, more homogeneous energy distribution throughout the material, higher quality of the product and reduced energy consumption (Sanga *et al.*, 2000; Zhang *et al.*, 2006). However, the microwave drying process can have very high capital costs. In addition, the technology requires relatively expensive electricity energy, and, due to these limitations, it is only used in the final stages of drying (finish drying), where it can be used more efficiently than hot air (Gunasekaran, 1999).

Microwave radiation generates rapid volumetric heating of a wet material by altering the electromagnetic field to interact primarily with polar water molecules and ions in food materials (Varith *et al.*, 2007). In comparison to convective air drying, microwave drying offers significant energy savings, with a potential reduction in drying time up to 50% in addition to the inhibition of surface temperature of treated material (McLoughlin *et al.*, 2003). Because of their special heating behavior and high heating efficiency, microwave fields have been applied successfully to assist many drying processes.

This new process has been successfully used to dehydrate over 100 different fruits, vegetables, and other foods at temperatures below 54.4 °C (Vega-Mercado *et al.*, 2001). Several studies have shown that using pretreatments prior to microwave drying could decrease the drying time, and thus the drying costs (Drouzas and Schubert, 1996). Microwave-assisted convective drying of a thin layer of carrots reduced the total drying time by 25–90% (Prabhanjan *et al.*, 1995). To improve microwave-assisted drying, there are many combinations that can be considered for study. Among these combinations, researchers have shown that osmotic drying prior to microwave-assisted drying leads to lower energy consumption and a better quality dried product (Venkatachalapathy and Raghavan, 1998; Prothon *et al.*, 2001; Beaudry *et al.*, 2003). From the energy conservation point of view, a combination of osmotic dehydration with microwave-convective drying appears as a promising possibility for the production of dried fruits and vegetables with energy reduction benefits. Partial dehydration by osmosis has been widely employed prior to microwave drying, as a means of reducing processing time, and thus limiting energy consumption and improving sensory characteristics (Piotrowski *et al.*, 2004; Erle and Schubert, 2001).

The dielectric properties of materials are the key governing factors in microwave-assisted drying processes. It is reported that osmotic treatment reduces water content and increases soluble solids content within the sample, thus resulting in a decrease in

the dielectric constant (ε') and an increase in the effective loss factor ($\varepsilon''_{\text{eff}}$) as compared to the fresh sample (Heredia *et al.*, 2007). The amount of electromagnetic energy converted to heat per unit of volume in the dielectric material can be approximated (Rowley, 2001; Vicente and Castro, 2007) as:

$$P_V = 2 \cdot \pi \cdot f \cdot \varepsilon_0 \cdot \varepsilon''_{\text{eff}} \cdot E^2 \tag{3.1}$$

where, P_V is the rate of heat generated per unit of volume (W m^{-3}), f is the frequency of the electromagnetic wave applied (Hz), ε_0 is the dielectric constant of free space ($8.854 \times 10^{-12}\,\text{F m}^{-1}$), $\varepsilon''_{\text{eff}}$ is the effective relative loss factor of the material, and E is the electric field intensity (V m^{-1}).

From the above equation it can be understood that the power dissipation in microwave heating is proportional to the effective relative loss factor ($\varepsilon''_{\text{eff}}$) of the material. Therefore, osmotic pretreatment increases the effective loss factor ($\varepsilon''_{\text{eff}}$) that enhances the heat generation in the sample and accelerates the rate of the drying process. Al-Harashan *et al.* (2009) evaluated the osmotic pretreatment of tomato to eventually enhance the drying rate of microwave-dried tomato pomace. They found that the dielectric properties of the product were modified, resulting in an increase in dielectric loss factor and decrease in dielectric constant. Torringa *et al.* (2001), in their study on osmotic dehydration of mushrooms with salt solutions of 10 and 15% with bath temperatures of 20 and 45 °C, showed that the osmotically treated samples resulted in a 30% moisture loss prior to the MW drying. According to the authors, the drying time for microwave dehydration can be reduced by 10–20% as a result of the lower initial moisture content by osmotic pretreatment. Prothon *et al.* (2001) treated apple cubes osmotically in 50% (w/w) sucrose and then dried them in a microwave-assisted drier to demonstrate a significant reduction in the time required to reach 10% moisture.

Simultaneous microwave heating and osmotic dehydration have been carried out in recent years by Li and Ramaswamy (2006a, b), who demonstrated an acceleration of the moisture loss and a reduction in the solid gain for apple cylinders immersed in the osmotic solution under continuous flow conditions. More recently, Azarpazhooh and Ramaswamy (2010a, b) compared the osmotic drying effect under different conditions: microwave osmotic drying in spray mode, microwave osmotic drying in immersion mode, conventional osmotic drying in spray mode, and conventional osmotic drying in immersion mode. Experiments were conducted at two sucrose concentration and temperature combinations (40° Brix/40 °C and 50° Brix/50 °C). They reported that the moisture loss in microwave osmotic drying spray mode was around 35% as compared to conventional spray and immersion drying methods having moisture loss of less than 12% after 30 min of drying. The MW medium was better than the conventional one, and the spray mode was better than the immersion mode.

Increase in power absorbed during microwave heating results in an increase in the energy consumption rate per unit mass of water during microwave-assisted drying. Equation 3.2 can be used for the energy consumption (DE) per unit mass of water during microwave assisted intermittent power supply (Beaudry *et al.*, 2003; Yongsawatdigul and Gunasekaran, 1996). This equation is specific to intermittent

microwave irradiation, and does not account for the energy supplied by hot air (Beaudry *et al.*, 2003) or for the energy demand for the vacuum (Yongsawatdigul and Gunasekaran, 1996) during the drying process:

$$\mathrm{DE} = \frac{t_{\mathrm{on}} P(1-X_{\mathrm{f}}')}{m_{\mathrm{i}}(X_{\mathrm{i}}'-X_{\mathrm{f}}')} \tag{3.2}$$

Here, t_{on} is the total time that the microwave power is on (s); P is the input microwave power (W); m_{i} is the initial mass of the material (kg); and X_{i}' and X_{f}' are the initial and final material moisture content (wet basis), respectively. From the equation it can be inferred that the higher power and lower initial moisture content of osmotically treated food will yield a higher DE value as compared to an osmotically untreated one. An increase in the drying rate by increasing the power was also indicated by Drouzas and Schubert (1996).

In addition to microwave-convective drying, nowadays, microwave-vacuum drying technology also provides an alternative to other methods with respect to cost and food quality (Drouzas *et al.*, 1999). The use of microwaves helps to overcome the common problem associated with poor heat transfer in vacuum drying. The dehydration rate for microwave vacuum drying is always fast. It takes 33 min to dry carrot slices from 91.4 to 10% (wet basis) with microwave-vacuum, while 8 and 72 h are necessary to dry them with hot air and freeze-drying, respectively, according to Lin *et al.* (1998). Drouzas and Schubert (1996) showed that increasing the pressure or microwave power level reduced the final quality of dried banana slices, but the drying rate was significantly raised with increased microwave power level and reduced pressure.

The application of an osmotic treatment prior to microwave vacuum drying combines the advantages of both unit operations in a unique way: since no phase transition takes place in osmotic dehydration, energy consumption is especially low, even if the diluted solution needs to be re-concentrated by evaporation (Erle and Schubert, 2001). Drying performance results (defined as mass of evaporated water per unit of supplied energy) on cranberries showed that microwave vacuum drying is more energy-efficient than microwave convective drying (Sunjka *et al.*, 2004). Based on this, hybrid technology combining osmosis with microwave vacuum drying can be used to produce dehydrated high quality products with reduced energy cost. The combined application of osmotic dehydration, microwave energy, and vacuum creates food products with properties comparable to freeze drying, in a shorter time and, thus, at lower cost. In comparison to other advanced drying technologies (i.e., freeze drying) microwave vacuum drying is more economical, as drying is much faster and thus allows a higher throughput for the same plant dimensions (Ahrens *et al.*, 2006).

3.5.2.4 **Osmotic-Vacuum Drying**

In the vacuum drying method the food is subjected to a low pressure and simultaneous low heating source (conductive or radiative). The vacuum allows the water to vaporize at a lower temperature than under atmospheric conditions, thus foods can be dried without exposure to high temperature, and the low level of oxygen in the

atmosphere diminishes oxidation reactions during drying. In general, color, texture, and flavor of vacuum or vacuum-freeze dried products are improved as compared with air-dried products.

Pressure-driven flow is the major mechanism for moisture removal from a food. Because of the need to create reduced pressure in a drying chamber the technique is more expensive, and often used as a secondary dryer. The duration of the vacuum drying process mainly depends on the level of moisture to be removed, and the level of reduced pressure to be maintained. The energy and reduced pressure demand to remove moisture from a food can be minimized by combining osmotic treatment before the actual vacuum drying. This method is more advantageous for fruits and vegetables which are very rich in moisture, so that osmotic dehydration can reduce the percentage of original moisture to be removed by vacuum drying by 50%. For fruits with high water activity and porosity, the application of osmotic dehydration under vacuum was found to be advantageous compared to atmospheric osmotic dehydration (Mujica-Paz *et al.*, 2003). Shi *et al.* (1995) evaluated the influence of vacuum on mass transfer during the osmotic dehydration of fruits, and they confirmed that osmotic dehydration under vacuum makes it possible to obtain a higher diffusion rate of water transfer at lower solution temperatures for fruits with high porosity. Beaudry *et al.* (2004) compared four drying methods (osmo-vacuum, osmo-microwave, osmo-freeze and osmo-convective) and found that the drying rate of osmo-vacuum treated cranberries is the next highest after the osmo-microwave drying method. Moreover, reduction in pressure causes the expansion and escape of gas enclosed in the pores, and the pores can then be occupied by osmotic solution, thus increasing the mass transfer rate (Rahman and Perera, 2007). The process strongly favors solute uptake through an effective increase of mass transfer surface, caused by replacement of gas in the pores with osmotic solution (Fito *et al.*, 1994; Chiralt *et al.*, 1999). Therefore, the advantage of osmotic dehydration at vacuum pressures over atmospheric osmotic dehydration is that the solid/liquid interface area and the mass transfer between both phases can be increased (Fito *et al.*, 2002). The cumulative sum of the above benefits of enhanced rate of drying and rapid mass transfer leads to significant energy reduction in the osmo-vacuum drying method as compared to conventional vacuum drying.

3.6 Conclusions

Osmotic dehydration is a simultaneous mass transfer process which promotes the flow of water from the food to osmo-active solution and solute from the solution into the food. Different factors influence the overall mass transfer kinetics during the dehydration process. The structural matrix of foods and their modification through various treatments and methods determine the extent of mass transfer. The purpose of osmotic treatment has been traditionally to give the product a quality advantage. The treatment generally results in a better acid–sugar blend, the solids gain generally

limits the product shrinkage, and the treatment in solution prevents direct exposure to air and minimizes oxidative degradation. Finally, the bulk of the moisture is removed at relatively low temperature, and directly in the form of liquid water rather than vapor, providing a means for reducing the energy needs. In general, the osmotically treated dehydrated products have better color, flavor, texture and taste as compared to untreated ones.

The moisture content of fruits and vegetables can be as high as 75–95% and over 50% of this moisture can be removed by the osmotic treatment. Since the vaporization process is a very energy demanding process, this treatment prior to conventional dehydration can result in significant energy savings. Some estimates place the energy savings at over 1000 MJ per ton. Reduction of costs associated with energy is one means to maximize the economic performance of the food processing industry. For instance, energy saving in drying by 1% could result in as much as a 10% increase in profit margin. Osmotic dehydration can help to achieve this.

Even though osmotic dehydration is a novel approach to enhance drying and reduce energy cost, it is not free from limitations. The major limitation is that it increases the saltiness or sweetness of the product, which may ultimately affect the product's organoleptic properties. In addition to this, the cost of osmotic agent, osmotic agent dilution, reconstitution, sirup reuse and waste disposal are some of the additional steps which should be considered during the osmotic dehydration process. In particular, recycling of sirup, and microbial contamination, as well as the energy demand for reconstitution, are additional limitations for wide application of the method. Furthermore, disposal of the waste in large scale application of the method should be considered from the environmental point of view.

3.7 Additional Notation Used in Chapter 3

DE	specific energy demand	$J\,kg^{-1}$
E	electric field intensity	$V\,m^{-1}$
f	frequency	s^{-1}
X'	solids moisture content (wet basis)	–

Greek Letters

ε'	dielectric constant	–
$\varepsilon''_{\text{eff}}$	effective loss factor	–
ε_0	dielectric constant of free space	$F\,m^{-1}$

Subscripts and Superscripts

i	initial
f	final
on	power on

Abbreviations

MW	microwave
SG	solids or solutes gain
WL	water loss
WR	weight reduction

References

Ahrens, G., Kriszio, H., Langer, G., 2006. Microwave vacuum drying in the food processing industry. *Report from the 8th International Conference on Microwave and High Frequency Heating*, Bayreuth, Germany, pp. 426–435.

Al-Harashan, M., Al-Muhtaseb, A. H., Magee, T. R. A., 2009. Microwave drying kinetics of tomato pomace: Effect of osmotic dehydration. *J. Chem. Eng. Process.* **48**: 524–531.

Alibas, I., 2007. Microwave, air and combined microwave-air-drying parameters of pumpkin slices. *LWT-Food Sci. Technol.* **40**: 1445–1451.

Azarpazhooh, E., Ramaswamy, H. S., 2010a. Microwave-osmotic dehydration of apples under continuous flow medium spray conditions: Comparison with other methods. *Drying Technol.* **28**(1): 49–56.

Azarpazhooh, E., Ramaswamy, H. S., 2010b. Evaluation of diffusion and Azuara models for mass transfer kinetics during microwave-osmotic dehydration of apples under continuous flow medium-spray conditions. *Drying Technol.* **28**(1): 57–67.

Azuara, E., Cortes, R., Garcia, H. S., Beristain, C. I., 1992. Kinetic model for osmotic dehydration and its relationship with Fick's second law. *Int. J. Food Sci. Technol.* **27**: 239–242.

Beaudry, C., Raghavan, G. S. V., Rennie, T. J., 2003. Microwave finished drying of osmotically dehydrated cranberries. *Drying Technol.* **21**: 1797–1810.

Beaudry, C., Raghavan, G. S. V., Ratti, C., Rennie, T. J., 2004. Effect of four drying methods on the quality of osmotically dehydrated cranberries. *Drying Technol.* **22**(3): 521–539.

Beedie, M., 1995. Energy saving – a question of quality. *S. Afr. J. Food Sci. Technol.* **48**(3): 14–16.

Camirand, W., Krochta, J. M., Pavlath, A. E., Wong, D., Cole, M. E., 1992. Properties of some edible carbohydrate polymer coatings for potential use in osmotic dehydration. *Carbohyd. Polym.* **17**: 39–49.

Chiralt, A., Fito, P., Andres, A., Barat, J. M., Martinez-Monzo, J., Martinez-Navarrete, N., 1999. Vacuum impregnation: A tool in minimally processing of foods, in *Processing of foods: Quality optimization and process assessment* (eds F. A. R. Oliveira, J. C. Oliveira). CRC Press, Boca Raton, USA, pp. 341–356.

Chiralt, A., Martinez-Navarrete, N., Martinez-Monzo, J., Talens, P., Moraga, G., Ayala, A., Fito, P., 2001. Changes in mechanical properties throughout osmotic processes cryoprotectant effect. *J. Food Eng.* **49**: 129–135.

Cohen, J. S., Yang, T. C. S., 1995. Progress in food dehydration. *Trends Food Sci. Technol.* **6**: 20–25.

Drouzas, A. E., Schubert, H., 1996. Microwave application in vacuum drying of fruits. *J. Food Eng.* **28**(2): 203–206.

Drouzas, A. E., Tsami, E., Saravacos, G. D., 1999. Microwave/vacuum drying of model fruit gels. *J. Food Eng.* **39**: 117–122.

Erle, U., Schubert, H., 2001. Combined osmotic and microwave-vacuum dehydration of apples and strawberries. *J. Food Eng.* **49**: 193–199.

Fito, P., Andres, A., Pastor, R., Chiralt, A., 1994. Vacuum osmotic dehydration of fruits, in *Minimal processing of foods and process optimization: An interface* (eds R. P. Singh, F. A. R. Oliveira). CRC Press, Boca Raton, USA, pp. 107–122.

Fito, P., Chiralt, A., Barat, J. M., Martinez-Monzo, J., 2002. Mass transfer and deformation-relaxation phenomena in plant tissues, in *Engineering and food for the 21st century* (eds J. Welti-Chanes, G. V. Barbosa-Canovas, J. M. Aguilera). CRC Press, Boca Raton, USA, pp. 235–252.

Fuente-Blanco, S., Sarabia, E. R. F., Acosta-Aparicio, V. M., Blanco-Blanco, A., Gallego-Juarez, J. A., 2006. Food drying process by power ultrasound. *Ultrason. Sonochem.* **44**: 523–527.

Giraldo, G., Talens, P., Fito, P., Chiralt, A., 2003. Influence of sucrose solution concentration on kinetics and yield during osmotic dehydration of mango. *J. Food Eng.* **58**: 33–43.

Grabowski, S., Marcotte, M., Poirier, M., Kudra, T., 2002. Drying characteristics of osmotically pretreated cranberries: Energy and quality aspects. *Drying Technol.* **22**: 1129–1151.

Gunasekaran, S., 1999. Pulsed microwave-vacuum drying of food materials. *Drying Technol.* **17**(3): 395–412.

Hammami, C., Rene, F., 1997. Determination of freeze-drying process variables for strawberries. *J. Food Eng.* **32**(2): 133–154.

Heredia, A., Barrera, C., Andres, A., 2007. Drying of cherry tomato by a combination of different dehydration techniques: Comparison of kinetics and other related properties. *J. Food Eng.* **80**: 111–118.

Hilderbrand, K. S., 1992. Fish smoking procedures for forced convection smokehouse. Special Report 887, Oregon State University Extension Service, Oregon, USA, 1–41.

Kudra, T., 2004. Energy aspects in drying. *Drying Technol.* **22**: 917–932.

Kudra, T., 2009. Energy aspects in food dehydration, in *Advances in food dehydration* (ed. C. Ratti). CRC Press, New York, USA, pp. 423–443.

Lazarides, H. N., 1995. Osmotic preconcentration as a tool in freeze preservation of fruits and vegetables. *Proceedings of 2nd International Seminar on Osmotic Dehydration of Fruits and Vegetables*, Poland, Warsaw, pp. 88–98.

Lazarides, H. N., Mavroudis, N., 1995. Freeze/thaw effect on mass transfer rates during osmotic dehydration. *J. Food Sci.* **60** (4): 826–829.

Lazarides, H. N., 2001. Reasons and possibilities to control solids uptake during osmotic treatment of fruits and vegetables, in *Osmotic dehydration and vacuum impregnation: Applications in food industries* (eds P. Fito, A. Chiralt, J. M. Barat, W. E. L. Spiess, D. Behsnilion). Technomic Publ., Lancaster, USA, pp. 33–42.

Le Maruer, M., Biswall, C. J., 1988. Multicomponent diffusion and vapour liquid equilibria of dilute organic components in aqueous sugar solutions. *AIChE J.* **18**(3): 513–519.

Le Maguer, M., Mazzanti, G., Fernandezm, C., 2002. *The cellular approach in modeling mass transfer in fruit tissues.* CRC Press, Boca Raton, USA, pp. 193–215.

Lenart, A., Flink, J. M., 1984. Osmotic concentration of potato, I. Criteria for the end-point of the osmosis process. *J. Food Technol.* **19**: 45–63.

Lenart, A., Lewicki, P. P., 1988. Energy consumption during osmotic and convective drying of plant tissue. *Acta Aliment. Pol.* **14**: 65–72.

Lewicki, P. P., Lenart, A., Pakua, W., 1984. Influence of artificial semi-permeable membranes on the process of osmotic dehydration of apples. *Food Technol. Nutr.* **16**: 17–24.

Lewicki, P. P., Lenart, A., 1992. Energy consumption during osmo-convection drying of fruits and vegetables, in *Drying of solids* (ed. A. S. Mujumdar). Intern. Sci. Publ., New York, USA, and IBH Publ., New Delhi, India, pp. 354–367.

Li, H. P., Ramaswamy, H. S., 2006a. Osmotic dehydration of apple cylinders: I. Conventional batch processing conditions. *Drying Technol.* **24**(5): 619–630.

Li, H. P., Ramaswamy, H. S., 2006b. Osmotic dehydration of apple cylinders: III. Continuous medium flow microwave heating conditions. *Drying Technol.* **24**(5): 643–651.

Lin, T. M., Durance, T. D., Scarman, C. H., 1998. Characterisation of vacuum-microwave air and freeze dried carrot slices. *Food Res. Int.* **31**(2): 111–117.

Liu, Y. Z., Zhao, Y. F., Feng, X., 2008. Exergy analysis for a freeze-drying process. *Appl. Therm. Eng.* **28**: 675–690.

Maestrelli, A., Lo Scalzo, R., Lupi, D., Bertolo, G., Torregiani, D., 2001. Partial removal of water before freezing: Cultivar and

pretreatments as quality factors of frozen muskmelons (*Cucumis melo*, cv reticulates Naud.). *J. Food Eng.* **49**: 255–260.
Mavroudis, N. E., Gekas, V., Sjöholm, I., 1998. Osmotic dehydration of apples: Shrinkage phenomena and the significance of the initial structure on mass transfer rates. *J. Food Eng.* **38**: 101–123.
McLoughlin, C. M., McMinn, W. A. M., Magee, T. R. A., 2003. Microwave drying of multi-component powder systems. *Drying Technol.* **21**: 293–309.
Moy, J. H., Lau, N. B. H., Dollar, A. M., 1978. Effects of sucrose and acids on osmovac-dehydration of tropical fruits. *J. Food Process. Preserv.* **2**: 131–135.
Mujica-Paz, H., Valdez-Fragoso, A., Lopez-Malo Palou, A. E., Welti-Chanes, J., 2003. Impregnation and osmotic dehydration of some fruits: Effect of the vacuum pressure and syrup concentration. *J. Food Eng.* **57**: 305–314.
Mujumdar, A. S., Menon, A. S., 1995. Drying of solids: Principles, classification, and selection of dryers, in *Handbook of industrial drying* (ed. A. S. Mujumdar). Marcel-Dekker, New York, USA, pp. 1–39.
Mujumdar, A. S., Beke, J., 2003. Grain drying: Basic principles, in *Handbook of postharvest technology: Cereals, fruits, vegetables, tea, and spices* (eds A Chakraverty, A. S. Mujumdar, G. S. V. Raghavan, H. S. Ramaswamy). Marcel Dekker, New York, USA, pp. 119–139.
Mujumdar, A. S., 2007. Principles, classification and selection of dryers, in *Handbook of industrial drying*, 3rd edn (ed. A. S. Mujumdar). Taylor and Francis, Boca Raton, USA, pp. 3–32.
van Nieuwenhuijzen, N., Zareifard, M. R., Ramaswamy, H. S., 2001. Osmotic drying kinetics of cylindrical apple slices of different sizes. *Drying Technol.* **19**(3–4): 525–545.
Nunes, Y., Moreira, R. G., 2009. Effect of osmotic dehydration and vacuum-frying parameters to produce high-quality mango chips. *Food Eng. Phys. Prop.* **24**: 355–362.
Ochoa-Martinez, C. I., Ramaswamy, H. S., Ayala-Aponte, A. A., 2007. A comparison of some mathematical models used for the prediction of mass transfer kinetics in osmotic dehydration of fruits. *Drying Technol.* **25**(10): 1613–1620.
Panagiotou, N. M., Karathanos, V. T., Maroulis, Z. B., 1999. Effect of osmotic agent on osmotic dehydration of fruits. *Drying Technol.* **17**: 175–189.
Piotrowski, D., Lenart, A., Wardzynski, A., 2004. Influence of osmotic dehydration on microwave-convective drying of frozen strawberries. *J. Food Eng.* **65**: 519–525.
Prabhanjan, D. G., Ramaswamy, H. S., Raghavan, G. S. V., 1995. Microwave assisted convective air drying of thin layer carrots. *J. Food Eng.* **25**(2): 283–293.
Prothon, F., Ahrne, L. M., Funebo, T., Kidma, S., Langton, M., Sjöholm, I., 2001. Effects of combined osmotic and microwave dehydration of apple on texture, microstructure and rehydration characteristics. *Lebensm. Wiss. Technol.* **34**(2): 95–101.
Rahman, M. S., Lamb, J., 1990. Osmotic dehydration of pineapple. *J. Food Sci. Technol.* **27**: 150–152.
Rahman, M. S., Perera, C. O., 2007. Drying and food preservation, in *Handbook of food preservation*, (ed M. S. Rahman). CRC Press, USA, pp. 403–432.
Ramaswamy, H. S., Nsonzi, F., 1998. Convective-air drying kinetics of osmotically pretreated blueberries. *Drying Technol.* **16** (3–5): 743–759.
Ramaswamy, H. S., van Nieuwenhuijzen, N. H., 2002. Evaluation and modeling of two-stage osmo-convective drying of apple slices. *Drying Technol.* **20**(3): 651–667.
Rastogi, N. K., Raghavarao, K., 1997. Water and solute diffusion coefficients of carrot as a function of temperature and concentration during osmotic dehydration. *J. Food Eng.* **34**: 429–440.
Rastogi, N. K., Niranjan, K., 1998. Enhanced mass transfer during osmotic dehydration of high pressure treated pineapple. *J. Food Sci.* **63**: 508–511.
Rastogi, N. K., Eshtiaghi, M. N., Knorr, D., 1999. Accelerated mass transfer during osmotic dehydration of high intensity electrical field pulse pretreated carrots. *J. Food Sci.* **64**: 1020–1023.
Rastogi, N. K., Angersbach, A., Niranjan, K., Knorr, D., 2000. Rehydration kinetics of high pressure pretreated and osmotic dehydrated pineapple. *J. Food Sci.* **65**(5): 838–841.
Robbers, M., Singh, R. P., Cunha., L. M., 1997. Osmotic-convective dehydrofreezing

process for drying kiwifruit. *J. Food Sci.* **62** (5): 1039–1042.

Rodrigues, S., Gomes, M. C. F., Gallao, M. I., Fernandesc, F. A. N., 2009. Effect of ultrasound-assisted osmotic dehydration on cell structure of sapotas. *J. Sci. Food Agric.* **89**: 665–670.

Rowley, A. T., 2001. *Thermal technologies in food processing.* Woodhead Publishing, Cambridge, U.K, pp. 163–177.

Salvatori, D., Andres, A., Albors, A., Chiralt, A., Fito, P., 1998. Structural and compositional profiles in osmotically dehydrated apple. *J. Food Sci.* **63**(4): 606–610.

Sanga, E., Mujumdar, A. S., Raghavan, G. S. V., 2000. Principles and applications of microwave drying, in *Drying technology in agriculture and food sciences* (ed. A. S. Mujumdar). Science Publ., Enfield, USA, pp. 253–286.

Shi, X. Q., Fito, P., Chiralt, A., 1995. Influence of vacuum treatment on mass transfer during osmotic dehydration of fruits. *Food Res. Int.* **28**(5): 445–454.

Shi, J., 2008. Osmotic dehydration of foods, in *Food drying science and technology: Microbiology, chemistry, applications* (eds Y. H. Hui, C. Clary, M. M. Farid, O. O. Fasina, A. Noomhorm, J. Welti-Chanes). DEStech Publ., Lancaster, USA, pp. 275–295.

Sormani, A., Maffi, D., Bertolo, G., Torreggiani, D., 1999. Texture and structural changes of dehydrofreeze thawed strawberry slices: Effects of different dehydration pretreatments. *Food Sci. Tech. Int.* **5**: 479–485.

Spiazzi, E. A., Raggio, I., Bignone, K. A., Mascheroni, R. H., 1998. Experiments on dehydrofreezing of fruits and vegetables: Mass transfer and quality factors. *Advances in the Refrigeration Systems, Food Technologies and Cold Chain, IIF/IIR* **6**: 401–408.

Strumillo, C., Adamiec, J., 1996. Energy and quality aspects of food drying. *Drying Technol.* **14**(2): 423–448.

Sunjka, P. S., Rennie, T. J., Beaudry, C., Raghavan, G. S. V., 2004. Microwave-convective and microwave-vacuum drying of cranberries: A comparative study. *Drying Technol.* **22**: 1217–1231.

Tedjo, W., Taiwo, K. A., Eshtiaghi, M. N., Knorr, D., 2002. Comparison of pretreatment methods on water and solid diffusion kinetics of osmotically dehydrated mangos. *J. Food Eng.* **53**: 133–142.

Torreggiani, D., 1993. Osmotic dehydration in fruit and vegetable processing. *Food Res. Int.* **26**: 59–68.

Torringa, E., Lourenco, F., Scheewe, I., Bartels, P., 2001. Application of microwave drying after osmotic dehydration: Effect of dielectric properties on heating characteristics, in *Osmotic dehydration and vacuum impregnation* (eds P. Fito, A. Chiralt, J. M. Barat, W. E. L. Spiess, D. Behsnilia). Technomic Publ., Lancaster, USA, pp. 217–225.

Toupin, C. J., Le Maguer, M., 1989. Osmotically-induced mass transfer in plant storage tissues: A mathematical model. Part II. *J. Food Eng.* **10**: 97–121.

Varith, J., Dijkanarukkul, P., Achariyaviriya, A., Achariyaviriya, S., 2007. Combined microwave-hot air drying of peeled longan. *J. Food Eng.* **81**(2): 459–468.

Vega-Mercado, H., Marcela Gongora-Nieto, M., Barbosa-Canovas, G. V., 2001. Advances in dehydration of foods. *J. Food Eng.* **49** (4): 271–289.

Venkatachalapathy, K., Raghavan, G. S. V., 1998. Microwave drying of osmotically dehydrated blueberries. *J. Microwave Power E.E.* **33**(2): 95–102.

Vicente, A., Castro, I. A., 2007. Thermal and non-thermal food preservation technologies, in *Advances in thermal and non-thermal food preservation* (eds G. Tewari, V. K. Juneja). Blackwell, Iowa, B USA, pp. 99–144.

Welti-Chanes, J., Vergara-Balderas, F., Bermudez-Aguirre, D., 2005. Transport phenomena in food engineering: Basic concepts and advances. *J. Food Eng.* **67** (1–2): 113–128.

Wong, W. S., Tillin, S., Hudson, J. S., Pavlath, E., 1994. Gas exchange in cut apples with bilayer coatings. *J. Agr. Food Chem.* **10** (42): 2278–2285.

Yongsawatdigul, J., Gunasekaran, S., 1996. Microwave-vacuum drying of cranberries: Part 1, Energy use and efficiency. *J. Food Process. Preserv.* **20**: 121–143.

Zhang, M., Tang, J. M., Mujumdar, A. S., 2006. Trends in microwave-related drying of fruits and vegetables. *Trends Food Sci. Tech.* **17**: 524–534.

4
Heat Pump Assisted Drying Technology – Overview with Focus on Energy, Environment and Product Quality

Sachin V. Jangam and Arun S. Mujumdar

4.1
Introduction

Drying is one of the most important unit operations in the chemical, food, biochemical, pharmaceutical, and several other industries. Thermal drying is an extremely energy intensive unit operation which ultimately contributes to the emission of green house gases (Baker, 2005; Kudra, 2004). The energy used in the drying operations is of the order of 15–20% of the total energy used for industrial production in developed countries (Mujumdar, 2006; Kudra and Mujumdar, 2009). This can be attributed to various reasons, such as poor design of dryers, non-uniform distribution of drying media which results in inefficient heat utilization, poor insulation of dryers, improper control of dryers, and, of course, the high latent heat of vaporization of water (Baker, 2005). In addition, in conventional drying systems using the convection mode of heat transfer, the evaporated moisture is usually vented off along with the drying medium, resulting in loss of both sensible and latent heat of vaporization of moisture. In view of the present energy scenario it is obligatory for the industrial sector to develop energy efficient drying operations. There have been numerous studies conducted on increasing the efficiency of the drying system and very useful guidelines have been suggested by various researchers (Kudra *et al.*, 2009; Baker, 2005; Mujumdar, 2006).

When heat pumps are used in the drying operation, the moist air (the most common drying medium) leaving the dryer is cooled/dehumidified and recirculated back with addition of heat, thus recovering both sensible and latent heat. Heat pumps have been around for many years and have been used in several applications for heat recovery (Gopichand and Devotta, 1988; Omideyi *et al.*, 1984; Supranto *et al.*, 1986). When the air leaving the dryer is recirculated via a heat pump, the added benefit of dehumidification of the drying air is also realized, increasing its moisture carrying capability and thus achieving faster drying. Although heat pump assisted drying (HPD) was initially used for grain drying (Lai and Foster, 1977; Harrison and Allen, 1980; Kato, 1981), timber drying was the first well-known application (Margaret, 1991; Shang *et al.*, 1995). Lately, the potential in heat pump drying has led to applications in the pharmaceutical, biotechnological and food industries as well (Schmid, 1994;

Modern Drying Technology Volume 4: Energy Savings, First Edition.
Edited by Evangelos Tsotsas and Arun S. Mujumdar

Alves-Filho and Strommen, 1996; Perera and Rahman, 1997; Alves-Filho *et al.*, 1997; Chua *et al.*, 2002a, b; Strommen *et al.*, 2004; Islam and Mujumdar, 2008a, 2008b; Alves-Filho *et al.*, 2008; Gungor et al., 2011). Any type of dryer working in the convective mode can be fitted with a heat pump. Figure 4.1 shows a number of possibilities that can be exploited with a heat pump drying system. Batch tray and shelf dryers are the most common but heat pumps have also been used with fluid bed, spray and various other continuous dryers (Prasertsan and Saen-Saby, 1998a, b; Alves-Filho, 2002; Raghavan *et al.*, 2003; Chou and Chua, 2006; Claussen *et al.*, 2007b; Erbay *et al.*, 2010). Most common applications of HPD use air, however, other drying media have also been used for various reasons which will be discussed in detail in later sections. Mujumdar (1990) was the first to report the use of vapor compression in superheated steam drying. Heat pump dryers can be used in an open as well as a closed loop manner, depending on the application. The closed loop configurations have the added advantages of retention of aroma in the dried product during drying of some special high value products, and even the recovery of the solvent removed during drying of many pharmaceutical drugs which otherwise would pose danger if vented out along with the drying air.

The major factors which affect the properties of food, pharmaceutical and bio-products are the drying temperature and the drying time (Rossi *et al.*, 1992; Alves-Filho and Strommen, 1996; Strommen *et al.*, 2004). It has also been reported that some pharmaceutical products have a tendency to form polymorphs under certain drying air conditions. Heat pump dryers are of immense help in drying such heat-sensitive materials due to the possibility of controlled drying conditions – both temperature, from subzero to as high as 90 °C (using supplementary heating), and humidity, from 10 to 85% (by controlled mixing with steam) (Strommen *et al.*, 2004; Claussen *et al.*, 2007b). Thus, heat pump drying is beneficial in improving product quality, due to flexibility in operating conditions and independence from ambient conditions (Chua *et al.*, 2000; Perera and Rahman, 1997; Islam and Mujumdar, 2008a, b). Although electrical energy is used for driving heat pumps, high values of the coefficient of performance (COP) can make HPD cost-effective.

4.2
Heat Pump Drying System – Fundamentals

A heat pump dryer system is a combination of a heat pump system and a drying system. Before discussing further about HPD, it is essential to know the fundamentals of the heat pump cycle.

4.2.1
Heat Pump

Heat can only be transferred from a low temperature level to a higher temperature level with the addition of mechanical work. The device used for such a function is called a refrigerator. The refrigerator and the heat pump operate essentially on the

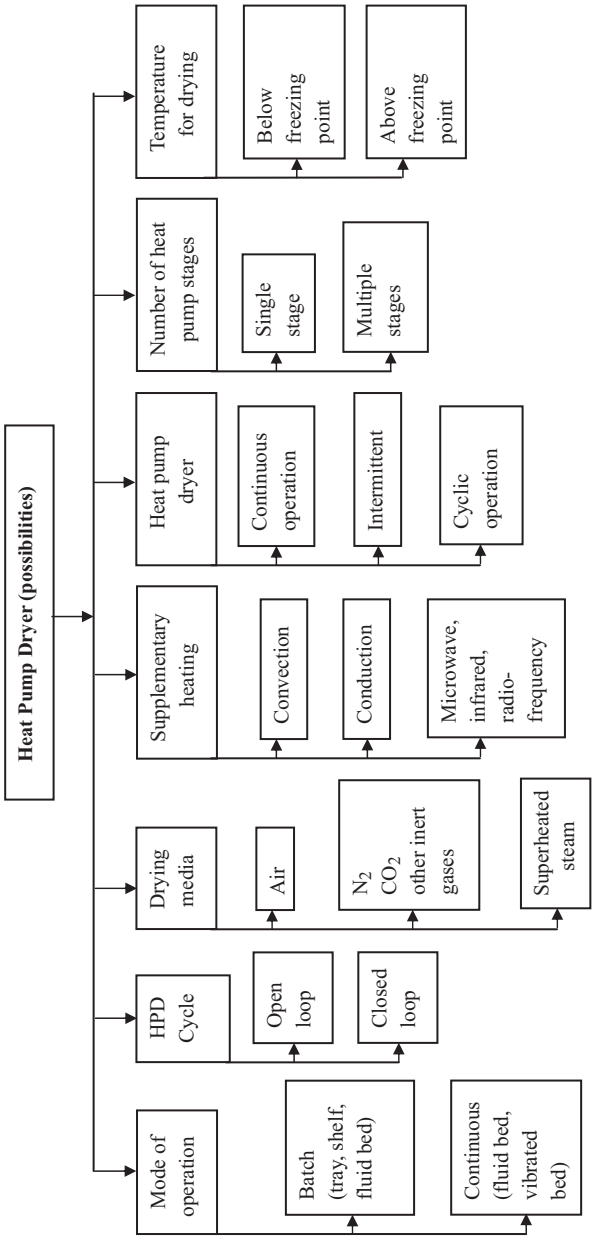

Fig. 4.1 Classification of heat pump dryers.

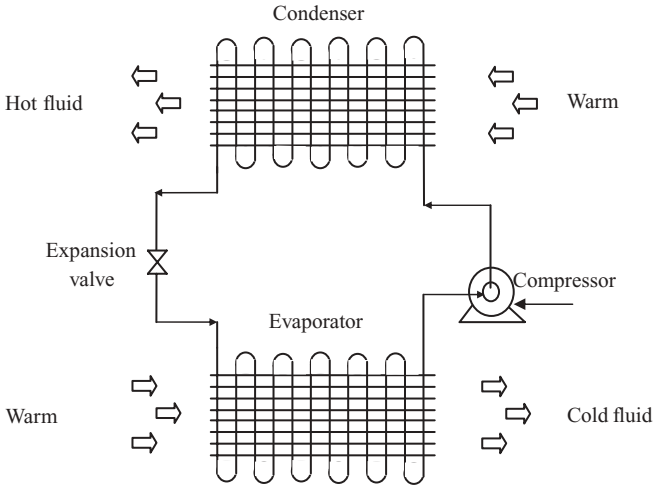

Fig. 4.2 Heat pump cycle.

same principle. The refrigerator is used to remove heat from the refrigerated space or to remove heat from a low energy source and transfer it to a high energy source. However, the rejection of heat to a high energy sink is not a goal but an essential part of the refrigeration cycle. On the other hand, heat pumps are used with the objective of supplying heat to a higher temperature sink by absorbing heat from a low temperature sink with additional mechanical work. This transfer of energy is achieved using a working fluid called the refrigerant (Whitman *et al.*, 2005; Hundy *et al.*, 2008; Wang, 2000; ASHRAE, 2002).

Figure 4.2 shows the different components of a simple vapor compression refrigeration/heat pump cycle while Fig. 4.3 shows the same cycle on a pressure–enthalpy

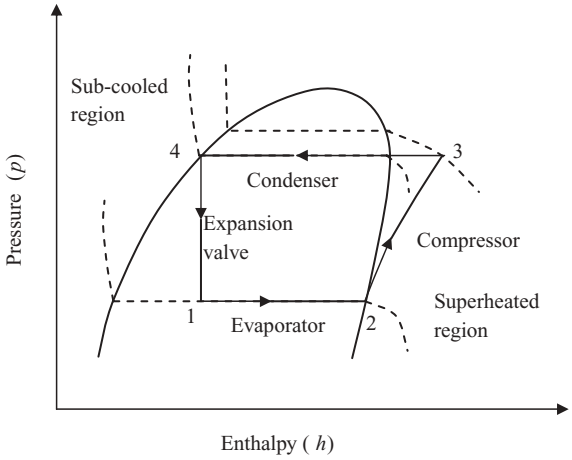

Fig. 4.3 Refrigerant cycle on *p–h* diagram.

diagram for a refrigerant undergoing variations in pressure and other properties after the different components. The main components of the vapor compression refrigeration cycle are the evaporator, compressor, condenser and the expansion valve (Wang, 2000). The sub-cooled liquid refrigerant at lower temperature is heated in an evaporator, extracting latent as well as sensible heat from the surrounding fluid which produces a cooling effect. The vapor refrigerant coming out of the evaporator goes through a mechanical compression to reach a high pressure state, as in the condenser, which is done using electrical energy. The refrigerant enters the condenser in a superheated state at high pressure, dissipates out heat to the surrounding fluid, and condenses. The condensed refrigerant at high pressure is expanded through an expansion valve to reach the lower pressure level of the evaporator where it absorbs heat again and the cycle continues. This is the simplest saturated vapor compression cycle; the real refrigeration cycle deviates a bit as a result of pressure losses in the evaporator and the condenser (Whitman *et al.*, 2005; Hundy *et al.*, 2008; Wang, 2000).

Details of the process steps are shown in Fig. 4.3 on a pressure–enthalpy diagram. The performance of a refrigerator or heat pump is described using the coefficient of performance (COP) which is defined as the ratio of either the heating effect (Eq. 4.1) or the cooling effect (Eq. 4.2) to the total work input:

$$\mathrm{COP}_{\text{heat pump}} = \mathrm{COP}_{\text{heating}} = \frac{\text{Heating effect}}{\text{Work input}} = \frac{h_3 - h_4}{h_3 - h_2} \tag{4.1}$$

$$\mathrm{COP}_{\text{refrigerator}} = \mathrm{COP}_{\text{cooling}} = \frac{\text{Cooling effect}}{\text{Work input}} = \frac{h_2 - h_1}{h_3 - h_2} = \mathrm{COP}_{\text{heating}} - 1 \tag{4.2}$$

The expansion of the refrigerant is a constant enthalpy steady process that is represented by a vertical line on the p–h diagram ($h_4 = h_1$). It can be seen from the p–h diagram that the heating effect of a heat pump ($h_3 - h_4$) is the sum of the energy absorbed by the refrigerant in the evaporator ($h_2 - h_1$) and the energy given to the compression ($h_3 - h_2$). The COP of a heat pump generally lies between 4 and 7, which means that the heating output is 4 to 7 times higher than the energy invested in the compressor. Although the higher grade electrical energy is converted to lower grade thermal energy; high values of the COP can make such "degradation" of energy cost-effective.

4.2.2 Refrigerants

Refrigerants are the working fluids used in a mechanical vapor compression cycle. Refrigerants should have desired thermodynamic properties such as boiling point below the required temperature, high critical temperature, high latent heat of vaporization, and so on. For many years, chlorofluorocarbons (CFCs) and hydro-chlorofluorocarbons (HCFCs), also known as "Freons", have been used as the working fluid for refrigeration, heat pumps and air conditioning

units because of their excellent chemical and thermodynamic properties. The most common CFC in use is dichlorodifluoromethane (R12), and the most commonly applied HCFC is difluoromonochloromethane, also known as R22. The use of these refrigerants in the food industry is enormous. However, there have been several environmental issues raised in recent decades due to possible depletion of the ozone layer caused by CFCs and HCFCs (Montreal protocol, 1987; Molina and Rowland, 1974; Devotta, 1995). The commonly used criteria for distinguishing the environmental impacts of particular refrigerants are the ozone depletion potential (ODP) and the global warming potential (GWP). The CFC and HCFC refrigerants are thus completely restricted in the developed countries because of high ODP and GWP values, while still in use in many developing countries. There have been numerous studies of substitution by, for example, ammonia and carbon dioxide, which are classical working fluids for industrial applications (Mujumdar, 2006; Devotta, 1995; Lorentzen, 1994). These refrigerants have either no (ammonia, see ASHRAE (2006)) or very little (CO_2) environmental impact (Neksa, 2002; Devotta, 1995). Mohanraj *et al.* (2009) have given a good review of alternate refrigerants which have low environmental impact. The hydrocarbons (HC) and mixtures of HC and HFC are becoming common for industrial as well as household applications. Propane has been proposed to give better efficiency compared to ammonia without any environmental impact. Mohanraj *et al.* (2009) have listed the possible options of refrigerants for various applications in coming years. However, they have also pointed out major difficulties in using these mixtures, which includes the occurrence of pinch points in the condenser and evaporators due to nonlinear variation of refrigerant properties, reduced effectiveness of condenser and evaporator, difficulty in sizing and selecting the components, and so on. Steam and air have also been used as the working fluids in heat pumps. It has been shown that the air cycle heat pump can give an evaporator temperature as low as $-40\,^{\circ}C$ and condenser temperature as high as $200\,^{\circ}C$. This can increase the versatility of the heat pump which can be used even for freeze drying.

Refrigerants are assigned a number for identification. Each identification number starts with the prefix "R" which means refrigerant. The suffix is a number which is defined based on the organic or inorganic nature of the substance. For organic refrigerants the suffix contains three numbers: the first equals the number of fluorine (F) atoms, the second is one more than the number of hydrogen atoms, and the third is one less than the number of carbon atoms. If the third number is zero, it is generally omitted. On the other hand, for inorganic refrigerants, the identification number is formed by adding the molecular mass of the compound to 700. To give an example, chlorodifluoromethane ($CHClF_2$) is an organic refrigerant with two fluorine, one hydrogen and one carbon atom, hence it is numbered as R22. Ammonia is an inorganic refrigerant with a molecular mass of 17, hence it is numbered as R717. Table 4.1 shows some of the commonly used refrigerants with their properties. ASHRAE (2004) classifies the refrigerants based on toxicity and flammability.

Tab. 4.1 Properties of commonly used refrigerants.

Classification	Name	Boiling Point (°C)	Latent Heat of Vaporization (kJ kg^{-1})	Critical Temperature (°C)	Critical Pressure (bar)
Natural					
R717	Ammonia	−33.34	1369	132.4	111.5
R744	Carbon dioxide	−57	574	31.1	73.8
R290	Propane	−42.1	428.31	96.6	42.5
R718	Water	100	2260	374	220.6
CFC/HCHC/HFCs					
R22	Chlorodifluoromethane	−40.7	233.95	96.2	49.36
R12	Dichlorodifluoromethane	−29.8	166.95	112	41.15
R11	Trichlorofluoromethane	23.8	—	198	43.8
R134a	1,1,1,2-Tetrafluoroethane	−26.3	215.9	101.3	40.7
R32	Difluoromethane	−51.6	360.24	78.45	58.3
Azeotropic mixtures					
R502	R22 (48.8%) + R115(51.2%)	−45.3	163.3	82.2	40.75
R507	R125 (50%) + R143a (50%)	−46.3	186.07	70.8	37.2

4.2.3 Heat Pump Dryer

In the drying process, it is essential to maintain the drying conditions, temperature and humidity of the drying air. Figure 4.4 shows a simple convective dryer coupled with a heat pump system. The main components of the dryer are: air blower, auxiliary heater, drying chamber and heat pump system (Alves-Filho and Efremov, 2009; Mujumdar, 2006; Islam and Mujumdar, 2008a, b). The thermodynamic path of air in the heat pump drying system is shown in Fig. 4.5 on a psychrometric chart. A part of the hot and moist air coming from the drying chamber goes through the evaporator, while the remaining air by-passes the evaporator. This is done so as to control the humidity of the air which is to be recirculated to the dryer by adjusting the flow rate of air over the evaporator and the flow rate of air by-passed (Islam and Mujumdar, 2008a, b; Alves-Filho and Efremov, 2009; Chou and Chua, 2006). The volumetric flow of air over the evaporator and the bypass are controlled commonly with butterfly dampers. When the air passes over the evaporator coils, the refrigerant takes out heat and the temperature of the air falls. Initially, the air is cooled without change in its absolute humidity (state 1–2 of Fig. 4.5). However, the relative humidity of the air increases, reaching 100% saturation or the dew point. As the air is cooled below the dew point temperature, condensation of moisture starts. If the air is cooled further, the temperature and absolute humidity decrease, following the saturation line on the psychrometric chart (state 2–3 of Fig. 4.5). On the other side, the refrigerant absorbs both sensible and the latent heat of condensation from the air and evaporates to a saturated or sometimes superheated state. This refrigerant is then compressed to a

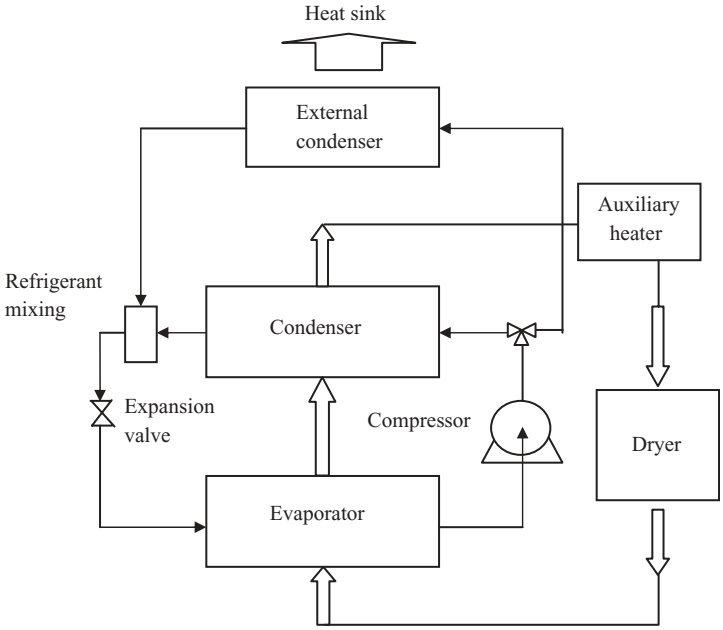

Fig. 4.4 Simple heat pump drying cycle.

high energy level. The condensed water from the air side, which has a temperature the same as that at state 3, is drained off.

The cold and dehumidified air which comes out from the evaporator is adiabatically mixed with the by-pass air before it is re-heated (state 3′ of Fig. 4.5). In some special applications this mixed air at lower temperature is used for

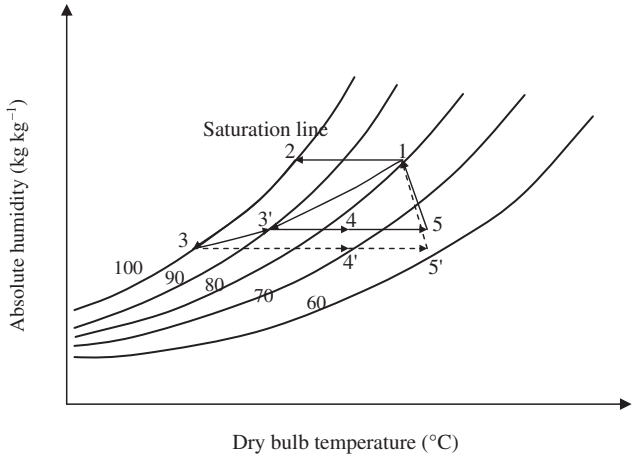

Fig. 4.5 Air cycle on a psychrometric chart.

drying, while in most cases it is passed over a condenser in order to be re-heated to the required temperature. The compressed refrigerant at higher pressure rejects heat in the condenser and heats up the air. Generally, the refrigerant coming out from the compressor is split into two condensers. The main condenser is used for re-heating the process air. The absolute humidity of the air remains the same while the relative humidity goes down as the air is heated in the condenser (path 3′-4 of Fig. 4.5). The secondary condenser is used to reject the remaining heat which is not required for the process air. The flow of refrigerant in these two condensers is controlled by a three-way valve, depending on the required temperature of the process air before the auxiliary heater. The air coming out of the condenser is then again heated to the dryer inlet temperature using auxiliary heating (4–5 of Fig. 4.5). The path 5–1 represents the drying process. The mass and energy balances of the different components and their use in sizing will be discussed in later sections.

The performance of a heat pump is defined by COP; however the performance parameter commonly used for a HP dryer is the specific moisture extraction rate (SMER) (Prasertsan and Saen-Saby, 1998a, b; Alves-Filho and Efremov, 2009; Islam and Mujumdar, 2008a, b). The SMER of a dryer is defined as the ratio of the amount of water evaporated in the dryer to the amount of energy input to the dryer:

$$\mathrm{SMER}\left(\frac{\mathrm{kg}}{\mathrm{kWh}}\right) = \frac{\text{Amount of water evaporated}}{\text{Energy input to the dryer}} \tag{4.3}$$

However, another parameter, known as specific energy consumption (SEC) – or heat pump dryer efficiency – is also used to compare the performance of various dryers. SEC is a reciprocal of SMER, that is, the energy used to evaporate a unit mass of water; it is generally related to COP as follows:

$$\mathrm{SEC} = \frac{W}{\text{water evaporated}} = \frac{Q_{\mathrm{ev}}/\left(\mathrm{COP}_{\mathrm{heating}}-1\right)}{M_{\mathrm{a}}\left(Y_1-Y_2\right)} = \frac{h_1-h_2}{\left(\mathrm{COP}_{\mathrm{heating}}-1\right)\left(Y_1-Y_2\right)} \tag{4.4}$$

For HPD, the SMER ranges from 1.0 to 4.0 and depends on various factors, such as the ambient conditions, the drying air conditions, the product moisture content and its thermo-physical properties, the refrigeration cycle, and the compressor efficiency. The value of the SMER decreases with decrease in the drying air temperature, as the COP of refrigeration decreases at lower evaporator temperature (Prasertsan and Saen-Saby, 1998a, b). Hence, it is advisable to use a higher drying temperature provided the product can tolerate it. A typical SMER value reported for HPD is $3\,\mathrm{kg\,kW^{-1}\,h^{-1}}$, whereas the SMER for convective dryers is in the range 0.5–1 kg $\mathrm{kW^{-1}\,h^{-1}}$. The value of SMER for HPDs can be as high as $10\,\mathrm{kg\,kW^{-1}\,h^{-1}}$ for advanced heat pump systems with optimized drying conditions (Islam and Mujumdar, 2008a, b). This definition of SMER only takes into account the work done in the compressor; however, the fan/blower power is not included. If a low drying temperature is used then the drying time is longer and the amount of energy consumed for blowing the air becomes significant and should be taken into account.

4.2.4
Advantages and Limitations of the Heat Pump Dryer

The major advantages of the heat pump dryer can be summarized as follows:

1) **Higher Efficiency**: The energy lost with moisture-laden air leaving the dryer is recovered and re-used, resulting in improved energy efficiency of the dryer. Lower humidity can enhance the drying rates.
2) **Drying Conditions**: A wide range of temperature from −20 to 90 °C and relative humidity from 10 to 90% can be achieved.
3) **Better Control**: HPD can offer accurate control of air flow, temperature and humidity. Different air condition cycles can be employed.
4) **Product Quality**: Low temperatures result in better product quality. The possibility of using an inert atmosphere also results in better quality by, for example, retention of aroma.

Table 4.2 (Mujumdar, 2006) shows a comparison of the heat pump dryer with commonly used hot air and vacuum dryers in terms of parameters such as SMER, drying efficiency, operating range of humidity and temperature, and various costs. Of course, the numerical values listed are sensitive to the operating conditions used.

However, HPD also has certain limitations due to:

1) **Environmental Effects**: The use of CFCs and HCFCs in most of the heat pump systems is of great environmental concern. However, recently developed environmentally friendly HCFCs and natural refrigerants may be used.
2) **Capital Cost**: The capital cost of a heat pump dryer is quite high compared to simpler hot air dryers. The main cost involved is in the procurement of various components of the heat pump such as the compressor, heat exchangers and controllers.

Tab. 4.2 Comparison of HPD with other commonly used dryers.

	Type of Dryer			
Parameter	**Heat Pump Dryer**	**Hot Air Dryer**	**Vacuum Dryer**	**Freeze Dryer**
SMER (kJ kg^{-1})	1.0–4.0	0.1–1.3	0.7–1.2	0.4 and lower
Operating temperature (°C)	−10 to 80	40 to very high	30–60	−35 to >50
Operating humidity (% RH)	10–80	Varies depending on temperature	Low	Low
Dryer Efficiency (%)	Up to 95	35–40	Up to 70	Very low
Product quality	Very good	Average	Good	Excellent
Capital cost	Moderate	Low	High	Very high
Drying rate	Faster	Average	Very slow	Very slow
Operating cost	Low	High	Very High	Very high
Control	Very good	Moderate	Good	Good

3) **Maintenance**: The components of a heat pump require regular maintenance.
4) **Refrigerant leak**: Can be a serious problem and involve recurring cost.

4.3
Various Configurations/Layout of a HPD

In this section different possible configurations of a HPD are discussed (Prasertsan and Saen-Saby, 1998a, b). The configuration shown in Fig. 4.6a is one of the most commonly used; ambient air is dehumidified in the evaporator and heated in the condenser before it enters the dryer. The air entering the dryer is, therefore, warmer and dryer all the time. Due to the low humidity of the air, the mass transfer driving force is raised in the dryer. Figure 4.6b shows a similar arrangement to Fig. 4.6a, but the moisture in the air is not extracted before entering the dryer. The working air is hotter than that in case (a). The air leaving the dryer is very moist and hot, which increases the heat recovery in the evaporator. The configurations shown in Fig. 4.6c

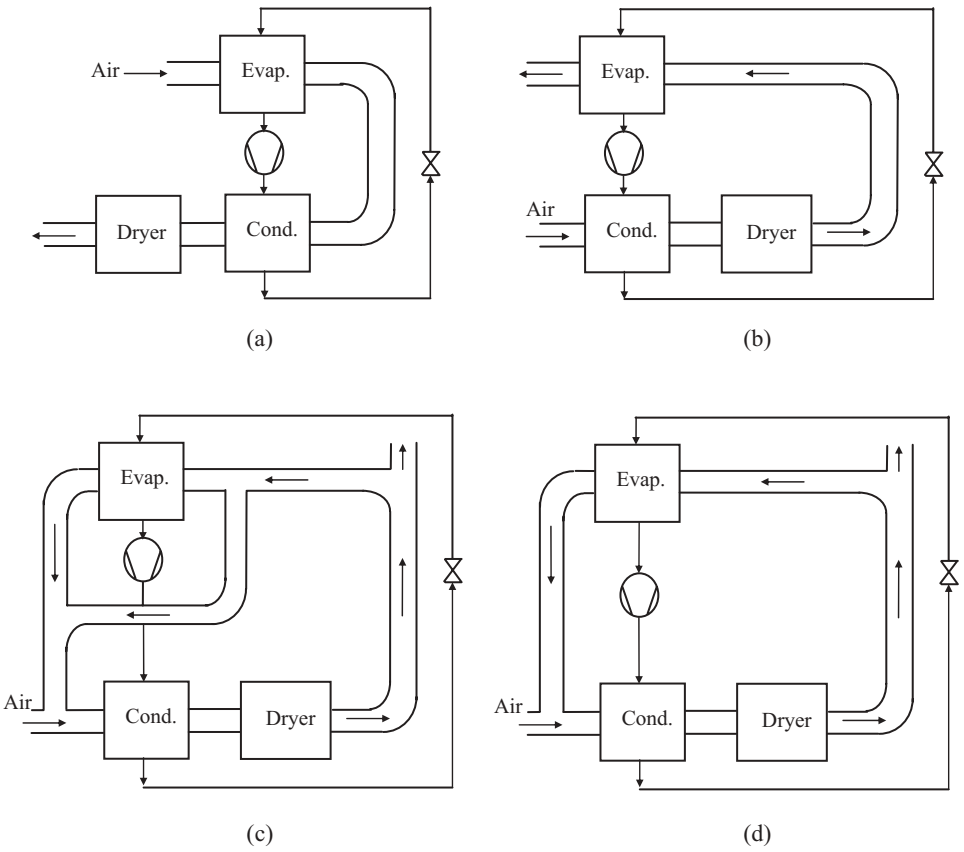

Fig. 4.6 Various configurations of HPD.

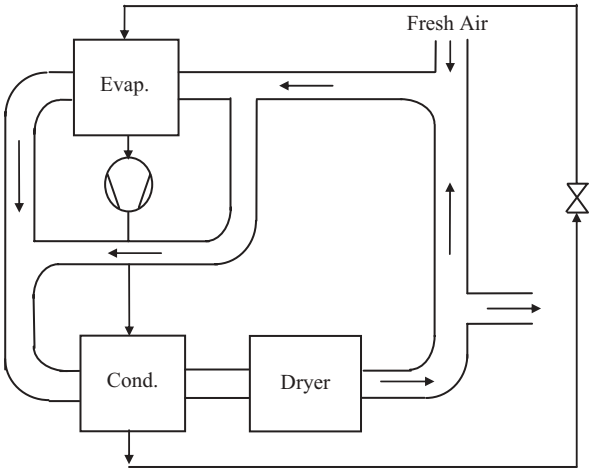

Fig. 4.7 A commonly used HPD configuration.

and d represent closed systems with partial purging of air and intake of fresh air before and after the evaporator, respectively. Configurations (a) and (b) are the simplest arrangements as these are open systems. The most commonly used HPD system is shown in Fig. 4.7.

4.4
Heat Pumps – Diverse Options and Advances

4.4.1
Multi-Stage Heat Pump

Commonly used heat pump dryers are based on a single stage compression refrigeration cycle. In these systems only one evaporator is used for cooling and dehumidification of the process air. Once the sizing of the evaporator is completed, it becomes a constraint on the maximum heat removed from the drying air. In addition, the single evaporator can supply only one air stream at a certain temperature and humidity. Multi-stage heat pumps can be used to produce multiple air streams of different drying conditions which can enter at different sections of the dryer, depending on the drying requirement. Multi-stage heat pumps can, moreover, reduce the energy consumption of the drying process as the COP values for such systems are high (Chua *et al.*, 2002a, b; Islam and Mujumdar, 2008a, b; Mujumdar, 2006; Alves-Filho and Efremov, 2009). Figure 4.8 shows the ranges of COP values of single and multi-stage heat pump systems (Chua *et al.*, 2002a, b).

To elaborate the working system of a multi-stage heat pump system, consider the example of a two-stage heat pump dryer. The refrigerant coming out of the condenser passes through two different expansion valves with different discharge pressure. One

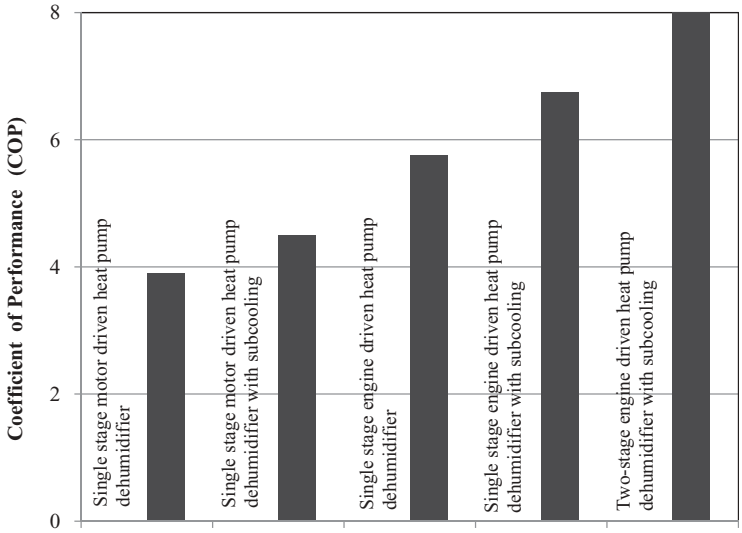

Fig. 4.8 COP values for various multi-stage heat pumps.

of the streams comes out at low temperature and the other at comparatively high temperature, and they enter two different evaporators, namely a high pressure and a low pressure evaporator (as shown in Fig. 4.9). The air is cooled to a different temperature and humidity level at the exit of each evaporator, producing two different air streams which can enter two different sections of the dryer. The pressure at the exit of the high pressure evaporator is regulated, by a backpressure regulator, to that of the low pressure evaporator before mixing of the two streams takes place. The refrigerant streams from both evaporators are then mixed and passed through a compressor to give a discharge pressure equal to that of the condenser, and the cycle follows (Islam and Mujumdar, 2008a, b).

Some drying applications need a very low temperature of the evaporator to reduce the moisture of the drying air to moderately low values. However, the drying air temperature required is high enough to require re-heating in the condenser. This corresponds to a high pressure difference between the evaporator and the condenser. In such applications multi-stage compression is used (Islam and Mujumdar, 2008a, b; Mujumdar, 2006; Alves-Filho and Efremov, 2009; Chua *et al.*, 2002a, b). The refrigerant is expanded to very low pressure to satisfy the cooling in the evaporator coil; then it goes through a low and a high pressure compressor to reach a sufficiently high discharge pressure to achieve re-heating in the condenser coil.

4.4.2 Cascade Heat Pump System

As discussed previously, in the multi-stage compression refrigeration cycle the same refrigerant is used, although the pressure difference between the evaporator

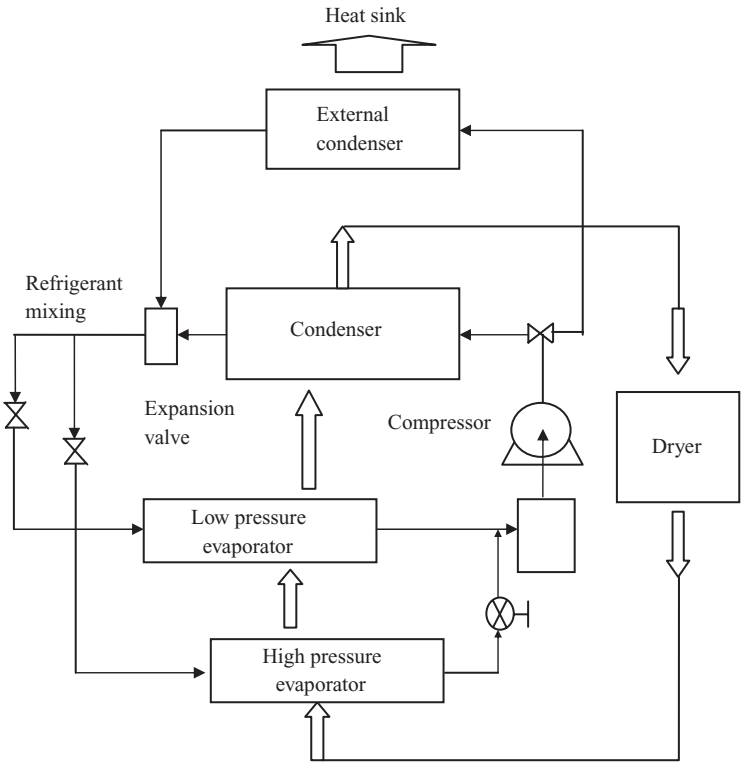

Fig. 4.9 A typical two-stage heat pump system.

and the condenser is high in some applications. The cascade heat pump configuration is another way to achieve high and low pressures of the refrigerant. In such a system, two different refrigerants of desired properties are used with different saturation levels for each refrigerant (Fig. 4.10). The high and low pressure cycles are connected with a heat exchanger which serves as a condenser for the low pressure cycle and evaporator for the high pressure cycle. The evaporator pressure of the high pressure cycle should be somewhat lower than the condenser pressure of the low pressure cycle so as to achieve good heat transfer. It is essential to control both the cycles to achieve the maximum heat transfer. Similar to multi-stage compression, cascade heat pumps also have better COP (Islam and Mujumdar, 2008a, b; Mujumdar, 2006).

4.4.3 Use of Heat Pipe

The heat pipe is a heat exchange device which is externally divided into two sections with a working fluid inside the pipe. The lower part contains the working fluid in a liquid state which takes out heat from the external fluid and goes into the vapor form in the upper

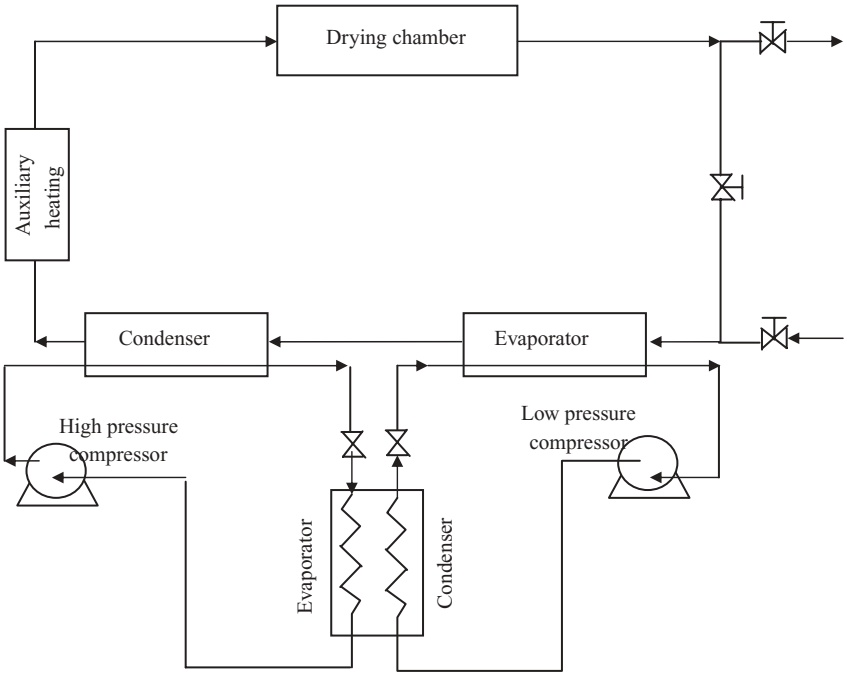

Fig. 4.10 Schematic of a cascade heat pump dryer.

section. The cold fluid flows externally over the upper part, taking out heat from the vapor form of the working fluid and resulting in condensation. This cycle goes on continuously. A certain pressure is maintained inside the heat pipe so as to achieve this heating and cooling effect. Heat pipes used in combination with the heat pump system can result in improved COP values. The same compressor of the heat pump cycle can be used to maintain a certain pressure inside the series of heat pipes to achieve pre-cooling and heating of drying air in a heat pump dryer. The functioning of such a system is very similar to that of the multi-stage heat pump system (Shah *et al.*, 2001).

4.4.4 Chemical Heat Pump (CHP)

Mechanical heat pumps are most commonly used in drying applications. High electric power consumption for compression and use of non-eco-friendly CFCs are their major limitations. A chemical heat pump (CHP) is an eco-friendly replacement option for mechanical heat pumps (Ogura and Mujumdar, 2000; Ogura *et al.*, 2003). The chemical heat pump stores or absorbs thermal energy in the exhaust from convective dryers, solar energy, or geothermal energy in the form of chemical energy via endothermic reactions in specially designed reactors, and rejects heat at a desired level via exothermic reactions. CHPs operate using thermal energy from the heat source and do not release any gases which may have an environmental impact.

Reversible reactions are utilized in the operation of CHPs (Wongsuwan *et al.*, 2001; Wang *et al.*, 2008) such as

$$A + B \leftrightarrow C + \Delta H \tag{4.5}$$

A, B and C are the reacting components and ΔH is the consumption or generation of heat during the reaction. The involved substances can be in the same phase or in different phases. Commonly, A and B react to give C through an exothermic reaction (heat pump) while substance C decomposes into A and B by an endothermic reaction (refrigeration). Figure 4.11 shows a simple gas–solid chemical heat pump concept (Wongsuwan *et al.*, 2001; Ogura and Mujumdar, 2000). This is a closed system consisting of a low and a high temperature reactor connected to each other. The heat storage and release reactions occur at different pressure levels. The low temperature side reactor has a higher reaction equilibrium pressure line. The CHP appears as a batch system with heat storing and heat rejection steps. For example, hydration and carbonation reactions are used for the high temperature side reactor. Evaporation/condensation of the reactant media are often used for the low temperature (0–200 °C) side reactor. The reaction on the left-hand side of Fig. 4.11 is an endothermic reaction which acts as a refrigeration process, and the reaction on the right hand side is an exothermic reaction which effectively has a heat pump function. Wang *et al.* (2008) and Wongsuwan *et al.* (2001) have classified chemical heat pumps based on characteristics of the reactions which may be mono-variant or bi-variant. Interested readers can refer to the relevant literature for more details (Wang *et al.*, 2008; Ogura and Mujumdar, 2000). The main advantages of energy storage by this route are low heat losses, high storage capacity and long term storage of both reactants and products (Wongsuwan *et al.*, 2001).

Figure 4.12 shows a simplified schematic of a chemical heat pump dryer proposed by Ogura and Mujumdar, 2000. In this dryer, which operates in a heat transfer enhancement mode, the $CaO/H_2O/Ca(OH)_2$ reaction was used for the refrigeration and heat pump effects. In the chemical heat pump 1 (CHP1), high temperature heat is stored in the CaO reactor using a suitable amount of heat input. The water vapor from this reactor is condensed by rejecting heat to the drying air, which in turn is heated. However, in chemical heat pump 2 (CHP2) the liquid water

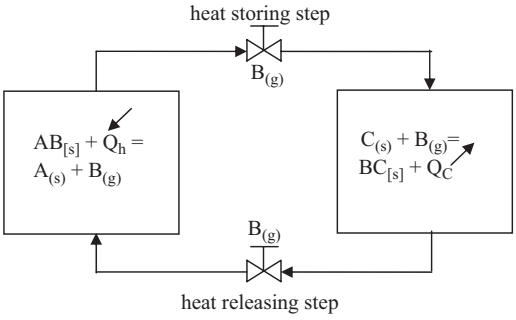

Fig. 4.11 The chemical heat pump concept.

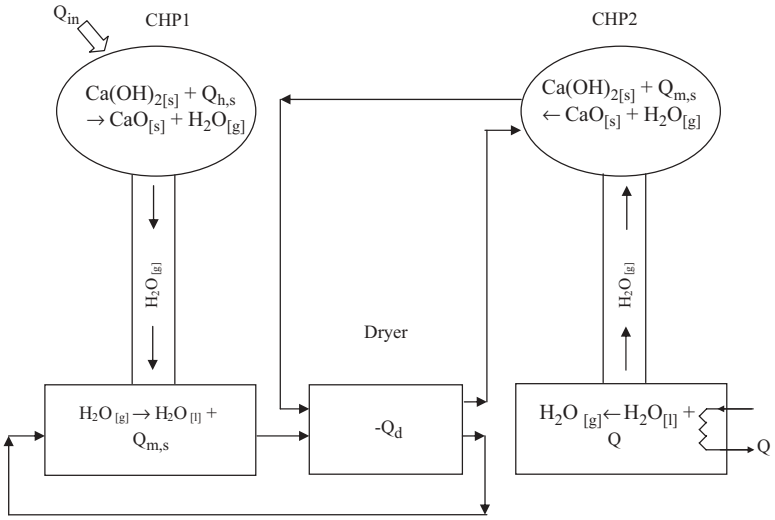

Fig. 4.12 Chemical heat pump drying system.

takes up heat, resulting in cooling and dehumidification. The CaO is converted to $Ca(OH)_2$ with low grade heat, which is also used for air heating (second air stream in Fig. 4.12).

Recently, much work has been carried out on improving the efficiency of chemical heat pumps, mainly in terms of heat and mass transfer enhancement, new working materials, reactions with high heat rejection rates and higher refrigeration effect, and integrated components for making the system compact (Wang *et al.*, 2008). Wang *et al.* (2008) have reviewed recent patents on the enhancement of heat and mass transfer in chemical heat pumps which mainly use absorption and desorption reactions. Ogura *et al.* (2003) have carried out energy enhancement studies of chemical heat pumps by developing new reactor designs. They found that shallow bed reactors which perform up to 94% chemical heat storage can produce air temperatures as high as 100 °C. The system was found to have very high efficiency over a wide temperature range of drying air.

In another study, Ogura *et al.* (2005) studied experimentally the control strategy for two different reaction systems for chemical heat pump drying applications viz. $CaO/H_2O/Ca(OH)_2$ hydration/dehydration system and $CaSO_4/H_2O/CaSO_4{\cdot}1/2H_2O$ hydration/dehydration system. They confirmed experimentally that heat supply to and from a chemical heat pump can be controlled by suitably selecting the pressure/temperature in the two chemical reactors. In particular, in the case of $CaO/H_2O/Ca(OH)_2$ it was found that up to 80 °C level heat can be produced in the heat storing step, however, the heat releasing step produces heat up to 125–130 °C. They reported that the chemical heat pump can produce drying air of controlled temperature. Ogura *et al.* (2004) have also carried out cost analysis for the chemical heat pump drying of ceramics in Japan and found that the CHP drying can reduce the cost to nearly half compared to the conventional drying process with gas-fired boilers. It was further

reported that use of a chemical heat pipe in addition to a heat pump can reduce the cost by 12%. Some of the commonly used materials for reactions in chemical heat pumps are ammonia derivatives, sulfur dioxide systems, water systems (magnesium oxide/water, calcium oxide/water and sodium carbonate/water), carbon dioxide systems and hydrocarbon–hydrocarbon derivatives systems (Wongsuwan *et al.*, 2001). There have been numerous efforts to find new materials for reactions in chemical heat pumps. Yu *et al.* (2008) have critically reviewed different solid–gas reactions for heat transformation in chemical heat pumps. Fujioka *et al.* (2008) have discussed the importance of increasing the heat transfer rate to enhance the rate of reaction in the packed bed reactor of a chemical heat pump. They have studied the use of composite reactants, such as combination of calcium chloride with expanded graphite and activated carbon fiber (ACF) and found that the effective conductivity of expanded graphite composite was 60% higher than that of the untreated calcium chloride. Ishitobi *et al.* (2010) have recently proposed that the use of lithium chloride (LiCl) modified magnesium hydroxide ($Mg(OH)_2$) can reduce the activation energy of the pure magnesium hydroxide.

Daghigh *et al.* (2010) have carried out an extensive review of solar-assisted heat pump drying of agricultural products. They report that solar energy can be stored as chemical energy using a suitable chemical substance in heat pumps. The energy from a low temperature source, such as solar collectors, can be upgraded for high temperature heating using the additional exothermic heat from the chemical heat pump. There are very few reports on the commercial application of solar-assisted chemical heat pump systems. Daghigh *et al.* (2010) reviewed a system recently developed in Malaysia for drying lemongrass (Ibrahim *et al.*, 2009). It should be noted that chemical heat pumps have huge potential for drying in high temperature applications with variable control of temperature. There are several opportunities to utilize better reactions or to enhance heat and mass transfer by better design of the reactors. Wongsuwan *et al.* (2001) have explained the potential of CHP to utilize renewable energy and waste heat over a wide range of temperature, which can then be used for a drying operation.

Despite their promise, CHP-assisted drying systems are not yet commonplace, based on our review of the relevant literature. Much R&D is needed before CHPs can replace, or can be utilized in conjunction with mechanical heat pumps in drying applications.

4.4.5
Absorption Refrigeration Cycle

Absorption refrigeration is another attractive refrigeration cycle which can use waste heat and/or solar energy as a driving force (Srikhirin *et al.*, 2001; Whitman *et al.*, 2005). It has two sections: absorber/evaporator and generator/condenser (Fig. 4.13). The system basically involves a mixture of refrigerant and the absorbent, with circulation of the refrigerant. In the generator, heat is added externally to the mixture of the refrigerant and absorbent. This results in evaporation of the refrigerant, which gives out heat to the external fluid to

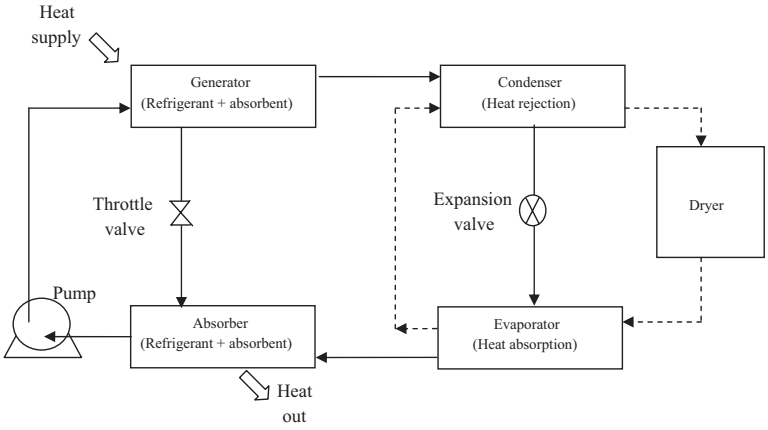

Fig. 4.13 Schematic of a typical absorption refrigeration cycle for HPD.

be heated, the drying air in this case (see Fig. 4.13), in the condenser. The condensed refrigerant flows through the expansion valve to the evaporator where it takes out heat from the external medium, exhaust air from the dryer in this case. In the absorber/evaporator section, the pressure is kept low. This causes absorption of the refrigerant in a strong solution of the absorbent, which in turn becomes weak. This is the reason why the cycle is known as an absorption/refrigeration cycle. The weaker solution is then pumped back to the generator section and the cycle is repeated. As the separation in the generator occurs at higher pressure a circulation pump is used to connect the absorber to the generator.

There are many refrigerant/absorbent combinations reported in the literature. Over 40 combinations have been reported for this type of refrigeration system. The important factors considered for selecting the combination are: the difference in boiling point, the latent heat of vaporization of the refrigerant, the stability of the mixture, the environmental impact, and the lack of crystallization or solidification inside the system. The most widely used pairs are ammonia–water or lithium bromide–water (Srikhirin *et al.*, 2001; Al-Rabghi and Akyurt, 2004). Ammonia and water are both very stable over a wide range of operating temperature and pressure. In addition, this combination is environmentally friendly and low cost. However, a rectifier is needed as water also evaporates along with ammonia. The lithium bromide–water system is better in this sense, as lithium bromide is non-volatile so that a rectifier is not needed for their separation. Since the water is a refrigerant in this case, the main constraint is to operate the system under vacuum for most of the applications. CFCs, mainly R22 and R21, can also be used as they have good solubility in various organic solvents. Recently, researchers have used multiple effect absorption refrigeration systems to improve performance. In these refrigeration systems, the absorber is the most crucial section, since the circulation rate of solution is limited by the absorption of evaporated refrigerant in the absorbent. Much work has been carried out to enhance the absorption process. Recently, Martin and Bermejo (2010) have

investigated combinations of ionic liquids with supercritical CO_2 for absorption refrigeration in which the ionic liquid acts as an absorbent for CO_2. Ionic liquids have negligible vapor pressure which eases their separation from a mixture with supercritical CO_2. Energy efficiency calculations (COP) have been carried out for combinations of various ionic liquids with CO_2 using a group contribution method. It was reported by these authors that the energy efficiency of the cycle using CO_2-[-mpyrr][Tf2N] was less than the efficiency of the commonly used NH_3–H_2O and LiBr–H_2O cycles. This was mainly due to the higher circulation rates required for the combination studied. More research is needed in this area.

Srikhirin *et al*. (2001) have critically reviewed various absorption refrigeration technologies with the emphasis on improving the process by various ways, such as better design of the absorber by better contact between refrigerant and absorbent, use of multi-effect absorption, an absorption refrigeration cycle with GAX (generator/absorber heat exchanger), half effect absorption refrigeration, combined vapor absorption and vapor compression, a dual cycle process, and a few other options. However, they report that, except for the single effect system, all other systems are very complicated and only the double effect absorption system with lithium bromide–water seems to be commercialized. A combined ejector–absorption system is promising but has low COP and is used only for small scale refrigeration (Hong *et al*., 2010). Multiple effect absorption cycles have potential for commercial applications. Al-Rabghi and Akyurt (2004) have recommended the use of absorption systems whenever economical heat sources are available, particularly for industrial applications. The increased COP of the heat pump cycle using absorption refrigeration can result in increased SMER values for heat pump dryers.

4.5
Miscellaneous Heat Pump Drying Systems

As discussed previously, a heat pump can be used in combination with any convective dryer. However, the refrigerants available commercially cannot go to very high temperature levels and one has to use additional heating. In addition, the drying rates in the final stages of drying are very sluggish which results in extended drying times. The efficiency of heat pump dryers can be increased significantly by application of external heat in various ways. There are many types of heat pump dryers reported in the literature which will be discussed in detail in this section. Some form of hybridization of HPD can be expected to yield more cost-effective solutions.

4.5.1
Solar-Assisted Heat Pump Drying

Recently, there is a trend towards making all systems sustainable, which basically means energy efficient, using renewable energy sources with minimal environmental impact. Solar-assisted heat pump dryers (SAHPD) can be used efficiently both

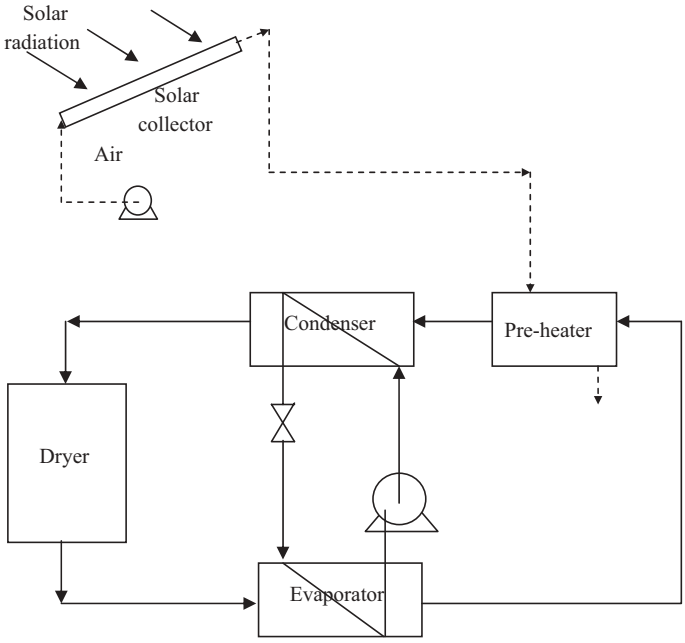

Fig. 4.14 A simple solar-assisted heat pump dryer.

with and without heat storage (Daghigh *et al.*, 2010; Sharma *et al.*, 2009; Hawlader *et al.*, 2008; Slim *et al.*, 2008; Fan et al., 2007). Basically, in SAHPD solar energy is used to heat the drying air, either before or after the condenser of a conventional heat pump. The simplest flow diagram of a solar-assisted heat pump dryer is shown in Fig. 4.14 (Daghigh *et al.*, 2010; Mujumdar, 2006). The dryer exhaust air first follows the usual path through the evaporator, where dehumidification takes place. Then it is pre-heated through a heat exchanger using another stream of air or some other fluid which is heated by means of solar energy. This pre-heated air is then heated further to the required temperature before entering the dryer. An auxiliary heater can also be added for better control of temperature in the absence of solar heat. This is especially useful when high drying temperatures are required. The main advantages of SAHPD are: effective utilization of renewable energy for direct heating, and storage with an easy control strategy. The higher capital cost involved in the installation of solar panels, regular maintenance of solar panels and irregular availability of solar energy are some of the limitations (Daghigh *et al.*, 2010; Hawlader *et al.*, 2008).

There are various configurations of SAHPDs reported in the literature. Hawlader *et al.* (2003a), Hawlader and Jahangeer (2003b) have reported a solar-assisted HPD which uses solar energy for heating of air as well as evaporation of the refrigerant. This system offers better control of a heat pump as well as the air cycle. Their suggested scheme is represented in Fig. 4.15. It can be seen that the refrigerant from the throttle valves goes through two evaporators at different pressures. In EV1 the refrigerant is evaporated by cooling and

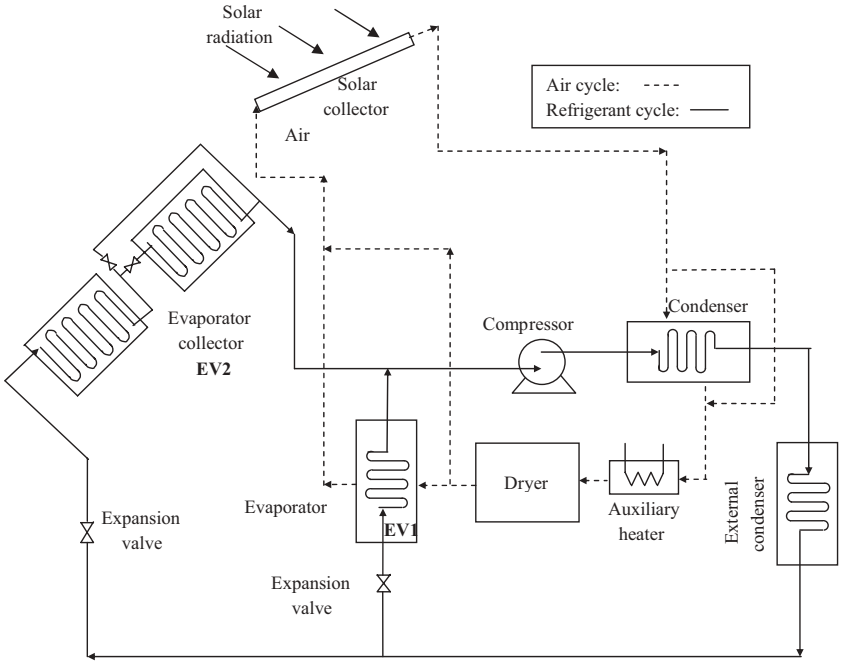

Fig. 4.15 Simplified schematic of solar-assisted heat pump dryer (Hawlader *et al.*, 2008).

dehumidification of the drying air, while in EV2 the refrigerant is evaporated by utilizing solar energy. Both refrigerant streams are then passed through the compressor; the pressure is regulated at the exit of both the evaporators. The air from EV1 goes through a solar heater where it is pre-heated to a certain level before it enters the condenser for further addition of sensible heat. The compressed refrigerant rejects heat in two condensers, one for reheating of dehumidified air from the solar pre-heater and the other – a water condenser – utilizing the remaining heat for heating of process water. It was observed that the COP of this system falls from a maximum value of 7 during the initial stages of drying to a value of 6 during the final stages of drying (Hawlader *et al.*, 2003a; Hawlader and Jahangeer, 2003b; Hawlader *et al.*, 2008).

In places where solar energy is available abundantly, and when high drying temperatures are necessary, a SAHPD with heat storage can enhance the overall energy efficiency of the process. The auxiliary heating required in this HPD system can be accomplished by the stored heat. Generally, solar energy is stored using a phase change material, such as paraffin wax or a bed of rocks. The stored solar energy is then supplied as sensible heat to the air used for drying. Such a system offers considerable flexibility of operating conditions. SAHPD with heat storage using water has also been reported. In such a system, the dryer exhaust air is cooled normally through the evaporator of a heat pump cycle. However, the condenser heat is extracted using cooling water which flows in a storage tank. This water from the storage tank is heated by passing through a solar collector. Depending on the

requirement, the cold and dehumidified air is heated using this water, while the remaining hot water is stored in a storage tank (Daghigh *et al.*, 2010).

There is scope for research and development of SAHPDs. The main component for these systems is the solar collector. It is thus necessary to invent new, highly efficient solar collectors for better performance. The geothermal heat pump system is also highly energy efficient, next to the solar system. Hence, it could be very interesting to couple these two systems to develop a sustainable technique mainly for drying applications with less environmental impact (Daghigh *et al.*, 2010; Bi *et al.*, 2004).

4.5.2
Infrared-Assisted Heat Pump Dryer

Infrared energy can be selectively used for heating of solids during convective drying (Mujumdar, 2006; Chua *et al.*, 2002a, b; Kudra and Mujumdar, 2009; Islam *et al.*, 2003a, b). IR heating can speed up the drying process as the additional sensible heat is supplied to the drying solid directly (Chua *et al.*, 2002a, b). Islam *et al.* (2003a, b) carried out a mathematical analysis of multi-mode heat transfer in convective drying. According to their results, IR combined with HPD can provide a highly efficient drying process. The main advantages of using IR are: high heat transfer rates, ease of directing energy from the heat source, quick response time, hence better control, and easy compatibility with a heat pump dryer.

Figure 4.16 shows a schematic of a simple IR-assisted heat pump dryer. It can be seen that the infrared sources are connected to the electric power through a control system. The IR radiation is directed to the product on trays, while the hot and dehumidified air coming from the heat pump system takes out the moisture. The IR-assisted HPD can be operated in batch as well as in continuous mode. In a continuous dryer a moving belt replaces the trays, and the required residence time will decide the belt speed. For heat-sensitive products convective drying can be combined with intermittent IR radiation (Islam *et al.*, 2003a, b). In such cases IR is used continuously in the initial stages for the fast removal of surface moisture, but only intermittently during the falling rate period. This mode of operation results in faster drying. IR-assisted HPD offers various advantages, such as compactness, ease of control, and low installation cost. However, it must be noted that the IR-assisted heat pump dryer needs careful control of heating so as to avoid overheating, resulting in product quality loss. A good feedback control of the IR power is, therefore, necessary in order to keep a required temperature in the drying chamber, as shown in Fig. 4.16, and to avoid overheating of the product. Recently, Alves-Filho and Goncharova-Alves (2010) have reported that the use of IR radiators in fluidized bed atmospheric freeze drying of green peas results in faster drying.

4.5.3
Microwave-Assisted Heat Pump Drying

The mechanism involved in microwave heating is different from that involved in conduction and convection heating. Microwaves can penetrate dielectric material and

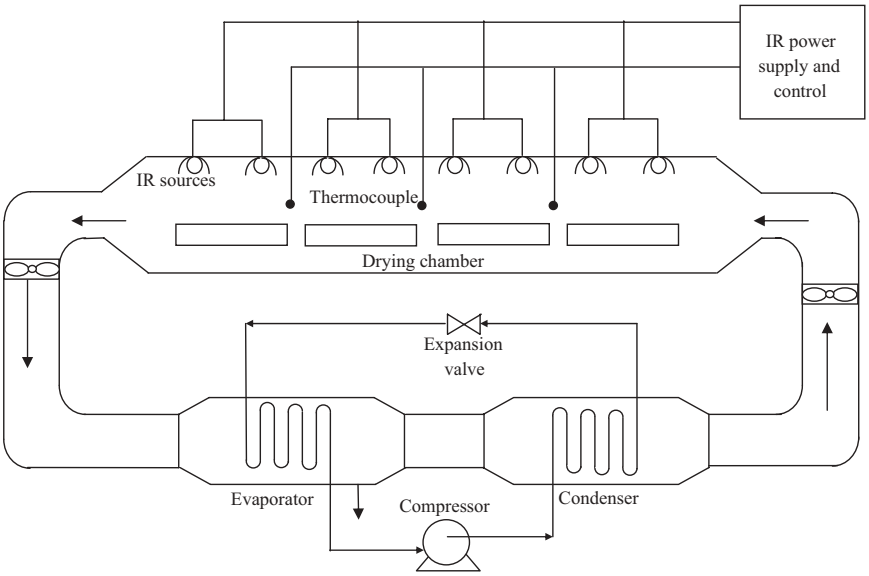

Fig. 4.16 IR-assisted heat pump drying system.

achieve volumetric heating (Mujumdar, 2006; Jia *et al.*, 2003). This kind of heating of the material "pumps" the moisture outwards because of a vapor pressure difference and prevents case hardening during drying. Because of the unique advantage of volumetric heating, microwave drying has become popular in some sectors, such as ceramics, food, and pharmaceuticals. However, certain limitations, such as insufficient absorption of MW radiation, high cost, and low energy efficiency have resulted in limited industrial applications. To make microwave drying more attractive for industrial applications by increasing its energetic efficiency, it is necessary to combine it with some other technique such as a heat pump dryer. In addition, because of volumetric heating, microwaves can be used to remove the final traces of moisture, which otherwise is a very energy consuming stage. Microwave-assisted convective drying has proven to be faster and more efficient (Turner and Jolly, 1991; Jia *et al.*, 1993; Kudra and Mujumdar, 2009). The microwave radiation can be used both in continuous as well as an intermittent manner, depending on the requirement of the process. Operation can be near atmospheric or in vacuum.

Figure 4.17 shows a schematic of a microwave-assisted HPD employed by Jia *et al.* (1993). The microwave energy is supplied by the magnetron and waveguide system to a product placed on a moving belt; the air cycle follows the usual path of a heat pump dryer. Jia *et al.* (1993) used this technique for drying foam rubber and some vegetables, such as carrot and ginger. Interestingly, they observed that the SMER of MW-assisted HPD was similar or somewhat lower than in the case of normal HPD, but with higher throughput. It was reported that for non-hygroscopic materials, such as foam rubber, the position of the MW source did not affect the drying. For hygroscopic products such as carrot and ginger it did, with lower values of

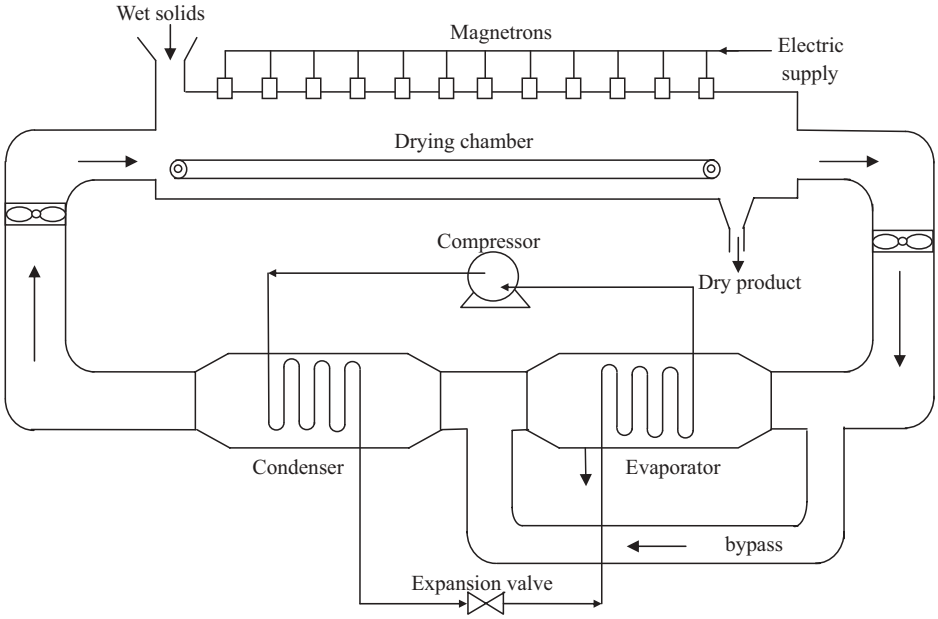

Fig. 4.17 Microwave-assisted heat pump drying system.

SMER. Further research in this area is necessary to increase the efficiency and lower the costs of such innovative drying systems.

4.5.4 Time-Varying Drying Conditions and Multi-Mode Heat Pump Drying

Conventional drying systems generally use fixed steady drying conditions, such as air velocity, temperature, and humidity throughout the entire batch drying cycle. During the initial phase of drying, when the moisture content is high and most of the moisture is surface moisture, the use of higher temperature, higher velocity, and lower humidity drying air is appropriate as it enhances the evaporation rate. In the initial stages of drying the evaporation rate depends on the external driving potential for vapor transfer, which is the partial pressure difference. Hence, low moisture air from a heat pump enhances the drying rate. However, during the later stages of drying, when the moisture content is low, internal diffusion dominates, and the effect of temperature or humidity is less significant. Instead, higher temperature can result in hardening and shrinkage in many food products (Mujumdar, 2006). Islam *et al.* (2003a, b) have carried out a numerical investigation of the effect of varying drying conditions, such as air temperature, velocity, and humidity on the drying of fruit and vegetable slices in batch heat pump mode. Islam *et al.* (2003b) simulated, using a simple diffusion model, various time varying cycles of air velocity, temperature, and humidity for the drying of potato slices. They found that higher

temperature, lower humidity, and relatively high velocity during the initial stages help remove the moisture at a faster rate. However, continued use of high temperature during later stages results in increased thermal energy consumption, heating of the product, and potential damage to product quality. It was also reported that low humidities during the later stages of drying are not useful, add to the evaporator rate, and, in turn, reduce the SMER values for HPD. Use of low humidity in later drying stages may not be advantageous.

The findings of Islam *et al.* (2003b) give very useful guidelines that essentially demonstrate via modeling that use of a heat pump over the entire drying cycle is not necessary. Dehumidified air at comparatively high temperature should be mainly used during the initial drying period, while ambient heated air can replace it during later stages of drying when the evaporation rate slows down. Islam *et al.* (2003b) have also suggested a multiple drying chamber arrangement that uses dehumidified air from a heat pump alternately with ambient heated air, which can result in reduced capital as well as running costs. As the time varying or intermittent cycle is used, the required compressor size decreases. Based on the type of material to be dried in a particular drying chamber, the relative humidity and the duration of the supply of dehumidified air to this drying chamber can be adjusted, while hot ambient air is supplied over the remaining cycle time. Figure 4.18 shows a simple arrangement of multiple drying chambers with a single heat pump which operates on a time varying drying cycle. It should be noted that the system suggested by Islam *et al.* (2003b) can provide better control of humidity and temperature; hence the advantages of the heat pump dryer can be optimally utilized.

Although not discussed here, work at the National University of Singapore has also shown that it is possible to enhance the energy efficiency and the product quality concurrently during heat pump assisted drying of heat-sensitive materials by use of

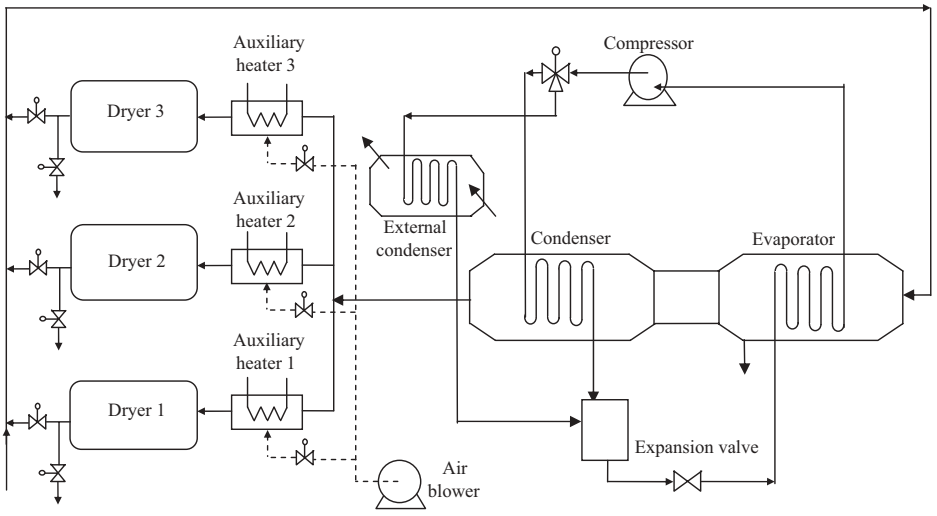

Fig. 4.18 Multiple drying chambers with time varying cycle in heat pump dryer.

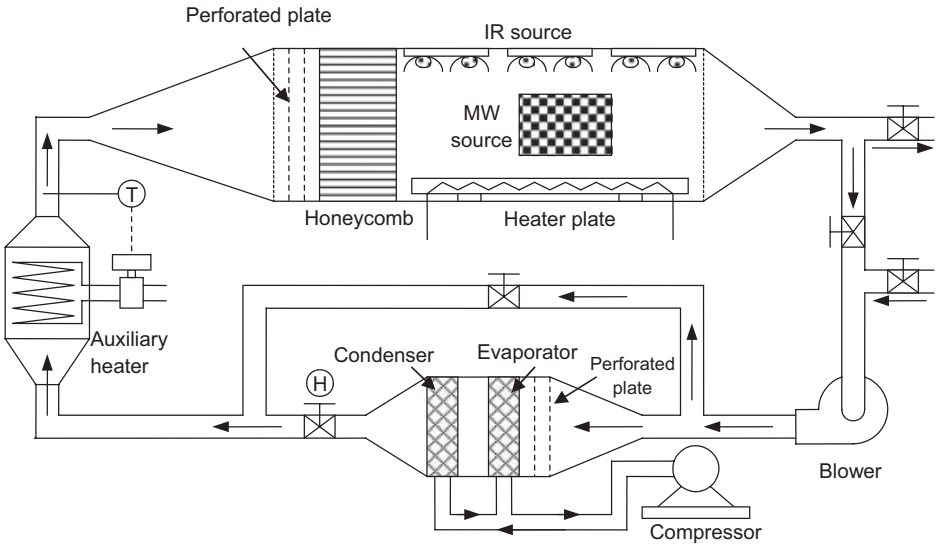

Fig. 4.19 Multi-mode heat pump drying system (Islam and Mujumdar, 2008b).

time-varying heat input which may be by radiation and conduction together with convection.

The multi-mode heat pump drying system suggested by Islam and Mujumdar (2008a, b) allows better control of the drying conditions (Fig. 4.19). The main components of such a drying system are air blower, heat pump, auxiliary air heater (for better temperature control), drying chamber, conduction heating by heater plate located at the bottom of the drying chamber, and infrared lamps located at the top of the drying chamber for supplying radiation heat. It should be noted that such a system has huge potential for optimal use of the heat pump dryer. Islam and Mujumdar (2008b) have also suggested a concept of flipping the product on a solid tray. Flipping the product every hour resulted in considerable reduction in drying time. If not flipped, the moisture from the bottom surface migrates slowly to the top surface, which needs a long time. Flipping reduces the diffusion path for the moisture to reach the surface for evaporation and, hence, reduces the drying time.

4.5.5
Heat Pump Assisted Spray Drying

In industrial spray dryers huge volumes of air are used, taking out considerable amounts of latent and sensible heat when purged. The heat pump has not been commonly used for spray dryers as the volume of air to be handled is very large. Hence, it is generally not recommended for such a system. However, some researchers have used a refrigeration system for dehumidification of drying air which is then heated, mainly using auxiliary heaters as the spray drying inlet temperatures are quite high. The main purpose of such a system is to get better

flow characteristics of the spray dried powder, and retention of color and some important components which otherwise are difficult to retain using normal heated air. One such application is for drying tomato paste (Goula and Adamopoulos, 2005). Dehumidified air was used for better color retention, flowability and better retention of lycopene. It is worth noting here that heat pump assisted spray drying systems can be used for small scale production of high value products, such as some pharmaceutical drugs, some high value bio-products, and some products where inert gas is used as a drying medium.

Recently Alves-Filho *et al.* (2009) have carried out a theoretical analysis of different arrangements of heat pump assisted spray drying. They found that the SMER for certain heat pump assisted units can go as high as 1.63 kJ kg^{-1} compared to a SMER value of only 0.78 for the basic spray drying system considered. In addition, their calculations showed the possibility to achieve definite temperature levels and energy transport using a heat pump system.

4.5.6
Modified Atmosphere Heat Pump Drying

Dehydration of food products is the biggest sector in the field of drying. The most common drying methods employed for food dehydration use hot air as the drying medium. Freeze drying gives the best quality products but is an extremely expensive choice. In convective air drying most of the food products undergo quality degradation due to various unwanted physical and chemical changes occurring during the drying. Most common are the browning reaction and shrinkage of the products due to case hardening (Perera and Rahman, 1997; Mujumdar, 2006). Browning can be due to enzymatic or non-enzymatic reactions. The most common enzyme present in fruits and vegetables is polyphenol oxidase causing such unwanted quality effects. There are numerous ways to reduce the activity of PPO, for example, by changing pH, using ascorbic acid, or using some sulfating agents. During drying, considerable structural changes occur as the water comes out (Chen and Mujumdar, 2008). Shrinkage occurs as the structure of the food polymers collapses due to surface tension effects when moisture is removed, which ultimately results in a change in porosity and the unacceptable sensory and rehydration properties of the dried products. Generally, low temperatures are used to avoid these problems, which leads to longer drying times and reduced energy efficiency. Another way to overcome these problems is to use inert atmosphere in a heat pump dryer (Hawlader *et al.*, 2006a, b, c). In such systems, an inert gas, such as nitrogen or carbon dioxide, is used for drying in a closed cycle, similar to the HPD using air. The absence of oxygen eliminates the chances of oxidative reactions, resulting in better sensory properties. Hawlader *et al.* (2006a) have carried out modified atmosphere HPD of various food products, such as apple, guava, and potato. It was observed that the product quality was much superior compared to heat pump and air drying in terms of color and shrinkage. In addition, the drying rate was observed to be faster than for the normal heat pump dryer. In another study (Hawlader *et al.*, 2006b), the drying of ginger in a modified atmosphere was found to retain more 6-gingrol.

4.5.7 Atmospheric Freeze Drying Using Heat Pump

Vacuum freeze drying is a well established drying technique and much research has been done to improve the process. Vacuum freeze drying is considered as the benchmark as far as product quality is concerned (Mujumdar, 2006). However, freeze drying is also possible at atmospheric pressure as the diffusion of water vapor to the surface through the dried shell occurs mainly due to the vapor pressure gradient rather than the difference in the absolute pressure (Claussen *et al.*, 2007b). Atmospheric pressure freeze drying is much more efficient as far as energy is concerned. Figure 4.20 illustrates the moisture movement in an atmospheric freeze-dried product. Much research has been carried out in the field of atmospheric freeze drying of food, pharmaceutical and biological products. Claussen *et al.* (2007b) have critically reviewed the concept of atmospheric freeze drying and the recent developments. A heat pump system can be efficiently used to carry out AFD using air at very low temperature, below the freezing point (generally between -3 and $-10\,^{\circ}C$). The process is very similar to the common heat pump drying except the air is cooled to a very low temperature before using it for drying. However, temperatures below $-10\,^{\circ}C$ are not recommended, because the moisture carrying capability of air becomes too low and the SMER value goes down as the temperature is decreased.

A continuous production line is a key factor for the development of such a technique, and the first continuous plant for drying of vegetables was started in 2005 in Hungary, designed by a Norwegian company (Claussen *et al.*, 2007b). There are various applications of heat pumps for atmospheric pressure freeze drying of vegetables, fruits, fish, and lactic acid bacteria to high quality products (Alves-Filho and Strommen, 1996; Strommen *et al.*, 2004; Alves-Filho *et al.*, 2007; Claussen *et al.*, 2007a, c). The AFD offers several advantages over vacuum freeze drying, such as low investment cost, higher productivity at lower operating cost, use of different temperature cycles because of the heat pump system, and the possibility of using an

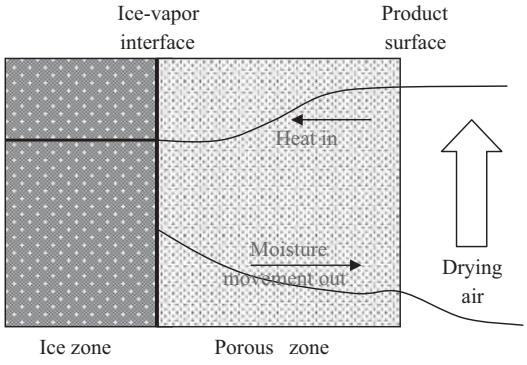

Fig. 4.20 Schematic of atmospheric freeze drying process inside drying material.

inert atmosphere for drying. It is also reported that the SMER of the atmospheric pressure freeze drying process ranges from 1.5 to 4.6 kg of water per kWh, when the value is in the range of 0.4 or below for vacuum freeze drying.

4.6 Applications of Heat Pump Drying

4.6.1 Food and Agricultural Products

In the food industry the most important criterion for dryers is the quality of the dried food products, which is assessed in terms of color, flavor, nutritional value, and texture (Mujumdar, 2006; Chen and Mujumdar, 2008). In dehydration processes these quality attributes are affected mainly by the temperature, drying time, and, in some cases, the drying medium due to presence of oxygen. As discussed earlier in this chapter, heat pump dryers offer many advantages to preserve these quality attributes of food products. In addition, food products also lose aroma and some nutritional content when exposed to higher temperature for a longer time to reach a certain moisture content. Heat pump dryers can help retain such volatile components as the system operates in a closed manner. Any volatile component removed during drying can be retained. The heat pump tray dryer is the most common one for small scale food drying. Recently, fluidized bed dryers have also been fitted with HP. Table 4.3 shows some recent applications of the heat pump drying technique for food and agricultural products.

4.6.2 Drying of Wood/Timber

It should be mentioned that the drying of wood/timber was the first major industrial application of heat pump dryers (Sun *et al.*, 2004; Shang *et al.*, 1995; Mujumdar, 2006). Drying of wood is a highly time-consuming process which requires very long drying times, especially since the drying temperature is necessarily low. This results in high drying cost. It should also be noted that large amounts of energy are wasted from the dryer exhaust as the volume of wood dried in a typical kiln is more than 50–60 m^3 which needs a tremendous amount of drying air. It is also necessary to develop high quality timber to comply with the market demands. Heat pump drying can be used very efficiently and effectively for drying timber. The use of a heat pump for wood drying was reported back in the 1970s, however, it has become popular only in the last two decades. The main advantages of heat pump drying are better quality of the dried timber, better energy efficiency, reduced drying time, and increased throughput because of the increased drying rate using low humidity air. Figure 4.21 shows a typical heat pump drying system for timber (Ceylan *et al.*, 2007). Table 4.4 lists different studies reported on the drying of timber.

Tab. 4.3 Recent applications of HPD in the food and agriculture sector.

Product Dried	Observations	Reference
Mushroom and chili	Vacuum heat pump dryer; Temperature and pressure have significant effect on color. Temperature has little effect on rehydration but decreasing pressure increases rehydration capacity.	Artnaseaw *et al.*, 2010a
Chili	Vacuum heat pump dried product quality was much better than sun dried. Drying temperature has less significant effect than pressure on quality attributes.	Artnaseaw *et al.*, 2010c
Tom Yum herbs	Thin layer vacuum heat pump drying; pressure of 0.2 bar and drying temperatures ranging from 50 to 65 °C.	Artnaseaw *et al.*, 2010b
High moisture paddy	Heat pump dryer can save 40% energy compared to far-infrared low temperature diesel-powered hot air drying for the same capacity and final product quality.	Jinjiang and Yaosen, 2010
Longan	Far-infrared-assisted heat pump drying and hot air drying were used to reduce the drying time; Porous structure of longan was obtained.	Nathakaranakule *et al.*, 2010
Maize (Grain drying)	Solar-assisted heat pump drying was used with reduced drying time, uniform drying of maize and very high energy efficiency. The COP of the heat pump was found to be 5.4.	Li *et al.*, 2010
Ginger	Tray, heat pump, two-stage drying and mixed mode solar drying; Heat pump dried ginger had shorter drying time, better rehydration and maximum retention of the active component 6-gingerol.	Phoungchandang *et al.*, 2009; Phoungchandang and Saentaweesuk, 2010
Apple	Heat pump dryer and solar dryer were used. It was recommended to use solar dryer in daytime and HPD during nighttime to make the operation energy efficient.	Aktas *et al.*, 2009
Olive leaves	Heat pump continuous dryer was successfully used; optimum conditions for minimum anti-oxidant activity loss and maximum exergetic efficiency were obtained.	Erbay and Icier, 2009
Green sweet paper	More retention of total chlorophyll content and ascorbic acid content using heat pump dryer.	Pal *et al.*, 2008
Hazelnut	PID controlled HPD was used with energy utilization as high as 65%.	Ceylan and Aktas, 2008
Shrimp	Peeled, headed and whole shrimps were dried using HPD; shrimps dried using HPD had better rehydration characteristics and better water-holding capacity.	Zhang *et al.*, 2008

(*Continued*)

Tab. 4.3 (*Continued*)

Product Dried	Observations	Reference
Herbs	Heat pump drying was used for drying of Jew's mallow, spearmint and parsley with low specific heat consumption value.	Fatouh *et al.*, 2006
Apple, guava, potato slices	Modified atmosphere heat pump drying using nitrogen and carbon dioxide at around 45 °C and 10% relative humidity, resulted in better structure and faster drying.	Hawlader *et al.*, 2006a
Carrot slices	Heat pump in combination with fluidized bed for granular carrot, SMER was observed to be 2.35 kg kWh^{-1}.	Zhang *et al.*, 2006
Guava and papaya slices	Drying using HPD, vacuum dryer and freeze dryer; Using modified atmosphere resulted in 44% increase in diffusivity of guava and 16% increase for papaya with less browning, better rehydration and better nutrient retention.	Hawlader *et al.*, 2006c

4.6.3 Drying of Pharmaceutical/Biological Products

In the pharmaceutical industry the product quality cannot be compromised, hence freeze drying is most commonly used (Mujumdar, 2006). However, there are various low value active pharmaceutical ingredients, mainly in powder form, for which the use of a very expensive technique such as freeze drying is not affordable, so that fluidized bed dryers, or similar suitable techniques are applied. In many cases an organic solvent is also removed during drying and must be recovered before purging out the dryer exhaust gas. Heat pump dryers can be useful for drying such APIs. Pharmaceutical products can be dried at lower temperature using HPD, hence the

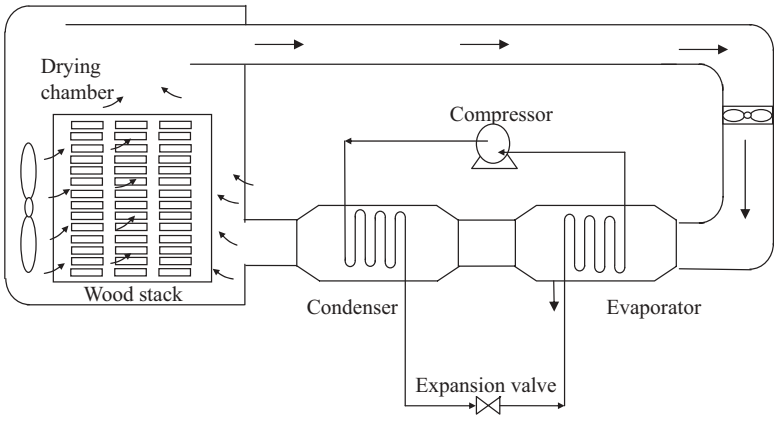

Fig. 4.21 Drying of wood using heat pump dryer.

Tab. 4.4 Some applications of heat pump dryers.

Product Dried	Observations	Reference
Wood chips	Absorption heat pump system was used and compared with wood burning furnace and waste heat recovery system; single stage absorption heat pump is useful only for air temperature less than 60 °C, otherwise it was recommended to use two-stage heat pump	Lostec *et al.*, 2008
Softwood	Average reduction in specific energy costs, compared to the costs of conventional softwood drying cycles, ranged around 35%. The COP was 3.9 while SMER ranged from 2.35–2.95 kg kW h^{-1}	Minea, 2008
Poplar and pine timbers	Effect of various operating parameters on energy utilization and energy loss was evaluated; as the recycled air ratio increased the energy loss decreased.	Ceylan *et al.*, 2007
Wood drying	Solar-assisted dehumidification drying was used; high volume capacity of 60 m^3 and high temperature of 95 °C were used. SMER as high as 3.08 kg kW h^{-1} was obtained.	Shang *et al.*, 1995
Wood drying kiln	Study of dehumidified air distribution in wood dryer; The recirculation of air in the dehumidifier was reduced by changing the duct design which otherwise reduces the efficiency by 14–18%.	Sun *et al.*, 2004

activity is retained. Recovery of solvent with ease is the main advantage of HPD for drying pharmaceutical products.

Some of the APIs have a tendency to form polymorphs (different crystal forms) during the drying step. The important operating parameters responsible for this are air temperature and humidity. As discussed earlier, heat pump dryers can be operated over a wide range of humidity and temperature. Hence, a proper drying path can be followed to obtain a particular form of a polymorph, which may be either stable or metastable (Laurent *et al.*, 1999). Both single and multi-stage heat pump dryers have been used for drying of proteins and celluloses. Claussen *et al.* (2007b) have noted that atmospheric freeze drying using heat pumps can be very useful for various pharmaceutical products which are very heat sensitive. Alves-Filho (2010) has recently reported a numerical mass transport analysis of atmospheric freeze drying of protein. It was reported that the numerical analysis allows better control of the particle–gas contact time in order to reach a proper time schedule for each stage in the atmospheric freeze drying as well as better scale-up. Table 4.5 summarizes various applications of heat pump dryers.

4.7 Sizing of Heat Pump Dryer Components

As discussed so far, heat pump dryers have numerous applications, mainly in the drying of heat-sensitive products such as food, pharmaceuticals and biomaterials, to

Tab. 4.5 Application of heat pumps for pharmaceutical/biological products.

Product Dried	Observations	Reference
Protein (myoisin)	Two-stage atmospheric freeze drying using heat pump resulted in manifold increase in diffusivity and water removal rate; Two-stage drying with proper residence time resulted in improved dryer capacity and better quality.	Alves-Filho *et al.*, 2008
Probiotic	Comparison of heat pump fluidized bed drying with hot air drying; Better retention of activity.	Joshi and Thorat, 2010
Sulfate and sulfite cellulose	Comparison of properties of dried product.	Strommen *et al.*, 2004
Enzyme and active bacteria	Heat pump fluidized bed and shelf dryers were used with bacteria reaching 100% viability and with biomolecules attaining full biological activity; improvement in survival rate, rehydration at optimum conditions.	Alves-Filho and Strommen, 1996

achieve better quality. However, the application of heat pumps to the prolonged drying of wood and related products mainly targets improved energy efficiency and faster drying. The sizing of each component of a heat pump dryer is very important. The design of the drying chamber is carried out in a similar fashion as for a normal convective dryer; however, the air distribution system is very important for better efficiency of HPD. In sizing the components of a heat pump dryer, one has to make a few assumptions. Commonly, it is assumed that the refrigerant is at saturated conditions at the exit of the evaporator and the condenser, while the compression and expansion processes of the refrigerant are isentropic, and regarded as isenthalpic processes, respectively. In addition, it is assumed that the pressure drop in the tubes connecting the heat pump components is negligible, and that these tubes are well insulated. At the dryer side it is generally assumed that the dryer is adiabatic and that the air conditions do not change when the air flows from one component to the other. Various researchers have given design protocols for heat pump dryers (Pal and Khan, 2010; Pal and Khan, 2008; Teeboonma *et al.*, 2003; Achariyaviriya *et al.*, 2000; Prasertsan *et al.*, 1997). Subsequently the general steps to be followed in designing a heat pump dryer are summarized as:

1) Calculate the amount of moisture to be evaporated, which is application specific:

$$\dot{M}_{\mathrm{w}} = \frac{\dot{M}_{\mathrm{P}}(X_{\mathrm{d,in}} - X_{\mathrm{d,out}})}{t_{\mathrm{d}}} \tag{4.6}$$

2) Calculate the heat required for evaporation of the moisture to be removed, which in turn gives the volume of air required at a selected temperature.

3) Calculate the properties of the air at the dryer exit using the heat and mass balance equations for the dryer

$$t_{\mathrm{d}}\dot{M}_{\mathrm{a}}(Y_{\mathrm{d,out}}-Y_{\mathrm{d,in}}) = \dot{M}_{\mathrm{P}}(X_{\mathrm{d,in}}-X_{\mathrm{d,out}}) \tag{4.7}$$

$$c_{p,\mathrm{a}}T_{\mathrm{a,d,in}} + Y_{\mathrm{d,in}}(\Delta h_{\mathrm{v}} + c_{p,\mathrm{w,v}}T_{\mathrm{a,d,in}}) = c_{\mathrm{p,a}}T_{\mathrm{a,d,out}} + Y_{\mathrm{d,out}}(\Delta h_{\mathrm{v}} + c_{p,\mathrm{w,v}}T_{\mathrm{a,d,out}}) \tag{4.8}$$

and the psychrometric relations (see Fig. 4.22 and Pal and Khan (2008)).

4) Using a suitable evaporator model (Jolly *et al.*, 1990; Prasertsan *et al.*, 1997; Clements *et al.*, 1993; Achariyaviriya *et al.*, 2000), calculate the evaporator area required, based on the maximum cooling to be carried out below the dew point temperature of the drying air. For a selected refrigerant cycle, the refrigerant mass flow can be calculated for a certain evaporator cooling load. Existing correlations for the heat transfer coefficient can be used to predict the heat transfer area. The mass and heat balance for air in the evaporator can be expressed by the following simple equations

$$\dot{M}_{\mathrm{w,e}} = \dot{M}_{\mathrm{a}}(Y_{\mathrm{d,out}}-Y_{\mathrm{e,out}})(1-\mathrm{BP}) \tag{4.9}$$

$$\dot{Q}_{e} = \dot{M}_{\mathrm{a}}(1-\mathrm{BP})(h_{\mathrm{a,d,out}}-h_{\mathrm{a,e,out}}) - \dot{M}_{\mathrm{w,e}}h_{\mathrm{w,e,out}} \tag{4.10}$$

5) For selected refrigerant flow and pressure levels calculate the power requirement for the compressor using existing equations from literature (ASHRAE, 2002).

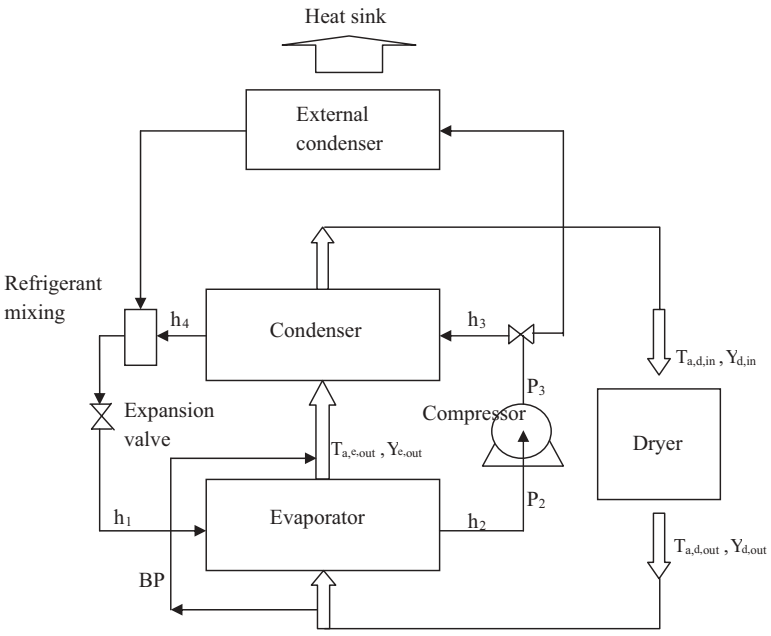

Fig. 4.22 Heat pump dryer sizing.

6) The heat transfer in the condensers can be calculated by simple heat balance equations as there is no change in the absolute humidity of the air while it is heated. Depending on the maximum heating requirement in the internal condenser

$$\dot{Q}_c = \dot{M}_a(c_{p,a} + Y_{d,in}c_{p,w,v})(T_{a,d,in} - T_{a,e,out}) \tag{4.11}$$

as shown in Fig. 4.22, the area for heat transfer can be calculated. The design of the internal condenser also gives the maximum heating load on the external condenser and, hence, its heat transfer.

7) Selection of a type of compressor, the material of construction for heat exchanger tubes, and the size and capacity of the fan can be done by referring to related handbooks (ASHRAE, 2002; Achariyaviriya *et al.*, 2000; Prasertsan *et al.*, 1997).

This is the general protocol suggested for design of the components of a heat pump dryer; however, the procedure may differ, based on the assumptions made and the heat pump dryer cycle followed. As discussed earlier, uniformity of air flow in the dryer is critical. Non-uniformity of air distribution results in different drying rates in a dryer, which gives variable moisture content. Especially, in a tray dryer the design and arrangement of trays is crucial for air distribution. Islam and Mujumdar (2008a, b) have suggested a certain arrangement of trays in a batch dryer which uses netted trays, allowing evaporation of moisture from the bottom as well as from the top surface. In addition, perforated plates and honeycombs are generally placed at the entrance of the evaporator, condenser and auxiliary heaters to make the drying air flow uniform (Islam and Mujumdar, 2008a, b). However, these are the major reasons for pressure drop in the system. Hence, the extra pumping cost because of the use of such flow obstacles should be compensated by the reduced drying time and the uniform product quality. As discussed in earlier sections, heat pump fluidized beds are also used for drying various food and pharmaceutical products (Alves-Filho *et al.*, 1997, 2008). However, these kinds of dryers have poor air distribution design which results in non-uniform moisture in the dried products. Recently, Jangam *et al.* (2009) have reported various ways to improve the air distribution in fluidized bed dryers. Interested readers can refer to the related literature for better design of a dryer unit.

4.8 Future Research and Development Needs in Heat Pump Drying

The present energy crisis has forced researchers around the globe to develop energy efficient and sustainable processes for all industrial sectors. Drying is one of those energy intensive processes which needs continuous development to make it more energy efficient. There have been numerous ways used to enhance the efficiency of existing drying systems, such as better insulation, better control of dryers, use of plant waste heat and recovery of exhaust heat using heat pump systems. Among these, heat pump drying has the biggest impact as it recovers a considerable amount of energy

which otherwise is wasted. However, there is still tremendous potential for research and development in this area. The main constraints in HPD are the use of environmentally unfriendly refrigerants in the conventional compression refrigeration cycle. Hence, it is necessary to make use of other refrigeration techniques, such as absorption refrigeration, chemical heat pumps, and solar and geothermal heat pumps which have very little or no environmental impact. It is necessary to develop and/or modify these systems to make them more energy efficient. Solar and geothermal energy are available freely, and should be used for making the heat pump dryers sustainable but considerable R&D is needed. Air distribution in heat pump dryers is another major concern which can enhance the efficiency of existing HPDs. Use of auxiliary heat by means or IR or MW radiation should be practised wherever possible to enhance the SMER.

Model-based optimal design and optimization of a multi-mode batch HPD, that is, one which incorporates an intermittent supply of radiative and convective heat along with conduction heating, has a strong potential for energy-efficient operation with slowly drying heat-sensitive materials like foods, fruits and vegetables. The supplementary heating, together with ON/OFF operation with dehumidified air will help to reduce the size of the heat pump for a single dryer chamber or allow the use of a single HP to service two or more drying chambers, drying the same or different materials, with only a marginal increase in drying time.

Additional Notation Used in Chapter 4

BP	bypass ratio	–
Q	amount of heat (thermal energy)	J
p	pressure	Pa
SEC	specific energy consumption	kWh kg^{-1}
SMER	specific moisture extraction rate	kg kWh^{-1}
W	work done in compressor	J

Subscripts

a	air
c	condenser
d	dryer/drying
e, ev	evaporator
h	heating
P	product
p	at constant pressure
1	evaporator inlet
2	compressor inlet
3	condenser inlet
4	expansion vale inlet

Abbreviations

AFD	atmospheric freeze drying
API	active pharmaceutical ingredient
CFC	chlorofluorocarbon
CHP	chemical heat pump
COP	coefficient of performance
GWP	global warming potential
HC	hydrocarbon
HCFC	hydrochlorofluorocarbon
HFC	hydrofluorocarbon
HP	heat pump
HPD	heat pump dryer/drying
IR	infrared
MW	microwave
ODP	ozone depletion potential
PPO	polyphenol oxidase
RH	relative humidity
SAHPD	solar-assisted heat pump dryer/drying

References

Achariyaviriya, S., Soponronnarit, S., Terdyothin, A., 2000. Mathematical model development and simulation of heat pump fruit dryer. *Drying Technol.* **18** (1&2): 479–491.

Aktas, M., Ceylan, I., Yilmaz, S., 2009. Determination of drying characteristics of apples in a heat pump and solar dryer. *Desalination* **238**(1–3): 266–275.

Al-Rabghi, O. M., Akyurt, M. M., 2004. A survey of energy efficient strategies for effective air conditioning. *Energ. Convers. Manage.* **45**: 1643–1654.

Alves-Filho, O., Strommen, I., 1996. The application of heat pump in drying of biomaterials. *Drying Technol.* **14** (9): 2061–2090.

Alves-Filho, O., Strommen, I., Thorbergsen, E., 1997. A simulation model for heat pump dryer plants for fruits and roots. *Drying Technol.* **15**(5): 1369–1398.

Alves-Filho, O., 2002. Combined innovative heat pump drying technologies and new cold extrusion techniques for production of instant foods. *Drying Technol.* **20** (8): 1541–1557.

Alves-Filho, O., 2010. Sweep numerical method and mass transport analysis in atmospheric freeze drying of protein particles. *Heat Mass Transfer* **46**(8–9): 923–928.

Alves-Filho, O., Efremov, G., 2009. *Heat pump drying: Experimentation, theory, design and practice*. CRC Press, Boca Raton, USA.

Alves-Filho, O., Eikevik, T., Mulet, A., Garau, C., Rossello, C., 2007. Kinetics and mass transfer during atmospheric freeze drying of red pepper. *Drying Technol.* **25**(7–8): 1155–1161.

Alves-Filho, O., Eikevik, T. M., Walberg, M., Fridberg, C., 2009. Energy and thermal efficiency analysis for combined spray drying and heat pump systems. *Proceedings of 4th Nordic Drying Conference*, Reykjavik, Iceland, pp. 1–12.

Alves-Filho, O., Goncharova-Alves, S., 2010. Infrared radiation and atmospheric freeze

drying of ocimum basilicum linnaeus. *Proceedings of 17th International Drying Symposium (IDS 2010)*, Magdeburg, Germany, pp. 1221–1224.

Alves-Filho, O., Eikevik, T. M., Goncharova-Alves, S. V., 2008. Single and multistage heat pump drying of protein. *Drying Technol.* **26**(4): 470–475.

Artnaseaw, A., Theerakulpisut, S., Benjapiyaporn, C., 2010a. Drying characteristics of Shiitake mushroom and Jinda chili during vacuum heat pump drying. *Food Bioprod. Process.* **88**(2–3): 105–114.

Artnaseaw, A., Theerakulpisut, S., Benjapiyaporn, C., 2010b. Thin layer modeling of Tom Yum herbs in vacuum heat pump dryer. *Food Sci. Technol. Int.* **16**(2): 135–146.

Artnaseaw, A., Theerakulpisut, S., Benjapiyaporn, C., 2010c. Development of a vacuum heat pump dryer for drying chili. *Biosystems Eng.* **105**(1): 130–138.

ASHRAE , 2002. *Handbook, refrigeration.* ASHRAE, Atlanta, USA.

ASHRAE , 2006. Ammonia as a refrigerant, position document, http://www.ashrae.org.

ASHRAE , Standard 34-2004, 2004. *Designation and safety classification of refrigerants.* ASHRAE, Atlanta, USA.

Baker, C. G. J., 2005. Energy efficient dryer operation – An update on developments. *Drying Technol.* **23**(9–11): 2071–2087.

Bi, Y., Guo, T., Zhang, L., Chen, L., 2004. Solar and ground source heat-pump system. *Appl. Energ.* **78**: 231–245.

Ceylan, I., Aktas, M., 2008. Energy analysis of hazelnut drying system-assisted heat pump. *Int. J. Energ. Res.* **32**(11): 971–979.

Ceylan, I., Aktas, M., Dogan, H., 2007. Energy and exergy analysis of timber dryer assisted heat pump. *Appl. Therm. Eng.* **27**: 216–222.

Chen, X. D., Mujumdar, A. S., 2008. *Drying technologies in food processing.* Blackwell Publishing, Oxford, UK.

Chou, S. K., Chua, K. J., 2006. Heat pump drying systems, in *Handbook of industrial dryers* (ed. A. S. Mujumdar). CRC Press, Boca Raton, USA.

Chua, K. J., Chou, S. K., Ho, J. C., Hawlader, M. N. A., 2002a. Heat pump drying: Recent developments and future trends. *Drying Technol.* **20**(8): 1579–1610.

Chua, K. J., Hawlader, M. N. A., Chou, S. K., Ho, J. C., 2002b. On the study of time-varying temperature drying – Effect on drying kinetics and product quality. *Drying Technol.* **20**(8): 1559–1577.

Chua, K. J., Mujumdar, A. S., Chou, S. K., Choy, H. J., Hawlader, M. N. A., 2000. Principles, applications and potentials of heat pump drying systems, in *Drying technology in agriculture and food sciences.* Oxford & IBH Publishing Co., New Delhi, India, pp. 213–248.

Claussen, I. C., Andresen, T., Eikevik, T. A., Strommen, I., 2007c. Atmospheric freeze drying – Modeling and simulation of a tunnel dryer. *Drying Technol.* **25**(12): 1959–1965.

Claussen, I. C., Strommen, I., Hemmingsen, A. K. T., Rustad, T., 2007a. Relationship of product structure, sorption characteristics, and freezing point of atmospheric freeze-dried foods. *Drying Technol.* **25** (5): 853–865.

Claussen, I. C., Ustad, T. S., Strommen, I., Walde, P. M., 2007b. Atmospheric freeze drying – A review. *Drying Technol.* **25** (6): 947–957.

Clements, S., Jia, X., Jolly, P., 1993. Experimental verification of a heat pump assisted continuous dryer simulation model. *Int. J. Energ. Res.* **17**(1): 19–28.

Daghigh, R., Ruslan, M. H., Sulaiman, M. Y., Sopian, K., 2010. Review of solar assisted heat pump drying systems for agricultural and marine products. *Renew. Sustain. Energy Rev.* **14**: 2564–2579.

Devotta, S., 1995. Alternative heat pump working fluids to CFCs. *Heat Recov. Syst. CHP* **15**(3): 273–279.

Erbay, Z., Icier, F., 2009. Optimization of drying of olive leaves in a pilot-scale heat pump dryer. *Drying Technol.* **27**(3): 416–427.

Erbay, Z., Icier, F., Hepbasli, A., 2010. Exergetic performance assessment of a pilot-scale heat pump belt conveyor dryer. *Int. J. Energ. Res.* **34**: 249–264.

Fan, Y., Luo, L., Souyri, B., 2007. Review of solar sorption refrigeration technologies: Development and applications. *Renew. Sustain. Energy Rev.* **11**: 1758–1775.

Fatouh, M., Metwally, M. N., Helali, A. B., Shedid, M. H., 2006. Herbs drying using a heat pump dryer. *Energ. Convers. Manage.* **47** (15–16): 2629–2643.

Fujioka, K., Hatanaka, K., Hirata, Y., 2008. Composite reactants of calcium chloride combined with functional carbon materials for chemical heat pumps. *Appl. Therm. Eng.* **28**: 304–310.

Gopichand, S., Devotta, S., 1988. Heat pump assisted distillation: Potential for industrial applications. *Int. J. Energ. Res.* **12**: 569–582.

Goula, A. M., Adamopoulos, K. G., 2005. Spray drying of tomato pulp in dehumidified air: II. The effect on powder properties. *J. Food Eng.* **66**(1): 35–42.

Gungor, A., Erbay, Z., Hepbaslic, A., 2011. Exergetic analysis and evaluation of a new application of gas engine heat pumps (GEHPs) for food drying processes. *Appl. Energ.* **88**(3): 882–891.

Harrison, R. E., Allen, W. H., 1980. Solar supplemented heat pump corn dryer. *Am. Soc. Agric. Eng.* ASAE Summer meet, San Antanio, USA, June 15–18, 19.

Hawlader, M. N. A., Chou, S. K., Jahangeer, K. A., Rahman, S. M. A., Eugene Lau, K. W., 2003a. Solar-assisted heat – pump dryer and water heater. *Appl. Energ.* **74**: 185–193.

Hawlader, M. N. A., Jahangeer, K. A., 2003b. Solar heat-pump drying and water heating in the tropics. *Sol. Energ.* **80**: 492–499.

Hawlader, M. N. A., Perera, C. O., Tian, M., 2006a. Properties of modified atmosphere heat pump dried foods. *J. Food Eng.* **74** (3): 392–401.

Hawlader, M. N. A., Perera, C. O., Tian, M., 2006b. Comparison of the retention of 6-gingerol in drying of ginger under modified atmosphere heat pump drying and other drying methods. *Drying Technol.* **24**(1): 51–56.

Hawlader, M. N. A., Perera, C. O., Tian, M., Yeo, K. L., 2006c. Drying of guava and papaya: Impact of different drying methods. *Drying Technol.* **24**(1): 77–87.

Hawlader, M. N. A., Rahman, S. M. A., Jahangeer, K. A., 2008. Performance of evaporator-collector and air collector in solar assisted heat pump dryer. *Energ. Convers. Manage.* **49**: 1612–1619.

Hong, D., Chen, G., Tang, L., He, Y., 2010. A novel ejector-absorption combined refrigeration cycle. *Int. J. Refrig.*, available online. (DOI: 10.1016/j.ijrefrig.2010.07.007).

Hundy, G., Hundy, G. H., Trott, A. R., 2008. *Refrigeration and air-conditioning*. Butterworth Heinemann, Jordan Hill, Oxford, UK.

Ibrahim, M., Sopian, K., Daud, W. R. W., Alghoul, M. A., 2009. An experimental analysis of solar-assisted chemical heat pump dryer. *Int. J. Low-Carbon Technol.* **4** (2): 78–83.

Ishitobi, H., Sato, Y., Uruma, K., Ryu, J., Kato, Y., 2010. Dehydration and hydration behavior of LiCl-modified $Mg(OH)_2$ as a material for chemical heat pumps. *Proceedings of Innovative Materials for Processes in Energy Systems*, Singapore, pp. 255–262.

Islam, M. R., Ho, J. C., Mujumdar, A. S., 2003a. Simulation of liquid diffusion-controlled drying of shrinking thin slabs subjected to multiple heat sources. *Drying Technol.* **21**(3): 413–438.

Islam, M. R., Ho, J. C., Mujumdar, A. S., 2003b. Convective drying with time-varying heat input: simulation results. *Drying Technol.* **21**(7): 1333–1356.

Islam, M. R., Mujumdar, A. S., 2008a. Heat pump-assisted drying, in *Drying technologies in food processing* (eds. X. D. Chen, A. S. Mujumdar). Blackwell Publishing, Oxford, UK, pp. 190–224.

Islam, M. R., Mujumdar, A. S., 2008b. Heat pump-assisted drying, in *Guide to industrial drying* (ed A. S. Mujumdar). Three S Colors Publication, Mumbai, India, pp. 157–180.

Jangam, S. V., Mujumdar, A. S., Thorat, B. N., 2009. Design of an efficient gas distribution system for a fluidized bed dryer. *Drying Technol.* **27**(11): 1217–1228.

Jia, L. W., Islam, M. R., Mujumdar, A. S., 2003. A simulation study on convection and microwave drying of different food products. *Drying Technol.* **21**(8): 1549–1574.

Jia, X., Clements, S., Jolly, P., 1993. Study of heat pump assisted microwave drying. *Drying Technol.* **11**(7): 1583–1616.

Jinjiang, Z., Yaosen, W., 2010. Experimental study on drying high moisture paddy by heat pump dryer with heat recovery. *Int. J. Food Eng.* **6**(2): art. no. 14.

Jolly, P., Jia, X., Clements, S., 1990. Heat pump assisted continuous drying. Part 1. Simulation model. *Int. J. Energ. Res.* **14** (7): 757–770.

Joshi, V. S., Thorat, B. N., 2010. Formulation and cost effective drying of probiotic yeast. *Drying Technol.* Accepted for publication.

Kato, K., 1981. Energy savings in grain drying – A thermodynamic evaluation. *Energ. Dev. Jpn.* **4**(2): 153–182.

Kudra, T., 2004. Energy aspects in drying. *Drying Technol*. **22**(5): 917–932.

Kudra, T., Mujumdar, A. S., 2009. *Advanced drying technologies*. CRC Press, Boca Raton, Florida, USA.

Kudra, T., Platon, R., Navarri, P., 2009. Excel-based tool to analyze the energy performance of convective dryers. *Drying Technol*. **27** (10–12): 1302–1308.

Laurent, S., Couture, F., Roques, M., 1999. The use of local thermodynamic path for quality problems during convective drying. *Drying Technol*. **17**(7): 1327–1345.

Lai, F. S., Foster, G. H., 1977. Improvement in grain-dryer fuel efficiency through heat recovery. *Trans. Am. Soc. Agric. Eng*. **20**(3): 579–584.

Li, H., Li, Y., Dai, Y., Gao, S., Wei, L., Li, Z., 2010. Experiment on hybrid solar drying system assisted by heat pump for grain in-store drying. *Trans. Chin. Soc. Agric. Machin*. **41**(7): 109–113.

Lorentzen, G., 1994. Revival of carbon dioxide as a refrigerant. *Int. J. Refrig*. **17** (5): 292–301.

Lostec, B. L., Galanis, N., Baribeault, J., Millette, J., 2008. Wood chip drying with an absorption heat pump. *Energy* **33**: 500–512.

Margaret, T. B., 1991. Optimization of humidity conditions in timber drying kilns using heat pump dehumidifiers. *Proceedings of 7th International Drying Symposium*, Prague, Czech, pp. 535–545.

Martin, A., Bermejo, M. D., 2010. Thermodynamic analysis of absorption refrigeration cycles using ionic liquid and supercritical CO_2 pairs. *J. Supercrit. Fluids*, available online.

Minea, V., 2008. Energetic and ecological aspects of softwood drying with high-temperature heat pumps. *Drying Technol*. **26** (11): 1373–1381.

Mohanraj, M., Jayaraj, S., Muraleedharan, C., 2009. Environment friendly alternatives to halogenated refrigerants – A review. *Int. J. Greenhouse Gas Control* **3**: 108–119.

Molina, M., Rowland, F. S., 1974. Stratospheric sink for chlorofluoromethane: Chlorine atom catalyzed destruction of ozone. *Nature* **249**: 810.

Montreal protocol on substances that deplete the ozone layer, 1987. *United Nations Environment Programme*.

Mujumdar, A. S., 1990. Superheated steam drying: Principles, practice and potential for use of electricity. *Report for the Canadian Electrical Association*. Quebec, Canada, pp. 73–81.

Mujumdar, A. S., 2006. *Handbook of industrial drying*. CRC Press, Boca Raton, USA.

Nathakaranakule, A., Jaiboon, P., Soponronnarit, S., 2010. Far-infrared radiation assisted drying of longan fruit. *J. Food Eng*. **100**(4): 662–668.

Neksa, P., 2002. CO_2 heat pump systems. *Int. J. Refrig*. **25**: 421–427.

Ogura, H., Hamaguchi, N., Kage, H., Mujumdar, A. S., 2004. Energy and cost estimation for application of chemical heat pump dryer to industrial ceramics drying. *Drying Technol*. **22**(1): 307–323.

Ogura, H., Ishida, H., Kage, H., Mujumdar, A. S., 2003. Enhancement of energy efficiency of a chemical heat pump-assisted convective dryer. *Drying Technol*. **21**(2): 279–292.

Ogura, H., Mujumdar, A. S., 2000. Proposal for a novel chemical heat pump dryer. *Drying Technol*. **18**(4): 1033–1053.

Ogura, H., Yamamoto, T., Otsubo, Y., Ishida, H., Kage, H., Mujumdar, A. S., 2005. A control strategy for a chemical heat pump dryer. *Drying Technol*. **23**(6): 1189–1203.

Omideyi, T. O., Parade, M. G., Kasprzycki, J., Devona, S., 1984. The economics of heat pump assisted distillation system: Part III: A comparative analysis on three alcohol mixtures. *J. Heat Recov. Syst*. **4**: 281–286.

Pal, U. S., Khan, M. K., 2008. Calculation steps for the design of different components of heat pump dryers under constant drying rate condition. *Drying Technol*. **26**(7): 864–872.

Pal, U. S., Khan, M. K., 2010. Performance evaluation of heat pump dryer. *J. Food Sci. Tech*. **47**(2): 230–234.

Pal, U. S., Khan, M. K., Mohanty, S. N., 2008. Heat pump drying of green sweet pepper. *Drying Technol*. **26**(12): 1584–1590.

Perera, C. O., Rahman, M. S., 1997. Heat pump dehumidifier drying of food. *Trends Food Sci. Technol*. **8**(3): 75–79.

Phoungchandang, S., Nongsang, S., Sanchai, P., 2009. The development of ginger drying using tray drying, heat pump-dehumidified drying, and mixed-mode solar drying. *Drying Technol*. **27**(10): 1123–1131.

Phoungchandang, S., Saentaweesuk, S., 2010. Effect of two stage, tray and heat pump

assisted-dehumidified drying on drying characteristics and qualities of dried ginger. *Food Bioprod. Process*. Available online.

Prasertsan, S., Saen-Saby, P., 1998a. Heat pump drying of agricultural materials. *Drying Technol*. **16**(1): 235–250.

Prasertsan, S., Saen-Saby, P., 1998b. Heat pump dryers: Research and development needs and opportunities. *Drying Technol*. **16**(1): 251–270.

Prasertsan, S., Saen-Saby, P., Ngamsritrakul, P., Prateepchaikul, G., 1997. Heat pump dryer Part 2: Results of the simulation. *Int. J. Energ. Res*. **1**: 1–20.

Raghavan, G. S. V., Sosle, V., Kittler, R., 2003. Low-temperature drying using versatile heat pump dehumidifier. *Drying Technol*. **21** (3): 539–554.

Rossi, S. J., Neves, L. C., Kieckbusch, T. G., 1992. Thermodynamic and energetic evaluation of heat pump applied to the drying of vegetables. *Proceedings of the 8th International Drying Symposium*, Montreal, Quebec, Canada, Volume B, pp. 1475–1484.

Schmid, M., 1994. Industrial drying of food and non-food products by gas dehumidifier heat pumps. *Powder Handling Process*. **6** (1): 80–83.

Shah, S. H., Bhetasiwala, Y., Mehta, D., 2001. Low energy 100%-outside-air dryer. *Air Cond. Refrig. J*. **4**(2): 31–36.

Shang, D.-K., Rasmuson, A., Zhang, X.-D., 1995. Design of solar-dehumidification wood drying kiln characterized by high capacity and temperature. *Drying Technol*. **13** (5–7): 1431–1445.

Sharma, A., Chen, C. R., Vu Lan, A., 2009. Solar-energy drying systems: A review. *Renew. Sust. Energ. Rev*. **13**: 1185–1210.

Slim, R., Zoughaib, A., Clodic, D., 2008. Modeling of a solar and heat pump sludge drying system. *Int. J. Refrig*. **31**: 1156–1168.

Srikhirin, P., Aphornratana, S., Chungpaibulpatana, S., 2001. A review of absorption refrigeration technologies. *Renew. Sust. Energ. Rev*. **5**: 343–372.

Strommen, I., Eikevik, T., Alves Filho, O., Syverud, K., 2004. Heat pump drying of sulphate and sulphite cellulose. *Proceedings of the 14th International Drying Symposium (IDS 2004)*, Sao Paulo, Brazil, Volume B, pp. 1225–1232.

Sun, Z. F., Carrington, C. G., Anderson, J. A., Sun, Q., 2004. Air flow patterns in dehumidifier wood drying kilns. *Chem. Eng. Res. Des*. **82**(10): 1344–1352.

Supranto, S., Chandra, I., Unde, M. B., Diggory, P. J., Holland, F. A., 1986. Heat pump assisted distillation: Part III: Experimental studies using an external heat pump. *Energ. Res*. **10**: 255–276.

Teeboonma, U., Tinasuwan, J., Soponronnarit, S., 2003. Optimization of heat pump fruit dryers. *J. Food Eng*. **59**: 369–377.

Turner, I. W., Jolly, P., 1991. Combined microwave and convective drying of a porous material. *Drying Technol*. **9** (5): 1209–1270.

Wang, C., Zhang, P., Wang, R., 2008. Review of recent patents on chemical heat pump. *Recent Pat. Eng*. **2**: 208–216.

Wang, S. K., 2000. *Handbook of air conditioning and refrigeration*. McGraw-Hill, New York, USA.

Whitman, W. C., Johnson, W. M., Tomczyk, J. A., 2005. *Refrigeration and air conditioning technology*. Thomson Delmar Learning, New York, USA.

Wongsuwan, W., Kumar, S., Neveu, P., Meunier, F., 2001. A review of chemical heat pump technology and applications. *Appl. Therm. Eng*. **21**: 1489–1519.

Yu, Y. Q., Zhang, P., Wu, J. Y., Wang, R. Z., 2008. Energy upgrading by solid-gas reaction heat transformer: A critical review. *Renew. Sust. Energy Rev*. **12**: 1302–1324.

Zhang, G., Arason, S., Arnason, S. V., 2008. Physical and sensory properties of heat pump dried shrimp (Pandalus borealis). *Trans. Chin. Soc. Agric. Eng*. **24**(5): 235–239.

Zhang, X., Mao, Z., Li, H., Xu, G., Xiong, K., Gu, Z., 2006. Combined heat pump and fluidized bed drying of granular carrots. *Trans. Chin. Soc. Agric. Machin*. **37**(3): 68–71.

5
Zeolites for Reducing Drying Energy Usage

Antonius J. B. van Boxtel, Moniek A. Boon,
Henk C. van Deventer, and Paul J. Th. Bussmann

5.1
Introduction

Drying systems take about 15% of the energy consumption in industrial production (Kemp, 2005). The energy efficiency for most convective drying systems is in the range 40–60%. Drying systems with high air inlet temperatures are on the high side of this range, while systems with low air inlet temperatures are on the low side. In the food industry there is a tendency for lower air inlet temperatures to maintain vulnerable and volatile components which are essential for the product quality and value. Moving to a lower dryer air inlet temperature will result, for current drying systems, in less energy efficient systems. These figures and trends show that the development of energy efficient alternatives is a real challenge for drying technology.

The energy efficiency of drying systems can be improved by using zeolite as an intermediate. Zeolites have a strong affinity to water and can adsorb a considerable amount of water or water vapor. Together with water uptake, a significant amount of adsorption heat is also released. Zeolites can, therefore, be used to dehumidify the air for drying, or be mixed with the product to be dried.

Dehumidification of air used in drying yields a higher driving force for drying and an increased water uptake capacity. At the same time, due to the release of the adsorption heat, the temperature of the air increases (to 40–70 °C, depending on zeolite type and the humidity of the used air) and, therefore, less energy is required for drying. Mixing zeolite with product particles results in an improved micro-climate on a particle level with a high driving force for the release of water in the product, while the heat required for water release from the product is provided by the emitted adsorption enthalpy.

For example, zeolites type 13X and 4A raise ambient air from 20 °C, 70% RH (relative humidity), to a temperature around 60 °C, and a RH below 1%. This reduces the necessity for additional heating and enhances water transfer. As a result, the required amount of energy for drying is significantly reduced. However, the

Modern Drying Technology Volume 4: Energy Savings, First Edition.
Edited by Evangelos Tsotsas and Arun S. Mujumdar

regeneration of zeolite for reuse requires energy, so that the energy profit obtained for drying would be lost, if not making use of the following two opportunities:

- Zeolites are regenerated/dried at high temperatures (250–300 °C) and therefore regeneration is a more energy efficient drying process than product drying at low and medium temperatures;
- Energy from the regenerator exhaust air can be recovered/reused.

With these properties, a drying system with low energy efficiency is shifted to a system which has much better energy efficiency. As such, the application of zeolites in drying systems may result in a 30–50% lower energy usage. Consequently, this technology can make an important contribution to the reduction of industrial energy usage and CO_2-emission.

The present chapter discusses the use of zeolites to increase the energy efficiency in drying systems. First, zeolites and their properties for water uptake and release are discussed. Then the principles of direct contact drying systems and air dehumidification systems for drying are described, and two approaches for energy recovery are given. In the following section the technical realization of using zeolites in drying systems is considered. Then the potential for energy savings is illustrated by examples from demonstration projects from Dutch research and collaboration with industries (milk powder, seed coating, manure/sludge processing). Finally, the economic feasibility is evaluated and the potential of the technology is reviewed.

5.2 Zeolite as an Adsorption Material

5.2.1 Zeolite

Many adsorbents are available to bind water, for example silica gel, zeolites, alumina and activated carbon. Zeolite is a molecular sieve built up from crystalline aluminosilicates. The structure is based on an infinitely extendable three-dimensional framework of AlO_4 and SiO_4 units, which share the oxygen ions (Flanigan, 1991). The SiO_4 in the crystal is uncharged, while AlO_4 has a net negative charge. This charge is balanced by mobile cations (Na^+, K^+, Ca^{++}) in the crystal. The ratio between AlO_4 and SiO_4 structures in the crystal determines whether the zeolite is hydrophobic (high-silica zeolites) or hydrophilic (low-silica zeolites). The cation, among others, determines the pore size of the crystal. Especially, the hydrophilic zeolite 4A ($Si/Al = 1$) is used for water adsorption.

The "unit cell" in the molecular sieve (see Fig. 5.1) consists of 12 SiO_4 and 12 AlO_4 units, which enclose small and larger spaces. The negative charge introduced by the aluminum ion is compensated by the sodium ion. When the zeolite is completely saturated, 27 molecules of water are adsorbed in the "unit cell". Most water molecules (20) are present in the α space (inner core), while in the β space (around the corners) 4 molecules can be present. The other 3 molecules are adsorbed on the side surface.

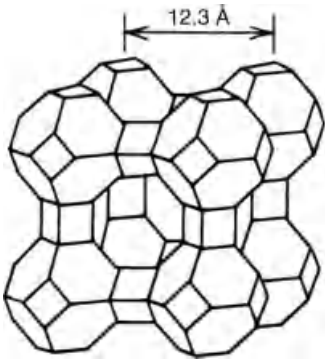

Fig. 5.1 Representation of zeolite structure, type A zeolite "unit cell" (Ruthven, 1984).

Measurements have shown that the adsorption heat for water molecules in the β spaces is higher than for the α spaces (Muller *et al.*, 1998; Morris, 1968). The adsorption heat for zeolites is generally lower than the value of 4000 kJ kg^{-1} that is often reported in the literature. Figure 5.2 gives the adsorption heat for 1–25 adsorbed molecules (Morris, 1968). In industrial applications, the zeolite is often not fully regenerated but still has a loading of 2–4 wt%, which corresponds to 3–5 molecules. Thus, 3320 kJ kg^{-1}, as determined by Morris (1968) is a good value for the sorption heat.

Most industrial zeolite applications use composites in which the zeolite crystallites are bound together with a binder in a particle (sphere or cylinder) with a dimension of a few millimeters. Figure 5.3 shows a particle where crystals have a cubic shape and a size of about 5 μm. The binder is present as a thread-like structure. The composites contain 10–20% of clay binder (Dyer, 1988). The theoretical water loading on zeolite 4A crystals is 28 wt%. On the composite the theoretical loading is 23–25 wt%, but sorption isotherms show mostly an effective maximum loading of 20 wt%.

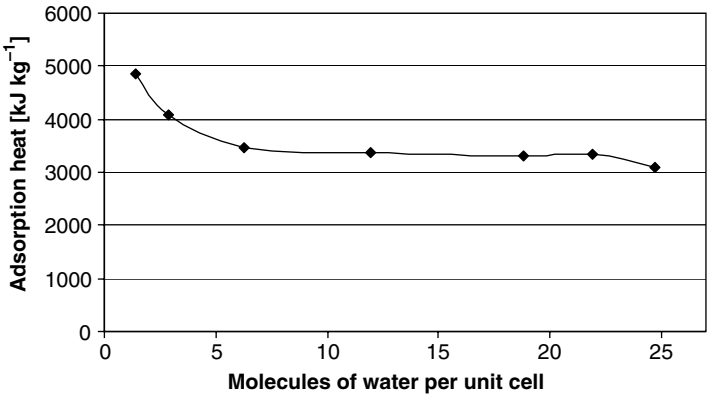

Fig. 5.2 Sorption heat on 4A zeolite as a function of the number of water molecules (Morris, 1968).

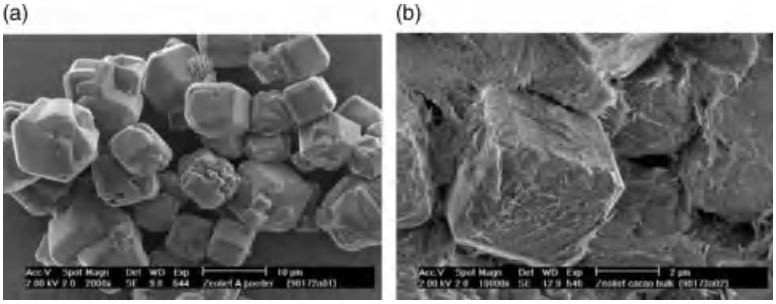

Fig. 5.3 SEM photographs of zeolite A: (a) smooth crystal surfaces without binder material, (b) crystals covered with binding material (Vente, 1999).

5.2.2
Comparing the Main Sorption Properties of Zeolite with other Adsorbents

The suitability of adsorption materials as an intermediate in drying depends, among others, on the sorption properties. Figure 5.4 gives the sorption isotherms for five different adsorbent materials. The maximum water uptake capacity of zeolite (D) is below the maximum capacity for granular alumina, silica gel and activated carbon (B, C, E) at high relative humidity. The advantage of zeolite is, however, in the low relative humidity area where zeolite has a much higher water uptake capacity than the other adsorbents. This part of the relative humidity range is especially relevant in drying.

Another advantage is revealed by examination of the adsorption capacity over an adsorption–regeneration cycle as a function of partial vapor pressure and temperature. Figure 5.5 (see also Appendix) gives the sorption isotherms of zeolite 4A as a

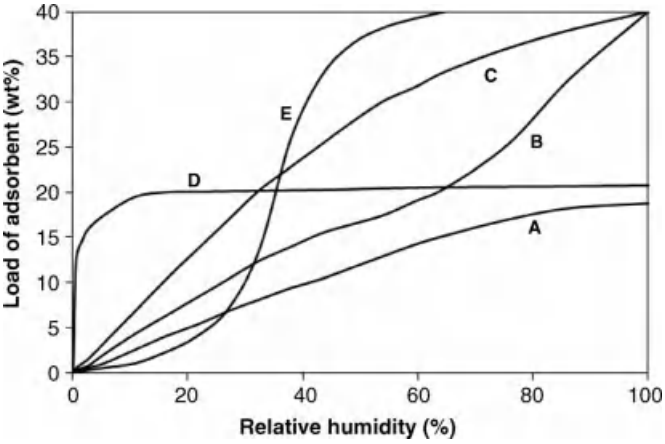

Fig. 5.4 Water adsorption isotherm from atmospheric air at 25 °C; (A) granular alumina, (B) spherical alumina, (C) silica gel, (D) 5A zeolite, (E) activated carbon (Yang, 1997).

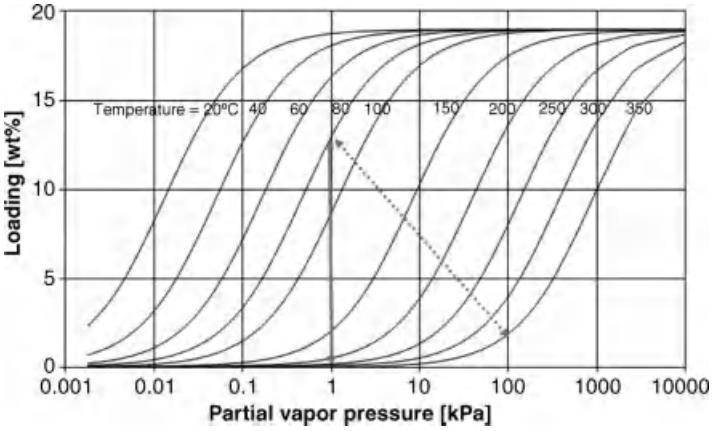

Fig. 5.5 Experimentally determined sorption isotherms for zeolite 4A as function of the partial vapor pressure and temperature. The solid arrow shows the capacity for an adsorption–regeneration cycle with ambient air, the dotted arrow for regeneration with superheated steam.

function of the partial vapor pressure and temperature. Suppose that adsorption concerns air with a partial water vapor pressure of 1 kPa (20 °C, RH 50%) on zeolite at 80 °C. Then, the zeolite has a load capacity of 13 wt%. Regeneration can take place by heating ambient air to 250 °C, then the water load of zeolite is below 1 wt%. The net adsorption capacity is, in this case, just above 12 wt%. As an alternative, superheated steam can be used for regeneration (see also Section 5.4.4). For example, 1 bar steam at 350 °C has a partial water vapor pressure of 100 kPa, resulting in a load capacity of 2 wt%. In this case the zeolite has a net capacity of 11 wt%.

The regeneration capacity of silica gel over an adsorption–regeneration cycle differs from that of zeolite. Figure 5.6 (see also Appendix) shows the sorption isotherms for silica gel. The isotherms illustrate that silica adsorbs the best at low temperatures; high temperatures are not suitable. For example: suppose that adsorption concerns air with a partial water vapor pressure of 1 kPa (20 °C, RH 50%) and silica gel at a temperature of 80 °C, then silica gel has only a load of 2 wt% and adsorbs hardly any water. Therefore, the silica must be cooled, for example to 30 °C, then it has a capacity of 14 wt%. Regeneration with ambient air at 100–150 °C results in a load of 1 wt%; the loading capacity over an adsorption–regeneration cycle is 13 wt%. The maximum temperature for regeneration for silica gel is 150 °C. Above that temperature silica gel will break down. The loading of silica gel in regeneration with steam is 7 wt%, and so the loading capacity over an adsorption–regeneration cycle with steam is 7 wt%.

Zeolite is thus, in contrast to silica gel, not critical in regard to the adsorption temperature, and it is not necessary to cool the zeolite as far as silica gel. Moreover, zeolite can be regenerated by using a high temperature and moist environment, such as superheated steam. This property gives zeolite advantages in energy efficient drying, see the next sections.

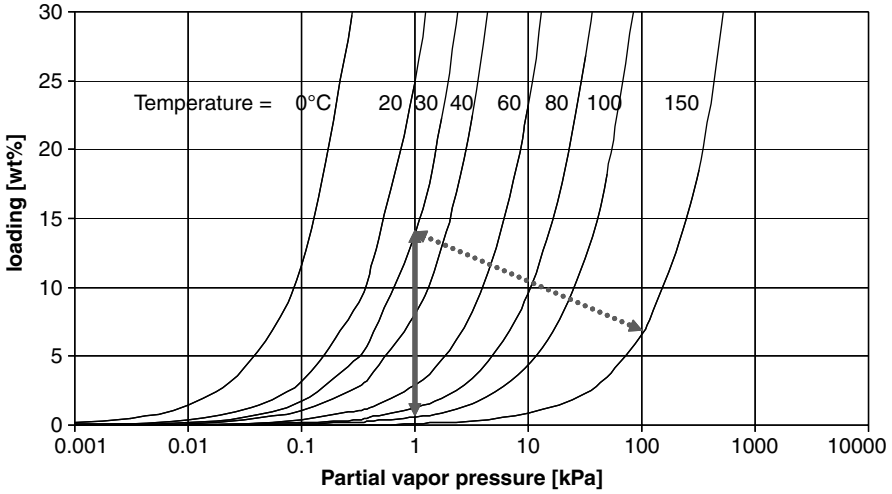

Fig. 5.6 Experimentally determined sorption isotherms for silica gel as a function of the partial vapor pressure and temperature. The solid arrow shows the capacity for an adsorption–regeneration cycle with ambient air, the dotted arrow for regeneration with superheated steam.

5.3
Using Zeolites in Drying Systems

5.3.1
Drying Systems

In "direct contact drying" adsorbents are mixed with the products to be dried. The adsorbent adsorbs water from the product, and at the same time heat is released. The intensive contact between the heat transferring medium and the product leads to fast drying and a homogeneous product. After drying, the product is separated from the zeolite by using a suitable sieve and, after regeneration, the zeolite is reused (see Fig. 5.7a).

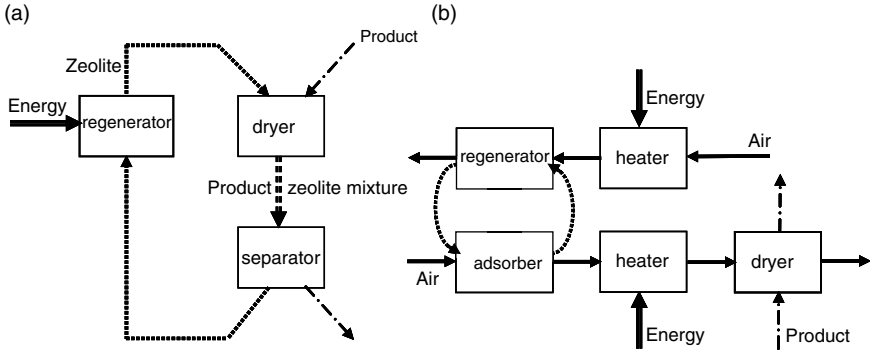

Fig. 5.7 Concepts of (a) direct contact drying and (b) drying with dehumidified air.

Tab. 5.1 Characteristics and requirements of "direct contact drying" and "drying with dehumidified air".

	Direct Contact Drying	**Drying with Dehumidified Air**
Units (excl. heat generation and emission treatment)	Solid/solid mixer, solid/solid separator and adsorbent regeneration unit	Dryer and adsorption–regeneration unit
Solids handling	Need for solid handling	No need for solid handling
Conditions	Same conditions for drying product and adsorption on zeolite	Different conditions for drying product and adsorption on zeolite possible
Dryer size	Zeolite-product mixture requires a small volume (up to 1000 times smaller)	Air–product mixture requires a substantial volume
Operation mode dryer	Batch or continuous	Continuous
Operation mode regeneration	Batch or continuous	Batch or continuous
Dryer off-gas volume	Small	Medium to large
Product	Heat is generated in the product–zeolite mixture. Product temperature must be controlled for heat-sensitive products.	Suitable for heat-sensitive products; after cooling, drying at low temperatures is possible.
Cross-contamination	Product can contain zeolite particles.	Product is free of zeolite particles.
Drying rate	High drying rates resulting from local heat generation	Low drying rates resulting from low temperatures
Emission	Very low emission of volatile components	Low emission of volatile components because drying at low temperatures is possible.
Fire and explosion risk	Low risk	Low risk
Complexity of the equipment	Simple dryer	Simple dryer, smaller volume than conventional dryers

The other option for the use of zeolites in drying concerns "drying with dehumidified air". Here, ambient air contacts zeolites and is dehumidified. At the same time the air temperature increases due to the released heat of adsorption. If necessary, the air can be heated further and then fed to the dryer (see Fig. 5.7b). Zeolite undergoes a cycle in which the zeolite is loaded with water in the adsorber and unloaded in the regenerator. The characteristics and requirements of both methods are summarized in Tab. 5.1.

5.3.2 Direct Contact Drying

The affinity of zeolite for water is high compared to other adsorbents, so that drying can be conducted at a low dew point. In addition, zeolite particles release heat when

water is adsorbed and, as a result, the drying rate is enhanced. Because of size exclusion, zeolites are very selective for water and do not adsorb large molecules. Consequently, only water is removed in the drying process, whereas all aromatic compounds are preserved.

In traditional processing of foodstuffs such as cocoa and nuts, the products are often first dried with hot air and subsequently roasted. The high temperatures during air-drying and roasting easily result in undesired changes in color, and loss of functional properties or aromatic compounds. These undesired changes of product quality do not occur when drying and roasting take place in oxygen-free environments. An alternative is to apply direct contact drying of foodstuffs by thoroughly mixing the product with spherical or cylindrical zeolite particles. Depending on the process conditions, and the amount of zeolite applied, the final temperature can reach roasting levels. Hence, drying and roasting can be combined effectively in one operation.

Subsequently, the zeolite particles are separated from the product on a suitable sieve and regenerated by heat treatment in dry air or with superheated steam. Although zeolite particles are not harmful for human consumption, it is still essential to avoid the presence of zeolite particles, dust and fragments in food products. In these applications the separation step is of the utmost importance and demands much attention. In the selection of the most suitable zeolite the particle size and strength must be taken into account (see Section 5.5).

Comparison of conventionally processed product and zeolite-processed product (cereals, cocoa, herbs, nuts and seeds) showed that the quality of the zeolite-processed product was at least equal in terms of color, taste and microbial quality. Moreover, the water transfer rate in direct contact drying is faster than in conventional drying. Therefore, direct contact systems with zeolite are more compact and reduce the process time. Other advantages of direct contact systems with zeolite are the reduced energy requirements and the reduced emission of odorous gases, especially at low process temperature. The energy savings which can be realized are strongly dependent on the product and the desired end moisture content. The lower the end moisture content, the larger the energy saving compared to conventional air drying (see also Section 5.6 for some examples).

Direct contact adsorption drying with zeolite can also be applied to manure and sludge. The reduced drying temperature and the inert process environment result in a fireproof system. Moreover, because of the selectivity of zeolite for water, the emission of volatiles and odor in the regeneration exhaust air is low. Therefore, off-gas treatment is not required. In conventional processes the investment costs for off-gas treatment are considerable and can be responsible for 40 to 50% of the total investment costs. So, the drying system fulfills more than one function.

5.3.3
Air Dehumidification

Zeolites can also be used for dehumidification of air before feeding it to the dryer (see Fig. 5.7b). In this case the vapor pressure difference between the product and air

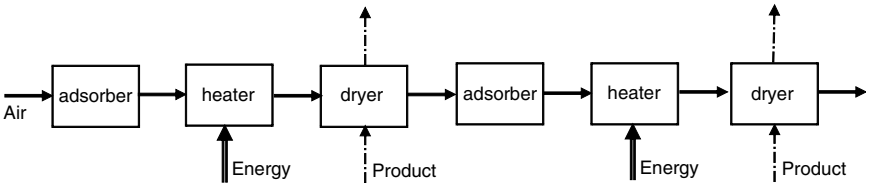

Fig. 5.8 Flows in a multi-stage dryer; The sequence can be repeated several times.

increases and the drying rate is enhanced. The adsorption heat for water by zeolites is above the heat of evaporation of water, and with dehumidification the air temperature increases to temperatures in the range 50–70 °C. Air dehumidification reduces the amount of energy required to reach the required drying temperature significantly, however, energy is required for the regeneration step.

The air at the exit of the dryer has a significant energy content of both sensible and latent heat. The sensible heat is of low temperature level, with limited possibilities of recovery. The latent heat can be recovered by condensation. Recovery from low temperature air by heat exchangers is not effective if there is no requirement for low temperature heat. Holmberg and Ahtila (2004), Spets (2001), and Spets and Ahtila (2001) discuss the possibility of multi-stage drying systems in which the energy content from the dryer exhaust air is retained by reheating the air and then reusing it for drying in a succeeding stage. A similar approach can be achieved in adsorption drying (Djaeni *et al.*, 2007a, b). Both latent and sensible heat can be fully recovered in a multi-stage adsorption-dryer system. Thereby the exhaust air from the dryer is dehumidified again, see Fig. 5.8. With the obtained low vapor pressure and increased temperature the air regains its drying capacity.

Another alternative to recover energy from the dryer exhaust is partial recirculation of air over an adsorber with zeolite (see Fig. 5.9). In this way latent heat is partly recovered. The heater in Fig. 5.9 is required for high temperature drying and to realize a quick start-up.

At this point adsorption drying with zeolite seems beneficial with regard to energy consumption, but the water accumulated in the zeolite must be removed from the system. Figure 5.10 describes a multi-stage dryer with regeneration. Zeolite passes in every stage through a sequence of adsorbing and regeneration. The preferred air temperature for regeneration is above 150 °C (see Fig. 5.5). Regeneration is an energy

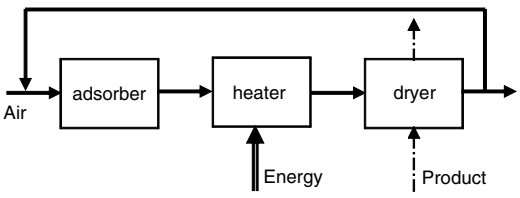

Fig. 5.9 Flows in a dryer with air dehumidification; The exhaust air from the dryer is partly/fully recycled.

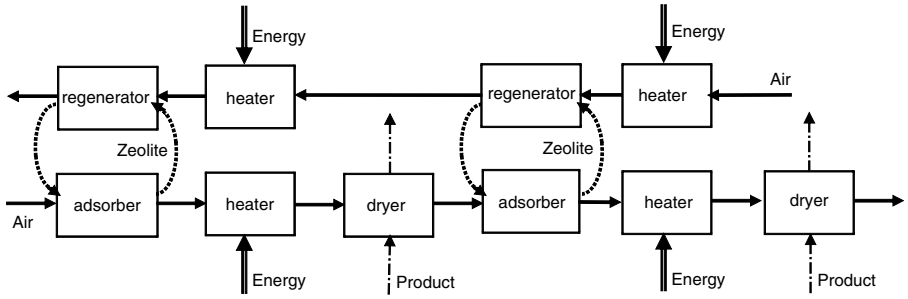

Fig. 5.10 Flows in a multi-stage dryer with air dehumidification and zeolite regeneration.

demanding step and to realize a higher energy efficiency heat recovery is necessary (see Section 5.4).

Besides the potential for energy savings, air dehumidification has three other advantages:

- No disturbances from ambient air conditions,
- Increased drying capacity due to the lower vapor pressure,
- Lower temperature load on the products.

The performance of conventional drying systems using ambient air is related to the moisture content of the used air. Figure 5.11 shows the variations in the ambient air moisture content in a moderate climate over one year. Drying companies have to deal with these variations. In practice, the process settings are chosen in such a way that the resulting product is never off-spec. This implies that the process is not optimized and that most of the time more water is removed from the product than necessary (the product is over-dried). Air dehumidification cancels the variations in air moisture content (see for example the continuous line in Fig. 5.11), which enables the residual moisture content of the product to be maintained at specification, and ensures that a higher return on the resources is obtained.

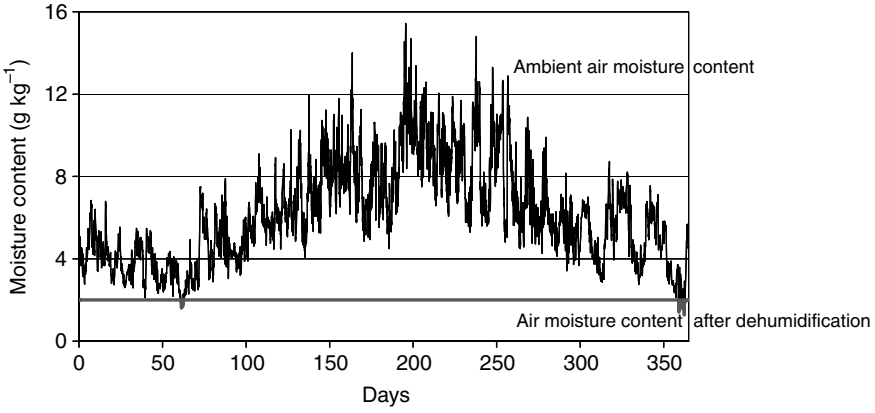

Fig. 5.11 Moisture content of ambient air in moderate climates and after air dehumidification.

The drying capacity of dehumidified air is higher than that of ambient air. Therefore, a second advantage of air dehumidification is the ability to increase the capacity of dryers. During summer, in moderate climates, dehumidification can increase the capacity of dryers by up to 30%; in winter the increase is smaller. Under tropical conditions, the gain in capacity is all year round, and even more spectacular, depending on the level of fixation of the moisture content, which is determined by the intake air conditions and the regeneration temperature.

Products leaving a dryer reach equilibrium with the humidity of air. Consider two cases: (i) ambient air and (ii) dehumidified air are heated to the same temperature and, in both cases, the exhaust air has the same relative humidity. The psychometric chart teaches that in these cases the dehumidified air has a lower exhaust air temperature. As a consequence, the product temperature for drying with dehumidified air will also be lower than that of ambient air drying. Thus, the temperature load on the product is lower and deterioration of heat sensitive products can be reduced.

5.4
Energy Efficiency and Heat Recovery

5.4.1
Defining Energy Efficiency

In convective drying, the air is heated to the operational temperature. In contact with product, the energy content of the air remains constant, but sensible heat is exchanged for latent heat by the evaporation of water from the product. The common definition for drying energy efficiency is based on the sensible-to-latent heat exchange against the amount of heat used to raise air to the operational temperature[1)]:

$$\text{Energy efficiency} = \frac{\text{energy used for evaporation of water from product}}{\text{energy added to the flows towards the dryer}} \times 100\%$$

Dryer exhaust air is not saturated, and therefore not all energy that is used to heat ambient air to the operational condition is exchanged for latent heat. As a result the efficiency is below 100%. However, considering the efficiency for a dryer with heat recovery *within* the dryer system or *in another unit operation* at the production site the effectiveness becomes:

$$\text{Energy efficiency with heat recovery} = \frac{\text{energy used for evaporation of water from product}}{\text{energy added to the flows towards the dryer} - \text{energy recovered}} \times 100\%$$

With this definition, if enough energy is recovered the efficiency can rise to values above 100%.

1) As heat usage is often dominant in the energy consumption of a dryer, the definition is limited to the efficiency for heat usage. Electrical energy for pumps and fans is not considered in this definition.

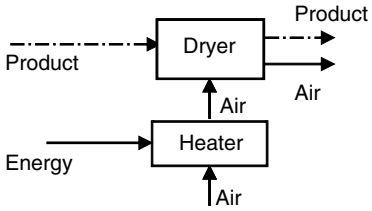

Fig. 5.12 Conventional dryer system; air is heated before contacting the product.

Example:
Consider the dryer system given in Fig. 5.12. Ambient air (humidity 0.010 kg water per kg air and 25 °C) is heated to 70 °C. During product drying, the temperature of air decreases to 42 °C, 0.021 kg water per kg air and a RH of 40%. For 1200 kg air per hour in total 55 000 kJ h^{-1} is used to heat the ambient air to the operational temperature from which 34 000 kJ h^{-1} are used to dry the product. The efficiency of the dryer is then 62%. The exhaust air has a temperature of about 42 °C and has hardly potential for recovery.

5.4.2
Energy Recovery for a Single-Stage System

The single- and multi-stage systems, as described before, are not yet efficient in energy usage. This is illustrated for a single-stage adsorption dryer with zeolite in Fig. 5.13. Ambient air is fed to the adsorber, heated and fed to the dryer. By feeding dry air to the dryer, the water uptake capacity of the air is increased and therefore 1000 kg h^{-1} ambient air flow is sufficient, instead of 1200 kg h^{-1} in the conventional dryer. At the exit of the dryer the air exit temperature is 35 °C, air water content is 0.014 kg water per kg air and the relative humidity of the air is 40%. Zeolite is recycled over the adsorber and the regenerator, which is also fed by ambient air. In accordance with the sorption isotherms of zeolite, the regeneration temperatures have to be relatively high (150 °C or higher), in this example 300 °C.

Despite the increased water uptake rate in the dryer the efficiency of the system is only 47%. The low energy efficiency is the result of the energy requirements for regeneration, especially of the energy lost with the exhaust air from the regenerator. Therefore, it is necessary to consider possibilities of heat recovery in the system.

Pinch analysis is a systematic methodology to find the potential for heat recovery (see for example Linnhoff (1994) and Kemp (2005)). The analysis considers hot and cold streams in a system. The cold streams are the streams that have to be heated and require energy, the hot streams have energy in excess and can be cooled. In composite graphs the energy requirement of all cold streams together, and available energy from all hot streams together, are combined into lines for hot and cold streams; (the methodology to construct these composite curves is explained by Linnhoff (1994), as

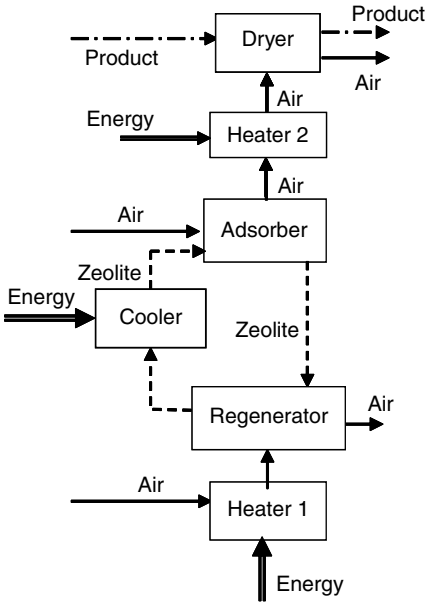

Fig. 5.13 Dryer system with air dehumidification by zeolite in the adsorber and regeneration of zeolite. Energy supply is required for the heaters 1 and 2, cooling energy is used to decrease the temperature of the zeolite.

well as in Chapter 1 of this book). Djaeni *et al.* (2007a) derived the composite curves for several dryer systems, among them the system of Fig. 5.13. The composite curves in Fig 5.14 are based on a minimum temperature difference between hot and cold streams of 10 K. Where the two lines are above each other (region II), energy can be exchanged between hot and cold streams and thus energy can be recovered. In this

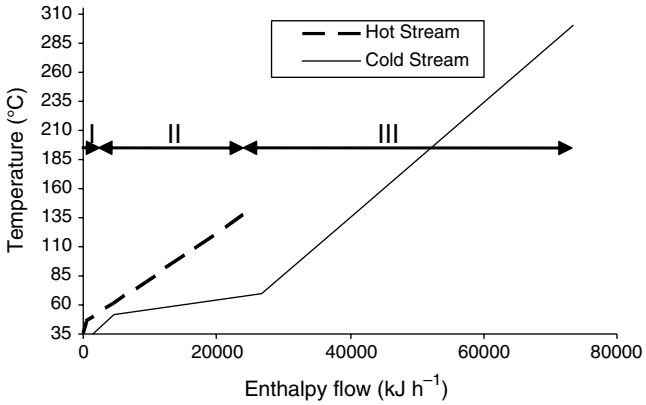

Fig. 5.14 Pinch analysis for a single-stage dryer using zeolite for air dehumidification (Djaeni *et al.*, 2007a); I: energy to be removed, II: energy to be recovered, III: energy to be supplied.

case about 23 000 kJ h^{-1} can be recovered. Thus, the efficiency of the total system comes to 70%, that is, 8% above that of the conventional system.

There are several options to realize heat recovery with heat exchangers. A simple recovery system is used to split the regenerator exhaust flow: one part for heating up the air in heater 1, the other part for preheating the air used for regeneration. In this way 89% of the heat that can be recovered is utilized. Thus 11% of the recoverable heat is then lost, but with an extended heat exchanger network all heat can be recovered (Djaeni *et al.*, 2007a).

5.4.3
Energy Recovery in a Multi-Stage System

The other flow in the system with a significant amount of energy (latent and sensible) is the dryer exhaust. Traditionally, this flow is not regarded as a candidate for energy recovery due to the low temperature level. However, the energy content in this flow can be fully recovered by dehumidification; either by returning the dryer exhaust air to the adsorber or by applying a multi-stage system (Djaeni *et al.*, 2007b), see Figs. 5.9 and 5.10.

Figure 5.15 illustrates a co-current multi-stage system in which product is dried at 70 °C (Djaeni *et al.*, 2007b). Ambient air is dehumidified and the temperature at the adsorber exhaust reaches about 55 °C. Additional heating is then required to achieve the operational temperature of 70 °C. In the first drying stage the air water content rises to about 0.015 kg water per kg air. Together with the first stage dryer exhaust air temperature, the exhaust moisture content is enough to raise the temperature at the exit of the second adsorber to about 70 °C. Therefore, in this example, no additional heating is required; if higher drying temperatures are required additional heating is necessary.

In this system heat is required for the first dryer heater, and for the regenerators; heat is available from the coolers and the exhaust from the regenerators. The heat recovery unit at the bottom of the figure is used to retrieve energy. The potential for heat recovery is derived from a pinch analysis similar to that of Fig. 5.14. The coolers in Fig. 5.15 are connected with the heat recovery unit, but it is also an option to skip the coolers and to retrieve the energy in the adsorbers.

The multi-stage system can be operated in a co-current configuration (product and air have the same sequence of flow through the equipment), counter-current (air is fed to stage 1, product to stage n, so that they move in opposite directions) and cross-current (air passes through the multi-stage configuration, fresh product is fed to each stage and passes only one stage) (Djaeni *et al.*, 2007b). An overview of efficiency values for these three configurations is given in Tab. 5.2. The energy efficiency increases with the number of stages, but above three stages the improvement is marginal. The best results are obtained for a counter-current system.

One option for heat recovery remains. The exhaust air from the last regenerator of a multi-stage system has a significant amount of latent heat which can be recovered by condensation. The temperature is in the range 140–160 °C and water content is 0.10–0.15 kg water per kg air. The condensation temperatures for these conditions

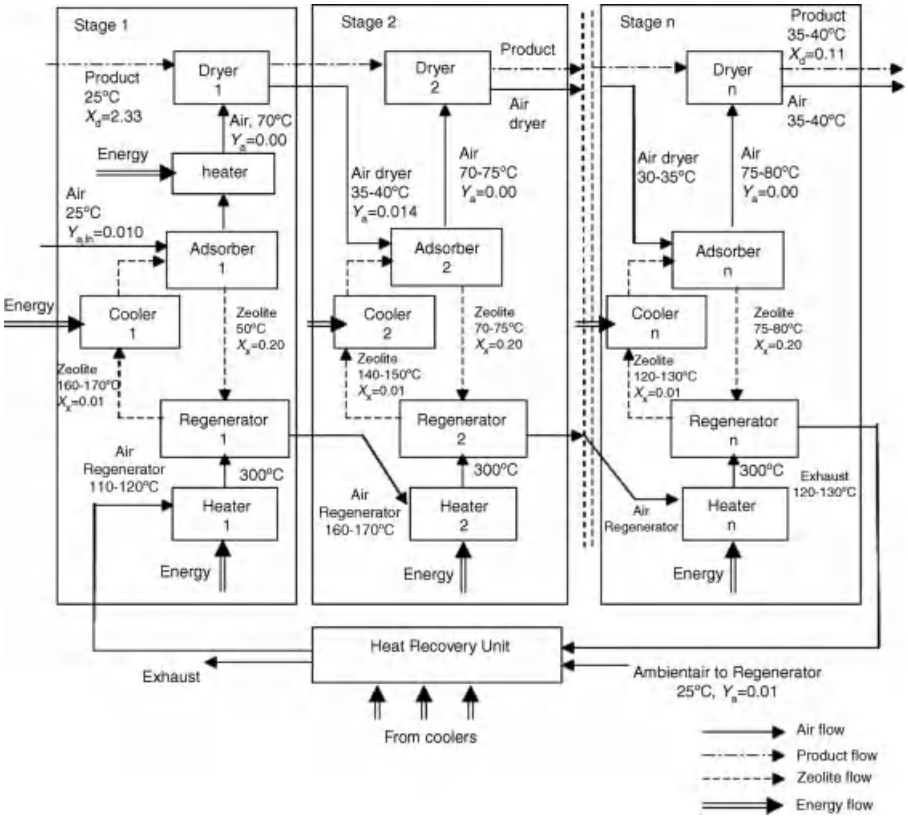

Fig. 5.15 Co-current multi-stage dryer system with air dehumidification by zeolite in the adsorber and regeneration of zeolite. Energy supply is required for the heaters, cooling energy is used to decrease the temperature of the zeolite returned to the adsorber. Energy is recovered and used to heat the air flows (Djaeni *et al.*, 2007b).

Tab. 5.2 Energy efficiency for zeolite adsorption dryer systems operating at air inlet temperature of 70 °C.

	Efficiency (%)		
Conventional dryer (Section 5.4.1)	62.3		
1-stage zeolite with heat recovery (Section 5.4.2)	70.0		
Multi-stage (Section 5.4.3)	Cross-current	Co-current	Counter-current
Number of stages			
2	80.5	77.6	80.2
3	82.6	81.7	88.1
4	83.5	82.2	90.0
Superheated steam regeneration (Section 5.4.4)	101%		

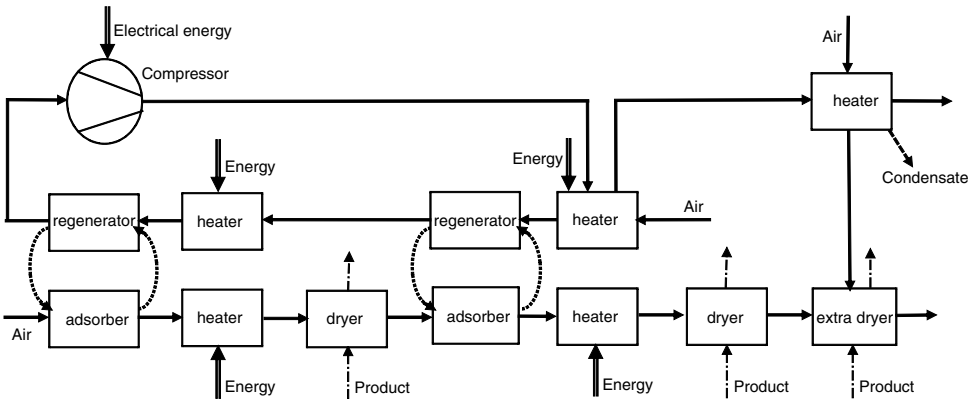

Fig. 5.16 Multi-stage dryer with regenerator air compression. The dew point after compression to 2–2.5 bar is 70–80 °C and is high enough to heat air for an extra drying stage.

are between 50 and 60 °C, which are not very suitable for heat recovery. The condensation temperature can, however, be raised by increasing the pressure of the regenerator exhaust air to about 2–2.5 bar (compressor or fan) which results in condensation temperatures in the range 70–80 °C (Djaeni *et al.*, 2007b). This level is high enough to preheat air fed to an additional drying stage (see Fig. 5.16). The additional drying stage can be part of the sequence of the dryer.

The effectiveness of this solution depends on the energy input for the compressor/fan. Djaeni *et al.* (2007b) consider the electrical energy input of the compressor unit and the benefits that can be gained by the water removal in the extra dryer unit. Due to the extra drying stage, the efficiency of the dryer increases, for a pressure of 1.5–2.0 bar, to 120% for a three-stage system with an extra stage. Higher pressures are not beneficial due to the increasing amount of energy for air compression. However, if primary energy usage (energy for electricity generation) is considered, then the energy efficiency hardly improves, unless a combined heat–power system is used.

5.4.4
Energy Recovery with Superheated Steam

A disadvantage of using hot air for regeneration (see Sections 5.4.2 and 5.4.3) is that the latent heat of the desorbed water vapor in the regenerator exhaust is available at relatively low temperatures. At the end of Section 5.4.3 a solution is proposed by compressing the regenerator exhaust air. With further heat recovery, the efficiency of the system can improve, but from a primary energy usage point of view (usage of fuel to generate electricity) the energy efficiency gain is minimal.

An alternative is to use superheated steam (SHS), as described in Bussmann (2002). Figure 5.17 illustrates the regeneration system. Zeolite passes the adsorber, regenerator and cooler cycle continuously. In the regenerator the zeolite is contacted with steam that is superheated in an indirect heater. The partial vapor pressure of the superheated steam is higher than that of ambient air. The sorption isotherms in

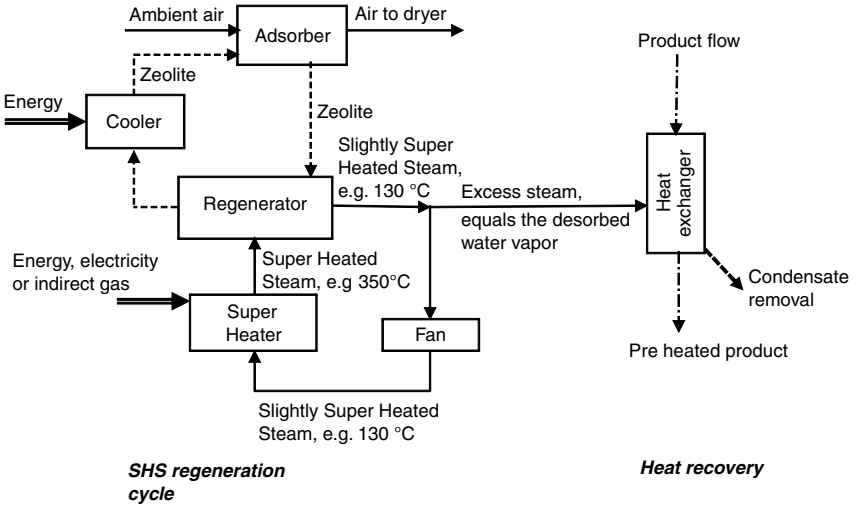

Fig. 5.17 Scheme of superheated steam (SHS) regeneration including heat recovery which, in this example, is used to heat an arbitrary product.

Fig. 5.5 (Section 5.2.2) show that zeolite regenerated with superheated steam at 350 °C contains 2 wt% of water. So the zeolite can be regenerated sufficiently.

Steam leaves the exhaust of the regenerator just above the saturation temperature and is partly recycled. The surplus of steam, with an energy content equal to the latent heat of desorbed water is available for usage in other operations at the production site. For example: (pre)heating of liquid flows, evaporators, heating of cleaning systems, or feeding back to the central power/heat generation systems.

The advantage of the SHS regeneration originates from the full recovery of the latent heat of the removed water from the zeolite in the regenerator. This latent heat is available at a relatively high temperature, 100 °C at atmospheric pressure, and suitable for usage in other processes at the production site. If energy is required at a higher temperature level then the pressure in the SHS regeneration cycle or the excess steam can be raised.

The superheated steam system replaces heater 1 in Fig. 5.13. The energy supplied for desorption of 1 kg of water in the super-heater is 3320 kJ per kg water. At the same time desorption delivers vapor with about 60 kJ kg^{-1} sensible heat and 2400 kJ kg^{-1} latent heat. The efficiency of the SHS cycle is, therefore, 74%. Current experiences, however, show that the efficiency of the SHS cycle is about 50%. SHS efficiency losses arise from the indirect gas heating system for the super-heater, heat loss through the insulation, and fan power to overcome pressure differences. With 50% efficiency for the SHS-cycle (i.e., 50% of the 3320 kJ kg^{-1} used to remove water from the zeolite is available as excess steam) the total efficiency of the dryer system in Fig. 5.13 becomes 101%.

A comparison of the systems with the same operational conditions is given in Tab. 5.2. The calculated efficiency values in Tab. 5.2 concern open systems where, except in the multistage system, the dryer exhaust air is no longer used. The results

are, furthermore, related to the operational conditions in the considered example. The dryer inlet temperature (70 °C) is an essential factor for the efficiency value. If the operational temperature goes to a higher value, then more energy is required and efficiency decreases.

5.5
Realization of Adsorption Dryer Systems

5.5.1
Adsorption Dryer Systems for Zeolite

Adsorption with zeolite can be realized in several ways. Figure 5.18 gives four options. Options (a) to (c) concern air dehumidification and option (d) direct

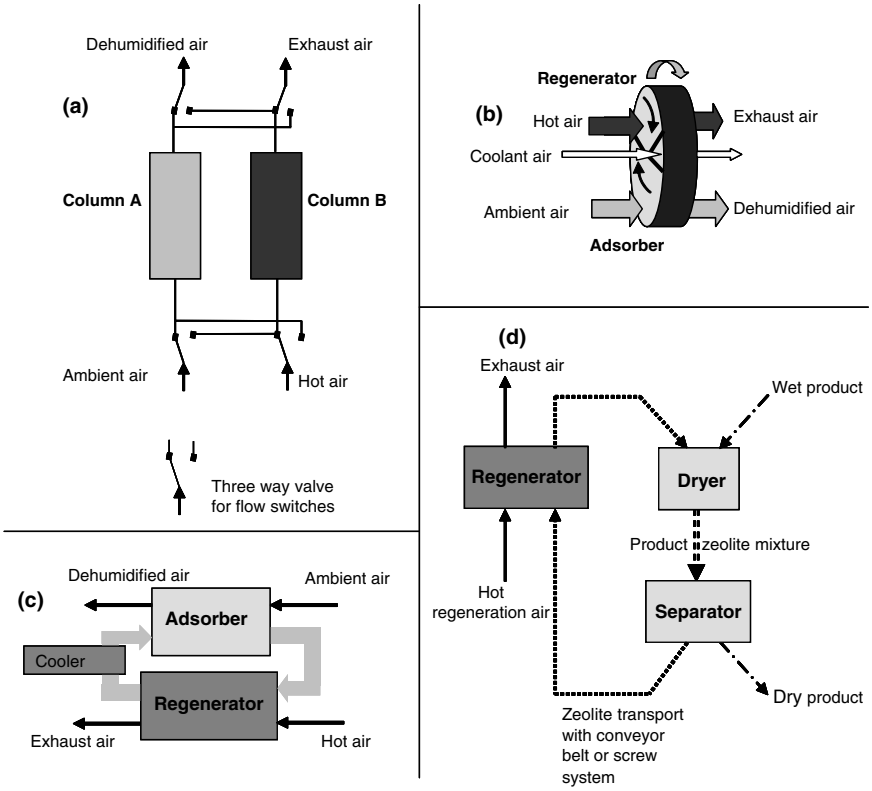

Fig. 5.18 (a) Adsorption bed system with controlled three-way valves to switch between the columns. (b) Rotating wheel system in which the zeolite passes the adsorption, regeneration and cooling function. (c) Conveying bed system in which the zeolite is mechanically moved through the adsorption–regeneration cycle. (d) Direct contact drying system. Note: instead of air the systems can be based on other gas media.

contact drying. The first option (Fig. 5.18a) uses two or more adsorption beds with zeolite particles. By switching the air flows with three-way valves the columns are alternately used for air dehumidification and regeneration. Cooling of the zeolite takes place during the adsorption cycle. If required, an additional third column can be added for cooling. The second option (Fig. 5.18b) is the use of a rotating wheel with zeolite coating on a glass fiber structure, where the zeolite passes through its rotation the regenerator, cooling, and adsorber functions. The third option (Fig. 5.18c) is a system with a mechanical transport mechanism (conveyor belt or screw) for the zeolite through the different functions. Although zeolite particles are quite strong, mechanical transport of the particles can lead to gradual breakdown and must be limited. Therefore, a wheel construction or the adsorption bed system are to be preferred.

A system for direct contact drying is given in Fig. 5.18d. Product and regenerated zeolite are mixed in the dryer and at the same time product is dried. Product and zeolite are batch-wise or continuously fed to the separator. Then zeolite is transported to the regenerator by a conveyor belt and product is gathered for further treatment.

5.5.2
Adsorption Wheel Versus Packed Bed

The technical realization of a column system with packed beds of zeolite requires, for large production systems, large three-way valves to switch between air flows. Due to the large dimensions the costs rise more than proportionally. Splitting the air flows in sub-flows is an option but will also result in increased investment costs. In a wheel system the size of the wheel increases with the square root of the air flow rate and the costs are proportional to the wheel size. The wheel size is nowadays restricted to a maximum diameter of 4 m and, for large capacities, it might be necessary to split the air flow over two or more wheels.

The mass and heat transfer properties in the wheel and packed bed system are totally different. This is illustrated using the Biot number for mass, $Bi = (\beta d)/D$, which gives the ratio between the mass transfer resistances inside the adsorbent and at the surface of the adsorbent; (β: mass transfer coefficient ($m\,s^{-1}$), *d:* characteristic length for diffusion (m), *D*: diffusion coefficient water vapor in air ($m^2\,s^{-1}$). For adsorbents with small Biot numbers (lower than 0.1) the resistance lies outside the adsorbent, for large Biot numbers (larger than 40) the resistance lies inside the adsorbent.

The Biot number for mass is calculated for a packed bed and an adsorption wheel, both based on zeolites. The mass transfer coefficient was estimated using the Lewis analogy between mass and heat transfer. The heat transfer coefficient in the packed bed was estimated using the appropriate Nusselt relationships (HEDH, 1989). In wheel systems there is laminar flow with a Nusselt number of 2.12 (Shah and London, 1978). The diffusion coefficient of water vapor in air is estimated, using the equation of Fuller for diffusion coefficients in low-pressure gas, to be 2.5×10^{-5} $m^2\,s^{-1}$ at 25 °C (Reid *et al.*, 1988). The characteristic length for diffusion in a packed

Tab. 5.3 Calculation of Biot number for mass in a packed bed and an adsorption wheel with zeolite.

	Packed Bed	Adsorption Wheel
Characteristic length [m]	2.5×10^{-3}	90×10^{-6}
Mass transfer coefficient [m s^{-1}]	3.3	0.4
Biot number	165	1.8

bed is the diameter of the particles (2.5 mm). In the adsorption wheel, where the zeolite is coated on a glass fiber structure, the thickness of the adsorbent layer is 90 μm. The results are shown in Tab. 5.3.

These properties result for a packed bed in a Biot number for mass of 165. This means that the resistance for mass transfer in a packed bed lies completely within the particle. The resistance can be decreased by reducing the granular size. However, this will result in an increasing pressure drop. For the adsorption wheel a Biot number for mass of 1.8 is obtained. The resistance for mass transfer in the wheel is, therefore, determined by the external film layer and by the diffusion resistance in the macropores.

These Biot numbers for mass show that the resistance for mass transfer is larger in a packed column than in an adsorption wheel. This implies that the adsorption capacity available in the wheel is more easily accessible than in a packed column, which is eventually reflected in the size and cost of the equipment.

5.5.3 Zeolite Mechanical Strength

The use of zeolites at high temperatures and in the presence of water vapor can result in a deterioration in the adsorption properties of the material (Ruthven, 1984). Physical stress occurs when the zeolite is heated quickly and the internal pressure builds up quickly due to fast water evaporation. As a result, the zeolite structure might crack. The strength of the clay binder decreases when the zeolite is in prolonged contact with liquid water. Therefore, even in applications of zeolite under mild regeneration conditions (<300 °C and dry air) zeolite will degrade and form dust. Zeolites have to be replaced after a period of use (up to several years).

The mechanical strength of particles can be quantified by measuring attrition and the crushing strength. A crushing strength above 40 N is normally regarded as the lower limit. Figure 5.19 gives zeolite sample measurement results for the crushing strength over 300 cycles of regeneration with superheated steam (1 bar, 350 °C) and vapor adsorption from air at 80 °C. As the crushing load is distributed over a larger contact area, the strength of larger particles is greater than for small particles. Overall, a decrease in the crushing strength can be seen in time, but in all cases the crushing strength remains above the threshold of 40 N. Results of attrition measurements are summarized in Tab. 5.4.

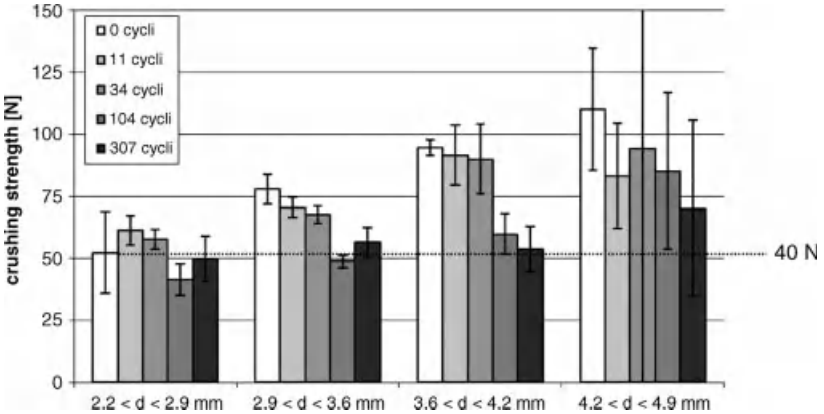

Fig. 5.19 Crushing strength of zeolite particles after a varying number of cycles of adsorption from ambient air at 80 °C and regeneration with superheated steam (350 °C, 1 bar).

5.5.4
Long Term Capacity of Zeolite

Ruthven (1984) presents results on the performance of zeolite systems in accelerated experiments over up to 750 cycles. For industrial applications in adsorption wheels these tests are equivalent to about two weeks of continuous operation. Therefore, new accelerated regeneration experiments with SHS regeneration (300 °C) in a zeolite adsorption wheel were performed. The results showed a decrease in the adsorption capacity of only 7.5% after 22 400 cycles. Other adsorption wheels that have been tested in accelerated regeneration experiments consisted of a mixture of silica and zeolite in which the silica is used as binder. For these wheels a strong decrease in the adsorption capacity was found (50%) after 27 000 cycles.

5.5.5
Zeolite Adsorption Wheel

Figure 5.20 is a full design of a zeolite adsorption wheel system with required devices (Akkerman *et al.*, 2008). Process air (1) is heated in a heat exchanger (5) and

Tab. 5.4 Sieve fractions after attrition test with 1000 rotations performed on the original zeolite particles and particles after 300 cycles of adsorption from moist air and desorption with superheated steam.

Particle Size	Original Material (%)	After 300 Cycles (%)
$d > 2$ mm	98.5	97.6
1 mm $< d <$ 2 mm (breakage)	1.3	2.0
0.5 mm $< d <$ 1 mm (breakage)	0.1	0.2
$d <$ 0.5 mm (dust)	0	0.1

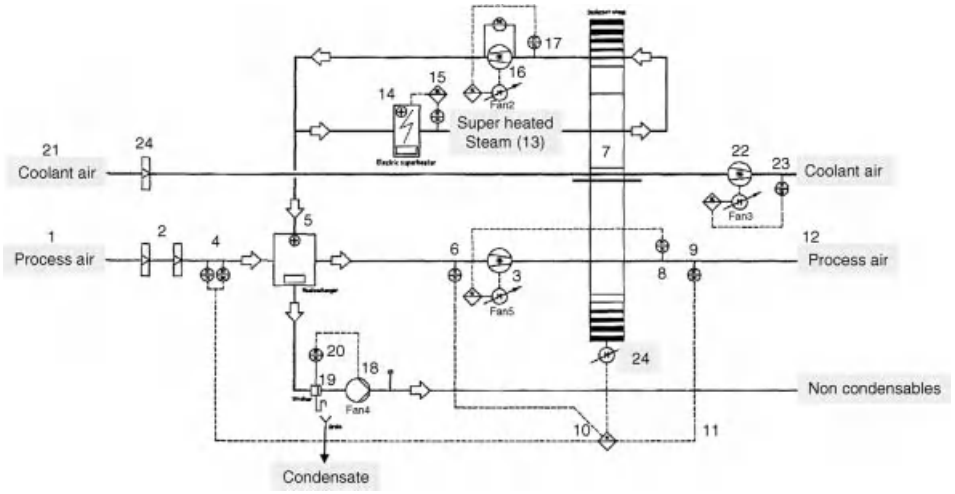

Fig. 5.20 Process diagram for a zeolite adsorption wheel with rotation control and regeneration by superheated steam.

conducted through a rotating zeolite adsorption wheel (7) where the zeolite adsorbs water. The temperature and moisture content of the air can be measured (4). The rotational speed of the wheel is adjusted constantly (24) using a feed-forward control loop (10) in which the measurements are combined with the sorption isotherm of zeolite. By regulating the rotational speed, dry air with constant moisture content is produced. Zeolite in the adsorption wheel is regenerated using superheated steam (13) that passes the regeneration section two times. The regeneration energy is transferred to the superheated steam using a regulated steam heater (14). The desorbed water provides surplus steam, which is condensed in the heat exchanger (5). The warm zeolite is then cooled using regeneration air (21), whereby the zeolite further regenerates.

The zeolite adsorption wheel has a very high surface to volume ratio ($>2000\,m^2\,m^{-3}$) and is mounted in a casing that has a number of physical divisions. The wheel in Fig. 5.20 is divided into three sections, each of which can be individually regulated in terms of temperature and gas flow.

- In the adsorption section, which comprises 50% of the wheel surface area, the zeolite adsorbs moisture from the drying air, whereby the adsorption energy released is transferred to the drying air. The speed at which the wheel rotates is regulated such that the moisture content of the outgoing drying air is constant. For this, a process model of the adsorption wheel is needed. Such a model is described in section Nb 1 of the VDI-Wärmeatlas ().
- In the regeneration section, which takes up 46.5% of the surface area, most of the adsorbed moisture is subsequently removed from the zeolite using superheated steam. The desorbed moisture creates surplus steam, which can be used internally in a condenser to heat the drying air. In this way the latent heat, which

in other systems is lost, is recovered. To obtain the best efficiency in regeneration the superheated steam is conducted through the wheel in two passes and is regulated such that the outgoing steam is still superheated.
- In the cooling section (3.5% of the surface area) the moisture still present in the wheel after the regeneration section is purged with ambient air. Due to the low water vapor pressure in the air, which is by a factor of 100 lower than the vapor pressure of steam, the zeolite releases a little more moisture and at the same time cools to a level fit for the adsorption section.

The various sections of the wheel are separated with static seals. These seals must prevent leakage between steam and process air. At regeneration temperatures lower than 300 °C silicones can be used, at higher temperatures other materials must be used.

5.6 Cases

In the past years, several demonstration projects on drying with zeolites have been performed. This section gives an impression of some of these projects.

5.6.1 Zeolite-Assisted Drying in the Dairy Industry

Dairy powders are spray dried in large dryers using enormous quantities of air. The resulting product has to fulfill strict quality specifications in terms of bulk density, moisture content, wettability, dispersibility, insolubility, and so on. All these quality characteristics are influenced by the conditions imposed on the product during its residence time in the dryer, that is, during the transformation of the droplets that leave the nozzle into agglomerated powder at the dryer outlet. Thermal load to the product may result in unwanted Maillard reactions, while on the other hand insufficient drying causes malfunctions due to fouling and clogging of the process equipment. This implies that the operating window (temperature, moisture content and flow rates) of spray dryers is limited.

In spray dryers, sensible heat is adiabatically converted into latent heat and, for most spray dryers, the air exhaust conditions (temperature and relative humidity) are fixed. Suppose that for a spray dryer the exhaust temperature conditions are represented by point A in the Mollier diagram given in Fig. 5.21. The adiabatic is given by line B–A, B′–A and B″–A for, respectively, a tropical climate, a moderate climate and after air dehumidification. The length of the adiabatic lines is determined by the difference in moisture content of the exhaust air and the fresh incoming air. Under tropical conditions, where the ambient moisture content of the air is high (point C), only a limited quantity of water can be transferred from the product to the air (distance I between A and B on the humidity axis). In moderate climates (point C′) more moisture can be transferred from the product to the air (distance II). Finally,

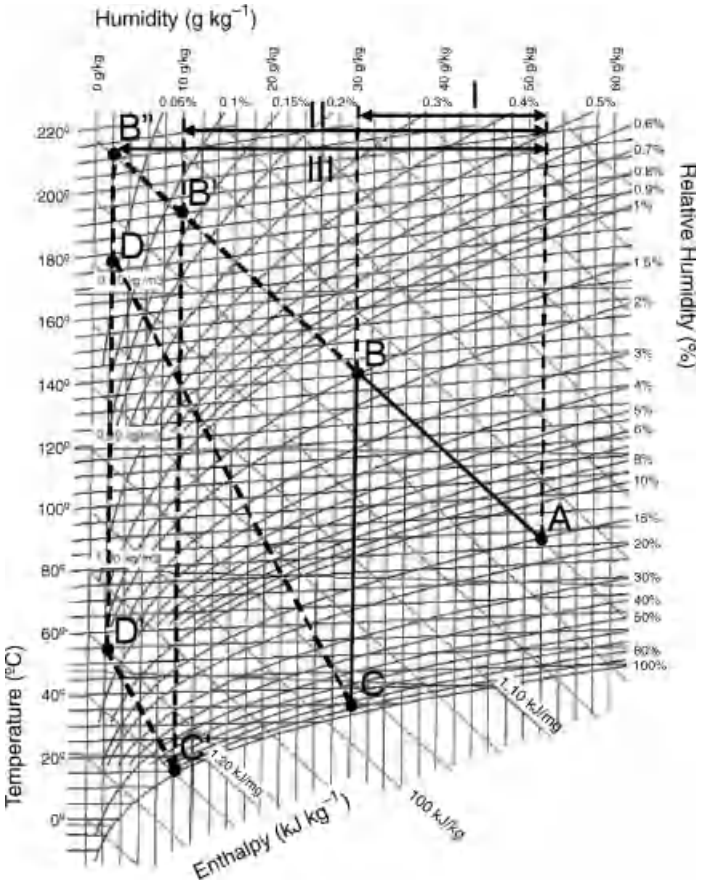

Fig. 5.21 Mollier diagram for process air in a spray dryer (see text).

when the incoming air is dehumidified by a zeolite adsorption unit (points D and D′ which are obtained after the release of adsorption heat during dehumidification of air in, respectively, a tropical climate and moderate climate) the maximum absorption capacity of the process air can be used (distance III).

According to the adiabatic line a higher water drying capacity allows a higher temperature of the incoming process air as indicated in the figure ($T_B < T_{B'} < T_{B''}$). In the zeolite unit the moisture content from the ambient air is adsorbed by the zeolite and the latent heat is converted into sensible heat. This results in a considerable energy saving if the regeneration of the zeolite is done by using superheated steam (see Section 5.4.4) and the surplus steam can be utilized elsewhere in the process or plant. Figure 5.22 gives an impression of a prototype unit based on these principles that has been tested at a dairy company.

The energy efficiency results (according to the definition in Section 5.4) for a moderate and tropical climate are given in Tab. 5.5. For the SHS cycle, just as in

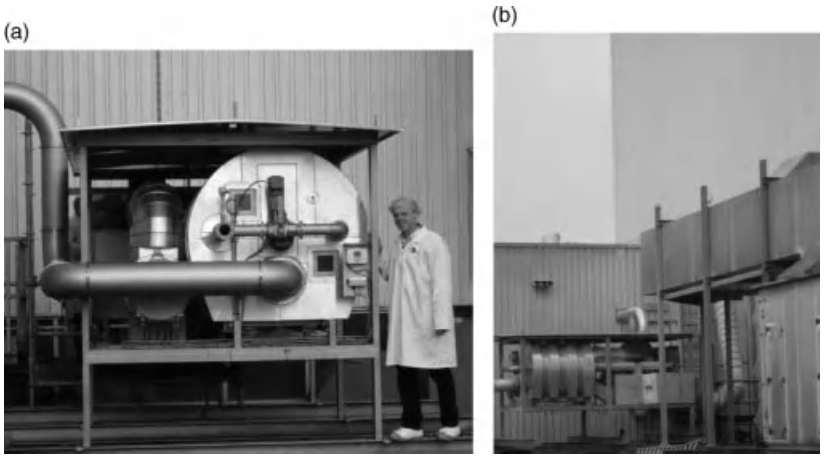

Fig. 5.22 Demonstration unit for a superheated steam system with zeolite for air dehumidification in a dairy powder production plant; (a) front view, (b) side view.

Tab. 5.5 Overview of efficiency calculations for a conventional dairy spray dryer and a spray dryer with adsorption system and SHS-cycle.

Conventional spray drying system				
	Moderate climate		Tropical climate	
Energy for air heating (kJ per kg air)	Line C′–B′	175	Line C–B	100
Energy effectively used for evaporation (kJ per kg air)	Line B′–A	96	Line B–A	48
Energy efficiency (%)		55		48
Spray dryer with adsorption system and SHS-cycle with 50% recovery of heat used for regeneration				
	Moderate climate		Tropical climate	
Energy for air heating (1) (kJ per kg air)	Line D′–B″	157	Line D–B″	25
Energy required for SHS-cycle (2) (kJ per kg air)		33		100
Energy obtained from surplus of steam (3) (kJ per kg air)		16		50
Total energy input (1 + 2 − 3) (kJ per kg air)		174	Line B″–A	75
Energy effectively used for evaporation (kJ per kg air)	Line B″–A	120	Line B″–A	120
Energy efficiency (%)		69		160

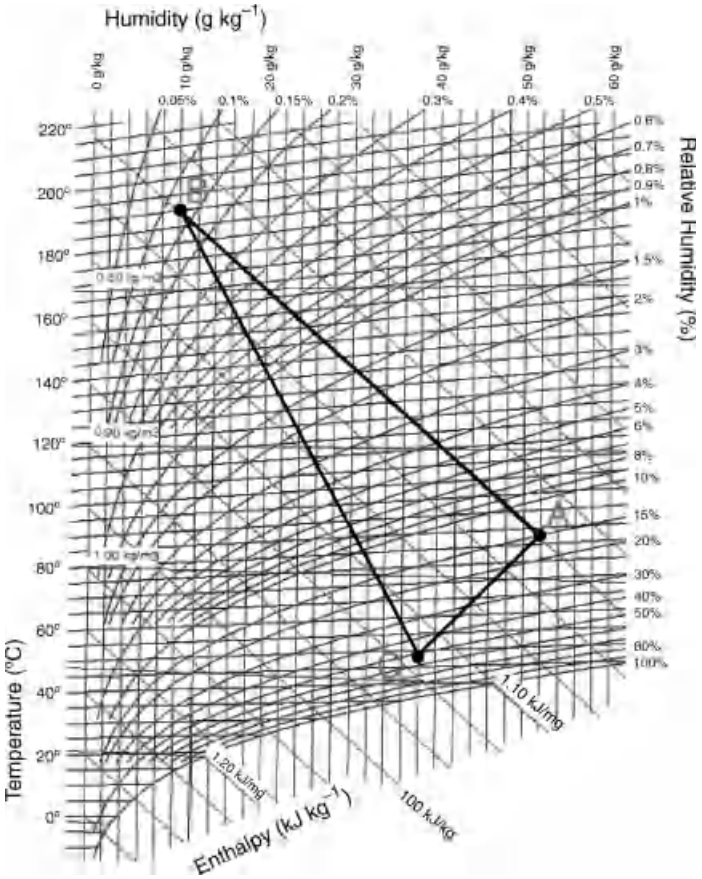

Fig. 5.23 Mollier diagram for process air over an adsorber–spray dryer cycle with partial air recirculation.

Section 5.4.4, 50% recovery of latent heat is applied. Recovery of the latent heat from the regenerator exhaust is significant and results in high energy efficiency values. The efficiency of 160% for the tropical climate indicates that a large amount of latent heat is gained from the ambient air.

The superheated steam sorption unit is used as an add-on to existing spray dryers for dehumidifying and preheating the incoming ambient air. However, the unit can also be used in a closed loop system in which the wet outgoing process air is regenerated by the sorption unit and recycled to the spray dryer. Schematically this process is shown in the Mollier diagram of Fig. 5.23.

Wet process air at the exhaust of the dryer passes the sorption unit where the latent heat is converted to sensible heat (line C–B). Thereby, latent heat in the exhaust air is recovered. During drying, the conditions of the air change along the adiabatic line B–A. Sensible heat from the process air is converted into latent heat. As the heat of adsorption is somewhat higher than the heat of evaporation, the lines do not coincide

and a gap exists between the points C and A. Thus, to make the cycle complete, an additional unit operation is required which, in practice, is to purge a part of the wet air and supply some fresh air to the recycle. This cools and reduces the moisture content of the process air to what is required (line A–C). As a result not all latent heat can be recovered, but energy savings are still substantial.

Calculation of the energy efficiency for Fig. 5.23 shows that the amount of water evaporated from the product requires 96 kJ per kg air, while 92 kJ per kg air are needed to regenerate the zeolite. Half of the energy for regeneration is recovered as steam that is, 46 kJ per kg air. So the net energy input is 46 kJ per kg air. This brings the system efficiency to 208%. This value is much higher than the result of Section 5.4.4, but in that case the SHS-cycle was applied to an open system with energy loss from the dryer air exhaust.

5.6.2
Zeolite-Assisted Manure and Sludge Drying

The application of large quantities of animal manure and sludge from waste water treatment installations to agricultural soils has created environmental problems such as pollution of ground water and eutrophication (over-fertilization) of surface water. Regionally, a surplus of animal manure and sludge exists while elsewhere there is a strong demand for products containing organic matter. Thus, to tune supply and demand, manure and sludge transport is required.

To limit the cost of transport, storage and supply, it is necessary to reduce the volume and weight of the manure/sludge or, in other words, the manure must be dried. Most drying systems involve air dryers which are directly or indirectly heated. Air dryers need large flows of air to provide the required amount of heat for water uptake from the manure. Besides water vapor, the exhaust air of the dryer contains large amounts of volatile components. Consequently, to meet emission regulations, large, expensive and energy-consuming off-gas treatment installations are required.

In contact drying systems (for example a steam-heated drum dryer), heat is transferred from a heat transporting medium, such as steam or oil, through a wall to the product. In these systems a limited amount of air is required to remove the water vapor. Such contact drying systems need long contact times and, as a consequence, there is a risk of overheating and scaling. A large heat transferring area is needed and the possibilities for scale-up of the equipment to large units are limited. Contact dryers are complex in their operation and expensive.

However, by utilizing zeolite, a dryer system was developed in which the advantages of direct and contact drying systems were combined and in which water is removed by adsorption on the zeolite (Bussmann and Boot, 2000). A process scheme is shown in Fig. 5.24. The advantages of this adsorption drying process are faster heat transfer, less off-gas, and lower energy consumption.

The direct contact adsorption system with zeolite for liquid manure or sludge drying uses a decanter to separate the solid and liquid fraction. The liquid fraction contains relatively low amounts of dry substance, some phosphate, and dissolved salts. The solid fraction is further processed in a mixer in which the manure is dried

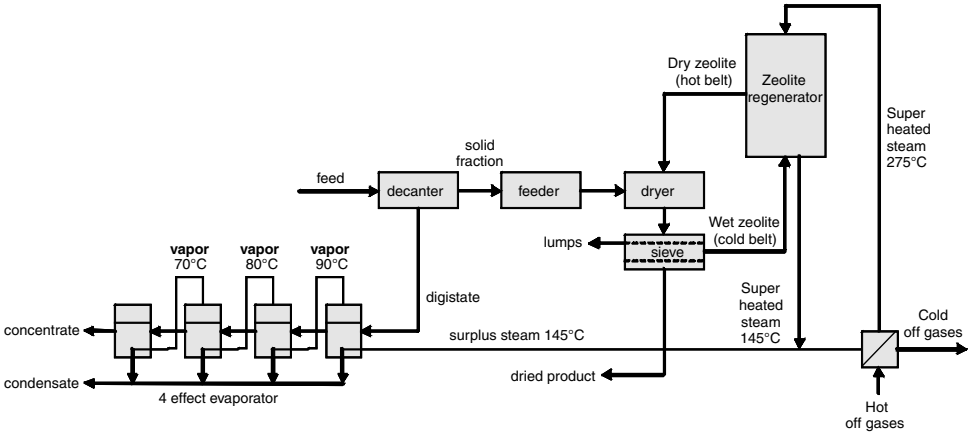

Fig. 5.24 A direct contact drying system in which zeolite is mixed with manure or sludge. Superheated steam is used for regeneration. The resulting steam is used to heat a 4-effect evaporator.

under the addition of, and in direct contact with zeolite particles. Zeolite and manure/sludge are separated on a sieve. The zeolite is regenerated with superheated steam which is obtained from an electricity generating unit. The liquid effluent from the decanter is fed to a four-effect evaporator which uses the surplus steam coming from the zeolite regenerator. A pilot plant to process the solid fraction has been built and operated (see Fig. 5.25 for a technical realization).

The energy consumption of the full plant (both solid and liquid fraction) is 0.8 GJ per ton of water removed. This energy consumption is quite low, moreover the plant operates on waste heat from a small scale power plant and, therefore, the energy costs are negligible. The zeolite consumption due to attrition is also important. Mined

Fig. 5.25 Technical realization for direct contact drying of manure and sludge with zeolite, including zeolite regeneration. Zeolite transport from separator to regenerator to dryer is realized by two conveyor belts.

mineral zeolites with costs of about 50 € per ton are too soft for application in the envisaged process. Synthesized granulated zeolites are much stronger but also much more expensive (up to 2000 € per ton). The decision on the material to use should be based on the crushing strength of zeolite granules, which should be 40 N at minimum (see Section 5.5.3).

An important advantage of the proposed zeolite dryer concept is the low emission level. Zeolite adsorbs water from the manure or sludge and the steam produced during regeneration of the zeolite is condensed in the evaporator section. As a consequence the system is almost completely closed and undesired emissions to the environment are minimal.

5.6.3
Direct Contact Drying of Seeds with Zeolites

Seeds are traditionally dried in batch or continuous processes, where beds of seeds contact flows of warm air. Bed heights vary from 100 to 300 mm and the seeds are sometimes mixed by vibration. Seed drying may take 1–5 h or more and air temperatures at the inlet are 30–50 °C. At the beginning of the drying air leaves the dryer at temperatures of 15–25 °C; the efficiency is then about 50%. Later, when the seeds only contain internal moisture, the dryer exhaust temperature raises gradually, and at the end of the drying time the exhaust temperature is close to the air inlet temperature, making the final efficiency very low. The average efficiency for drying of seeds is estimated at about 20%.

A closed drum system (see for example Fig. 5.26), in which seeds are in direct contact with zeolite, is an alternative solution to traditional approaches for seed drying. The drying procedure requires special attention in its initial phase to ensure that the seeds and zeolite particles are well distributed and mixed. Over-drying, under-drying and overheating of part of the batch are then avoided.

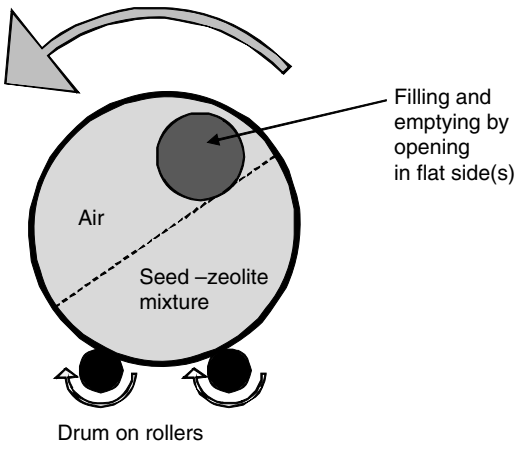

Fig. 5.26 Schematic example of a closed drum dryer for seeds.

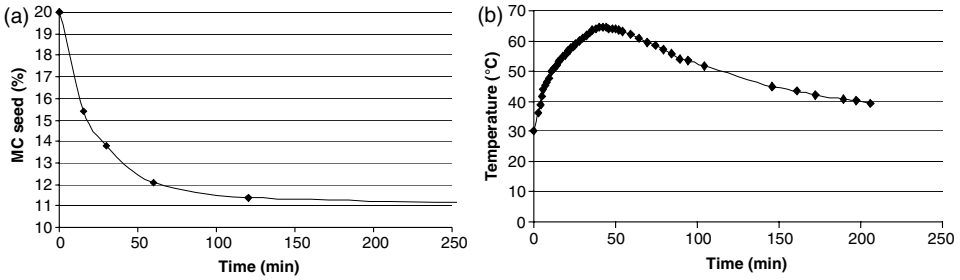

Fig. 5.27 Direct contact drying of seeds (400 g seeds with 200 g dry zeolite, ambient temperature 32.5 °C). (a) Seed moisture content as a function of drying time, (b) temperature response in the bulk of the seeds.

The direct contact between the dry zeolites and the wet seeds causes fast drying. Figure 5.27a gives the measured moisture content of seeds during drying. The drying curve deviates strongly from the exponential drying curves that are commonly observed in drying systems. In the initial phase, with wet seeds, the microclimate with low vapor pressure around the seeds is beneficial for the removal of the surface and superficially bound water. The removal of the last part of the moisture from the product is limited by the moisture transport in the seeds and is not enhanced by the beneficial microclimate around the seeds. Complete drying would take a long time, but because it is sufficient to dry seeds to a final moisture content between 10 and 15%, complete drying is not necessary.

The temperature of the seed–zeolite mixture increases due to the adsorption heat. Figure 5.27b illustrates the temperature variation in the product over the drying time. In the first period, where most moisture is removed from the product, the temperature rises to over 60 °C. The temperature increase can be controlled for heat-sensitive products by increasing the heat loss to the environment or by pre-cooling the seeds and the zeolites. In the following phase the heat loss to the environment is above the heat release due to the low moisture adsorption. As a result, the temperature decreases gradually. The temperature curve also shows the suitability of zeolite for this application. The sorption isotherms in Figs. 5.5 and 5.6 show that zeolite can contain much more water than silica gel at elevated temperatures.

Seed drying with zeolite also allows a tight control of the final moisture content by proper choice of the zeolite-to-seed ratio. From the mass balance over the seeds and zeolites follows:

$$\text{kg seed} \times (\text{start product moisture} - \text{aimed final moisture content}) = \text{kg of zeolite} \times (\text{max. load zeolite} - \text{load of zeolite after regeneration})$$

Figure 5.5 gives information on the maximum load of zeolite and the load after regeneration (depends on the regeneration conditions).

Direct contact drying of seeds itself does not need any energy input. The energy input occurs at the zeolite regeneration step. Because seed drying is a rather small scale process, the zeolites are regenerated in an oven and the hot oven gases are

vented to the environment. Zeolite regeneration is more energy efficient than seed drying.

5.7 Economic Considerations

The foregoing sections demonstrate the potential improvement in energy consumption, the technical feasibility and potential applications of zeolite drying. The economic feasibility is another issue. Zeolite systems have quite a potential for energy savings and, at the same time, costs for CO_2-emission can be reduced. The investment costs for an add-on unit are not easy to estimate and depend highly on the local situation. Therefore, the economic feasibility is expressed in terms of energy savings and reduced costs for CO_2-emission per year (Djaeni *et al.*, 2009).

Table 5.6 gives the operational conditions for a small-to-medium-sized standard dryer used in a moderate climate region and considers different levels of costs for energy and CO_2-emission. Figure 5.28 demonstrates the potential savings for energy and CO_2-emission. For example, compared to a conventional dryer operated at 70 °C inlet temperature and a standard efficiency of 55%, a two-stage adsorption dryer operated at 85% efficiency yields for 7.5 € per GJ energy and 20 € per ton CO_2 about 54 000 € (= 48 000 € energy + 6000 € CO_2-emission) savings per year. The potential savings on energy costs are dominating.

Furthermore, the energy savings and reduced costs for CO_2-emission are linear with respect to the air flow rate, production hours per year, the costs for energy and CO_2-emission, CO_2-emission per GJ, efficiency for energy generation from fuel, and payback time. For other values of these parameters the savings can, therefore, be calculated from the results in Fig. 5.28 by using a proportionality factor.

For a two year payback period, the dryer system using zeolite as adsorbent has, for an energy price of 7.5 € per GJ and 20 € per ton CO_2-emission at 70 °C, an extra investment potential of about 2 times 54 000 € = 108 000 €. The costs for a wheel system with all related requirements (insulation, heat exchanger, control, etc.) as an

Tab. 5.6 Operational conditions of a small-to-medium-sized dryer system for which the potential energy savings and reduced costs for CO_2-emission are estimated.

Air flow rate ($m^3\ h^{-1}$)	50 000
Ambient air temperature (°C)	15
Ambient air moisture (kg per kg)	0.008
Dryer inlet air temperature (°C)	70
Water removal capacity at inlet temperature 70 °C (kg h^{-1})	500
Hours per year (h)	5000
Energy costs (€ per GJ)	5, 7.5, 10, 15
Efficiency energy generation (%)	85
CO_2-emission (kg per GJ)	50
Costs for CO_2-emission (€ per ton)	10, 20, 50

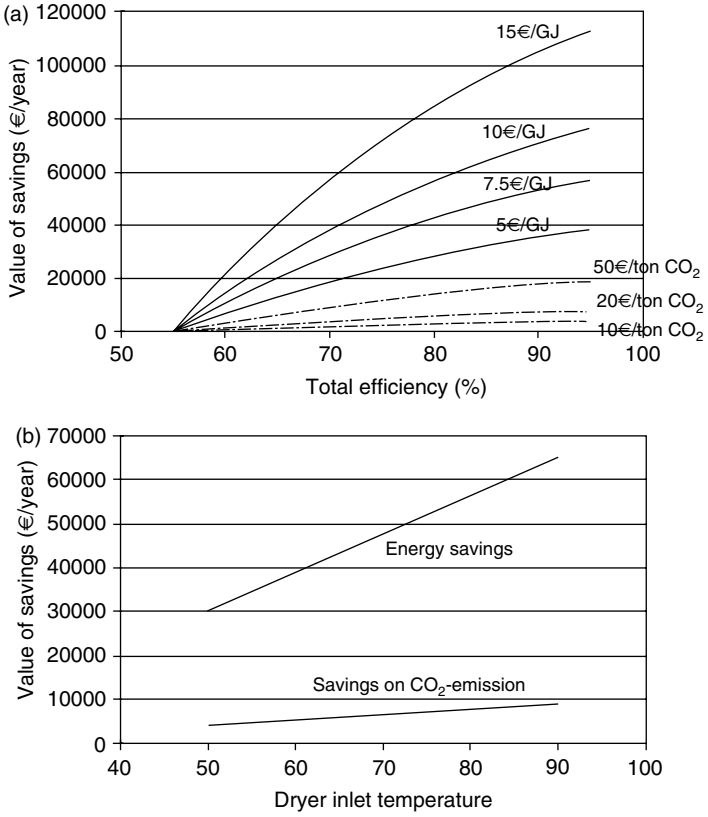

Fig. 5.28 Comparison of a zeolite dryer system with different energy efficiency values with a conventional dryer operating at an efficiency of 55%. (a) Potential savings for different cost levels for energy and CO_2-emission, (b) potential savings as a function of air inlet temperature for a zeolite dryer system operating with an efficiency of 85%, energy costs 7.5 € per GJ and 20 € per ton CO_2.

add-on to a current dryer are certainly within this budget. Moreover, installation of the add-on unit will result in a capacity increase of 20% for the given case.

Considering the tendency for increasing energy prices, and the pressure to reduce carbon emissions (for example the European Union decided in December 2008 to reduce carbon emissions by 2020 by 20%, Australia strives for a reduction of 15% in the long term), the savings with an adsorption system are expected to increase, resulting in a shorter payback time. Moreover, a step from a dryer operating at an efficiency of 55% to a dryer operating at 85% results in a reduction of energy use and CO_2-emission by over 50%. With such an investment in the dryer system the overall energy usage and CO_2-emission at a production site would quickly reach the required targets.

5.8 Perspectives

Energy takes over the most important and increasing part in the operational costs of drying. Together with the necessity to limit the worldwide energy consumption, there is a need to develop energy efficient drying technologies. In the present chapter the use of zeolites as an intermediate medium in drying has been discussed. The adsorption of water from air and products by zeolites, in combination with regeneration techniques, allows an efficient energy management for drying systems. Energy management is the key, and usage of zeolites results in a substantial energy reduction in drying. A systems approach and a changed view on system boundaries, like producing steam for other processes, are essential for the development of energy management systems.

Energy management with zeolite is demonstrated in the multi-stage application by heat recovery within a dryer–adsorption–regeneration system. Latent and sensible heat from the dryer exhaust are recovered multiple times. The other way for energy management is based on regeneration with superheated steam. In drying, latent heat in air is, as a rule, accepted as a loss of energy, but the superheated system is one of the few systems able to recover latent heat in air.

Furthermore, the chapter has presented the background of using zeolites in drying and three application examples. The different areas of the case studies (dairy, manure/sludge, seeds) illustrate the potential. With the given general background there are also possibilities for drying textiles, chemicals, resins, detergents, and so on. The presented technical solutions are designed in such a way that they can be installed as an add-on to existing drying equipment in small and large scale applications. The current technology has been tested and proved to be reliable, the first industries are considering its application.

Drying with zeolites is emerging. The significance for the reduction of energy usage and CO_2-emission is obvious. There is a future for new generations of zeolite systems in drying applications, for example advanced wheel systems, closed-loop drying systems to retain volatiles, extra product advantages by drying with dehumidified air, process intensification in direct contact systems, and so on. Fundamental and applied research and technical developments in these fields are ongoing.

Appendix 5.A: Sorption Isotherm Data

For a commercial zeolite (CeCA, 4A) the sorption isotherm data were measured and fitted to a Langmuir isotherm equation:

$$q = \frac{q_{\max} b P}{1 + bP}$$

$$b = b_0 \mathrm{e}^{-E/RT}$$

q	amount of water adsorbed per 100 kg dry zeolite (kg per 100 kg)	
q_{max}	maximum amount of water adsorbed per 100 kg zeolite (kg per 100 kg)	18.96
P	partial water vapor pressure in equilibrium with zeolite (kPa)	0.001–10 000
b	Langmuir constant	
b_0	constant	5.62×10^{-11}
R	gas constant (J mol^{-1} K^{-1})	8.314
T	absolute temperature (K)	20–350 °C
E	Arrhenius constant (J mol^{-1})	−51 240

The sorption isotherm of a commercial silica gel (Engelhard) was measured and fitted to a Freundlich isotherm:

$$q = k\mathrm{e}^{-E/RT}P^{1/n}$$

q	amount of water adsorbed per 100 kg dry silica gel (kg per 100 kg)	
k	pre-exponential factor	1.02×10^{-9}
P	partial water vapor pressure in equilibrium with silica gel (kPa)	0.001–10 000
n	constant	1.12
R	gas constant (J mol^{-1} K^{-1})	8.314
T	absolute temperature (K)	20–350 °C
E	Arrhenius constant (J mol^{-1})	−43 200

Acknowledgment

The main funding for the developments reported in this chapter was obtained from the Energy Research Program of the Dutch Ministry of Economics (projects NEOT01005 and KO20444).

References

Akkerman, J. C., Boon, M. A., Bussmann, P. J. T., 2008. Process for controlling the moisture content of a supply gas for use in drying a product, WO 08/044932 A1, Priority date 12 October 2006.

Bussmann, P. J. T., Boot, J., 2000. Method for processing a watery substance with zeolites, WO 00/02822, Priority date 10 July 1998.

Bussmann, P. J. T., 2002. Method for drying a product using a regenerative adsorbent, WO 03/097231 A1, Priority date 15 May 2002.

Djaeni, M., Bartels, P., Sanders, J., van Straten, G., van Boxtel, A. J. B., 2007a. Process integration for food drying with air dehumidified by zeolites. *Drying Technol.* **25**(1): 225–239.

Djaeni, M., Bartels, P., Sanders, J., van Straten, G., van Boxtel, A. J. B., 2007b. Multi-stage zeolite drying to enhance heat efficiency of food drying. *Drying Technol.* **25**(6): 1063–1077.

Djaeni, M., Bartels, P., Sanders, J., van Straten, G., van Boxtel, A. J. B., 2009. Assessment of a two-stage zeolite dryer for energy efficient drying. *Drying Technol.* **27**(11): 1205–1216.

Dyer, A., 1988. *An introduction to zeolite molecular sieves*. Wiley, New York, USA.

Flanigan, E. M., 1991. Zeolites and molecular sieves: An historical perspective, in *Introduction to zeolite science and practice* (eds H. van Beckum, E. M. Flanigan, J. C. Jansen). Elsevier, Amsterdam.

HEDH , 1989. *Heat exchanger design handbook*. Hemisphere, New York, USA.

Holmberg, H., Ahtila, P., 2004. Comparison of drying costs in biofuel drying between multi-stage and single-stage drying. *J. Biomass Bioenerg.* **26**(6): 515–530.

Kemp, I. C., 2005. Reducing dryer energy use by process integration and pinch analysis. *Drying Technol.* **23**(9): 2089–2104.

Linnhoff, B., 1994. *User guide on process integration for the efficient use of energy*. The Institution of Chemical Engineers, Rugby, UK.

Morris, B., 1968. Heats of sorption in the crystalline Linde-A zeolite-water vapor system. *J. Colloid Interface Sci.* **28**(1): 149–155.

Muller, J. C. M., Hakvoort, G., Jansen, J. C., 1998. DSC and TG study of water adsorption and desorption on zeolite NaA: Powder and attached as layer on metal. *J. Therm. Anal. Cal.*, **53**(2): 449–466.

Reid, R. C., Prausnitz, J. M., Poling, B. E., 1988. *The properties of gases and liquids*. McGraw-Hill, New York, USA.

Ruthven, D. M., 1984. *Principles of adsorption and adsorption processes*. Wiley, New York, USA.

Shah, R. K., London, A. L., 1978. *Laminar flow forced convection in ducts*. Academic Press, New York, USA.

Spets, J. P., 2001. New multi-stage drying system. *Proceedings of the 1st Nordic Drying Conference*. Trondheim, Norway, June 21–29, paper no. 13.

Spets, J. P., Ahtila, P., 2001b. Preliminary economical examinations for a new multistage biofuel drying system integrated in industrial CHP-power plant. *Proceedings of the 1st Nordic Drying Conference*. Trondheim, Norway, June 21–29, paper no. 14.

VDI-Wärmeatlas, 2002. Springer, Berlin, Germany.

Vente, J. A., 1999. Drying processes for manure based on adsorption with zeolite. *TNO-MEP R99-259*, TNO, The Netherlands.

Yang, R. T., 1997. *Gas separation by adsorptive processes*. Imperial College Press, London, UK, pp. 352.

6
Solar Drying

Joachim Müller and Werner Mühlbauer

6.1
Introduction

World agriculture shows a contrasting situation between industrialized and developing countries. This disparity also greatly influences the potential of solar energy for drying agricultural products. In industrialized countries, the use of highly efficient harvesters also requires adequate dryers, which allow preserving of the crop immediately after harvest. Consequently, high-temperature dryers have displaced natural drying almost completely. High-temperature batch and continuous-flow dryers require significant quantities of fuel oil or gas for heating the drying air, as well as electricity for operating the fans. To maximize the drying capacity, these dryers are operated round-the-clock during the drying season. Automatic temperature control systems prevent losses and guarantee the required product quality. On this background, solar dryers are only competitive when the drying costs are reduced without lowering the drying efficiency and reliability. Even with currently increasing energy prices, there are only special niches where solar drying is competitive with conventional drying systems in industrialized countries.

In developing countries, spreading the drying material in thin layers on mats, trays or paved ground to expose it to sun and wind is still the most common drying method. Since the drying process is relatively slow, considerable losses occur. Furthermore, insect infestation, enzymatic reactions, microorganism growth, and mycotoxin production cause significant reduction of the product quality. Non-uniform and insufficient drying also leads to deterioration of the crop during storage. Serious drying problems occur, especially in humid tropical regions where some crops have to be dried during the rainy season. In order to ensure continuous food supply to the growing population, and to enable the farmers to produce high quality products, the development of efficient drying methods is an urgent necessity. However, high-temperature dryers are mostly not applicable, due to high investment and lack of energy supply. Therefore, the introduction of low-cost and locally manufactured solar dryers offers a promising alternative to reduce post-harvest losses. The opportunity to produce marketable products seems to be a chance to improve the economic situation

Modern Drying Technology Volume 4: Energy Savings, First Edition.
Edited by Evangelos Tsotsas and Arun S. Mujumdar

of the farmers. However, taking into consideration the low income of the rural population in developing countries, the relatively high investment for solar dryers still remains a barrier to a wide application. Currently, the introduction of solar dryers is limited to high-value cash crops for international markets. Widespread dissemination of solar dryers also requires a change in prevailing marketing systems, because farmers are only willing to invest in new technologies if they get higher prices for better product quality.

6.2 Solar Radiation

Solar drying differs fundamentally from conventional drying as the energy source is not available at will. Solar energy, in spite of being Earth's greatest energy supply, is fluctuating and of low power in terms of energy density per area. In the following, the properties of solar radiation, relevant for solar drying, will be described.

Extraterrestrial solar radiation, that is, solar radiation before entering the atmosphere, holds an average energy density of $1353\,W\,m^{-2}$, which is called the solar constant, although the value varies by $\pm 3\%$ during the year due to the eccentricity of the Earth's orbit (Thekaekara and Drummond, 1971). Terrestrial solar radiation on a horizontal surface at ground level is less than the solar constant and depends on several geographic and climatological parameters: (i) with increasing latitude, the incident angle of the sun increases, whereby solar radiation is reduced according to the cosines law; (ii) with decreasing altitude, optical airmass increases, whereby solar radiation is reduced by absorption, reflection and scattering by gas molecules; (iii) air pollution aggravates the effect of optical airmass by aerosols; and (iv) clouds reduce solar radiation considerably by reflection back to outer space. A world map showing the mean values of annual cumulative solar radiation in $kWh\,m^{-2}$ reveals major impacts such as latitude and cloud cover, Fig. 6.1. In desert areas like the Sahara, Atacama, Namib or the Australian deserts along the tropics of Cancer and Capricorn, respectively, annual solar radiation is highest with values above $2200\,kWh\,m^{-2}$. In spite of the lower latitude of the rainforest areas along the Equator, the annual solar radiation is lower with values of $1700\,kWh\,m^{-2}$ because of the cloud cover.

Due to the Earth's axial tilt of 23.45°, higher latitudes are characterized by seasons with low solar radiation during the winter because of short day length and the large incident angle of the sun, and the opposite conditions during the summer. The lower the latitude, the less pronounced are the seasonal effects. At the Equator the day length is 12 hours all year round with small variations. Moderate differences in solar radiation are caused by varying cloud cover between the dry and rainy seasons. For illustration, Fig. 6.2 gives the monthly means of daily cumulative solar radiation for Jakarta, as an example for equatorial conditions, and for Berlin and Sydney for the northern and southern hemisphere, respectively.

On a cloudless day, the Earth's rotation causes a sinusoidal course of solar radiation with a maximum at noon, the absolute value depending on the latitude and season. Figure 6.3 shows the daily course of solar radiation for Stuttgart (Germany) on a

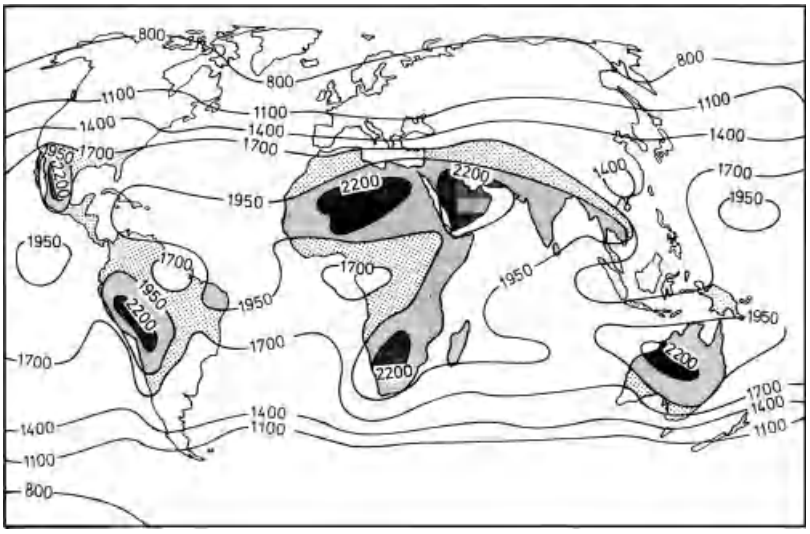

Fig. 6.1 Annual cumulative solar radiation on a horizontal surface in kWh m^{-2} (Stoy, 1988).

cloudless and a cloudy day, in July and November. Cumulative solar radiation with a value of 7.3 kWh m^{-2} is much higher on a cloudless day in summer than in winter with 2.0 kWh m^{-2}. However, on a cloudy day in summer, solar radiation may even be lower than on a cloudless day in winter.

When solar radiation is used as the energy source for drying, systematic fluctuations such as summer/winter and day/night have to be taken into consideration, as well as stochastic variations such as cloud cover, and arbitrary effects such as air pollution. Although the systematic fluctuations of solar radiation are

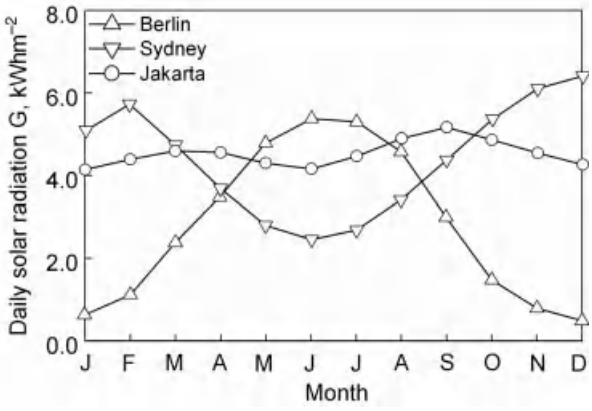

Fig. 6.2 Monthly mean value of the daily cumulative solar radiation of Jakarta (6.12 °S, 106.48 °E), Berlin (52.30 °N, 13.25 °E), and Sydney (33.51 °S, 151.12 °E).

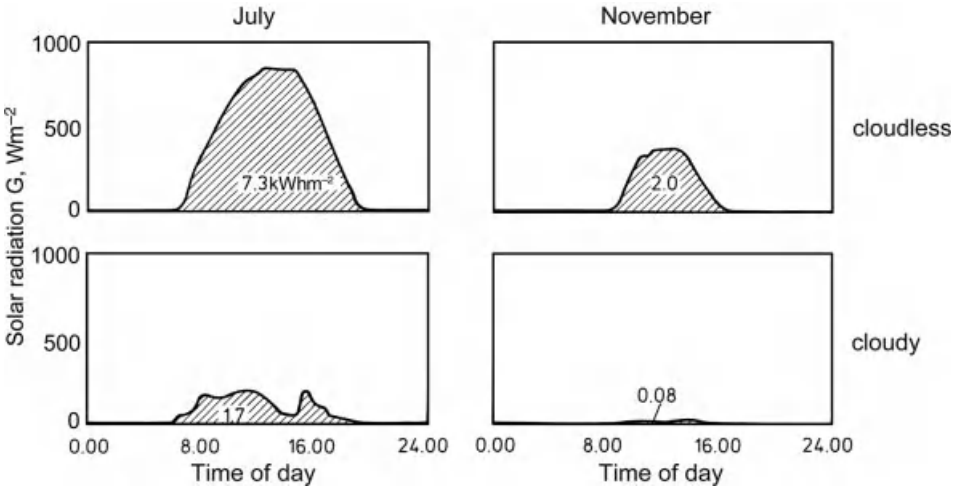

Fig. 6.3 Course of solar radiation in Stuttgart, Germany (48.77 °N, 9.18 °E) on a cloudless and a cloudy day in July and November; value below curve indicates daily cumulative solar radiation in kWh m^{-2} (Mühlbauer, 1979).

computable, time series of measured solar radiation data are required to estimate the solar energy potential of a certain location because cloud cover and air pollution are site-specific.

Solar radiation G, as measured on a horizontal plane at ground level, is composed of direct beam radiation G_{beam} and diffuse sky radiation G_{diffuse}. Beam radiation reaches the ground as parallel beams without being scattered in the atmosphere, whereas sky radiation originates from scattering by gas molecules and aerosols in the atmosphere and reaches the ground omnidirectionally. Therefore, it does not cast any shadow and neither can it be focused. The higher the optical airmass that has to be penetrated by the sun beams, the higher is the share of diffuse radiation. The share of diffuse radiation is up to 100% on cloudy days and, typically, still higher than 50% on cloudless days.

Solar radiation data of weather stations are measured on a horizontal plane. Solar collectors, however, are frequently inclined – either for optimizing energy harvest or for integrating the device into the roof of a building. Therefore, solar radiation on surfaces with any slope and orientation has to be estimated from available time series data. Figure 6.4 shows a tilted surface with slope β and azimuth γ, where the azimuth is 0° for south orientation and −90° for east and 90° for west, respectively.

Beam radiation on a tilted surface $G_{\text{beam},\beta}$ can be calculated from knowledge of the angle of incidence θ between the sun and the normal to the tilted surface and the angle of incidence θ_Z between the sun and the zenith:

$$G_{\text{beam},\beta} = \frac{\cos\theta}{\cos\theta_Z} \cdot G_{\text{beam}} \tag{6.1}$$

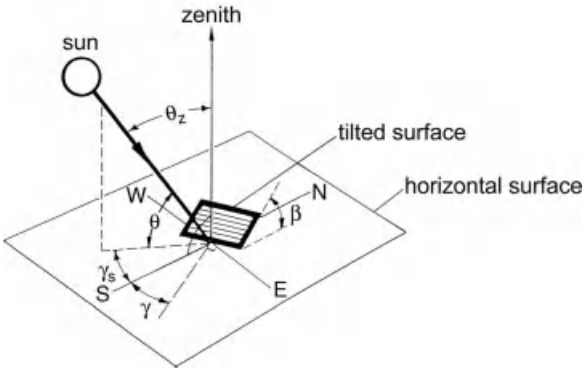

Fig. 6.4 Slope β and azimuth γ of a tilted surface and angle of incidence θ_Z between the sun and the zenith (Duffy and Beckmann, 1980).

where $\cos\theta$ is calculated for slope β and azimuth γ of the tilted surface:

$$\begin{aligned}\cos\theta = &+\sin\delta\cdot\sin\phi\cdot\cos\beta\\ &-\sin\delta\cdot\cos\phi\cdot\sin\beta\cdot\cos\gamma\\ &+\cos\delta\cdot\sin\phi\cdot\sin\beta\cdot\cos\gamma\cdot\cos\omega\\ &+\cos\delta\cdot\sin\beta\cdot\sin\gamma\cdot\sin\omega\\ &+\cos\delta\cdot\cos\phi\cdot\cos\beta\cdot\cos\omega\end{aligned} \tag{6.2}$$

with latitude φ of the location, declination δ according to the season and hour angle ω according to the time of the day. The hour angle ω is 0° at solar noon and changes at 15° per hour, with morning being negative and afternoon being positive. The incidence θ_Z between the sun and the zenith can be calculated by the same equation with $\beta = 0°$.

The declination δ of the Earth's axis is calculated for the nth day of the year:

$$\delta = 23.45\cdot\sin\left(360\cdot\frac{284+n}{365}\right) \tag{6.3}$$

The total solar radiation G_β on a tilted surface can be calculated by:

$$G_\beta = \frac{\cos\theta}{\cos\theta_Z}\cdot G_{\text{beam}} + \left(\frac{1+\cos\beta}{2}\right)\cdot G_{\text{diffuse}} + \alpha_{\text{albedo}}\cdot G\cdot\left(\frac{1-\cos\beta}{2}\right) \tag{6.4}$$

where α_{albedo} is the coefficient of ground reflectance.

As weather stations most typically record total solar radiation G only, the share of diffuse sky radiation G_{diffuse} has to be estimated. In an approach of Orgill and Hollands (1977), diffuse radiation is estimated based on the clearness index k_{clear}:

$$G_{\text{diffuse}} = \begin{cases}(1-0.249\cdot k_{\text{clear}})\cdot G & \text{for} \quad k_{\text{clear}} < 0.35\\ (1.557-1.84\cdot k_{\text{clear}})\cdot G & \text{for} \quad 0.35 < k_{\text{clear}} < 0.75\\ 0.177\cdot G & \text{for} \quad k_{\text{clear}} > 0.75\end{cases} \tag{6.5}$$

with

$$k_{\text{clear}} = \frac{G}{G_{\text{ex}}} \tag{6.6}$$

where G_{ex} is the extraterrestrial radiation outside the atmosphere on a horizontal plane:

$$G_{\text{ex}} = G_0 \cdot \left(1 + 0.033 \cdot \cos\left(\frac{360 \cdot n}{365}\right)\right) \cdot \cos\theta_{\text{Z}} \tag{6.7}$$

with the solar constant $G_0 = 1353\,\text{W}\,\text{m}^{-2}$.

As the calculation of diffuse sky radiation G_{diffuse} bears some uncertainty, separate measurements of beam and diffuse sky radiation should become standard for meteorological stations. If precise data for tilted solar air heaters is required, ones own measurements of solar radiation G_β are recommended by tilting the measurement device.

6.3 Solar Air Heaters

Solar collectors are operated with heat transfer fluids like air, water or oil. Whereas solar collectors based on liquid heat transfer fluids are occasionally used as a supplementary heat source in conventional dryers, flat plate solar air heaters are typically used in solar drying for direct heating of the drying air without a heat exchanger. In the following, the design and function of solar air heaters as the principal component of solar dryers will be described.

In general, a flat plate solar air heater consists of an absorber with insulation at the back and a front cover made of glass or transparent plastic, Fig. 6.5. Solar radiation passes through the transparent front cover and hits the absorber. A certain amount is reflected or absorbed by the transparent front cover. The major portion of the solar radiation is absorbed by the black absorber surface and converted into heat. To harvest useful energy, an airflow is generated by a fan and channeled between the absorber and the transparent cover, where it is heated by convective heat transfer from the absorber

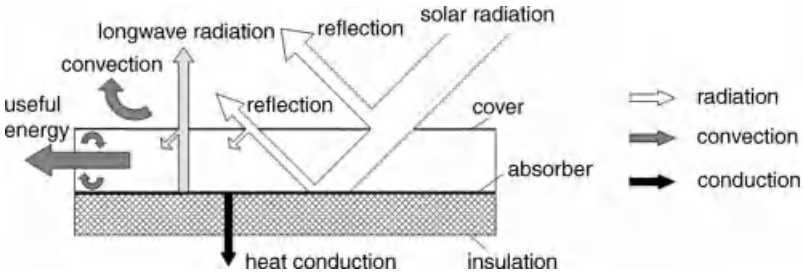

Fig. 6.5 Energy flow of a typical flat plate solar air heater with airflow between a black absorber and a transparent front cover.

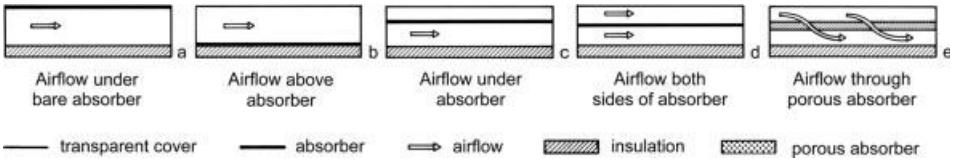

Fig. 6.6 Flat plate collectors with different absorber arrangements and modes of airflow.

surface. The heat insulation at the back reduces losses caused by heat conduction. Further losses are caused by long-wave radiation from the absorber to the sky, and are reduced by reflection and absorption at the front cover material. Finally, losses are caused at the front cover by convective heat transfer, which is aggravated by wind.

As shown in Fig. 6.6, solar collectors may deviate from the standard design (b), where air is ducted between the absorber and the front cover. The most basic type of solar air heater is a bare plate collector (a), which is designed without any transparent front cover. The absorber is exposed directly to the open sky and the airflow is channeled underneath, where it is heated at the back by convective heat transfer. Due to the high convection and radiation losses at the front, those low-cost collectors achieve only a limited temperature rise of 3 to 5 K above ambient temperature. The front losses are reduced considerably when the absorber is covered by a transparent material (c), because it prevents convective heat transfer from the absorber to ambient air. Whereas the front cover reduces solar radiation according to the material's transmittance for shortwave radiation, long-wave radiation losses are reduced according to its transmittance for long-wave radiation. When materials such as glass or polycarbonate are used, the reduction in heat losses outweighs the reduced solar radiation by far, and a temperature rise of 20 to 50 K above ambient temperature can be achieved. Convective heat transfer from the absorber can be improved when the airflow is channeled on both the front and the back, because of the double the heat transfer area (d). Therefore, the absorber temperature is lower and, consequently, long-wave radiation losses are reduced. However, in contrast to absorbers with flow exclusively on the back, dust from the front airflow will deposit on the absorber surface and reduce its absorptance. Heat transfer can even be intensified by forcing the airflow through a porous absorber material (e). As the heated air passes underneath the absorber, convective losses at the front cover are reduced. However, the absorber will filter dust from the airflow and – besides losing absorptance – flow resistance will increase by clogging and, consequently, the air flow rate will decrease.

Solar air heaters vary in efficiency according to their design and the materials used, where efficiency η is defined as the quotient of useful power Q_{use} and the solar radiation G_β arriving at the surface of an optionally inclined solar air heater. Useful power occurs in the form of a temperature rise ΔT of the specific airflow m_{fluid}, which is given in kg air per s and m^2 absorber area:

$$\eta = \frac{m_{\text{fluid}} \cdot c_p \cdot \Delta T}{G_\beta} \tag{6.8}$$

According to the ASHRAE standard (ANSI/ASHRAE, 1986) solar air heaters are characterized by efficiency curves, where the efficiency η is plotted versus the reduced parameter Ω, which relates the difference of average airflow temperature T_{fluid} and ambient temperature T_{ambient} to solar radiation G_β:

$$\Omega = \frac{T_{\text{fluid}} - T_{\text{ambient}}}{G_\beta} \tag{6.9}$$

The efficiency η is the ratio of useful power in the form of temperature rise of the airflow in the collector, and irradiated solar energy, quoted as a function of the reduced parameter:

$$\eta = F' \cdot [(\tau\alpha)_e - U \cdot \Omega] \tag{6.10}$$

where the optical losses are accounted for by the transmittance τ of the front cover and the absorptance α of the absorber by the effective transmittance absorptance product $(\tau\alpha)_e$, and the heat losses are accounted for by the overall heat loss coefficient U. The air heater efficiency factor F' considers the conductive, convective and irradiative energy flux between the absorber and the ambient:

$$F' = \frac{h_{a-f}(h_{f-c} + h_{a-c} + U_{\text{front}}) + h_{f-c} \cdot h_{a-c}}{(h_{a-f} + h_{a-s} + U_{\text{back}})(h_{f-c} + h_{a-c} + U_{\text{front}}) + h_{a-c}(h_{f-c} + U_{\text{front}})} \tag{6.11}$$

with the convective heat transfer coefficients h_{a-f} from the absorber to the fluid and h_{f-c} from the fluid to the front cover, the radiative heat transfer coefficients h_{a-c} from the absorber to the front cover and h_{a-s} from the absorber to the sky, as well as the combined heat transfer coefficients U_{back} and U_{front} for energy losses on the back and front sides of the air heater, respectively. A thermal network for the energy fluxes in the system is depicted in Fig. 6.7b.

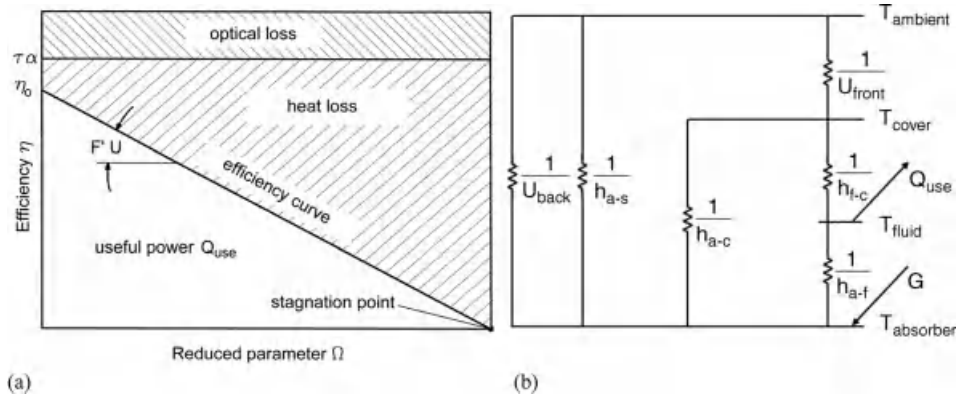

Fig. 6.7 (a) Idealized efficiency curve of a solar air heater, and (b) thermal circuit of energy flux; convective heat transfer coefficient h_{a-f} from absorber to fluid and h_{f-c} from fluid to front cover; radiative heat transfer coefficient h_{a-c} from absorber to front cover and h_{a-s} from absorber to sky; combined heat transfer coefficient U_{back} for energy losses at back of the air heater and U_{front} at the front; temperature T of absorber, fluid and ambience; solar radiation G; useful power Q_{use}.

Figure 6.7a shows an idealized efficiency curve of a solar air heater. The intercept on the ordinate η_0 indicates a virtual value, where the collector airflow is infinite and, hence, the temperature rise is zero. Therefore, the efficiency is dominated by the transmittance absorptance product $(\tau\alpha)_e$. The slope of the efficiency curve represents the product of the efficiency factor F' and the overall heat loss coefficient U. Increasing the reduced parameter Ω means decreasing the collector airflow and, consequently, increasing the temperature rise and heat losses. When the airflow is decreased to zero, efficiency η will also become zero, although the temperature rise reaches a maximum, the so-called stagnation temperature. The stagnation temperature is an essential design parameter as it indicates the maximum heat stress of collector materials that occurs when the fans of a solar air heater are out of operation. The stagnation temperature for given solar radiation can be calculated from the intercept on the abscissa by transposing Eq. 6.9.

Figure 6.8a shows, as an example, the efficiency curve of a solar air heater with airflow between a black absorber and a transparent front cover. Collector efficiency increases with increasing specific airflow, Fig. 6.8b. The higher efficiency is a result

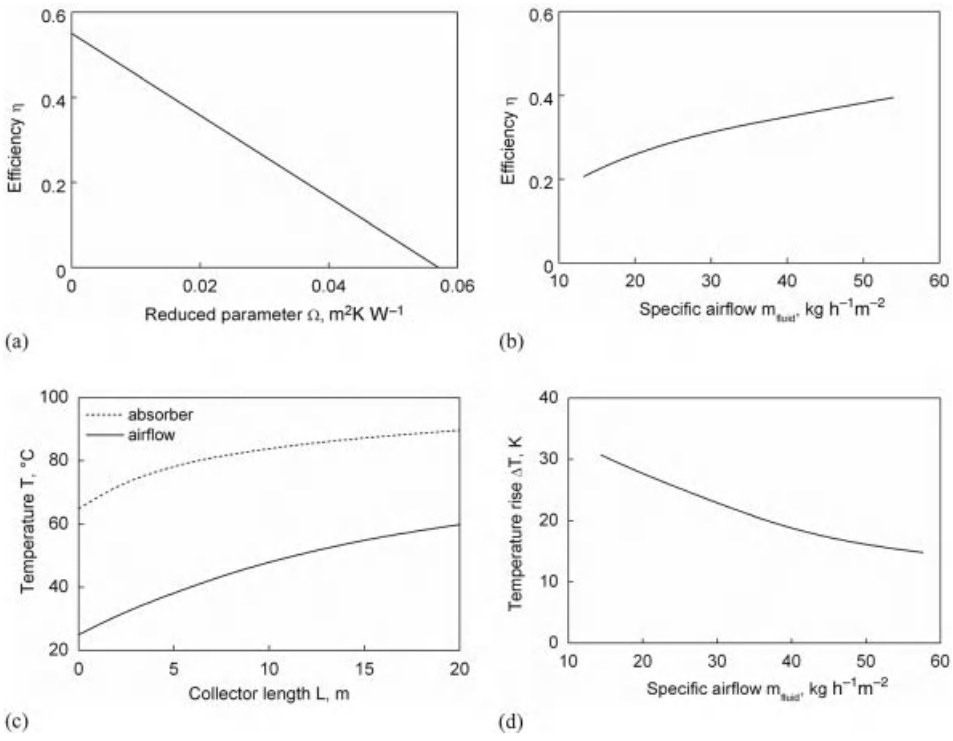

Fig. 6.8 Performance of a solar air heater with airflow between a black absorber and transparent front cover at solar radiation of 400 W m^{-2} and ambient temperature of 25 °C; (a) efficiency η vs. reduced parameter Ω, (b) efficiency η vs. specific airflow m_{fluid}, (c) temperature T of absorber and fluid vs. length of collector L and (d) temperature rise of fluid ΔT vs. specific airflow m_{fluid}.

of the reduced heat losses due to a lower temperature rise at a higher specific airflow, Fig. 6.8d. Heated by the absorber, air temperature rises along the length of the collector. However, this rise is not linear but digressive due to the increasing heat losses at a higher temperature difference from ambient. Thereby, the temperature of the absorber, acting as a heat source, is considerably higher than the temperature of the air, which is acting as a cooling agent, Fig. 6.8c.

As temperature is one of the strongest driving parameters in drying, optimizing a solar air heater does not mean maximizing efficiency – which would be achieved by high specific airflow and short collector length – but heating the required airflow to the target drying air temperature. From the intercept η_0 and the slope $F'U$ of the efficiency curve, the temperature of the airflow at a certain length L of a solar air heater with breadth b can be calculated:

$$T_{\text{fluid},L} = T_{\text{ambient}} + \frac{G \cdot \eta_0}{F' \cdot U} + \left(T_{\text{ambient}} - \frac{G \cdot \eta_0}{F' \cdot U} \right) \exp\left(- \frac{b \cdot F' \cdot U}{m_{\text{fluid}} \cdot c_p} \right) \tag{6.12}$$

The physical properties of the materials used for the absorber and the transparent cover are decisive for the efficiency of solar air heaters. The absorber material should have a high absorptance for solar radiation, which is mainly short-wave radiation in the visible range. Therefore, suitable absorber materials have a black surface. The emittance for long-wave radiation, on the contrary, should be low, to minimize energy losses by long-wave radiation. The quotient of shortwave absorptance and long-wave emittance is called the selectivity and materials with high absorptance and low emittance are said to be selective. To maintain favorable absorptance and emittance properties, the absorber material should be dust-repellent. If the airflow is on the back of the absorber the heat conductivity of the material should be high. Further properties are desirable for construction purposes and longevity: high temperature resistance, low thermal expansion, high corrosion resistance, and low aging of the absorbing surface. The physical properties of selected absorber materials are listed in Tab. 6.1. While the absorptance is high for all the listed materials, the emittance is advantageously low for black nickel (NiS–ZnS), which is why it is marketed as a selective absorber. Selective absorbers show a considerably higher efficiency than simple ones, Fig. 6.9.

Transparent cover materials should have a high transmittance for solar radiation, that is, the absorptance and reflectance of short-wave radiation should be low. In contrast, transmittance for long-wave radiation should be low to reduce radiation heat

Tab. 6.1 Properties of absorber materials (Linckh, 1993).

Absorber Material	Absorptance α	Emittance ε	Temperature Resistance, °C
Polyester fabric, black	0.96	0.72	100
Solar paint on steel, black	0.95	0.89	250
Aluminum film, black	0.93	0.64	>300
Black nickel (NiS-ZnS), selective	0.94	0.09	>300

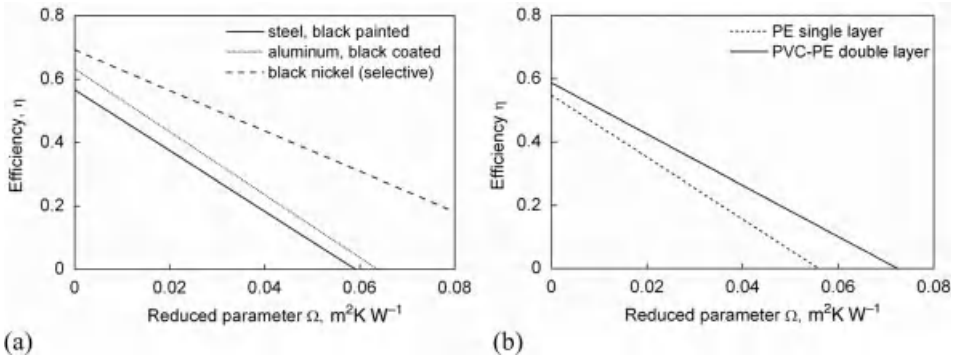

Fig. 6.9 Efficiency curves of solar air heaters with (a) different absorbers and (b) different front covers (Mühlbauer and Esper, 1995).

losses from the absorber. In analogy to absorber materials, high temperature resistance and low thermal expansion are required. As the cover is exposed directly to the environment, further properties are essential: materials and fixing systems have to be watertight and of high mechanical strength to protect the collector from rain, hail, snow, and wind. At the same time it should be of low weight to reduce the cost of the substructure. Furthermore, the material should be of high UV-resistance, because solar collectors are exposed permanently to the energy-rich UV-radiation of the sun. If the transparent material is translucent to UV-radiation, the absorber surface has to be UV-resistant to prevent aging. The physical properties of selected transparent cover materials are listed in Tab. 6.2. Polyethylene (PE) and polyvinyl chloride (PVC), both available as low-cost transparent plastic foils, show a similar transmittance for short-wave radiation. Transmittance of long-wave radiation, however, is much lower for PVC. Due to the reduced radiative heat losses, air heaters covered with PVC achieve higher efficiencies than those covered with PE, Fig. 6.9b. Rigid transparent materials, such as poly(methyl methacrylate) (PMMA) and sheet glass, show favorable optical properties and long useful life due to high

Tab. 6.2 Properties of transparent cover materials (Linckh, 1993).

Cover material	Thickness mm	Transmittance short-wave 380–780 nm	Transmittance long-wave 2–40 µm	Temperature Resistance °C	UV Resistance year
PE Polyethylene	0.2	0.89	0.45	80	3
PVC Polyvinyl chloride	0.3	0.86	0.08	70	4–5
PTFE Polytetrafluoroethylene	0.1	0.91	0.25	150	>15
PMMA Poly(methyl methacrylate)	3.0	0.91	0.01	95	10–15
Sheet glass	6.0	0.90	0.02	>500	>15

UV-resistance. However, the price is higher than for plastic foil and expensive sub-constructions are required, both to support the higher load and to facilitate an airtight connection of the panes.

Figure 6.9 shows efficiency curves of solar air heaters with different materials for the absorber and front cover. The positive influence of a selective absorber on efficiency is most distinct, and outweighs even a double front cover layer made of PE and PVC foil. However, selective absorber materials are expensive and should only be used when deposition of dust, which would increase the emittance of long-wave radiation, can be prevented effectively.

In general, the use of solar air heaters puts certain limitations on the drying process. The temperature rise in solar air heaters, even at high efficiency, is limited to 40 to 50 K. Consequently, solar drying is appropriate for products that are best dried at temperatures below 70 °C. To achieve those temperatures, the length of an absorber has to be at least 5 m, which requires corresponding installation space. Large ground area is also required, because of the low energy density of solar radiation. Therefore, to stay within the size of common buildings, solar air heaters for drying are typically below 50 kW power. A further consequence of solar characteristics on drying is the lack of energy during the night, which requires heat storage or robust drying products that do not perish when drying is interrupted for several hours.

6.4 Design and Function of Solar Dryers

During the last decades, numerous types of solar dryers have been developed to reduce post-harvest losses and to improve product quality. However, only a few types are used on a scale beyond demonstration projects or have been commercialized. In the following, a system to classify solar dryers is developed, and types of solar dryers relevant for practical use are described in more detail.

6.4.1 Classification of Solar Dryers

To classify the various types of solar dryers, it is necessary to simplify the complex constructions and various modes of operation to basic principles, such as mode of air movement (natural or forced convection), exposure to solar radiation (direct or indirect) and structural arrangement of the dryer (open-air or structure-integrated), as shown in Fig. 6.10.

The air movement in solar dryers can be provided either by natural or by forced convection. Natural convection is based on the reduction of the specific weight of air due to heating and vapor uptake. The difference in specific weight between the drying air and the ambient air promotes a vertical air flow. Natural convection type solar dryers are exclusively operated with solar energy and wind, and, therefore, their use is independent of the mains electricity supply. However, the airflow in this type of dryer is not sufficient to penetrate higher material bulk. Furthermore, the air flow ceases

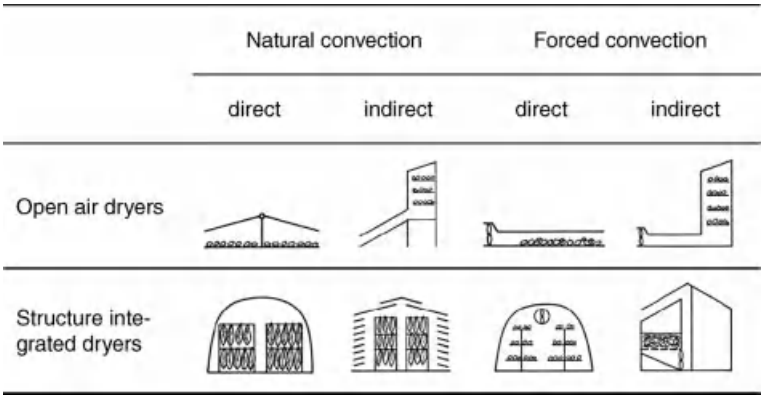

Fig. 6.10 Classification of solar dryers.

completely during the night and adverse weather conditions. Therefore, the risk of product deterioration due to mold attack and enzymatic reactions is high. In contrast, forced convection solar dryers are operated by fans driven either by electric motors or internal combustion engines. Air flow can be provided in the dryer on demand throughout the drying process, independent of the weather conditions. Furthermore, the bulk depth is no longer restricted to thin layers, and the airflow rate can be controlled. Hence, the capacity and reliability of the dryers are increased considerably compared to natural convection type dryers.

The bulk of the drying material can either be ventilated in flow-through or flow-over mode. In almost all mechanical dryers, the drying air is forced through the bulk, causing high pressure drop. Guiding the air over the drying material reduces the pressure drop significantly, and also the power requirement of the fan. However, this drying method is limited to the drying of thin layers, since the drying air penetrates only superficially into the bulk, which has to be mixed in short intervals to guarantee uniform drying.

The mode of drying can either be direct or indirect, depending on whether the product is directly exposed to solar radiation or dried in the shade by solar heated air. In the direct mode, the product itself serves as the absorber, that is, the heat transfer is affected not only by convection but also by radiation, according to the albedo of the product surface. Therefore, the surface area of the product being dried has to be maximized by spreading the drying material in thin layers. To obtain uniform final moisture content, the drying material has to be turned frequently. Using the direct mode of drying, sunlight might affect valuable components of the product, for example, chlorophyll is quickly decomposed. Therefore, it is advisable not to use the direct mode in drying products like most medicinal and aromatic plants in which the green color has to be preserved. However, for products like apricots and grapes, in which the decomposition of chlorophyll causes a positive color effect, the use of direct mode is recommended. Due to the limitation of the bulk depth, such dryers require large ground surface areas. If grounds are scarce, indirect mode dryers are preferred for drying larger quantities.

Solar dryers for small capacities, known as box, tent, cabinet or tunnel dryers are installed outdoors. Since the complete handling takes place in the open air, such dryers should be applied preferably in regions without precipitation during the drying season. Out of season, the equipment can be detached and stored to prevent seasoning or damage caused by weather. For larger harvest quantities structure integrated dryers are used. In contrast to outdoor solar dryers, these dryers are placed in weatherproof, permanent, and accessible buildings, such as barns or greenhouses. The roof and walls serve as components of the air heater. All handling takes place under cover and is, therefore, independent of weather conditions. Out of the drying season, the buildings can be used for alternative purposes, such as storing, processing, and even for plant production if a greenhouse is used as the structure.

6.4.2
Solar Dryers with Natural Convection for Direct Solar Drying

An ancient method of drying, still widely practiced in less developed regions, is by spreading the drying material on the ground to expose it to the sun. During sun drying, heat is transferred by convection from the ambient air, and by absorption of solar radiation at the surface of the drying material, which acts as an absorber according to its optical properties. Solar radiation that is not reflected is converted to heat, which is conducted to the interior of the bulk, increasing the temperature of the drying material and providing energy for evaporation of water. Heat losses occur due to radiation and convection at the surface of the bulk, and by conduction to the ground, Fig. 6.11a. The evaporated water has to be removed by natural convection supported by wind. Due to the hygroscopic properties of agricultural products, the drying material can either be dried or remoistened. Especially during the night, when the ambient temperature is decreasing, remoistening effects can occur, either by vapor sorption or by condensation of dew. When the drying material is spread directly on the ground, as typically practiced for drying hay in the grasslands, water may even be transported from the soil to the drying material by evapotranspiration of the sward. In adverse weather conditions, water in the form of rain or fog may precipitate on the unprotected drying material, Fig. 6.11b.

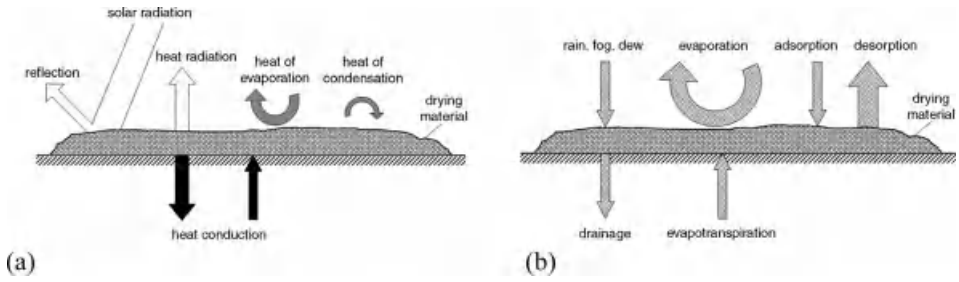

Fig. 6.11 (a) Heat transfer, and (b) water transport during sun drying.

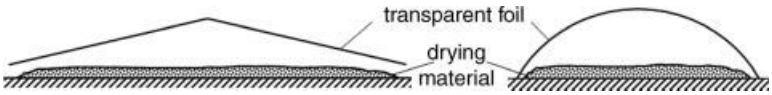

Fig. 6.12 Tent-type solar dryers with natural convection for direct solar drying (Eissen, 1983; Eissen *et al.*, 1985).

Solar drying, in contrast to sun drying, needs certain investment. The simplest form of solar drying is by covering the drying material with a transparent plastic foil. To drain rain water, the cover has to be tilted or curved by a simple substructure made out of wood, bamboo or metal. To ensure the transport of the evaporated water, openings should be oriented in the main wind direction. The drying material is spread out in a thin layer on the plain ground or on concrete floors, which should be raised above ground level to prevent flooding in case of heavy rain. After the drying season the foils should be removed and stored to prevent degradation. Figure 6.12 shows a typical transparent cover for drying grapes in Greece. A polyethylene foil, 3.5 m wide and 10 m long, is stretched over a ridge 60 cm above ground, and anchored with ropes at both sides, leaving 20 cm high openings. The fresh grapes are spread on a fabric in a bulk density of 20 kg m^{-2}. For spreading, turning and final collection of the raisins, the cover foil has to be removed (Eissen, 1983; Eissen *et al.*, 1985).

Using a transparent cover, drying time can be reduced by 20% compared to traditional sun drying, because heat losses by convection and long-wave radiation are reduced. Even more important than the reduction of drying time is the improvement of product quality in terms of color and hygienic status, avoiding both rewetting during the night by dew, and contamination by dust. Moreover, the risk of a total loss caused by sudden rainfalls is minimized. This kind of solar drying in direct mode and natural convection is favorable for fruits like grapes and apricots that need direct exposure to solar radiation for full development of product quality by degradation of chlorophyll. Construction requires low investment because locally available materials and labor can be employed.

6.4.3
Solar Dryers with Natural Convection for Indirect Drying

Light-sensitive products have to be dried in indirect mode, that is, drying air is heated by extra solar air heaters and applied to the drying material that is protected from the sun. A basic type of such drying equipment, operated by natural convection, is the solar cabinet dryer, as shown in Fig. 6.13. The inclined solar air heater has to be mounted facing the sun and tilted at an optimum angle, depending on the latitude of the location. The drying air is heated by passing the absorber of the solar air heater, enters the drying chamber at the base, and passes through the drying material that is spread in thin layers on vertically stacked trays. Natural convection can be enforced by a chimney.

Solar cabinet dryers are propagated frequently for small-scale farmers and drying industries at village level. Numerous versions have been developed worldwide, however, their use is still sporadic.

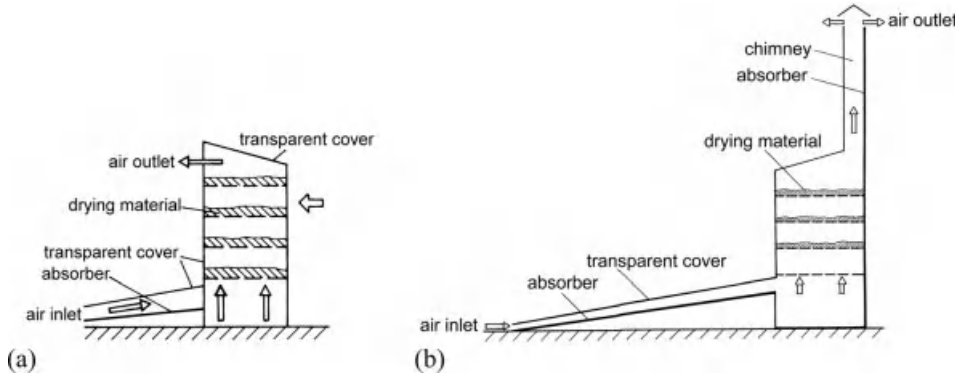

Fig. 6.13 Solar cabinet dryer for indirect solar drying with natural convection; (a) basic type, and (b) construction enforced with a solar chimney (Eissen, 1983; Eissen *et al.*, 1985; Sodha *et al.*, 1987).

6.4.4

Solar Dryers with Forced Convection for Direct Drying

A promising concept of forced convection type solar dryers is represented by the solar tunnel dryer that was developed at University of Hohenheim. This tunnel dryer is intended for use on small farms or farmer cooperatives. The solar tunnel dryer consists basically of a plastic foil-covered flat plate solar air heater, a drying tunnel and small axial flow fans (Esper, 1995; Häuser *et al.*, 1995; Schirmer *et al.*, 1996), Fig. 6.14. To simplify the construction and to reduce the production costs, the solar air heater is connected directly to the drying tunnel without additional air ducts. Both the air heater and the drying tunnel are installed on concrete block substructures for ease of loading and unloading the dryer. All parts of the dryer, including the back heat insulation and metal frames, are in a modular design that facilitates transport and installation of the equipment.

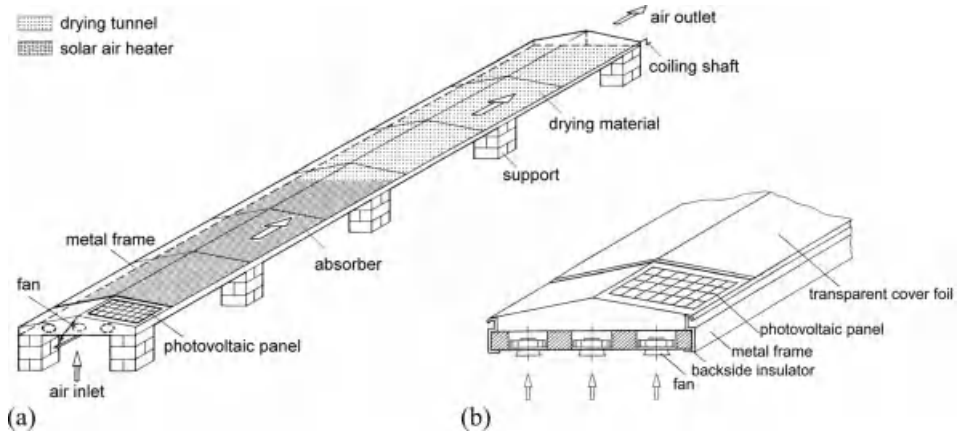

Fig. 6.14 (a) Solar tunnel dryer for direct solar drying with forced convection in full view, and (b) detail view of air heater inlet with fans and photovoltaic panel (Esper and Mühlbauer, 1996).

The floor of the solar tunnel dryer consists of plastic foam sandwiched between two metal sheets with a tongue and groove system. For dryers produced locally in developing countries, concrete or waterproofed plywood boards provided with heat and water resistant insulation material can be alternatively used as the substructure and back heat insulation. The insulator sheets are connected by a corrugated metal frame which also enables easy fixing and replacement of the transparent plastic cover foil by using reinforced plastic clamps.

The solar air heater and dryer are covered with a transparent plastic foil. In a standard design using a 0.2 mm thick UV-stabilized PE foil, the useful life is 1 to 2 years before UV radiation and mechanical stress cause damage. On one length side of the dryer the plastic foil is fixed to the metal frame, and on the other side to a metal tube that allows the foil to be coiled for loading and unloading the dryer. To convert solar radiation into heat, the top surface of the absorber is painted black, achieving an absorptance of about 90%. In humid tropical countries with frequent rainfall the covering sheet is tilted roof-like to prevent water entering the dryer. In arid regions a flat cover is sufficient. In the solar tunnel dryer the drying material is spread on a wire mesh placed 20 mm above the floor. Alternatively, trays can be used for ease of loading and unloading. By this arrangement the drying material is exposed to the drying air from all sides.

Depending on the solar radiation available, two or three axial fans are incorporated into the sandwich substructure to suck ambient air into the air heater, Fig. 6.14b. Due to the low pressure drop of 20 Pa, a maximum 20 to 30 W electrical energy is required to force 800 to 1000 $m^3 h^{-1}$ of air between the floor and the foil cover, which is sufficient to ensure drying to safe storage conditions. The drying material spread in a thin layer in the tunnel dryer itself acts as an absorber, enabling the drying air to gain additional heat, when passing through the dryer. The heat losses caused by evaporation of the moisture during drying are compensated by this additional energy gain, resulting in an almost uniform drying. The air inlet and outlet are covered with plastic net or wire mesh to prevent insects from entering the solar tunnel dryer.

Figure 6.15a shows an example of the daily course of air temperature at the inlet and outlet of the air heater of the solar tunnel dryer, as measured in Khartoum (Sudan) for different airflow rates (Adam, 1998). At an airflow rate of 900 $m^3 h^{-1}$ a maximum temperature of slightly above 60 °C was achieved, whereas at a reduced airflow rate of 600 $m^3 h^{-1}$ the temperature exceeded 70 °C. The temperature rise in the solar air heater was proportional to the solar radiation and reached 26 K at an airflow rate of 900 $m^3 h^{-1}$ and 32 K at an airflow rate of 600 $m^3 h^{-1}$ for peak radiation of 990 $W m^{-2}$, Fig. 6.15b.

Figure 6.16 shows the gradient of temperature and relative humidity of the drying air in the solar tunnel dryer along the solar air heater and the dryer section, as measured in Khartoum (Sudan) at a solar radiation of 985 $W m^{-2}$ (Adam, 1998).

When the dryer was empty, the temperature increased steadily from the ambient condition of 38 °C at the inlet of the solar air heater to 68 °C at the outlet of the dryer. When the dryer was freshly filled with onion slices, and the average moisture content was still high at 75%, the drying air was cooled by evaporative cooling due to water vapor uptake to 45 °C. During the final phase of drying, at 10% average moisture

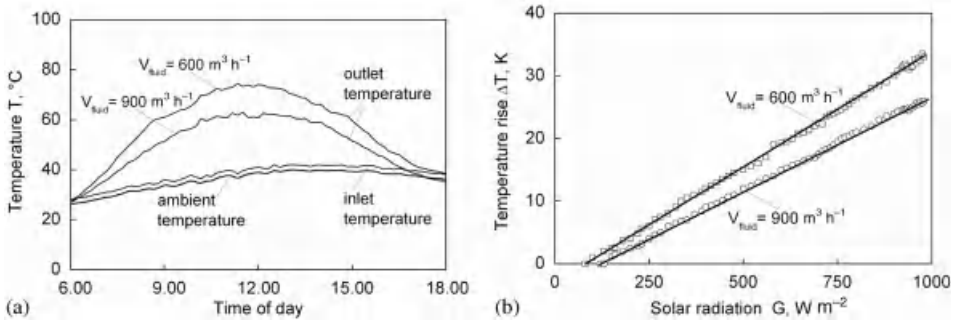

Fig. 6.15 (a) Daily course of air temperature at the inlet and outlet of the solar air heater, and (b) temperature rise in the solar air heater vs. solar radiation at different airflow rates V_{fluid}, as measured in Khartoum, Sudan (15.63 °N, 32.53 °E), (Adam, 1998).

content of the onion slices, the cooling effect was considerably lower due to the reduced drying rate. As a consequence of the increasing temperature along the solar air heater, the relative humidity of the air decreases. During the initial phase of drying, the relative humidity of the air in the dryer section does not decrease further but remains about constant, which provides enough drying potential for uniform drying.

Due to the low power requirement for driving the fans, photovoltaic (PV) generators can be economically used to provide the required electrical energy in remote areas. The PV panel is installed at the inlet of the solar air heater. Cooling of the panel by forcing ambient air underneath the back side increases its efficiency. The solar tunnel dryer can be operated with one PV panel in the case of direct coupling of a generator and a DC-motor, when continuous operation of the fan is not required. Despite their comparatively low efficiency, car cooling fans with DC-motors are the cheapest and most adequate solution, since they are available in all developing countries at low prices. Continuous operation of the fan is only required for perishable fruits, such as

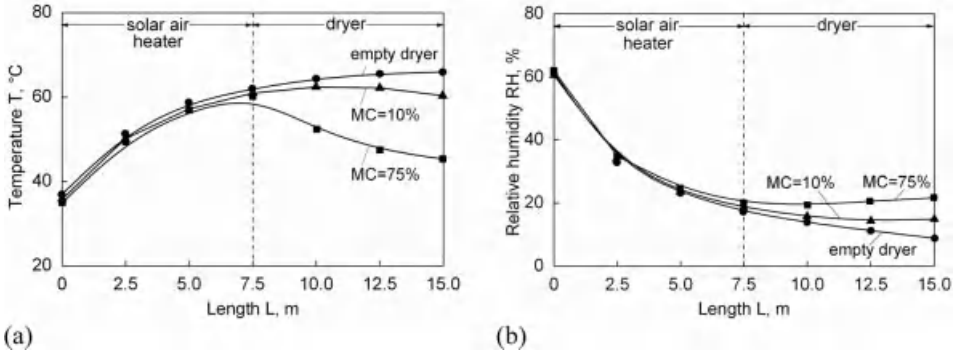

Fig. 6.16 Gradient of (a) temperature *T*, and (b) relative humidity RH along the solar air heater and dryer section of the solar tunnel dryer operated in Khartoum, Sudan (15.63 °N, 32.53 °E) at a solar radiation of 985 W m^{-2}; curves are for the empty dryer and for initial (MC = 75%) and final phase (MC = 10%) during drying of onion slices (Adam, 1998).

grapes or cocoa beans, during the first phase of the drying process. In that case the photovoltaic system has to be equipped with battery storage to provide the energy necessary for air ventilation during the night or in adverse weather.

The standard version of the solar tunnel dryer is 2.0 m wide. Both, the solar air heater and the tunnel dryer are 10 m long. The drying area of 20 m^2 is sufficient for labor-intensive products like mangos, pineapples and papayas, which require pre-treatments such as washing, peeling, dipping, or slicing before drying. Due to the modular design, the dryer can be enlarged in length up to 20 m for drying raisins, figs or apricots in arid regions. The capacity of the dryer is mainly influenced by the size, shape and moisture content of the fruit to be dried. The loading capacity ranges from 100 kg for medicinal plants to 300 kg for figs, apricots or coffee (Esper and Mühlbauer, 1996; Häuser, 1995; Häuser *et al.*, 1995; Schirmer *et al.*, 1996). The solar tunnel dryer is one of the few types of solar dryers that is commercialized and manufactured in various countries.

Another type of solar dryer with forced convection for direct drying has been developed by Janjai *et al.* (2010) in the form of a walk-in solar tunnel dryer for tropical fruit, such as mango, papaya, banana, and longan. The dryer is based on a small-scale greenhouse and consists of a parabolic roof structure covered with polycarbonate sheets on a concrete floor, Fig. 6.17. The tunnel is 8.0 m wide, 20.0 m long and 3.5 m high with a loading capacity of about 1 t of fruit, which are dried within 3–4 days. Depending on the required capacity, the dryer can be extended in length. Nine DC fans operated by three 50 W PV-modules are installed in the wall opposite to the air inlet to ventilate the dryer. A 100 kW LPG-burner was installed in a housing at the rear side of the dryer to heat the drying air which is guided through two air ducts installed in a legthways direction on the concrete floor inside the dryer. The burner is equipped with

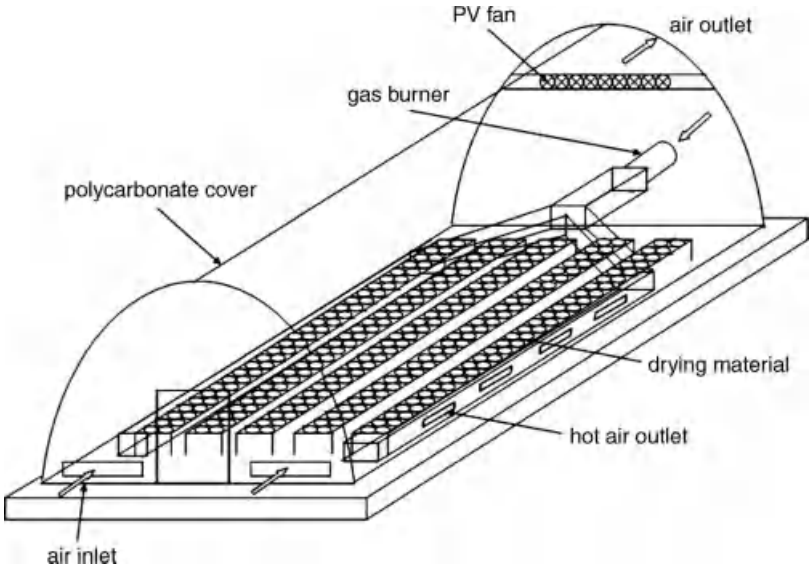

Fig. 6.17 Walk-in type solar tunnel dryer covered with polycarbonate sheets for drying of tropical fruit (Janjai *et al.*, 2010).

a thermostat to control the drying air temperature. Due to the use of a supplementary gas heater, the solar dryer can be operated continuously, even during adverse weather conditions. As the dryer is walk-in, the drying material can also be handled during rainy weather. Therefore, this dryer is particularly suitable for humid climates.

Solar radiation passing through the polycarbonate roof heats the air and the drying material inside the dryer as well as the concrete floor. The 6 mm thick polycarbonate sheets have a transmissivity for solar radiation of about 80% and a heat transfer coefficient of $3.2\,W\,m^{-2}\,K^{-1}$ thus reducing the heat losses significantly during periods when the gas heater is in operation. Ambient air is drawn in through a small opening at the bottom of the front side of the dryer and is heated by the floor and the drying material exposed to solar radiation. The heated air absorbs moisture while passing through and over the material. Due to the low air flow, the drying air inside the dryer can be heated to 60 °C during periods of high solar radiation, which guarantees the desired high drying rate.

Moist air is sucked from the dryer by the fans at the top of the rear side of the dryer. In the case of rain or cloudy weather, the LPG burner is manually started and the fan of the burner blows hot air through an air duct into the dryer. The solar greenhouse dryer is successfully used by cooperatives and small scale industry, mainly for drying high value crops. During the last few years several units were disseminated in Thailand and Laos.

6.4.5
Solar Dryers with Forced Convection for Indirect Drying

To meet the requirements of larger farms and cooperatives, several efforts have been made to increase the capacity of solar drying by incorporating solar air heaters into greenhouse structures covered either by glass or by plastic foils (Chen and Helton, 1989; Guzman *et al.*, 1985; Huang *et al.*, 1981; Marais, 1982; Oliveira *et al.*, 1982; Trim and Ko, 1982). In spite of promising results, up to now none of these systems has been commercialized. The obstacles are the high investment cost of glass covered greenhouses, and the low reliability of the considerably cheaper plastic foil greenhouses.

To eliminate these disadvantages a new type of greenhouse dryer was developed at Hohenheim University, using a high quality plastic foil in combination with a special fastening system that guarantees the required reliability (Müller *et al.*, 1993; Müller *et al.*, 1989). Figure 6.18 shows the solar greenhouse dryer being commercially applied for medicinal and aromatic plants in some European countries, as well as in Egypt and Chile. A batch dryer, taking about one third of the base, is integrated into a commercially available greenhouse structure with vertical side walls, a span roof and a transparent cover made of a PE/EVA air-bubble foil. Due to the protection against UV radiation, the foil has a useful life of at least 10 years.

The solar air heaters are incorporated into the roof by installing a black woven fabric as absorber, and a second air-bubble foil to reduce heat losses from the back, Fig. 6.19. To increase the air heater area, the roof is extended to the ground on the sun-facing side. The frame, made out of rectangular galvanized steel profiles, is structured along the ridge into 2 m wide segments to obtain a modular design. The

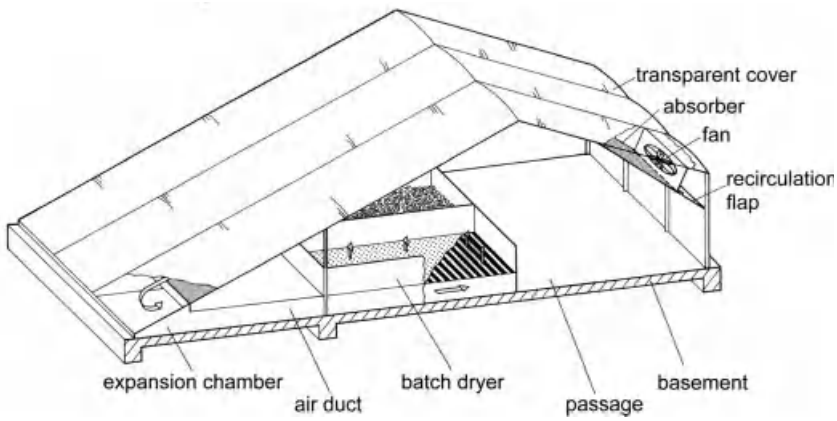

Fig. 6.18 Solar greenhouse dryer for medicinal and aromatic plants (Müller, 1992b).

greenhouse is 4 m high and 15 m wide, the length depends on the chosen number of modules. Each module has a flatbed dryer with a drying area of 12 m^2 and is operated separately by a 500 W axial fan, providing an air flow of 7000 $m^3\,h^{-1}$ at a pressure drop of 60 Pa. At a typical size of 10 modules the greenhouse dryer is 20 m long and has a loading capacity of 10 t of medicinal plants at initial moisture content.

Ambient air is sucked in at the sun-averted eaves and blown between the upper foil and the absorber. The heated air is reversed at the sun-facing eaves and directed to the batch dryer, ventilating the drying material vertically. The moistened air escapes through outlets at both gables. To achieve an additional rise in temperature, the dryer can be operated with recirculating air by a flap at the air inlet.

Figure 6.20 shows a typical daily course of the drying temperature for opened and closed recirculation flap, measured on a cloudless day with a maximum global irradiation of 760 $W\,m^{-2}$. When sucking in fresh air the drying temperature reaches 45 °C at real noon, exceeding the ambient temperature by 15 K. When air is recirculated completely, the temperature inside the greenhouse dryer will reach a maximum of 70 °C. In practice, drying air can only be recirculated partly to prevent excessive accumulation of humidity and to keep certain temperature limits dependent on the drying product. Therefore, the ratio of recirculating air is controlled by humidity and temperature sensors.

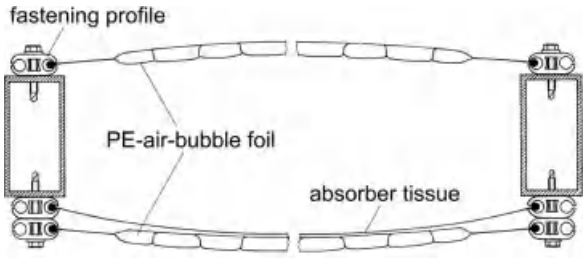

Fig. 6.19 Cross-section of an air heater of the solar greenhouse dryer (Müller, 1992b).

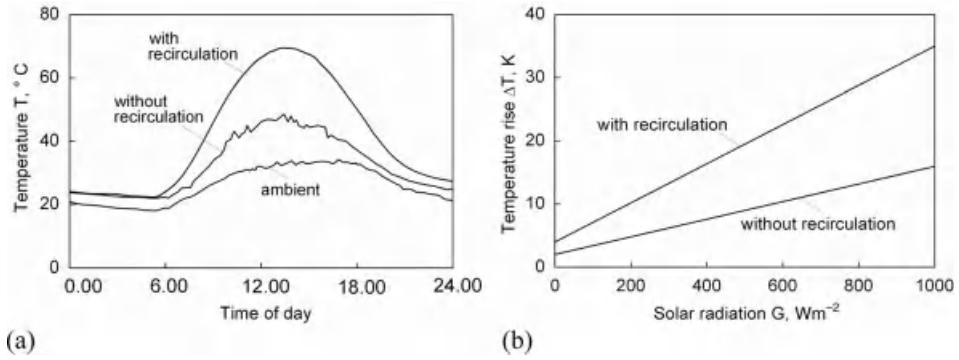

Fig. 6.20 Influence of recirculation of drying air in the solar greenhouse dryer: (a) daily course of temperature T at ambient and at the outlet of the solar air heater and (b) temperature rise ΔT in the solar air heater vs. solar radiation as measured in Novi Sad, Serbia (45.25 °N, 19.85 °E) (Müller, 1992b).

Certain products, like tobacco for cigars, or timber, require a specific temperature/humidity regime for curing and drying. Therefore, a special greenhouse type solar dryer was developed, based on a plastic film greenhouse, which is 10 m wide, 16 m long and 6.6 m high, with a solar air heater incorporated in the roof, a humidifier, a supplementary biomass furnace, a heat exchanger and four axial flow fans (Bux, 1996). Inside the solar barn, horizontal beams are placed at five different heights to serve as racks for the tobacco leaves, Fig. 6.21. A black absorber tissue is mounted below the girders, serving a double function: as a shade for the tobacco leaves, and as an aperture for absorbing solar radiation. The axial flow fans, each of 500 W power, are installed in an air conditioning unit at one of the gables to blow air in the attic. Three of the fans ensure a permanent supply of circulating air. The collector fan forces air through the absorber tissue for heat transfer when thermal solar energy is available and needed. The circulating air passes downwards through the tobacco leaves in a vertical direction and is finally forced back over the ground to the air conditioning unit. As a result of the upside down airflow, warm and dry air enters the attic, preventing condensation of water on the cold roof during the night. A supplementary firewood furnace of 80 kW calorific power, with a hot water circuit and a heat exchanger installed in the air conditioning unit, maintains the optimum temperature during the night or periods of low radiation. To provide sufficient humidity even at varying temperatures, a humidifier is integrated into the system.

Humidity is controlled by means of a recirculation flap incorporated into the gable. In recirculation mode the flap is closed and the air is circulated in the barn. During this mode of operation the humidity rises and fresh air has to be mixed in certain amounts. In ambient air mode, the flap is completely opened and only ambient air is sucked in. Since the water content of the ambient air is generally lower than the water content of the recirculated air, the humidity decreases if the temperature is kept constant. By electronic control of the recirculation flap, any ratio of fresh and circulating air can be adjusted in order to provide the required curing conditions. Thus, curing in the solar barn is widely independent of weather conditions.

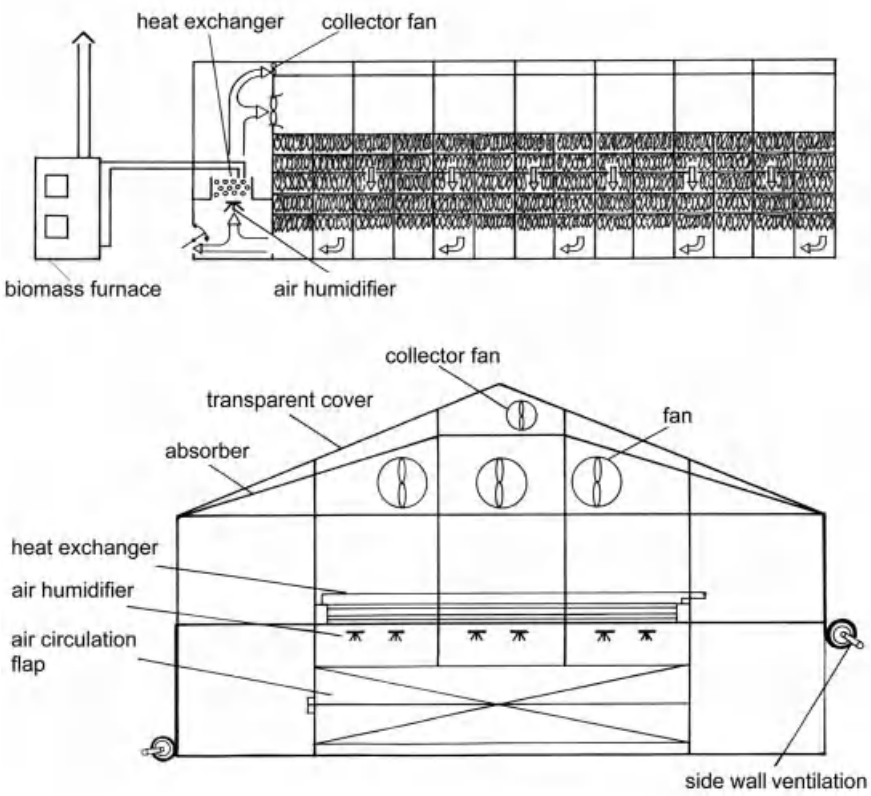

Fig. 6.21 Longitudinal and cross sectional view of the greenhouse-type solar dryer for tobacco (Bux, 1996; Bux *et al.*, 1997).

In a down-draught firewood furnace, water is heated and pumped to an insulated heat storage tank or to the heat exchanger inside the air conditioning unit of the solar dryer. The calorific power of the furnace is controlled thermostatically via control of the combustion air fan. Individual control of primary and secondary combustion air and the division of the drying, gasification and burning zones ensures an efficient combustion and low emissions. A reservoir for 200 kg of firewood provides sufficient fuel for at least 10 hours of operation.

The use of the solar greenhouse type dryer for curing tobacco showed several advantages compared to the traditional curing method applied in Brazil. Curing in the sensor-controlled solar dryer allowed the use of a higher temperature to accelerate the biochemical processes without the risk of drying the tobacco too fast. Thus, the curing process can be finished after 15 to 20 days without any impact on quality, while conventional curing takes 30 to 40 days. Furthermore, the forced air circulation in the solar barn allows a closer spacing of the leaves, facilitating a bulk density of 20 kg m^{-3} compared to 4–5 kg m^{-3} in conventional curing barns, resulting in a reduction in the required barn capacity from 122 to 17 m^3 per ha cropping area. The firewood consump-

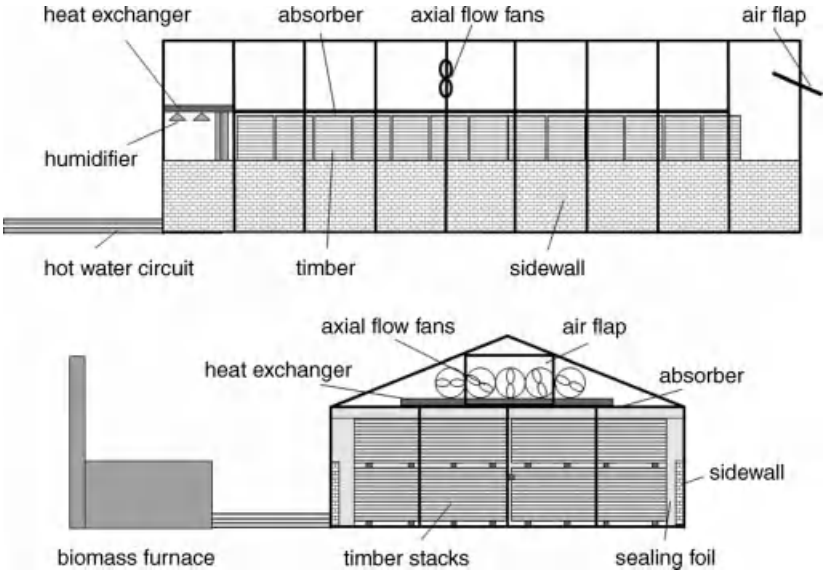

Fig. 6.22 Longitudinal and cross-sectional view of the solar-assisted timber dryer (Bauer, 2003).

tion can be reduced from 30 to 2 kg per kg dried tobacco. The usual leaf losses, by barn rot, of about 10% can be reduced considerably (Bux, 1996; Bux *et al.*, 1997).

The same type of dryer was adapted for drying timber in Brazil (Bauer, 2003; Bux, 2001; Bux *et al.*, 2001). Instead of a porous absorber tissue, black-coated corrugated aluminum sheets were used. The axial flow fans force a horizontal airflow over the absorber from the front to the rear of the solar dryer, where it passes through the heat exchanger down to the drying chamber, Fig. 6.22.

During daytime the temperature of the absorber surface increased to a maximum of 65 °C and was thereby about 30 K higher than the ambient temperature. The airflow temperature reached a maximum of 50 °C, Fig. 6.23a. The energy rate by solar radiation irradiated on the air-heater area reached a maximum of 200 kW, where 60%

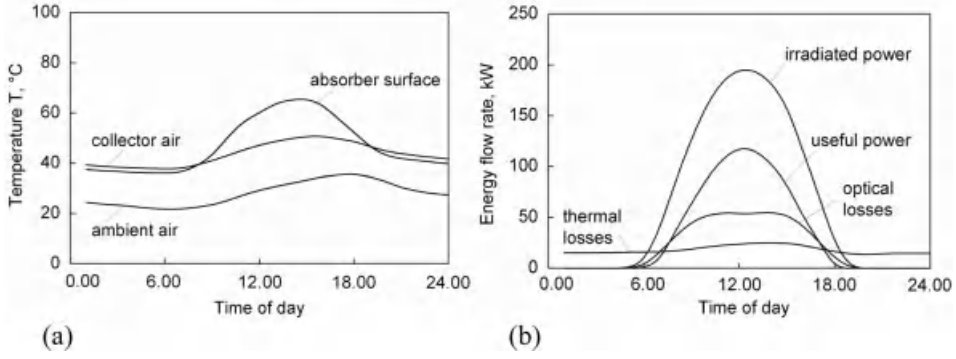

Fig. 6.23 Daily course of (a) temperature and (b) energy flow rate in the solar greenhouse-type timber dryer in Martinho Campos, Brazil (19.19 °S, 45.14 °W) (Bauer, 2003).

was converted to useful power. During daytime, optical losses exceeded the heat losses, however, during nighttime heat losses prevailed, causing a negative energy balance, Fig. 6.23b.

For drying, up to 250 m^3 of freshly sawn timber are loaded in the drying chamber. Timber stacks with 40 mm thick boards and 15 mm thick stacking laths are arranged over the whole width of the dryer of 10 m, with a length of 14 m and a height of 3.20 m. To prevent the airflow bypassing the timber stacks, sealing foils are installed between the walls of the solar dryer and the timber stacks. For timber loading and unloading, two revolving doors are installed at the front of the dryer over the full width of the drying chamber. The air is forced through the timber stacks in a horizontal direction to the front of the dryer where it moves back to the attic.

During daytime the circulating drying air is heated by solar energy while passing the absorber. The preheated air moves over the heat exchanger, where it is heated additionally to the desired drying air temperature, if necessary. As the drying air passes the timber load, moisture is evaporated, causing a decrease in temperature and an increase in the relative humidity of the drying air along the load. When the humidity of the circulating drying air exceeds the set maximum value, a part of the drying air is substituted by outside air. By opening the air flap, humid drying air leaves the dryer while ambient air is sucked into the drying chamber. Thereby, the relative humidity and the temperature of the drying air decrease due to the lower water content and temperature level of the ambient air. If the relative humidity decreases below the set minimum value, the air flap is closed. The humidifying system is used to maintain the relative humidity of drying air whenever it falls below the minimum value, to prevent deformation and splitting of the boards by too fast drying. Since the control of the drying conditions is essential for quality timber drying, a microprocessor was applied to control the air flap, humidifier and back-up heating system.

With the solar greenhouse-type timber dryer, within 27 days a batch of 250 m^3 eucalypt wood sawn into 27 mm thick boards could be dried from a moisture content of about 60 to 12% d.b. (note that wood moisture content is customarily given in dry base). Drying time was about 20% greater than in a conventional hot-air dryer. The electric energy consumption in the solar dryer was about 20 kWh per m^3 dried timber, which is 80% less than usually consumed in a hot-air dryer. The thermal energy consumption was 1.2 GJ per m^3 of dried timber, which is 60% less than required in hot-air dryer. Nowadays, approximately 35 000 m^3 of eucalypt hardwood is dried annually in two solar-assisted drying plants.

6.4.6
Dryers with Roof-Integrated Solar Air Heaters

Integration of solar air heaters into existing structures of farm buildings shows two major advantages: (i) no additional ground area is required for the installation of the solar air heater, and (ii) the investment can be reduced by dual use of the roof structure. In Switzerland around 4000 units of such solar assisted in-storage drying systems have been installed for hay production during the last two decades. Since hay is dried during periods of maximum solar radiation and only a small temperature rise

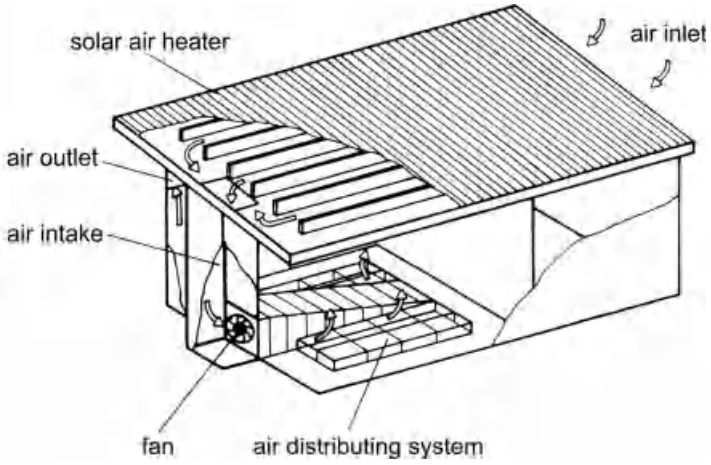

Fig. 6.24 Drying system for hay with solar air heater incorporated into the roof of a farm building (Pfister, 1986).

of 5 to 10 K is required, the application of solar energy is an economic viable alternative to conventional heating systems. The desired temperature rise can be achieved by non-sophisticated solar air heaters, incorporated into the roof of the farm building, Fig. 6.24 (Pfister, 1986). As transparent roof covers would be in disturbing contrast to the traditional style of farm buildings in Switzerland, typically dark roof covers are used as a bare absorber with panels mounted with spacing on the back side to form an air duct. Ambient air is sucked through the air duct by a fan and forced to a conventional flatbed batch dryer inside the barn. The air velocity inside the solar air heater should be high to intensify heat transfer, but pressure drop should not exceed 100 Pa to limit the electric energy consumption of the fan.

Solar dryers with roof-integrated air heaters have also been developed for tropical countries. In Indonesia a solar processing center for cocoa and coffee found wider distribution (Mulato *et al.*, 1999). This unit consists of a low cost substructure sheltering all postharvest operations, such as fermentation, drying, grading, and storage under a common roof. The prototype was designed to cover a yearly processing capacity of 250 ons of wet cocoa beans, equivalent to 85 tons of dried beans, collected from 150 ha of smallholders farming area. To substitute scarce and expensive firewood that is commonly used as a fuel for high-temperature dryers on estates, a solar air heater is incorporated into the roof, Fig. 6.25.

The total effective surface area of the solar air heater installed on a 25° saddle roof is 144 m^2. Experiments showed that this angle provides good self-cleaning effects and optimal solar energy conversion. The solar air heater has a modular design using common construction materials, such as C-profile steel, plywood and sheet metal. Transparent corrugated polycarbonate sheets of 0.8 mm thickness and a transmittance for solar radiation of about 92% were used as the front cover, Fig. 6.26a.

The efficiency of the solar air heater was remarkably high with an intercept η_0 of more than 75% and a stagnation point of 0.08 K m^2 W^{-1}. Due to dust deposition and

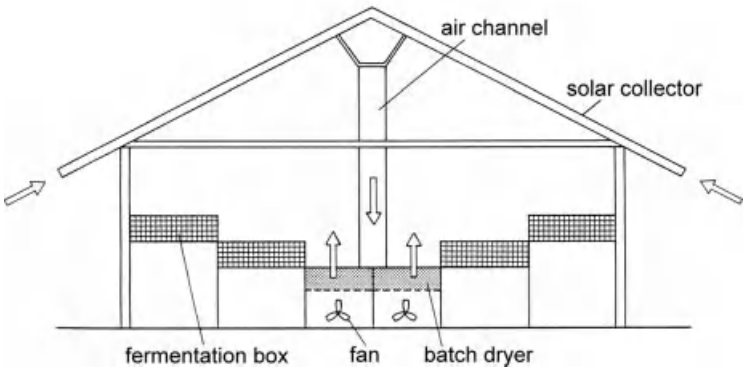

Fig. 6.25 Solar processing center with roof-integrated solar air heaters for cocoa in Indonesia (Esper and Mühlbauer, 1998).

discoloration by unavoidable chemical degradation, the transmittance of the polycarbonate sheets was reduced from 92 to 81% after 6 years of operation. However, the efficiency of the solar air heater was still higher than the efficiency of plastic foil solar air heaters after that time, Fig. 6.26b.

The solar air heaters are connected at the gable to a 12 m long horizontal air collecting duct. At the gable end a vertical air duct is installed, which is connected to the dryer by lateral ducts. To reduce heat losses the air ducts are heat insulated. Ambient air is sucked through the air gap between the transparent front cover and the absorber surface at an airflow rate between 2500 and 10 000 $m^3 h^{-1}$, depending on the number of fans in operation. The temperature of the drying air is maintained between 40 and 50 °C to prevent significant losses in fructose and glucose content of the cocoa. The time required to dry cocoa beans from 55 to 6% moisture content is 80 to 96 hours, whereas sun drying takes 120 to 140 hours. The increase in drying rate reduces the risk of spoilage and microbial infestation. Electricity requirement for the fans is 25 to 30 kWh, which is a small amount compared to the amount of water removed.

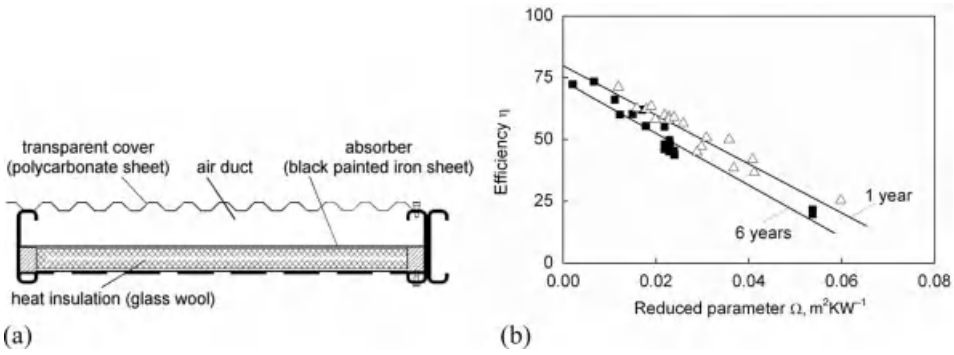

Fig. 6.26 (a) Cross-section of the roof-integrated solar air heater, and (b) efficiency curves for different periods of aging (Mulato, 2001).

6.5
Solar Drying Kinetics

Conventional high-temperature drying systems are continuously operated at set temperature and flow rate of the drying air and fluctuating weather conditions have no influence on the drying process. Various models are available to predict the course of drying under these stationary conditions (Mühlbauer, 2009). In contrast, drying kinetics in solar drying systems are characterized by a cascaded course of drying governed by the diurnal cycle of solar radiation as a major driving parameter for the drying air temperature and, hence, drying rate.

6.5.1
Empirical Drying Curves in Solar Drying

Figure 6.27 shows the drying kinetics of bananas in the solar tunnel dryer compared to traditional sun drying. In both cases, the drying product is spread in a single layer and exposed to solar radiation. In the solar tunnel dryer, however, incoming solar radiation is slightly reduced by the transparent cover foil. The drying rate accelerates with sunrise, passes through a maximum at noon, decelerates towards sunset, and ceases during the night. This drying behavior with decreasing moisture content during the day and stagnation during the night is known from traditional sun drying. In solar drying, however, the decrease during the day is more distinct due to the rise in drying air temperature in solar air heaters.

In contrast to the tunnel dryer, in the solar greenhouse dryer, the drying product is dried in thick layers, and not exposed directly to solar radiation, as the drying air is heated in roof-integrated solar air heaters. Figure 6.28a shows the typical cascaded drying characteristics for chamomile flowers dried in the solar greenhouse dryer. The drying time is increasing with specific load m_{spec} of the flatbed dryers, where m_{spec} is given in kg dry matter of drying material per m^2 of flatbed area. As long as the moisture content is high, drying progresses during the night, however, at a very low rate. At low moisture content, towards the end of drying, the drying material might even be remoistened by humid night air. As shown in Fig. 6.28b, the drying rate

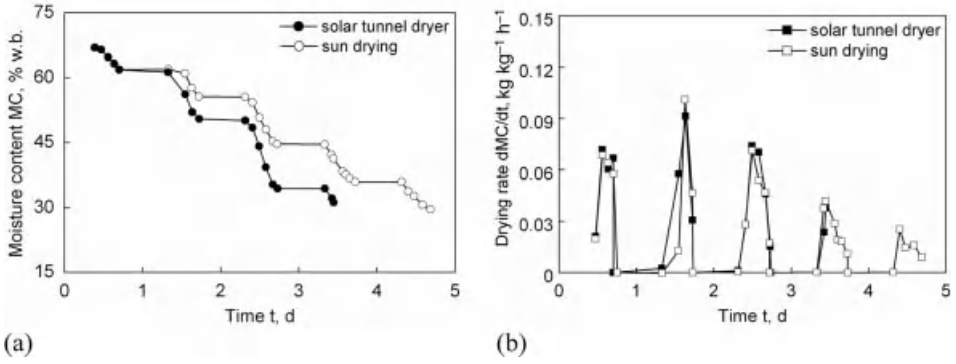

Fig. 6.27 Course of (a) moisture content MC and (b) drying rate dMC/d*t* of bananas in the solar tunnel dryer compared to traditional sun drying (Schirmer *et al.*, 1996).

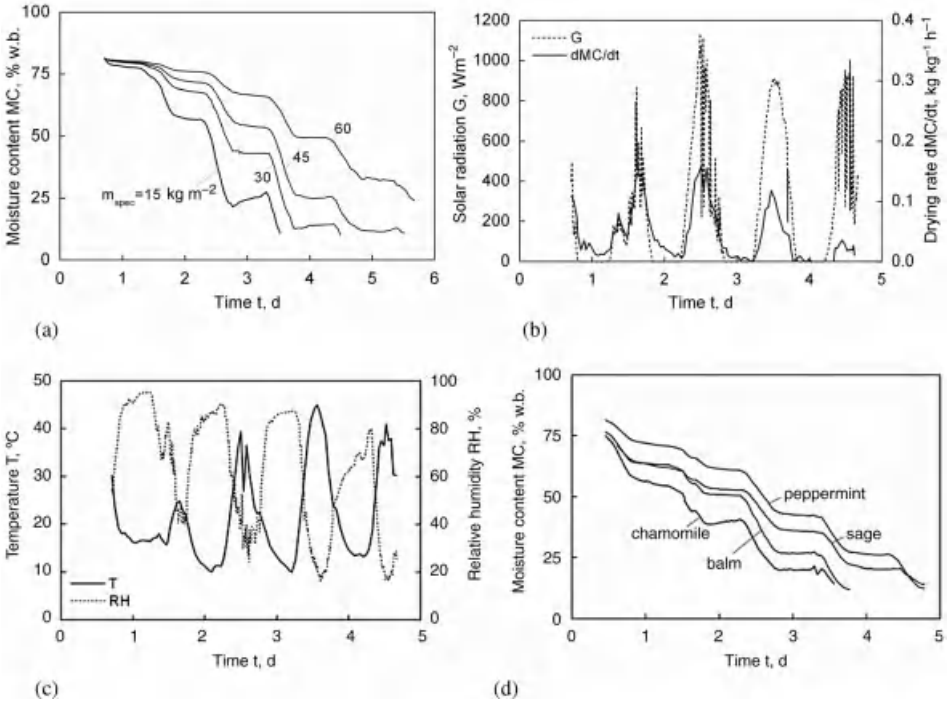

Fig. 6.28 Drying kinetics of medicinal plants in the solar greenhouse dryer; (a) course of moisture content MC of chamomile flowers for different specific loads, (b) course of solar radiation G and drying rate dMC/dt of chamomile flowers at a specific load m_{spec} of 45 kg m^{-2}, (c) course of temperature T and relative humidity RH of the drying air and (d) course of moisture content MC of chamomile, balm, sage and peppermint at a specific load m_{spec} of 20 kg m^{-2} (Müller, 1992b).

follows the course of solar radiation, not only in the systematic diurnal variation but also in the fluctuations caused by cloudiness, in which the potential daily maximum decreases with drying progress, as known from drying theory. In this way, solar radiation is the primary driving force for drying, because it governs the temperature and, thus, the relative humidity of the drying air, Fig. 6.28c. Although the drying behavior depends on the drying material, as shown for various medicinal plant species in Fig. 6.28d, the cascaded pattern of the drying curves does persist.

In spite of the fluctuating temperature in the solar greenhouse dryer there was no loss in product quality in terms of essential oil content measured before and after drying of various medicinal plants, as shown in Tab. 6.3.

6.5.2
Equilibrium Model for Solar Drying Kinetics

Both unsteady drying conditions and episodes of remoistening of the drying product are the reasons why drying models from high-temperature drying are not suitable to describe solar drying kinetics. Equilibrium models, developed for low-temperature in-storage drying systems are more suitable to be adapted to solar drying (Sharp, 1982).

Tab. 6.3 Drying characteristics of peppermint, balm, chamomile and sage in the solar greenhouse dryer.

Material		Peppermint	Balm	Chamomile	Sage
Initial moisture	%	82	77	75	71
Drying time	h	104	80	75	100
Capacity	$kg\,m^{-2}\,d^{-1}$	4.6	6.0	6.4	4.8
Heat requirement	$kJ\,kg^{-1}$	16 900	12 900	13 700	22 400
Evaporated water	$kg\,m^{-2}$	16.0	14.8	14.4	13.5
Essential Oil					
wet	%	2.52	0.13	0.46	2.37
dry	%	2.67	0.18	0.38	2.46

Due to the low temperature and airflow rate, these equilibrium models are based on the assumption that the saturation deficit of drying air is more decisive for drying than diffusion processes inside the drying material. As in monovalent solar drying systems, that is, in systems without back-up heating, higher temperatures around 50 °C are only achieved during short periods at high-noon, assumptions from low-temperature drying can be adopted. In that way an empirical model for approximation of solar drying curves was developed, based on three parameters: (i) the adjusted saturation deficit of the drying air ΔY_{adj} as the driving force for drying, (ii) the moisture content X d.b. of the drying material as the decelerating factor over the course of drying, and (iii) a drying coefficient c to consider specific drying behaviors (Müller, 1992a). The instantaneous drying rate $dX(t)/dt$ is estimated as:

$$\frac{dX(t)}{dt} = c \cdot X(t) \cdot \Delta Y_{adj} \tag{6.13}$$

where the average moisture content in the bulk $X(t)$ vs. drying time is calculated stepwise by time increments Δt:

$$X(t+\Delta t) = X(t) - \frac{dX(t)}{dt}\Delta t \tag{6.14}$$

In contrast to the common saturation deficit, the adjusted saturation deficit ΔY_{adj} is not calculated until total saturation of the air is reached (100% RH) but reaching instantaneous equilibrium relative humidity (ERH) of the drying material, which is given by the sorption isotherm. In Fig. 6.29 the determination of adjusted saturation deficit ΔY_{adj} is demonstrated in the Mollier diagram that represents a psychrometric chart. The adjusted saturation deficit changes sign as soon as the relative humidity of the drying air exceeds the ERH, resulting in a negative drying rate, which indicates episodes with remoistening of the drying material.

The falling characteristic of the drying rate dX/dt is taken account of by introducing the moisture content $X(t)$ of the drying material as a factor. This is justified because the drying rate is the first derivative of moisture content and, therefore, shows analogous exponential decrease with time. The specific drying behavior of drying

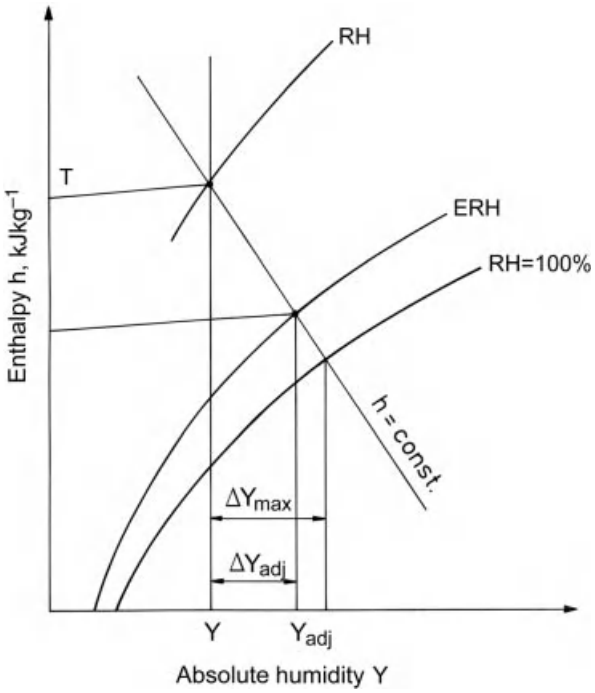

Fig. 6.29 Determining the adjusted saturation deficit ΔY_{adj} in a Mollier diagram.

products, the influence of bulk depth, and characteristics of the dryer are accounted for in the drying coefficient c that has to be established experimentally.

The model fits satisfactorily the experimental data of laboratory dryers with steady-state drying conditions, and of solar dryers with unsteady drying conditions, Fig. 6.30.

Drying coefficients c have been established for a couple of drying products and drying conditions, Tab. 6.4. When thick layers of drying material are dried in through-

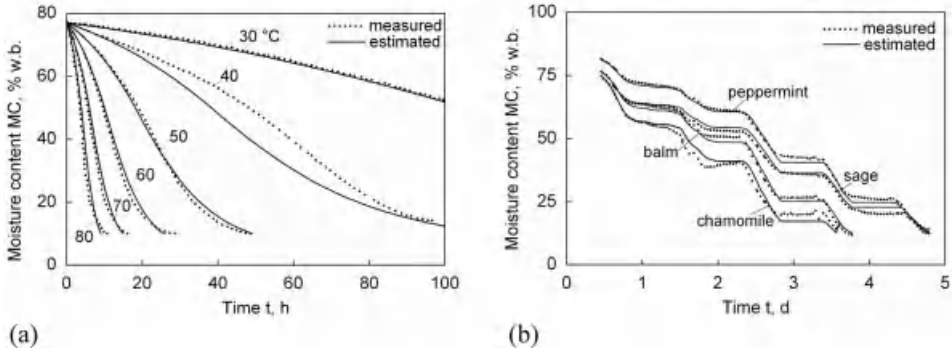

Fig. 6.30 Measured and estimated drying curves of grapes (a) for steady-state drying conditions in a laboratory dryer (Linckh, 1993), and (b) for unsteady drying conditions in the solar greenhouse dryer (Müller, 1992b).

Tab. 6.4 Drying coefficient c for different drying products and drying conditions (temperature T in °C, specific load m_{spec} in kg m^{-2}, air velocity v in m s^{-1}).

Product	Coefficient c	Drying process
Peppermint	$0.0089 + \frac{0.0185}{m_{spec}}$	Solar greenhouse dryer, bulk, through-flow, $v = 0.1$ m s^{-1} (Müller, 1992b)
Sage	0.0126	Solar greenhouse dryer, bulk, through-flow, $v = 0.1$ m s^{-1}, $m_{spec} \leq 40$ kg m^{-2} (Müller, 1992b)
Chamomile	$\frac{0.11}{m_{spec}}$	Solar greenhouse dryer, bulk, through-flow, $v = 0.1$ m s^{-1} (Müller, 1992b)
Chamomile	$0.045 \cdot T^2$	Laboratory dryer, thin layer, through-flow (Linckh, 1993)
Grapes	$0.014 \cdot \frac{T^2}{\ln(T)}$	Laboratory dryer, thin layer, through-flow (Linckh, 1993)
Grapes	$0.008 \cdot \frac{T^2}{\ln(T)}$	Laboratory dryer, thin layer, over-flow (Linckh, 1993)
Apricots	$0.2 \cdot \ln^3(T)$	Laboratory dryer, thin layer, over-flow (Linckh, 1993)
Apricots	$0.183 \cdot \ln^3(T) \cdot v^{0.45}$	Solar tunnel dryer, thin layer, over/under-flow (Esper, 1995)

flow mode, as in the flatbeds of the solar greenhouse dryer, the bulk depth has to be considered, which was done by introducing a specific load into the drying coefficient. When thin layers are dried, like in the solar tunnel dryer, bulk depth can be neglected but temperature is introduced into the drying coefficient to amplify the driving force of the adjusted saturation deficit.

By introducing the air velocity in the drying coefficient c, drying curves for unsteady airflow in a photovoltaic driven solar tunnel dryer can also be predicted with high accuracy, Fig. 6.31a. Hence, the model can be used to predict the drying behavior as soon as the drying coefficient c is established for a specific drying product and drying process. Figure 6.31b shows predicted drying curves for apricots in the

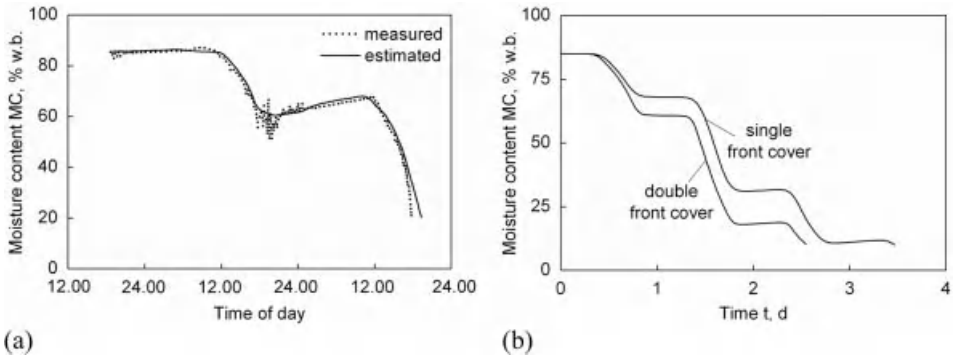

Fig. 6.31 (a) Estimated and measured drying curve of apricots in a solar tunnel dryer with photovoltaic driven fans (Esper, 1995), and (b) predicted drying curve for apricots in a solar tunnel dryer with different solar air heaters (Linckh, 1993).

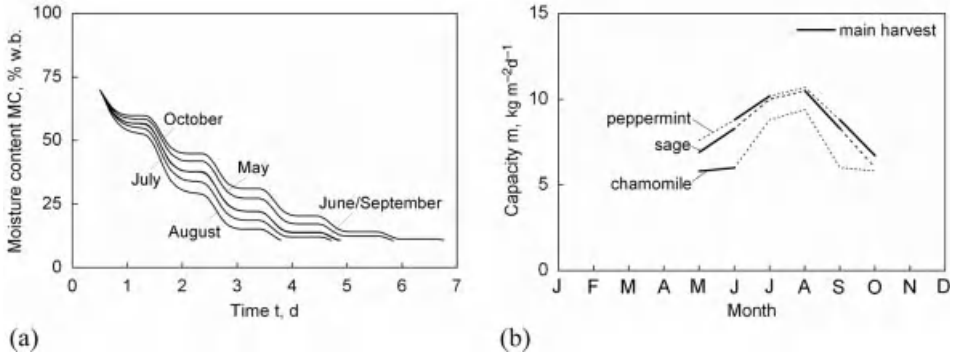

Fig. 6.32 (a) Estimated drying curves for sage ($m_{spec} = 40\,kg\,m^{-2}$) in the solar greenhouse dryer for different months under climate conditions of Novi Sad, Serbia (45.25 °N, 19.85 °E) and (b) estimated capacity of the solar greenhouse dryer for peppermint, sage and chamomile under climate conditions of Novi Sad (Müller, 1992b).

solar tunnel dryer when different air heater configurations are applied. Using a high-performance solar air heater with a double front cover, for example, reduces drying time by 30% compared to a version with a single front cover.

As the drying air conditions of solar dryers can be estimated on the basis of climate data and knowledge of the solar air heater performance, drying curves can be predicted for different seasons, Fig. 6.32a. Due to the strong influence of temperature on drying rate, drying time is shortest and, hence, dryer capacity is highest during the summer months. However, the harvest season of the drying product does not necessarily coincide with the maximum dryer capacity, which has to be considered in the sizing of drying facilities, Fig. 6.32b.

The model for solar drying kinetics based on saturation deficit of air shows a good quality of fitting for the investigated drying products and drying conditions. Further empirical research is required to establish the drying constant c for a wider range of drying products.

6.6 Control Strategies for Solar Dryers

In contrast to hot-air drying systems, where the flow rate and temperature of the drying air are kept within narrow ranges around set values by conventional control systems, solar drying systems require more complex control strategies to cope with the fluctuating characteristics of solar radiation. In the following, control strategies are discussed for damping the effect of system-inherent power lacks.

6.6.1 Airflow Management During the Night

During the night solar air heaters show no temperature rise, but rather a temperature decrease when the absorber is cooling down below ambient temperature due to long-wave radiation to clear sky. Therefore, solar dryers with natural convection show not

only low temperature during the night, but are also lacking exchange of air. This might lead to condensation of water on cool surfaces, especially when the moisture content of the drying product is still high, and drying still proceeds at low temperature. This might lead to corrosion of the construction and loss of quality of the drying material by fermentation and microbial growth. Management options are quite limited. In the case of small solar cabinet dryers, the drying product can be removed during the night to be stored indoors. For larger solar dryers this will not be practicable. Here, drying of a new batch should be started in the early morning to make use of a full day to reduce the moisture content of the drying material before the first night. As a consequence, however, the drying material has to be prepared during a night shift.

For solar dryers with forced convection a decision has to be made, whether the fans are operated during the night. On the one hand, the fans are consuming energy during the night without contributing to water removal. On the other hand ceasing the airflow could lead to spontaneous heating of the drying product, particularly when the moisture content is still high and bulks are dried, as in the solar greenhouse dryer. The recommended control strategy is overnight shutdown of the fans and temperature control inside the bulk to operate the fans when the temperature rises by spontaneous heating. A sensor can be placed in the bulk to detect the temperature rise. For drying medicinal plants, no heating occurred during the nights and 50% of the electrical energy input could be saved without loss of product quality. However, as a precautionary measure, the fans should be operated during the first night, to prevent fermentative processes in the drying product by the cooling effect of ventilating.

6.6.2
Recirculation of Drying Air

Due to the falling drying rate, the water vapor saturation of the exhaust air decreases during the course of drying. Therefore, the exhaust air that is still of higher temperature than the ambient air can be recirculated to the solar air heater for further temperature rise. By passing the bulk of the drying material, the specific humidity will rise as well. Therefore, the recirculation rate has to be controlled, with a trade-off between rising temperature and rising specific humidity in terms of maximizing drying rate having to be considered. As the saturation deficit, which is determined by both parameters, represents the driving force in drying very well, the recirculation rate can be controlled by maximizing the saturation deficit. As the saturation deficit cannot be measured directly, a microprocessor is required to calculate this parameter from the temperature and relative humidity of the drying air. Such a control algorithm increases the drying rate considerably. For example, the drying time of peppermint in the solar greenhouse dryer was reduced from 7 to 4 days, Fig. 6.33.

6.6.3
Back-Up Heating Systems

The capacity of solar dryers can be increased considerably by installing a fuel-fired back-up heating system that allows operation of the dryer round-the-clock and even in rainy weather conditions. These hybrid solar dryers, however, require additional investment and fossil energy.

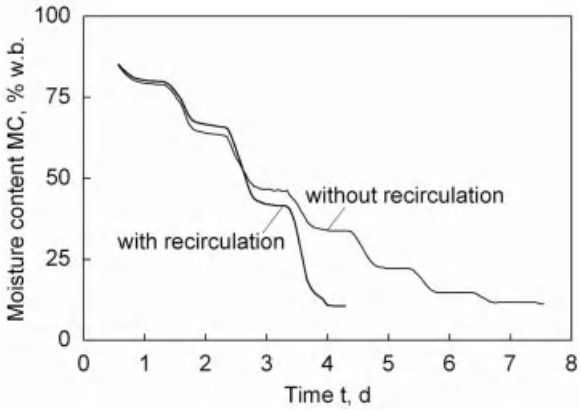

Fig. 6.33 Drying curve of peppermint in the solar greenhouse dryer with and without recirculation of drying air (Müller, 1992b).

The solar greenhouse dryer has a 110 kW oil-burning back-up heating system with a consumption of 11.5 l fuel oil per hour. The temperature rise in the heat exchanger is 30 K at an airflow of 6300 $m^3 h^{-1}$. This heated airflow is mixed with the drying air after having passed the solar air heater, Fig. 6.34. In this set-up, fossil back-up power of 1.75 kW per m^2 of absorber area is available.

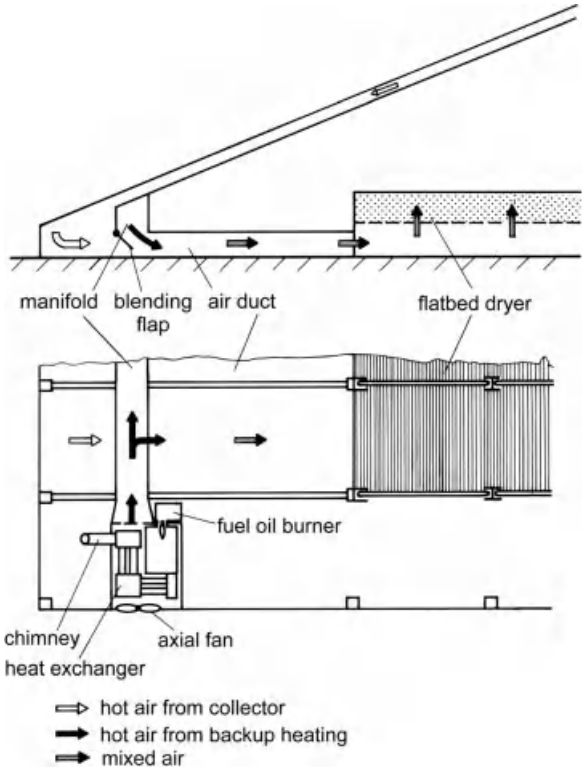

Fig. 6.34 Oil burning back-up heating system of the solar greenhouse dryer (Müller, 1992b).

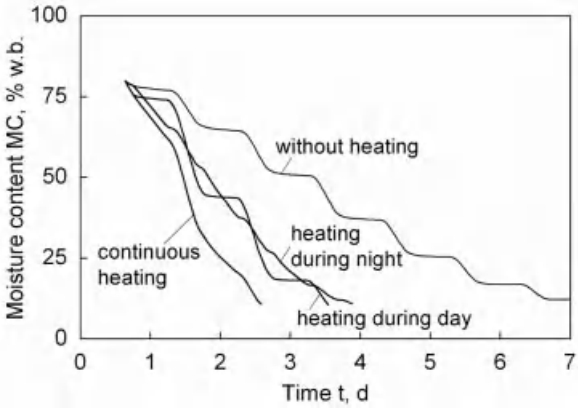

Fig. 6.35 Drying curves of peppermint in the solar greenhouse dryer with back-up heating system in different modes of operation: with and without additional heating as well as with additional heating during the day (6 am to 6 pm) or during the night (6 pm to 6 am) (Müller, 1992b).

Tab. 6.5 Capacity of the solar greenhouse dryer with back-up heating system together with specific consumption of fuel oil and electric energy per kg dried material for different modes of operation (Müller, 1992b).

Mode of Operation	Capacity ($kg\,m^{-2}\,d^{-1}$)	Fuel Oil ($l\,kg^{-1}$)	Electricity ($kW\,kg^{-1}$)
Without heating	4.4	—	1.10
Heating during night	9.2	1.1	0.71
Heating during day	10.3	1.0	0.31
Continuous heating	15.3	1.3	0.43

By thermostatic control, a threshold for drying air temperature can be set to avoid quality losses of the drying material due to overheating. For drying of peppermint, the drying time could be reduced from 7 to 2 days by operating the back-up heating system continuously, in which the threshold temperature of 50 °C was only reached during daytime, Fig. 6.35.

If the back-up heating is only to be operated for half the day to boost drying capacity, then daytime is more preferable than night time. When the back-up heating system is operated during daytime, the capacity of the solar dryer is higher at a lower specific consumption of electric energy because the fans are shut down at night, Tab. 6.5.

6.7 Economic Feasibility of Solar Drying

The method of evaluating the economic feasibility of solar drying facilities depends on whether they are competing with natural sun drying or with conventional hot air drying. When compared with natural sun drying, the investment costs of a solar drying system have to be outweighed by reduced deterioration of drying material and

by higher prices for better quality of the dried product. When compared to conventional hot-air drying and the same quality of the dried product is expected, the investment costs of solar air heating have to be outweighed by fuel savings. Consequently, the economic feasibility of solar drying depends on site-specific frame conditions and should be evaluated by the cost comparison method. The lower the costs per unit of a dried product the higher is the profitability of this drying method. Total drying costs result from variable and fixed costs. Variable costs arise from thermal and electrical energy demand and labor, while fixed costs are the costs of investments, calculated as annuity AN:

$$\mathrm{AN} = (A - S \cdot q^{-n}) \cdot \frac{q^n \cdot (q-1)}{q^n - 1} + A \cdot \frac{r}{100} \tag{6.15}$$

with total investment cost A, salvage value S, depreciation period n, repair cost rate r and the interest coefficient q that is based on an interest rate i:

$$q = 1 + \frac{i}{100} \tag{6.16}$$

To compare solar drying systems with traditional drying systems that are causing quantitative and qualitative losses of drying product, the payoff period PO of the additional investment can be calculated (Finck and Oelert, 1983):

$$\mathrm{PO} = \frac{\ln \frac{\Delta C}{\Delta A} - \ln\left(1 + \frac{\Delta C}{\Delta A} - q\right)}{\ln q} \tag{6.17}$$

where ΔA are the additional investment costs of a solar dryer compared to traditional drying and ΔC is the difference in drying costs per unit including the opportunity costs OC caused by quantitative product losses and lower producer price due to reduced product quality when sticking to traditional drying.

In the following, case studies of cost comparisons between solar and conventional hot air drying are presented.

6.7.1 Drying of Timber in Brazil

In Brazil, eucalypt timber for the furniture industry is mostly dried in hot-air dryers that are imported from Europe or the USA. In an economic study, the solar-assisted timber dryer was compared with a hot-air dryer, both exported from Germany to Brazil in a sea freight container. The chamber capacity of the solar dryer was 220 m^3 and that of the hot-air dryer 130 m^3 (Bauer, 2003). Table 6.6 shows the composition of investment costs for both dryers.

In spite of the larger chamber capacity, the purchase price was lower for the solar dryer, mainly because a greenhouse was used as housing instead of a steel plate housing as used for the hot-air dryer. Taxes contributed considerably to the investment costs, so that the total investment costs of the solar dryer were about one third lower than that of the hot-air dryer.

The drying costs per unit, calculated in US$ per m^3 of dried eucalypt timber, are listed in Tab. 6.7. The annuity for the transparent cover foil of the solar dryer has been

Tab. 6.6 Investment costs for the solar dryer and a hot-air dryer for timber in Brazil (Bauer, 2003).

Cost Category	Solar Dryer US$	Hot-air Dryer US$
Purchase price	51 445	88 534
Taxes	24 863	42 085
Fees and insurance	2703	2890
Transport (sea freight)	3849	3849
Heating system	13 818	17 960
Construction work	3370	2855
Total	100 047	158 172

calculated separately, because the depreciation period is shorter than that of the other system components.

Although drying time per batch of timber in the solar dryer (27 days) was longer than in the hot-air dryer (22 days), the annual drying capacity was higher in the solar dryer (2970 m^3 per year) than in the hot-air dryer (2140 m^3 per year), because of the larger drying chamber of the solar dryer. Consequently, the fixed costs per unit resulting from the annuity were considerably higher for the hot-air dryer than for the solar dryer. The variable costs comprise, beside expenditures for fuel wood, electricity, and labor, also the interest for timber as drying is causing a dryer specific delay of the purchase according to the required drying time. The costs for electrical energy were noticeably higher in the hot-air dryer than in the solar dryer due to the higher velocity of the drying air, and a corresponding high pressure drop. In total, the drying cost per unit was considerably lower for the solar dryer with 9.13 US$ per m^3 than for the hot-air dryer with 21.29 US$ per m^3. However, the difference is mainly caused by the higher investment costs of the hot-air dryer, and its high consumption of electrical energy for the fans. The fuel cost savings by the use of solar energy for heating is limited to 0.70 US$ per m^3.

Tab. 6.7 Fixed and variable drying costs per m^3 eucalypt timber in the solar dryer and in a hot-air dryer for timber in Brazil (Bauer, 2003).

Cost category	Solar dryer US$ per m^3	Hot-air dryer US$ per m^3
Fixed Costs		
Investment dryer ($n = 15$ yr)	4.10	9.01
Investment cover foil ($n = 10$ yr)	0.12	—
Maintenance and repairs ($r = 5\%$)	1.40	3.04
Variable Costs		
Fuel wood	0.35	1.05
Electricity	1.40	6.32
Labor	0.59	0.82
Interest for timber ($i = 12\%$)	1.17	1.05
Total	9.13	21.29

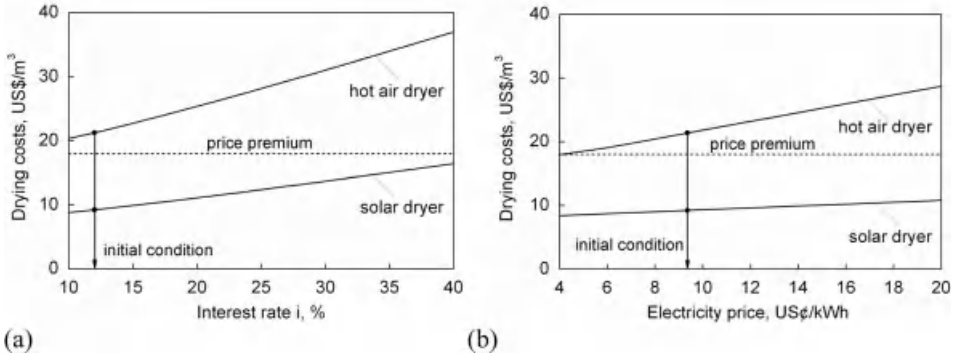

Fig. 6.36 Sensitivity of drying costs of the solar dryer and the hot-air dryer in terms of (a) the interest rate for Brazilian bank credits and (b) electricity prices (Bauer, 2003).

To estimate the sensitivity of drying costs to changing frame conditions, results of a sensitivity analysis are shown for interest rate and electricity price in Fig. 6.36.

Due to the unstable currency in many developing countries, interest rates are typically high, and might even exceed 50%. For this study special credits from the Brazilian bank of development (BNDES) at an interest rate of 12% were available. Since this type of credit is not available for all investors, the influence of the interest rate on the total drying cost for investment credits between 10 and 40% was analyzed. Due to the higher investment costs, a rising interest rate has a higher influence on the absolute drying costs in the case of the hot air dryer compared to those of the solar dryer.

The electricity price in Brazil was 0.94 US$ per kWh during the time of the study. However, higher prices are expected in the future. An increase in the electricity costs would have a bigger influence on the hot-air dryer than on the solar dryer due to its significantly higher electrical energy consumption. At a price premium of 18 US$ that was paid for dried over fresh sawn timber, only solar drying was profitable under the prevailing frame conditions.

6.7.2
Drying of Tobacco in Brazil

In Brazil high quality tobacco leaves for cigar wrappers are traditionally dried in curing barns heated by open charcoal fires. In an economic study, the greenhouse-type solar dryer for tobacco was compared with such a conventional curing barn. Both systems were designed for an annual capacity of 5350 kg dried tobacco leaves, which is achieved by different sizes because of differences in loading density and drying time. For the solar dryer 220 m^2 ground area is sufficient, whereas for the conventional curing barn 960 m^2 is required. In Table 6.8 the investment costs of both systems are listed.

Although the solar dryer is smaller than the conventional curing barn, the investment costs are considerably higher, due to the more sophisticated steel construction, the back-up heating system and the electrical installation, including a sensor-based control system.

Tab. 6.8 Investment costs for the solar dryer and a conventional curing barn for tobacco in Brazil (Bux, 1996; Bux *et al.*, 1997).

Cost Category	Solar Dryer US$	Curing Barn US$
Foundation	383	1470
Building	11 639	7997
Interior fitting, drying rack	12 174	5147
Construction work	3005	2668
Back-up heating system	2833	—
Electrical installation	7577	—
Total	37 611	17 282

Drying costs per kg of tobacco were calculated based on an interest rate i of 14% and a depreciation period n of 20 years for the steel construction of the solar dryer and 10 years for all other building components. The repair rate was set to 2% for the solar dryer and 8% for the curing barn because the latter requires frequent maintenance and repairs.

As shown in Tab. 6.9, fixed costs are higher for the solar dryer than for the conventional curing barn. Among the variable costs, expenses for energy are higher for the curing barn because of the requirement for charcoal. In total, drying costs are higher in the conventional curing barn, mainly because of the opportunity costs, which are caused by a 5.2% loss of tobacco leaves and a lower price of 19.5 US$ per kg of conventionally dried tobacco compared to 21.0 US$ per kg for solar dried tobacco.

Under prevailing conditions in Brazil the pay-off period of the solar dryer was 2.2 years. As the profitability of the solar dryer is mainly governed by investment costs and opportunity costs, the sensitivity of the pay-off period for those two parameters is depicted in Fig. 6.37.

Tab. 6.9 Fixed and variable drying costs per kg tobacco in the solar dryer and in a conventional curing barn as well as opportunity costs by loss of benefits when using a conventional curing barn instead of a solar dryer (Bux, 1996; Bux *et al.*, 1997).

Cost Category	Solar Dryer US$ per kg	Curing Barn US$ per kg
Fixed Costs		
Investment dryer	1.06	0.55
Maintenance and repairs	0.14	0.26
Variable Costs		
Energy	0.16	0.45
Labor	0.80	0.78
Opportunity Costs		
Quantitative loss	—	1.20
Qualitative loss	—	1.50
Total	2.16	4.74

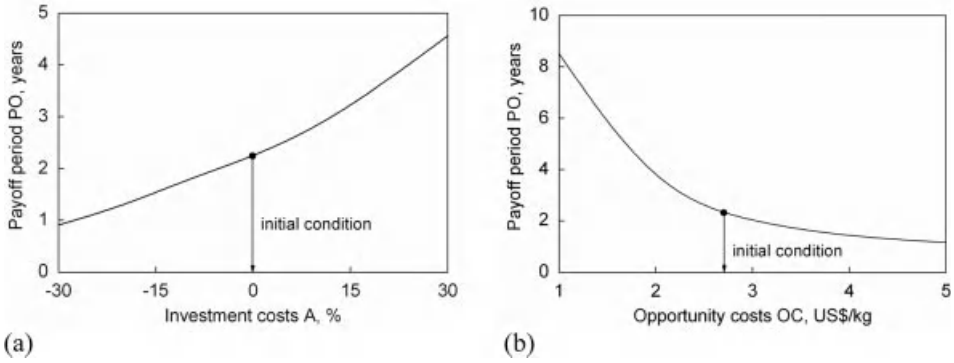

Fig. 6.37 Sensitivity of the pay-off period PO of the solar tobacco dryer for (a) investment cost *A* and (b) opportunity costs OC (Bux, 1996; Bux *et al.*, 1997).

A 30% increase in investment costs would prolong the pay-off period from 2.2 to 4.5 years. However, as the lifetime of the solar dryer is more than 10 years, the investment would still be profitable. Increasing opportunity costs of conventional curing barns are causing an exponential decrease in the pay-off period of the solar dryer. Decreasing opportunity costs would prolong the pay-off period markedly. This could happen, for example, if no price premium was paid for the higher quality of solar dried tobacco. The benefits of solar drying would then be limited simply to prevention of quantitative losses.

The example of solar drying of tobacco depicts a typical situation in developing countries where solar drying is replacing natural sun drying or other low-cost traditional drying methods. Here, the profitability of solar drying depends on low investment costs for the solar dryer and price premiums for the higher quality of solar dried products. This requires local production of solar dryers to avoid sea freight costs and tax on imports, and a marketing system with graduation of prices according to product quality.

6.8 Conclusions and Outlook

Solar drying is an essential improvement of natural sun drying by enforcing air flow and drying temperature by the use of solar air heaters. Besides increasing the drying rate, which reduces the risk of fermentative heating and mold development, the drying product is protected from environmental impacts such as rain, dew, dust, insects and rodents. However, even basic improvements, such as using plastic foils as transparent cover, lead to investment costs that have to be compensated by reduced quantitative and qualitative losses of drying products. Typically, in developing countries, incentives for improved drying of stable crops are missing, because better quality of the dried product does not realize higher prices. For high-value crops, such

as fruit, medicinal plants, or spices the situation is more favorable, because high quality of dried products offers access to international markets.

In industrialized countries solar air heaters can be integrated into conventional hot-air drying systems to substitute fossil fuel. However, the integration of an energy source of fluctuating power, such as solar radiation, requires additional efforts in terms of investment and management skills, so that, at current energy prices, the use of solar energy in drying is still limited to certain niche applications.

For the next decades, social and environmental development will be increasingly affected by population growth, increasing food requirements, depletion of fossil energy resources, and climate change by greenhouse gas emissions. Consequently, the need for efficient food processing on the one hand, and the need for reduction of fossil energy consumption on the other hand, will increase considerably. With this background there are bright prospects for a broad dissemination of solar drying technologies. Fortunately, research and development in this field, which has seen early heydays following the oil crisis in the 1970s, is already gaining momentum by increasing energy prices and emission taxes.

6.9 Additional Notation Used in Chapter 6

A	investment cost currency	
AN	annuity currency	
b	collector breadth	m
C	cost currency	
c	drying coefficient	s^{-1}
ERH	equilibrium relative humidity	–
F'	air heater efficiency factor	–
G	solar radiation	$W\ m^{-2}$
i	interest rate	%
k_{clear}	clearness index	–
MC	solids moisture content (wet basis)	
m	dryer capacity per time and area	$kg\ m^{-2}\ s^{-1}$
m_{fluid}	airflow rate per absorber area	$kg\ m^{-2}\ s^{-1}$
m_{spec}	dryer load per area	$kg\ m^{-2}$
n	day of year	–
n	depreciation period	–
OC	opportunity cost currency	
PO	payoff period	years
Q	power per area	$W\ m^{-2}$
q	interest coefficient	–
RH	relative humidity	–
r	repair cost rate	%
S	salvage value currency	
U	overall heat loss coefficient	$W\ m^{-2}\ K^{-1}$

Greek Letters

α	absorptance	–
α_{albedo}	coefficient of ground reflectance	–
β	slope of collector surface grad (°)	
γ	azimuth of collector surface grad (°)	
δ	declination grad (°)	
ε	emittance grad (°)	
θ	angle of incidence grad (°)	
τ	transmittance	–
φ	latitude grad (°)	
Ω	reduced solar air heater parameter	$m^2\,K\,W^{-1}$
ω	hour angle grad (°)	

Subscripts

a	absorber
adj	adjusted
ambient	ambient
back	at the back
beam	beam radiation
c	cover
diffuse	diffuse sky radiation
e	effective
ex	extraterrestrial
f	fluid
front	at the front
L	at a certain axial position
S	to the south
s	sky
use	useful
Z	to the zenith
β	on the surface with slope β
0	intercept
0	solar constant

Abbreviations

DC	direct current
E	east
EVA	ethylene-vinyl acetate
LPG	liquefied petroleum gas
N	north

PE	polyethylene
PMMA	poly (methylmethacrylate)
PTFE	polytetrafluoroethylene
PV	photovoltaic
PVC	polyvinyl chloride
S	south
UV	ultraviolet
W	west

References

Adam, E., 1998. *Solar drying of sliced onion and quality attributes as affected by the drying process and storage conditions.* Diss., Universität Hohenheim, Germany.

ANSI/ASHRAE , 1986. Methods of testing to determine the thermal performance of solar collectors. ASHRE 93-1986, Atlanta, USA, 41 pp.

Bauer, K., 2003. *Development and optimisation of a low-temperature drying schedule for Eucalyptus grandis (Hill) ex Maiden in a solar-assisted timber dryer.* Diss., Universität Hohenheim, Germany.

Bux, M., 1996. *Entwicklung eines solargestützten Trocknungsverfahrens für Zigarrentabak*. Diss., Universität Hohenheim, Germany.

Bux, M., 2001. Solar-assisted drying of timber in industrial scale. *Agr. Eng*. **7** (1–4): 7–15.

Bux, M., Arnold, M., Serrano, P., Mühlbauer, W., 1997. Curing cigar tobacco with solar energy. *Tob. J. Int*. **2**: 22–25.

Bux, M., Bauer, K., Mühlbauer, W., Conrad, T., 2001. Solar-assisted drying of timber in industrial scale. *S. Afr. Forest. J*. **192**: 73–78.

Chen, P. Y. S., Helton, C. E., 1989. Design and evaluation of a low-cost solar kiln. *Forest Prod. J*. **39**(1): 19–22.

Duffy, J. A., Beckmann, W. A., 1980. *Solar energy of thermal processes.* John Wiley & Sons, New York.

Eissen, W., 1983. *Trocknung von Trauben mit Solarenergie.* Diss., Universität Hohenheim, Germany.

Eissen, W., Mühlbauer, W., Kutzbach, H. D., 1985. Solar drying of grapes. *Drying Technol*. **3**(1): 63–74.

Esper, A., 1995. *Solarer Tunneltrockner mit photovoltaischem Antriebssystem*. Diss., Universität Stuttgart, Germany.

Esper, A., Mühlbauer, W., 1996. Solar tunnel dryer for fruits. *Plant Res. Dev*. **44**: 61–80.

Esper, A., Mühlbauer, W., 1998. Solar drying – An effective means of food preservation. *Renew. Energ*. **15**: 95–100.

Finck, H., Oelert, G., 1983. *Leitfaden zur Berechnung der Wirtschaftlichkeit von Investitionsvorhaben zur Energieversorgung.* Gesellschaft für Technische Zusammenarbeit (gtz), Eschborn, Germany.

Guzman, J. A., Lauterbach, A., Jordan, R. C., 1985. Performance of wood solar kilns with box type collector. *Energy Agric*. **4**: 243–252.

Häuser, M., 1995. *Trocknung von Aprikosen mit Solarenergie.* Diss., Universität Hohenheim, Germany.

Häuser, M., Oechsle, P., Mühlbauer, W., 1995. Solar drying of apricots in Morocco. *Acta Hortic*. **384**: 645–649.

Huang, B. K., Ozisik, M. N., Toksoy, M., 1981. Development of greenhouse solar drying for farm crops and processed products. *AMA* **12** (1): 47–52.

Janjai, S., Intawee, P., Kaewkiew, J., Sritus, C., Khamvongsa, V., 2010. A large-scale solar greenhouse dryer using polycarbonate cover: Modeling and testing in a tropical environment of Lao Peoplele's Democratic Republic. *Renew. Energ*. **36**: 1053–1062.

Linckh, G., 1993. *Thermodynamische Optimierung von Luftkollektoren für solare Trocknungsanlagen*. Diss., Universität Hohenheim, Germany.

Marais, G., 1982. Solar drying tunnel. *Wood S. Am*. **7**(9): 26.

Mühlbauer, W., 1979. Drying of agricultural products with solar energy in the Federal Republic of Germany. *Proceedings of the German-Greek Solar Conference*, 24 April 1979, Chania, Greece, pp. 1–18.

Mühlbauer, W., 2009. *Handbuch der Getreidetrocknung – Grundlagen und Verfahren*. Agrimedia GmbH, Clenze, Germany.

Mühlbauer, W., Esper, A., 1995. Solar air heaters – State of the art and future perspective. *Proceedings of the ISES Solar World Congress*, 11–15 Sept. 1995, Harare, Zimbabwe, pp. 310–321.

Mulato, S., 2001. *Development and evaluation of a solar cocoa processing center for cooperative use in Indonesia*. Diss., University of Hohenheim, Germany.

Mulato, S., Atmawinata, O., Yusianto, Handaka, Pass, T., Mühlbauer, W., Esper, A., 1999. Development of a solar cocoa processing center for cooperative use in Indonesia. *The Planter* **75**(875): 57–74.

Müller, J., 1992a. Prediction of drying rate for solar drying. *American Society of Agricultural Engineers: International Summer Meeting*, 21–24 June 1992, Charlotte, North Carolina, ASAE-Paper No. 926040, pp. 1–7.

Müller, J., 1992b. *Trocknung von Arzneipflanzen mit Solarenergie*. Diss., Universität Hohenheim, Germany.

Müller, J., Conrad, T., Tesic, M., Sabo, J., 1993. Drying of medicinal plants in a plastic-house type solar dryer. *Acta Hortic*. **344**: 79–85.

Müller, J., Reisinger, G., Kisgeci, J., Kota, E., Tesic, M., Mühlbauer, W., 1989. Development of a greenhouse-type solar dryer for medicinal plants and herbs. *Sol. Wind Technol*. **6**(5): 523–530.

Oliveira, L. C. S., Skaar, C., Wengert, E. M., 1982. Solar and air lumber drying during winter in Virginia. *Forest Prod. J*. **32** (1): 37–44.

Orgill, J. F., Hollands, K. G. T., 1977. Correlation equation for hourly diffuse radiation on a horizontal surface. *Sol. Energy* **19**(4): 357–359.

Pfister, T., 1986. *Heubelüftung mit Sonnenkollektoren*. Flawil, Switzerland.

Schirmer, P., Janjai, S., Esper, A., Smitabhindu, R., Mühlbauer, W., 1996. Experimental investigation of the performance of the solar tunnel dryer for drying bananas. *Renew. Energ*. **7** (2): 119–129.

Sharp, J. R., 1982. A review of low temperature drying simulation models. *J. Agr. Eng. Res.* **27**: 169–190.

Sodha, M. S., Bansal, N. K., Kumar, A., Bansal, P. K., Malik, M., 1987. *Solar crop drying*. CRC Press, Boca Raton, USA.

Stoy, B., 1988. *Wunschenergie Sonne*. Energie-Verlag, Heidelberg, Germany.

Thekaekara, M. P., Drummond, A. J., 1971. Standard values for the solar constant and its spectral components. *Nature Phys. Sci*., **229**, 6–9.

Trim, D. S., Ko, H. Y., 1982. Development of a forced convection solar dryer for red peppers. *Trop. Agr. (Trinidad & Tobago)* **59** (4): 319–323.

7
Energy Issues of Drying and Heat Treatment for Solid Wood and Other Biomass Sources

Patrick Perré, Giana Almeida, and Julien Colin

7.1
Introduction

This chapter is devoted to energy issues related to biomass processing, more specifically to the drying and heat treatment of biomass. Section 7.2 is a rapid overview of production, harvesting, technological properties, and processing of biomass as an engineering material, and/or for energy purposes. Section 7.3 is more specifically devoted to the energy consumption during the wood drying operation, namely for solid wood. Section 7.4 presents two important processing operations of biomass, drying and heat treatment, when used for energy purposes: their impact on properties and the energy issues of the process itself.

7.2
Wood and Biomass as a Source of Renewable Material and Energy

In 2007, the world carbon dioxide emissions from human activities are estimated to be 35 Gt, of which 80% are due to the use of fossil hydrocarbons (UN Statistic Division, 2010). About one third of this additional atmospheric greenhouse gas is absorbed in the biosphere by photosynthesis. However, the other part remains in the atmosphere and contributes to global warming (IPCC, 2007). Moreover, the renewal of the reserves of hydrocarbons is very slow leading to a progressive exhaustion of fields. Some studies evaluate the total exhaustion of oil by 2050 and of coal in 150 years (IFP, 2008). The increase in the atmospheric carbon dioxide content and the rarefaction of the hydrocarbons encourage society to develop new ways of energy and materials production.

In this context the authorities encourage the use of renewable energies and agreed on objectives for the replacement of fossil fuels. In 1997, many countries ratified the Kyoto protocol, which fixes objectives for reduction of greenhouse gases emissions for 2012 compared to 1990: most of the European Union countries must reduce their emission by 8% (UN, 1997).

Modern Drying Technology Volume 4: Energy Savings, First Edition.
Edited by Evangelos Tsotsas and Arun S. Mujumdar

On the scale of humanity, the solar energy can be considered as renewable, or at least perennial. For comparison, the yearly consumption of energy is about 11.3 Gtoe, whereas the yearly solar flux at the surface of the Earth is about 92×10^3 Gtoe (BP, 2010). The energy received at the surface of the Earth being about 10^4 times higher than consumption, the sun has a great potential to cover our needs if we can exploit a tiny part of this flux. To that end, we have to be able to harvest, to store, and to distribute it. Obviously, this energy can be exploited directly by means of solar panels (photovoltaic or thermal). However, there are also alternative methods, such as using the mechanical energy of wind or chemical energy from biomass. In the latter case, plants harvest and store, naturally and efficiently, the solar energy by photosynthesis: each year about 105 Gt of atmospheric carbon dioxide is reduced to organic molecules (Field, 1998) which amounts to 71 Gtoe (FAO, 1997) that is, seven times the world energy consumption. So the plant kingdom is the most important primary producer of organic fuels in the biosphere. The biomass can be oxidized via various processes (natural or artificial) and release the stored energy. The carbon dioxide emissions from the utilization of bioresources are then balanced by the photosynthesis, which explains the renewable character of the energy coming from biomass.

Nowadays, energy recovery from biomass accounts for only 10% of the global energy consumption. However, it corresponds to about 50% of the renewable energy consumed on Earth (IFP, 2008). A policy promoting bioenergies will thus have a significant impact on the proportion of total energy consumption covered by renewable energies. Furthermore, the biosphere is the only renewable source of carbon molecules. So, because it is the only alternative to oil for the production of liquid fuels and carbon chemistry, the biosphere, and in particular the plants, will be more and more involved as raw resources.

Currently the combustion of wood represents the main part of bioenergies (World Energy Council, 2007). Traditionally, the produced energy is used for heating and cooking. For example, in France the authorities encourage the increase in the production of heat from wood, mainly in communal housing and in industry. This will also result in an increase in electricity production from biomass by cogeneration. Concerning the individual housing, it is planned that the wood fuel consumption should remain constant until 2020. However, thanks to improvement in the equipment, a doubling of homes heated with wood is expected (MEEDDAT, 2008).

Meanwhile, in the coming decades, the proportion of biomass converted to biofuels will increase. At the end of 2010, the use of biofuels has to reach 7% in France. First generation biofuels can, thus, substitute the fuels of fossil origin to a more or less large extent. On the one hand, ethanol is produced in biorefineries from saccharose (from sugar cane, beet, etc.) or starch (from cereals, potatoes, etc.) and is added to petrol (E10, E85). On the other hand, diester is produced from vegetable oils (rapeseed, sunflower, etc.) as an additive to diesel oil. In 2006, their production was 24.4 Mtoe divided into 40 Mm^3 of ethanol and 3 Mm^3 of diester (IEA, 2008). The yields of the processes depend strongly on the raw material. The production of ethanol as a fuel from sugar cane is proof of the efficiency of the conversion of biomass to energy: the EROEI (energy returned on energy invested) is estimated from

3 to 10 (Solomon, 2010; Hammerschlag, 2006; Dias De Oliveira *et al.*, 2005). The conversion of corn is another example of a first generation biofuel production which is common in the USA. Unfortunately, the relevance is arguable: the EROEI is often in the range of only 1.1 to 1.65 (Hall *et al.*, 2009; Dias De Oliveira *et al.*, 2005; Solomon, 2010). Though in both cases ethanol is obtained by alcoholic fermentation thanks to microorganisms, the amount of fermentable sugar is higher in sugar cane than in corn. Furthermore, the raw materials used for these syntheses are also basic ingredients for human food. As a result, the society, through numerous environmentalist organizations, has questioned the sustainability of such productions.

Thus, it is planned that a second generation of biofuels will replace the first one. These biofuels will be produced from lignocellulosic material. Except in seeds and in storage organs, this is the major constituent of the higher plants: for example we can find it in large quantities in wood and agricultural wastes (straw, pulp, bagasse, etc.). The lignocellulosic material, naturally synthesized by plants in their cell wall, is an entanglement of polymers among which cellulose and lignin are two of the main components. They are carbohydrates and polyphenols, respectively, which are hardly hydrolyzable and non-digestible by humans. Their energy recovery is, therefore, not in direct competition with agri-food uses. Cellulose is the most abundant organic matter on Earth. The world resource is estimated at more than 10^{11} tons, 80% being in forests. Lignin is the second most common biopolymer. Together, both components represent more than 70% of the biosphere (Stevanovic and Perrin, 2009). Moreover, lignocellulosic material has an interesting higher heating value, about 19–20 MJ kg^{-1} (Demirbas, 1997). So, it is an interesting and huge source of carbonaceous polymers which can be used as energy, as materials or as molecules for chemistry.

Cropping systems have been developed to produce lignocellulosic biomass in abundance. First, they can be dedicated to the production of biomass. In this case, the used crop plants are often not edible (*Miscanthus* × *giganteus*, hemp, eucalyptus, poplar, etc.). Second, the agricultural or silvicultural wastes can be accumulated and then converted into biofuels, which optimizes the added value of the harvest because all the plant is used. Indeed, these residues can represent an important part of the plant: the production of wheat straw can reach 10 t ha^{-1} $year^{-1}$ and, in high forests, the crop of oak and beech represents 0.8 to 1.5 tons of wood per m^3 of timber. Systems of biomass production with a long cycle are considered as ecologically beneficial because they are not, or only moderately, man-made: ecosystems have then time to develop. From this point of view the traditional forest management (40 to 200 year long cycle) has to be preferred to short or very short rotation coppice (2 to 10 year long cycle) and annual or bi-annual crop. In any case, a sustainable production of biomass will be of the utmost importance (Patzek and Pimentel, 2005).

The energy recovery from lignocellulosic biomass seems at first sight perfectly suited to replace fossil fuels: this biomass is renewable, abundant, and does not compete directly with human food. Nevertheless, the production of bioenergies must be conducted in a framework of sustainable development. The quantity of biomass used must be reasonably low, so that the surfaces of primary production can remain constant: on Easter Island, manufacture and transport of the monolithic statues

ended when the island was completely cleared of trees. The collection of agricultural and forest residues makes sense only if the durability of soil fertility can be ensured (ADEME, 2005). Moreover, all the biomass produced is not available for energy. Some areas have to be protected from any human activity to preserve ecosystems, and being the primary producers of the biosphere, plants are the first link of most tropical nutrition chains. Animals consume a large part of the lignocellulosic biomass and we must be careful not to disturb the equilibrium by an overexploitation of this natural resource. Finally, even if the energetic use of lignocellulosic material does not compete directly with nutrition, it is necessary to consider that, with the development of new ways of biomass valuation, and with world population growth, a strong pressure will be applied on farmlands. Indirectly, bioenergies and biomaterials are going to compete with food production. The fact remains that the harvest of biomass must be increased on a fundament of sustainable development.

Two conversion route types can be implemented to produce liquid fuel from the lignocellulosic material. Cellulosic ethanol is obtained by addition of synthetic enzymes in the aqueous phase. Biomass to liquid (BTL) is a dry multistage process thanks to which synfuels (by gasification and Fischer-Tropsch synthesis) or bio-oil (by flash pyrolysis) are produced. These second generation processes can use the whole plants and do not produce such a large quantity of waste as the first generation ones, which use only the fermentable sugars or the oils. This explains why their yield is usually higher. Today, the EROEI for cellulosic ethanol reaches values between 4.4 and 6.1 (Hammerschlag, 2006) and it will continue to rise with further improvement of the processes.

Moreover, we should not lose sight of the fact that energy production is not the only use of lignocellulosic material. A significant part is used for materials manufacturing. In 2009, 257 Mm^3 of timber were sawn and used for construction or furniture fabrication (FAO, 2010). The material integrity is unchanged, and its quality depends mainly on the properties it has acquired during its synthesis (stiffness, breaking strength, density, etc.). The original material can also be deconstructed and implemented in composites. In 2009, the world production of medium density fiberboard (MDF) panels was estimated to be 55 Mm^3 (FAO, 2010). Hemp fibers can also be incorporated into plastics to improve their mechanical properties and reduce their carbon footprint. These are just a few examples of the use of lignocellulosics as engineering materials.

Different technological properties of lignocellulosic materials must be considered, depending on their use: as *engineering material* or for *energy*. Hereafter, some important properties concerning the mentioned uses will be presented.

The principal components of lignocellulosic materials are cellulose (glucose polymer, with an average molecular weight of around 100 000), hemicelluloses (mixtures of polysaccharides, with an average molecular weight of $<30\,000$) and lignin (an irregular polymer composed of phenyl-propane units). The concentration of each component (Tab. 7.1) varies largely among species, plant tissues, and is also dependent on growing conditions (soil, season, geographic location, growth rate) and the plant's stage of development. These factors will contribute to the heterogeneity of the technological properties of these materials.

Tab. 7.1 Chemical composition of several lignocellulosic materials.

Material		Chemical Composition (% dry weight basis)					Ref.
		Cellulose	Hemicelluloses	Lignins	Ash	Silica	
Wood	Hardwood	38–49	23–30	19–26	<1	—	1
	ex: *Eucalyptus saligna*	41.57	32.56	25.40	0.23	—	2
	Softwood	40–45	26–34	7–14	<1	—	1
	ex: *Picea abies*	46	26	28	<1	—	3
Bast fiber	Hemp	64	15	4	4		4
	Seed flax	43–47	21–23	24–26	5	—	1
Straw	Rice	28–48	12–16	23–28	15–20	9–14	1
	Wheat	29–51	26–32	16–21	4.5–9	3–7	1
Cane	Sugar cane bagasse	32–48	27–32	19–24	1.5–5	0.7–3.5	1
	Bamboo	26–43	21–31	15–26	1.7–5	0.7	1
Seed wool	Coton	85–96	0.7–1.6	1–3	0.8–2	—	1

1: Rowell *et al.* (2000); 2: Abreu *et al.* (2004); 3: Bertaud and Holmbom (2004); 4: Thygesen *et al.* (2007).

In order to determine the potential and better use of a combustible material, one needs to know its thermochemical elemental properties. Thus, the most relevant properties of biomass destined to produce *energy* are ultimate elemental composition, proximate composition, and heating value. Depending on the system of conversion of biomass to energy (combustion, gasification, pyrolysis, liquefaction. . .), other properties must also be taken into account, for example, the size of particles ($<100\,\mu m$) in the case of gasification, and the proportions of cellulose and lignin in biomass in the case of biochemical conversion processes.

The ultimate elemental composition of a biomass is the amount of dry mass (as a percentage) of carbon (C), hydrogen (H), sulfur (S), oxygen (O), nitrogen (N), chlorine (Cl) and inorganic matter (ash). Jenkins *et al.* (1998) give the combustion properties of biomass and highlight that the composition of biomass is complex, involving six major elements in the organic phase, and at least ten other elements, not including heavy metals, in the inorganic phase important to ash characterization. Table 7.2 gives the ultimate composition of some biomass materials, data on fossil fuels (coals) are added for comparison. Table 7.2 shows that the principal components of biomass are carbon and oxygen (about 80%); due to the carbohydrate structure, biomass is highly oxygenated compared to fossil fuels. Certain inorganic elements can be found in high concentration, for example, silica in rice straw can represent more than 10% of the dry matter (Jenkins *et al.*, 1998).

The proximate composition of biomass is the amount of fixed carbon and volatile matter, where the volatile matter (VM) of a solid fuel is that portion driven off as a gas (including moisture) by heating (to 950 °C for 7 min), and the fixed carbon content (FC) is the mass remaining after the release of volatiles, excluding the ash and moisture contents (McKendry, 2002a). These properties are relevant in the thermoconversion processes, for example, the volatiles are important during the ignition and

Tab. 7.2 Chemical and energy properties of some lignocellulosic materials used as energy source. Data of coal is included for comparison purposes.

		Ultimate analysis (% dry basis)						Proximate analysis (% dry basis)				
Material		**C**	**H**	**O**	**N**	**S**	**Cl**	**FC**	**VM**	**Ash**	**GCV (MJ kg^{-1})**	**Ref.**
Wood	Wood (aver.)	51.9	6.0	41.8	0.12	0.009	0.015	20–25	75–80	≈0.6	21 (soft.) 20 (hard.)	1,2
	Salix spp	49.90	5.90	41.80	0.61	0.07	<0.01	16.07	82.22	1.71	19.59	3
	Populus spp	50.18	6.06	40.43	0.60	0.02	0.01	12.49	84.81	2.70	19.02	3
	Eucalyptus spp	49.00	5.87	43.97	0.30	0.01	—	17.82	81.42	0.79	19.42	4
	Bark	51.2	6.0	37.8	0.4	—	—	12.2	81.6	6.2	17.1	5,6
	Torrefied wood	54.4	5.2	42.9	0	0	—	24.8	75.1	0.1	21.5	6,7
	Charcoal	73.67	3.08	17.45	0.80	0	—	73	23	3.3	27.8	8,9
Straw	Wheat	44.92	4.75	35.47	0.52	0.05	0.12	17.71	75.27	7.02	17.94	3
	Rice	38.24	5.20	36.26	0.87	0.18	0.58	15.86	65.47	18.67	15.09	3
Cane	Sugar cane bagasse	48.64	5.87	42.82	0.16	0.04	0.03	11.95	85.61	2.44	18.99	3
Fossil fuel	Anthracite coal	83.67	3.56	2.84	0.55	1.05	—	84.59	7.09	8.32	32.86	10
	Lignite coal	63.89	4.97	24.54	0.57	0.48	—	46.03	49.47	4.50	25.10	10

1: Nordin (1994); 2: Barker (1983); 3: Jenkins *et al.* (1998); 4: Cortez *et al.* (2008); 5: Brito and Barrichelo (1978); 6: Almeida *et al.* (2010); 7: Couhert *et al.* (2009); 8: Yatim and Hoi (1987); 9: Pastor-Villegas *et al.* (2010); 10: Parikh *et al.* (2005).

first steps of combustion. The volatile matter of biomass is very high (65–83%) compared to that of fossil fuels.

The calorific value (or heat value) of a material is an expression of the energy content that is released when the material is burned in air. The GCV (gross calorific value) is the total energy content released when a fuel is burned in air, including the latent heat contained in the water vapor and, therefore, represents the maximum amount of energy potentially recoverable from a given biomass source. In practice, the effective use of the latent heat contained in the water vapor is difficult. Depending on the technology used, the NCV (net calorific value) may be a more appropriate value for energy purposes. It is normal practice to quote both the calorific value and crop yield on the basis of dry matter, which assumes zero percent moisture content (McKendry, 2002a). As will be discussed in Section 7.4, if any moisture is present in the material, the calorific value decreases proportionally to the moisture content. Note that the significance of the O:C and H:C ratios on the calorific value of solid fuels can be illustrated using a van Krevelen diagram. This diagram shows that higher proportions of O and H compared with C (as in biomass fuels) reduce the energy value of a fuel, due to the lower energy contained in C−O and C−H bonds, than in C−C bonds. Table 7.2 gives the proximate composition and GCV of some biomass materials in comparison with data for fossil fuels (coals).

Lignocellulosic materials are frequently used as *engineering materials*, mainly as a source of fibers. Knowledge of the physicochemical properties of these materials is of extreme importance in order to obtain their highest potential. Thus, taking into account the large variability of technological properties of lignocellulosic materials, some important properties of fibers that must be known before their use as an engineering material are: fiber anatomy, dimension, strength and crystallinity. It must be noted that the values cited here are averages; due to their biological origins, the technological properties of lignocellulosic materials vary largely between different plants of the same species, and even inside the same plant. As an example, reaction wood in hardwoods (called tension wood) has fibers presenting a "gelatinous layer" composed of more than 90% of cellulose.

Physical properties of fibers are highly influenced by their morphology. First, there is a fundamental difference in the anatomical structure between the monocotyledonous and dicotyledonous plants. A monocotyledonous plant does not present secondary growth (vascular cambium). Its stem structure has numerous vascular bundles scattered in a ground tissue of parenchymatic cells, surrounded by a strong and dense epidermis. Vascular bundles are composed of vascular cells (assuring the sap circulation) surrounded by thick-walled sclerenchyma fibers. In the case of dicotyledonous plants, a primordial anatomical difference can be made between woody and non-woody species (hemp, flax, ramie, jute, etc.). In non-woody dicotyledonous species, fibers of economic interest are located in the secondary phloem (outer part of the vascular cambium), also called bast fibers. In the case of woody species, fibers of economic interest are located in the secondary xylem (inner part of the vascular cambium). Figure 7.1 presents some examples of the anatomical structure of monocotyledonous (sugar cane, wheat straw) and dicotyledonous (flax, softwood and hardwood) plants.

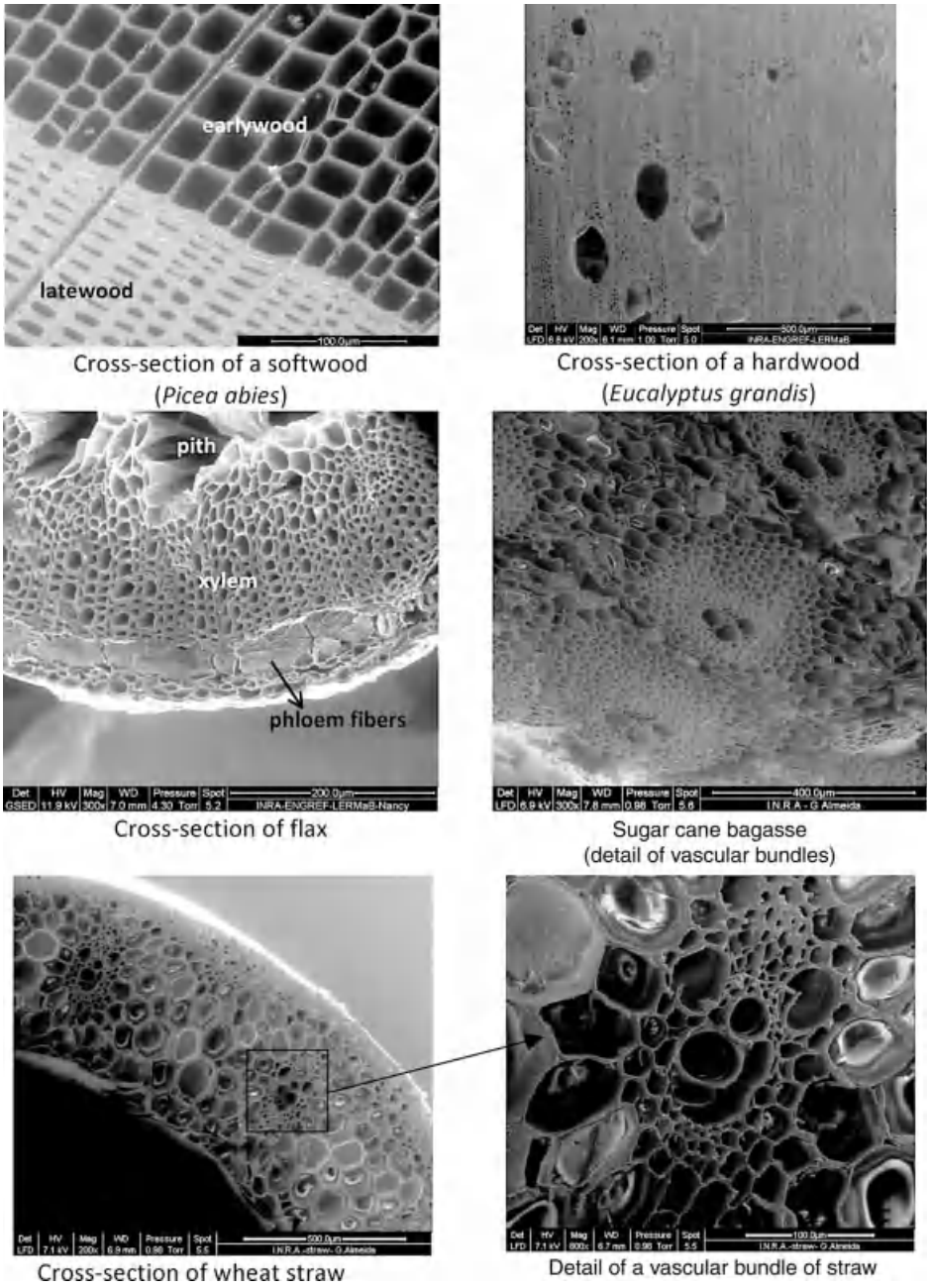

Fig. 7.1 Example of the anatomical structure of some lignocellulosic materials (ESEM images from G. Almeida, F. Huber and P. Perré, INRA/AgroParisTech).

Tab. 7.3 Dimensions of fibers from various lignocellulosic materials.

Fiber		Length (mm)	Width (µm)	Ref.
Wood	Hardwood (libriform fiber)	1.5	15	1,2
	Softwood (tracheid)	3.5	35	1,2
Bast fiber	Hemp	25	25	3
	Flax	33	19	3
	Ramie	120	50	3
Straw	Wheat	1.4	15	3
	Rice	1.4	8	3
Cane	Sugar cane	1.7	20	3
	Bamboo	27	14	3
Seed wool	Cotton lint	18	20	3

1: Panshin and de Zeeuw (1980); 2: Siau (1984); 3: Rowell *et al.* (2000).

Knowledge of fiber length is very important in several industrial fields (fiberboard, pulp and paper, textile) and the aspect ratio (length/width) gives some indication of its strength. Table 7.3 presents some examples of the large size variability among lignocellulosic fibers. This large variability can also be observed in the mechanical properties of these fibers (Fig. 7.2).

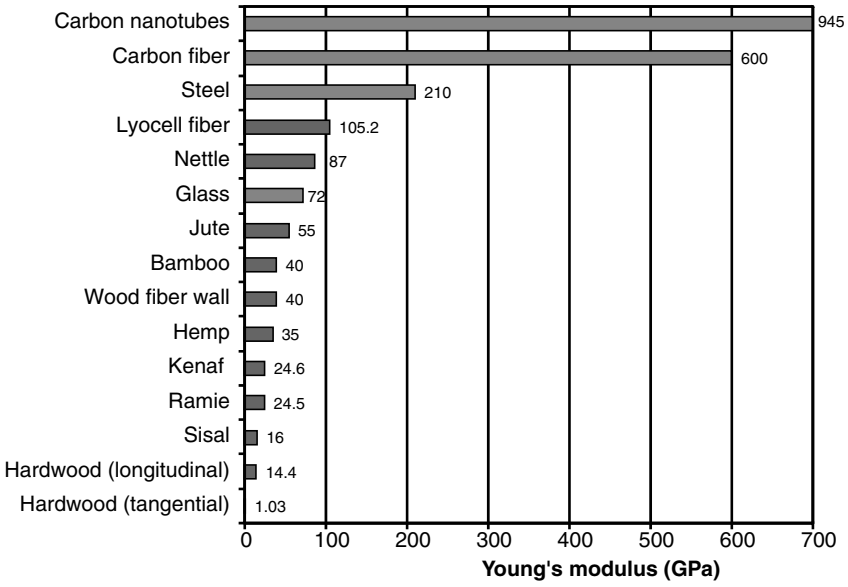

Fig. 7.2 Elastic properties of some lignocellulosic and synthetic fibers (Guitard, 1994; Jacobsen *et al.*, 1995; Bodros *et al.*, 2007; Bodros and Baley, 2008; Goda and Cao, 2007; Cheng *et al.*, 2009; Meo and Rossi, 2006).

As will be discussed in the following sections, whatever the way of realizing the value of the biomass, drying is a necessary step for its use. For example, it helps to restrict the cost of transportation by reducing the weight carried, and to preserve perishable matter.

7.3
Energy Consumption and Energy Savings in the Drying of Solid Wood

7.3.1
Kiln-Drying of Solid Wood: A Real Challenge

Within trees, the moisture content (MC) of wood is between about 50 and 200%, depending on the species and on the position within the log (the difference is especially dramatic between sapwood and heartwood). During the product use, the MC ranges between 8 and 15%, depending on the place (climatic conditions, external versus internal use). For several reasons (preservation, dimensional stability, mechanical properties, finishing ability, etc.), the removal of this huge amount of water is required after sawing before any subsequent wood processing operation. Although natural drying is still widely applied, this section is focused on the industrial drying operation, namely on the so-called conventional drying.

Behind the complexity of this operation, the industrial point of view is rather simple to understand (Fig. 7.3). Three major issues are involved in evaluating the quality of the drying process (Perré, 2001).

- The *drying time* is certainly the most simple to evaluate. However, it has many important implications: fixed capital, possibility to satisfy demands of the customers, storage capacity...

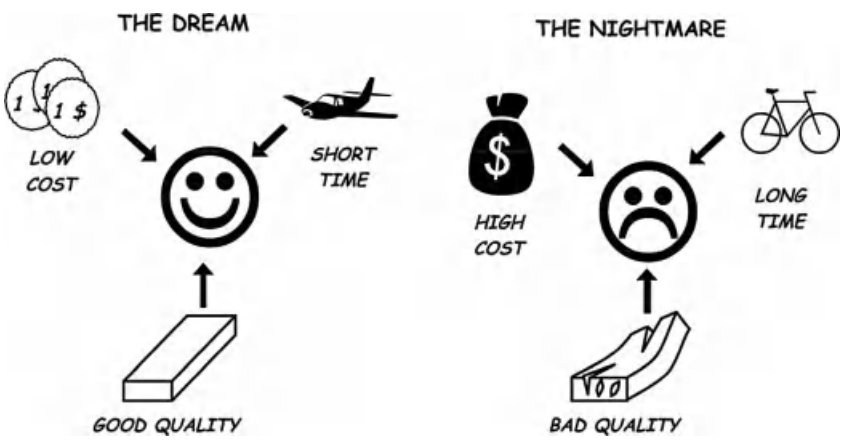

Fig. 7.3 The wood drying process: the industrial point of view (after Perré, 2001).

- The *product quality* concerns mainly moisture content specifications (average value, variance, MC gradient along the thickness), and mechanical quality (straightness, stability, absence of case hardening, absence of checking). Depending on the species, other aspects can be of dramatic importance too: discoloration, sticker staining, collapse, cementation, and so on.
- The *drying cost* results from the choice of the equipment and the compromise chosen between drying time and quality of the dried product. Several topics are to be considered:
  - Labor input (sticking, loading, supervision, etc.)
  - Energy consumption, heat source and electricity,
  - Timber losses due to distortion and degradation,
  - Maintenance, repair and depreciation of the equipment,
  - Interest on the timber and the technical investment.

Obviously, it is more than difficult to combine all advantages at the same time. In practice, a compromise has always to be found between cost, quality and time. In addition, the right compromise depends on the industry, on the country, and on the market, and evolves in time. So, for a factory already equipped with dryers, the satisfactory compromise has just to be found between time and product quality. In the case of overloaded equipment, some losses due to low quality may be tolerated to save time (Fig. 7.4a). In contrast, in spite of longer drying times, careful drying schedules will be used in order to make the most of valuable species (Fig. 7.4b).

Obviously, this discussion supposes that a kind of optimum has been achieved in the use of the equipment: inappropriate drying schedules always increase the drying cost because of a poor balance between product quality and drying time (Fig. 7.5a). Some other situations may occur, in which both the drying time and the product quality can be improved (Fig. 7.5b). Such a situation has two possible explanations:

- The previous situation was really bad. In that case, the path from (a) to (b) is a question of know-how transfer (training and technical formation). People situated midway between research and practice are in charge of this effort (in France, this is the typical task of scientists belonging to the Technical Centre for Cellulose, Wood and Furniture, FCBA).
- The previous situation was already rather good. Then the explanation lies in innovation. In theory, this is the job of fundamental and applied research.

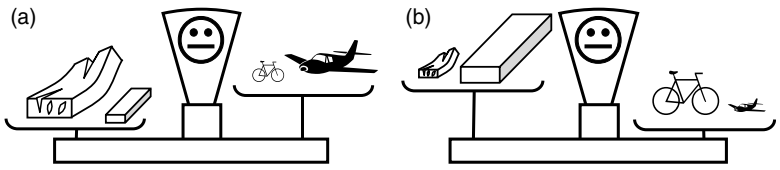

Fig. 7.4 The compromise between drying time and product quality: two acceptable situations, depending on the production priorities.

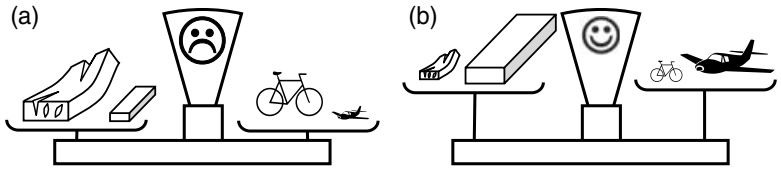

Fig. 7.5 Depending on the situation, the balance between drying time and product quality may range between (a) poor and (b) excellent.

Fundamental research deals with understanding, and hence predicting, while applied research provides the industry with tools able to implement and adjust new procedures.

In terms of material sciences (biology, physics, chemistry, mechanical and chemical engineering, etc.) the simple schematic depicted in Fig. 7.3 hides very complex and coupled phenomena. A detailed description of these phenomena, including transfers and mechanics, together with the relevant physical formulation, are available elsewhere (see, for example, Perré, 1996, 2007a). The most important phenomena involved in wood drying and their intricate connections are outlined in Fig. 7.6, namely:

- Coupled heat and mass transfers in porous media,
- Shrinkage induced drying stresses,
- Chemical degradation, like discolorations, thermal degradation,
- Specific effects (cementation, collapse, etc.).

Along this complexity, the direct coupling between transfer and mechanical stresses explains why the air conditions have to be controlled during the drying of solid wood. The general idea is to limit the external transfers and to ease the internal transfers in order to have flat variable fields within the section, hence low levels of drying stresses (Perré, 2001).

The empirical way to dry common wood species gradually accounted for all these intricate mechanisms. In this sense, we may consider that, nowadays, a kind of optimal situation has evolved, that accounts for a whole set of constrains such as the species properties and variability, the section thickness and the kiln characteristics. Due to the latter point, this optimum is only a local optimum, tied to the conventional way solid wood is dried in industry.

The improvement gap is, therefore, limited as far as the basic principles of industrial drying remain the same. A typical example for this situation is when a stepwise regulation (drying schedule) is exchanged by a modern regulator with continuous variation of the drying conditions.

Significant improvements are necessary when changes allow the local optimum to be left. Respective examples can be found in innovative techniques (high pressure convective vacuum drying, drying with internal heat sources such as microwaves or radiofrequencies, glass transition drying, etc.) or when improving the drying control for poorly known species.

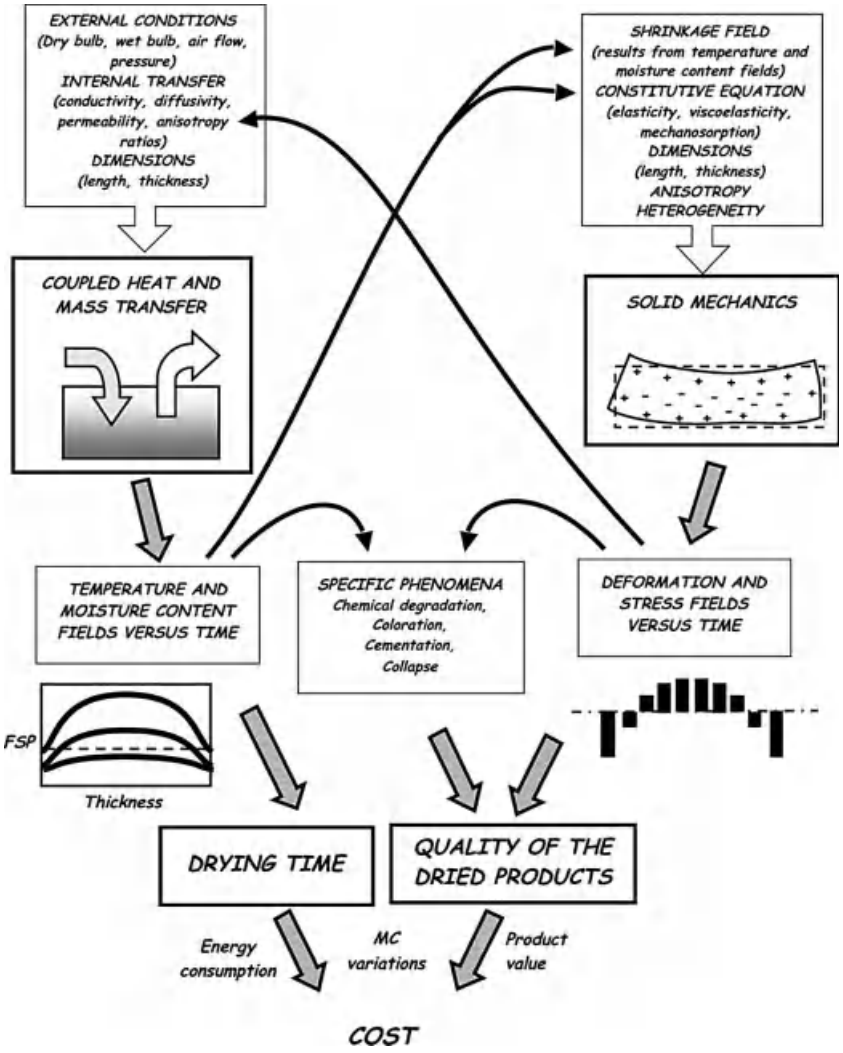

Fig. 7.6 Some of the coupled phenomena involved in wood drying.

Due to this complexity, the energy issues were of almost no concern in the domain of wood drying. The situation has obviously changed over the last decade due to the increasing price of energy and the regulations linked to global warming. In the future, R&D in the domain of solid wood drying will certainly be driven by energy concerns: energy savings, use of energy with low exergy, use of recompressed superheated steam, and so on.

These new fields of investigation emphasize the need for a good description of the present situation in terms of energy consumption. This is the purpose of Sections 7.3.2 and 7.3.3, which are mainly focused on conventional drying.

7.3.2 The Conventional Drying of Wood

7.3.2.1 The Design of Conventional Kilns

In the industry, the most widespread drier technology is the so-called conventional kiln. Basically, this kind of lumber kiln consists of a special-purpose room, the drier chamber, fitted with overhead fans for circulating the drying air, and heating coils for maintaining the air (and thus the wood) temperature at the set levels. The moisture in the air is controlled by means of opening vents in the kiln's roof, thus governing the amount of moist air that returns to the fan to be mixed with the fresh air drawn in (Perré and Keey, 2006). Humidification of the air is sometimes required, namely at the beginning of drying, hence the presence of nozzles, for droplets or steam injection.

The lumber is stacked externally in a rectangular pile on a low, flat-bed trolley, with rows of boards separated by wooden stickers of uniform thickness to provide spaces between the boards for the kiln air to flow through. These trolleys are put on rails to ease the kiln loading and unloading after external stacking. For smaller kilns, the boards may be stacked in separate packages on bearers and loaded into the kiln by a forklift vehicle. The boards are butted up, with their long faces incident to the airflow. The stack is squared off as far as possible to provide a uniform resistance to the airflow, and thus minimize variations in drying throughout the kiln. In Scandinavian practice, kiln stacks are normally built from boards of random length, so that every second board is placed flush at one end of the stack, and the other boards flush at the other end (Salin, 2001). Kilns may be single-tracked with a 2.4 m-wide stack, or twin-tracked, with two stacks side by side, to yield a double-width stack of 4.8 m. Figure 7.7 illustrates a vertical cross-section through a single-tracked, batch kiln.

To obtain as uniform an air distribution to the air-inlet face of the stack as possible, the plenum spaces at each side of the stack must be sufficiently wide (Nijdam and Keey, 2000). An internal ceiling directs the air though the lumber stack or stacks, with baffles or curtains to direct the airflow through the lumber pile. Inward-swinging baffles and contoured, right-angled bends to the plenum space from the ceiling zone improve the uniformity of this airflow (Nijdam and Keey, 2002). Bypass of air around the stack is minimized by the fitting of side baffles or curtains. The kiln is designed so that the pressure loss though the heating coils and other ancillary fittings is small compared with that through the stack of lumber. Usually, the airflow in the duct-like space between the board rows lies in the range 2 to 5 m s^{-1}. The higher velocity values are required for fast-drying species. To attain these values, the electrical power of fans can be evaluated by the observed ratios of 0.15 to 0.20 kW m^{-3} of wood for hardwoods and 0.30 kW m^{-3} for softwoods (Aléon *et al.*, 1990).

The set of constrains resulting from the design of conventional kilns is important to evaluate the ratio between the lumber volume and the kiln volume. Depending on the kiln and the board characteristics, the filling factor varies between 0.15 and 0.35 (Joly and More-Chevalier, 1980). This factor is better for thick boards, as the relative volume of the spaces provided by the stickers decreases with the board thickness.

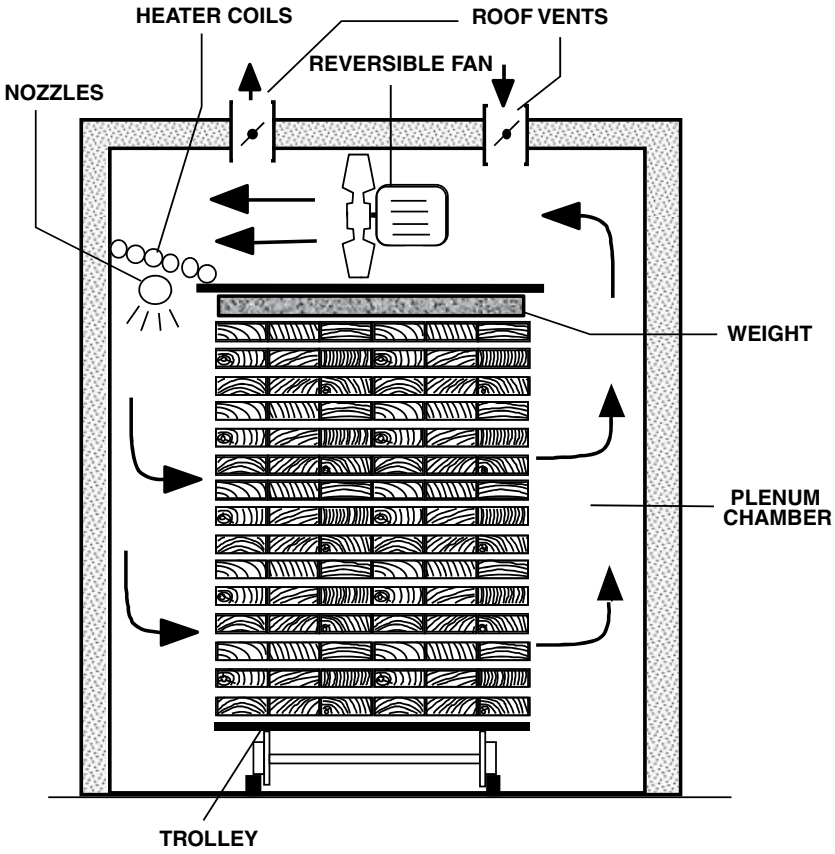

Fig. 7.7 A vertical cross-section through a single-tracked, box kiln (from Perré, 1993).

7.3.2.2 **Drying Time and Energy Efficiency**

As explained in Section 7.3.1, the time required to dry solid wood when the mechanical quality matters results from a subtle equilibrium between wood properties, board thickness, drier characteristics, and production priorities. This balance between all involved constraints has been improved over the years, based on empirical knowledge, and is embedded in the so-called drying schedules. The basic principle is to keep the relative humidity of the air high at the beginning of the process. During this period, the kiln acts just as a reactor that lowers the external heat and mass transfer to avoid any damage. The air RH then gradually decreases as the timber load dries. Obviously, these schedules depend on the species. Table 7.4 summarizes the schedules recommended for two contrasting situations. One may notice that difficult species need the temperature level to be low, and the relative humidity level to be close to saturation, especially at the beginning of the process. Resulting from these differences in drying conditions, the drying times depend dramatically on the species. Table 7.5 reports some typical drying times usually

Tab. 7.4 Two examples of drying schedules proposed for contrasting situations: (a) fast-drying softwood species, such as fir, (b) problematic hardwood species, such as European oak.

MC (%)	T_{db} (°C)	T_{wb} (°C)	RH (%)	EMC (%)
(a)				
>50	35	32	95	19
50–40	35	31	93	18
40–30	35	30	90	17
30–27	40	37	81	16
27–24	40	36	76	14
24–21	40	35	70	12
21–18	45	37.5	63	10
18–15	45	36	54	9
15–12	45	34.5	49	8
12–8	45	30.5	34	6
(b)				
>50	70	64	75	11
50–40	70	63	71	10
40–30	70	61	64	9
30–27	80	70.5	65	8
27–24	80	68	58	7
24–21	80	65	50	6
21–18	85	66	43	5
18–15	85	61	34	4
15–12	85	59	31	3,5
12–8	85	55	23	3

MC is the actual moisture content (dry basis) of the load, T_{db} and T_{wb} are the recommended dry and wet bulb temperatures, RH and EMC are the corresponding relative humidity of air and the equilibrium moisture content of wood (according to Joly and More-Chevalier, 1980).

Tab. 7.5 Typical times (in days) observed in the industry for the drying of 27 mm thick solid wood; S = softwoods, M = middle-density hardwoods, H = high-density hardwoods (adapted from Joly and More-Chevalier, 1980, and Aléon *et al.*, 1990).

Drying Technique		Green to 18%	Green to 10%	30% to 10%
Natural drying	S	25 to 60	Impossible	
	M	150 to 250		
	H	190 to 340		
Conventional drying	S	2	3	1.5
	M	9 to 12	10 to 16	5 to 8
	H	15 to 20	20 to 30	10 to 15
Dehumidifier	S	7 to 8	10 to 12	5 to 7
	M	12 to 14	18 to 21	9 to 12
	H	20 to 25	25 to 35	18 to 20
Continuous vacuum drying	S	1.5	2	1
	M	2 to 3	3 to 4	1.5 to 2
	H	4 to 5	5 to 6	2.5 to 4

observed in the industry for three categories of species (softwoods, middle-density hardwoods, high-density hardwoods), different dryer technologies, and different drying goals (initial and final moisture contents). From this table, it is obvious that natural drying, even though it does not need any energy source, is very long and out of control. In particular, it does not allow low final moisture content to be obtained, and the drying time is very dependent on the weather, summer/winter time, hence the huge variability in the drying times reported in Tab. 7.5. For all technologies, the drying time depends dramatically on the species category. Finally, one has to notice that a factor up to 4 or 5 can be observed between different technologies. In this table, the continuous vacuum drying (low pressure vacuum drying with contact heating) always produces the fastest drying. Note that more innovative technologies, such as radio-frequency drying, are even more efficient because they supply the heat required for evaporation directly at the right place, avoiding the need for conduction (Rémond and Perré, 2008).

In Tab. 7.5, all data are given for 27 mm-thick lumbers. The relative effect of thickness (with a reference value of unity for 27 mm) is depicted in Fig. 7.8. For comparison purposes, the effect of thickness for two ideal situations was also plotted (constant drying rate period, where the drying time is proportional to the thickness, and pure internal diffusion, where the time varies as the thickness squared). One can observe that the drying time for conventional drying consistently lies between these two theoretical situations. On the contrary, the experimental observations for vacuum drying are less than the best ideal situation (CDR); in this case, one important part of

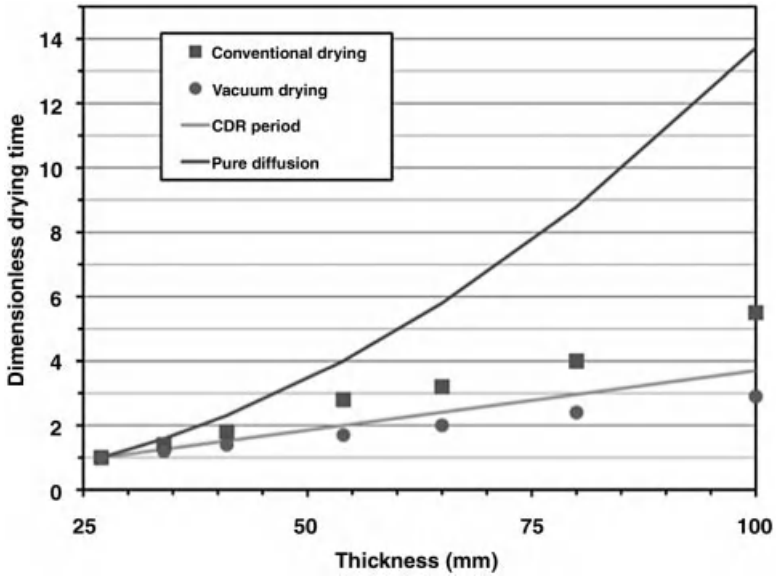

Fig. 7.8 Effect of the board thickness on the total drying time (CDR = constant drying rate period). Adapted from Joly and More-Chevalier (1980).

the moisture migrates in the longitudinal direction, which is independent of the board thickness.

The energy efficiency is usually expressed as the amount of energy required to remove a certain amount of water from the load, in $kWh\,kg^{-1}$. Remembering that the latent heat of vaporization equals $2503\,kJ\,kg^{-1}$ at $0\,^{\circ}C$ and $2257\,kJ\,kg^{-1}$ at $100\,^{\circ}C$, the energy required to evaporate 1 kg of liquid water at a medium temperature (say $50\,^{\circ}C$) equals $2380\,kJ\,kg^{-1}$, or $0.66\,kWh\,kg^{-1}$. If all water is removed from the load as water vapor and extracted from the kiln as it is, it is impossible to obtain a ratio below this theoretical value. Only some processes, such as dehumidifiers, that use a heat pump to heat the air and condense water vapor, or superheated steam dryers with mechanical compression can theoretically go beyond this limit.

In practical situations, the real amount of energy required per kg of evaporated water is not so simple to measure. For such studies, the kiln needs a comprehensive instrumentation to quantify all possible energy consumption, such as fans, heating elements, humidifiers. Additional difficulties arise when one single boiler supplies several kilns simultaneously. For these reasons, studies reporting reliable consumption figures are quite rare. The numbers reported in Tab. 7.6 come from different studies carried out on many industrial kiln cycles by FCBA, in Paris.

Depending on the species and the board thickness, Tab. 7.6 depicts values ranging from 1.00 to $2.73\,kWh\,kg^{-1}$. The huge range of drying times between these configurations (refer to Tab. 7.5) is part of the explanation for these variations. Indeed, the drying time has a direct impact on the kiln efficiency, as the fan consumption and thermal losses increase linearly with time. The ratio reported for pine is higher than that reported for beech and seems surprisingly high. However, these numbers come from two different studies in different kilns. The one used for pine was certainly of quite poor characteristics. The next section is devoted to a detailed theoretical analysis of the energy consumption in conventional kilns.

Tab. 7.6 Typical energy ratios (energy consumption per kg of evaporated water) observed in conventional dryers (adapted from Aléon *et al.*, 1990; Chanrion and Davesne, 1991).

	Moisture Content (%)			
Lumber	**Initial**	**Final**	**Heating Consumption ($kWh\,kg^{-1}$)**	**Electrical Consumption ($kWh\,kg^{-1}$)**
Oak 27 mm	30	10	2.65	0.49
Oak 27 mm	60	10	2.10	0.36
Oak 54 mm	40	14	2.73	1.27
Beech 27 mm	30	10	1.20	0.16
Beech 27 mm	60	10	1.00	0.15
Beech 54 mm	40	14	1.10	0.36
Pine 27 mm	90	10	1.35	0.06

7.3.3
Theoretical Evaluation of the Kiln Efficiency

In the case of conventional dryers, the energy balance is quite straightforward, as the different energy needs are supplied directly to the kiln. The energy consumption of this kind of kiln can, therefore, be evaluated quite accurately, provided the kiln has no significant defaults, such as air leakages, thermal bridges or cold points, for example, due to doors with poor maintenance or mistakes in the conception of the structure. The energy consumption can be divided into six components:

1) Latent heat of vaporization,
2) Differential heat of sorption,
3) Thermal losses,
4) Air renewal,
5) Fan consumption,
6) Heating of the timber load and the kiln structure.

Latent heat of vaporization

In a conventional kiln, as is the case for any thermal drying principle, the water is removed from the product as water vapor. In the case of the so-called "free water", the enthalpy ΔH_v required to go from the liquid to the gaseous state is simply the evaporated mass times the latent heat of vaporization at the drying temperature $L_v(T)$:

$$\Delta H_v = \Delta m_{water} L_v(T) \tag{7.1}$$

Differential heat of sorption

In the case of bound water removal, a further term has to be added to Eq. 7.1, the so-called differential heat of sorption H_s. For wood, the differential heat of sorption at moisture content X can be obtained with a good approximation by a second order polynomial:

$$H_s(X) = 0.4\Delta H_v(T)\left(\frac{X_{fsp}-X}{X_{fsp}}\right)^2 \tag{7.2}$$

The integration of this value from the final moisture content to the FSP (fiber saturation point) content allows the averaged value of the differential heat of sorption $\langle H_s \rangle$ to be determined:

$$\begin{aligned}\langle H_s \rangle &= \int_X^{X_{fsp}} H_s(X)\mathrm{d}X \\ &= \frac{0.4\Delta H_v}{X_{fsp}^2}\left[\frac{2X_{fsp}^3}{3} - X_{fsp}^2 X + \frac{X^3}{3}\right]\end{aligned} \tag{7.3}$$

Thermal losses

Thermal losses have to be evaluated for all external surfaces of the kiln: roof, walls and soil. For each surface, the thermal loss per unit of surface area q_{th} ($\mathrm{W\,m^{-2}}$) equals

Tab. 7.7 Characteristics of the heat transfer in the wall of a conventional kiln (example based on a compound wall).

Element	Thermal Conductivity ($W K^{-1} m^{-1}$)	Thickness (mm)	Heat Transfer Coefficient ($W K^{-1} m^{-2}$)	Comment
Internal convection	—	—	25	The forced convection produced by the fans explains the high value chosen here
Aluminum sheet	200	1	—	
Rock glass	0.04	60	—	
Aluminum sheet	200	1	—	
External convection	—	—	12	Reasonable value that accounts for transfer by radiation and the presence of a moderate wind

the global thermal conductance K_{th} ($W K^{-1} m^{-2}$) resulting from layers placed in series, times the temperature difference (Bird *et al.*, 1960):

$$q_{th} = K_{th}(T_{int} - T_{ext}) = \frac{1}{\frac{1}{h_{int}} + \sum_i \frac{\ell_i}{\lambda_i} + \frac{1}{h_{ext}}} \times (T_{int} - T_{ext}) \tag{7.4}$$

As an example, Tab. 7.7 summarizes the characteristics of a compound wall composed of rock wool placed between two aluminum sheets. With these values, the global thermal conductance determined by Eq. 7.4 is equal to $0.62\,W K^{-1} m^{-2}$.

The total heat flux through a wall is simply the product of q_{th} and the surface area of the wall. For example, with the previous compound wall, assuming a temperature difference of 50 K (i.e., $T_{int} = 65\,°C$ and $T_{ext} = 15\,°C$) and a $3 \times 10\,m^2$ wall, we obtain:

$$\begin{aligned} q_{th} &= K_{th}(T_{int} - T_{ext}) = 31\,W m^{-2} \quad \text{and} \\ Q_{th} &= q_{th} A = 930\,W \end{aligned} \tag{7.5}$$

The enthalpy to be supplied to compensate for these thermal losses, ΔH_{loss}, is therefore:

$$\Delta H_{loss} = Q_{th} t_{drying} \tag{7.6}$$

Air renewal

In a conventional kiln, the control of the internal relative humidity, or more precisely the reduction of this value, required due to the vapor flux removed from the timber load, is achieved by air renewal. During this process, the opening of vents allows hot and moist air to exit the kiln and cold and dry air to enter the kiln. The price to pay for this moisture removal is the heating of the external air flux to the dry bulb

temperature inside the kiln. Due to the air dilatation and to the difference in moisture content of these two fluxes, the mass balance has to be written in terms of the mass flux of dry air: when fresh air enters the kiln, an equivalent volume of hot air exits the kiln, hence a smaller mass of air. However, when the fresh air heats up to the kiln temperature, its dilatation forces an additional volume of air to exit. Assuming a perfect balance between the vapor removed from the kiln by air renewal and the vapor added to the air by evaporation from wood (constant relative humidity), the total mass of air inside the kiln remains constant. For an elementary amount of air mass Δm_a exchanged between the kiln and the exterior, the amount of water vapor removed from the kiln is given by:

$$\Delta m_v = \Delta m_a (Y_{int} - Y_\infty) \tag{7.7}$$

Here Y_{int} and Y_∞ are the absolute humidities of the air inside the kiln and in the atmosphere, respectively. It should be remembered that absolute and relative humidities at a dry bulb temperature T, are related by the following formula:

$$Y = \frac{\rho_v}{\rho_a} = \frac{RH P_{v,S}(T) M_v}{\left\{P_{atm} - RH P_{v,S}(T)\right\} M_a} \tag{7.8}$$

which includes the molar mass of air and vapor, the atmospheric pressure and the saturated pressure of vapor.

For a drying stage at constant drying conditions (one step of a drying schedule for example), the enthalpy ΔH_a to be supplied to the incoming air to extract the amount of water removed from the wood load Δm_v is therefore:

$$\Delta H_a = \frac{\Delta m_v}{Y_{int} - Y_\infty} (c_{P,a} + Y_\infty c_{P,v})(T_{int} - T_{ext}) \tag{7.9}$$

Fan consumption

The fan consumption simply equals the electrical power times the drying time

$$\Delta W_{fan} = P_{fan} t_{drying} \tag{7.10}$$

Note, however, that due to viscous dissipation most of this electrical power (the efficiency of industrial electrical motors is excellent) eventually turns into heat. In the calculation presented hereafter, the consumption of electrical energy is computed (the cost of electricity is generally much higher than the cost of heat and its impact on the environment depends on the way it was produced) but it is not considered in the evaluation of the energy ratio ($kWh\,kg^{-1}$).

Heating of the timber load and the kiln structure

For each stage of drying, the dry wood and its actual water content have to be heated to the drying temperature:

$$\Delta H_{heating} = (c_{P,s} + X_{ini} c_{P,w})(T_{int} - T_{kiln}) \tag{7.11}$$

The energy to dry the structure is trickier to evaluate. If starting from a cold kiln, the establishment of the steady-state temperature profile would allow us to determine the

Tab. 7.8 Geometrical and thermal characteristics of the kiln used for the case studies.

	Kiln	Stack
Width (m)	4.5	2.5
Length (m)	10	8
Height (m)	6.5	4
Volume (m^3)	292.5	80
K_{th} walls and roof ($W\,m^{-2}\,K^{-1}$)	0.62	
K_{th} floor ($W\,m^{-2}\,K^{-1}$)	4.17	

temperature variation of each part of the envelope. The analytical method used to obtain Eq. 7.4 is suitable for this. In the particular case of a symmetrical wall, with the same heat transfer coefficient for the internal and external surface, the energy required to heat the wall exactly equals the heat capacity of the wall times half the temperature increase between the initial value and the final kiln temperature.

The same procedure can be applied to the walls and to the roof. The floor is in contact with the soil, whose temperature is more difficult to evaluate.

Note, however, that in the case of a continuously operating kiln, this heating energy has more or less to be supplied only once. Consequently, the energy needed to heat the kiln structure will not be taken into account in the following section.

7.3.4
Two Case Studies of Kiln Efficiency

In this section, the previous formulation will be applied to two contrasting situations:

- Case study 1: the drying of 27 mm-thick spruce boards,
- Case study 2: the drying of 54 mm-thick oak boards.

In order to focus our attention on the coupled effect of species/thickness, the geometrical and thermal characteristics of the kiln (Tab. 7.8), as well as the external conditions (Tab. 7.9) are the same for both case studies (except the fan power).

Several parameters allow the drying of spruce and oak to be distinguished (Tab. 7.10). The most important differences lie in the drying time, the drying temperature and relative humidity, and the species density. The initial moisture content is higher in the case of spruce for two reasons; (i) the moisture content in standing trees is rather high for spruce, and (ii) the timbers are usually dried just after

Tab. 7.9 External conditions used for the case studies.

External temperature	10 °C
Initial wood temperature	10 °C
Soil temperature (beneath the floor)	25 °C
External RH	80%

Tab. 7.10 Representative parameters chosen for case studies 1 and 2 (spruce and oak).

	Spruce	**Oak**
Density (kg m^{-3})	400	580
Board thickness (mm)	27	54
Sticker thickness (mm)	20	25
Volume of wood (m^3)	46.0	54.7
Fan power (kW m^{-3})	0.30	0.15
X_{ini} (kg kg^{-1})	1	0.5
X_{fin} (kg kg^{-1})	0.15	0.08
Drying temperature (°C)	75	40
Drying RH	0.6	0.8
Drying time (days)	3	60

sawing. In the case of oak, the timbers are generally stored on park for a while before drying, to lower the moisture content. The final moisture content also differs, according to the general use of these species: structure for spruce and flooring or furniture for oak. Notice that, for the sake of simplicity, and although the formulation proposed in Section 7.3.3 could be applied stepwise using a drying schedule, the drying process is supposed to be made up of one single stage. This is why representative values of the whole process were selected as drying conditions.

Using the formulation of Section 7.3.3 in a spreadsheet allowed the energy partition to be computed. A graphical plot of this partition is depicted in Figs. 7.9 and 7.10, for spruce and oak, respectively. On these graphs, the electrical consumption of fans is plotted using open bars because, as explained above, this consumption was not considered when computing the energy ratio. The respective energy ratios are 1.02 and 1.84 kWh kg^{-1}. These values are in quite good agreement with those reported from industrial studies (Fig. 7.6). In the case of spruce, in spite of the higher temperature level, the thermal losses are quite low (8.5%) just because the drying is fast. The air renewal and the load heating each represent about 10% of the total energy needs. Consistently, for this fast-drying species, the most important demand is simply the energy for water evaporation (68%).

The figure obtained for oak is quite different: as a consequence of the process duration, the thermal losses (42%) are higher than the need for evaporation (38%). Due to the low temperature level and the higher energy ratio, the load heating represents now only 4% of the total energy needs. As another effect of the lower drying temperature, the absolute moisture content of air within the kiln is much less, and the air renewal is less efficient: heating the fresh air represents now 15% of the total energy.

Note that, in spite of these additional needs, the ratio calculated for oak remains quite a bit smaller than those measured on an industrial kiln (2.73 kWh kg^{-1} for a thickness of 54 mm). There are two reasons for this huge experimental consumption:

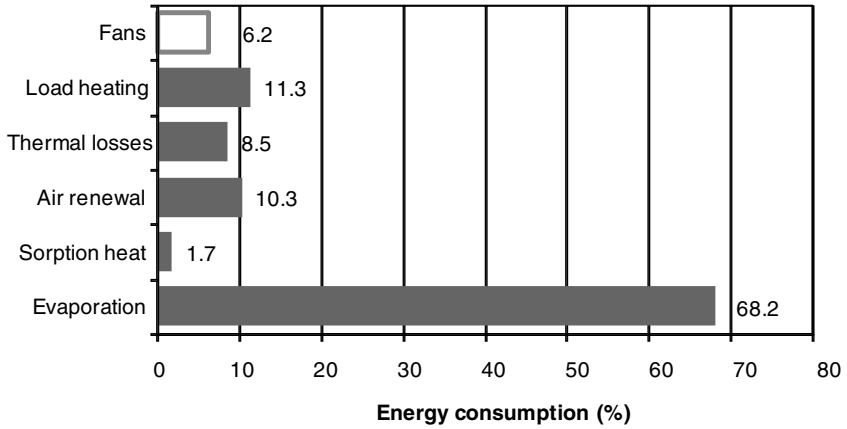

Fig. 7.9 The distribution of energy consumption (%), obtained for case study 1 (spruce). In this case, the energy ratio equals 1.02 kWh per kg of water.

1) *Poor thermal insulation* of the kiln walls: in our model, if we changed the compound wall for a brick one (say 20 cm thick with thermal conductivity $0.5\,W\,K^{-1}\,m^{-1}$), the respective ratios, for spruce and oak, rise to 1.11 and $2.82\,kWh\,kg^{-1}$.
2) *Poor air-tightness* of the kiln: in the case of oak, due to the drying duration, the average rate of air renewal is 1.01 kiln volumes per hour. This value is rather low and the leakages, namely at the doors, can easily be higher. Just imagine the leakage to be twice the required value. As a consequence, the energy required to heat the air will obviously be twice as high, but the worse effect is that the humidifier of the kiln will have to supply water to maintain the desired relative humidity: the need for water evaporation would also be

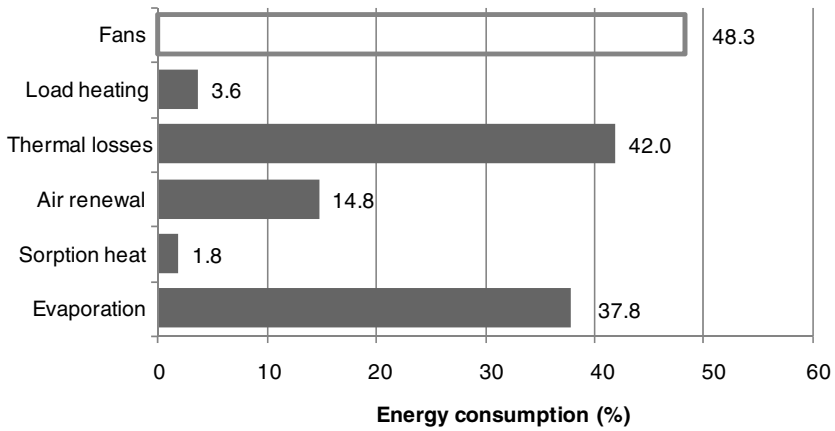

Fig. 7.10 The distribution of energy consumption (%), obtained for case study 2 (oak). In this case, the energy ratio increases to 1.84 kWh per kg of water.

doubled! Due to such a leakage, the energy ratio would be shifted from 1.84 to 2.81 kWh kg^{-1}.

Finally, it is worth noting that, contrary to some common affirmations, the energy due to the differential heat of sorption is almost negligible in both case-studies.

7.3.5 Rules for Saving Energy

7.3.5.1 Energy Savings in Conventional Kilns

Following the previous section, the ways to save energy in conventional kilns are straightforward. As nothing can be changed concerning the latent heat of evaporation, the possibilities lie in the other significant consumption categories, namely air renewal and thermal losses.

Concerning air renewal, the amount of air to be exchanged with the exterior is determined by the external conditions and the drying conditions. The only possibility to reduce this energy consumption is to add an air heat exchanger: in this way the inlet flux can be preheated up to approximately the wet bulb temperature of the kiln thanks to the condensation of one part of the water vapor contained in the outlet flux. Such exchangers exist in cold climates, such as Canada.

As seen above, it is interesting to reduce thermal losses, especially for low-drying species. The insulation of the walls is a straightforward means of doing this (see above for the difference obtained for two different wall structures in the case of oak drying). Another possibility to reduce the thermal losses is to increase the size of the kiln, as the volume of timber increases faster than the wall surface area when increasing the kiln size. This can be one of the explanations for the lower consumption reported in the very large continuous kilns operating in Scandinavia compared to batch kilns (Salin and Wamming, 2008). In the two case studies presented before, increasing the kiln size to a twin-tracked kiln with dimensions of $7 \times 20 \times 6.5$ m^3 (W × L × H) leads to a decrease in the energy ratios from 1.02 to 0.98 kWh kg^{-1} and from 1.84 down to 1.49 kWh kg^{-1} for spruce and oak, respectively.

As already stated, the fan consumption is eventually converted into heat and reduces the need for heating energy, even though not involved in the energy ratio. However, the cost of electricity is generally much higher than that of heat. It is, therefore, interesting to reduce this consumption. The fact that the number of mass transfer units along the stack is reduced dramatically as the drying progresses (Perré, 2010), allows the airflow to be decreased without degradation of the moisture content homogeneity. By applying this principle, significant reductions in electricity consumption can be obtained without deterioration of the product quality (Perré *et al.*, 2007).

Following this principle, one has to remember that the drying schedules used in the industry have mainly been adapted to get a good balance between drying time and product quality. It is, therefore, possible to revisit these drying schedules to focus on energy issues (Hwang *et al.*, 1994; McCurdy and Pang, 2007). The graphs of energy consumption (Figs. 7.9 and 7.10) represent an interesting guide for this.

In particular, they show that drying time and temperature level are important. By increasing the temperature level during drying, one can gain on two energy components: thermal losses due to a reduced drying time, and air renewal due to an increased absolute humidity in the air of the kiln (Rosen, 1980; Fortin *et al.*, 2004; Salin and Wamming, 2008).

7.3.5.2 Energy Saving by Alternative Technologies

Dehumidification drying is an interesting alternative in terms of energy consumption. In such a kiln, one part of the air is passed through the cold exchanger of the heat pump, thus recovering partly the latent heat of vaporization (the air has to be heated after being cooled). Together with the efficiency factor of the heat pump, the consumption can be dramatically lowered. Aléon *et al.* (1990) reported energy ratios ranging from 0.4 to 0.6 $kWh\,kg^{-1}$ for the drying of softwood and 0.9 to 1.0 $kWh\,kg^{-1}$ for the drying of oak. Note, however, that the whole energy consumption is electrical energy.

One drawback of this technology is the limited temperature level that can be attained with the usual heat pumps, resulting in long drying times. This lowers the productivity and increases thermal losses. A combination of conventional and dehumidification drying has been proposed to combine the advantages of both methods, finally obtaining an energy consumption 20% less than in conventional drying for the same drying time (Zhang *et al.*, 2007).

In vacuum drying, the energy is required for heating the wood, the evaporation of water and its removal by condensation/vacuum pump. In this process, quite good energy ratios, below 1 $kWh\,kg^{-1}$ were measured (Jung *et al.*, 2000; Aléon, 2008).

Superheated steam drying using mechanical steam compression produces an efficient thermodynamic cycle able to reduce significantly the energy needed per kg of water removal down to 20 to 45% of the base-line energy consumption of dryers (Palandre and Clodic, 2003).

Although difficult to control, and in spite of the lack of energy during the night, solar drying may be of interest in the future to address energy issues (Bux *et al.*, 2001; Raghavan *et al.*, 2005). In the same spirit, the possibility to dry with energy of low exergy, such as residual energy from industrial processes, may be of double interest: the use of energy at a very low price, and reduction of thermal pollution associated with the use of such energy sources (for example, the temperature increase of river water due to nuclear plants). With solar energy and energy with low exergy, the problem will be to adapt the process control as a function of the available energy. Embedded computational models with predictive possibilities would certainly be of great help in addressing this problem.

New technologies such as radiofrequency drying and microwave drying, at atmospheric pressure or under vacuum, allowed the total drying time to be reduced by orders of magnitude (Dedic and Zlatanovic, 2001; Leiker and Adamska, 2004; Rémond and Perré, 2008). In these technologies, the energy efficiency of the volumetric heat source is of the order of 50%, with electrical energy. This is not excellent, but the very short drying time allows all the other energy components except the load heating to be almost negligible.

7.4
Preconditioning of Biomass as a Source of Energy: Drying and Heat Treatment

7.4.1
Importance of Biomass Drying as a Preconditioning Step

The initial moisture content of a type of biomass is very important in the choice of the energy conversion process (McKendry, 2002a). Thus, algae, manures and some herbaceous biomass (sugar-cane) are high-moisture matters and are more suited to wet conversion routes (alcoholic fermentation, methanogenesis, enzymatic hydrolysis, etc.) (McKendry, 2002b). Other annual and pluriannual plants (wood, straw, sugar-cane bagasse, etc.) are considered to have a lower MC and are more economically suited to gasification, pyrolysis or combustion (McKendry, 2002b, c). In the case of biomass used as a combustible, its moisture content is usually expressed on a wet basis (mass of water over total mass).

The residual water causes a drop in the lower heating value (LHV) per dry mass because a part of the energy released by combustion of the lignocellulosic material is used to evaporate the water contained in the fuel. The drop becomes spectacular when the LHV is reported to the total mass, as the water embedded in the product does not contain any energy (Núñez-Regueria *et al.*, 2001; Rogaume, 2005). This unit (kJ per kg of total mass) is, however, relevant only for unit operations such as transportation and storage. Figure 7.11 gives an example of the influence of moisture content on the lower calorific value for two types of wood: *Pinus pinaster* (softwood) and *Eucalyptus globules* (hardwood). In most facilities, this water must remain as vapor along the chimney, as its liquefaction would cause corrosion. In addition to the simple energy balance, one has also to keep in mind that the moisture content has several negative side-effects such as a decrease in the flame temperature, a decline in energy efficiency (Ståhl *et al.*, 2004), and an increase in soot and tar production (Bryden and Hagge, 2003). The latter present multiple inconveniences, (i) they

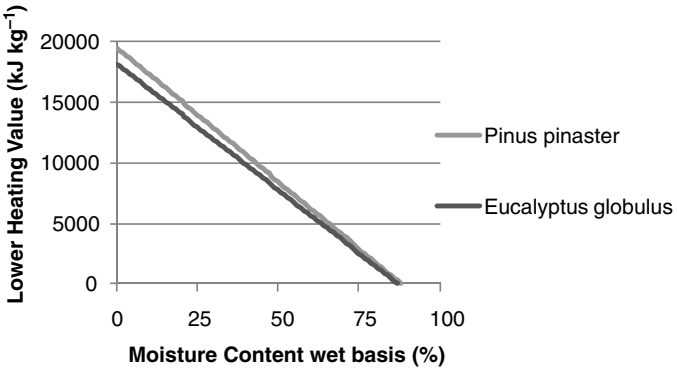

Fig. 7.11 Influence of moisture content on LHV for two types of wood: *Pinus pinaster* (softwood) and *Eucalyptus globulus* (hardwood); adapted from Rogaume (2005).

Tab. 7.11 Required moisture content, dry basis, for thermochemical conversion (McKendry, 2002b; Pang, 2008).

	Combustion	Gasification	Pyrolysis
Required MC (db)	Up to 50%	10–15%	5–10%

provoke material damage: fouling of reactors or wear of turbine blades working with the syngas, and (ii) their emission into the atmosphere is a public health problem: skin or lung cancer risk after prolonged exposure (Fontaine, 2009).

Thus, for many reasons, the technologies used for the thermochemical conversion of biomass require a raw material with low and homogeneous moisture content (Tab. 7.11).

In the case of combustion, the required moisture content depends on the size of the boiler. It can reach 50% for fuel intended for industrial plants, which can be supplied just-in-time with wood chips produced from logs. However, the individual housing boilers need combustibles with lower moisture content. The optimum is about 15–20% (Pang, 2008).

However, at harvest time, the moisture content of the biomass can be high. As an example, the moisture content of pine can reach values higher than 100% db. This explains why a preconditioning step that includes drying is compulsory.

Furthermore, the dried biomass has mechanical properties that are interesting for its energetic conversion. As an example, the strength impact decreases with decreasing moisture content: the energy saving during grinding attains 40% if the biomass is pre-dried (Bergman *et al.*, 2005; Repellin *et al.*, 2010). This is of great advantage for the pressurized fluidized bed gasification, a process that requires a maximum particle size of about 500 μm. Such a small size is very difficult to obtain, and energy demanding because of the fibrous nature of lignocellulosic products.

Finally, because of its biological origin, the lignocellulosic material is perishable, especially in the presence of water. In this case, a microbial population develops that degrades biomass with exothermic reactions. This represents a danger for the storage of biomass stocks, where a phenomenon of self-ignition can occur (Li *et al.*, 2005). Furthermore, the biological degradation of biomass represents a mass loss up to 3% per month (Hamelinck *et al.*, 2005). Drying the lignocellulosic material before storage prevents this biological degradation. On the other hand, the described exothermic process can be used to convert one part of the biomass into energy to dry wood chips (Ast, 2009).

As the distribution map of biological production does not overlap that of energy consumption, worldwide fluxes of biomass are expected (IEA Bioenergy, 2010). Transportation will, therefore, be decisive in the global life cycle assessment of the energy recovery process. Drying helps to restrict the cost of transportation by reducing the weight carried (McIlveen-Wright *et al.*, 2001).

In conclusion, whatever the way of thermochemical conversion of the biomass, the drying enables one to increase the efficiency of the process while preventing

pollution. Thus, it is one of the key steps of the biomass energy recovery, which have to be keenly mastered in order to optimize the production line.

7.4.1.1 Dryers for Biomass

More than three quarters of the biomass harvested each year is converted into heat by combustion (World Energy Council, 2007). Compared to other processes, combustion can tolerate a raw material with relatively high and heterogeneous moisture content. Moreover, the low added value requires the preconditioning to be as cheap as possible. This explains why natural drying of the biomass is common: it is neither fast nor easy to control, but requires only simple infrastructures. It can be easily improved if the biomass is dried under a hangar or a breathable cover.

However the need for industrially dried biomass will increase in the near future: this is the only way to quickly obtain a raw material with a low and homogeneous moisture content. Such feedstock is essential to supply large plants for the production of biofuels by thermochemical conversion. This kind of production is planned to increase fivefold between 2006 and 2030 (IEA, 2008). Compared to batch dryers, the continuous dryers need of course a higher investment, but they are often preferred because of their better integration into the production line: the handling and the intermediate storage are reduced which allows savings on space and workforce.

Hereafter, we present concisely the main types of convective dryers for biomass (Arlabosse, 2008; Ast, 2009; Mujumdar, 2007; Pang, 2008). For more information, refer to Mujumdar (2007).

Conveyor Dryers The biomass crosses, on a conveyor belt or in carts, a drying tunnel in which hot air is circulated. With this transport mode, the residence time does not depend on the particle size and geometry, which is a great advantage if these parameters are not constant from one particle to another. Moreover, the dryer can easily be adapted for a wide range of particle sizes: taking into account the characteristic drying time for a given particle size, the conveyor speed can be adjusted. It can also accept large particles because the dryer is robust due to the immobility of the particles within the bed. Flexibility is the main advantage of conveyor dryers.

The effectiveness of this type of dryer is mostly determined by the configuration of the airflow. Hot air can be injected around or through the bed. In the first case, heat and mass transfer between the biomass and the air is not optimal: there is a wide disparity of climatic conditions across the bed, causing a heterogeneity of moisture content between the core and the periphery at the dryer outlet. So the bed has to be thin. In the second configuration, the heterogeneity is lower because the air is forced across the bed. Moreover, to further reduce this heterogeneity the tunnel can be partitioned, allowing air to circulate through the bed from top to bottom in one part of the dryer, and inversely in the other part. Thus the bed can be thicker, which results in compact dryers.

In a conveyor dryer, the air velocity sets the minimum size of particles: they must not be blown away. For example, this technology is not suitable for drying sawdust or wood shavings.

Two types of configurations can be designed: parallel or counter-flow (Tab. 7.12).

Tab. 7.12 Comparison between counter and parallel flow configurations for a conveyor dryer.

	Drying Parameters	Parallel-Flow Configuration	Counter-Flow Configuration
Beginning of the tunnel	Airflow temperature	High	Low
	Relative humidity	Low	High
	Biomass temperature	Low	Low
	Consequences	No condensation	Condensation at the particles surface
End of the tunnel	Airflow temperature	Low	High
	Relative humidity	High	Low
	Biomass temperature	High	High
	Consequences	High equilibrium moisture content	Low equilibrium moisture content
	Conclusion	More efficient if the residence time is short	More efficient if the residence time is long

Rotary Dryers This type of dryer consists of a large cylinder, slightly inclined to the horizontal, rotating around its axis. The biomass enters the raised end of the cylinder and, due to gravity and the rotation, moves to the dryer outlet at the lower end. Thus the intrinsic parameters of the biomass (particle size, sphericity, density, etc.) significantly influence the speed of the biomass along the dryer and, therefore, the residence time. Adjusting the inclination of the cylinder and the rotation speed can regulate the residence time. The mode of moving requires the biomass to be well calibrated to obtain an even residence time, otherwise, a homogeneous moisture content at the exit cannot be guaranteed.

The rotating cylinder continuously mixes the biomass. Thus, all the particles are subjected to the same profile of climatic conditions along the dryer. This mixing can be improved by peripheral flights on the inside face of the cylinder: the biomass is lifted and tipped. This is an efficient way to reach the desired homogeneity of the biomass moisture content. However, one should note that rotary dryers cannot take large size particles, such as logs.

Based on the different ways of supplying the heat, we can differentiate between direct and indirect rotary dryers. In the first case, hot air is injected inside the cylinder: the biomass and the drying medium come into contact with each other. In the second case, either the wall of the dryer is heated (with fire or electricity) or steam flows through tubes inside the cylinder. These indirect rotary dryers are useful if the biomass is finely ground, to avoid entrainment of the particles by the airflow.

However, the heat transfer by convection (direct type) is more efficient than by conduction (indirect type), so the direct rotary dryers give a better yield. The presence of peripheral flights helps to improve this performance: when they fall, the particles pass through the air stream, which promotes heat and mass exchange between the drying medium and the biomass. If the biomass caliber is adequate, as is the case for wood chips, direct rotary dryers have to be preferred. In addition to their design and manufacture being easier, the investment is lower.

Rotary dryers are suitable for the preconditioning of small to medium size particles of biomass (sawdust, shavings, chips, etc.).

Fluidized Bed Dryer In a fluidized bed dryer, granular biomass is suspended by a drying medium. Usually the drying medium is a powerful upward hot air stream which passes through the biomass bed: the bed then behaves like a liquid. The *sine qua non* condition is that the air velocity must be greater (two to four times) than the minimum fluidization velocity, which depends on air viscosity and, mostly, on particle parameters: the fluidization is easier when the particles are relatively small, spherical, and with a low density. Thus the maximum particle size is limited by the available flow of hot gas: usually, the particle size ranges from 50 to 2000 μm. Smaller particles would be blown away.

The conventional fluidized bed dryer design consists of a vertical drying tower. The wet granular biomass is fed at the top of the tower and the dry product is discharged at the bottom: this is a counter-flow configuration. For the air velocity to be uniform in the dryer, the base of the tower must be equipped with a distributor. For a given type of particles, the role of the distributor is to obtain identical residence times wherever the particle is injected across the tower section. In any case, variable particle sizes would produce different residence times and result in a heterogeneous final moisture content.

Due to this intense mixing of the particles, the external transfer coefficients reach high values, which explains why fluidized bed drying is one of the most efficient processes of drying by convection. Moreover, the low residence time reduces the inertia of the system and facilitates the drying control by adjusting the airflow rate and its temperature. Nevertheless, the injection of air at relatively large flow rates requires a significant amount of electric energy.

Fluidized bed dryers are suitable for the preconditioning of small size particles of biomass. For example, they are used for sawdust or wood shavings drying in pelletizing plants.

Fixed Bed Dryer A non-agitated particle bed is crossed by a moderate stream of hot gas, lower than the minimum fluidization velocity: the biomass is not suspended. The biomass moves inside the tower by gravity: the biomass is fed at the top and is discharged at the bottom. The residence time is directly regulated by the exhaust flow of dry biomass and the air stream has no influence on the residence time. Even though it is usually the case, the airflow does not necessarily circulate from bottom to top. The particles are immobile relative to each other, so it is very important that the airflow is uniform across the tower section. The role of the air distributor is, therefore, of the utmost importance for the homogeneity of the moisture content.

The main advantage of fixed bed dryers is their ability to use air at a low temperature (40 to 200 °C). For example, energy can come from solar facilities, or from recovery heat produced by neighboring industrial plants (carbonization tower, etc.). Such flexibility reduces the cost of drying as a dedicated heat source is not essential. However, the residence time becomes long (some hours to several days). As a drawback, this technology causes a delay cost of the biomass, partly offset from an economic point of view by the low investment cost and by the high rate of filling. Nevertheless, if the bed is thick, the pressure drop of the air along the dryer can be high. So the electric power consumption of the fan is not negligible.

Fixed bed dryers are suitable for the preconditioning of medium size particles of biomass. As their cost of drying is low, they are a good alternative to natural air-drying for combustion.

7.4.1.2 Numerical Approach to the Continuous Drying of Woody Biomass

Whatever the conveying system, the design of continuous dryers for biomass and the choice of climatic conditions are tedious for engineers because the spatial evolution of the air parameters depends on the temporal evolution of the wood parameters. The optimization of the airflow configuration allows a low moisture content at the exit of the dryer to be guaranteed while avoiding overdrying in order to reduce the drying time and to save energy: we have to keep in mind that up to 70% of the life cycle cost of a convective dryer is due to energy (Mujumdar, 2007).

Numerical tools can be helpful for engineers to adjust the size of their equipment and to optimize the ventilation conditions. To simulate the drying of woody biomass, the stack is considered as a particulate medium: the basic element corresponds to the fragment of wood, whatever its size (from a fiber to a log). The use of a dual-scale model is perfectly suited to simulatation of the drying of such a particle system (Perré, 2007b; Perré and Rémond, 2006) as this formulation allows the variability of particles (initial moisture content, shape, size. . .), and the absence of local equilibrium to be accounted for.

At the Particle Scale: The Local Model Before considering the process modeling as a whole, it is essential that the behavior of a single particle can be predicted as a function of the climatic conditions.

Computational models are helpful tools to predict the evolution of the moisture content field and the stress in the woody particle. The control-volume approach has been widely used for this purpose (Patankar, 1980; Perré and Degiovanni, 1990; Prat, 1991; Turner, 1996) but its computational time would be huge when applied to hundreds of particles, and some phenomena are difficult to consider, such as the impact of open checks on mass migration, and hence on the drying kinetics.

This is why analytical models based on the concept of characteristic drying curves (van Meel, 1958; Chen, 2005; Sander, 2007) are often employed in the case of biomass preconditioning. Indeed, once implemented in the dual-scale model, their low computing time is suitable to simulate the simultaneous drying of a large number of particles. However, in these analytical models it is often assumed that all the heat transferred from the air to the wood is used solely for the evaporation of water: the

coupling between heat and mass transfer is, therefore, implicit. However, without considering the sensible heat, the model is not able to predict faithfully the evolution of the moisture content when the product temperature varies significantly, nor to predict condensation. This lack leads to a poor agreement with experimental results during the heating of the product (Chen, 2005; Saastamoinen and Impola, 1997).

In order to become a suitable particle model for continuous kilns, the van Meel model was enhanced by taking into account the coupling between heat and mass transfer in an explicit way, Fig. 7.12 (Colin *et al.*, 2008):

The global mass balance allows the evolution of the particle moisture content to be related to the vapor flux through the boundary layer:

$$m_0 \frac{d\bar{X}}{dt} = -h_m c M_v A_{particle} \ln \frac{P_{atm} - P_v^{\infty}}{P_{atm} - a(\phi, RH) P_{v,s}(\bar{T})} \tag{7.12}$$

In this equation, m_0 is the dry mass of the particle, c the molar concentration in the boundary layer and $A_{particle}$ is the area of the exchange surface. The vapor pressure at the surface of the particle is evaluated through the water activity:

$$P_v^{surf} = a P_{v,S}(\bar{T}) \tag{7.13}$$

The values of a are calculated from experimental results. During the drying, its value decreases from unity when the particle surface is supplied with free water to RH when the wood is in equilibrium with its surrounding air. Following the concept of a characteristic drying curve, the water activity is indentified as a function of RH and ϕ, the dimensionless moisture content (Eq. 7.14), and input in the enhanced van Meel model:

$$\phi = \begin{cases} 1 & \text{if} \quad \bar{X} \geq X_{cr} \\ \dfrac{\bar{X} - X_{eq}}{X_{cr} - X_{eq}} & \text{if} \quad \bar{X} < X_{cr} \end{cases} \tag{7.14}$$

This drying activity function contains all the heat and mass transfer properties of the material, and the geometry of the sample, and takes into account the mechanical phenomena which could have an influence on the kinetics, such as shrinkage, checks, deformations, and so on.

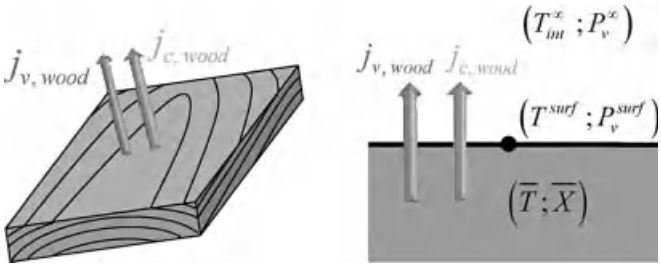

Fig. 7.12 Heat and mass fluxes at the surface of the particle.

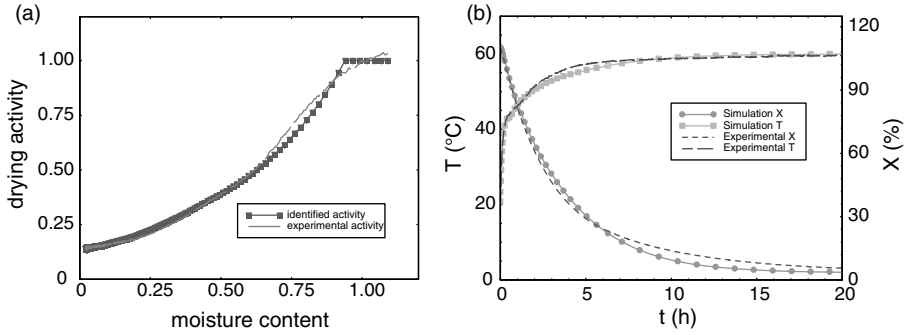

Fig. 7.13 (a) Identification of the drying activity and (b) simulation of the drying of a single particle.

The energy balance (Eq. 7.15) involves the latent heat of water evaporation and the heat capacity of wet wood:

$$m_0\left(c_{P,\text{wood}}+\bar{X}c_{P,\text{water}}\right)\frac{\mathrm{d}\bar{T}}{\mathrm{d}t}-m_0L_\text{v}\left(\bar{T}\right)\frac{\mathrm{d}\bar{X}}{\mathrm{d}t}=h_\text{c}A_\text{particle}\left(T_\text{int}^\infty-\bar{T}\right) \tag{7.15}$$

The numerical solution of the set of balance equations (Eqs. 7.12 and 7.15) allows the drying of one particle to be simulated. Figure 7.13a depicts the experimental and the identified drying activity function obtained from a drying test of one single particle. Using this function, the computational model is able to simulate faithfully the drying of a single particle (Fig. 7.13b) while keeping a low computing time. In this case, the activity has been identified for a thin quartersawn board of beech (80(R) × 10 (T) × 100(L) mm^3) subjected to a drying temperature of 60 °C at low relative humidity.

At the Dryer Scale: The Global Model On an industrial scale, the evolution of climatic conditions along the dryer depends on the drying of all particles and *vice versa*. Therefore, to simulate the continuous drying of a whole bed of particles, a two-way coupling between particle and bed has to be solved.

The global model (Colin *et al.*, 2009) calculates the evolution of the air parameters from the local heat and vapor fluxes at the surface of each particle, and at the surface of the wall, according to the equations:

$$\frac{\partial q_{\text{m},v}}{\partial x}=\frac{\sum_{i=1}^{M}\left(j_{\text{v,wood}}A_\text{particle}\right)_i+j_{\text{v,wall}}A_\text{wall}}{\mathrm{d}x} \tag{7.16}$$

$$\frac{\partial}{\partial x}\left(\left(q_{\text{m},v}c_{P,v}+q_{\text{m},a}c_{P,\text{a}}\right)T_\text{int}^\infty\right)=\frac{\sum_{i=1}^{M}\left(\left(j_{\text{c,wood}}-j_{\text{v,wood}}c_{P,v}\left(T_\text{int}^\infty-\bar{T}\right)\right)A_\text{particle}\right)_i}{\mathrm{d}x}+\frac{\left(j_{\text{c,wall}}-j_{\text{v,wall}}c_{P,\text{v}}\left(T_\text{int}^\infty-T_\text{int}^\text{wall}\right)\right)A_\text{wall}}{\mathrm{d}x} \tag{7.17}$$

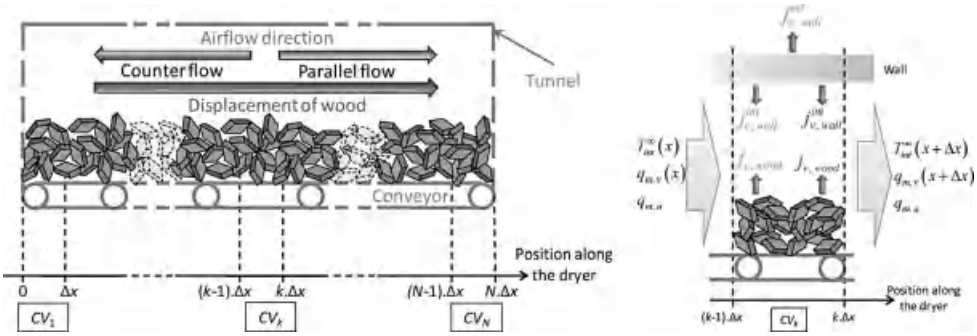

Fig. 7.14 Schematic diagram of a thin bed of wood chips in a conveyor dryer.

In this approach, the global model is connected to hundreds or thousands of local models, one for each particle.

In the following, we present results obtained with this global model for one configuration example (Fig. 7.14). A 10 cm thick bed of beech chips passes through a 5 m long drying tunnel on a 1.5 m wide conveyor belt. The 15 cm thick walls are made of concrete and the outside temperature is assumed constant (20 °C). The particle is considered as a parallelepiped ($55 \times 25 \times 10\,mm^3$) with an stochastic initial moisture content (90% ± 10%, following a Gaussian distribution).

The inlet temperature of the airflow is 120 °C and its relative humidity is 0.6%. The input airflow is $1\,m^3\,s^{-1}$ and the speed of the conveyor belt varies from 1 to $4\,m\,h^{-1}$. The heat and mass transfer coefficients are equal to $32\,W\,m^{-2}\,K^{-1}$ and $0.032\,m\,s^{-1}$, respectively. The bed is considered thin enough to assume that there is no gradient of air temperature and relative humidity along its thickness.

In the case of counter-flow (Fig. 7.15), we can notice that a condensation zone exists at the beginning of the dryer, where the particles entering with their initial temperature meet the airflow humidified during its course along the drying particles. This condensation zone does not exist in the parallel-flow configuration (Fig. 7.15), due to the low value of the inlet relative humidity. In the first part of the tunnel, the drying rate is higher in the case of parallel-flow. Thus, the parallel-flow configuration is more efficient if the residence time is short (high throughput of wood). In the second part of the kiln (Fig. 7.15), the trend is inverted and the counter-flow configuration becomes more efficient if the residence time is long (low throughput of wood or long kiln). Furthermore, the equilibrium moisture content of wood at the end of the dryer is the lowest in the case of the counter-flow configuration. With this model it is easy to identify the most efficient configuration: in this example this is the counter-flow configuration with a wood velocity of $2\,m\,s^{-1}$. If the velocity is higher, the woody biomass is not dry enough and, if the velocity is lower, overdrying occurs.

Because of its dual-scale structure, the model is able to predict the decrease in the biomass moisture content heterogeneity along the dryer (Fig. 7.16): it decreases from 60 to less than 3%.

More importantly, such a model is suitable both to design a dryer or to optimize its use, for example in the difficult problem of tuning the compromise between drying

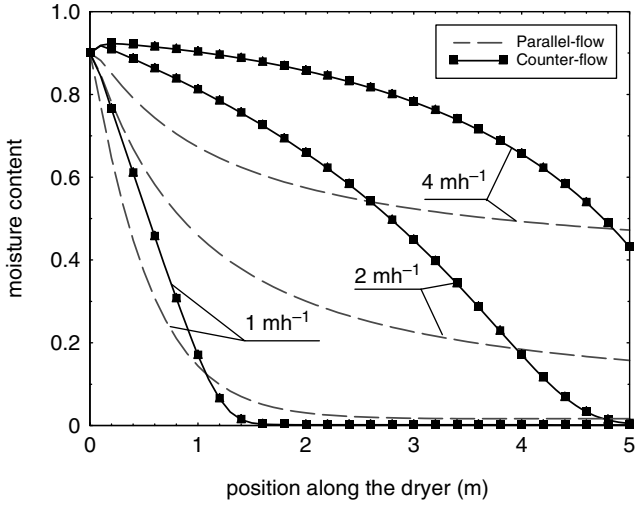

Fig. 7.15 Simulation of the spatial evolution of the average moisture content of wood along the tunnel in counter- or parallel-flow configuration.

quality (low and homogeneous final moisture content) and energy consumption (Tab. 7.13). The same characteristics as before were used in these simulations (outside temperature = 20 °C, inlet air temperature = 120 °C, inlet air flow rate = 1 $m^3 s^{-1}$). With the chosen bed dimensions, the rate of oven-dry mass ranges from 1.35×10^{-2} to 5.41×10^{-2} $kg\,s^{-1}$ when the bed velocity increases from 1 to 4 $m\,h^{-1}$. Table 7.13 shows that the counter flow configuration always leads to better energy efficiency. Moreover, it is not surprising that, for this open loop design, the energy ratio increases when the mass flow rate of product decreases. With a low mass flow rate, the final

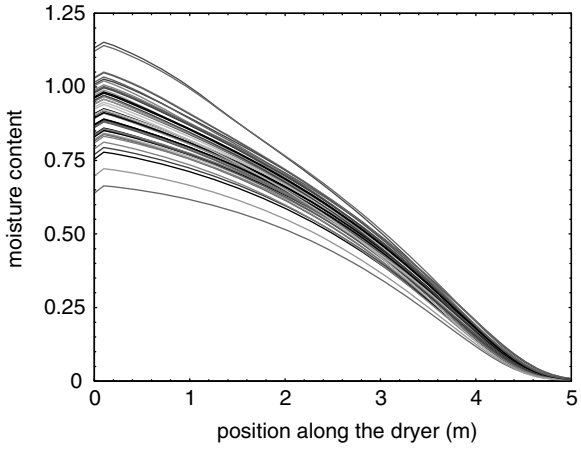

Fig. 7.16 Simulation of moisture content heterogeneity along the tunnel in counter-flow configuration (wood velocity of 2 $m\,s^{-1}$).

Tab. 7.13 Some outputs of the continuous drying model in terms of energy issues.

Configuration	Bed Velocity ($m\ h^{-1}$)	Outlet Moisture Content (%)	Outlet air Characteristics		Efficiency (%)	Energy Ratio ($kWh\ kg^{-1}$)
			T (°C)	RH (%)		
Counter flow	1	0.16	76.6	8.1	34.0	2.09
Parallel flow	1	1.69	80.0	7.0	33.5	2.13
Counter flow	2	0.50	45.0	56.2	66.4	1.05
Parallel flow	2	15.76	58.2	25.6	55.6	1.26
Counter flow	4	43.15	38.4	82.5	69.1	1.00
Parallel flow	4	47.23	48.0	46.8	63.6	1.10

moisture content is reduced, but the outlet air temperature increases dramatically, leading to important energy losses. Our model indeed allows us to know that the energy embedded in the air leaving the dryer is by far the most important explanation for energy loss (ca. 90%), whereas the other 10% is due to thermal losses through the walls (simply 20 cm of concrete in the present test) and in the energy used to heat the dry mass, and the final moisture content. From such observations, it is obvious that no satisfactory energy efficiency can be achieved at low final moisture content, unless a more expensive closed loop design is chosen, possibly combined with a heat pump.

Such a model may be useful to understand malfunctioning of existing dryers for biomass preconditioning, to choose adapted drying schedules, to help design of new kilns (length, air flow configuration, etc.), or to optimize kiln use (speed of wood, input airflow parameters, etc.). Moreover, it opens the possibility of predicting the benefit of mixed configurations (parallel-flow in the first part of the dryer and then counter-flow) or air recycling. And, due to the CPU efficiency of the local model, the dual-scale model remains interactive, despite the large number of particles: it needs about 10 min of computing time on a PC to simulate the drying of 350 000 chips.

7.4.2 Interest of Heat Treatment as a Preconditioning Step

Heat treatment of lignocellulosic materials by mild pyrolysis subjects the material to temperature levels up to 300 °C. The application of this process to wood has been intensively studied due to several technological advantages that this treatment can bring to this material. Several studies have demonstrated that heat treatment of wood permanently changes several of its chemical and physical properties. The change in properties is mainly caused by thermal degradation of hemicelluloses and amorphous cellulose, together with condensation of lignins (Windeisen *et al.*, 2007). Due to these changes, the OH groups available for water adsorption are significantly reduced, which in turn reduces the hygroscopicity (reduces water uptake, swelling and shrinkage). Almeida *et al.* (2009) demonstrated the decrease in hygroscopicity with increase in heating temperature in samples of eucalyptus (Fig. 7.17). Heat

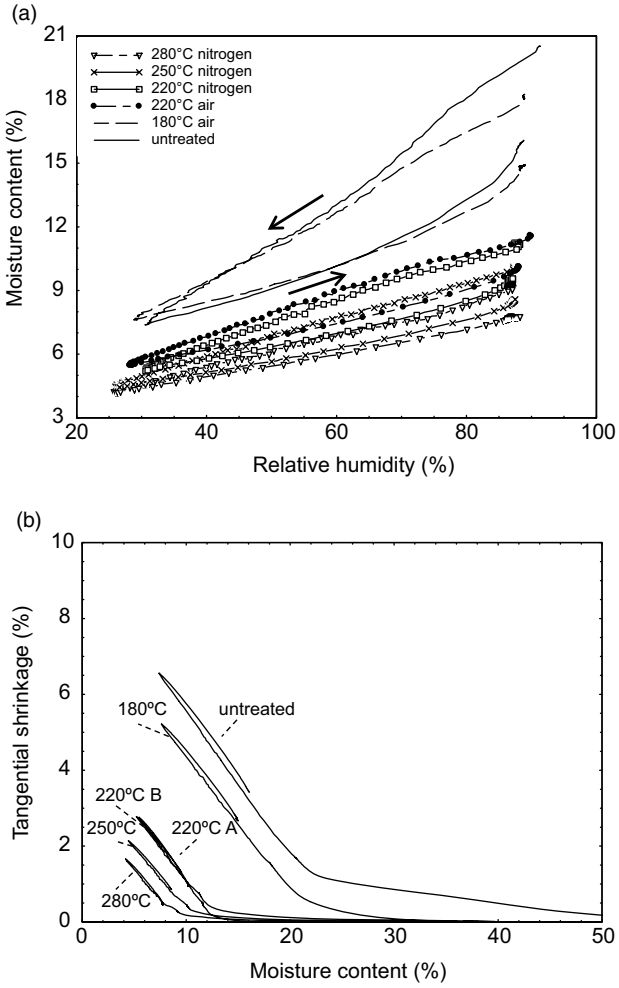

Fig. 7.17 Hygroscopic behavior of heat-treated *Eucalyptus saligna* wood. (a) Sorption curves, (b) tangential shrinkage as a function of moisture content (220 °C A = 220 °C air atmosphere; 220 °C B = 220 °C nitrogen atmosphere) (Almeida *et al.*, 2009).

treatment decreases the ratio of tangential to radial shrinkage (T/R), resulting in a decrease in wood transverse anisotropy. Reduction in wood hygroscopicity, decrease in wood transverse anisotropy, and increase in wood stability bring significant advantages to wood transport and storage. These advantages can be explored for several end-uses of wood: solid wood (inside and outside furniture, doors, windows, etc.) and wood as an energy source.

Heat treatment is a possible pre-treatment prior to further processes (grinding, combustion, gasification, etc.) to generate energy or biofuels. Almeida *et al.* (2010) studied the alterations in structural and energy properties of three eucalyptus species (wood and bark) subjected to heat treatment. Their results demonstrated that the

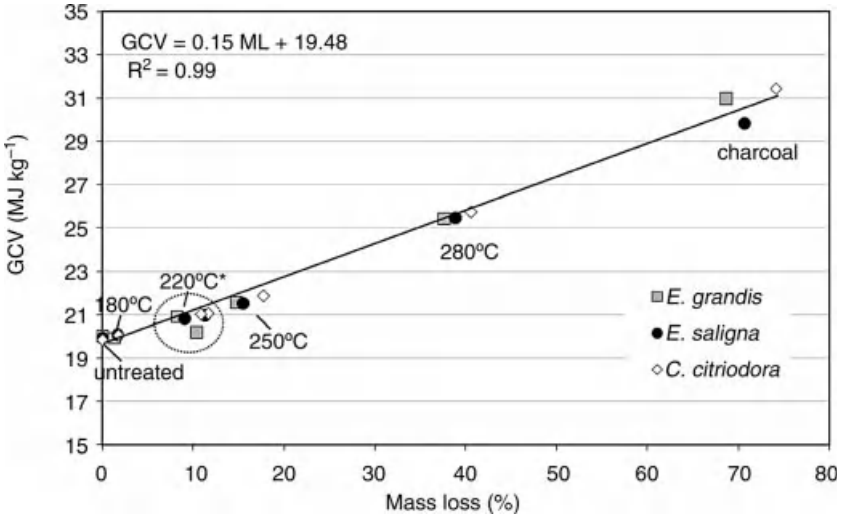

Fig. 7.18 Gross calorific value as a function of mass loss of Eucalyptus woods treated at several temperature levels (Almeida *et al.*, 2010). Charcoal data is taken from Brito and Barrichelo (1977) and Arantes *et al.* (2008).

process parameters (temperature levels and durations) can be tuned to obtain various products, ranging from native biomass to charcoal (Fig. 7.18). Energy yields were always higher than mass yields, thereby demonstrating the benefits of heat treatment in concentrating biomass energy (Fig. 7.19). The analysis of the whole data set also proved that the mass loss is an excellent indicator of the treatment intensity.

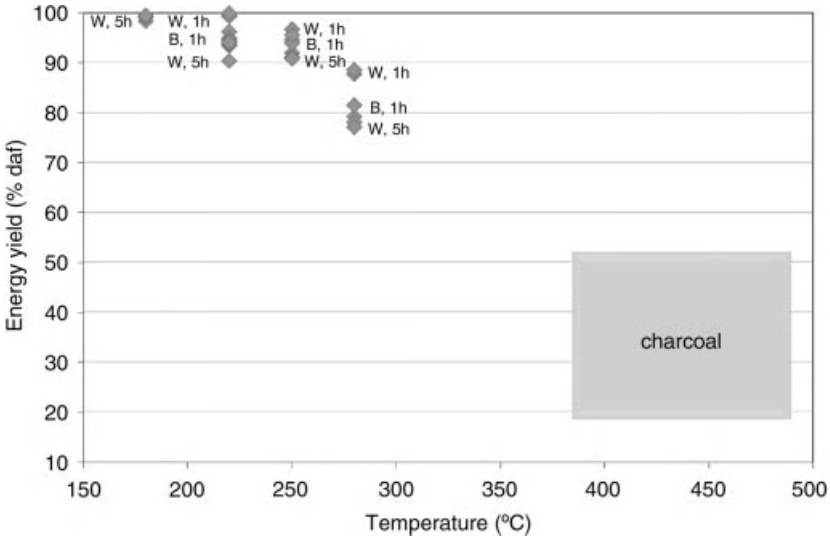

Fig. 7.19 Energy yield of wood (W) and bark (B) heat-treated under different conditions (Almeida *et al.*, 2010). Charcoal data is taken from Schenkel *et al.* (1997) (daf: dry ash free).

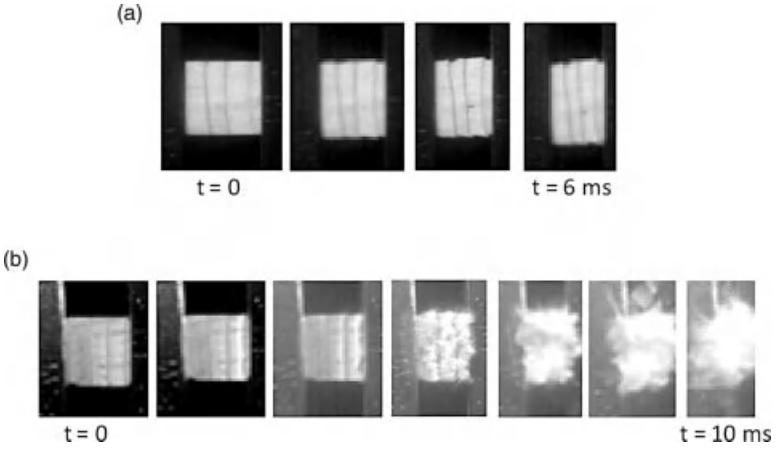

Fig. 7.20 Deformation of (a) untreated and (b) heat-treated (280 °C, 5 h) maritime pine wood during the impact (Pierre *et al.*, 2010).

Another consequence of the heat treatment is a decrease in the wood stiffness and the maximal compression stress. This decrease in mechanical properties is a disadvantage to solid wood uses, but is sometimes highly desired for energy use. In order to feed a gasifier, for example, the particle size has to be of the order of 500 μm, which requires a large amount of energy for native wood. In order to study the grindability of biomass, Pierre *et al.* (2010) designed and built an impact test device equipped with accelerometers and a high-speed camera. The brittle character of heat-treated wood is obvious, both on the strain–stress curves (not presented here) and when observing the sample with the high-speed camera (Fig. 7.20).

In principle, the heat-treatment of biomass resembles the drying operation and usually starts with a drying phase. The two main differences lie in the temperature level (roughly speaking between 200 and 280 °C) and the nature of gas (the oxygen level has to be very low above 220 °C to avoid combustion). From a practical point of view, the control of the process is very tricky due the exothermic reactions that take place above 240–250 °C. Thermal runaway easily occurs in industrial plants, completely ruining the expected product quality.

This field, with very little empirical knowledge, is suitable for computational-aided design and control of reactors. In order to be operational, the model has to combine several features (Turner *et al.*, 2010; Rémond *et al.*, 2010):

1) a comprehensive macroscopic formulation of coupled transport phenomena in the product (effect of internal pressure, effect of product anisotropy),
2) a relevant description of the chemical reactions and heat of reactions, expressed at the microparticle level,
3) a two-way coupled resolution of transport phenomena and reactions (thermo-activation of chemical reactions, source of heat and volatiles due to these reactions)

4) a dual-scale approach.

Altogether, the model is able to account for important mechanisms such as water evaporation, thermo-activation of the chemical reaction and heating of the particles due to exothermic reactions. Note that this effect is strongly tied to the design of the reactor and to the size of the particles. Internal heating of thick particles is the most obvious effect of the exothermic reactions, as biomass is usually a good thermal insulator. Additionally, more subtle effects can be of the utmost importance for the reactor process, such as:

- at low gas flow rates, the thermal runaway of a particle bed, even with small particles, due to the cumulative effect of reaction heats and thermo-activation,
- at higher gas flow rate, the increasing temperature of the gas along the flow due to the heat transferred from the particles, which may result in a thermal runaway at the outlet of the bed.

Figure 7.21 depicts a typical result obtained with one wood board submitted to a hot flow of gas (250 °C). During the drying and subsequent heating phase, the board temperature is less than the gas temperature. The transfer of heat by conduction within the board also explains why the core remains colder than the surface. Once the temperature level is enough to activate the exothermic reactions, the production of heat inside the board inverts this temperature profile, with a temperature level that decreases from the core to the surface, and to the gas (Fig. 7.21a). A double pressure peak is observed in experiment and simulation: the first peak is due to water evaporation, and the second to the production of volatiles by the chemical reactions. The comprehensive model formulation and a detailed discussion can be found in Turner *et al.* (2010).

A dual-scale modeling of the heat treatment of wood was proposed recently (Rémond *et al.*, 2010). On the local scale the computational code solves the coupled heat and mass transfer, and the thermal degradation mechanisms of wood components. On the global scale, the conditions along the channels formed by two adjacent board layers are computed.

Figure 7.22 depicts a simulation example in which the stack consists of 20 boards with a width of 25 cm (hence 2 m of stack depth). During the drying and heating period, the gas flow supplies heat to the stack, for water evaporation, which explains the decrease in dry-bulb temperature along the stack. The drying period is not completed at the end of the plateau at 110 °C. When the temperature increases above 110 °C, a massive and sudden evaporation of the remaining water occurs, which gives rise to an important pressure peak.

When the temperature level is sufficient to trigger the reactions, the behavior of board no. 1 (stack inlet) is similar to that observed for one single board (Fig. 7.21). The temperature of this board reaches 267 °C. However, the simulation results highlight that the exothermic reactions occurring in each single board can be accumulated along the stack: the temperature overshoot of one board triggers more intensively the exothermic reactions of the next boards in the direction of the gas flow. The situation is, therefore, much more severe for the board situated at the

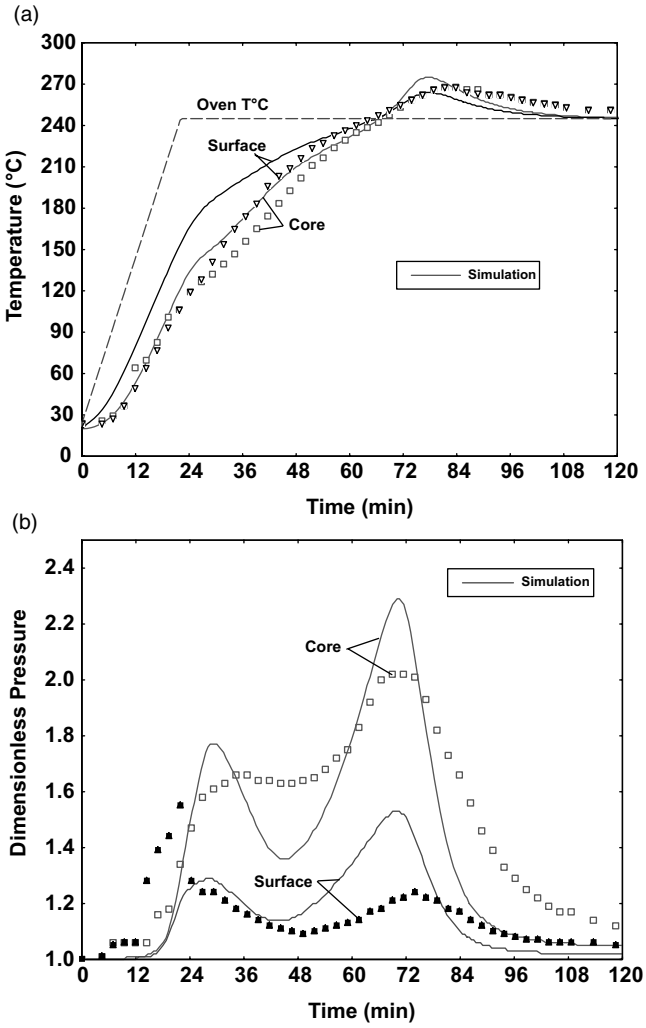

Fig. 7.21 Comparison between experimental and simulated (a) temperature curves and (b) dimensionless pressure at the core and beneath the exchange surface during the heat treatment of a quartersawn beech board ($24 \times 75 \times 250\,mm^3$ in T, R and L directions, respectively) with an initial MC of 5%, heated at 250 °C for 100 min (from Turner *et al.*, 2010).

outlet of the stack, with a temperature peak equal to 295 °C. In this case, the process heterogeneity due to the stack effect is obvious. To improve the industrial process, such a comprehensive dual-scale model can be used as a tool to decrease this heterogeneity (Rémond *et al.*, 2010).

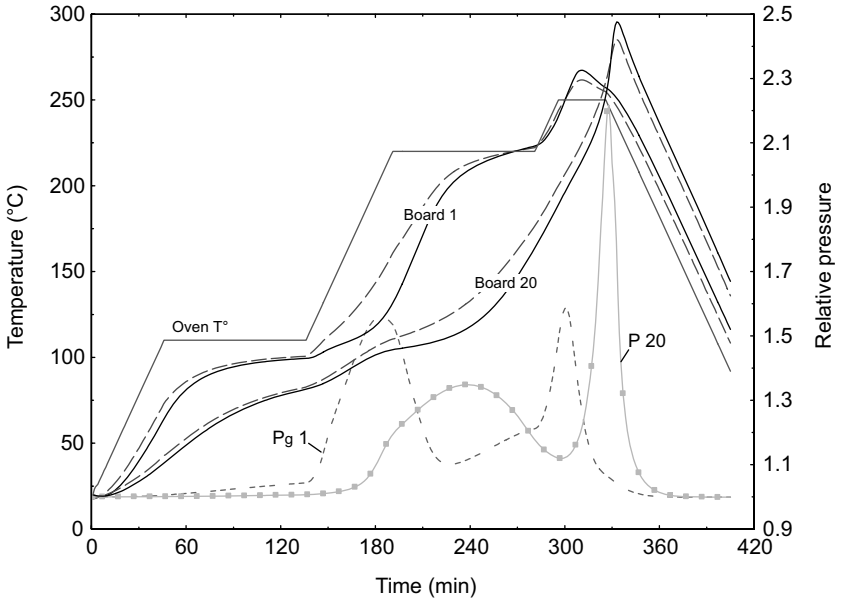

Fig. 7.22 Evolution of temperature and relative pressure (P/P_{atm}) at the surface and at the core of the boards located at the stack inlet (board no.1) and at the stack outlet (board no. 20). Initial moisture content is 25%, and gasflow velocity 2 m s^{-1} (from Rémond *et al.*, 2010).

7.5 Conclusions

This chapter has tried to provide an overview of the energy issues related to lignocellulosic biomass. This is a wide field of investigation, because complementary aspects have to be considered simultaneously:

- the *energy content*: the energy that can be gained from biomass, namely by combustion and gasification,
- the *energy consumption*: the energy that needs to be spent by different processing operations, such as transportation, storage, drying, heat treatment, grinding, and so on,
- the possibility of different processing operations to change both the energy content and the energy consumption, which implies a difficult optimization procedure from harvest to final use.

Drying appears to be a key process in both aspects, as the amount of water always present in harvested biomass alters its gross calorific value and requires a large amount of energy to be removed. Because of shrinkage, the water present in trees also needs to be removed down to the equilibrium moisture content when wood is used as an engineering material.

Except for the conventional drying of solid wood, very little empirical knowledge is available for the continuous drying and treatment of biomass for energy purposes, or for the drying of solid wood with innovative technology. Therefore, a fantastic field of applications exists for modeling approaches, and computational simulations, provided that these tools have a predictive potential.

Acknowledgements

The authors would like to thank the international cooperation programs between Brazil and France FAPES/INRA and CAPES/COFECUB.

Additional Notation Used in Chapter 7

a	drying activity function	–
c	molar density	$\mathrm{mol\,m^{-3}}$
h_m	mass transfer coefficient	$\mathrm{m\,s^{-1}}$
j	flux of mass or heat	$\mathrm{kg\,m^{-2}\,s^{-1}}$, $\mathrm{W\,m^{-2}}$
K	overall heat transfer coefficient	$\mathrm{W\,m^{-2}\,K^{-1}}$
l	layer width	m
L_v	specific enthalpy of evaporation	$\mathrm{J\,kg^{-1}}$
P	pressure (total or partial)	Pa
Q	amount of heat	J
q_m	mass flow rate	$\mathrm{kg\,s^{-1}}$
q_{th}	heat loss flux	$\mathrm{W\,m^{-2}}$
RH	relative humidity	–
W	work	J

Greek Letters

ϕ	dimensionless moisture content	–

Subscripts and Superscripts

a	air
atm	atmospheric
c	convection
db	dry bulb
ext	external
fsp	fiber saturation point
ini	initial
int	internal
s	sorption
th	thermal
0	reference value (dry mass)

Abbreviations

ADEME	Agence de l'Environnement et de la Maîtrise de l'Énergie
BTL	biomass to liquid
CDR	constant drying rate period
CV	control volume
db	dry basis
EMC	equilibrium moisture content
EROEI	energy returned on energy invested
ESEM	environmental scanning electron microscopy
FAO	Food and Agriculture Organization of the United Nations
FC	fixed carbon
FCBA	Institut Technologique Forêt Cellulose Bois-construction Ameublement
FSP	fiber saturation point
GCV	gross calorific value
Gtoe	gigatons of oil equivalent
IEA	International Energy Agency
IFP	Institut Français du Pétrole
IPCC	Intergovernmental Panel on Climate Change
L	longitudinal direction
LHV	lower heating value
MC	moisture content
MDF	medium density fiber panels
NCV	net calorific power
R	radial direction
T	tangential direction
UN	United Nations
VM	volatile matter

References

Abreu, L. R. C., Igarza, U. O., Machado, E. C., 2004. Composición química de tres maderas en la provincia de Pinar del Río, Cuba a tresalturas del fuste comercial. Parte 4: Estudio comparativo de la composición química. *Revista Chapingo* **10**: 77–81.

ADEME, 2005. *La récolte raisonnée des rémanents en forêt*, guide pratique. 35 p.

Aléon, D., Chanrion, P., Négrié, G., Perez, J., Snieg, O., 1990. *Séchage du bois: guide pratique*, CTBA, Paris, France.

Aléon, D., 2008. Réduction de la consommation énergétique du séchage sous vide du bois. Research report no. 03-74-C0159, FTBA, Paris, France.

Almeida, G., Brito, J. O., Perré, P., 2009. Changes in wood-water relationship due to heat treatment assessed using micro-samples of Eucalyptus. *Holzforschung* **63**(1): 80–88.

Almeida, G., Brito, J. O., Perré, P., 2010. Alterations in energy properties of eucalyptus wood and bark subjected to torrefaction: the potential of mass loss as a synthetic indicator. *Bioresour. Technol.* **101**(24): 9778–9784.

Arantes, M. D. C., Mendes, L. M., Rabelo, G. F., Silva, J. R. M., Mori, F. A., Barbosa, A. M., 2008. Gaseificação de materiais lignocelulósicos para geração de energia elétrica. *Ciência Florestal* **18**: 525–533.

Arlabosse, P., 2008. *Séchage industriel - Aspects pratiques*. Techniques de l'Ingénieur, J2455. 24 p.

Ast, J., 2009. Étude de l'évolution des caractéristiques physico-chimiques des plaquettes forestières en fonction des modalités de stockage et de séchage. Diss. Université Henri Poincaré, Nancy, France, 209 p.

Barker, A. J., 1983. Wood fuel properties and fuel products from woods. *Proceedings of fuelwood management and utilization seminar*, East Lansing, Michigan State University, pp. 14–25.

Bergman, P. C. A., Boersma, A. R., Kiel, J. H. A., Prins, M. J., Ptasinski, K. J., Janssen, F. J. J. G., 2005. Torrefaction for entrained-flow gasification of biomass. Report ECN-C-05-067, Energy Research Centre of the Netherlands, 50 p.

Bertaud, F., Holmbom, B., 2004. Chemical composition of earlywood and latewood in Norway spruce heartwood, sapwood and transition zone wood. *Wood Sci. Technol.* **38**: 245–256.

Bird, R. B., Steward, W. E., Lightfoot, E. N., 1960. *Transport phenomena*. John Wiley and Sons, New York.

Bodros, E., Pillin, I., Montrelay, N., Baley, C., 2007. Could biopolymers reinforced by randomly scattered flax fibre be used in structural applications? *Compos. Sci. Technol.* **67**: 462–470.

Bodros, E., Baley, C., 2008. Study of the tensile properties of stinging nettle fibres (*Urticadioica*). *Mater. Lett.* **62**: 2143–2145.

BP, 2010. Statistical Review of World Energy. 45 p.

Brito, J. O., Barrichelo, L. E. G., 1977. Correlações entre características físicas e químicas da madeira e a produção de carvão vegetal: i. Densidade e teor de ligninadamadeira de eucalipto. *IPEF* **14**: 9–20.

Brito, J. O., Barrichelo, L. E. G., 1978. Características do eucalipto como combustível: análise química imediata da madeira e dacasca. *IPEF* **16**: 63–70.

Bryden, M. K., Hagge, M. J., 2003. Modeling the combined impact of moisture and char shrinkage on the pyrolysis of a biomass particle. *Fuel* **82**(13): 1633–1644.

Bux, M., Bauer, K., Mühlbauer, W., Conrad, T., 2001. Solar-assisted drying of timber at industrial scale. *S. Afr. Forest. J.* **192**: 73–78.

Chanrion, P., Davesne, A., 1991. *Le séchage des feuillus, une nécessité économique*. CTBA, Paris, France.

Chen, X. D., 2005. A discussion on a generalized correlation for drying rate modeling. *Drying Technol.* **23**(3): 415–426.

Cheng, Q., Wang, S., Harper, D. P., 2009. Effects of process and source on elastic modulus of single cellulose fibrils evaluated by atomic force microscopy. *Composites: Part A* **40**: 583–588.

Colin, J., Rémond, R., Perré, P., 2008. An enhanced van Meel model implemented in a dual scale model for the continuous drying of biomass. *Proceedings of 16th International Drying Symposium* (IDS2008), Hyderabad, Volume A, pp. 273–279.

Colin, J., Rémond, R., Perré, P., 2009. A computational model for the continuous drying of wood chips for energy use. *Cahier de l'AFSIA* **23**: 12–13.

Cortez, L. A. B., Lora, E. S., Gomez, E. O., 2008. Caracterização da biomassa, in *Biomassa para energia*. Editorada UNICAMP, Chapter 2 (eds. L. A. B. Cortez, E. E. S. Lora, E. O. Gomez), Campinas, São Paulo, Brazil.

Couhert, C., Salvador, S., Commandré, J.-M., 2009. Impact of torrefaction on syngas production from wood. *Fuel* **88**: 2286–2290.

Dedic, A., Zlatanovic, M., 2001. Some aspects and comparisons of microwave drying of beech (*Fagus moesiaca*) and fir wood (*Abies alba*). *Holz als Roh- und Werkstoff* **59**(4): 246–249.

Demirbas, A., 1997. Calculation of higher heating values of biomass fuels. *Fuel* **76**(5): 431–434.

Dias De Oliveira, M. E., Vaughan, B. E., Rykiel, E. J. Jr., 2005. Ethanol as fuel: energy, carbon dioxide balances, and ecological footprint. *Bioscience* **55**(7): 593–602.

FAO, 1997. Renewable biological systems for alternative sustainable energy production. *FAO Agricultural Services Bulletin* 128.

FAO, 2010. http://faostat.fao.org, accessed on 1st November 2010.

Field, C. B., 1998. Primary production of the biosphere: integrating terrestrial and oceanic components. *Science* **281**: 237–240.

Fontaine, B., 2009. Traduction de la liste des évaluations faites par le centre international sur le cancer sur les risques de

cancérogénicité pour l'homme et commentaire sur l'utilisation des agents cités, Pôle Santé-Travail, Lille, France, 33 p.
Fortin, Y., Defo, M., Nabhani, M., Tremblay, C., Gendron, G., 2004. A simulation tool for the optimization of lumber drying schedules. *Drying Technol.* **22**(5): 963–983.
Goda, K., Cao, Y., 2007. Research and development of fully green composites reinforced with natural fibers. *J. Solid Mech. Mater. Eng.* **1**: 1073–1084.
Hall, C. A. S., Balogh, S., Murphy, D. J. R., 2009. What is the minimum EROI that a sustainable society must have? *Energies* **2**: 25–47.
Hamelinck, C. N., Suurs, R. A. A., Faaij, A. P. C., 2005. International bioenergy transport costs and energy balance. *Biomass Bioenerg* **29**: 114–134.
Hammerschlag, R., 2006. Ethanol's energy return on investment: a survey of the literature 1990-Present. *Environ. Sci. Technol.* **40**: 1744–1750.
Hwang, B. J., Wang, C.-H., Liou, C.-T., 1994. Optimal operational strategy for wood in batch drying system. *Can. J. Chem. Eng.* **72**(4): 594–601.
IEA, 2008. World Energy Outlook, 569 p.
IEA Bioenergy, 2010. Annual report 2010, 136 p.
IFP, 2008. Charbon: ressources, réserves et production, 9 p.
IPCC, 2007. Climate change, synthesis report, 4th assessment, 104 p.
Jacobsen, R. L., Tritt, T. M., Guth, J. R., Ehrlich, A. C., Gillespie, D. J., 1995. Mechanical properties of vapor-grown carbon fiber. *Carbon* **33**: 1217–1221.
Jenkins, B. M., Baxter, L. L., Miles, T. R. Jr., Miles, T. R., 1998. Combustion properties of biomass. *Fuel Process. Technol.* **5**: 17–46.
Joly, P., More-Chevalier, F., 1980. *Théorie, pratique et économie du séchage des bois.* H. Vial, Dourdan, France.
Jung, H., Lee, J., Lee, N., 2000. Vacuum-press drying of thick softwood lumbers. *Drying Technol.* **18**(8): 1921–1933.
Guitard, D., 1994. Comportement mécanique du bois. Capter 3 in: P. Jodin. *Le bois, matériau d'ingénierie,* Editions *A.R.B.O.L.O.R.* 433 p.
Keey, R., Langrish, T., Walker, J., 2000. *The kiln-drying of lumber.* Springer, Berlin.
Leiker, M., Adamska, M., 2004. Energy efficiency and drying rates during vacuum microwave drying of wood. *Holz als Roh - und Werkstoff* **62**(3): 203–208.
Li, X.- R., Koseki, H., Momota, M., 2005. Evaluation of danger from fermentation-induced spontaneous ignition of wood chips. *J. Hazard. Mater.* **135**(1–3): 15–20.
McCurdy, M., Pang, S., 2007. Optimization of kiln drying for softwood through simulation of wood stack drying, energy use, and wood color change. *Drying Technol.* **25**(10): 1733–1740.
McKendry, P., 2002a. Energy production from biomass, Part 1: Overview of biomass. *Bioresour. Technol.* **83**: 37–46.
McKendry, P., 2002b. Energy production from biomass, Part 2: Conversion technologies. *Bioresour. Technol.* **83**(1): 47–54.
McKendry, P., 2002c. Energy production from biomass, Part 3: gasification technologies. *Bioresour. Technol.* **83**(1): 55–63.
McIlveen-Wright, D. R., Williams, B. C., McMullan, J. T., 2001. A re-appraisal of wood-fired combustion. *Bioresour. Technol.* **76**: 183–190.
MEEDDAT, 2008. Grenelle Environnement: Réussir la transition énergétique, 50 mesures pour un développement des energies renouvelables à haute qualité environnementale, 26 p.
Meo, M., Rossi, M., 2006. Prediction of Young's modulus of single wall carbon nanotubes by molecular-mechanics based finite element modelling. *Compos. Sci. Technol.* **66**: 1597–1605.
Mujumdar, A. S., 2007. *Handbook of industrial drying.* 3rd edn, CRC Press, USA, p. 1280.
Nijdam, J. J., Keey, R. B., 2000. The influence of kiln geometry on flow maldistribution across timber stacks in kilns. *Drying Technol.* **18**: 1865–1877.
Nijdam, J. J., Keey, R. B., 2002. New timber kiln designs for promoting uniform airflows within the wood stack. *Trans. IChemE* **80**(A): 739–744.
Nordin, A., 1994. Chemical elemental characteristics of biomass fuels. *Biomass Bioenerg* **6**: 339–347.
Núñez-Regueria, L., Rodríguez-Añon, J. A., Proupín-Castiñeiras, J., Vilanova-Diz, A., Montero-Santoveña, N., 2001. Determination of calorific values of forest

waste biomass by static bomb calorimetric. *Thermochim. Acta* **371**(1–2): 23–31.

Palandre, L., Clodic, D., 2003. Comparison of heat pump dryer and mechanical steam compression dryer. *Proceedings of International Congress of Refrigeration*, Washington D.C., USA.

Pang, S., 2008. Drying of woody biomass for bioenergy: drying technologies for an integrated bioenergy plant. *Proceedings of 16th International Drying Symposium (IDS2008)*, Hyderabad, Volume A, pp. 25–35.

Panshin, A. J., de Zeeuw, C., 1980. *Textbook of wood technology*. 4th edn, McGraw Hill, New York, USA.

Parikh, J., Channiwala, S. A., Ghosa, G. K., 2005. A correlation for calculating HHV from proximate analysis of solid fuels. *Fuel* **84**: 487–494.

Pastor-Villegas, J., Meneses Rodríguez, J. M., Pastor-Valle, J. F., Rouquerol, J., Denoyel, R., García-García, M., 2010. Adsorption–desorption of water vapour on chars prepared from commercial wood charcoals, in relation to their chemical composition, surface chemistry and pore structure. *J. Anal. Appl. Pyrol.* **88**: 124–133.

Patankar, S. V., 1980. *Numerical heat transfer and fluid flow*. Hemisphere Publishing Corporation, New York, 192 p.

Patzek, T., Pimentel, D., 2005. Thermodynamics of energy production from biomass. *Crit. Rev. Plant Sci.* **24**(5–6): 327–364.

Perré, P., 1993. Le séchage du bois. Teaching notes, ENGREF, Nancy, France.

Perré, P., 1996. The numerical modelling of physical and mechanical phenomena involved in wood drying: an excellent tool for assisting with the study of new processes. *Proceedings of 5th International IUFRO Wood Drying Conference*, Québec, Canada, pp. 9–38.

Perré, P., 2001. The drying of wood: The benefit of fundamental research to shift from improvement to innovation. *Proceedings of 7th International IUFRO Wood Drying Conference*, Tsukuba, Japan, pp. 2–13.

Perré, P. (ed.) 2007a. *Fundamentals of wood drying*, COST E15 and ARBOLOR, Nancy, France.

Perré, P., 2007b. Multiscale aspects of heat and mass transfer during drying. *Transport Porous Med.* **66**(1–2): 59–76.

Perré, P., 2010. Multiscale modelling of drying as a powerful extension of the macroscopic approach: Application to solid wood and biomass processing. *Drying Technol.* **28**: 944–959.

Perré, P., Degiovanni, A., 1990. Simulation par volumes finis des transferts couplés en milieu poreux anisotropes: séchage du bois à basse et à haute température. *Int. J. Heat Mass Tran.* **33**(11): 2463–2478.

Perré, P., Keey, R., 2006. Drying of wood: Principles and practice, in *Handbook of Industrial Drying*, 3rd edn (ed. A. S. Mujumdar). Marcel Dekker, New York, pp. 821–877, Ch. 36.

Perré, P., Rémond, R., 2006. A Dual scale computational model of kiln wood drying including single board and stack level simulation. *Drying Technol.* **4**(1–6): 1069–1074.

Perré, P., Rémond, R., Aléon, D., 2007. Energy saving in industrial wood drying addressed by a multi-scale computational model: Board, stack and kiln. *Drying Technol.* **25**: 75–84.

Pierre, F., Almeida, G., Brito, J. O., Perré, P., 2010. Grindability behavior of torrefied biomass for energy purpose. *18th European Biomass Conference and Exhibition*, Lyon, France, 3 –7 May 2010.

Prat, M., 1991. 2D modelling of drying of porous media: Influence of edge effects at the interface. *Drying Technol.* **9**(5): 1181–1208.

Raghavan, G. S. V., Rennie, T. J., Sunjka, P. S., Orsat, V., Phaphuangwittayakul, W., Terdtoon, P., 2005. Overview of new techniques for drying biological materials with emphasis on energy aspects. *Braz. J. Chem. Eng.* **22**: 195–201.

Rémond, R., Perré, P., 2008. High frequency heating controlled by convective hot air: Toward a solution for on-line drying of softwoods. *Drying Technol.* **26**: 530–536.

Rémond, R., Turner, I., Perré, P., 2010. Dual-scale model for heat treatment of wood: Evidence of thermal run-away due to the cumulative effect of exothermic reactions. *Proceedings of 17th International Drying*

Symposium (IDS 2010), Magdeburg, Germany, pp. 1311–1316.

Repellin, V., Govin, A., Rolland, M., Guyonnet, R., 2010. Energy requirement for fine grinding of torrefied wood. *Biomass Bioenerg.* **34**: 9923–9930.

Rosen, H. N., 1980. High-temperature initial drying of wood: Potential for energy recovery. *Forest Prod. J.* **30**: 29–35.

Rowell, R. M., Han, J. S., Rowell, J. S., 2000. Characterization and factors effecting fiber properties, in *Natural Polymers and Agrofibers Composites*, São Carlos, Brazil, pp. 115–134.

Rogaume, Y., 2005. Production de chaleur à partir du bois: combustible et appareillage. *Techniques de l'Ingénieur*, 15 p.

Saastamoinen, J., Impola, R., 1997. Drying of biomass particles in fixed and moving beds. *Drying Technol.* **15**(6–8): 1919–1929.

Salin, J. G., 2001. Global modelling of kiln drying; taking local variations in the timber stack into consideration. *Proceedings of 7th International IUFRO Wood Drying Conference*, Tsukuba, Japan, pp. 34–39.

Salin, J. G., Wamming, T., 2008. Drying of timber in progressive kilns: Simulation, quality, energy consumption and drying cost considerations. *Wood Mater. Sci. Eng.* **3**: 12–20.

Sander, A., 2007. Thin layer drying of porous materials: Selection of the appropriate model and relationships between thin-layer models parameters. *Chem. Eng. Process.* **46**: 1324–1331.

Schenkel, Y., Bertaux, P., Vanwijnsberghe, S., Carré, J., 1997. Une évaluation de la technique de la carbonisation en meule. *Biotechnol. Agron. Soc. Environ.* (1): 113–124.

Siau, J. F., 1984. *Transport processes in wood*. Springer, New York, USA.

Solomon, B. D., 2010. Biofuels and sustainability. *Ann. N. Y. Acad. Sci.* **1185**: 119–134.

Ståhl, M., Granström, K., Berghel, J., Renström, R., 2004. Industrial processes for biomass drying and their effects on the quality properties of wood pellets. *Biomass Bioenerg.* **27**: 621–628.

Stevanovic, T., Perrin, D., 2009. *Chimie du bois*, Presses Polytechniques et Universitaires Romandes, p. 242.

Thygesen, A., Thomsen, A. B., Daniel, G., Lilholt, H., 2007. Comparison of composites made from fungal defibrated hemp with composites of traditional hemp yarn. *Ind. Crop. Prod.* (25): 147–159.

Turner, I. W., 1996. A two-dimensional orthotropic model for simulating wood drying processes. *Appl. Math. Model.* **20**(1): 60–81.

Turner, I. W., Rousset, P., Rémond, R., Perré, P., 2010. An experimental and theoretical investigation of the thermal treatment of wood in the range 200–260 °C. *Int. J. Heat Mass Transfer* **53**: 715–725.

UN, 1997. Kyoto Protocol to the United Nations framework convention on climate change, 20 p.

UN Statistic Division, 2010. Carbon dioxide emissions, Update 23rd June 2010.

Van Meel, D. A., 1958. Adiabatic convection batch drying with recirculation of air. *Chem. Eng. Sci.* **9**: 36–44.

Windeisen, E., Strobel, C., Wegener, G., 2007. Chemical changes during the production of thermo-treated beech wood. *Wood Sci. Technol.* **41**: 523–536.

World Energy Council, 2007. Survey of Energy Resources, 586 p.

Yatim, B. B., Hoi, W. H., 1987. The quality of charcoal from various types of wood. *Fuel* **66**: 1305–1306.

Zhang, B. G., Zhou, Y. D., Ning, W., Xie, D. B., 2007. Experimental study on energy consumption of combined conventional and dehumidification drying. *Drying Technol.* **25**(3): 471–474.

8
Efficient Sludge Thermal Processing: From Drying to Thermal Valorization

Patricia Arlabosse, Jean-Henry Ferrasse, Didier Lecomte, Michel Crine, Yohann Dumont, and Angélique Léonard

8.1
Introduction to the Sludge Context

8.1.1
Origin, Production and Valorization Issues

The constituents removed in a wastewater treatment plant (WWTP) include screenings, grit, scum, solids, and biosolids, collectively called sludge. Of all these constituents, biosolids produced during the biological treatment represent the largest amount in volume. Indeed, an excess of biomass generated through the assimilation of biodegradable materials by a flora of microorganisms has to be removed from the system. The treatment of the wastewater of one so-called "population equivalent", PE, will produce annually between 15 and 20 kg of sludge, expressed in dry matter. However, these solids and biosolids are in the form of a liquid or semi-solid liquid, containing from 0.25 to 12% solids by weight. According to regulations, the sludge is a waste product that has to be first treated and then reused or disposed of by the municipalities. Sludge management is an ever-increasing problem due to the environmental pollution and energy consumption that result from progressive generation of industrial and municipal sludge. For example, 11.7 million tons of municipal sludge (expressed as dry matter) are produced each year in the European Union (Milieu Ltd *et al.*, 2008). In China, the total amount of urban sludge generated annually was around 8.4 million tons of dry matter in 2010 and should further increase in the following years. The same amount was projected for the municipal wastewater in the United States in 2010 (Zsirai, 2010).

Within WWTPs, the first treatment applied to sludges consists in reducing their water content by thickening, conditioning, mechanical and/or thermal dewatering. Table 8.1 clearly shows that the energy demand related to drying is much higher than the energy consumption of gravitational or mechanical techniques. Ideally, the highest possible amount of water should have been removed at the end of mechanical dewatering in order to save energy during the drying process. Taking sludge with 25%

Modern Drying Technology Volume 4: Energy Savings, First Edition.
Edited by Evangelos Tsotsas and Arun S. Mujumdar.

Tab. 8.1 Techniques used to decrease water content in sludges (Moller, 1990).

Technique	Energy demand kWh per ton of water	Dry solids content range
Thickening	10^{-3}–10^{-2}	≤5–6%
Mechanical dewatering	1–10	≤20–25%
Thermal drying	10^{3}	≤95%

dry solids content as a reference, Permuy Vila (2008) showed that the drying energy costs increased by 92% when the initial dry solids content fell to 15%, and decreased by 23% for an inlet dry solids content of 30%. However, it should be noted that the situation is much more complex, and in some cases the shear stresses undergone by the sludge in centrifuges, for example, will alter its drying behavior.

Various techniques can be used to treat the organic material present in the sludge, such as digestion in order to produce biogas, or composting. Liming can also be used to stabilize the product and enhance its structure. A huge number of combinations of these methods are possible (Metcalf & Eddy Inc., 2003). Furthermore, several reuse possibilities are available: utilization of sludge as a raw material for industrial production, energy recovery, or soil amendment. Energy recovery may refer to thermal valorization via incineration (see below), pyrolysis, or gasification.

Sludge processing, reuse, and disposal represent the most complex technical problems facing the engineer in the field of wastewater treatment. Besides available technologies, the selection of the optimal sludge management strategy should take into account the legislation, economy, culture, and social structure of the society (Poulsen and Hansen, 2003; Bengtsson and Tillman, 2004). Table 8.2 indicates that sewage sludge is commonly land spread as complementary fertilizer in agriculture, subjected to a thermal treatment, or disposed of in landfills. Thermal treatment refers to the various ways of recovering energy from sludge, mainly by using sludge as a fuel or co-fuel in cement kilns, coal-fired power plants, municipal waste incinerators, and mono-incinerators. Sludge gasification or pyrolysis processes are still under development or exist only on a small scale. Disposal in landfills is continuously decreasing within the European Union according to the European Landfill Directive, which stipulates that material with an organic content greater than 5% must no longer be disposed of to landfill (European Community, 1999). Other methods of sludge treatment and disposal are wet oxidation, storage, and dumping at sea, this latter being now prohibited in Europe.

Tab. 8.2 Estimates of sludge use and disposal (Turovskiy and Mathai, 2006; Milieu Ltd *et al.*, 2008; Wang, 2010).

Sewage sludge disposal methods	China	Europe	USA
Agricultural and land application (%)	48.2	42	53
Thermal treatment (%)	3.5	27	22
Landfill (%)	34.5	14	17
Other (%)	13.8	16	8

Sludge chemical composition has been extensively investigated. Typical data for organic content (Jarde *et al.*, 2003; Réveillé *et al.*, 2003), nutrients (Jarde *et al.*, 2003; Réveillé *et al.*, 2003; Bengtsson and Tillman, 2004; Warman and Termeer, 2005), pathogens (Gantzer *et al.*, 2001; Sahlstrom *et al.*, 2004), heavy metals (Fjallborg and Dave, 2003; Fuentes *et al.*, 2004), pesticides (Delmas *et al.*, 2000), or hydrocarbons (Villar *et al.*, 2004) that affect the suitability either for land application or for incineration are available in the literature.

To face the demonstrations of public disapproval of agricultural spreading, the legislation was strengthened. Nevertheless, doubts and uncertainties remain. Several European countries, such as Germany, The Netherlands, Denmark and Sweden, turn determinedly towards energy recovery systems, according to the high organic content of the matter, and its high heating value on a dry basis. Environmental analyses show that thermal disposal routes present less environmental impact than agricultural spreading when energy is recovered (Poulsen and Hansen, 2003), or when sludges are substituted for fossil fuels (Houillon and Jolliet, 2005). As a consequence, thermal processes will become widespread for sewage sludge treatment in the near future, especially for medium- to large-sized wastewater treatment plants. But conventional combustion technologies require a minimal lower heating value (between 6 and 10 $GJ\,t^{-1}$) to compensate thermal losses and the phenomena of incomplete combustion, a minimum which can only be reached by partial drying of the mechanically dewatered sludge. Sludge drying is also of interest for countries still promoting sludge use in agriculture. Indeed, drying produces dried pellets which are easy to store, handle, and transport, in contrast to pasty dewatered sludge. Moreover, the product is stabilized due the low water activity and will not produce bad odors along the fields. Destruction of pathogens may even be achieved provided the drying temperature and the residence time are high enough.

Nowadays, drying can be considered as an essential step after mechanical dewatering, prior to agricultural or energy valorization. As an example, in France (Chabrier, 2008) 40% of the dried sludge is spread in agriculture while 42.5% is disposed of thermally (12.5% incinerated, 15% co-incinerated with municipal solid waste, and 15% incinerated in cement plants). The number of sludge drying facilities is continuously increasing worldwide, reaching about 1500 lines (Chabrier, 2010).

8.1.2
Sludge: A Complex Material

Sewage sludges are quite different from the products usually dried in industry. Sludges are heterogeneous mixtures of microorganisms, mineral particles, colloids, organic polymers, cations, fibers, and so on, the composition of which varies considerably, depending on their origin, the season, and so on. The biomass and the refractory suspended matter are joined together within a complex mucilage, a by-product of the bacterial metabolism. These structures (see Fig. 8.1) are called the bacterial flocs. A large amount of water can be trapped in this polymeric network, both around and inside the bacteria, including osmotic effects. This makes the water

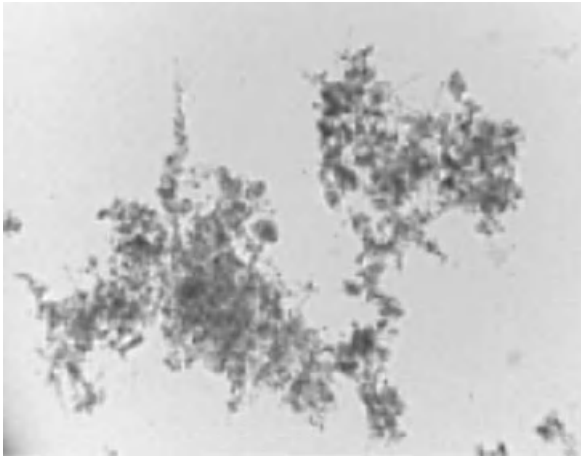

Fig. 8.1 Picture of an activated sludge floc (da Motta *et al.*, 2001).

classification more complex than the four categories which are usually adopted, as reviewed by Vaxelaire and Cézac (2004):

- Free water: water not associated with solid particles and including void water not affected by capillary force;
- Interstitial water: water trapped inside crevices and interstitial spaces of flocs and organisms;
- Surface (or vicinal) water: water held on the surface of solid particles by adsorption and adhesion;
- Bound (or hydration) water.

The use of one single index such as bound water content, or water distribution within the sludge was proved to be insufficient to describe all the acting phenomena during the solid–liquid separation, so several tests coexist to determine the water distribution (Vaxelaire and Cézac, 2004). It remains really challenging to correlate the properties of sludge to its ability to dewater and then to dry.

Sludges are also characterized by complex rheological properties, evolving with their water content, as indicated in Tab. 8.3:

- Most sludges have a pasty consistency and a high water content. It is usual to obtain sludges with 20 to 25% of dry solids content (DS) after mechanical dewatering by centrifugation or belt filters. The performance of filter presses is usually better (with solids contents typically around 30 to 35%) but their discontinuous operation makes them unsuited for large wastewater treatment plants;

Tab. 8.3 Evolution of rheological state with dryness.

	Dry solids content				
% DS	<10	10–40	40–60	60–90	>90
State	Liquid	Viscous liquid, Pasty	Glue phase	Granular solid	Dry solid

- Several operations may greatly affect sludge rheology and drying behavior: pumping, liming, and so on (Huron *et al.*, 2010; Royer *et al.*, 2010);
- For the same initial water content, corresponding to around 20% of solids content, some sludges will be suited for extrusion and others not, forming a pile once in the dryer (Léonard *et al.*, 2008);
- At around 45–60% of dry solids content, most of the sludges become sticky (Ferrasse *et al.*, 2002), affecting the hydrodynamic characteristics of the dryer, the gas to solid contact area and the local solids hold-up.

Moreover, specific phenomena may occur due to the organic content of sludges. On the one hand, the product can evolve during storage due to both aerobic and anaerobic fermentation, affecting the rheology and drying behavior (Fraikin *et al.*, 2010b). On the other hand, heating induces breakdown of part of the organic matter, leading to the emission of volatile organic compounds and malodorous substances, such as hydrogen sulfide (Ferrasse *et al.*, 2003a; Léonard *et al.*, 2007; Deng *et al.*, 2009a; Fraikin *et al.*, 2010a). The non-condensable parts of the vapor have to be treated in biofilters, biowashers, absorption/adsorption facilities, or by thermal oxidation, while the condensates are sent back to the head of the wastewater treatment plant.

These specificities, along with the legal status of waste, accentuate the traditional problems in drying, like the energy consumption or the dryer design.

8.1.3
Useful Properties for Energy Valorization

The heating value (HV) is the chemical enthalpy content of a fuel. The higher heating value (HHV) considers liquid water as a combustion product. The lower heating value (LHV) considers water in the vapor phase. To calculate the HHV in MJ per kg of dry sludge, the relationship

$$\mathrm{HHV_{db}} = (1-i)\mathrm{HHV_{daf}} \tag{8.1}$$

is used, where the subscript db indicates dry basis, and daf indicates dry and ash-free; i corresponds to the mass fraction of inerts or ash on a dry basis.

For a wet sludge, Eq. 8.2 can be used where ar indicates as received, with w representing the moisture mass fraction:

$$\mathrm{HHV_{ar}} = (1-w)\mathrm{HHV_{db}} \tag{8.2}$$

Equation 8.2 shows that the HHV decreases linearly with the moisture fraction due to the dilution effect. For the lower heating values, similar equations can be used:

$$\mathrm{LHV_{db}} = (1-i)\mathrm{LHV_{daf}} \tag{8.3}$$

$$\mathrm{LHV_{ar}} = (1-w)\mathrm{LHV_{db}} - 2.44\,w \tag{8.4}$$

The LHV decreases linearly with the moisture fraction due to the dilution effect and the energy used to evaporate the moisture.

The relationship between the two heating values on an ash-free basis is

$$\mathrm{LHV_{daf}} = \mathrm{HHV_{daf}} - 21.96[\mathrm{H}] \tag{8.5}$$

with [H] representing the mass fraction of hydrogen in the sludge.

The typical calorific value of a dry sewage sludge is close to 16 MJ kg^{-1} for a digested sludge and reaches 20 MJ kg^{-1} for non-digested sludge. The heating value of dry sewage sludge can be estimated according to numerous correlations from ultimate or proximate analysis results (Niessen, 1995; Sheng and Azevedo, 2005; Thipkhunthod *et al.*, 2005).

The dry ash-free value may be estimated from ultimate analysis (i.e., the elementary analysis on a dry ash-free basis). For example, the relation developed by Sheng and Azevedo (2005) gives:

$$\mathrm{HHV_{daf}}\left(\mathrm{MJ\ kg^{-1}}\right) = -136.75 + 31.70[\mathrm{C}] + 70.09[\mathrm{H}] + 3.18[\mathrm{O}] \tag{8.6}$$

For a dry sewage sludge, the HHV obtained by a calorimetric bomb is comparable to the value calculated from ultimate analysis. As a practical rule, the Boie formula, Eq. 8.7, or the Dulong equation, Eq. 8.8, recommended by US EPA (1979) can be used:

$$\mathrm{HHV_{db}}\left(\mathrm{MJ\ kg^{-1}}\right) = 35.160[\mathrm{C}] + 116.225[\mathrm{H}] - 11.09[\mathrm{O}] + 6.280[\mathrm{N}] + 10.485[\mathrm{S}] \tag{8.7}$$

$$\mathrm{HHV_{db}}\left(\mathrm{MJ\ kg^{-1}}\right) = 0.3386[\mathrm{C}] + 1.4317\left([\mathrm{H}] - \frac{[\mathrm{O}]}{8}\right) + 0.0941[S] \tag{8.8}$$

In the previous equations, [C], [H], [N], [S], [O], are the mass fractions, on a dry basis, of carbon, hydrogen, nitrogen, sulfur and oxygen, respectively.

For the case when an ultimate analyzer is not available, Parikh *et al.* (2005) introduced a general correlation, based on proximate analysis of solid fuels,

$$\mathrm{HHV_{db}}\left(\mathrm{MJ\ kg^{-1}}\right) = 0.3536\, m_1 + 0.1559\, m_2 - 0.0078\, m_3 \tag{8.9}$$

where m_1 stands for the percentage of fixed carbon, m_2 for the percentage of volatile matter, and m_3 for the percentage of ash, on a dry basis. The amount of volatile matter is obtained from the mass lost from the dry sample heated to 550 °C. The ash content corresponds to the residue after ignition of the pyrolyzed sample under air at oven with onset temperature of 900 °C. The fixed carbon is calculated from the difference between the two previous tests.

8.2 Sludge Drying Technologies

8.2.1 General Remarks

The design of the unit operations and processes for sludge treatment requires knowledge of the characteristics of the sludge that will be processed, even before this

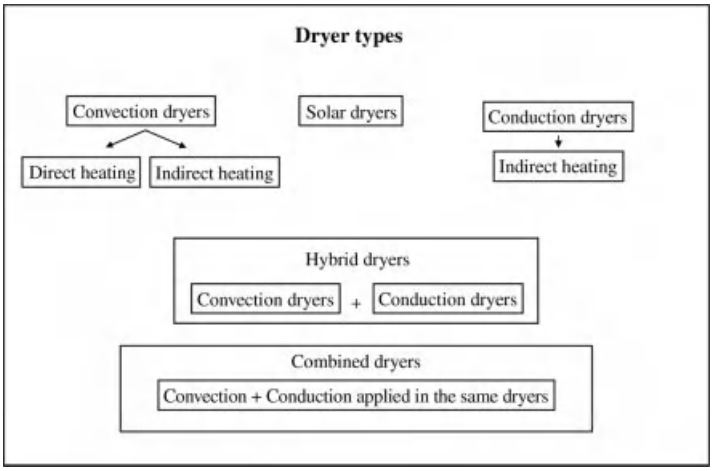

Fig. 8.2 Types of sludge dryers.

specific sludge may exist. As explained above, these characteristics vary, depending on the origin of the solids and biosolids, the aging that has taken place, the type of processing to which they have been subjected, the location of the plant, and the period of the year. Furthermore, some of these characteristics, such as composition, density, and so on, are related to intrinsic properties, while others, like thermal conductivity, water diffusion, or rheological behavior, are affected by sludge consistency and morphology.

As a consequence, most sludge dryers have evolved from standard drying processes, but adaptation of existing technologies is not straightforward owing to the unusual stickiness of the sludge (for indirect dryers) or to the unpleasant odors and risk of explosion (for direct dryers). Nowadays, few companies possess expertise and successful experience in thermal processing of sewage sludge. Dryer design relies too often on empirical considerations, sometimes leading to inefficient systems, unable to face sludge property changes due to any modification within the WWTP.

Drying technologies can be classified into four groups, depending on the way the energy is supplied to the sludge, as illustrated by Fig. 8.2:

- convection or direct dryers
- conduction or contact or indirect dryers
- radiation dryers (solar)
- combined systems (convection and conduction in the same dryer) and hybrid systems (convection and conduction dryers put in series).

8.2.2 Convective Drying Methods and Dryer Types

In convective systems, the heat is transferred to the product by a gaseous medium, air or steam, which is put in direct contact with the sludge. The evaporated water, and

possibly released volatile organic compounds (VOC), are mixed with the drying medium. These exhaust gases have to be treated using wet scrubbers or biofilters. A convection dryer can operate with direct or indirect heating (Fig. 8.2). Three heating alternatives are possible: direct heating with a burner using fossil fuel, biogas or biomass; indirect heating with a burner and a heat exchanger; indirect heating with a heat exchanger. The sludge feed has to be prepared in order to maximize the exchange area available for heat and mass transfer. Extrusion or granulation are commonly used to obtain cylindrically-shaped pellets or granules, respectively. Back-mixing is sometimes realized when the sludge texture is too soft to keep well defined cylinders after extrusion (Léonard *et al.*, 2008), to produce strong granules, or to avoid the sticky phase (see below) (CEN European Committee for Standardization, 2007).

Industrial dryers can operate in high or low temperature ranges, depending on the way the air is heated: burner, heat exchanger using hot water produced by cogeneration, and so on. In order to avoid dust explosion, it is often required to limit the oxygen concentration in the warm gas, for example, by recycling a part of the exhaust gas. The most common convection dryers are: belt dryers, flash dryers, fluidized bed dryers, and drum or rotary dryers.

Belt dryers have the widest range of applications. The wet sludge is distributed on the belts by extrusion: the sludge is pressed across the holes (6 to 12 mm in diameter) of cylindrical dyes disposed across the belts. Since the material is not subjected to mechanical stresses during drying, it hardly matters whether the sludge is very sticky. However, sludges must be rigid enough to ensure the formation of a bed with a high permeability after extrusion. Back-mixing, that is, recirculation of dried product, can be realized in the case of soft sludge, in order to promote extrudate stiffness. The sludge is transported through several drying chambers on one or more perforated conveyor belts across which the drying medium circulates, Fig. 8.3. At the outlet, the exhaust gases are cooled to below the dew-point temperature in order to condense the

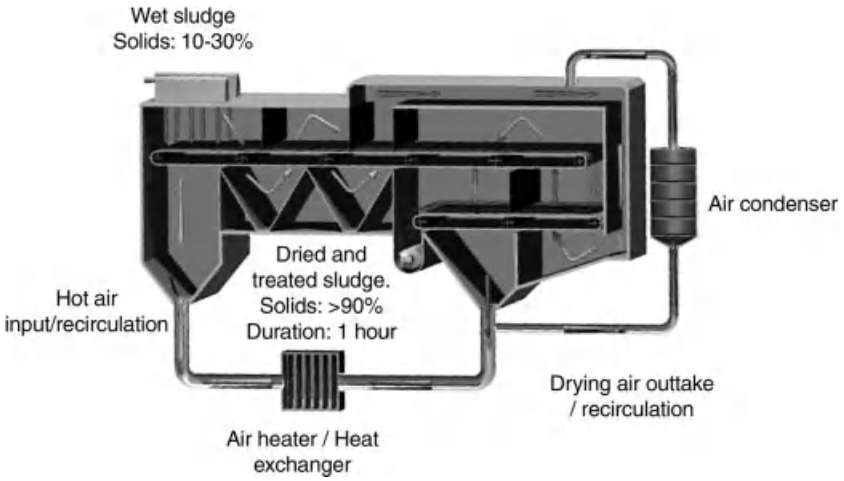

Fig. 8.3 Belt dryer (BioCon®, with courtesy of Krüger Inc., USA).

vaporized water, together with some VOC. The drying air is usually pre-heated in the exchanger with heat from the condensate. These systems can be operated between ambient temperature and 180 °C, and the residence time of the sludge and the size of the dryer vary accordingly. Due to this range of operating temperature, waste heat can be used, gases, hot water or low-pressure steam, either directly or as a secondary energy source (Jacobs *et al.*, 2003).

Belt dryers have a rather good flexibility because there are three ways of controlling the process: by adjusting the input sludge quantity, the belt speed and the heat energy supplied in each chamber (CEN European Committee for Standardization, 2007).

Belt dryers are distributed by several companies: Sevar Anlagentechnik (Germany), Andritz AG (Austria), Krüger Inc. (USA), Maguin SAS (France), Sistemas de Transferencia de Calor, S.A. (Spain), Huber SE (Germany), Watropur AG (Switzerland), Thermal Energy International Inc. (Canada), Imtech DryGenic (The Netherlands), Siemens Water Technologies (USA), Stela Laxhuber GmbH (Germany).

In flash dryers, also called pneumatic dryers, the drying medium (hot air, superheated steam) supplies energy and transports the product in the system. The dewatered sludge is finely pulverized and moves upwards, in co-current flow with a high temperature gas stream. Back-mixing is performed in the case of sludge particles sticking to the tower walls. Separation of the dried product is by the use of cyclones or fabric bags, Fig. 8.4.

Flash dryers are provided by GEA Niro (Denmark), or GEA Barr-Rosin (UK) for example. Systems combining mechanical dewatering by centrifugation and flash drying have also been developed, for example, Centridry® (Euroby Ltd, UK).

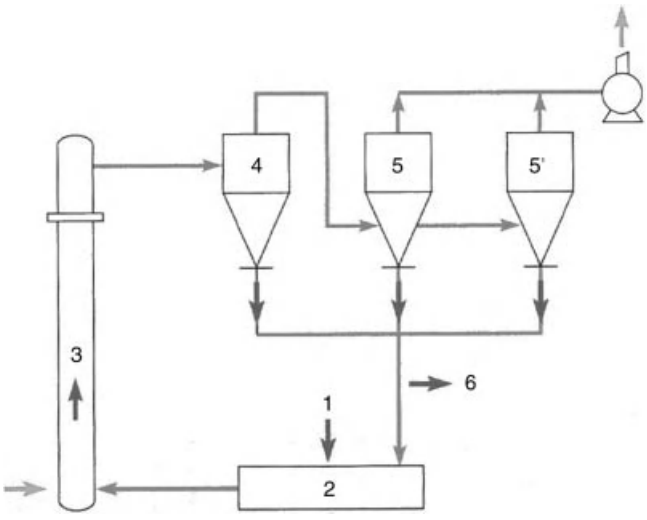

Fig. 8.4 Flash dryer, 1: inlet of wet product, 2: mixing with recirculated dried product, 3: zone of product air conveying, 4: cyclone, 5: dedusters, 6: outlet of dried product. (Adapted from ADEME and CETIAT (2000).)

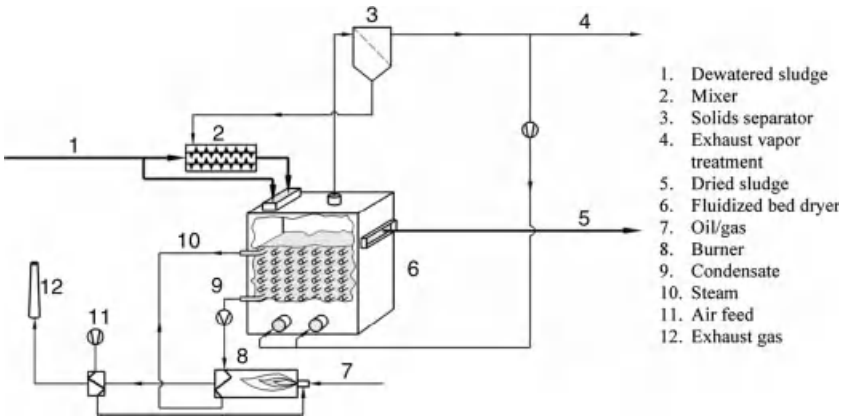

Fig. 8.5 Fluidized bed dryer (CEN European Committee for Standardization, 2007).

Fluidized bed dryers for sludge are indirectly heated convection dryers operating in a closed inert gas loop. A granulation device is used to form sludge granules. In some processes, back-mixing of dried sludge, available as dust and screened fines, is realized to produce strong granules, and to stabilize the drying operation. Sludge granules are distributed from the top; they are held in suspension and intensively blended by the gas stream passing through the product layer, Fig. 8.5. Energy for water evaporation is supplied by means of submerged heated tubes located inside the sludge fluidized bed. The fluidizing gas leaving the dryer carries fines and evaporated water from the fluidized bed dryer. The fines are separated in a cyclone and the evaporated water is condensed from the gas stream, this latter being recycled to the dryer. The dried sludge is usually removed laterally from the dryer and directly transported to a silo without any sieving, due to its dust-free character. This type of dryer is very compact due to improved heat transfer by combined conduction through contact with heated tubes, and convection via the heated turbulent gas stream.

Among others, fluidized bed dryers are provided by Andritz (Austria), GEA Niro (Denmark), Imtech DryGenic (The Netherlands), Thema Process BV (The Netherlands).

Drum or rotary dryers, Fig. 8.6, are usually used for drying to low outlet moisture content. A system for back-feeding already dried material into the wet sludge is employed to avoid the sticky phase. This also gives the possibility to compensate for variations of sludge cake water content at the inlet. Transport through the drum is ensured by guide blades, or through an inclined position of the drum. A large amount of warm air is blown through the drum, either in parallel or in counter-flow. The exhaust gas is separated, using a bag filter or cyclone, from the dried product which is fed to a sieving unit. The coarse fraction is crushed in a grinder and fed to the granulator with the sieved-off fine material.

Drum dryers often operate with inlet temperatures of more than 400 °C and are most economical to purchase if designed with direct heating (Jacobs *et al.*, 2003). Oil,

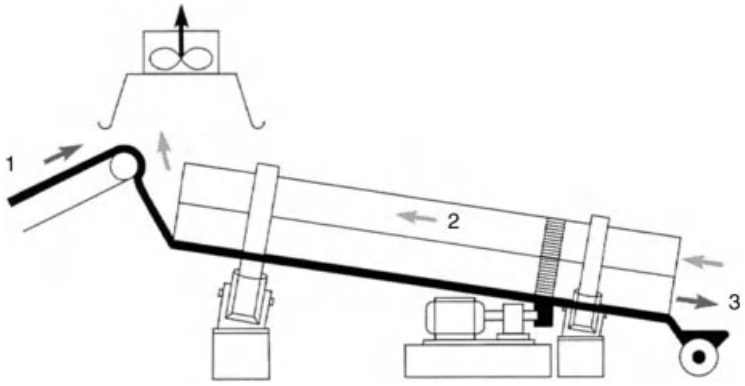

Fig. 8.6 Direct drum dryer, 1: inlet of wet product, 2: air in counter-flow, 3: outlet of dried product. (Adapted from ADEME and CETIAT (2000).)

biogas or natural gas burning can be used, as well as exhaust gas from a combined heat and power plant (CHP).

Continuous rotary dryers can also be heated indirectly. Most of the time, steam flowing inside heat-transfer tubes set along the circumference of the horizontal cylindrical shell is used as the heating fluid. Steam, with a pressure in the range 0.4–1 MPa, is introduced into the tubes through a manifold located at the discharge end of the cylinder. Like radial flights, the steam tubes serve to agitate the product in the dryer. Up to three staggered, concentric rows of tubes are usually available. The diameter of the tubes increases from the inner row to the outermost row. In conventional applications, a pitch-to-diameter ratio of the tubes of 2:1 is used to ensure that the solids can flow freely around them. However, for sticky materials like sludge, single row tubes and back-mixing are frequently applied. The construction of an indirect-heat rotary dryer is more complicated but heat losses to the surroundings are smaller than in a direct rotary dryer, since the outer wall is not in contact with the heating fluid.

Single or three pass systems are available on the market and are distributed by several companies such as Andritz (Austria), Comessa (France), ELINO Industrie-Ofenbau Carl Hanf GmbH (Germany), GEA Barr Rosin (UK), SC Technology GmbH (Switzerland), Maguin SAS (France), Mitchell Dryers Ltd (UK), Siemens Water Technologies (USA), TechTrade GmbH (Germany), Vandenbroek International (The Netherlands), among others.

Performance characteristics of direct dryers for sludge are summarized in Tab. 8.4.

8.2.3
Indirect Contact Drying Methods and Dryer Types

In the case of contact dryers, the heat necessary to vaporize the moisture is transferred to the sludge through a heated surface, over which the product is

Tab. 8.4 Performances of direct dryers.

Dryer type	Operating range (in terms of water content X, expressed on a dry basis)	Specific drying rate ($kg\,m^{-2}\,h^{-1}$)	Specific energy consumption ($kWh\,t^{-1}$)
Belt dryer	Full drying	from 5 to 30	700 to 1140
Direct drum dryer	Full drying, with dry product back-mixing: $0.1 \leq X \leq 0.54$	from 3 to 8	900 to 1100
Flash dryer	Full drying	from 0.2 to 1	1200 to 1400

transported. Thermal oil or steam, saturated up to 0.85 MPa, is used as the heating fluid. Usually, the fluid is heated in a boiler fired with fossil fuel or biomass. The drying process can take place in an atmosphere containing only the liquid's vapor (under partial vacuum or at atmospheric pressure) but air or inert gas can also be used as a sweeping gas (the vapor fraction is then close to 80% in volume).

8.2.3.1 Rotor Design and Operation of the Drying Process

Three indirect drying technologies are mainly encountered for sludge drying: disc, paddle and thin film dryers. These dryers are composed of an internal rotor inserted in a cylindrical double wall external envelope. The *design of the rotor*, which is specific to each technology, is crucially important for overcoming the sticky phase and thus for the operation of the drying process.

The rotor of a disc dryer is composed of a hollow shaft with hollow discs, shaped as plates and welded on the shaft. Usually, transport paddles are mounted on the discs to ensure the product transport in the longitudinal direction. Paddle dryer rotors consist of two shafts rotating in opposite directions. Each shaft bears hollow paddles (wedge-shaped elements or discs segmented with bar-scrapers for instance) which overlap with the paddles of the other shaft. Thus, the design of the paddles not only induces a high shearing of the product, but also an almost total self-cleaning of the rotor. As a result, complete drying without recycling some dry product upstream can only be performed in paddle dryers. In a disc dryer, overcoming the sticky phase should be achieved outside the dryer: the drying process should be stopped before the sticky phase (before 40% of solids content) or a part of the dry solids should be mixed with the mechanically dewatered sludge before its insertion into the dryer, to dry past the sticky region. To avoid clogging, the dry solids content of the sludge at the dryer inlet is usually around 70%. This means that the rate of recirculation, defined as the ratio of solids flow recycled in the installation to the entering flow, is classically close to 2.

Disc and paddle dryers are distributed by several companies (non-exhaustive list): Andritz (Austria), Buss-SMS-Canzler (Germany), Fenton Environmental Technologies (USA), GEA Barr Rosin (UK), GMF Gouda (The Netherlands), Komline-Sanderson (USA), SIL - DS Engineers & Contractors (France), Haarslev Industries

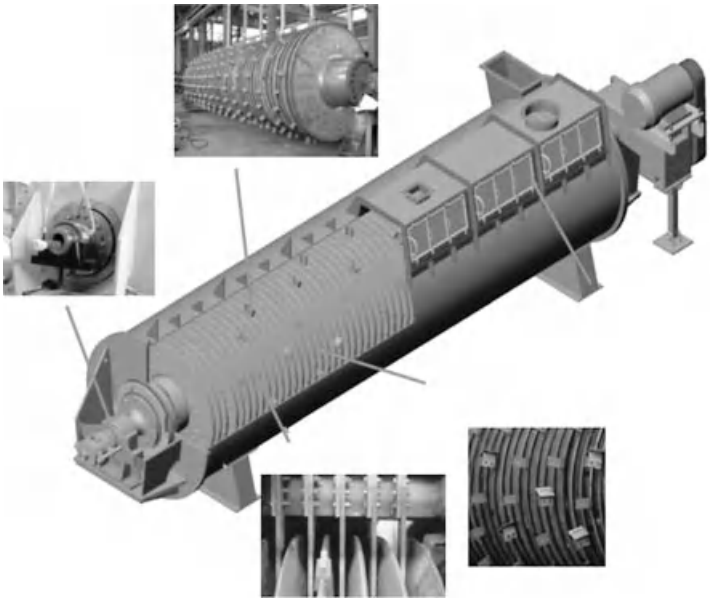

Fig. 8.7 Disc dryer (with courtesy of SIL, DS Engineers & Contractors, France).

(Denmark), Siemens Water Technologies (USA), Waterleau (Belgium). Equipment examples are shown in Figs. 8.7 and 8.8.

In thin film dryers (Fig. 8.9), the function of the rotor is to spread the sludge in a 5 to 15 mm thick layer on the inner wall of the heated stator and to convey the thin layer of sludge in a helical flow path along the jacketed wall. The blade configuration includes feed transfer elements located at the dryer inlet to distribute the pasty sludge onto the stator, twisted transportation elements to convey the sludge through the dryer with a controlled residence time, and cleaning elements to scour the heated wall. Freely

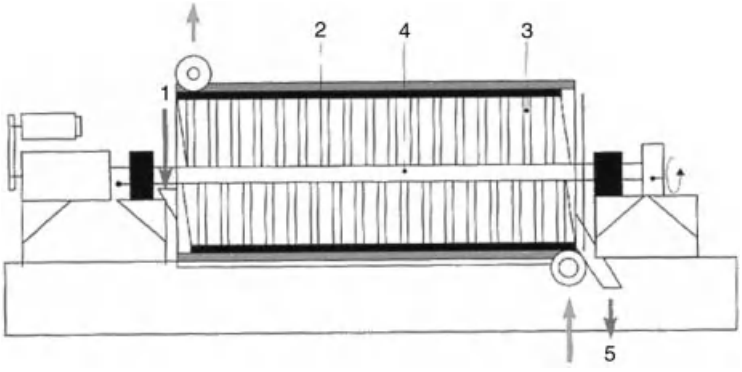

Fig. 8.8 Paddle dryer, 1: inlet of wet product, 2: double jacket, 3: paddles, 4: hollow arm, 5: outlet of dried product. (Adapted from ADEME and CETIAT (2000).)

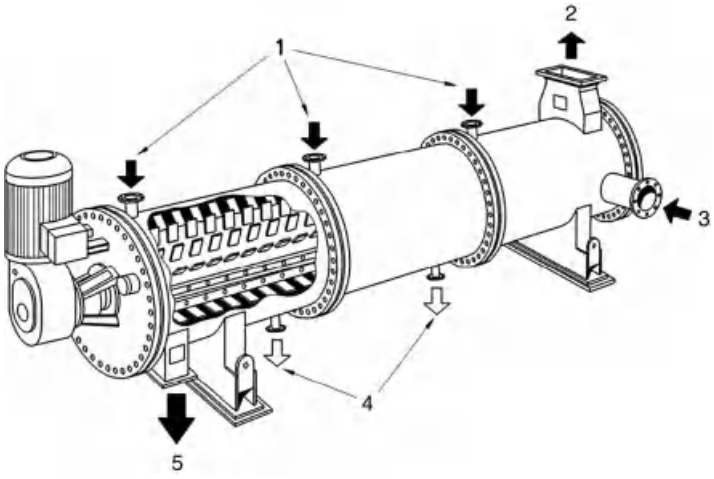

Fig. 8.9 Thin film dryer (Buss-SMS), 1: steam, 2: exhaust vapor: 3: wet product, 4: condensate, 5: dried product.

moving pivoted flaps are added on the rotor in the sticky region to ensure a continuous blending and breakdown of agglomerates. Basically, full drying is possible with a thin film dryer, but in practice the compactness of these dryers is low, so that they are mostly used for partial drying of sludge up to 65% dry solids content. Indeed, in paddle and disc dryers the heating fluid is fed simultaneously in the shafts, the hollow paddles or discs, and, most of the time, in the dryer horizontal housing. Discs or paddles provide around 80% of the heating area. Related to the dryer volume, the large surface area for heat transfer, provided by the discs or paddles, makes these types of equipment very compact. In a thin film dryer, the heating fluid is only fed in the double jacket of the housing and thus the available heating area is low compared with the other indirect drying technologies. Thin film indirect dryers are distributed by companies such as Buss-SMS-Canzler (Germany) and GMF Gouda (The Netherlands), among others.

8.2.3.2 **Drying Performances**

Inlet and outlet moisture contents being quite different for the three technologies, the specific drying rates change a lot from a disc to a paddle, and to a thin film dryer. In the European context, the specific evaporation performances are well documented. As a general rule, the values reported in Tab. 8.5 are used for dryer design.

These empirical design criteria can be checked and the discussed drying technologies can be improved by using the penetration theory to model the drying rate curves. Developed to describe the heat transfer from heated surfaces to dry moving packings (Wunschmann and Schlünder, 1980), the penetration theory, which rests on the description of the random particle motion effect, was extended to contact drying of free flowing granular material (Schlünder and Mollekopf, 1984; Tsotsas and Schlünder, 1986a, b). The continuous mixing process is replaced by a sequence of

Tab. 8.5 Specific evaporation performances of disc, paddle and thin film dryers in Europe (AFNOR, 2008).

Dryer Type	Operating range (in terms of water content *X*, expressed on a dry basis)	Specific drying rate ($kg\,m^{-2}\,h^{-1}$)	Specific energy consumption ($kWh\,t^{-1}$)
Disc dryer	Partial drying: $1.25 \leq X \leq 4.5$ Full drying, with recycling of dry product upstream: $0.1 \leq X \leq 0.54$	from 10 to 12 from 7 to 10	from 855 to 955
Paddle dryer	Full drying: $0.1 \leq X \leq 4.5$	from 15 to 20	from 800 to 885
Thin film dryer	Partial drying: $0.54 \leq X \leq 4.5$	from 25 to 35	from 800 to 900

unsteady mixing steps. During a fictitious time period t_R, the bulk is assumed to be static and a drying front is assumed to penetrate from the hot surface into the bulk. Thereafter, an instantaneous perfect macro-mixing of the bulk occurs, followed by the same static period again. The apparent resting time, t_R, is a mechanical property of the system (dryer type, stirrer, product). Specifically, t_R is defined as the ratio of a mixing number, N_{mix}, which indicates how often the stirrer must have turned around before the product has been ideally mixed, to the number of revolutions per second of the stirrer. Empirical power laws, which correlate the mixing number to the Froude number, *Fr*, are available for some conventional drying technologies (paddle, tray and drum dryers).

An approach similar to that of Dittler *et al.* (1997), who extended the penetration theory to pasty materials like china clays, was developed to compute the drying kinetics of municipal sewage sludge (Arlabosse and Chitu, 2007; Deng *et al.*, 2009b). Even if the drying process is a solid-forming process with a "reverse granulation" period from the wet to the dry solid, so that the particle size distribution of the sludge evolves during drying, the pasty sludge is assumed to be a mono-dispersed saturated particulate phase. As a consequence, the dry matter is the same both in the pasty and granular regimes. The size of the largest particles in the pasty sludge proves to be the characteristic dimension to consider. This dimension depends on many factors (location of the WWTP, eating habits, type and length of sewers, wastewater treatment processes, sludge treatment processes) and thus, even if the wastewater treatment is identical, its value can change significantly from one context to another. For instance, the most common wastewater treatment process in both China and France is extended aeration. But the composition of Chinese effluents entering the wastewater treatment plant is appreciably different from those met in Europe. As a result, the Chinese sewage sludge contains half the organic matter of European sludges, and the silica and silicate contents are higher. Thus, after mechanical dewatering, the particle size distribution of the pasty material ranges from some micrometers to around 200 μm in China. In European countries, the particles in the pasty sludge are larger, and the particle size distribution ranges from some micrometers to around 1000 μm. On the assumption of a mono-dispersed particulate phase, and as for granular packing, the contact resistance between heated walls and

particles is rate controlling for sludges with coarse particles ($d \approx 1$ mm) whereas the penetration resistance of the bulk is rate controlling for sludges with fine particles ($d \approx 100\,\mu$m). Thus, the efficient operation of contact dryers inevitably results from different settings of the processing parameters. Contact drying becomes faster as the temperature difference between the heated wall and the bed increases. But, for the coarse particles, the drying rate is directly proportional to the temperature difference whereas, for fine materials, it depends approximately upon the square root of this difference. In contrast, an enhancement of the mixing intensity increases the drying rate of fine particles but does not have any influence on the drying rate of coarse ones.

8.2.4
Solar Drying and Dryer Types

Solar dryers, such as those depicted in Fig. 8.10, can be used to increase sludge solids content in a range typically between 70 and 80%. They constitute a good alternative to thermal drying for small to medium size WWTPs, that is, between 2000 and 50 000 PE. A typical process consists in putting in contact, under a greenhouse, a regularly renewed amount of air and sludge distributed over an area sealed from the subsoil. The space is heated through solar radiation. A ventilation system ensures both air renewal and the evacuation of removed water vapor. It also promotes heat and mass transfer with the air. A special sludge turning system is used in order to spread, turn and aerate the sludge. Turning is essential to avoid crust formation at the outer surface, and enhance transfer with the air. Depending on the process, the sludge is transported from one side to the other as drying proceeds ("tunnel solar dryer") or fresh sludge is mixed with (partially) dried sludge. The height of the sludge bed may vary between 25 and 60 cm. The amount of water evaporated depends on the characteristics of the air (temperature, humidity), of the sludge (temperature, water content, mechanical properties), and the greenhouse design. For non-tunnel systems, the discharge of the greenhouse is usually made once a year after the summer period, to profit the most from the solar energy.

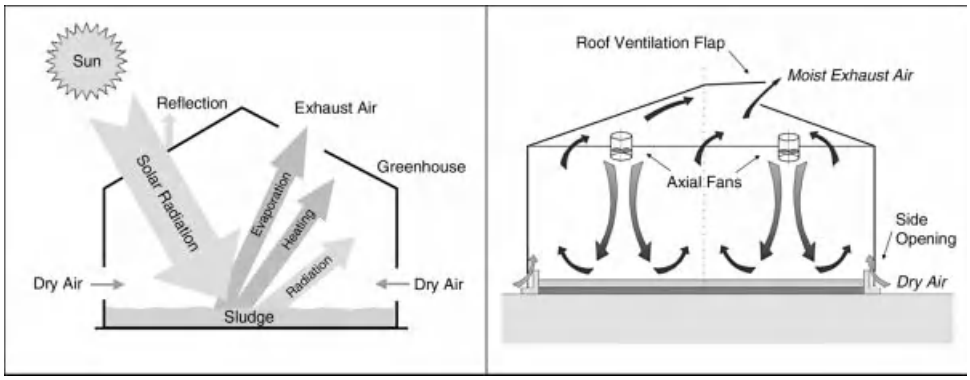

Fig. 8.10 Principle of sludge solar dryer (with courtesy of IST-Anlagenbau GmbH, Germany).

There exist three main types of solar dryers: open greenhouses, closed greenhouses, and solar dryers combined with a heated floor, using heat pump or hot air injection.

The energy demand for the process ranges between 30 and 200 kWh per ton of evaporated water, depending on whether ventilation and/or biological odor treatment are applied. Higher energy consumption is needed in the case of chemical deodorization, up to 1000 kWh per ton of evaporated water (Canler, 2010).

Solar dryers are distributed by several companies among them: Degrémont (France), Huber (Germany), IST-Anlagenbau GmbH (Germany), Stereau (France), Thermo-System (Germany), Veolia Eau Solutions & Technologies (France), Vinci-Sogea (France).

8.2.5
Combined and Hybrid Drying

Combined systems refer to dryers including both convective and conductive heat transfer in the same process. One industrial realization is the so-called turbo-dryer (VOMM, Italy), associating thin film drying, that is, conduction, and fluidization, that is, convection with the carrier gas. Due to intense agitation, the sludge in contact with the heated walls is continuously renewed and the breakdown of the film increases the surface area exposed to the hot drying medium. The process operates with a closed loop circuit. The residence time is very short due to the high intensity of the combined heat transfer. Nevertheless, one must pay attention to the possible formation of dust due to the mechanical action of the rotor because such dust may affect the carrier gas circulation.

In hybrid systems, convective and conductive dryers are put in series. In the sludge domain, this approach is used in the Innodry® 2E process (Degrémont, France) including three main parts: thin film dryer, intermediate chopper, and belt dryer, Fig. 8.11. At the outlet of the thin film evaporator, sludge has a dry solids content around 45–55%, starting from 15 to 35% DS. After extrusion, the semi-dried product is sent to the belt dryer in order to reach a dry solids content ranging between 65 and 95%, depending on the sludge use. The belt dryer operates with a closed air circuit, including heat recovery from the vapor produced during the first indirect drying stage. The closed loop also comprises vapor condensation and a re-heating step using the same heating medium (oil or steam) as that used in the thin film dryer. The energy recovery between the two drying units allows reduction of the energy demand per ton of water from 900 to less than 700 kWh (Cousin, 2010). Typical capacities range from 0.5 to 4 ton water per hour.

8.2.6
Sludge Frying, an Alternative to Conventional Drying

Frying can be an alternative to the thermal drying of sewage sludge. Fry-drying is an innovative technique for the thermal treatment of sewage sludge. The process consists of immersing a mechanically dewatered sludge in a bath of hot immiscible

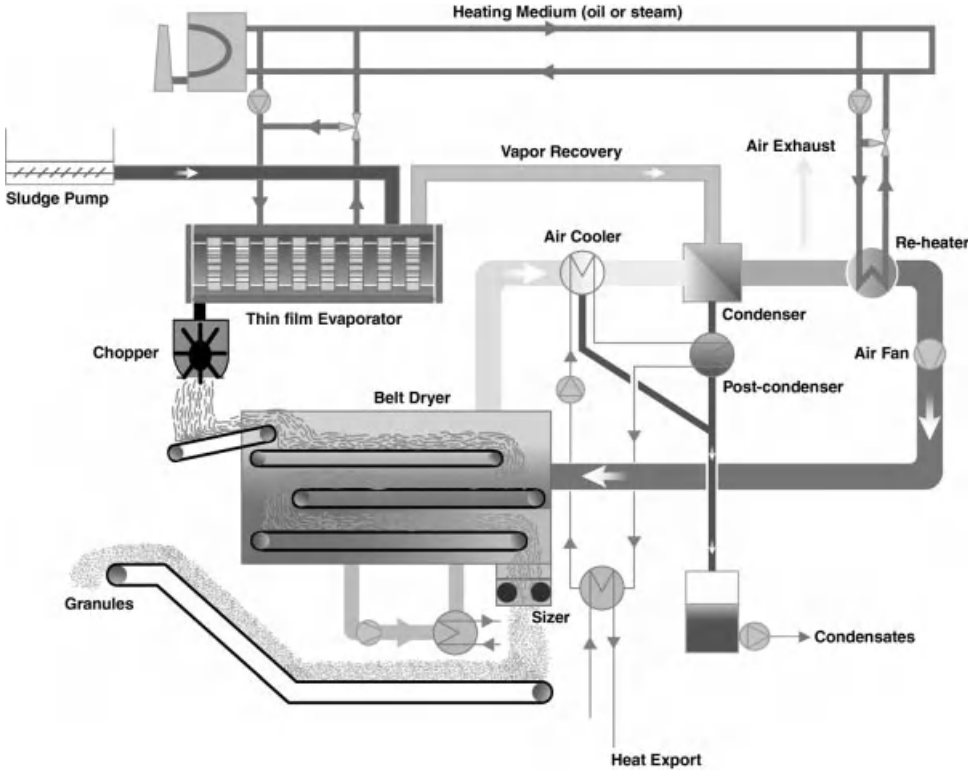

Fig. 8.11 Hybrid dryer according to the Innodry® technology (with courtesy of INNOPLANA, Degrémont Technologies).

oil maintained at a few degrees above the water boiling point (Peregrina *et al.*, 2006a, b), thus removing water by internal boiling. Because of the oil impregnation which occurs simultaneously with the boiling process, fry-dried sludge is a high specific energy fuel. Frying limits fermentation, and enables pathogen destruction, thus limiting risks for handling, storage and transportation. In a recent study, kinetic parameters for the thermal inactivation of pathogens were chosen from the literature for pathogen reduction modeling in sludge processes (Romdhana *et al.*, 2009b). When applied to the vacuum fry-drying process, it was shown that 10 min treatment at 85 °C was sufficient to inactivate even the most temperature-resistant pathogens (Hepatitis A viruses). The frying process is intensive and allows energy recovery using mechanical vapor compression and condensation. The use of a waste oil (recycled cooking oil) as frying medium allows co-disposal and valorization into energy by combustion.

8.2.6.1 **Heat and Mass Transfer During Fry-Drying**

Frying has been largely used in the food industry, and heat and mass transfer phenomena in food frying have been the objects of abundant research work in the

past decades (Moreira *et al.*, 1999). Knowledge of the heat and mass transfer rates during the frying process is essential in order to design frying equipment, and to ensure good quality of the final product. The need for high heat and mass transfer rates and for a favorable energy balance of the process is specific to sludge fry-drying, because of the large throughputs involved, and the low value of the processed material. The control of porosity changes and oil uptake, which is a key factor for processing a mixture of wastes into a valuable solid fuel, is highly dependent on the fry-drying conditions.

Peregrina *et al.* (2006a) examined the fry-drying of municipal sewage sludge cylinders using recycled cooking oil. The experimental tests were carried out by immersion of cylindrical samples of 15, 20 and 25 mm in an oil bath at operating temperatures between 120 and 180 °C. A continuous on-line weight measuring method was developed, and the temperature profile in the sludge was recorded simultaneously. The weight loss allowed computation of the boiling rate, and thus an overall heat transfer coefficient was derived from an energy balance of the sample, with a maximum of 2.5 $MW\,m^{-2}\,K^{-1}$. Micrographs of the cylindrical sample clearly showed a receding front inside the sample with a dry shell soaked with oil, and a wet core.

The combination of heat and mass transfer with physical changes of the product (porosity, permeability) makes the theoretical treatment of simultaneous water removal and oil intake complicated. Heat is transferred from the surrounding oil to the product surface by convection and through the product by conduction. Water is removed in vapor form as oil penetrates the generated porous solid structure. Romdhana *et al.* (2009a) used similar experiments in the range 110–140 °C with small samples (4, 8 and 12 mm) and developed a simple model based on diffusion mass transfer. The moisture diffusion coefficient was assumed constant during frying but a function of the oil temperature and initial moisture content (i.e., the experimental conditions). Another important assumption was the volumetric replacement of the removed water by the impregnating oil, which was confirmed experimentally. Romdhana *et al.* (2010b) also showed the relationship between heat transfer and moisture loss rate in the form of a dimensionless correlation.

8.2.6.2 **Energy and Environmental Aspects**

The LHV of a partially fry-dried sludge (pds) was established by Peregrina *et al.* (2006a, b) for municipal sludge to be:

$$\mathrm{LHV_{pds}(MJ\ kg^{-1})} = 15.9(1-o)\mathrm{S} + 36.43\ o.S + 2.26(1-S) \tag{8.10}$$

for the range $0.35 < S < 0.95$ and $0.7 < o < 1.1$, where S is the solid mass fraction of the sludge and o is the oil content per kg dry solid.

The LHV for autothermal combustion (4–6 $MJ\,kg^{-1}$ depending on the combustion technology) can be reached with a larger moisture content than for conventional drying. When full fry-drying is achieved, the LHV may be as large as 24 $MJ\,kg^{-1}$ for municipal sludge, which makes it comparable to dry hardwood. The optimal moisture content and oil uptake depends on the valorization route, and oil availability and price. To obtain a positive energy balance in the overall waste to energy process,

energy recovery is essential in the fry-drying process. In a study of the economics, Peregrina *et al*. (2008) compared three process designs for autothermal combustion, one (P1) with just condensation of the vapors and the two others (P2 and P3) with mechanical vapor compression. The use of a compressor reduces the fuel gas needed by more than 50% and avoids the large cooling water requirement to condense the exhaust vapors which is characteristic for option P1. On the other hand, the compressors in the P2/P3 cases create a higher electrical energy consumption.

Compared to indirect and direct dryers, fry-dryers need less maintenance and fossil fuels, but running costs are determined by the waste oil price. Therefore, one way to improve the fry-drying running costs is to find more economical frying oils, for example trap waste from WWTP. Another is to find more economical and renewable heating sources operating at lower temperatures (solar energy, heat pumps). At 85 °C, vacuum frying is achieved at 0.58 bar. Lower pressures also allow lower temperatures in the compressor and Roots compressors may be used for small scale biofuel fry-drying units (Romdhana *et al*., 2009a).

Life cycle assessment has been applied at the early stages of the design of a fry-drying unit (Peregrina *et al*., 2006b). The study compared aspects of environmental performance with conventional disposal of sludge by incineration. Data were obtained on the laboratory scale (VOC) and extrapolated to full scale. Four impact categories were selected to assess the environmental profile of the operation – abiotic, depletion of resources, climate change, eutrophication and acidification. More recent works on the association of a fry-dryer with a combustion system completed this study and new categories of impact were examined (Romdhana *et al*., 2010a). It was shown that impacts on toxicity were very much dependent on the quality of combustion of the biofuel, thus suggesting the use of the best available technologies, such as fluidized bed combustion with flue gas treatment.

8.2.7 Pathogen Reduction

Micro-organisms present in sludge are composed of bacteria, viruses, protozoa and helminths. An infinitesimal part of these micro-organisms can be pathogenic. The number of pathogens per kilogram is estimated at 10^3 viruses, 10^7 bacteria, 10^2 protozoa and 10^3 helminths at the final clarifier exit (Courtois, 2000). Temperature, moisture and residence time are three of the parameters affecting the inactivation of pathogens. Thermal drying is considered by the United States Environmental Protection Agency as one of the seven processes to further reduce pathogens (PFRP). The sludge treated in a PFRP is considered as Class A biosolids, which are defined as biosolids that meet "the highest quality" pathogen reduction requirements (Office, 1997). To meet this requirement, the sludge should be dried to 90% solids or greater, and either the temperature of the sludge particles, or the wet bulb temperature of the gas in contact with the sludge as the sludge leaves the dryer, should exceed 80 °C. The factors in sludge treatment processes that generate lethal effects on pathogens were also investigated for the European Commission Directorate-General Environment (Carrington, 2001). The study emphasizes that thermal

drying could be considered as an effective process to kill/inactivate pathogens if the sludge is heated to at least 80 °C for 10 min to a moisture content of less than 10%.

For convective systems, hygienization can be obtained in the case of full drying within rotary dryers and fluidized bed dryers, due to long retention times and controlled outlet temperature. A prolonged drying zone can be required in belt dryers to ensure the destruction of pathogens (Jacobs *et al.*, 2003). For conductive systems, sludge residence time is rather large in disc and paddle dryers, around 1 h in disc dryers and up to 4 h in paddle dryers. In thin film dryers, the retention time is only 4 to 10 min. In these three cases, the sludge is released from the dryer at a temperature between 80 and 95 °C. Thus, disc and paddle drying could be considered as processes capable of achieving sludge hygienization, if the final dry basis moisture content is less than 0.11. Due to the rather low temperature, solar drying usually fails to reach hygienization, all the more because the final siccity, that is, the dry solids content, hardly exceeds 70 to 80%. For frying, pathogen destruction has been assessed, as mentioned above. Nevertheless, in all cases, re-infection by micro-organisms as a result of rewetting is possible, depending upon the conditions of storage.

8.3
Energy Efficiency of Sludge Drying Processes

8.3.1
Specific Heat Consumption of Sludge Dryers

Dryer efficiency can be assessed through many performance factors. The specific heat consumption and the energy consumption ratio will be used in the following. The specific heat consumption (SHC) is defined as the ratio of the amount of heat supplied to the dryer, Q_D to the mass of evaporated water, m_v:

$$\mathrm{SHC} = \frac{Q_D}{m_v} \tag{8.11}$$

Consequently, SHC is inversely proportional to the specific moisture extraction rate, or SMER. The energy consumption ratio (R_D, an inverse efficiency) compares the specific heat consumption and the latent heat of vaporization, taken at 0 °C:

$$R_D = \frac{\mathrm{SHC}}{\Delta h_v(0\,^\circ\mathrm{C})} \tag{8.12}$$

R_D ranges from 1.25 to 2.5 for conventional dryers (Schlünder, 1998). An operational audit was carried out on 12 installations of urban and industrial sludge drying in France and Germany a few years ago (Ressent, 2000). The operation conditions of conveyor dryers, indirect rotary dryers, and disc dryers were assessed. Measurements emphasize that R_D ranges from 1.15 to 1.65 but most of the drying facilities operate around a median value of 1.35. This tendency was confirmed by other studies (Arlabosse, 2001; Pimor, 2003). For solar dryers, R_D can be considerably reduced down to 0.05–0.4 (Arlabosse and Lecomte, 2008).

8.3.2
Towards the Reduction of Energy Consumption Associated with Sludge Drying

Several methods can be used to reduce the energy consumption (Kemp, 2005):

- Reduction of the energy requirement of the dryer by enhancing the solids content at the dryer inlet and adapting the outlet solids content to the final disposal route;
- Increase in the efficiency of the dryer by reducing heat losses and optimizing the operating conditions (for instance, air flow in convective dryers, heating fluid temperature and flowrate in conductive dryers);
- Heat recovery within the dryer system between the hot streams (the exhaust gas in convective dryers, the heating fluid in conductive dryers, the hot solids emerging from the dryer) and the cold ones (the drying air which has to be heated from ambient to the dryer inlet temperature, the solids which could be pre-heated before entering the dryer) by means of heat exchanger or heat pump;
- Heat recovery between the dryer and surrounding processes, like an anaerobic digestion process (by direct combustion of the purified biogas) or a combined heat and power unit (through gas turbine exhausts and/or cooling water of the engines) in the WWTP or like a MSW incinerator or any process providing low-grade heat sources in an industrial park (e.g., Suzhou or Shanghaï industrial park in China), if the dryer is located there.

8.3.3
Case Studies

The combination of several of these solutions can make it possible to achieve a neutral energy assessment on a WWTP. The plant located in Légué (Saint Brieuc, France, 140 000 PE) implements an anaerobic digestion of mixed sludges (mixture of primary sludges and middle-load activated sludges with simultaneous dephosphatation), a mechanical dehydration by centrifugation, and a thermal drying (Couturier, 2010). Two mesophilic anaerobic digestion units produced annually 900 000 m^3 of biogas, which represents an energy source of 5.1 GWh. 7000 m^3 of sludge, dewatered to 20% solids content, are sent to a Naratherm paddle dryer, designed to evaporate 2.02 tons of water per hour, and are transformed into an approved fertilizer, FERTI AMOR 4N®. As often in WWTP, the Naratherm paddle dryer was over-sized and is operated 2750 hours per annum. So, the energy consumption ratio reaches 1.38, against the 1.25 expected under nominal operation (Arlabosse, 2001). Before optimization, around 40% of the energy available from the biogas was used *in situ* as a low-cost fuel for heating the paddle dryer, natural gas providing the complement of energy necessary to the operation of the dryer. The remaining biogas was burned in a flare stack without any valorization. The temperature of the condensates from the superheated steam, used to provide the energy for drying, was high enough to heat the mesophilic digesters at 38 °C. Thus, 35% of the energy hold in the condensates was recovered, the remainder being lost. The overall energy assessment is presented in Fig. 8.12a. Improvement of the performances of the centrifugation units, with an increase in the

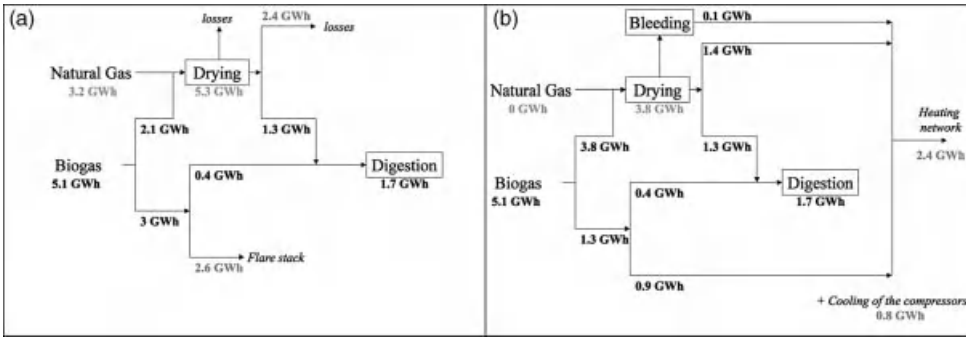

Fig. 8.12 Energy assessment (a) before and (b) after optimization (adapted from Couturier, 2010).

solids content from 20 to 23.7%, led to a reduction of 39% for the energy consumption of the dryer. As a consequence, an increase in the capacity of the gasometer makes it possible to remove the natural gas supplement, the energy stored in biogas being sufficient to heat the dryer. Finally, the waste energy from the condensates, the remaining biogas, and also from the bleeding of the evaporated vapor, and the cooling of the compressors of the combined heat and power unit can be recovered in two heating networks (low, 70/50 °C, and medium, 90/70 °C). Indeed, the WWTP is located near a zone of collective habitats and a public swimming pool, which in total require 7.4 GWh annually. Because of the seasonal variation of the needs (in heating mainly), the net thermal balance was improved from -3.2 to $+2$ GWh.

Heat recovery from surrounding processes or within the drying system is rather commonly found in low-temperature belt dryers (Permuy Vila, 2008, 2010). In the area of Alicante (Spain), the sludges produced by four WWTP located within 14 km of a cement factory are collected and dried on the site of the cement factory. Annually, 46 785 MWh are recovered from the kiln exhaust gases and the clinker cooling gases to evaporate 40 235 tons of water. Taking into account their dust content, combustion gases cannot be introduced directly into the dryer. A gas-water heat exchanger is thus placed in parallel to the gas cooler of the cement manufacturing process to produce hot water between 75 and 90 °C. With a specific heat consumption of 4186 kJ kg^{-1}, the energy consumption ratio of this dryer is close to 1.67. Even if R_D is quite high, no primary energy is consumed in the drying system. Moreover, the dry sludges, the LHV of which is 12.54 MJ kg^{-1}, are directly burned in the cement kiln, improving the carbon footprint of the factory. In addition to the use of the general services of the cement factory (lorry access zone, weighing systems, gas emission measurements), this integrated solution combines recovery of waste energy with perennial elimination of sewage sludges, and energy production. Following the same idea, thermal energy is recovered from the gas engine CHP plant (on the engine block and the exhaust fumes) and used to heat the drying air of the four low-temperature belt dryers implemented in the WWTP of Metrofang (Barcelona, Spain). These dryers replaced high-temperature belt dryers, and the decrease in the temperature has doubled the quantity of energy available for drying. A heat pump can also be coupled to these low-temperature belt dryers, such as, for instance, in the WWTP of Louis Fargues (Bordeaux, France).

To highlight the energy benefit, let us take the example of a WWTP producing 25 000 tons per annum of mechanically dewatered sludges, which have to be dried from 25% to 70% solids. The drying air is assumed to be introduced at a temperature of 70 °C with a relative humidity of 8%. At the dryer outlet, the temperature and relative humidity of the drying air are 35 °C and 80%, respectively. Before it is recycled in the drying system, the gas stream is dehumidified in contact with a cold surface at 20/30 °C and then heated in an exchanger at 75/90 °C. According to these assumptions, the specific heat consumption of the dryer is close to 4110 kJ kg^{-1}, which leads to an energy consumption ratio of 1.64. For the same drying facility coupled to a heat pump, functioning between a hot source at 80 °C and a cold source at 20 °C, the specific heat consumption of the dryer falls to 775 kJ kg^{-1}, leading to an energy consumption ratio of 0.52. The capital cost is, of course, higher but the operating costs are significantly reduced (Permuy Vila, 2010). This solution is particularly interesting for intermediate-size WWTP. If fatty acids are present in the exhaust vapor, special attention must be paid to the grade of steel used in the condenser.

8.4
Thermal Valorization of Sewage Sludge

As mentioned earlier, the water content at the end of mechanical dewatering is still very high. This water content depends mostly on the origin of the sludge. According to experience, the water content for a non-digested sludge can be as high as 20% and can reach 30% for digested sludge. These values depend mainly on the waste water process used. Another point is that, during anaerobic digestion, methane is produced, leading to a decrease in carbon content and an increase in the mineral part: this results in a decrease in the heating value. The mineral part is mainly composed of Fe, P, Ca, Al, Si and other alkalis and heavy metals. Their behavior during thermal treatment is complex but does not depend on the drying process, except if clay or limestone is used (Elled *et al.*, 2007; Ischia *et al.*, 2011).

8.4.1
General Description of the Thermal Processes Available for Sewage Sludge

Since sewage sludge is a waste, its thermal processing must be integrated in the entire scheme or route towards final treatment, such as landfilling, composting, soil amendment and so on. In this frame, incineration, pyrolysis and gasification are used to reduce the volume, facilitate disposal and serve as the ultimate waste processing. Thermal processes for valorization, mainly incineration, have been well investigated for sewage sludge (Werther and Ogada, 1999), even though the dry mass available is weak compared to other biomass or waste. The high initial water content of sewage sludge means that a drying step is essential. The basic idea is to use the carbonaceous matter as a source of renewable energy in the near future. The main thermal valorization processes are incineration, wet air oxidation, pyrolysis, and gasification. Distinctions between these processes are based on the prevailing temperature and gaseous atmosphere.

For *incineration*, temperatures are kept close to 900 °C and the gaseous atmosphere is air. The air ratio used is close to 200%. The outputs of the process are flue gas and a solid phase (ash). The reactions are exothermic. At least regarding combustion, it is advisable to derive conditions for the auto-ignition of the wet sewage sludge from an enthalpy balance with a flame temperature of 600 °C. This generally gives values of siccity close to 50%.

Wet air oxidation (Lendormi *et al.*, 2001) consists in contacting air or oxygen with humid sewage sludge at a mild temperature (150–300 °C) and high pressure (15–30 MPa). As this oxidation occurs in the liquid phase, oxygen transfer from the vapor phase to the liquid phase is limited due to very low Hatta numbers. Thus industrial processes are currently working with very high air ratios (up to 500%), and use catalysts in order to perform at the lower temperature of the mentioned range.

Pyrolysis is realized at temperatures ranging from 400 to 800 °C. The output products are a combustible gas composed mainly of methane, hydrogen, CO and CO_2, an oil that is a mixture of many compounds with an average heating value close to that of the initial sewage sludge, and so-called char, a solid phase containing the mineral matter and a high content of carbon. Some distinctions can be made according to the power density received. At high density, the oil fraction is the most important. Classical compositions of output products and their associated heating values can be found in Jacobs *et al.* (2003). Reactions are slightly endothermic at 500 °C and slightly exothermic at higher temperatures.

Finally, *gasification* is realized at temperatures close to 900 °C and can be carried out under various initial atmospheres (air ratio up to 0.3, H_2O and air, CO_2 and H_2O, pure steam). The basic idea is to use either steam or CO_2 to react with carbon:

$$C + CO_2 \rightarrow 2CO$$
$$C + H_2O \rightarrow CO + H_2$$

Air is generally insufflated to give a partial oxidation, and then to produce internal heating via $C + O_2 \rightarrow CO_2$, this reaction being exothermic. Outputs of the process are a combustible gas called *syngas* and ash. Composition and heating value for syngas can be found in Ferrasse *et al.* (2003b) for different configurations.

Both last mentioned processes are, in the field of sewage sludge, still under development but, in contrast, incineration is well developed, with, for example, about 170 incinerators installed in the United States of America.

8.4.2
Desired Water Content for Thermal Processes

Drying is essential to increase the dry solids content of the product prior to thermal valorization, depending on the considered process, as summarized in Tab. 8.6.

If the only purpose of incineration is to treat the sludge on site, the water content has to be adjusted to reach autothermicity, otherwise fuel has to be added. When combustion is coupled with municipal solid waste (MSW) incinerators or other thermal needs, the highest possible siccity is required, because the heating value of the sludge as a fuel is used to regulate MSW incineration.

Tab. 8.6 Dry solids contents (DS) required for various valorization processes.

Process	Dry solids content	LHV_{ar} (kJ kg^{-1})
Incineration in specific furnace	$30\% < DS < 45\%$	3000–5000 Autothermicity
Co-incineration with municipal domestic waste	$60\% < DS < 90\%$	8400–17 000
Pyrolysis/Gasification	$DS > 95\%$	≅14 000

The pyrolysis of wet product is never desired because water is produced by pyrolysis and concentrated in the oil phase. This oil has, thus, a natural content of water close to 20 wt%, even when starting with a completely dry product. Adding more water means a decrease in the heating value. Consequently, sludges must have been dried to a minimum 95% DS before any pyrolysis process.

As gasification is endothermic, heat will have to be furnished to the process. As in the case of dryers, two ways can be distinguished: direct heating realized by adding air in the gasification atmosphere, leading to the partial combustion already mentioned, or indirect heat transfer by heating the bed materials in an auxiliary reactor (case of a fluidized bed) or by the wall. When wet sludge enters the reactor, it is generally accepted that there exists a drying zone producing steam. This steam then acts as a gasification agent. An optimal ratio between steam and raw biomass is generally determined by studying the composition of the syngas at the outlet of the gasifier. This study is done by equilibrium calculations (Li *et al.*, 2001) and depending on the chosen criteria (hydrogen production, hydrogen to carbon monoxide ratio) a desired ratio is defined. The ratio of steam to sewage sludge corresponds to water contents close to unity (50% water, 50% dry sludge) in studies performed with pure steam. If air is added, the dilution by nitrogen will lead to poor syngas quality, but no more external heat will have to be furnished. As a consequence, it is favorable to let sludge with an initial dry solids content between 50% and 100% enter a gasification process.

Wet air oxidation requires no pre-drying. On the contrary, to be successful in keeping the autothermicity of the process, humid sewage sludge is required, leading sometimes to deliberately sub-optimal operation of the mechanical dewatering.

8.4.3 Including a Drying Step Before Thermal Valorization

As wet sludge is a paste, a great advantage of the drying step is the formatting: pellets with a rather constant mean diameter can be obtained. These pellets can be easily conveyed and eventually fluidized. Matter losses during drying mainly concern water. Losses of some minerals, like K, or N, via ammonia release, are generally observed. Such losses can be problematic on a long-term operation period for dryers, but they do not modify significantly the general composition of the sludge to present any kind of advantages or disadvantages regarding the subsequent thermal treatment.

The use of dryers before a thermal treatment should be evaluated by consideration of the following aspects:

- the heat input required by the dryer
- the increase in heating value
- the formatting
- the already conducted and "paid" phase change of water

8.5
Energy Efficiency of Thermal Valorization Routes

8.5.1
Importance of Dryer Efficiency

Regarding thermal valorization of any type of biomass, the energy efficiency of the disposal routes depends mainly on:

- the calorific value of the dry biomass, related to the organic fraction;
- the water content at the dryer inlet;
- the energy efficiency of the dryer, characterized by the ratio between the energy required to dry the product and the latent heat of vaporization, R_D.

The influence of the biomass on the thermal efficiency of the disposal routes is illustrated in Figs. 8.13 and 8.14 for the case of incineration. A lower heating value of 8 MJ kg^{-1} is assumed for all the fuels at the boiler inlet, which implies various water contents at the boiler inlet. The initial water contents and the lower heating values of the dry matter used for this assessment are reported in Tab. 8.7. The results clearly show the importance of the dryer efficiency. Even with a dryer considered as efficient,

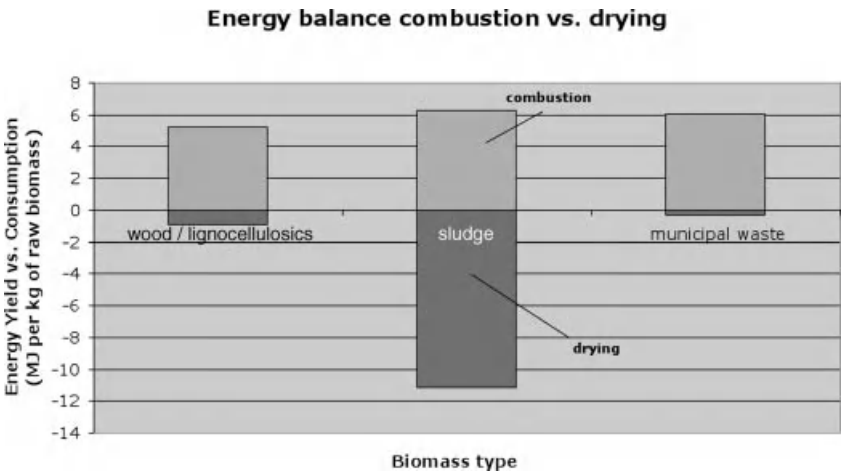

Fig. 8.13 Energy assessment of a thermal disposal route including moderately efficient thermal drying ($R_D = 1.25$) and specific combustion for 1 kg of fuel with LHV= 8 MJ kg^{-1} (Lecomte and Arlabosse, 2009).

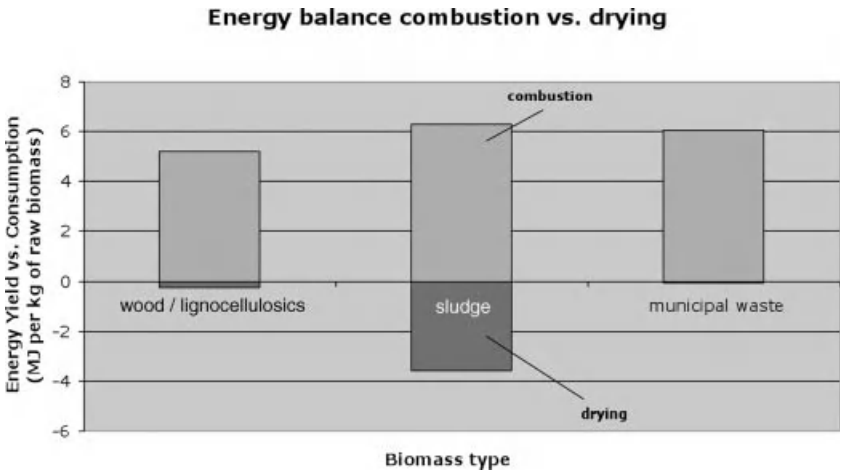

Fig. 8.14 Energy assessment of a thermal disposal route including highly efficient thermal drying ($R_D = 0.4$) and specific combustion for 1 kg of fuel with LHV = 8 MJ kg^{-1} (Lecomte and Arlabosse, 2009).

Tab. 8.7 Initial water content and lower heating value of dry lignocellulosic biomass, sludge and municipal waste.

	$X_{initial}$ (dry basis)	LHV of dry matter (MJ kg^{-1})
Dry lignocellulosic biomass	0.5	18
Sludge	4	9
Municipal waste	0.5	12

that is, $R_D = 1.25$, the net energy assessment of the thermal disposal route becomes negative for very wet materials like sludge. Optimization has to be performed, see Sections 8.3.2 and 8.3.3, in order to drastically decrease R_D, so that a moderate net energy production can be achieved. In order to get a neutral energy balance for sludge combustion, dewatering and drying technologies with about $R_D = 0.7$ are required. With a better efficiency (for instance $R_D = 0.4$), energy production from sludges can even become viable.

8.5.2
Combining Sludge Drying and Thermal Valorization by Integrating on Site

Combining a thermal process and a sewage sludge dryer depends, of course, on the location of the dryer relative to the wastewater treatment plant, and on the aim of the installation. We will focus on energy integration for neighboring process. Energy integration can be studied by pinch analysis. Pinch analysis (which is basically also an exergetic analysis) is a guide to calculating the minimum energy (heat, work) needed, and possible maximum recoverable energy for a plant. Following the pinch analysis

several methods exist to design the plant in an optimal manner (Kemp, 2007). Coupling the pinch analysis with a process simulator allows rapid parameter studies. Several algorithms can be used to interrogate the simulator in a relevant way (Lefèvre *et al.*, 2011; Gassner and Marechal, 2009).

Examples of results combining an air dryer and an incinerator on the one hand, and a steam dryer and a gasifier on the other hand, are given below. These results illustrate the effect of the product dryness entering the dryer for simplified schemes that include the principal apparatuses. To be complete, such studies should integrate the wastewater treatment plant. Integration is provided here for two cases. In both cases, the R_D is equal to 1.25 and the LHV_{db} of the sewage sludge is 17 MJ kg^{-1}. First, an incinerator is coupled with an air convective dryer and the moist air is partially (the stoechiometry is kept constant) used as an oxidizer. Second, a gasifier is coupled with a steam dryer. The steam flow is used to activate gasification in a ratio of 1 kg of steam per 1 kg of dry biomass and the gas is burned with an air ratio of 1.06. The results presented in Fig. 8.15 show the evolution of the energy needed to get autothermicity of the whole coupled processes with changing inlet product dryness. Zero means that no additional energy is required to run the whole coupling. Negative values represent available heat. Increasing the inlet dryness above the autothermicity limit would increase the amount of available heat and the temperature from which this heat would be available.

It must be kept in mind that coupling a combustor or gasifier with a dryer makes heat available at high temperature. Thus there is a real possibility of considering sludge as a tank of energy. But if the whole waste water treatment plant is considered, this conclusion should be moderated: the total energy consumption of the plant, mainly for

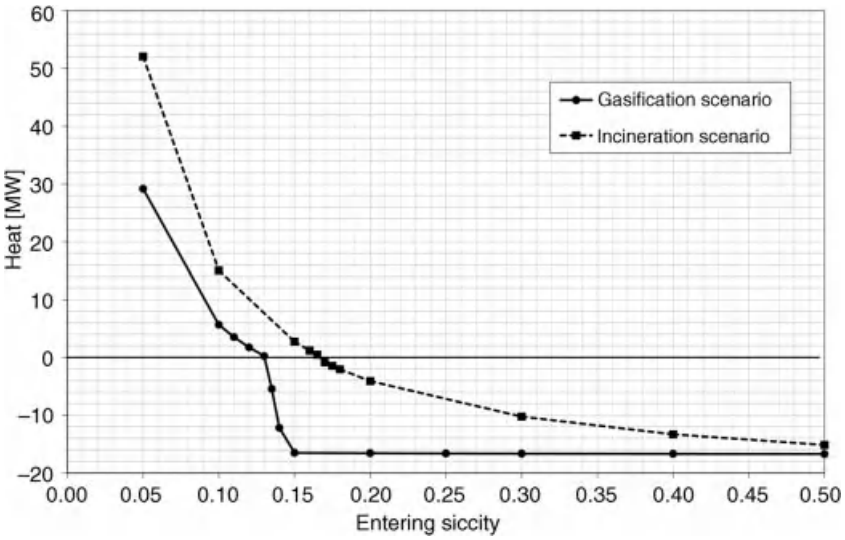

Fig. 8.15 Influence of sludge dryness at the inlet of the dryer on the energy balance.

aeration, brings the energy balance close to zero. Some heat at moderate temperature (300–400 °C) remains available, which could fulfill district heating demands.

8.6 Conclusions

Following the current trends which promote waste valorization routes, processes allowing energy recovery from sludge are expected to develop. Within this context, drying constitutes a crucial step upstream from incineration, gasification or pyrolysis, due to its large impact on the global energy balance. However, efforts have to be made to optimize the whole treatment chain, from sludge production, dewatering, drying, to energy recovery. Each stage and their coupled effects have to be examined for the design of sustainable "zero energy wastewater treatment plant". One of the most challenging parts remains the better understanding of the mechanisms governing sludge drying, depending on the sludge origin and previous treatment. Any improvement of the knowledge in this area should lead to the conception of dedicated sludge dryers in a more rational way, contributing to the success of the whole valorization process.

Additional Notation Used in Chapter 8

[A]	mass fraction of element A, on dry basis	–
HHV	higher heating value	$MJ\,kg^{-1}$
i	mass fraction of inerts or ash	–
LHV	lower heating value	$MJ\,kg^{-1}\,m$
N_{mix}	mixing number	–
o	oil content per mass of dry solids	–
Q	amount of heat	J
R_D	dryer energy consumption ratio	–
S	mass fraction solids	–
SHC	specific heat consumption	$J\,kg^{-1}$
t_R	duration of fictitious static period	s
w	mass fraction of water	–

Subscripts and Superscripts

ar	as received (wet)
D	dryer
daf	dry and ash-free
db	on a dry basis
pds	fry-dried sludge

Abbreviations

CHP	combined heat and power plant
DS	dry solids content
EE	evaporated water
HV	heating value
MSW	municipal solid waste
PE	population equivalent
PFRP	process to further reduce pathogens
VOC	volatile organic compound
WWTP	wastewater treatment plant

References

ADEME, CETIAT, 2000. *Les Procédés de séchage dans l'industrie*. ADEME Editions, Angers, France.

AFNOR, 2008. Caractérisation des boues - Bonne pratique pour le séchage des boues. FD X33-047.

Arlabosse, P., 2001. Etude des procédés de séchage des boues urbaines et industrielles. Study Contract No. 99-0217/1A for the association RE.CO.R.D.

Arlabosse, P., Chitu, T., 2007. Identification of the limiting mechanism in contact drying of agitated sewage sludge. *Drying Technol.* **25**(4): 557–567.

Arlabosse, P., Lecomte, D., 2008. Valorisation de la biomass humide: Problématique de la déshydratation et du séchage. *Proceedings of the 10èmes Journées Cathala-Letort de prospective scientifique et technique, Le Génie des Procédés au service de l'Environnement: Enjeux et défis*, Toulouse, France, October 1–2, 2008.

Bengtsson, M., Tillman, A.-M., 2004. Actors and interpretations in an environmental controversy: The Swedish debate on sewage sludge use in agriculture. *Resour. Conserv. Recy.* **42**(1): 65–82.

Canler, J.-P., 2010. Le séchage solaire des boues: Etat de l'art et retours d'expérience. *Proceedings of the Journées techniques de l'OIEau, Innovations technologiques et retours d'expérence en traitement des boues*, Paris, France, November 17, 2010.

Carrington, E. G., 2001. Evaluation of sewage sludge treatments for pathogens reduction. Study Contract No B4-3040/2001/322179/MAR/A2 for the European Commission.

CEN European Committee for Standardization, 2007. Characterization of sludges: Good practice for sludges drying. CEN/TR/15473:2007.

Chabrier, J. P., 2008. France sludge drying return experience: The consultant's point of view. *Proceedings of European Conference on Sludge Management (ECSM'08)*, Liège, Belgium, September 1–2, 2008 (CD-Rom).

Chabrier, J. P., 2010. Le séchage thermique industriel. *Proceedings of the Journées techniques de l'OIEau, Innovations technologiques et retours d'expérience en traitement des boues*, Paris, France, November 17, 2010.

Courtois, G., 2000. Biological contaminations. *Proceedings of "Sludges:Which stakes? Which solutions?"*, Pau, France, February 23–24, 2000, pp. 26–27.

Cousin, F., 2010. Innoplana: New developments of the highly efficient sludge drying process Innodry(r) 2E. *Proceedings of Second European Conference on Sludge Management (ECSM 2010)*, Budapest, Hungary, September 9–10, 2010 (CD-Rom).

Couturier, C., 2010. Stations d'épuration à énergie positive, vers l'optimisation exergétique: Illustration avec la station d'épuration de Saint Brieuc. *Proceedings of the Journées Techniques Nationales "Station d'épuration et énergie, Empreinte environnementale et vision intégrée"*, Toulouse, France, June 10–11, 2010.

da Motta, M., Pons, M. N., Roche, N., Vivier, H., 2001. Characterisation of activated sludge by automated image analysis. *Biochem. Eng. J.* **9**(3): 165–173.

Delmas, F., Maisonnave, V., Fulladosa, E., Villaescusa, I., Soleilhavoup, J. P., Murat, J. C., 2000. Comparative evaluation of the potential noxiousness in domestic sludge used in agriculture and in commercial fertilizers. *Ecotox. Environ. Safe.* **47**(3): 292–297.

Deng, W., Yan, J., Li, X., Wang, F., Zhu, X., Lu, S., Cen, K., 2009a. Emission characteristics of volatile compounds during sludges drying process. *J. Hazard. Mater.* **162**(1): 186–192.

Deng, W. Y., Yan, J. H., Li, X. D., Wang, F., Lu, S. Y., Chi, Y., Cen, K. F., 2009b. Measurement and simulation of the contact drying of sewage sludge in a Nara-type paddle dryer. *Chem. Eng. Sci.* **64**(24): 5117–5124.

Dittler, A., Bamberger, T., Gehrmann, D., Schlünder, E.-U., 1997. Measurement and simulation of the vacuum contact drying of pastes in a LIST-type kneader drier. *Chem. Eng. Process.* **36**(4): 301–308.

Elled, A. L., Amand, L. E., Leckner, B., Andersson, B. A., 2007. The fate of trace elements in fluidised bed combustion of sewage sludge and wood. *Fuel* **86** (5–6): 843–852.

European Community, 1999. Council Directive 1999/31/EC of 26 April 1999 on the landfill of waste.

Ferrasse, J. H., Arlabosse, P., Lecomte, D., 2002. Heat, momentum, and mass transfer measurements in indirect agitated sludge dryer. *Drying Technol.* **20**(4–5): 749–769.

Ferrasse, J. H., Chavez, S., Arlabosse, P., Dupuy, N., 2003a. Chemometrics as a tool for the analysis of evolved gas during the thermal treatment of sewage sludge using coupled TG-FTIR. *Thermochim. Acta* **404** (1–2): 97–108.

Ferrasse, J. H., Seyssiecq, I., Roche, N., 2003b. Thermal gasification: A feasible solution for sewage sludge valorisation? *Chem. Eng. Technol.* **26**(9): 941–945.

Fjallborg, B., Dave, G., 2003. Toxicity of copper in sewage sludge. *Environ. Int.* **28** (8): 761–769.

Fraikin, L., Herbreteau, B., Chaucherie, X., Nicol, F., Crine, M., Léonard, A., 2010a. Impact of storage at 4 °C on the study of sludge drying emissions. *Proceedings of Second European Conference on Sludge Management (ECSM 2010)*, Budapest, Hungary, September 9–10, 2010.

Fraikin, L., Herbreteau, B., Chaucherie, X., Nicol, F., Salmon, T., Crine, M., Léonard, A., 2010b. Impact of storage duration on the emissions of ammonia and VOC during the convective drying of urban residual sludges. *Proceedings of 17th International Drying Symposium (IDS2010)*, Magdeburg, Germany, October 3–6, 2010, Volume B, pp. 738–741.

Fuentes, A., Llorens, M., Saez, J., Aguilar, M. I., Ortuno, J. F., Meseguer, V. F., 2004. Phytotoxicity and heavy metals speciation of stabilised sewage sludges. *J. Hazard. Mater.* **108**(3): 161–169.

Gantzer, C., Gaspard, P., Galvez, L., Huyard, A., Dumouthier, N., Schwartzbrod, J., 2001. Monitoring of bacterial and parasitological contamination during various treatment of sludge. *Water Res.* **35**(16): 3763–3770.

Gassner, M., Marechal, F., 2009. Methodology for the optimal thermo-economic, multi-objective design of thermochemical fuel production from biomass. *Comput. Chem. Eng.* **33**(3): 769–781.

Houillon, G., Jolliet, O., 2005. Life cycle assessment of processes for the treatment of wastewater urban sludge: Energy and global warming analysis. *J. Clean Prod.* **13**(3): 287–299.

Huron, Y., Salmon, T., Crine, M., Blandin, G., Léonard, A., 2010. Effect of liming on the convective drying of urban residual sludges. *Asia-Pac. J. Chem. Eng.* **5**(6): 909–914.

Ischia, M., Dal Maschio, R., Grigiante, M., Baratieri, M., 2011. Clay-sewage sludge co-pyrolysis: A TG-MS and Py-GC study on potential advantages afforded by the presence of clay in the pyrolysis of wastewater sewage sludge. *Waste Manag* **31**(1): 71–77.

Jacobs, U., Haintz, J., Kappel, J., 2003. Selection criteria for sludge drying plants: Belt, drum and fluidised bed dryers. *Proceedings of VDI Meeting "Sewage sludge, Meat and bone meal, Manure, Biogenous wastes"*, Bamberg, Germany.

Jarde, E., Mansuy, L., Faure, P., 2003. Characterization of the macromolecular organic content of sewage sludges by thermally assisted hydrolysis and

methylation-gas chromatography-mass spectrometer (THM-GC/MS). *J. Anal. Appl. Pyrol.* **68**(9): 331–350.

Kemp, I. C., 2005. Reducing dryer energy use by process integration and pinch analysis. *Drying Technol.* **23**(9–11): 2089–2104.

Kemp, I. C., 2007. *Pinch analysis and process integration: A user guide on process integration for the efficient use of energy.* 2nd edn, Elsevier, Butterworth-Heinemann, Oxford, UK.

Lecomte, D., Arlabosse, P., 2009. Valorisation énergétique de la biomasse et des déchets humide. *Proceedings of Conférence Internationale sur la Valorisation des Déchets et de la Biomasse Résiduelle dans les Pays en Développement*, Ouagadougou, Burkina Faso.

Lefèvre, S., Ferrasse, J.-H., Boutin, O., Sergent, M., Faucherand, R., Viand, A., 2011. Process optimisation using the combination of simulation and experimental design approach: Application to wet air oxidation. *Chem. Eng. Res. Des.* **89**(7): 1045–1055.

Lendormi, T., Prevot, C., Doppenberg, F., Foussard, J. N., Debellefontaine, H., 2001. Subcritical wet oxidation of municipal sewage sludge: Comparison of batch and continuous experiments. *Water Sci. Technol.* **44**(5): 161–169.

Léonard, A., Martin, G., Nicolas, J., Romain, A.-C., Crine, M., 2007. Study of VOC and odour emissions during the convective drying of urban residual sludges. *Proceedings of Symposium International sur les Ecotechnologies appliquées aux boues résiduaires, Eco-process et Eco-utilisation*, Montoldre, France, October 2–3, 2007.

Léonard, A., Meneses, E., Le Trong, E., Salmon, T., Marchot, P., Toye, D., Crine, M., 2008. Influence of back mixing on the convective drying of residual sludges in a fixed bed. *Water Res.* **42**(10–11): 2671–2677.

Li, X., Grace, J. R., Watkinson, A. P., Lim, C. J., Ergudenler, A., 2001. Equilibrium modeling of gasification: A free energy minimization approach and its application to a circulating fluidized bed coal gasifier. *Fuel* **80** (2): 195–207.

Milieu Ltd, WRc, RPA, 2008. Environmental, economic and social impacts of the use of sewage sludge on land – Part I: Overview Report. Study Contract DG ENV.G.4/ETU/ 2008/0076r.

Moller U., 1990. *Klärschlammbehandlung - verwertung und Entsorgunug auf weiter gesteigertm Niveau unte Einsatz von Klarschlammtrocknung*, Abwassertechnik, Abfalltechnik & Recycling, **41**, pp. 16–22.

Metcalf & Eddy, Inc., 2003. *Wastewater engineering, treatment and reuse.* 4th edn, McGrawHill, New York, USA.

Moreira, R. G., Castell-Perez, M. E., Barrufet, M. A., 1999. *Deep-fat frying fundamentals and application*, Aspen Publisher, Maryland, USA.

Niessen, W. R., 1995. *Combustion and incineration processes.* Marcel Dekker, New York, USA.

Office, U. S. G. P., 1997. Code of Federal Regulations, Title 40: Protection of Environment, Chapter I: Environmental Protection Agency, Part 503: Standards for the use or disposal of sewage sludge.

Parikh, J., Channiwala, S. A., Ghosal, G. K., 2005. A correlation for calculating HHV from proximate analysis of solid fuels. *Fuel* **84** (5): 487–494.

Peregrina, C., Arlabosse, P., Lecomte, D., Rudolph, V., 2006a. Heat and mass transfer during fry-drying of sewage sludge. *Drying Technol.* **24**(7): 797–818.

Peregrina, C. A., Lecomte, D., Arlabosse, P., Rudolph, V., 2006b. Life cycle assessment (LCA) applied to the design of an innovative drying process for sewage sludge. *Process Saf. Environ.* **84**(B4): 270–279.

Peregrina, C., Rudolph, V., Lecomte, D., Arlabosse, P., 2008. Immersion frying for the thermal drying of sewage sludge: An economic assessment. *J. Environ. Manage.* **86**(1): 246–261.

Permuy Vila, D., 2008. Low temperature thermal drying: An opportunity for residual energies. *Proceedings of European Conference on Sludge Management (ECSM'08)*, Liège, Belgium, September 1–2, 2008 (CD-Rom).

Permuy Vila, D., 2010. Options de récupération énergétique dans un sécheur basse température. *Proceedings of Journées Techniques Nationales "Station d'épuration et énergie, Empreinte environnementale et vision intégrée"*, Toulouse, France.

Pimor, M., 2003. *Suivi du fonctionnement d'installation de séchage thermique de boues résiduaires urbaines.* MSc Thesis, Ecole des Mines de Douai.

Poulsen, T. G., Hansen, J. A., 2003. Strategic environmental assessment of alternative sewage sludge management scenarios. *Waste Manag. Res.* **21**(1): 19–28.

Ressent, S., 2000. Campagnes de mesures réalisées sur des sécheurs de boues de stations d'épuration urbaines et industrielles, Report for the Agence de l'eau Seine Normandie.

Réveillé, V., Mansuy, L., Jardé, E., Garnier-Sillam, E., 2003. Characterisation of sewage sludge-derived organic matter: Lipids and humic acids. *Org. Geochem.* **34**(4): 615–627.

Romdhana, M. H., Busset, G., Appin, Y., Montréjaud-Vignoles, M., Lecomte, D., Simon, V., Sablayrolles, C., 2010a. Life cycle assessment to design fry-drying process of indusrial biomass. *Proceedings of WasteEng 2010, 3rd International Conference on Engineering for Waste and Biomass Valorisation*, Beijing, China.

Romdhana, M. H., Hamasaiid, A., Ladevie, B., Lecomte, D., 2009b. Energy valorization of industrial biomass: Using a batch frying process for sewage sludge. *Bioresource Technol.* **100**(15): 3740–3744.

Romdhana, M. H., Lecomte, D., Ladevie, B., 2010b. Dimensionless formulation of convective heat transfer in fry-drying process of sewage sludge. *Proceedings of 17th International Drying Symposium (IDS 2010)*, Magdeburg, Germany, October 3–6, 2010, Volume A, pp. 221–226.

Romdhana, M. H., Lecomte, D., Ladevie, B., Sablayrolles, C., 2009b. Monitoring of pathogenic microorganisms contamination during heat drying process of sewage sludge. *Process Saf. Environ.* **87**(6): 377–386.

Royer, S., Blandin, G., Salmon, T., Fraikin, L., Crine, M., Léonard, A., 2010. Impact of liming operating conditions on the convective drying kinetics of urban residual sludges. *Proceedings of Second European Conference on Sludge Management (ECSM 2010)*, Budapest, Hungary, September 9–10, 2010.

Sahlstrom, L., Aspan, A., Bagge, E., Danielsson-Tham, M. L., Albihn, A., 2004. Bacterial pathogen incidences in sludge from Swedish sewage treatment plants. *Water Res.* **38**(8): 1989–1994.

Schlünder, E. U., 1998. *Heat-Exchanger Design Handbook, Section 3.13*. Hemisphere, New York, USA.

Schlünder, E. U., Mollekopf, N., 1984. Vacuum contact drying of free flowing mechanically agitated particulate material. *Chem. Eng. Process.* **18**(2): 93–111.

Sheng, C. D., Azevedo, J. L. T., 2005. Estimating the higher heating value of biomass fuels from basic analysis data. *Biomass Bioenerg.* **28**(5): 499–507.

Thipkhunthod, P., Meeyoo, V., Rangsunvigit, P., Kitiyanan, B., Siemanond, K., Rirksomboon, T., 2005. Predicting the heating value of sewage sludges in Thailand from proximate and ultimate analyses. *Fuel* **84**(7–8): 849–857.

Tsotsas, E., Schlünder, E. U., 1986a. Contact drying of mechanically agitated particulate material in the presence of inert gas. *Chem. Eng. Process.* **20**(5): 277–285.

Tsotsas, E., Schlünder, E. U., 1986b. Vacuum contact drying of free flowing mechanically agitated multigranular packings. *Chem. Eng. Process.* **20**(6): 339–349.

Turovskiy, I. S., Mathai, P. K., 2006. *Wastewater sludge processing*. John Wiley & Sons, Inc., Hoboken, NJ, USA.

US EPA, 1979. *Process design manual, Sludge treatment and disposal*. US Environmental Protection Agency.

Vaxelaire, J., Cézac, P., 2004. Moisture distribution in activated sludges: A review. *Water Res.* **38**(9): 2215–2230.

Villar, P., Callejon, M., Alonso, E., Jimenez, J. C., Guiraum, A., 2004. Optimization and validation of a new method of analysis for polycyclic aromatic hydrocarbons in sewage sludge by liquid chromatography after microwave assisted extraction. *Anal. Chim. Acta* **524**(1–2): 295–304.

Wang, F., 2010. Study on sludge drying and incineration in China. *Proceedings of Joint Seminar on Waste and Biomass Valorization between Zhejiang University and Ecole des Mines d'Albi Carmaux*, Hangzhou, China.

Warman, P. R., Termeer, W. C., 2005. Evaluation of sewage sludge, septic waste and sludge compost applications to corn and forage: Ca, Mg, S, Fe, Mn, Cu, Zn and B content of crops and soils. *Bioresource Technol.* **96**(9): 1029–1038.

Werther, J., Ogada, T., 1999. Sewage sludge combustion. *Prog. Energy Combust. Sci.* **25** (1): 55–116.

Wunschmann, J., Schlünder, E. U., 1980. Heat transfer from heated surfaces to spherical packings. *Int. Chem. Eng.* **20** (4): 555–563.

Zsirai, I., 2010. Sewage sludge as renewable energy. *Proceedings of ECSM 2010, Second European Conference on Sludge Management, Budapest*, Hungary, September 8–10, 2010.

Index

Modern Drying Technology Volume 4: Energy Savings, First Edition.
Edited by Evangelos Tsotsas and Arun S. Mujumdar.